



MONASH University

**Inhibitors of SPSB-iNOS Interactions as a
Potential Novel Class of Anti-infectives**

Beow Keat Yap

B.Pharm. (Hons), M.Med.Sc.

The thesis is submitted in total fulfilment of the
requirements for the degree of Doctor of Philosophy

2016

Medicinal Chemistry
Faculty of Pharmacy and Pharmaceutical Sciences
Monash University
Australia

Copyright notice

© The author (2016). Except as provided in the Copyright Act 1968, this thesis may not be reproduced in any form without the written permission of the author.

I certify that I have made all reasonable efforts to secure copyright permissions for third-party content included in this thesis and have not knowingly added copyright content to my work without the owner's permission.

Monash University

Declaration for thesis based or partially based on conjointly published or unpublished work

General declaration

In accordance with Monash University Doctorate Regulation 17.2 Doctor of Philosophy and Research Master's regulations the following declarations are made:

I hereby declare that this thesis contains no material which has been accepted for the award of any other degree or diploma at any university or equivalent institution and that, to the best of my knowledge and belief, this thesis contains no material previously published or written by another person, except where due reference is made in the text of the thesis.

This thesis includes 4 original papers published in peer-reviewed journals (3 first-author, 1 co-author). The core theme of this thesis is the design, synthesis and characterisation of novel cyclic peptide inhibitors of SPSB-iNOS interactions as a potential novel class of anti-infectives. The ideas, development and writing up of all the papers in the thesis were the principal responsibility of myself, the candidate, working within the Department of Medicinal Chemistry, Faculty of Pharmacy and Pharmaceutical Sciences under the supervision of Professor Raymond Norton and associate supervision of Professor Jonathan Baell.

The inclusion of co-authors reflects the fact that the work came from active collaboration between researchers and acknowledges input into team-based research.

In the case of **Chapter 4, 5 and 6**, my contribution to the work involved the following:

Thesis chapter	Publication title	Publication status	Nature and extent of candidate's contribution
4	A potent cyclic peptide targeting SPSB2 protein as a potential anti-infective agent	Published	Designed and performed the experiments, analysed the data and wrote the manuscript. Total contribution = 70%
5	Redox-stable cyclic peptide inhibitors of the SPSB2-iNOS interaction	Published	Designed and performed the experiments, analysed the data and wrote the manuscript. Total contribution = 80%
6	Design, synthesis, and characterization of cyclic peptidomimetics of the inducible nitric oxide synthase binding epitope that disrupt the protein-protein interaction involving SPRY domain-containing suppressor of cytokine signaling box protein (SPSB) 2 and inducible nitric oxide synthase	Published	Designed and performed the experiments, analysed the data and wrote the manuscript. Total contribution = 40%

I have not renumbered sections of submitted or published papers in order to generate a consistent presentation within the thesis.

Signed: 

Date: 10/06/2016

List of publications

Yap, B. K., Leung, E. W. W., Yagi, H., Galea, C. A., Chhabra, S., Chalmers, D. K., Nicholson, S. E., Thompson, P. E., and Norton, R. S. (2014) A potent cyclic peptide targeting SPSB2 protein as a potential anti-infective agent, *J. Med. Chem.* **57**, 7006-7015.

Yap, B. K., Harjani, J. R., Leung, E. W. W., Nicholson, S. E., Scanlon, M. J., Chalmers, D. K., Thompson, P. E., Baell, J.B. and Norton, R. S. (2016) Redox-stable cyclic peptide inhibitors of the SPSB2-iNOS interaction, *FEBS Lett.* **590**, 696–704

Yap, B. K., Harjani, J. R., Thompson, P. E., Chalmers, D. K., Baell, J. B. and Norton, R. S. (2016) Stable protein ligands as anti-infective agents, *Aus Patent (Provisional)*, 2016900201.

Harjani, J. R., **Yap, B. K.**, Norton, R. S. and Baell, J. B. (2016) An alternative approach to the synthesis of peptides containing a cystathionine bridge, *Tetrahedron* **72**, 3256-3261.

Harjani, J. R., **Yap, B. K.**, Leung, E. W., Lucke, A., Nicholson, S. E., Scanlon, M. J., Chalmers, D. K., Thompson, P. E., Norton, R.S., and Baell, J. B. (2016) Design, synthesis, and characterization of cyclic peptidomimetics of the inducible nitric oxide synthase binding epitope that disrupt the protein-protein interaction involving SPRY domain-containing suppressor of cytokine signaling box protein (SPSB) 2 and inducible nitric oxide synthase, *J. Med. Chem.* doi:10.1021/acs.jmedchem.6b00386

Acknowledgements

First and foremost, I would like to thank the Malaysian government and the Universiti Sains Malaysia for providing me with the financial support to do my PhD study in one of the highly reputable research institutions in the world.

I would also like to express my deepest gratitude to Professor Ray Norton for his excellent supervision and for being a great mentor. He not only provided me with a lot of intellectual support and constructive criticism throughout my PhD but was also a good role model as a highly enthusiastic, professional and successful scientist. His guidance and undivided support have allowed me to build myself into a more independent researcher and I am very grateful to him for giving me a lot of opportunities during my PhD years to expand my skill sets and to improve myself.

I would also like to thank my Associate Supervisor Professor Jonathan Baell for his supervision during my PhD. He has always been very critical and supportive of the project and I am greatly appreciative of his fruitful ideas, opinions and suggestions throughout the whole supervision.

My sincere thanks also to other SPSB team members, especially to Dr Eleanor Leung for being very supportive and helpful, both scientifically and personally. She has never declined to help when needed and has always been very friendly and caring. The same applies to Dr Sandra Nicholson, Dr Hiromasa Yagi and Dr Jitendra Harjani for their unfailing support in the success of some of the experiments. Special thanks also to Dr David Chalmers and Associate Professor Philip Thompson for their guidance and supports, and Associate Professor Martin Scanlon for his constructive ideas and inputs on the project.

I am also very grateful to Professor Sebastien Perrier for allowing me to spend some valuable time in one of the world's leading polymer chemistry groups in the Department of Chemistry, University of Warwick, United Kingdom. This opportunity has allowed me to pick up some useful skills and techniques on polymer chemistry. Special thanks also to Dr Kristian Kempe, Dr Paul Wilson and especially Joji Tanaka for accommodating me and for the guidance and help throughout my laboratory attachment in the UK.

A special note of thanks also to Dr Tony Wang for being there to share the ups and downs, and to light up my otherwise “nothing but research” monotonous lifestyles.

Not forgetting my fellow lab mates and officemates (both former and current): Dr Samuel Robinson, Krishnarjuna Bankala, Dr San Sui Lim, Dr Jeff Chang, Dr Rodrigo Morales, Dr Indu Chandrasekaran, Dr Sandeep Chhabra, Dr Christopher MacRaid, Dr Keith Khoo, Stephen Drane, Jeff Seow, Cael Debono, Maiada, Michela, Nisa, Dr Kade Roberts, Oscar Liu, Krithika Sundaram, Andy Horne, Jo-Ann, Lynn and Yasemin. I am grateful to share this journey with you all.

Last but not least, I would like to specifically thank my wife, Samanthha Chang for her support, understanding and patience; my parents, brother, sister-in-law, sister and brother-in-law for their loves and supports; and finally my parents-in-law for providing the best care and love to my daughter, Ying Yi. Without them, this journey will not be even possible. Thank you once again.

Abstract

The SPRY-domain of the SOCS box protein 2 (SPSB2) plays an important role in the proteasomal degradation of inducible nitric oxide synthase (iNOS). SPSB2 knockout mice show prolonged expression of iNOS and enhanced killing of persistent pathogens such as *Mycobacterium tuberculosis* and *Leishmania major*, suggesting that inhibitors of the SPSB2-iNOS interaction represent a potential novel class of anti-infectives.

In this study, attempts to discover small molecule inhibitors of SPSB2-iNOS interaction were performed using *in silico* guided fragment-based drug design (FBDD) approach. The best fragment hit STK441224, however, was found to bind promiscuously to SPSB2 by saturation transfer difference spectroscopy (STD), Carr-Purcell-Meiboom-Gill (CPMG), ^{19}F and $[^1\text{H},^{15}\text{N}]$ -HSQC NMR experiments, with an estimated K_D of 1.8 mM by surface plasmon resonance (SPR). Further predictions by SiteMap and FTMap revealed that the iNOS binding site of SPSB2 is less druggable, explaining the poor outcome from the current FBDD campaign. Thus, other approaches to discover potent and specific inhibitors of the SPSB2-iNOS interaction were explored.

Utilising an *in silico* structure-based drug design approach, a disulphide-bridged cyclic peptide Ac-c[CVDINNNC]-NH₂ was designed and synthesised. It was found to bind to the iNOS binding site on SPSB2 with a K_D of 4.4 nM, as shown by SPR, $[^1\text{H},^{15}\text{N}]$ -HSQC and ^{19}F NMR experiments, with approximately 70-fold improvement in affinity, compared to the linear peptide DINNN ($K_D \approx 318$ nM). An *in vitro* assay on macrophage cell lysates further showed a complete inhibition of SPSB2-iNOS interactions by the cyclic peptide. In addition, the solution structure of the cyclic peptide was found to closely match that of the crystal structure of SPSB2-bound linear peptide DINNN with a backbone RMSD of 1.21 Å. The designed peptide was also found to be stable against pepsin, trypsin and α -chymotrypsin, and in human plasma.

The disulphide-bridged cyclic peptide, however, is reductively labile. To generate redox-stable inhibitors of SPSB2-iNOS interaction that would retain activity in the cell cytoplasm, two cyclic peptide analogues, one containing a thioether bridge (**CP1**) and the other a lactam bridge (**CP2**), as well as four cyclic peptidomimetics (**M1-M4**), incorporating organic moieties as cyclisation linkers, were generated. All analogues were able to bind to the iNOS binding site of SPSB2, with five of the six analogues binding

with stronger affinities (3-15 fold) than the linear peptide DINNN (**CP1**, K_D 31 nM; **CP2**, K_D 21 nM; **M1**, K_D 29 nM; **M2**, K_D 99 nM; **M3**, K_D 54 nM; **M4**, K_D 465 nM), as determined by ^{19}F NMR and SPR, respectively. All analogues were able to compete with full-length iNOS for binding to SPSB2 in macrophage cell lysates.

As **CP2** is the most potent redox-stable analogue, with more sites for derivatisation and is easier to synthesise compared to other analogues, **CP2** is being used as the template to generate analogues for macrophage-targeted delivery studies. Binding studies by SPR and ^{19}F NMR revealed an approximately 5-fold improvement in binding affinity of rhodamine B isothiocyanate (RBITC)-conjugated cyclic peptide analogue **CP4** to the iNOS binding site of SPSB2 ($K_D \approx 4$ nM), while the oligohistidine-conjugated analogues **CP5** and **CP6** showed a modest 1-2 fold drop in their binding affinities to SPSB2 compared to **CP2** ($K_D \approx 33$ -51 nM). Imaging studies of mannose or GalNAc glycopolymer-conjugated analogues of **CP4** (i.e. **CP7** and **CP8**, respectively) by confocal laser scanning microscopy revealed that both analogues were taken up by bone marrow-derived macrophages but not HEK 293 cells. On the other hand, oligohistidine-conjugated analogue **CP6** showed signs of endosomal escape after 9 h of incubation, although coincident signs of cell necrosis or apoptosis were observed in some of these macrophages.

In summary, several potent and stable cyclic peptide and peptidomimetic inhibitors of SPSB2-iNOS interactions were identified in this study. One of these analogues was able to be derivatised for macrophage-targeted delivery studies without negatively affecting their binding to SPSB2. This study also showed that both mannose and GalNAc glycopolymers are viable choices for macrophage-targeted delivery although more work to improve the endosomal escape of this new class of cyclic peptide inhibitors of SPSB2-iNOS interaction to the cytoplasm of macrophages without causing cell injury is needed.

Table of contents

Copyright notice	ii
General declaration	iii
List of publications	v
Acknowledgements.....	vi
Abstract.....	viii
List of abbreviations	xiii
Chapter 1: Introduction	1
1.1 Introduction.....	2
1.2 Antimicrobial resistance: mechanisms and strategies	4
1.3 SPSB-iNOS system.....	5
1.3.1 SPSB-iNOS interaction as potential anti-infective drug target	5
1.3.2 Molecular interaction between SPSB-iNOS.....	9
1.4 Targeting protein-protein interaction.....	11
1.4.1 Small molecule inhibitors	12
1.4.2 Cyclic peptides and peptidomimetics	16
1.5 Drug delivery	20
1.5.1 Macrophage-targeted drug delivery.....	20
1.5.2 Endosomal escape.....	21
1.6 Scope of the thesis	23
Chapter 2: General materials and methods	26
2.1 Introduction.....	27
2.2 General materials	27
2.2.1 Chemical reagents.....	27
2.2.2 Bacterial strain	27
2.2.3 Plasmid.....	27
2.2.4 Bacterial media	28
2.2.5 Buffers and solution.....	29
2.2.6 Instrument/Software.....	30

2.2.7 Web resources.....	31
2.3 General methods	32
2.3.1 Computational studies.....	32
2.3.2 SPSB2 expression and purification.....	35
2.3.3 Cyclic peptide and peptidomimetic synthesis and purification	39
2.3.4 Surface plasmon resonance.....	45
2.3.5 Nuclear magnetic resonance	48
2.3.6 Macrophage cell lysate inhibition assay	50
2.3.7 Other methods.....	54
Chapter 3: Discovery of fragment hit targeting SPSB2 protein via <i>in silico</i> and NMR-guided FBDD	55
3.1 Introduction.....	56
3.2 Materials and methods	56
3.2.1 Computational drug design and docking studies	56
3.2.2 Nuclear magnetic resonance (NMR) experiments.....	58
3.2.3 Surface plasmon resonance (SPR) experiments	61
3.3 Results.....	62
3.3.1 Key interactions essential for SPSB2-iNOS binding.....	62
3.3.2 13 potential hits were identified from <i>in silico</i> screening.....	64
3.3.3 Two <i>in silico</i> hits gave positive responses in STD and CPMG.....	64
3.3.4 The two potential hits bound at low millimolar affinities	68
3.3.5 The potential hits bound weakly or promiscuously to SPSB2.....	70
3.3.6 The iNOS binding site of SPSB2 is less druggable	73
3.4 Discussion.....	74
3.5 Conclusions.....	75
Chapter 4: Disulphide-bridged cyclic peptide inhibitor of SPSB2-iNOS interaction	77
4.1 Declaration for Thesis Chapter 4.....	78
4.2 Introduction.....	79
Chapter 5: Redox-stable cyclic peptide inhibitors of SPSB2-iNOS interaction.....	80

5.1 Declaration for Thesis Chapter 5	81
5.2 Introduction.....	82
Chapter 6: Cyclic peptidomimetics targeting SPSB2 as potential anti-infectives agents.....	83
6.1 Declaration for Thesis Chapter 6	84
6.2 Introduction.....	85
Chapter 7: Design, synthesis and characterisation of cyclic peptide analogues for macrophage targeting	86
7.1 Introduction.....	87
7.2 Materials and methods	88
7.2.1 Synthesis and purification of cyclic peptide analogues CP3-CP6	89
7.2.2 Synthesis and purification of GalNAc and mannose glycopolymers	92
7.2.3 Mannose and GalNAc glycopolymers conjugation to the cyclic peptides	99
7.2.4 Cells	104
7.2.5 Confocal laser scanning microscopy	104
7.3 Results.....	104
7.3.1 Design of analogues for macrophage-targeted delivery studies	104
7.3.2 CP4, CP5 and CP6 bound to SPSB2 at low nanomolar affinities	105
7.3.3 CP4, CP5 and CP6 bound to the iNOS binding site of SPSB2	107
7.3.4 Mannose and GalNAc glycopolymers helped target CP4 to BMDM cells.	108
7.3.5 Oligohistidine facilitates the endosomal escape of CP4 into cytoplasm.....	110
7.4 Discussion.....	114
7.5 Conclusions.....	116
Chapter 8: Conclusions and future work	118
Chapter 9: References	123
Appendix I: Other cyclic peptide and peptidomimetic analogues	148
Appendix II: Other co-authored publication.....	157

List of abbreviations

1D	one-dimensional
2D	two-dimensional
3D	three-dimensional
BMDM	bone marrow-derived macrophage
BSA	bovine serum albumin
CPMG	Carr–Purcell–Meiboom–Gill
CPP	cell-penetrating peptide
DCM	dichloromethane
DIPEA	<i>N, N</i> -diisopropylethylamine
DMB	dimethoxybenzene
DMEM	Dulbecco’s modified Eagle’s medium
DMF	dimethylformamide
DMSO	dimethyl sulphoxide
DODT	3,6-dioxa-1,8-octanedithiol
DPBS	Dulbecco’s phosphate-buffered saline
DQF-COSY	double-quantum filtered correlation spectroscopy
DSS	3-trimethylsilyl-1-propanesulfonic acid sodium sulphate
EDC	1-ethyl-3-(3-dimethylaminopropyl)-carbodiimide
FBDD	Fragment-based drug discovery
FBS	fetal bovine serum
FID	free induction decay
FPLC	fast protein liquid chromatography
GalNAc	<i>N</i> -acetylgalactosamine
GPC	gel permeation chromatography
GST	glutathione- <i>S</i> -transferase
HBSS	Hanks' Balanced Salt Solution
HCTU	O-(1H-6-Chlorobenzotriazole-1-yl)-1,1,3,3-tetramethyluronium hexafluorophosphate
HFIP	hexafluoro-2-propanol
HSQC	heteronuclear single quantum coherence
HTS	high-throughput screening

IFN- γ	interferon- γ
iNOS	inducible nitric oxide synthase
IPTG	isopropyl β -D-1-thio-galactopyranoside
ITC	isothermal titration calorimetry
k_{on}	association rate
k_{off}	dissociation rate
K_{D}	binding affinity
LB	Luria Broth
LC-MS	liquid chromatography-mass spectroscopy
LE	ligand-efficiency
LPS	lipopolysaccharide
M-CSF	macrophage colony-stimulating factor
MeCN	acetonitrile
MGL	macrophage galactose-type lectin
MQ	Milli-Q water
MTPBS	mouse-tonicity phosphate-buffered saline
NDM	New Delhi metallo- β -lactamase
NHS	<i>N</i> -hydroxysuccinimide
NMR	Nuclear magnetic resonance
NO	nitric oxide
NOESY	nuclear Overhauser effect spectroscopy
PDB	Protein Data Bank
PMSF	phenylmethylsulphonyl fluoride
PPIs	protein-protein interactions
RBITC	rhodamine B isothiocyanate
RMSD	root mean square deviation
ROESY	rotating frame Overhauser effect spectroscopy
RP-HPLC	reversed-phase high-performance liquid chromatography
SDS	sodium dodecyl sulphate
SDS-PAGE	sodium dodecyl sulphate polyacrylamide gel electrophoresis
SP	standard precision
SPPS	solid-phase peptide synthesis
SPR	surface plasmon resonance

SPSB	SPRY domain of the SOCS box protein
STD	saturation transfer difference
TB	tuberculosis
TCEP.HCl	tris-(2-carboxyethyl)phosphine hydrochloride
TFA	trifluoroacetic acid
THF	tetrahydrofuran
TIPS	triisopropylsilane
TMS	trimethylsilyl
TOCSY	total correlation spectroscopy
XP	extra precision
WHO	World Health Organisation

CHAPTER 1

Introduction

1.1 Introduction

Antimicrobial resistance is an increasing global phenomenon. According to the World Health Organisation (WHO) report in 2014,¹ cases of antibiotic resistance had been reported in a large number of countries in 2013 (**Figure 1.1A**), presumably due to unregulated use of antibiotics in developing countries² and overprescribing by general practitioners worldwide.³ Over the past decades, many bacterial strains showing resistance to at least one of the clinically used antibiotics have been reported. These include *Escherichia coli*, *Staphylococcus pneumoniae*, nontyphoidal *Salmonella sp.*, *Shigella sp.*, *Neisseria gonorrhoea*¹ and the commonly dubbed ESKAPE pathogens (i.e. the *Enterococcus faecium*, *Staphylococcus aureus*, *Klebsiella pneumoniae*, *Acinetobacter baumannii*, *Pseudomonas aeruginosa* and *Enterococcus sp.*).⁴ In 2009, a carbapenem-resistant *K. pneumoniae* bacterial strain carrying the New Delhi metallo- β -lactamase (NDM)-mediated gene has been identified in India.⁵ The NDM-1 gene has been found to be resistant to all antibiotics except fluoroquinolone and colistin and has now spread to over 40 countries worldwide.⁶ Recently, *E. coli* with the multidrug-resistant gene MCR-1 has been reported in animals and human samples from China⁷ and Denmark.⁸ This bacterial strain has been found to show resistance to all Gram-negative antibiotics currently available in the clinic including polymyxin,⁹ an old antibiotic often used as a last resort due to its high neuro- and nephrotoxicity profiles. Similarly, some 3.6% of new tuberculosis (TB) and 20.2% of previously treated cases had also found to show multidrug resistance in 2012, of which half were in India, China and Russia (**Figure 1.1B**).¹ The resistance has been found to be primarily due to mutations in the *rpoB* gene of *Mycobacterium tuberculosis* for rifampicin¹⁰ and the *katG*¹¹ and *inhA*¹² genes for isoniazid. This breach in the last line of antibiotic and the increase in multidrug-resistant bacterial strains thus emphasises the critical need for urgent measures to tackle this problem.

Recently, the WHO came up with five key strategic plans to contain this issue, in which one of them is to renew investment in the research and development of new antimicrobial agents.¹³ The call for innovation and collaboration between policy-makers, academia and pharmaceutical industries was made as only two major new classes of antibiotic have been discovered since 1987 (i.e. the oxazolidinone (linezolid)¹⁴ and the cyclic lipopeptide (daptomycin)).¹⁵ Moreover, the number of antibacterials in the current

development pipeline is far too low to meet the challenge of the rise in multidrug resistance.¹³ A decreasing trend in the development of anti-infectives observed in the past decades has been found to be partly due to the switch in investment priorities by the majority of pharmaceutical companies to other more profitable drugs with less regulatory complexity, such as drugs for chronic diseases.¹⁶

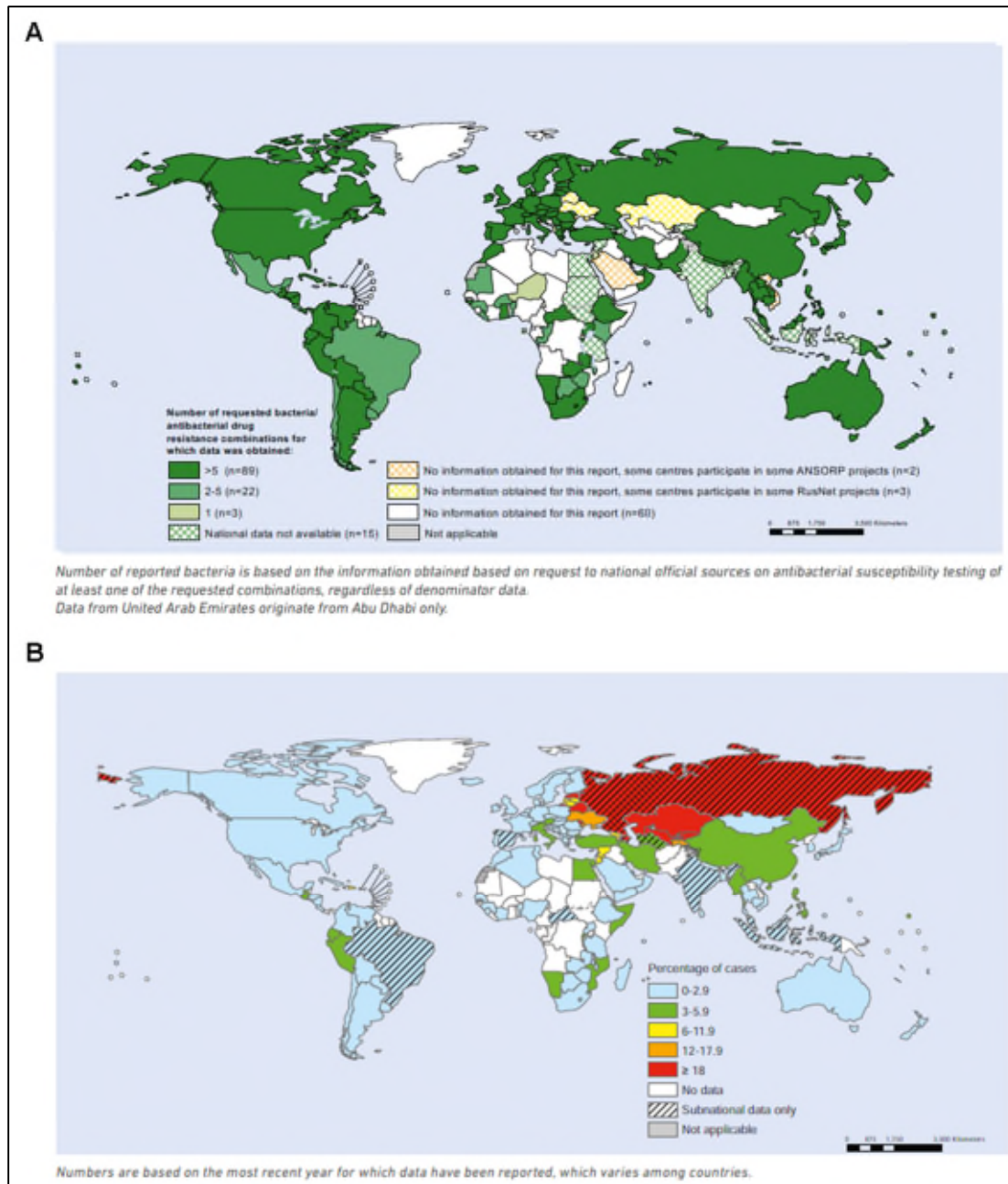


Figure 1.1. (A) Antimicrobial resistance data for selected bacterial-antibacterial drug combinations in 2013 and (B) Proportion of new TB with multidrug resistance cases worldwide. Both images were adapted from the WHO antimicrobial resistance global report on surveillance 2014.¹

Recently, signs of renewed interest from the companies on the research and development of anti-infectives have begun to emerge¹⁷ as more drugs are currently in phase II clinical trials. The number of first-in-class drugs, however, is still low as most of these drugs shared similar modes of actions as the old drug,^{18, 19} suggesting that bacteria showing resistance to the old drugs are likely to develop resistance to the new drugs from the same class. This has been observed in one recent example of a new drug, Perchlozone[®], developed for the treatment of multidrug-resistant TB.²⁰ A substantial effort is thus required to discover novel classes of anti-infective drugs with different mechanisms of action from the drugs currently available in the market.

1.2 Antimicrobial resistance: mechanisms and strategies

Multidrug resistance in bacteria has been reported to occur through two main mechanisms: (1) the acquisition and accumulation of resistance genes from other species on a single R-plasmid or a transposon, and (2) the action of the bacteria's intrinsic structural and functional characteristics.^{21, 22} In the first example, bacteria acquiring resistance genes modified their own protein target site(s) to disallow binding by the target antibiotics or directly inactivated the antibiotics (e.g. *via* hydrolysis or alteration in the antibiotic structure through transfers of chemical groups to the antibiotic). Intrinsically, multidrug-resistant bacteria prevented drug access to the target (e.g. by reducing membrane permeability to the antibiotics), increased the efflux of antibiotics *via* multidrug efflux pumps (e.g. the Resistance-Nodulation-Division pumps) or changed the physiological states of the infection sites (e.g. formation of biofilms).

In addition to the inherited resistance mechanisms, all tested microbes have also been reported to stochastically generate phenotypically different but genetically identical small subpopulation of cells that are highly tolerant to antimicrobials; these are known as persister cells.²³ As persister cells are non-growing dormant cells, they are not vulnerable to most (if not all) antibiotics as the current antibiotics mainly target the rapid dividing active bacterial cells. This subsequently allows the persister cells to survive and resume growth once the antibiotics are removed and consequently results in more drug resistant mutant cells.²⁴ This proposed mechanism is supported by a mathematical model by Levin and Rozen²⁵ which showed that cells displaying non-inherited resistance mechanism such as that demonstrated by persister cells have higher chances to acquire inherited resistance

in the long run. To date, persister cells have been observed in both biofilms and planktonic cells in chronic infections such as cystic fibrosis-associated lung infections and candidiasis, primarily caused by *P. aeruginosa*,²⁶ and the fungal pathogen *Candida albicans*,²⁷ respectively. Although no persister genes have been successfully isolated from microbes causing persistent infections such as in latent tuberculosis, at least 36 toxin-antitoxin loci, which have been proposed to be involved in formation of persister cells in *E. coli*,²⁸ have been reported in different variants of *M. tuberculosis*.²⁹

Various new antimicrobial approaches to treat infections from multidrug-resistant strains have been reported and summarised in recent reviews by Laxminarayan *et al.*³⁰ and Gill *et al.*³¹ Briefly, these strategies include the use of: (1) antibiotic adjuvants such as inhibitors of resistance mechanisms (e.g. the β -lactamase inhibitor), compounds that can exploit chemical genetic interactions to potentiate the antibiotic activities (e.g. efflux pump inhibitor, membrane permeabilisers) or agents that can overcome the bacterial functions in causing resistance (e.g. inhibitors of biofilm formation); (2) an anti-virulence inhibitor which has the ability to impair the ability of microbes to establish an infection in the first place (e.g. inhibitors of quorum sensing, type II/III secretion systems or the biosynthesis of glycolipid surface structures); and (3) the biologicals such as vaccines, monoclonal antibodies (targeting bacterial toxins or cell surface structures) or a host immune system modifier (e.g. the host defence regulator peptides or agonists of the innate immune system such as the Toll-like receptors and NOD-like receptors). Although less common, alternative strategies such as oral rehydration system, phage therapy, probiotics and prebiotics have also been proposed. In this thesis, attempts to develop a novel anti-infective targeting the host innate immune system, i.e. the SPSB-iNOS system are described.

1.3 SPSB-iNOS system

1.3.1 SPSB-iNOS interaction as potential anti-infective drug target

Nitric oxide (NO), which is produced biosynthetically from *L*-arginine *via* inducible nitric oxide synthase (iNOS) in cells such as macrophages and dendritic cells, plays an important role in combating infections.³² The expression of iNOS has been found to be significantly enhanced in animal models during infections such as salmonellosis,³³ tuberculosis,³⁴ and leishmaniasis.³⁵ In addition, Scharon-Kersten and co-workers³⁶

reported that the iNOS knockout mice succumbed to infections by intracellular pathogens 3 to 4 weeks post-infection. NO has also found to result in the dispersal of *P. aeruginosa* biofilms,³⁷ suggesting a potential role of NO in persistent and chronic infections.³⁸ These observations suggest that both iNOS and NO are essential in host immunity.

iNOS expression in human macrophages has been found to be regulated at both transcriptional and post-translational levels (i.e. the control of gene expression at the DNA and RNA levels, respectively).^{39, 40} At the transcriptional level, the binding of transcription factors (e.g. NFκB, STAT1) to DNA has been found to result in activation of the iNOS promoter, thus regulating the iNOS expression (**Figure 1.2**).

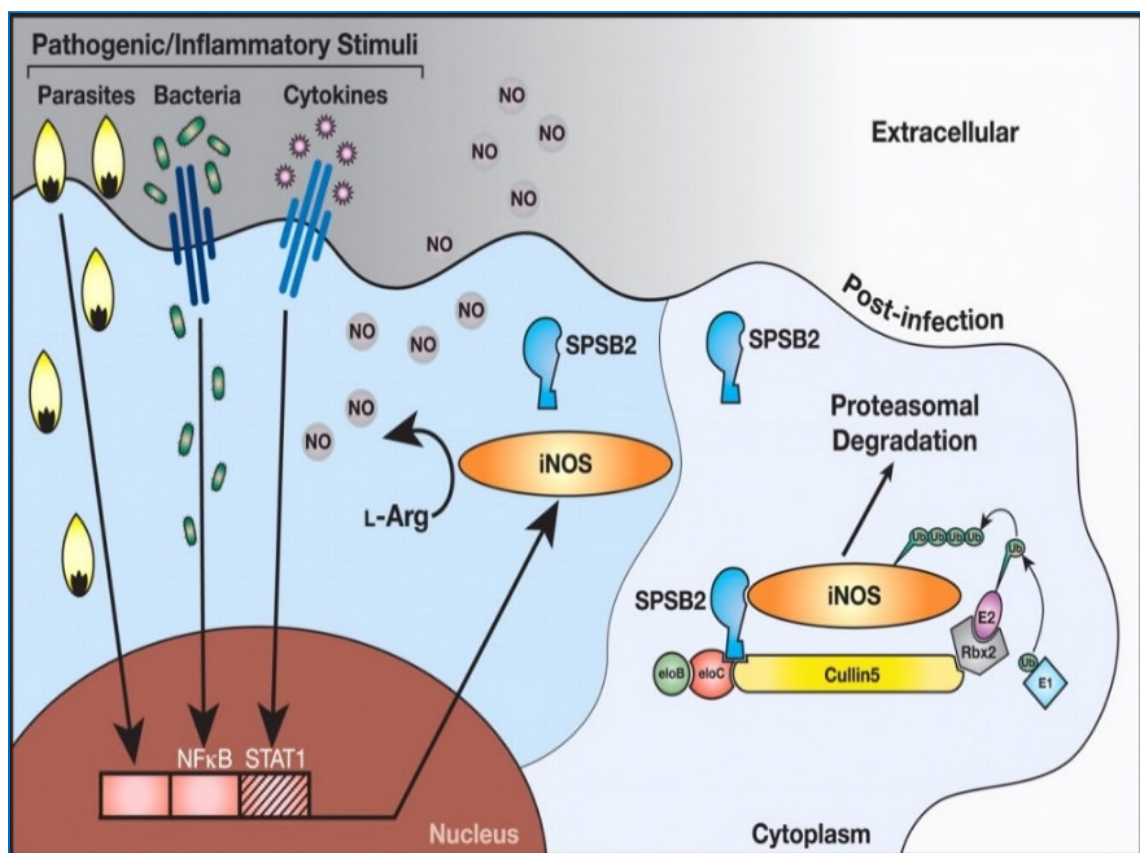


Figure 1.2. Transcriptional and post-translational regulation of iNOS expression in macrophages in response to microbial pathogens and cytokines. ©Kuang *et al.*, 2010. Originally published in *Journal of Cell Biology*. doi:10.1083/jcb.200912087.³⁹

At the post-translational level, iNOS expression has been found to be regulated through (1) modulation of iNOS mRNA stability *via* a complex network of RNA-binding

proteins such as AUF1, HuR, KSRP, PTB and TTP, or (2) modulation of iNOS protein stability through interaction with protein partners (e.g. Cav-1, Src) or the proteasome. Recently, iNOS has also been shown to be downregulated *via* aggresome formation as a consequence of overproduction of NO.⁴¹⁻⁴³ The role of the 26S proteasome in iNOS degradation was first described by Musial and Eissa⁴⁴ in 2001. iNOS has been found to be ubiquitinated *via* interaction with either the C-terminus of Hsp70-interacting protein (CHIP)^{45, 46} or the E3 ubiquitin ligases,^{39, 47, 48} resulting in its proteasomal degradation. For E3 ubiquitin ligases, one of the key protein mediating its interaction with the iNOS protein has been found to be the SPRY domain-containing SOCS box proteins or the SPSB (**Figure 1.2**).³⁹

SPSB is a four-member family of proteins (SPSB1-4) with SPSB1, SPSB2 and SPSB4 having a conserved β -sandwich structure formed by two seven-stranded β -sheets (**Figure 1.3**). The structure of the most phylogenetically distinct protein among the SPSB family members (i.e. the SPSB3, with amino acid sequence similarity of only 18% compared to SPSB1),⁴⁹ however, has yet to be determined. All four SPSB proteins have been initially found to interact with the hepatocyte growth factor receptor, c-Met,⁵⁰ whereas SPSB1, SPSB2 and SPSB4, but not SPSB3 have been found to interact with human prostate response apoptosis protein-4 (hPar-4).⁵¹ In addition, the *Drosophila* SPSB1 protein homologue, GUSTAVUS has been found to interact with the DEAD-box RNA-helicase VASA peptide.⁵² Both hPar-4 and VASA contain a similar sequence, i.e. ELN>NNL and DIN>NNN, respectively, suggesting that the SPRY domains of SPSB1, SPSB2 and SPSB4 recognise a common [D/E]-[I/L]-N-N-N motif in these proteins.⁵³ In contrast, c-Met, which does not contain the [D/E]-[I/L]-N-N-N motif, could have bound to a different site within the SPRY domain of SPSB proteins. The [D/E]-[I/L]-N-N-N motif, however, is not present in human or mouse VASA or in mouse Par-4, suggesting that both VASA and Par-4 may not be the key physiological target of the mammalian SPSB proteins. A subsequent search for additional SPSB binding partners *via* sequence analysis with ScanProsite,⁵⁴ discovered that the N-terminus region of iNOS, but not endothelial NOS (eNOS) or neuronal NOS (nNOS) from different species, contain the highly conserved peptide sequence DIN>NN.³⁹

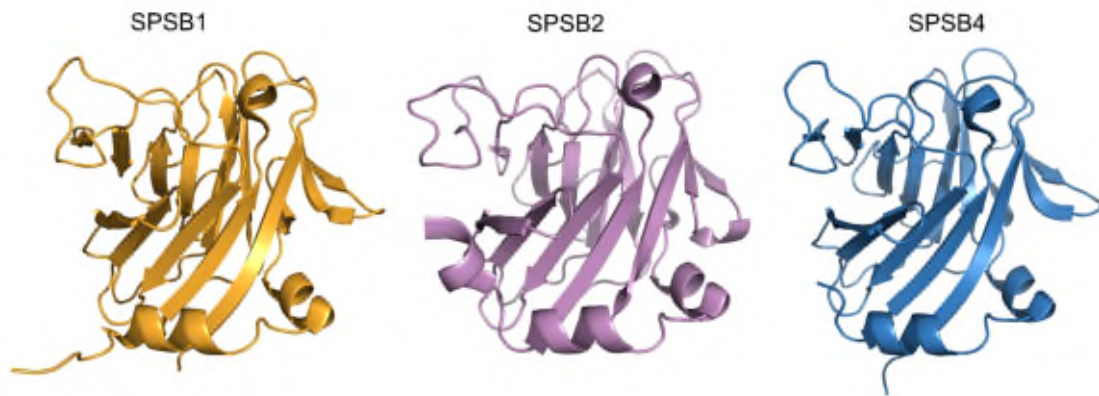


Figure 1.3. (A) Crystal structures of human SPSB1 (PDB ID: 2JK9),⁵⁵ SPSB2 (PDB ID: 3EMW),⁵⁵ and SPSB4 (PDB ID: 2V24).⁵⁵ A conserved β -sandwich structure formed by two seven-stranded β -sheets with a long loop was observed.

When SPSB2 knockout mice were infected with pathogens such as *M. tuberculosis* and *Leishmania major* parasites, prolonged iNOS expression was observed with a coincident increase in NO production and enhanced killing of the pathogens,³⁹ confirming the role of SPSB2 in proteasomal degradation of iNOS. Similarly, the SPSB1 and SPSB4 proteins were also found to be important in the negative regulation of iNOS expression in macrophages.^{56, 57} Consistent with previous observations, both SPSB1 and SPSB4 have been found to bind to the same peptide sequence DINNN in iNOS as SPSB2. In addition to the SPSB proteins, another ubiquitin ligase scaffolding F-box protein (i.e. the FBXO45 protein) has also been found to bind to the same peptide sequence DINNN, as mutation of Asn27 of DINNN in iNOS to alanine has been found to abrogate co-immunoprecipitation of FBXO45 with iNOS.⁵⁸ The FBXO45 protein recruited the E3 ligase complex for ubiquitination and subsequently resulted in the proteasomal degradation of iNOS, suggesting that both FBXO45 and the SPSB protein families share the same role in the negative regulation of iNOS.^{58, 59} The E3 ligase complex recruited by FBXO45, however, consists of different proteins from that recruited by the SPSBs, with the MYCBP2, SKP1 and Cullin-1 proteins in the case of FBXO45, and the Elongin B/C and Cullin-5 proteins in SPSBs, suggesting that FBXO45 acts differently from the SPSBs.⁵⁸ These observations suggest that inhibitors mimicking the peptide sequence DINNN would be advantageous in disrupting the proteasomal degradation of iNOS.

Figure 1.4. (A) Sequence alignment of SPRY domain structures in the SPSB family (except SPSB3), GUSTAVUS and FBXO45. Key hPar-4 (i.e. DINNN) contact residues (highlighted in yellow boxes) are conserved across the SPRY domain structures in SPSBs, GUSTAVUS and FBXO45 except Trp207, where the corresponding residue in FBXO45 is Tyr270, as indicated by an orange arrow. (B) Residues forming the iNOS peptide-binding site of SPSB2, as evidenced by site-directed mutagenesis and [¹H, ¹⁵N]-HSQC chemical shift perturbation studies, are labelled and mapped onto a surface (left) and cartoon (right) diagrams of murine SPSB2 (PDB ID: 3EK9)⁶⁰ in white.

Further comparison of the binding mode of VASA (DINNN) on hSPSB2 and hPar-4 (ELNNN) on hSPSB1 revealed that both VASA and hPar-4 bound similarly to the SPSB proteins, with seven conserved intermolecular hydrogen bonds between the NNN motif and the SPSB proteins (**Figure 1.5**). Although the two preceding residues of NNN motif are different in VASA and hPar-4, no significant changes in overall conformation of the peptides bound to SPSB proteins was observed, with an additional hydrogen bond noted between Glu84 side chain (hPar-4) and Tyr129 (hSPSB1), and between Asp184 side chain (VASA) and Tyr120 side chain (hSPSB2), respectively. As iNOS also contains similar [D/E]-[I/L]-N-N-N motif (DINNNV),³⁹ it was thus hypothesised that the peptide sequence DINNN of iNOS may also bind to the SPSB proteins in a similar manner as the VASA and the hPar-4 proteins. Indeed, mutational and structural studies with isothermal titration calorimetry (ITC) and nuclear magnetic resonance (NMR) at the binding interface of SPSB2-iNOS revealed that the SPSB2 protein was tightly bound to Asp23, Asn25 and Asn27 of the DINNN sequence in the *N*-terminus region of iNOS,³⁹ consistent with the structural requirements previously reported for the interaction between GUSTAVUS and VASA peptide, in which the corresponding residues are Asp184, Asn186 and Asn188.⁵³ In addition, Lys22, Val28 and Lys30, which flank the DINNN sequence of iNOS peptide, have also been reported by both NMR and ITC to be important for binding,³⁹ consistent with a stronger affinity observed between SPSB2 and iNOS, compared to the interactions between human SPSB2 and hPar-4 ($K_D \approx 1.5 \mu\text{M}$) or VASA ($K_D \approx 147 \text{ nM}$).⁵⁵ Based on these observations, the crystal structure of human SPSB2-bound VASA peptide was used as a template in the design of novel inhibitors of SPSB2-iNOS interaction in this study.

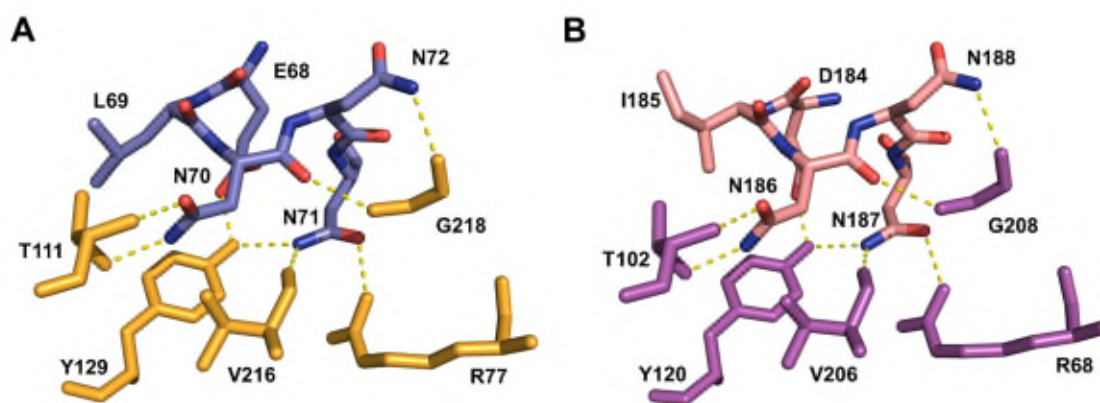


Figure 1.5. Crystal structures of the complex of (A) human SPSB1 (yellow sticks) and hPar-4 (blue sticks) (PDB ID: 2JK9)⁵⁵ and (B) human SPSB2 (purple sticks) and VASA (pink sticks) (PDB ID: 3EMW).⁵⁵ Eight conserved intermolecular hydrogen bonds (yellow dashes) are observed between the [D/E]-[I/L]-N-N-N motif and the SPSB proteins.

This high specificity in the molecular interaction between SPSB-iNOS thus suggests that inhibitors mimicking the peptide sequence DINNN would be advantageous in disrupting the proteasomal degradation of iNOS, thus prolonging the iNOS expression in target cell where iNOS is being produced in response to infection. Furthermore, the peptide sequence DINNN is only present in iNOS, but not eNOS and nNOS, suggesting that blocking SPSB-iNOS interaction would not affect other NOS subtypes⁴⁸ (unlike CHIP protein which ubiquitinates all NOS subtypes),^{62, 63} and thus potential toxicity associated with excessive systemic NO production from non-specific inhibitions may be avoided. These suggest that inhibitors targeting SPSB-iNOS interaction may be useful as a potential novel class of anti-infective agents.

1.4 Targeting protein-protein interactions

Various strategies have been reported in attempts to inhibit protein-protein interactions (PPIs). These include the use of small molecules,⁶⁴ peptides,⁶⁵ antibodies,⁶⁶ oligomers,⁶⁷ macromolecules such as dendrimers⁶⁸ and nanoparticles,⁶⁹ and miniproteins.⁷⁰ As PPI surfaces are usually much flatter and less well-defined compared to typical drug targets such as enzymes, targeting PPIs with small molecules is potentially challenging.^{71, 72} In the past decade, however, some success stories involving small molecules targeting PPIs have been reported, with some of these molecules now in clinical trials.⁶⁴ Small molecule

inhibitors of PPIs have been generally discovered through high-throughput screening from synthetic⁷³ or natural products libraries,⁷⁴⁻⁷⁶ although fragment-based drug discovery (FBDD),⁷⁷ peptidomimetics⁷⁸ and proteomimetics such as the topographical α -helix mimetics⁷⁹⁻⁸¹ have begun to gain popularity. To illustrate, Whitby *et al.*⁸² recently demonstrated the identification of high-affinity and selective small molecule leads from peptidomimetic libraries consisting of α -helix, β -turn and β -strand mimetics targeting the HIV-1/gp41 and κ -opioid receptors. Similarly, potent α -helix mimetic inhibitors of p53/hDM2 and Bcl-2 family PPIs have been successfully developed by Barnard *et al.*⁸³ from a library of *N*-alkylated aromatic oligoamide helix mimetic.

Apart from small-molecule inhibitors of PPIs, peptide-based inhibitors have also been reported.⁶⁵ These include the β -peptides,⁸⁴ α/β -peptide foldamers,^{85, 86} peptoids,^{87, 88} phylomers,⁸⁹ and constrained peptides such as stapled α -helix peptides,⁹⁰ cyclic peptides⁹¹ and bicyclic peptides.⁹² The use of protein epitope mimetics such as the scorpion toxin scaffold⁹³ and β -hairpin scaffolds as mimetics of α -helical epitopes targeting PPIs interactions have also been reported.⁹⁴ Although these strategies have all been shown to yield potent inhibitors of PPIs, success in targeting PPIs (with small molecules in particular) is highly dependent on the characteristics of the binding interface; proteins that are bound to a continuous epitope from a surface-exposed helix, flexible loops or chain extensions of the protein partner are more likely to have smaller or deeper pockets or grooves, and therefore a better chance of success.⁹⁵ As the SPSB-iNOS interaction is mediated by a short 5-residue linear peptide motif from the disordered loop region of the *N*-terminus of iNOS, with a small binding pocket observed on the SPSB proteins, it is likely that the SPSB-iNOS interactions can also be targeted with small molecules. Thus, in this study, an attempt was made to develop small-molecule inhibitors of SPSB-iNOS interactions using an FBDD approach. In parallel, cyclic peptides targeting the SPSB2 protein were also designed and characterised. The rationale for the design and the selection of screening strategies in this study are described below.

1.4.1 Small molecule inhibitors

Traditionally, high-throughput screening (HTS), which often involves the use of automation to rapidly assay the biological or biochemical activity of a large number of drug-like compounds, was used in drug discovery pipelines. HTS, however, only samples a minute fraction of drug-like chemical space, and thus has a much lower hit rate.⁹⁶ In

contrast, FBDD, a viable complementary approach to HTS, gives a more efficient sampling and the chances of getting a fragment with good complementarity to the target are higher.⁹⁷⁻¹⁰⁰ In addition, HTS compounds are usually larger in size and more lipophilic¹⁰¹ and these properties may limit the potential for further development.⁹⁶ Moreover, to purchase, maintain and screen millions of compounds in HTS is highly expensive compared to relatively small libraries of fragments required in FBDD.¹⁰²

A fragment, as defined by the Astex's "Rule of Three", is a chemical structure with a molecular mass of ≤ 300 Da, hydrogen bond donor ≤ 3 , hydrogen bond acceptor ≤ 3 , calculated $\log P \leq 3$, rotatable bond ≤ 3 and polar surface area $\leq 60 \text{ \AA}$.¹⁰³ In FBDD, these structures are used as basic building blocks to construct drug-like small molecule structures *via* either fragment linking or growing approaches.¹⁰⁴ Fragments, however, usually result in a high-quality (i.e. high binding energies per atom) but weak interactions ($K_D = 100 \text{ }\mu\text{M} - 10 \text{ mM}$)¹⁰⁵ and specialised methods are therefore required to detect fragment binding. These include NMR spectroscopy, X-ray crystallography, surface plasmon resonance (SPR), thermal denaturation, ITC, mass spectrometry, capillary electrophoresis and microscale thermophoresis.^{101, 106} As starting fragment hits usually have a low affinity (e.g. in mM), efficient optimisation of the fragment hit¹⁰¹ and substantial chemical modification are usually required before a biologically active compound can be obtained. These necessitate the use of X-ray crystallography or NMR spectroscopy to determine their binding mode to guide fragment optimisation.¹⁰⁵

NMR has been widely used in FBDD because it is very sensitive and able to detect weakly-bound fragments. It is also preferred to other biophysical methods because it does not require protein modification for analysis, in contrast to SPR analysis where the target protein has to be immobilised onto a sensor chip prior to analysis. In addition, samples can be prepared in solution, mimicking the native environment, unlike mass spectrometry, in which the sample has to be in a volatile buffer. Furthermore, NMR methods (specifically ligand-based) have high throughput and thus are suitable for screening compounds in fragment libraries.¹⁰⁷ In general, NMR methods can be classified into two key approaches: ligand-based and target-based. Both have pros and cons and are commonly used in tandem in FBDD campaigns.¹⁰⁰ In the ligand-based approach, the most commonly used NMR methods are saturation transfer difference (STD),^{108, 109} Carr-Purcell-Meiboom-Gill (CPMG)¹¹⁰⁻¹¹² and Water-LOGSY.^{113, 114} STD experiments allow

direct identification of the binding component in either a single ligand or a mixture of ligands with dissociation constants K_D from 10^{-3} to 10^{-8} M.¹⁰⁸ Due to the high sensitivity of STD experiments, only a small amount of protein is needed for analysis. On the other hand, CPMG allows more accurate determination of long nuclear transverse relaxation time (T_2) in liquid systems.¹¹¹ Hajduk *et al.*¹¹² discovered that at a spin-lock time of 400 ms, at least 99% of the protein signal intensity was eliminated compared to only a 17% drop in the ligand signal intensity, suggesting that CPMG can be useful to investigate ligand binding to the protein. As CPMG does not require isotope-labelled protein and there is a lower risk of false positives, it is gaining popularity in ligand binding studies.¹¹² Nevertheless, ligand-based approaches do not provide fragment-protein binding site information, so complementary studies are required.

One approach that can be used to identify the binding site of a fragment on its target protein is the [^1H , ^{15}N]-HSQC experiment, in which the chemical shift perturbations of residues in the binding site of the protein upon ligand binding are monitored. This target-based approach, however, requires the assignment of resonances from binding site residues. In the case of SPSB2, some of these resonances have not been assigned because of spectral overlap and intermediate conformational exchange.¹¹⁵ This suggests the need for complementary approaches to monitor the chemical shift perturbation of key residues in the binding site when small molecules bind. As both Tyr120 and Trp207 have been shown to be important for binding of iNOS peptide, with ~5,000-fold reduced affinity in Y120A-SPSB2 and a dramatic decrease in SPSB2-iNOS interaction by Western blot in W207A-SPSB2,³⁹ ^{19}F NMR studies on either fluorinated tyrosine analogues (e.g. 3-fluorotyrosine) or fluorinated tryptophan analogues (e.g. 5-fluorotryptophan) may be useful. Recent work from our group has shown that ligands targeting the iNOS binding site of SPSB2 induced chemical shift perturbations of the ^{19}F labelled Trp207 indole resonance of SPSB2,¹¹⁶ suggesting that ^{19}F NMR can be used complementarily to the [^1H , ^{15}N]-HSQC experiments to identify the binding site of the fragment on SPSB2.

In addition to the NMR experiments, SPR has also been used at multiple stages of FBDD campaigns, including fragment screening, hit validation and fragment elaboration. A significant advantage of SPR is its low protein consumption, as thousands of compounds can be screened sequentially on the same immobilised protein.¹¹⁷ In addition, SPR allows determination of binding kinetics (i.e. association rate constant, k_{on} ,

dissociation rate constant, k_{off} and equilibrium (affinity) constant, K_{D}) in one experiment.¹¹⁷ SPR is also reproducible, reliable and highly sensitive,¹¹⁸ and can also provide information about promiscuous, non-specific binders, as well as stoichiometry, reversibility and changes in compound behaviour over a range of concentrations.^{77, 119}

In addition to biophysical screening strategies, computational techniques have also been shown to contribute to the success of FBDD campaigns.¹²⁰ As has been extensively reviewed, the role of computational tools in FBDD ranges from fragment-focused library design to fragment hit identification and elaboration *via* docking or pharmacophore modelling.^{119, 121, 122} In fragment library design, collections of diverse compounds can be obtained using cheminformatics tools such as similarity-based clustering methods (e.g. Tanimoto coefficient) or grid-based methods. Filters can also be applied at this stage to remove compounds that do not follow the Astex's "Rule of Three", or contain reactive, toxic and other undesirable chemical substructures from databases. On the other hand, docking has been widely used in fragment hit identification from virtual fragment libraries and fragment elaborations. Although there are significant challenges in fragment docking due to their small size and low binding energy (less than -5 kcal/mol), a few studies have shown otherwise.¹²⁰ To illustrate, Sandor *et al.*¹²³ demonstrated that Glide^{124, 125} could effectively predict the conformations of 190 protein-fragment complexes with an average root mean square deviation (RMSD) between the docked and co-crystallised poses of 1.17 Å. Similarly, Loving *et al.*¹²⁶ found that Glide was able to accurately dock fragments, with RMSD of <1.0 Å to the crystal structure and successfully recovered known compounds from the database screen in the top 1% of the database (with average enrichment of 8.1). Nevertheless, weak correlations between experimental binding affinities and the GlideScore have been observed, suggesting that post-processing of protein-fragment docking poses with other methods such as filling potential (FP) method, smooth reaction path generation (SRPG) method or water maps may be useful to improve the prediction of binding affinities.^{123, 127} Recent work by Sastry *et al.*¹²⁸ emphasised the importance of full protein and ligand preparation and the influence of various parameters on virtual screening enrichment. This includes hydrogen bond network optimisation, geometry minimisation of the protein and inclusion of energetically accessible ligand ionisation/tautomeric states by Epik in the GlideScore (docking score = GlideScore + Epik penalty).¹²⁸ Glide SP (standard precision docking protocol) with default settings has also been shown to produce a better enrichment of actives over random sampling than

the Glide XP (extra precision docking protocol).¹²⁹ Nevertheless, expanded funnel sampling, post-docking processing with E_{model} ranking and molecular mechanics generalised Born surface area (MM-GBSA) rescoring did not significantly improve the docking accuracy.^{123, 129}

Based on the roles and advantages of the *in silico*, NMR and SPR techniques in FBDD, these techniques were used in this study to identify small molecule inhibitors of SPSB2.

1.4.2 Cyclic peptides and peptidomimetics

As previously described, various studies have exemplified the use of constrained peptides in targeting PPIs. Linear peptides with free carboxyl and amino termini have been thought to be unstable *in vivo* as they are susceptible to degradation by both endo- and exopeptidases¹³⁰ and they are highly flexible, rendering them entropically unfavourable for receptor binding and biological activity.¹³¹ Consistent with this, cyclic peptides have been found to be more resistant to enzymatic degradation and proteolytic digestion by proteases than their linear counterparts, with higher selectivity and binding affinity as they were conformationally restricted to the bioactive conformation of the peptide.¹³²⁻¹³⁶ In addition, macrocyclisation has also been found to increase cellular penetration and transmembrane passage *in vitro*¹³² via a decrease in polarity of the cyclic peptide, although a study by Kwon and Kodadek¹³⁷ has demonstrated otherwise. Recently, Clark and colleagues described an orally active cyclic peptide for the treatment of neuropathic pain.¹³⁸ These suggest that cyclic peptides can be useful as potential drug candidates.

In general, there are four common strategies (i.e. the classical methods) by which a linear peptide can be cyclised: side chain to side chain, *N*-terminus to side chain, side chain to *C*-terminus and *N* to *C*-terminus cyclisation approaches (**Figure 1.6A**).¹³⁹ Gilon and co-workers¹⁴⁰ have also proposed the concept of *N*-backbone cyclisation (*N* to *N*-backbone, *N*-backbone to side chain, *N*-backbone to *N*-terminus, *N*-backbone to *C*-terminus) (**Figure 1.6B**) and C^α -backbone cyclisation (C^α to C^α -backbone, C^α -backbone to side chain, C^α to *N*-backbone, C^α -backbone to *C*-terminus, C^α -backbone to *N*-terminus) (**Figure 1.6C**) which may be useful when all functional groups in the side chain, *N*-terminus or *C*-terminus are important for biological activity (**Figure 1.6**). Gilon and colleagues have also shown that backbone cyclisation, which involves cyclisation with *N*-alkylation, further enhanced the activity and stability of the linear peptide against the

proteolytic digestion. Nevertheless, the classical methods of cyclisation are more approachable as they are easier to synthesise and less costly compared to the backbone cyclisation method.¹⁴¹

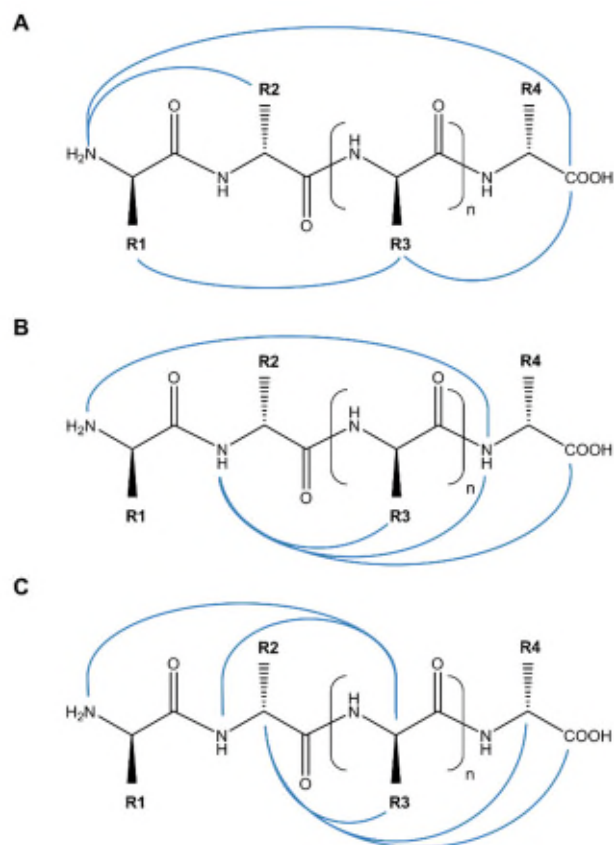


Figure 1.6. Common strategies to cyclise a linear peptide: (A) The “classical” methods, (B) *N*-backbone cyclisation methods and (C) *C*^α-backbone cyclisation methods. Possible cyclisation routes are depicted as solid blue lines.

As recently reviewed by White *et al.*,¹³⁹ there are various methods by which cyclic peptides can be synthesised. These include the ring-contraction strategies such as lactamisations, lactonisation and formation of disulphide bridge (one of the most common strategies), metal-ion-assisted cyclisations, sulphur-mediated cyclisations, azide-alkyne cycloadditions, ring-closing metathesis, multicomponent reactions (e.g. Ugi four-component reaction (U-4CR)) and electrostatically-controlled macrocyclisations.¹³⁹ These can be carried out in either a solution (solution-phase peptide synthesis) or by anchoring a reactive molecule to an insoluble polymer (solid-phase peptide synthesis or SPPS). As the solution-phase synthesis has to be carried out under high dilution (10^{-3} to 10^{-4} M) to minimise unwanted oligo- and polymerisations, reaction set-ups can be quite

complicated.¹⁴² This makes SPPS the preferable approach as it creates “pseudo-dilution phenomenon” and the purification method is much simpler. Other methods being developed for *N*-terminus to *C*-terminus cyclisation include the use of a soluble tag-assisted liquid-phase method¹⁴³ and enzyme-mediated cyclisation such as the use of Sortase A, a bacterial enzyme with transpeptidase activity^{144, 145} or other transpeptidases such as AEP, Glu-C, trypsin and proteasome, or other cysteine and serine proteases.¹⁴⁶

As linear peptide DINNN readily adopts a Type I β -turn conformation upon binding to SPSB2, with key hydrogen bonds between the carbonyl group of the backbone amide of Asp184 and the amino group of the backbone amide of Asn187, the amino group of the backbone amide of Asp184 and the carbonyl group of the backbone amide of Asn188, the carboxylic side chain of Asp184 and the amino group of the backbone amide of both Asn186 and Asn188, and a relatively small distance between the *N*- and *C*-terminus of the peptide (**Figure 1.7**), joining both ends together with a short linker to form a cyclic peptide is a feasible approach.

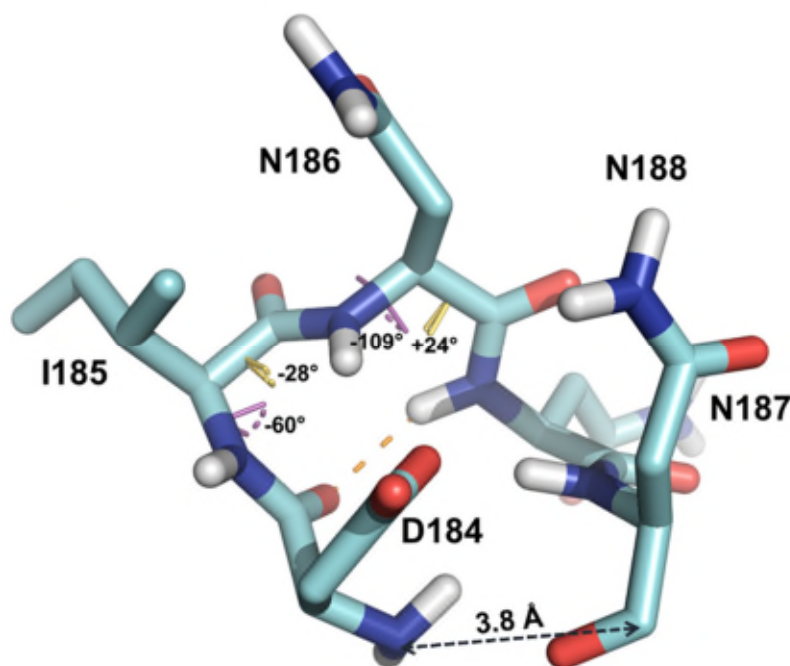


Figure 1.7. Intramolecular hydrogen bonds network connecting the DINNN peptide with hydrogen bonds dashed in yellow (PDB ID: 3EMW).⁵⁵ The linear peptide DINNN readily adopts a Type-I β -turn conformation upon binding to SPSB2 with a small distance between the *N*- and *C*-terminus of the peptide, suggesting its suitability to be designed into a cyclic peptide.

The use of linkers to join the *N*- and *C*-terminus of a linear peptide to form a cyclic peptide has also been previously reported. To illustrate, Baeza *et al.*¹⁴⁷ demonstrated that 3 out of the 6 designed cyclic peptides incorporating non-proteinogenic (unnatural) amino acid linker residues (*1S,2S*)-2-aminocyclohexanoic acid (BAc_{6c}), (*S*)-2-carboxylate-azetidine (Azg), (*S*)- and (*R*)-2-carboxylate-2-methylazetidine (Aza) between the *N*- and *C*-terminus of the β -turn-like brain-derived neurotrophic factor (BDNF) loop 2 and loop 4 were able to display significant inhibition of BDNF-induced tyrosine kinase (TrkB) receptor phosphorylation. In separate studies by the Borchardt group,^{148, 149} different organic linkers such as coumarinic acid, phenylpropionic acid and (acyloxy)alkoxy have been used to synthesise cyclic prodrugs of opioid linear peptides [Leu5]-enkephalin (YGGFL) and DADLE (YdAGFdL) to enhance their membrane permeability, as well as the metabolic stability to peptidases. Similarly, Rosengren *et al.*¹⁵⁰ have shown that cyclisation of a linear antibacterial peptide, pyrrococin *via* a 9-residue amino acid linker (KLPRPTPPR) retained its activity against Gram-negative bacteria and improved its activity against Gram-positive strains, although an improvement in resistance to degradation by proteases was not observed.

In addition to the use of linker residues to cyclise a linear peptide, few studies have also reported the use of linker residues to join the *N*- and *C*-terminus of an already cyclised peptide (e.g. *via* disulphide bonds) such as that in conotoxins to further improve their stability and selectivity. For example, Halai *et al.*¹⁵¹ reported that incorporation of a 6-residue amino acid linker (GGAAGG) between the *N*- and *C*-terminus of α -conotoxin RgIA not only maintained the overall structure of RgIA but also improved its stability in human serum and selectivity against GABA_B receptor. The same observation was noted for the α -conotoxin MII with a 7-residue amino acid linker (GAGAAGG) in which the same activity and selectivity as the native disulphide-bridged cyclic peptide were observed.¹⁵²

Thus, in this thesis, amino acid linkers, unusual amino acid linkers such as β -amino acids, as well as organic linkers (i.e. the peptidomimetic approach), were used to join the two ends of DINNN linear peptide. Ring-contraction strategies *via* disulphide bridge cyclisation and lactamisation were carried out to synthesise the designed cyclic peptides in which the linear peptides were first synthesised on SPPS, followed by cyclisation in solution. The effects of the introduced linkers on the overall conformation of the cyclic

peptides and ultimately their binding to SPSB2 were determined by SPR, ITC, ^{19}F NMR and [^1H , ^{15}N]-HSQC assays.

1.5 Drug delivery

While it is important to generate potent inhibitors of SPSB-iNOS interaction, it is also crucial to be able to deliver the generated inhibitors into the target cells (in this case, macrophages) to ensure that only the desired pharmacological responses at the target site are obtained, while undesirable interactions at other sites are avoided.¹⁵³ Various ligands have been conjugated to drugs for such purposes, including the integrins, nucleic acid aptamers, carbohydrates, vitamins, antibodies and peptides. Each of these ligands has different specificity to a different target with its own advantages and limitations.¹⁵⁴ In the majority of these studies, targeted drug delivery systems also consist of a delivery vehicle such as nanoparticles or DNA vectors¹⁵⁴ to protect the drug cargos from premature degradation by proteases in biological systems. As the interest of this thesis is to deliver inhibitors of SPSB2-iNOS interactions into the macrophages, strategies involved in macrophage-targeting are summarised below.

1.5.1 Macrophage-targeted drug delivery

Various approaches have been employed in targeting drugs to macrophages. A recent review by Jain *et al.*¹⁵⁵ found that the use of microspheres, liposomes, nanoparticles, dendrimers, niosomes, carbon nanotubes and polymersomes not only helped target delivery of biological agents to the macrophages but also extended the duration of action, thus reducing the therapeutic dose and subsequently the adverse effects of highly toxic, potent drugs. A more recent review by Costa *et al.*¹⁵⁶ re-emphasised the use of micro/nanotechnology approaches such as solid lipid nanoparticles, dendrimers, liposomes and polymeric particles in targeting the drug to the alveolar macrophages and outlined the specificity, advantages and disadvantages of each approach. Both reviews revealed that the majority of successful macrophage-targeting studies used mannose-sylated carriers, suggesting that targeting the mannose receptor on macrophages is a valuable approach.

The mannose receptor is a C-type lectin primarily expressed on the surface of tissue macrophages, dendritic cells and subsets of vascular and lymphatic endothelial cells.¹⁵⁷

It has been implicated in host immune responses by participation in endocytosis, phagocytosis, antigen processing and presentation, cell migration and intracellular signalling.¹⁵⁸ Many studies have demonstrated the exploitation of mannose receptor to deliver diagnostics and therapeutics into macrophages during chronic infections such as tuberculosis, as recently reviewed by Azad *et al.*¹⁵⁹ In addition to the mannose receptor, the macrophage galactose lectin (MGL) receptor which has an exclusive specificity to the terminal sugar GalNAc,¹⁶⁰ has also been found to be selectively expressed by immature dendritic cells¹⁶¹ and macrophages.¹⁶² The MGL expression pattern, carbohydrate specificities, role in internalisation and antigen presentation, pathogen pattern recognition, cell interaction, tumour recognition, signalling and immunomodulation are further described in a review by van Vliet *et al.*¹⁶³ Both mannose and MGL receptors, however, have been reported to be internalised into the macrophage or dendritic cells *via* a clathrin-dependent or receptor-mediated endocytosis and transported along the endosomal-lysosomal pathway.^{164, 165} This suggests that a mechanism to facilitate the endosomal escape of the endocytosed mannose- or GalNAc-conjugated cyclic peptide to the cytoplasm of macrophage (where the target SPSB2 protein is) will also be needed in this study.

1.5.2 Endosomal escape

Several mechanisms for endosomal escape have been proposed, and a wide selection of different endosomal escape agents have been summarised in reviews by Varkouhi *et al.*¹⁶⁶ and Shete *et al.*¹⁶⁷ Briefly, endosomal escape can be effected *via* (1) pore formation in the endosomal membrane by cationic amphiphilic peptides such as the cell penetrating peptides (CPP); (2) disruption of the endosomal membrane through an increase in osmotic pressure in the endosome, commonly known as the pH-buffering effect or the “proton sponge effect” by polyhistidine or polyetheneimine; (3) destabilisation of membrane by fusion of pH-sensitive fusogenic peptide such as GALA,¹⁶⁸ B18 and B15 peptides¹⁶⁹ and hemagglutinin HA2 (which changes conformation from coil at physiological pH to helical conformation at acidic pH) with the endosomal membrane; and (4) destruction of the endosomal membrane by the reactive singlet oxygen released by photosensitisers (e.g. TPPS₄ upon exposure to light), commonly known as the photochemical internalisation approach.¹⁷⁰

Although various endosomal escape agents have been proposed, each has its own limitations, making the issue of endosomal escape a significant challenge and a potential bottleneck in intracellular drug delivery campaign.¹⁶⁷ To illustrate, the use of CPPs such as the HIV-1 Tat peptide and nona-arginine as endosomal escape agents have been previously described, but the efficiency of the CPPs in enhancing the endosomal escape of its cargo has been found to be poor.¹⁷¹ Recently, various new strategies have emerged with the goal of improving the endosomolytic efficiency of CPP,¹⁷² such as the use of multivalent CPPs, and the conjugation of CPP with pH-sensitive fusogenic peptides, photosensitiser or fluorescence dyes.¹⁷³ For example, Salomone *et al.*¹⁷⁴ demonstrated the use of peptide chimaera consisting of Tat-peptide and cecropin-A-melittin peptide hybrids to effectively transport membrane-impermeable molecules such as Tat-EGFP fusion protein, calcein, dextrans, and plasmidic DNA to the cytoplasm of HeLa cells with no detectable cytotoxicity. Similarly, both Raagel *et al.*¹⁷⁵ and Mellert *et al.*¹⁷⁶ showed that their fluorescent and photosensitiser-conjugated CPP, respectively, were able to escape the endosome and remained intact and functional upon photo-activation. Recently, cyclic heptapeptide CPP, with the peptide sequence of c[FPhiRRRQ] has been reported to effectively deliver its cargo into the cytoplasm of the human cancer cells at 4-12 fold higher efficiency than the Tat, nona-arginine and penetratin peptides.¹⁷⁷ In addition, the 13-residue peptide, aurein 1.2 (GLFDIHKIAESF) has been found to successfully deliver cationic proteins into the cytoplasm of HeLa cells without causing cell toxicity.¹⁷⁸

In addition to CPP, the use of nanoparticle-mediated approaches for endosomal escape has gained considerable attention recently.¹⁷⁹ This includes the use of inorganic nanoparticles such as mesoporous silica nanoparticles¹⁸⁰ and bioconjugated quantum dots,¹⁸¹ zwitterionic polymer-based porous silicon nanocomposites,¹⁸² cationic lipid-based nanoparticles¹⁸³ and prickly nanodiamonds.¹⁸⁴ Recently, submicrometer (200 nm) nucleodendrimers have been shown to facilitate the endosomal escape of their cargos such as model drugs, proteins, sugars and nucleic acid without causing cell toxicity.¹⁸⁵ Furthermore, a novel strategy involving the use of plasmonic nanobubbles has also been demonstrated to assist the endosomal escape of an anti-cancer drug, Doxil, into the cytoplasm of drug-resistant cancer cells, with a coincident increase in therapeutic efficacy by 31-fold and a reduction of non-specific toxicity by 10-fold compared to the standard therapy.¹⁸⁶ Just like CPP, combination strategies such as the use of a stearylated IN7 peptide¹⁸⁷ or a neutral amphiphilic triblock copolymer Pluronic L64¹⁸⁸ with the

nanoparticles have been found to improve the release of the nanoparticles from the endosome or lysosome into the cytoplasm.

The use of oligohistidine to enhance the endosomal escape efficiency has also been described. Wen *et al.*,¹⁸⁹ Gu *et al.*¹⁹⁰ and Lachelt *et al.*¹⁹¹ showed that their polyhistidine-conjugated polyamidoamine/DNA complex (hPG4/DNA), poly(β -amino-ester)/DNA complex (PbAE/DNA), and oligo(ethanamino)amides/pDNA complex, respectively, had better transfection efficiency (10 to 100-fold), cell uptake, serum tolerance, endosomal escape and cytotoxicity profile than the non-polyhistidine-conjugated binary complex. Furthermore, Liu *et al.*¹⁹² discovered that an 18-residue oligohistidine-conjugated 20 kDa dsRBD protein in a siRNA aptamer chimera resulted in much higher endosomal escape than the non-oligohistidine-conjugated dsRBD protein, with a complete abolition of the RNA binding function of dsRBD observed. When oligohistidine was used together with other endosomal agents such as a CPP (e.g. oligoarginine, Tat),^{193, 194} a lipid (e.g. stearyl)¹⁹⁴ or a phospholipid (e.g. DPPE)¹⁹⁵ in nanoparticles, a higher transfection and better *in vitro* and *in vivo* activities have been observed. Nevertheless, the number of histidine residues and their distribution on the polymer backbone have been found to influence the endosomal escape efficiency. To illustrate, a 10-residue oligohistidine has been found to give better endosomolytic efficiency than the 5- and 20-residue oligohistidine-conjugated Tat-pDNA complex.¹⁹³ On the other hand, a polyhistidine-grafted polylysine has been found to produce higher gene transfection than the monohistidine-grafted polylysine with the same total number of histidine residues,¹⁹⁶ suggesting that the arrangement of the histidine residues on the polymer backbone is also important for optimum endosomal escape. Based on these observations, a 10-residue oligohistidine was grafted to the mannose or GalNAc glycopolymer-conjugated cyclic peptide in attempts to deliver the conjugated cyclic peptide to the cytoplasm of the macrophages. The uptake profiles and distributions of the glycopolymer-conjugated cyclic peptides in macrophages were explored by confocal laser scanning microscopy.

1.6 Scope of the thesis

SPSB2 has been found to play an important role in the proteasomal degradation of iNOS. SPSB2 knockout mice have been found to result in the enhanced killing of pathogens such as *M. tuberculosis* and *L. major* parasites in bone marrow-derived macrophages

(BMDM), suggesting the potential of the SPSB2-iNOS interaction as a novel drug target for anti-infective therapies. It is, however, not clear if inhibition of SPSB2-iNOS interactions would result in the same enhanced killing effect as that observed in pathogen-infected SPSB2 knockout mice. Therefore, the main aim of this study is to design inhibitors that could disrupt the SPSB2-iNOS interaction (in order to probe this possibility) and ultimately to discover a novel lead compound or peptide for development into a potentially new class of anti-infective agent.

In **Chapter 2**, all general materials and methods used in the design, synthesis and characterisation of the novel inhibitors of SPSB2-iNOS interactions are described. This includes the use of *in silico* approach in the design of the inhibitors; the synthesis, purification and characterisation of the designed cyclic peptide and peptidomimetic inhibitors; and the expression and purification of SPSB2 protein for binding analyses by SPR, ITC, NMR and macrophage cell lysate inhibition assays.

In **Chapter 3**, attempts to discover small molecule inhibitors targeting SPSB2 using both *in silico* and NMR-guided FBDD are described. Briefly, the *in silico* approach was first used to screen for fragments from a commercial compound library that were able to dock to the iNOS binding site of SPSB2 with ligand efficiency, $LE > 0.3$. The binding of shortlisted *in silico* fragment hits was then confirmed with both ligand-based (STD, CPMG) and target-based (^{19}F NMR, [^1H , ^{15}N -HSQC]) NMR methods. The binding affinities of both *in silico* and NMR-positive hits were subsequently quantified by SPR.

Chapter 4 describes the design of a disulphide-bridged cyclic peptide targeting SPSB2 based on the crystal structure of the SPSB2-bound DINNN peptide. The ability of this cyclic peptide to bind to the iNOS binding site was determined by ^{19}F NMR and [^1H , ^{15}N]-HSQC experiments, and its binding affinity on SPSB2 was estimated by SPR and ITC. The ability of the cyclic peptide to displace full-length iNOS from binding to SPSB2 in macrophage cell lysates, as well as its stability to three main digestive enzymes (i.e. pepsin, trypsin and α -chymotrypsin), human plasma and a redox environment, were determined.

In **Chapter 5**, the design and characterisation of two redox-stable analogues of the cyclic peptide are described. The effect of replacement of the disulphide bridge with other reduction-stable linkers such as a thioether and lactam bridge on their overall binding to

the iNOS binding site of SPSB2 was investigated by both SPR and ^{19}F NMR experiments. The stability of these analogues in both reducing and the oxidising environment *in vitro* was also explored.

Chapter 6 reveals an alternative approach to generating redox-stable inhibitors of SPSB2-iNOS interaction *via* the de novo design of cyclic peptidomimetics, incorporating different organic linkers joining the *N*- and *C*-terminus of the DINNN linear peptide. These cyclic peptidomimetics were synthesised using retrosynthetically-designed building blocks on SPPS and their identities were characterised by 2D NMR and liquid chromatography-mass spectroscopy (LC-MS). The effect of different length and characteristics of the linkers on their binding on SPSB2 was explored using SPR, ITC, ^{19}F NMR and macrophage cell lysate inhibition assays.

In **Chapter 7**, cyclic peptide analogues modified for macrophage targeting based on the most potent redox-stable cyclic peptide analogue as template are described. The effect of the oligohistidine and fluorophore moieties, which are required for endosomal escape and visualisation under confocal imaging studies, respectively, on cyclic peptide analogue binding to SPSB2, was investigated by SPR and ^{19}F NMR experiments. Subsequently, the uptake profiles of mannose and GalNAc glycopolymers-conjugated cyclic peptides, both in the absence and the presence of oligohistidine, by BMDM cells were investigated under the confocal laser scanning microscope.

Finally, all major findings from this study (including some preliminary findings involving other analogues outlined in **Appendix I**) are summarised in **Chapter 8**. Potential future directions of this project are discussed.

CHAPTER 2

General materials and methods

2.1 Introduction

In this Chapter, the materials and methods common to the work described in this thesis (Chapter 3-7) are described in detail. Other materials and methods that are (1) specific to certain chapters (e.g. fragment screening, structure calculation by NMR, plasma stability assay, redox stability assay, synthesis of glycopolymers and their cyclic peptide conjugates, imaging studies by confocal laser scanning microscope), or (2) conducted by other co-authors of the published paper or submitted manuscripts in Chapter 4-6 (e.g. proteolytic assays, isothermal titration calorimetry assays, ¹⁹F NMR assays, synthesis and characterisation of cyclic peptidomimetic building blocks) are described in the respective Chapters and therefore will not be included in this Chapter.

2.2 General materials

2.2.1 Chemical reagents

All chemical reagents used in the study were analytical grade or higher with purity \geq 95%. Salts and chemicals used in this study were mostly purchased from Sigma-Aldrich (St Louis, Missouri, USA), Amresco (Solon, Ohio, USA), Merck Millipore (Darmstadt, Germany) or Astral Scientific (New South Wales, Australia) unless stated otherwise in the text. Fmoc-protected amino acids and resins for peptide synthesis were purchased from Chem-Impex International (Wood Dale, Illinois, USA) or Mimotopes Pty Ltd (Victoria, Australia).

2.2.2 Bacterial strain

The bacterial strain used for transformation and protein expression of both unlabelled SPSB2 and ¹⁵N-labelled SPSB2 in this study is the Novagen[®] BL21 (DE3) competent *Escherichia coli* (*E. coli*) cells, containing a T7 RNA polymerase gene with the following genotypes: F⁻, *ompT*, *hsdS* ($r_{\text{BM}^{-}\text{B}}$), *gal*, *dcm*, λ DE3 (*lacI*, *lacUV5*-T7 gene 1, *ind1*, *sam7*, *nin5*) (Merck Biosciences, Madison, Wisconsin, USA).

2.2.3 Plasmid

The SPSB2 expression construct used in this study was the same as reported in Yao *et al.*,¹¹⁵ with the native sequence of mouse SPSB2 lacking the SOCS box and the first 11

residues (residues 12-224), and with an additional six (GSSARQ) and seven residues (TRRIHRD) at the *N*- and *C*-terminus, respectively, from the pGEX-2T vector, all expressed as a glutathione-*S*-transferase (GST) fusion protein in BL21 (DE3) *E.coli*.

2.2.4 Bacterial media

Bacterial media used in this study are summarised in **Table 2.1**. Luria Broth (LB), LB agar, 5 x M9 salts and Milli-Q[®] (MQ) water were autoclaved, while MgSO₄, CaCl₂, glucose, trace metals and vitamins were sterilised *via* filtration.

Table 2.1. Bacterial media used in this study with their respective compositions for 1 L media

Media	Reagent(s)	Amount to add (for 1 L)
LB	1% (w/v) casein peptone pancreatic digest, 0.5% (w/v) yeast extract, 0.5% (w/v) NaCl, pH 7.0-7.4	20 g
LB agar	LB	20 g
	Agar	15 g
5 x M9 salts	Na ₂ HPO ₄	30 g
	KH ₂ PO ₄	15 g
	NaCl	2.5 g
	MQ water	Add to final volume 1 L
M9 minimal media	5 x M9 salts	200 mL
	0.5 M MgSO ₄	4 mL
	1 M CaCl ₂	1 mL
	0.1 M FeCl ₃	400 µL
	0.1 M ZnCl ₂	250 µL
	10 mg/mL thiamine	500 µL
	<i>D</i> -glucose	4 g
	¹⁵ NH ₄ Cl	1 g
	LB	12.5 mL
	MQ water	Add to final volume 1 L
Ampicillin	100 mg/mL ampicillin	1 mL

Isopropyl β -D-1-thio galactopyranoside (IPTG)	IPTG (fresh)	0.23 mg
--	--------------	---------

2.2.5 Buffers and solution

Buffers and solutions used in this study are summarised in **Table 2.2**. In general, all except sodium dodecyl sulphate polyacrylamide gel electrophoresis (SDS-PAGE) running buffers were filtered (and degassed under vacuum and constant stirring for SPR and fast protein liquid chromatography (FPLC) buffers). Buffers and gradient used for purification of cyclic peptide and peptidomimetic analogues by reversed phase high performance liquid chromatography (RP-HPLC) are described in *Section 2.3.3.3*.

Table 2.2. Buffers and solutions used in this study. Amount to add to prepare 1 L buffer with stated compositions are given

Buffer	Compositions	Amount to add (for 1 L)
TN buffer, pH 8.0	20 mM Tris	2.4 g
	150 mM NaCl	8.8 g
	MQ water	Add to final volume 1 L
Thrombin cleavage buffer, pH 7.5	50 mM Tris	6.1 g
	2.5 mM CaCl ₂	0.4 g
	MQ water	Add to final volume 1 L
1 mM thrombin stock solution	Thrombin	14.3 mg
	HCl	420 μ L
10 mM Phosphate buffer, pH 7.0 (FPLC buffer)	NaH ₂ PO ₄	0.6 g
	Na ₂ HPO ₄	0.8 g
	50 mM NaCl	2.9 g
	MQ water	Add to final volume 1 L
SDS-PAGE running buffer	0.2 M glycine	14.4 g
	25 mM Tris base	3.0 g
	0.1% (w/v) SDS	1.0 g
	MQ water	Add to final volume 1 L
SDS staining solution	0.2% (w/v) Coomassie Brilliant Blue	2.0 g
	20% (v/v) methanol	200 mL

	5% (v/v) acetic acid	50 mL
	MQ water	750 mL
SDS de-staining solution	20% (v/v) ethanol	200 mL
	10% (v/v) acetic acid	100 mL
	MQ water	700 mL
HBS-EP, pH 7.4 (SPR running buffer)	10 mM HEPES	2.4 g
	150 mM NaCl	8.8 g
	3 mM EDTA·2Na·2H ₂ O	1.1 g
	0.05% (v/v) Tween 20	500 µL
	MQ water	Add to final volume 1 L

2.2.6 Instrument/Software

A list of key instruments and software used in this study is given in **Table 2.3**. Other common instruments such as the centrifuge, water bath, shaker, freeze dryer, etc. are not included in the table.

Table 2.3. Instrument and/or software used in this study

Instrument/Software	Version, supplier	Purpose
SYBYL-X	version 2.0, Tripos	<i>In silico</i> modelling
Maestro	version 9.3, 10.3, Schrödinger	<i>In silico</i> docking studies
PyMOL	version 1.5.0.4, Schrödinger	Molecular visualisation and image making
Novaspec II Visible Spectrophotometer	Pharmacia	Bacterial cell density measurement
PS3 TM Peptide Synthesizer	Protein Technologies, Inc.	Solid-phase peptide synthesis
ÄKTA FPLC / UNICORN	version 5.11, GE Healthcare	Protein purification
Waters PrepHPLC / Empower Pro (Empower 2)	version 6.0, Waters Corp.	Cyclic peptide and peptidomimetic purification

LCMS 2020 / LabSolutions	version 5.53 SP3, Shimadzu Corp.	LC-MS characterisation of cyclic peptide and peptidomimetic
NanoDrop [®] ND-1000 UV- Vis spectrometer	version 3.7, ThermoScientific	Protein concentration quantitation
Direct Detect [®] Infrared Spectrometer	version 2.0.0.28, EMD Millipore	Cyclic peptide or peptidomimetic concentration quantitation
Biacore [™] T200 Control/ Evaluation software	version 2.0, GE Healthcare	SPR binding studies and analysis
TopSpin	version 3.2, Bruker	NMR data processing
CcpNmr Analysis	version 2.1.5, CCPN	NMR data analysis, assignments

2.2.7 Web resources

Web resources used in this study are summarised in **Table 2.4**.

Table 2.4. Web resources used in this study

Web page address	Use
http://www.rcsb.org/pdb/	To extract structural information e.g. X-ray coordinates of the protein-ligand complex
http://web.expasy.org/protparam/	To estimate protein extinction coefficient, molecular mass and theoretical pI
http://www.peptidesynthetics.co.uk/tools/	To predict the mass of <i>N</i> -terminus modified, disulphide-bridged peptides of different amino acid sequences
http://ftmap.bu.edu	To predict ligand-binding hot spots for protein
http://spin.niddk.nih.gov/bax/nmrserver/talosn/	To predict protein backbone and side chain torsion angles from NMR chemical shifts (for structure calculation)

2.3 General methods

2.3.1 Computational studies

Methods described in this section are generally for *in silico* modelling and docking of cyclic peptide analogues. Methods used in the design of a library for fragment screening, fragment docking and post-docking analysis of the fragments are described in **Chapter 3**.

2.3.1.1 In silico modelling

The cyclic peptide models were generated using SYBYL[®]-X (version 2.0, Tripos). Firstly, the three-dimensional (3D) structure of the SPSB2-bound DINNN peptide was obtained from the crystal structure of the SPSB2-DINNNNN complex (PDB code 3EMW)⁵⁵ (File > Retrieve PDB > PDB Code: 3EMW; Selection > Select Atoms > Residues > Chain B; Edit > Extract > M2; Edit > Delete > Molecules > M1). Using the Biopolymer module, the monomer(s) of DINNNNN were mutated (Biopolymer > Composition > Mutate Monomers), deleted (Biopolymer > Composition > Delete Monomers) or built (Biopolymer > Build Protein) to yield different peptide sequences for cyclisation (Biopolymer > Build > Create Cycle). Peptides of different length and containing disulphide bridges (Biopolymer > Build > Create Disulphide) were designed. Hydrogen atoms were added to all residues in the peptide (Edit > Hydrogens > Add All Hydrogens).

The preliminary designed cyclic peptides were subjected to energy minimisation to correct the modelled bond lengths and angles, and to remove any steric clashes resulting from the modelling (Compute > Minimize > Molecule). Conjugate gradient energy minimisation method with termination gradient cut-off of 0.05 kcal/mol and maximum iterations of 10,000 were selected. The Ramachandran plot¹⁹⁷ (Maestro, version 9.3 or 10.3, Schrödinger) was inspected to ensure that the backbone ϕ and ψ angles were within the allowed regions. The optimised models were finally fitted to the backbone of the 3D structure of the DINNN peptide and the RMSD between the models and the original DINNN peptide was calculated (Biopolymers > Compare structures > Fit monomers). The most promising cyclic peptide analogues with the lowest RMSD were selected for synthesis.

2.3.1.2 Docking studies

2.3.1.2.1 Protein preparation

The crystal structure of the SPSB2-VASA peptide complex was loaded into Maestro (version 9.3 or 10.3, Schrödinger) (Project > Get PDB) and prepared using the Protein Preparation Wizard in Maestro, in which the water molecules beyond 5 Å of heteroatoms were removed, hydrogens were added to the structure, missing side chains were assigned (Tasks > Protein Preparation > Import and Process > Preprocess) and the complex was subjected to restrained minimisation (RMSD cut-off of 0.3 Å) to remove undesirable steric clashes in the structure (Tasks > Protein Preparation > Refine > Minimize). The VASA peptide was also removed prior to docking.

2.3.1.2.2 Receptor grid generation

A grid box of 28 x 28 x 28 Å³, with a default inner box of 10 x 10 x 10 Å³, centred at the putative binding site of SPSB2-VASA peptide (x = 11.3 Å, y = 30.7 Å, z = 61.6 Å) was generated using default parameters without constraint (Tasks > Docking > Grid Generation > Receptor > Pick to identify the ligand; Tasks > Docking > Grid Generation > Site > Centroid of Workspace Ligand > Dock ligands with length = 28 Å). For oligohistidine-conjugated cyclic peptide analogues (as in **Chapter 7**), a larger grid box of 76 x 46 x 46 Å³, with an inner box of 40 x 10 x 10 Å³ and a customised grid centre (x = 27.0 Å, y = 20.0 Å, z = 60.0 Å) were generated.

2.3.1.2.3 Ligand preparation

The *in silico* energy minimised cyclic peptide models from SYBYL-X were further prepared in a similar manner to the protein preparation with the Protein Preparation Wizard in Maestro prior to rigid ligand docking.

2.3.1.2.4 Docking

The superimposed cyclic peptide models were then docked with Glide^{124, 125, 198} (Maestro, version 9.3 or 10.3, Schrödinger) using the standard precision (SP) protocol and the “refine only” sampling method, in which the superimposed models were energy minimised in the presence of SPSB2 and scored (Tasks > Docking > Glide Docking > Settings > Ligand Sampling > None (refine only)). Selection of this docking method was

dictated by the failure of the initial docking attempt with Glide SP-Peptide (\pm MM-GBSA) (which was previously shown by Tubert-Brohman *et al.*¹⁹⁹ to be able to accurately predict the binding pose of up to 79% of the crystal structures tested), using the initial SPSB2-bound conformation of DINNNNN peptide in the crystal structure of the complex, to reproduce the binding pose of the crystal structure. The observed backbone RMSD between the crystal structure (a β -turn conformation) and the docked conformations (an extended conformation) was 3.3-3.5 Å (**Figure 2.1**).

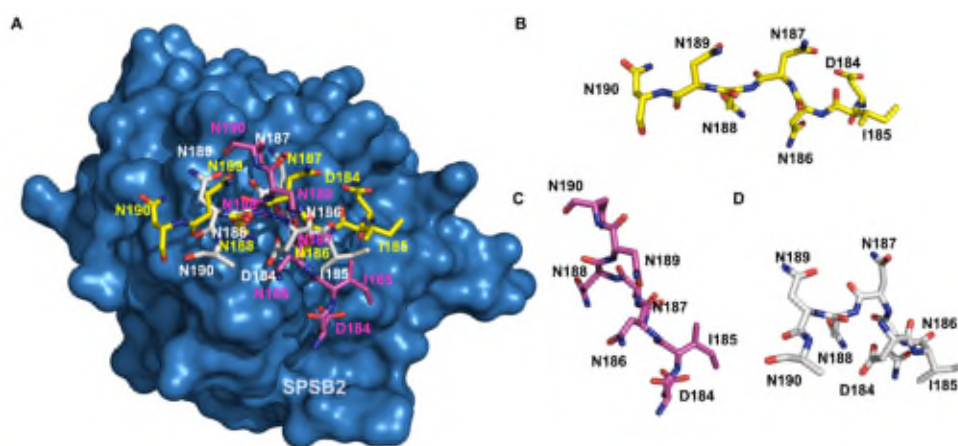


Figure 2.1. (A) Overlays of the crystal structure of the VASA peptide (white), Glide SP-Peptide docked VASA peptide (yellow) and Glide SP-Peptide + MM-GBSA-docked VASA peptide (magenta) on the crystal structure of the SPSB2 protein (blue) (PDB ID:3EMW). Both Glide SP-Peptide (\pm MM-GBSA)-docked VASA peptides (**B-C**) were found to adopt an extended conformation while the crystal structure of the SPSB2-bound VASA peptide (**D**) adopted a β -turn conformation, suggesting that the current ligand sampling methods are not very successful in reproducing the binding pose of the crystal structure of the VASA peptide on SPSB2 protein.

Another commonly used Glide SP “rigid” ligand sampling method also failed to produce any binding poses, presumably due to errors from steric clashes between the generated models and the iNOS binding site of SPSB2. Owing to the limitation of the current ligand sampling methods, the superimposed cyclic peptide models were thus “rigidly” docked using the SP protocol and the “refine only” sampling method.

2.3.1.3 Data analysis

The refined docking poses of the cyclic peptide models on SPSB2 protein were visualised by PyMOL (version 1.5.0.4).

2.3.2 SPSB2 expression and purification

2.3.2.1 Plasmid transformation

A 50 μ L aliquot of competent BL21 (DE3) cells (in 1.5 mL Eppendorf tube) stored at -80 °C were thawed on ice for 10 min. 1 μ L (100 ng) of plasmid construct pGEX-2T was added to the Eppendorf tube and left on ice for another 30 min. The competent cells/plasmid construct mixture in the Eppendorf tube was then immersed in the heat water bath at 42 °C for 45 s. Following the heat shock procedure, 1 mL of LB was added to the Eppendorf tube and further incubated at 37 °C under constant shaking for another 45 min. As the plasmid contains an antibiotic resistance gene against ampicillin, approximately 100 μ L of the plasmid-containing cells were pipetted out from the Eppendorf tube and plated onto an LB agar plate containing 100 μ g/mL ampicillin and incubated overnight at 37 °C. Only cells containing the plasmid will grow on the agar plate after overnight incubation.

2.3.2.2 GST-SPSB2 fusion protein expression

One isolated colony on the LB agar plate was picked using a sterile pipette tip. The pipette tip containing the isolated colony was dropped into a 50 mL Falcon tube containing 10 mL LB and 100 μ g/mL ampicillin and incubated at 37 °C under constant shaking overnight. To produce a 1 L culture, 10 mL of the cell culture was then transferred to a 2 L Erlenmeyer baffled cell culture flask containing 1 L LB (or M9 minimal media containing $^{15}\text{NH}_4\text{Cl}$ as the sole source of nitrogen for GST-tagged ^{15}N -SPSB2 protein expression) and 100 μ g/mL ampicillin with the flask loosely capped with a Drosophila Plug and further incubated at 37 °C under constant shaking until the OD_{600} reached 0.6-0.8. To induce the expression of the target protein, 1 mM IPTG was added to the flask and allowed to incubate at 28 °C under constant shaking for approximately 4-5 h. After induction, the cell cultures were transferred into Oak Ridge centrifuge tubes and the cells were spun down *via* centrifugation at 18,000 rpm for 16 min at 4 °C. Supernatants were removed and the cell pellets were transferred into a 50 mL Falcon tube for storage at -80 °C.

2.3.2.3 GST-SPSB2 fusion protein purification

Cell pellets in the 50 mL Falcon tube stored at -80 °C were thawed and resuspended on ice (with a transfer pipette) in lysis buffer containing Novagen's BugBuster[®] Master Mix

(5 mL/g cell pellet) and 1 tablet of Roche's cOmplete, Mini Protease Inhibitor Cocktail pre-dissolved in TN buffer. The resuspended cells were allowed to incubate in the cold room on a roller for approximately 30 min. After 30 min incubation, the resuspended cells were transferred to Oak Ridge centrifuge tubes and centrifuged at 18,000 rpm for 20 min at 4 °C. Supernatants, which contains the soluble proteins including the GST-SPSB2 protein, were transferred into a new 50 mL Falcon tube for purification.

To manually prepare a GST purification column, a clean Bio-Rad's Econo-Pac 20 mL gravity flow column was rinsed with MQ water, and approximately 2 mL of glutathione-Sepharose 4B beads (GE Healthcare) was added to the column. The beads were further washed with 20 mL MQ water to remove the residual ethanol in the beads, followed by equilibration with 2 x 20 mL TN buffer.

To purify the GST-SPSB2 protein from other soluble proteins in the cell lysate, the supernatants (in the 50 mL Falcon tube) were first filtered using an Acrodisc[®] syringe filter with a 0.8/0.2 µm Supor[®] membrane. The filtrate was then added to the pre-equilibrated GST purification column prepared earlier (with the bottom cap closed), capped and allowed to mix on a rocker for 10 min. To ensure that binding of the GST-SPSB2 to the glutathione beads is complete, the collected filtrate from the column was re-added to the column and mixed for another 10 min. The beads were then washed with approximately 150 mL of TN buffer to remove other unbound proteins.

To elute GST-SPSB2 fusion protein from the glutathione beads, approximately 1 mL of GST-tagged protein elution buffer containing 20 mM Tris, 20 mM reduced glutathione and 150 mM NaCl, pH 8.0, was added to the beads (0.5 mL elution buffer per 1 mL bed volume of resin) and incubated on a rocker for 10 min. Following incubation, the filtrate was collected into a 15 mL Falcon tube. The same elution procedure was repeated twice and the filtrate from each repeat was pooled in the same 15 mL Falcon tube. The purity of the GST-SPSB2 fusion protein was confirmed by SDS-PAGE.

2.3.2.4 GST-tag cleavage from GST-SPSB2 fusion protein

The GST-SPSB2 bound beads were equilibrated with approximately 20 mL of thrombin cleavage buffer. The beads were then transferred from the gravity column into a new 50 mL Falcon tube with approximately 30 mL of thrombin cleavage buffer, and 4.3 µL β-mercaptoethanol was added to the Falcon tube. A 40 µL of 1 mM thrombin stock solution

was then added to the Falcon tube and allowed to agitate overnight in the cold room at 4 °C on the roller. After cleavage by thrombin, all contents in the Falcon tube were transferred back into the gravity column (with bottom lid capped). The flow-through, which should contain both the untagged SPSB2 protein and thrombin, was collected into a new 50 mL Falcon tube. The beads were further rinsed with 5 mL of the thrombin cleavage buffer and the flow-through was again collected into the same Falcon tube. The same step was repeated again to ensure most of the cleaved SPSB2 protein was collected. The flow-through was further concentrated using a thrombin cleavage buffer pre-equilibrated 15 mL Amicon® Ultra centrifugal filter (molecular mass cut-off 10 kDa) *via* centrifugation at 3,500 rpm at 4 °C.

2.3.2.5 SPSB2 protein purification by size-exclusion

SPSB2 protein was further separated from other impurities such as thrombin by size-exclusion chromatography (Superdex® 75 10/300 GL) using a ÄKTA FPLC (UPC 900, Amersham Biosciences). The instrument pump, injector and lines were washed with filtered and degassed MQ water. The size-exclusion column was then assembled onto the instrument, washed with the MQ water followed by equilibration with the filtered and degassed FPLC buffer containing 10 mM phosphate, 50 mM NaCl, pH 7, at a flow rate of 0.8 mL/min. Prior to loading the concentrated protein sample, the 500 µL sample loop and needle were washed with MQ water and FPLC buffer, and the protein solution was filtered with an Acrodisc® syringe filter with a 0.45 µm Supor® membrane (to remove aggregated protein or insoluble impurities). 250 µL of filtered protein solution was then loaded into the sample loop using a 1 mL syringe attached to the needle. While the syringe and needle were still attached to the injector, the sample was injected into the system under a constant flow of the FPLC buffer at a flow rate of 0.5 mL/min. Each fraction of 1 mL was collected automatically using a fraction collector (Frac-950, Amersham Biosciences). Fractions with high absorbance were subjected to SDS-PAGE. An example of the FPLC chromatogram observed and SDS-PAGE gels of the high absorbance fractions are shown in **Figure 2.2**.

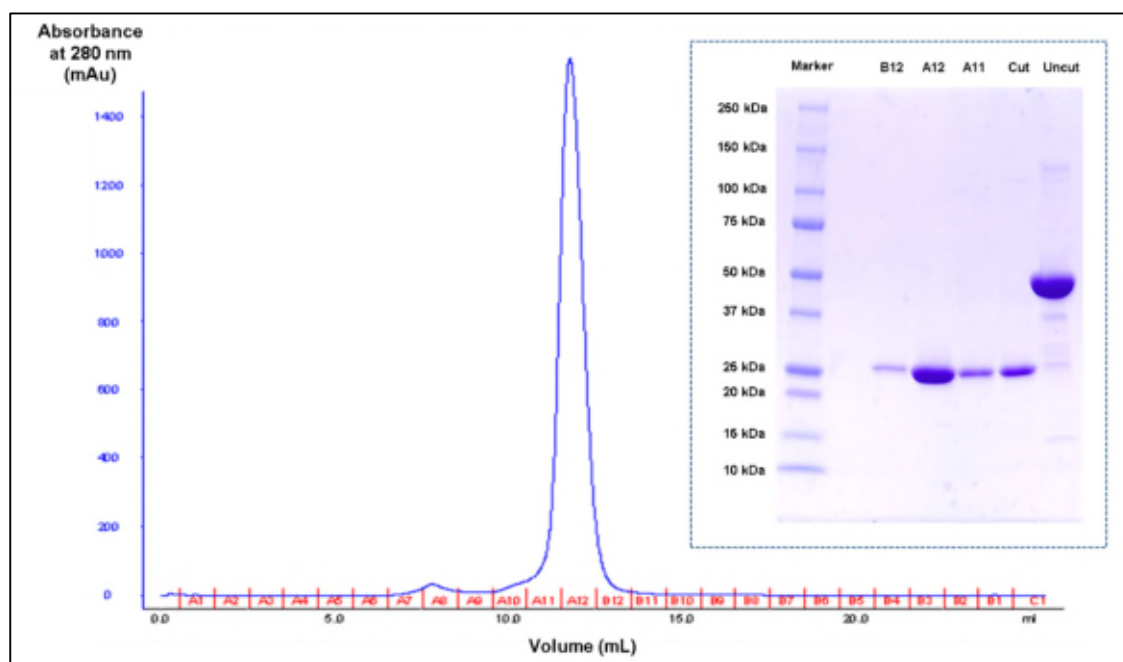


Figure 2.2. An example of FPLC chromatogram of SPSB2 purification by size-exclusion, with the fraction numbers in red and the absorbance of the separated protein samples at 280 nm in blue. SDS-PAGE gels of highly absorbed fractions (A11, A12 and B12) are shown with “Cut” = sample prior purification by size exclusion, and “Uncut” = sample prior GST-tag cleavage from GST-SPSB2.

2.3.2.6 Characterisation of purified SPSB2

Pure fractions corresponding to the protein with same molecular mass were pooled and their identity, purity and folding were confirmed by ^1H NMR. An example of the SDS-PAGE gel of the different fractions from size exclusion chromatography by FPLC and ^1H NMR spectra of the pooled fractions are shown in **Figure 2.3**. The protein concentration was determined *via* absorbance at 280 nm with a NanoDrop[®] spectrophotometer based on the Beer-Lambert Law (**Equation 2.1**) and the molar extinction coefficient value of $46,410 \text{ M}^{-1} \text{ cm}^{-1}$.

$$A = \epsilon cl \quad (2.1)$$

with ϵ is the molar extinction coefficient ($\text{M}^{-1} \text{ cm}^{-1}$), c is the concentration (M^{-1}) and l is the path length (cm).

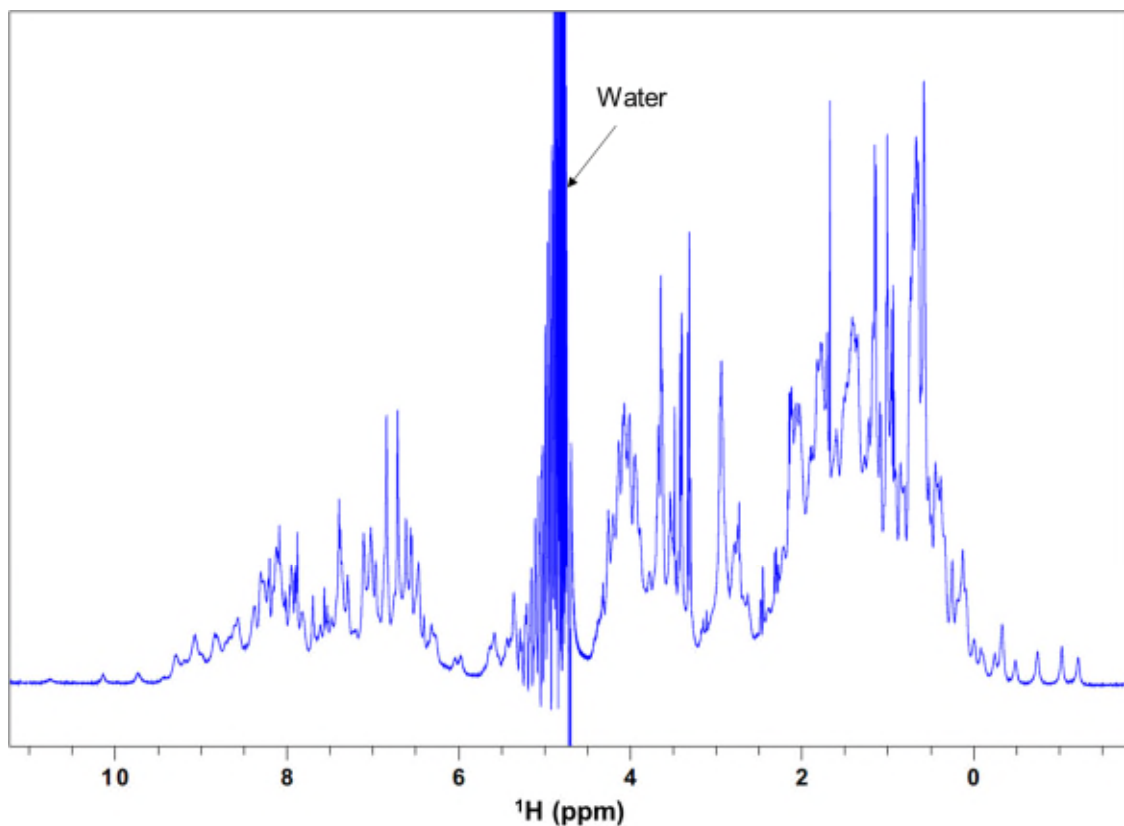


Figure 2.3. ^1H NMR spectra of the pooled pure fractions, corresponding to pure SPSB2 in 10 mM sodium phosphate, 50 mM NaCl, pH 7.0, at 10 °C. Large chemical shift dispersion in the methyl region between 1.0 and -1.0 ppm, as well as peaks in the amide region downfield of 8.5 ppm, indicate that the SPSB2 is well-folded.²⁰⁰

2.3.3 Cyclic peptide and peptidomimetic synthesis and purification

Syntheses of both cyclic peptide and peptidomimetics were carried out according to the general synthetic pathways shown in **Figure 2.4**, which will be summarised in the subsequent sections. In general, the synthesis can be divided into three major steps: (1) assembly of linear side chain protected peptides on resin; (2) cleavage of the linear peptides from resin and (3) linear peptide cyclisation in solution. For the disulphide-bridged cyclic peptide, cyclisation was carried out between the thiol side chains of Cys residues and therefore side chain protecting groups were removed prior cyclisation. In contrast, for the lactam-bridged cyclic peptide and peptidomimetics, cyclisation was carried out between primary amine of *N*-terminus and carboxylic acid of *C*-terminus and therefore side chain protecting groups were only removed after cyclisation.

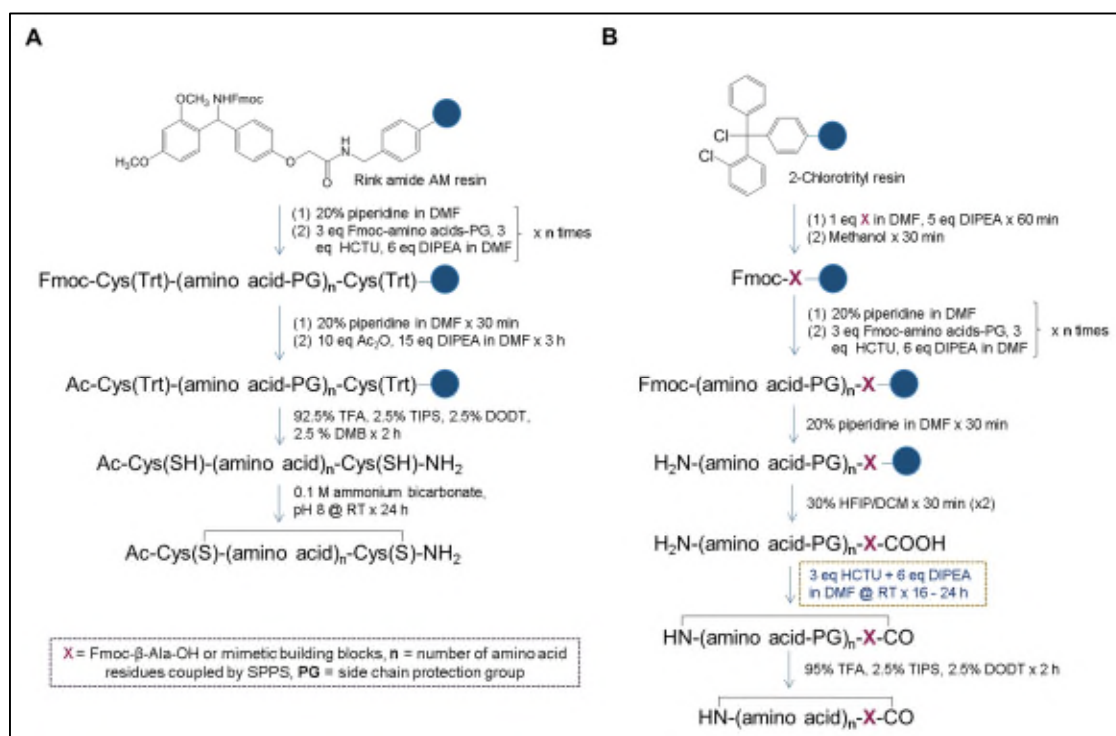


Figure 2.4. Common synthetic pathway used for (A) disulphide-bridged cyclic peptide and (B) lactam-bridged cyclic peptides and peptidomimetics

2.3.3.1 Disulphide-bridged cyclic peptides

The linear peptide was synthesised on resin (SPPS) using an automated Peptide Synthesizer 3 (PS3TM) *via* Fmoc chemistry.²⁰¹ Rink Amide resin was chosen for this class of analogues because C-terminus amidation was required. 213 mg (0.1 mmol) of Rink Amide AM resin (0.47 mmol/g loading) was weighed into a reaction vessel and swelled in dimethylformamide (DMF) (10 mL/g resin) for 30 min. 0.3 mmol (3 eq, 124 mg) of Fmoc-protected amino acids and O-(1H-6-Chlorobenzotriazole-1-yl)-1,1,3,3-tetramethyluronium hexafluorophosphate (HCTU) were weighed into vials (with one amino acid/HCTU powder mixtures per vial) and sealed using a PTFE/Silicone septa and cap. All vials were then queued (from C-terminus residue to N-terminus residue) on the carousel on PS3. To start the synthesis, each vial was assigned with Program 7 where the Fmoc protecting group on the resin was first removed by 20% (v/v) piperidine in DMF prior coupling to the amino acid residue for 50 min per coupling cycle under the activation of 0.3 mmol (3 eq) of HCTU and 7% (v/v) *N,N*-diisopropylethylamine (DIPEA) in DMF. For double coupling (which was carried out to couple the second Asn to the first Asn, as well as the third Asn to the second Asn, as single coupling resulted in substantial deletion of one Asn from the peptide sequence), an additional vial was queued

right after the first coupling and assigned as Program 9 where the Fmoc protecting group was not removed prior the coupling of amino acid. An example of the set-up of the synthesis sequence and program and the details of each program are illustrated in **Figure 2.5**.

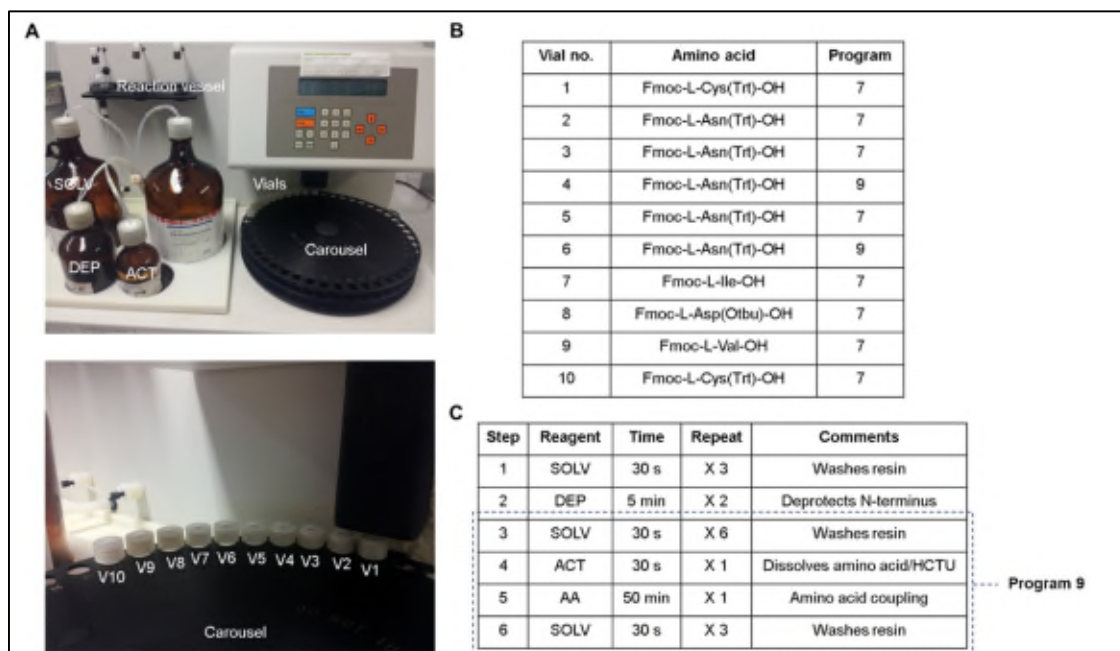


Figure 2.5. (A) Set up of Peptide Synthesizer 3 (PS3™) (upper panel) with the vials containing powder mixtures of amino acid and HCTU queued on the carousel (bottom panel). (B) An example of synthesis sequence and program used to synthesise side chain protected linear peptide Fmoc-CVDINNNC on Rink Amide AM resin. (C) Description of each step involved in Program 7 used is summarised in this table, with steps involved in Program 9 highlighted in a dotted rectangular box.

After synthesis of the linear peptide was complete, the linear peptide-bound resin was re-suspended in DMF and transferred from the reaction vessel to a 5 mL syringe equipped with a filter frit with a transfer pipette. The resin was washed 3 times with DMF under vacuum. Approximately 5 mL (10 mL/g peptide-resin) of 20% (v/v) piperidine was then added to the resin, and the syringe was sealed (at both end) with the syringe plunger and stopper, and allowed to shake for 30 min to remove the Fmoc protecting group at the *N*-terminus of the linear peptide. After 30 min, the resin was washed 6 times with DMF under vacuum to remove residual piperidine. For *N*-acetylation, 94.5 μ L (10 eq) acetic anhydride, 261.3 μ L (15 eq) DIPEA and 4.5 mL DMF were added to the syringe, capped and agitated for 3 h. The resin was again washed 3 times each with DMF, methanol and

diethyl ether and dried under vacuum (3-5 min). To cleave the *N*-acetylated linear peptide from the resin and to remove all side chain protecting groups from the peptide, a 5 mL cocktail solution containing 92.5% (v/v) trifluoroacetic acid (TFA) (4.625 mL) and scavengers 2.5% (v/v) triisopropylsilane (TIPS) (125 μ L), 2.5% (v/v) dimethoxybenzene (DMB) (125 μ L) and 2.5% (v/v) 3,6-dioxa-1,8-octanedithiol (DODT) (125 μ L) was added to the peptide-resin containing syringe and agitated for 2 h. After cleavage, the linear peptide in TFA solution was collected into a 50 mL Falcon tube and subjected to a stream of N₂ gas to remove as much TFA as possible from the peptide solution. Approximately 20-30 mL cold diethyl ether (i.e. at least 8-10 x volume of remaining TFA in the solution) was then added to the Falcon tube followed by centrifugation at 3,000 rpm for 5 min to precipitate the peptide, and the supernatant was removed. The same precipitation procedure was repeated twice prior redissolved in a water:acetonitrile (H₂O:MeCN) (1:1) mixture prior to lyophilisation. All reactions were carried out at room temperature. Cyclisation was carried out in solution with 0.1 M ammonium bicarbonate, pH 8.0, for 24 h at a peptide concentration of 0.5 mM under constant stirring in a 50 mL Falcon tube with holes on the cap.

2.3.3.2 Lactam-bridged cyclic peptide and peptidomimetic synthesis

For both lactam-bridged cyclic peptides and peptidomimetics, the 2-chlorotrityl resin was chosen to allow cyclisation between the *N*- and *C*-termini of the peptide. The use of 2-chlorotrityl resin, however, requires an additional step, i.e. the loading of the first amino acid on the resin. Thus, 167 mg (0.2 mmol) of 2-chlorotrityl resin (1.2 mmol/g loading) was weighed into a syringe with frit filter and swelled in DCM for 30 min. 0.1 mmol (1 eq) of the first residue Fmoc- β -alanine-OH (31.2 mg) (for lactam-bridged cyclic peptide) or the mimetic building block (for cyclic peptidomimetic) was then dissolved in minimal DMF and added to the syringe containing the mixtures of resin, 87.5 μ L DIPEA (5 eq) and 2.5 mL dichloromethane (DCM), capped and allowed to shake for 1 h. After 1 h, approximately 160 μ L (0.8 mL/g resin) methanol was added to the syringe and allowed to agitate for another 30 min to cap the remaining uncoupled resin. After 3 washes of the resin, each with DCM and DMF, it was transferred to a reaction vessel with DMF using a transfer pipette and subjected to SPPS using the same protocol as described in **Section 2.3.3.1**, in which subsequent amino acid residues were assembled on the resin under the activation of 0.3 mmol (3 eq) HCTU and 7% (v/v) DIPEA in DMF, with double coupling used to couple the second Asn to the first Asn, as well as the third Asn to the second Asn,

and the Fmoc protecting group at the *N*-terminus after each coupling/double coupling cycle removed with 20% (v/v) piperidine in DMF. After the completion of linear peptide synthesis by SPPS, the resin was transferred to a new syringe with filter frit with DMF and washed 3 times each with DMF, methanol and diethyl ether and dried under vacuum. Cleavage of the side chain-protected linear peptide from the resin was then carried out in the syringe with 30% (v/v) hexafluoro-2-propanol (HFIP) in DCM for 30 min twice (4 mL x 2) and the cleaved peptide was pooled together into a 50 mL Falcon tube and dried under a stream of N₂ gas. The cleaved side chain protected linear peptide was redissolved in H₂O:MeCN (1:9) and lyophilised. Cyclisation was carried out in solution at a concentration of 0.5 mM overnight with HCTU (3 eq) and DIPEA (6 eq) in DMF in a 50 mL Falcon tube at room temperature under constant shaking. The crude cyclic peptide was dried under vacuum and the side chain protecting groups were cleaved from the cyclic peptide with a cleavage cocktail solution containing 95% (v/v) TFA and scavengers 2.5% (v/v) TIPS and 2.5% (v/v) DODT. After cleavage, the volume of TFA was reduced *via* blowing of N₂ gas and the cyclic peptide was precipitated with cold diethyl ether twice *via* centrifugation at 3,000 rpm for 5 min each time followed by the removal of the supernatant. Finally, the crude precipitates were redissolved in an H₂O:MeCN (1:1) mixture prior to lyophilisation. All reactions were carried out at room temperature.

2.3.3.3 Purification of the cyclic peptide and peptidomimetic

The crude cyclic peptides were purified by RP-HPLC on a Phenomenex[®] Luna C18(2) column (100 Å, 5 µm, 100 x 10 mm). In general, a gradient of 20-50% B (A: 99.9% H₂O, 0.1% TFA; B: 80% MeCN, 19.9% H₂O, 0.1% TFA) over 30-60 min (**Table 2.5**) with a flow rate of 4 mL/min was used. The buffer and gradient used for purification, however, varied for each analogue depending on its retention on the RP-HPLC column and the purity of the crude (**Table 2.6**).

Table 2.5. An example of a method used for purification of cyclic peptide or cyclic peptidomimetic analogues by RP-HPLC

Time (min)	Flow rate (mL/min)	Buffer A (%)	Buffer B (%)
0.00	4.00	95	5
5.00	4.00	95	5
10.00	4.00	80	20

40.00	4.00	50	50
41.00	4.00	0	100
50.00	4.00	0	100
51.00	4.00	95	5
60.00	4.00	95	5

Buffer A: 99.9% H₂O, 0.1% TFA; Buffer B: 80% MeCN, 19.9% H₂O, 0.1% TFA

Table 2.6. Summary of buffers and gradient used for purification of cyclic peptide or cyclic peptidomimetic analogues by RP-HPLC

Analogues	Buffer A	Buffer B	Gradient
Disulphide-bridged cyclic peptide and its analogues, cystathionine analogue (CP1) and lactam-bridged cyclic peptide (CP2)	99.9% H ₂ O, 0.1% TFA	80% MeCN, 19.9% H ₂ O, 0.1% TFA	20-50% B over 30-60 min
Cyclic peptidomimetics (Mimetic M1)	10 mM ammonium acetate, pH 3.8	50% 10 mM ammonium acetate, pH 3.8, 50% MeCN	20-60% B over 40 min
Cyclic peptidomimetics (Mimetic M2-M4)	99.9% H ₂ O, 0.1% TFA	80% MeCN, 19.9% H ₂ O, 0.1% TFA	5-40% B over 35-70 min
Macrophage delivery analogues (CP3, CP5)	99.9% H ₂ O, 0.1% TFA	80% MeCN, 19.9% H ₂ O, 0.1% TFA	5-50% B over 25 min
Macrophage delivery analogues (CP4)	99.9% H ₂ O, 0.1% TFA	80% MeCN, 19.9% H ₂ O, 0.1% TFA	35-75% B over 20 min
Macrophage delivery analogues (CP6)	99.9% H ₂ O, 0.1% TFA	80% MeCN, 19.9% H ₂ O, 0.1% TFA	25-75% B over 25 min

2.3.3.4 Characterisation of identity and purity of cyclic peptide and peptidomimetic

The purity and molecular mass of the synthesised and cyclised peptide were confirmed with LC-MS at 214 nm on a Shimadzu LCMS2020 instrument, incorporating a Phenomenex® Luna C8 column (100 Å, 3 µm, 100 x 2 mm) and using a linear gradient of 100% H₂O (0.05% TFA) for 4 min, followed by 0-60% MeCN (0.05% TFA) in water over 10 min at a flow rate of 0.2 mL/min. For more hydrophobic cyclic peptide or peptidomimetic analogues, a linear gradient of 100% H₂O (0.05% TFA) for 4 min, followed by 0-100% MeCN (0.05% TFA) in water over 15 min at a flow rate of 0.2 mL/min was used instead.

2.3.4 Surface plasmon resonance

SPR experiments were set up and performed according to **Section 2.3.4.1 – 2.3.4.4**. In principle, SPR detects changes in the refractive index of the medium adjacent to the thin metal film (in this case, the sensor chip with gold film), which is dependent on the mass of the surface. When a polarised light hits the prism adjacent to the gold film, the incident light waves resonate with the surface-bound plasmon waves, and the photon energy of the incident light waves transfers to the surface plasmon waves. This results in a sharp attenuation of the reflected light and thus a minimum SPR intensity. When an analyte is bound to a pre-immobilised ligand on the surface, the overall surface mass changes and the difference in refractive index of the surface is produced. This results in a shift of the resonant angle and ultimately the observed SPR signals (**Figure 2.6**).²⁰²

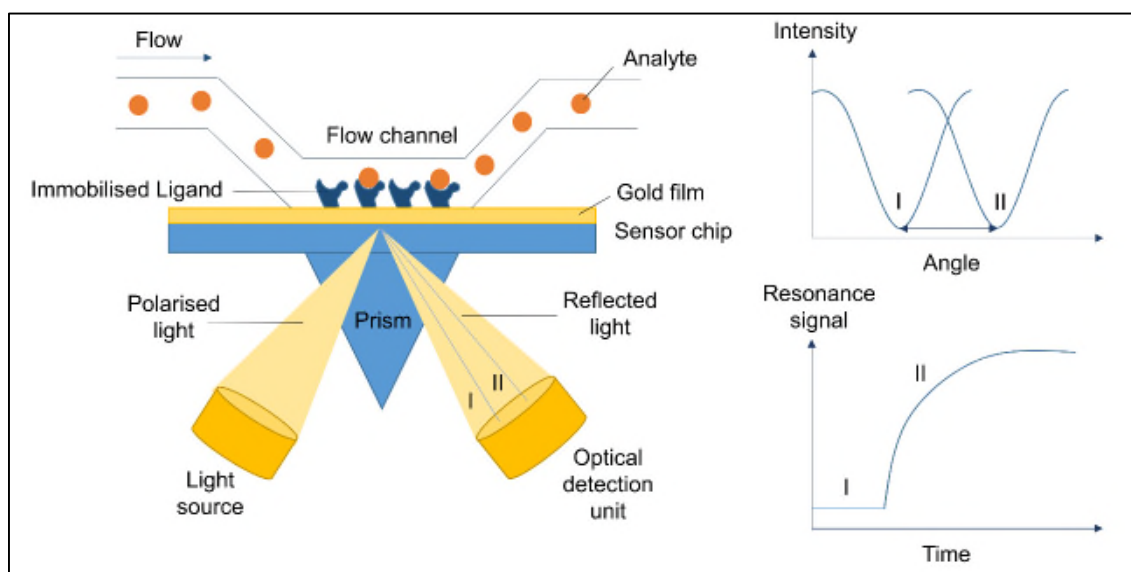


Figure 2.6. The principle of SPR. A change in the angle of reflected light (e.g. from I to II, upper right) upon binding of the analyte to the immobilised ligand on the surface of the gold film is detected by the optical detection unit and transformed into an SPR sensorgram (bottom right).

2.3.4.1 Preparation of SPR buffer and setting up instrument (Biacore™ T200)

Both MQ water and SPR running buffer containing 10 mM HEPES, 150 mM NaCl, 3 mM EDTA and 0.05% (v/v) Tween 20, pH 7.4, were prepared, filtered and degassed. To set up the instrument, a maintenance chip was first docked into the instrument using the Biacore™ T200 Control Software (version 2.0) (Tools > Insert Chip) and the instrument temperature was set to 25 °C (Tools > Set Temperature) and primed with water (Tools > Prime). To ensure the instrument was free from contamination prior to the run, the instrument was treated with the standard desorb procedure with 0.5% (w/v) SDS and 50 mM glycine, pH 9.5 (Tools > More Tools > Maintenance Tools > Desorb). Following the desorb procedure, the instrument was primed twice with water. As SPSB2 will be coupled to the chip using amine coupling, a dry CM5 sensor chip (GE Healthcare) was then docked into the instrument, replacing the maintenance chip (Tools > Eject chip), followed by priming with water and SPR running buffer (To change buffer, Tools > Stop Standby).

2.3.4.2 Immobilisation of SPSB2 protein on the SPR chip

Immobilisation was carried out using the Immobilization wizard (Run > Wizard > Surface Preparation > Immobilization) *via* standard amine coupling method on the CM5 sensor chip in the SPR running buffer with a flow rate of 10 µL/min and a contact time of 420 s. Both the target (SPSB2) and reference (blank) flow cells were activated for 7 min using a mixture of 0.2 M 1-ethyl-3-(3-dimethylaminopropyl)-carbodiimide (EDC) and 0.05 M *N*-hydroxysuccinimide (NHS). This was followed by an immediate injection of 150 µL of 100 µg/mL of SPSB2 protein, pre-dissolved in 10 mM of sodium acetate, pH 5.5, in the target flow cell. Finally, 150 µL of 1 M ethanolamine-HCl, pH 8.5, was injected into both target and reference flow cells to deactivate any remaining activated carboxyl groups on the surface. An example of immobilisation profile is shown in **Figure 2.7**.

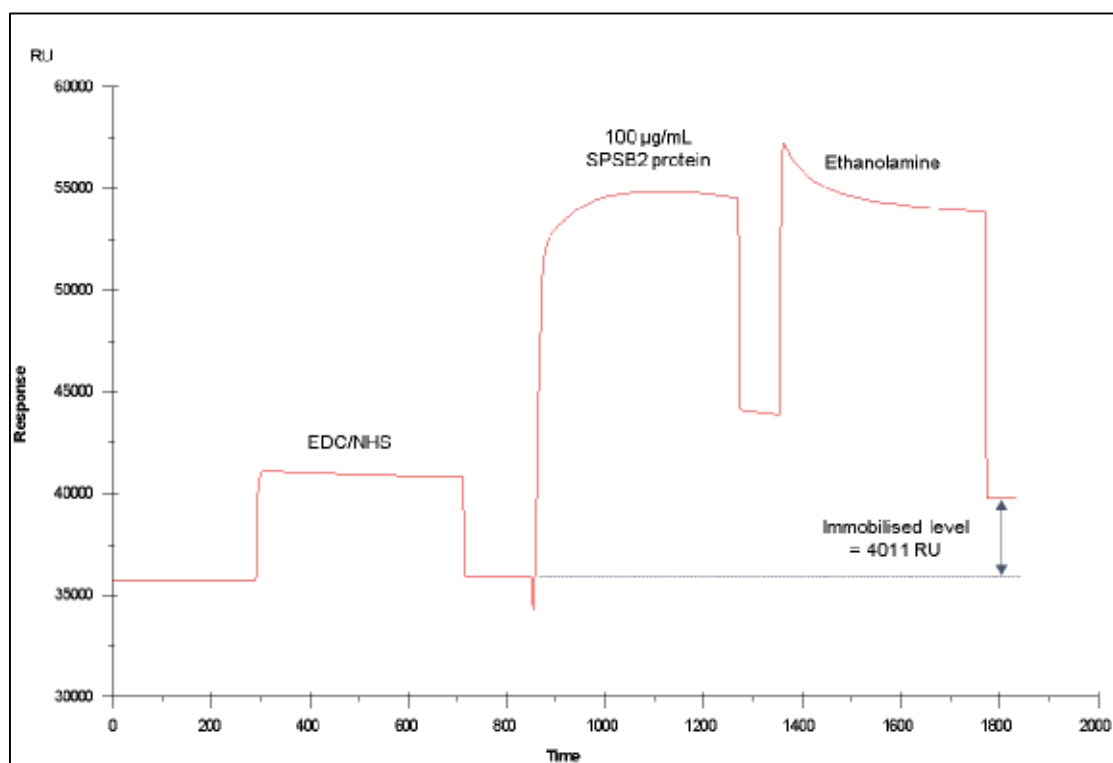


Figure 2.7. An example of an immobilisation profile of 100 $\mu\text{g/mL}$ of SPSB2 on the target flow cell on a CM5 sensor chip with each injection steps and the final immobilised level of the SPSB2 protein on the chip is labelled.

2.3.4.3 Setting up an analyte binding experiment

The binding of peptides (both linear and cyclic) and peptidomimetic was investigated in the SPR running buffer, while the binding of fragments and analogues with free thiol side chain such as that in the macrophage-targeted delivery analogues was carried out in SPR running buffer with addition of 5% (v/v) dimethyl sulphoxide (DMSO) or 0.1 mM tris-(2-carboxyethyl)phosphine hydrochloride (TCEP.HCl), respectively. To set up an analyte binding experiment, a method was first set on the instrument (Run > Method). Each compound (peptide or fragment) at 4-7 different concentrations (at 2, 3 or 5-fold dilutions) prepared in a 96-well plate was injected onto the surface with contact time of 30-100 s, flow rate of 100 $\mu\text{L/min}$, and dissociation time of 120-600 s, depending on the kinetic of the binding of each compound to SPSB2. No further regeneration step was carried out as all compounds were able to dissociate completely after 600 s. For fragment screening, the freshly immobilised SPSB2 were injected with blank samples (i.e. the SPR running buffer) overnight to ensure that the baseline stabilised prior to screening with weak binding fragments. A set of solvent correction solutions over a range of different

DMSO concentrations was prepared according to **Table 2.7** and included during the fragment screening to correct for higher DMSO bulk responses in the reference cell.

Table 2.7. Recipe to prepare solvent correction solutions to correct for high DMSO bulk responses in reference cell during fragment screening

Solvent correction solution	% DMSO	Volume to add (μL)	
		Stock Solution A	Stock Solution B
1	4.55	0	700
2	4.75	100	600
3	4.94	200	500
4	5.15	300	400
5	5.34	400	300
6	5.54	500	200
7	5.74	600	100
8	5.94	700	0

Stock solution A = 1 L SPR running buffer (+ 5% DMSO) + 10 μL 100% DMSO;

Stock solution B = 1 L SPR running buffer (+ 5% DMSO) + 100 μL MQ water

2.3.4.4 Analysis of binding results

For analysis, the Biacore™ T200 Evaluation software (version 2.0) was used. The sensorgrams were double-corrected (or double-referenced subtracted) for non-specific binding to the surface by subtracting the signals of the reference surface from those of the target protein surface, and the signals of the compound from those of the SPR running buffer alone (Kinetics/Affinity > Surface bound). The corrected signal was then fitted to a steady state 1:1 affinity model or a 1:1 kinetic model (if a significant kinetic profile, e.g. slow-on, slow-off, was observed) and K_D , k_{on} and k_{off} were estimated.

2.3.5 Nuclear magnetic resonance

NMR experiments were performed on a Bruker Avance 600 MHz spectrometer, equipped with $^1\text{H}/^{19}\text{F}$ - $^{13}\text{C}/^{15}\text{N}/^2\text{H}$ radiofrequency channels and a 5 mm TCI cryoprobe.

2.3.5.1 Sample preparation

For fragment screening by one-dimensional (1D) STD and CPMG NMR experiments, fragments were dissolved at 200 μM in a 10 mM phosphate, 50 mM NaCl, pH 7.0, buffer containing 10% $^2\text{H}_2\text{O}$ (for spin lock), 1% deuterated DMSO, both with and without 10 μM of purified SPSB2 in 500 μL NMR sample. For chemical shift perturbation studies, 100 μM ^{15}N -labelled SPSB2 was dissolved in 10 mM sodium phosphate buffer, pH 7.0, 50 mM NaCl, with 10% $^2\text{H}_2\text{O}$. The molar ratios of ^{15}N -SPSB2 to fragment and cyclic peptide were 1:10 (or 1:30) and 1:1, respectively. For chemical shift assignments of cyclic peptides and cyclic peptidomimetics, the peptides or mimetics was dissolved in water at pH 4.7-4.8 with 10% $^2\text{H}_2\text{O}$ (for 2D proton homonuclear total correlation spectroscopy ($^1\text{H}, ^1\text{H}$]-TOCSY), nuclear Overhauser effect spectroscopy ($^1\text{H}, ^1\text{H}$]-NOESY), rotating frame Overhauser effect spectroscopy ($^1\text{H}, ^1\text{H}$]-ROESY), double quantum filtered correlation spectroscopy ($^1\text{H}, ^1\text{H}$]-DQF-COSY) and [$^1\text{H}, ^{15}\text{N}$]-SOFASST HMQC) or 99.9% $^2\text{H}_2\text{O}$ (for 2D [$^1\text{H}, ^1\text{H}$]-DQF-COSY and [$^1\text{H}, ^{13}\text{C}$]-HSQC).

2.3.5.2 NMR experiments

All NMR experiments conducted in this study are summarised in **Table 2.8**. Conditions and acquisition parameters used for each experiment, however, varied for different analogues and thus will be described in detail in the respective chapters.

Table 2.8. NMR experiments carried out in this study, with the pulse sequence used for each experiment and the purpose of the experiments.

Type of NMR experiments	Pulse sequence	Purpose
^1H NMR (1D)	zgesgp ²⁰³	Purity check, temperature-dependence studies, reference spectra
STD (1D)	stddiffgp19.3 ^{109, 204, 205}	Fragment screening
CPMG (1D)	cpmges.poe	
[$^1\text{H}, ^{15}\text{N}$]-HSQC (2D)	hsqcNwg.hy	Chemical shift perturbation studies
[$^1\text{H}, ^1\text{H}$]-TOCSY (2D)	dipsi2esgpph ^{203, 206}	Chemical shift assignments of cyclic
[$^1\text{H}, ^1\text{H}$]-NOESY (2D)	noesyegpph	

[¹ H, ¹ H]-ROESY (2D)	roesygp ^{19.2} ^{204, 205, 207, 208}	peptides and peptidomimetics, structure calculation
[¹ H, ¹ H]-DQF-COSY (2D)	cosydfesgp ^{pp} ²⁰⁹	
[¹ H, ¹³ C]-HSQC (2D)	hsqcetgp	
[¹ H, ¹⁵ N]-SOFAS ^T HMQC (2D)	sfhmqcf3gp ^{pp} ²¹⁰	

2.3.5.3 Data analysis

The free induction decay (FID) of the 1D experiment was processed with an exponential window function with a line broadening of 2 Hz and phased. For processing of 2D spectra, a sine-bell squared window function was used. ¹H chemical shifts were referenced to 10 μM 3-trimethylsilyl-1-propanesulphonic acid sodium sulphate (DSS), while ¹³C and ¹⁵N chemical shifts were referenced indirectly through their gyromagnetic ratios²¹¹ unless stated otherwise. All data processing was performed using Bruker TopSpin (version 3.2) and analysed using CcpNmr-Analysis (version 2.1.5).

2.3.6 Macrophage cell lysate inhibition assay

The macrophage cell lysate inhibition assay was carried out according to **Figure 2.8A**. Briefly, bone marrow-derived macrophages were prepared according to **Section 2.3.6.1** and **2.3.6.2**. This was followed by stimulation of the macrophages with lipopolysaccharide and interferon-γ overnight to induce the production of iNOS. Following lysis of the stimulated cells, a GST-based pull-down assay was performed (**Section 2.3.6.3**) where recombinantly-expressed GST-tagged SPSB2 proteins and glutathione resin were added to the cell lysates. The amount of GST-tagged SPSB2-iNOS complex being “pulled down” from the cell lysates by the glutathione resin were determined by Western Blots (**Section 2.3.6.4**).

In principle, when no inhibitor of SPSB2-iNOS interaction is present, the majority of the iNOS protein in the cell lysates is expected to be bound to the GST-tagged SPSB2 and “pulled down” by the glutathione resin, resulting in a strong band corresponding to the anti-iNOS antibody on the Western Blot (**Figure 2.8B**). In contrast, in the presence of an inhibitor, a lower amount of iNOS is likely to bind to the GST-tagged SPSB2 (due to the competition for the iNOS binding site on the GST-tagged SPSB2) and be “pulled down” by the glutathione resin from the cell lysate, and thus, only a thin band corresponding to the anti-iNOS antibody is likely to be observed on the Western Blot.

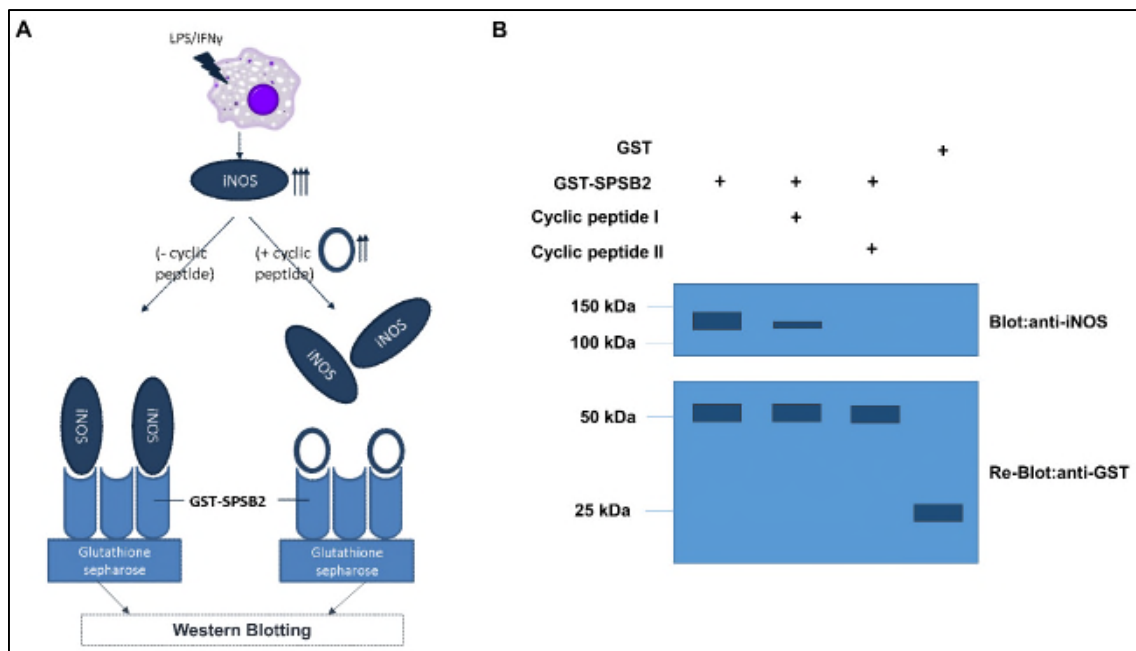


Figure 2.8. (A) A simplified diagram of the workflow and principle of the macrophage cell lysate inhibition assay carried out in this thesis. (B) An example of Western Blot of samples from GST-based pull-down assay. The presence of cyclic peptide I in the macrophage cell lysate during the pull-down assay results in a lesser amount of iNOS being “pulled down” by the GST-SPSB2-glutathione resin, and hence a thinner band on the blot detected by antibody anti-iNOS, compared to the sample collected in the absence of inhibitors. Cyclic peptide II completely displaces iNOS binding to GST-SPSB2, and thus no band is observed on the blot of anti-iNOS. Re-blot of the membrane with antibody anti-GST is performed to confirm the equivalent loading of the samples.

2.3.6.1 Preparation of macrophage cells

Preparation of macrophage cells was conducted by Dr Sandra Nicholson (Walter and Eliza Hall Institute of Medical Research, Parkville, Australia). Briefly, the macrophages were extracted from the bone marrow of both femur and tibia of C57BL/6 mice housed at the Walter and Eliza Hall Institute animal facility. The mice were asphyxiated in a closed container containing carbon dioxide gas. In a class II biological safety cabinet, the asphyxiated mice were sprayed with 80% (v/v) ethanol. The bone was cut on the hip joint and the skin of the leg was carefully cleared off with a pair of sterile scissors. The bone was further cut on the knee joint. Using a pair of sterile forceps, the femur or tibia was

held and a 5 mL syringe with a 26G needle, pre-filled with sterile Dulbecco's modified Eagle's medium (DMEM) was inserted into the bone marrow cavity of the femur or tibia and the entire media were flushed through the cavity into a clean 50 mL Falcon tube on ice. The cells were centrifuged at 500 g and 4 °C for 10 min. Supernatant was removed and the cell pellets were resuspended, plated and cultured in DMEM supplemented with 100 U/mL penicillin, 0.1 mg/ml streptomycin, 10% fetal bovine serum (FBS) and 20% *L*-cell conditioned medium (as a source of macrophage colony-stimulating factor (M-CSF)) at 37 °C and 10% CO₂ according to protocol described by Wormald *et al.*²¹² The cells and media were then added with 1 mL of *L*-conditioned media on day 3 and further incubated for 3-4 days until the cells were adherent to the plate.

2.3.6.2 Adherent macrophage cell harvesting and replating

To harvest the adherent macrophage cells from tissue culture plates, the media were first removed from the plate *via* suction under vacuum. The cells were then washed with approximately 5 mL of mouse-tonicity phosphate-buffered saline (MTPBS) or Dulbecco's phosphate-buffered saline (DPBS), followed by resuspension in approximately 4.5 mL of cell dissociation buffer, enzyme-free Hanks' balanced salt solution (HBSS) and incubation for 5 min at 37 °C. After 5 min of incubation, the cells were transferred to a 50 mL Falcon tube, and the plate was washed with a small amount of the filtered DMEM/10% FBS/20% *L*-conditioned media and its content was transferred to the same Falcon tube. To determine the number of cells in the Falcon tube, 100 µL of the sufficiently mixed cell-containing media were aliquoted into one empty well of a 96-well plate and mixed with 100 µL of trypan blue (0.5% solution) (1:1). The mixed sample was then added to a Neubauer chamber (with the glass cover slip over the counting chambers) and the cells were manually counted under a microscope (at four large corner squares). Based on the total cell counts from the four large corner squares, and the dilution factor of 2, the cell concentration in the Falcon tube was estimated using **Equation 2.2**.

$$\text{Cell concentration (cells/mL)} = \frac{\text{total cell count}}{\text{number of squares}} \times \text{dilution factor} \times 10^4 \quad (2.2)$$

To re-plate the cells into a petri dish for pull-down assays (e.g. 1-2 x 10⁷ cells/mL per plate), the cells were spun down at 15,000 rpm for 5 min at 4 °C and the supernatant was removed. The cells were resuspended in the filtered DMEM media with supplements to

make up the desired final cell concentrations, plated into the plates and incubated overnight at 37 °C at 5% CO₂. The media in each plate were then replaced with supplemented DMEM media containing 10 ng/mL murine interferon- γ (IFN- γ) and 20 ng/mL *Salmonella Minnesota*-derived lipopolysaccharide (LPS) overnight at 37 °C at 5% CO₂ to stimulate the expression of iNOS in the cells.

2.3.6.3 GST-based pull-down assay

Plates containing the LPS/IFN- γ stimulated BMDM cells were placed on ice and the media in the plate were completely removed *via* sucking using sterile pipette under vacuum. 1 mL of cold kinase assay lysis buffer (150 mM NaCl, 50 mM Tris, pH 7.4, 1% (v/v) Triton X-100, 1 mM EDTA)²¹³ containing freshly added Roche's cComplete Protease Inhibitor Cocktail (1 tab/50 mL buffer) and 1 mM phenylmethylsulphonyl fluoride (PMSF) was pipetted into each plate, carefully mixed to ensure that all cells adhered to the plate surface were in contact with the lysis buffer, and incubated on ice for 30 min. The cell lysates were then transferred to an Eppendorf tube and centrifuged at 13,000 rpm for 15 min at 4 °C. Supernatant was then pipetted into a 50 mL Falcon tube and 1 mL supernatant was then re-aliquoted into a new Eppendorf tube and incubated with 2.5 μ g/mL recombinantly expressed GST-SPSB2 protein (unless stated otherwise), in the absence and the presence of 10 μ M cyclic peptide or peptidomimetics for 2 h on a rotator in the cold room. After 2 h, the GST-tagged protein and cyclic peptide or peptidomimetic-containing cell lysates were added with 30 μ L of lysis buffer pre-washed 50% packed glutathione-Sepharose 4B beads (GE Healthcare) and further incubated for 1 h on the rotator in the cold room to pull down the GST-SPSB2-iNOS complex from the cell lysate. After incubation, the beads were washed 3 times with lysis buffer *via* repeated cycles of centrifugation at 13,000 rpm at 4 °C for 20 s, removal of supernatant by suction under vacuum with a glass pipette and resuspension with 1 mL of lysis buffer. To elute the bound protein from the beads, 30 μ L of 2 x SDS sample buffer was added to the beads in the Eppendorf tube and the samples were heated at 90 °C for 5 min prior centrifugation at 13,000 rpm for 2 min. 10 μ L samples were loaded into the wells of a 15-wells 1.5 mm thick 4-12% NuPAGE[®] Bis-Tris mini gel and proteins were separated by SDS-PAGE under reducing conditions (80 V for 30 min followed by 120 V for 2 h).

2.3.6.4 Western blots

Proteins separated by SDS-PAGE under reducing conditions were then electrophoretically transferred to nitrocellulose membranes (Millipore) using the BioRad Mini Trans-Blot[®] Cell in transfer buffer containing 25 mM Tris, 152 mM glycine, 20% (v/v) methanol, pH 8.3, for 3 h at 100 V under constant stirring. Membranes were then trimmed and put into a tube, with no overlap between the edges of the membrane, and the tube was half-filled with 10% (w/v) skim milk in water and incubated overnight on a roller in the cold room. After overnight blocking with skim milk, the membrane was washed 3 times with PBST buffer (PBS buffer + 0.1% (v/v) Tween 20) followed by incubation with approximately 4 mL of mouse monoclonal anti-iNOS (1:1000) (BD Biosciences) or mouse anti-GST primary antibody (1:3000) in fresh PBST buffer containing 1% (w/v) bovine serum albumin (BSA) on a roller at room temperature for 2 h. After 2 h incubation, the membrane was rinsed and washed 3 times with PBST with 10 min incubation on a roller per wash. 4 mL of secondary antibody peroxidase-conjugated sheep anti-mouse Ig antibody, diluted 1:10000 (GE Healthcare) in PBST+BSA buffer, was then added to the membrane and incubated for 1 h, followed by extensive washing with PBST every 20 min for 2-3 h. Finally, the buffer was removed and 1 mL each of Amersham Electrochemiluminescence (ECL) Western Blotting Detection Reagents (GE Healthcare) were added to the membrane and incubated on a roller for 3-5 min. ECL detection reagents were then discarded and the membrane was transferred to a film holder with transparency and subjected to ECL detection and film development with an Amersham Hyperfilm ECL (GE Healthcare). To reblot, the membrane was stripped of antibodies *via* incubation of the membrane in 0.1 M Gly, pH 2.9, for 20 min, followed by rinsing and washing the membrane 3 times with PBST prior incubation with primary and secondary antibodies for subsequent ECL visualisation.

2.3.7 Other methods

Other specific methods presented in the thesis, such as fragment screening, structure calculation by NMR, plasma stability assay, redox stability assay, synthesis of glycopolymers and their cyclic peptide conjugates and imaging studies by confocal laser scanning microscope are discussed in greater detail in the respective Chapters.

CHAPTER 3

**Discovery of fragment hit targeting SPSB2
protein *via in silico* and NMR-guided FBDD
approach**

3.1 Introduction

In attempts to discover small molecule inhibitors of SPSB2-iNOS interaction, FBDD approach was selected in this study. *In silico* approaches were first used to screen for fragments from a commercial library that bind to the iNOS binding site of SPSB2 with LE > 0.3. Fragment hits displaying key hydrogen bond interactions with SPSB2 as observed in the crystal structure of the linear peptide DINNN/SPSB2 complex (PDB ID: 3EMW)⁵⁵ were then selected for subsequent analysis by NMR. Both ligand-based (STD, CPMG) and target-based (¹⁹F, [¹H, ¹⁵N]-HSQC) NMR experiments were performed to confirm the binding of the *in silico* shortlisted fragment hits on the iNOS binding site of SPSB2. The binding affinity of the NMR-positive fragment hits on SPSB2 was subsequently determined by SPR.

3.2 Materials and methods

SPSB2 protein expression and purification were carried out according to **Section 2.3.2**.

3.2.1 Computational drug design and docking studies

3.2.1.1 Design of a virtual compound library for docking studies

A virtual library of compounds was designed from the 636,208 compounds of Vitas-M Laboratory Ltd, chemical compounds database, with molecular mass ranges between 75 and 300 Da.

3.2.1.2 Ligand and protein preparation

Energy-minimised 3D molecular structures of the virtual library compounds were prepared using LigPrep (version 2.5, Schrödinger). Tautomers and ionisation species at different ionisation states (pH 5.0-9.0) and stereoisomers were generated by Epik^{214, 215} and Stereoizer, respectively, to expand the chemical and structural diversity of the compounds. The crystal structure of the SPSB2-VASA peptide complex (PDB ID: 3EMW)⁵⁵ was prepared using the Protein Preparation Wizard in Maestro (version 9.3, Schrödinger), in which the water molecules were removed and hydrogens were added to the structure. Missing side chains were assigned and the complex was subjected to restrained minimisation (RMSD cut-off of 0.3Å) to remove undesirable steric clashes in

the structure. The VASA peptide was removed from the prepared crystal structure of SPSB2 complex prior to docking.

3.2.1.3 Receptor grid generation

A grid box of 28 x 28 x 28 Å³, with a default inner box of 10 x 10 x 10 Å³, centred at the putative binding site of SPSB2-VASA peptide was generated using default parameters without constraint.

3.2.1.4 Docking protocol

Docking studies were carried out with Glide^{124, 125, 198} using the SP protocol and the default sampling method. The SP protocol was chosen over Glide extra precision (XP) protocol because recent work by Sandor and colleagues¹²³ showed that Glide SP gave similar results to that of the computationally more intensive Glide XP. Similarly, the effect of expanded sampling on the docking performance was not significant, with a success rate of 82% versus 80% in default sampling.

3.2.1.5 Post-docking analysis

Docked compounds were re-sorted based on the calculated LE (Glide score/number of heavy atoms) using an in-house script. Docking poses of each compound in the library with LE > 0.3 were further analysed using the Select Top Poses and Pose Filter scripts in Maestro (version 9.3, Schrödinger), in which only the best pose of each compound that makes hydrogen bonds (i.e. hbond_dist_max = 2.5Å; hbond_donor_angle = 90°; hbond_acceptor_angle = 60°) with the key residues Arg68, Thr102, Val71/Tyr120/Val206 and Gly208 of SPSB2 was retained. Selected compounds were subjected to clustering with Molsoft ICM Chemist software to remove compounds that are highly similar to each other (i.e. with Tanimoto coefficient > 0.8). In this case, the clustering method used was the default rigorous tree approach which consists of 2 steps: calculation of distance matrix (based on chemical fingerprints for chemical data) and the hierarchical clustering itself. The type of linkage method used in this study was UPGMA (unweighted pair group method using averages), in which the distance calculated is the average of all elements. In addition, compounds with absorption, distribution, metabolism, excretion and toxicity (ADMET) reactive functional groups (such as vinyl ketones, vinyl ethers, enamines, secondary alkyl halides, β-haloamines, pyrole-2,5-dione, hydrazones, halomethyl ethers, linear dithiocarbamates, acrylonitriles, acrylates,

acrylamides, positively charged heterocycles, α -haloketones, thiones, thioamides, sulphonyl halogenides, oxiranes, nitroso, linear thioureas, benzylhalogenides, azo, aziridines, *N*-oxides and alkylsulphonates) and undesirable physicochemical properties were filtered out by the Bad Groups filter of Molsoft ICM Chemist Software and the Lipinski's Rule of Five (Ro5)²¹⁶ (molecular mass ≤ 500 Da, calculated log P ≤ 5 , number of hydrogen bond donor ≤ 5 and number of hydrogen bond acceptor ≤ 10) respectively.

The Lipinski's Ro5 was selected over the Astex's Rule of Three (Ro3) (which is commonly used in the design of fragment libraries as hits identified using this approach generally obey the criteria set in Ro3)¹⁰³ as a filter in this study because there is growing evidence that hard application of Ro3 in FBDD may unnecessarily limit the chemical space being sampled and restrict further lead optimisation *via* fragment growing or linking, which occasionally requires functional groups with hydrogen bond donor or acceptor properties. To illustrate, one recent study by Köster *et al.*²¹⁷ showed that 7 of the 11 fragment hits co-crystallised with endothiapepsin protein violate the Ro3. These fragment hits, however, conform to properties closer to Ro5, suggesting that the use of Lipinski's RoF as a filter in FBDD may be more appropriate than Ro3 even at this early stage of drug discovery.

Compounds with the highest LE in each cluster were then selected for further analysis with PyMOL (version 1.5.0.4, Schrödinger) and reasonable hits were selected for further analysis with NMR (i.e. STD, CPMG, ¹⁹F and [¹H, ¹⁵N]-HSQC) and SPR analysis.

3.2.2 Nuclear magnetic resonance (NMR) experiments

NMR spectra (STD, CPMG) were recorded separately for the compound alone, the compound in the presence of SPSB2 protein, and the compound with SPSB2 protein and peptides (DINNN peptide and KEEKDINNVKKT) at 283 K. All spectra were processed using an exponential window function with a line broadening of 2 Hz.

The principle of STD was first introduced by Mayer and Meyer^{108, 109} and is illustrated in **Figure 3.1**. In general, when a protein is selectively irradiated, i.e. at a frequency where only protein resonates (e.g. in the upfield region) (on-resonance), proton magnetisation transfers intramolecularly *via* spin-diffusion, resulting in complete protein saturation (i.e. an equal population of excited and ground states), and ultimately a complete loss of protein signals. When a ligand is bound to the magnetisation-saturated protein, the

saturation is transferred intermolecularly from the protein to the ligand. This results in a total loss or decrease in signal intensities of the ligand, depending on the proximity of the ligand's protons to the protein surface. When these on-resonance signals are subtracted from the reference spectrum (off-resonance) (e.g. when saturation pulse was applied at 30 ppm, where no protein signals are present), the proton signals of both protein and ligand (at different intensities) will be observed (difference spectrum). To facilitate analysis, a T1ρ filter (e.g. a 30 ms spin-lock pulse) is incorporated in STD NMR experiments to remove all background protein resonances, as the protein with much larger size than the ligand has a higher transverse relaxation rate (R_2) than ligand, and thus a faster FID decay rate. This results in only resonances of protein-bound ligand protons being observed in the difference (STD) spectrum.

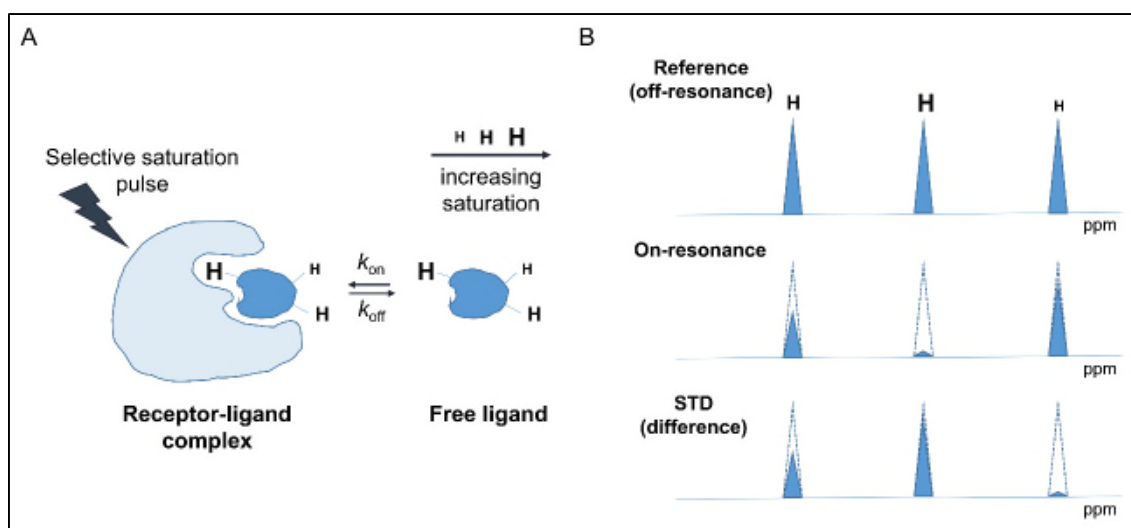


Figure 3.1. The principle of STD NMR experiment. Signal intensity of ligand proton that is closer to magnetisation-saturated protein in **A** (represented as larger “H”) is higher in the STD spectrum as shown in **B** (represented as solid blue triangles). The reference signal intensities of the ligand protons in both on-resonance and STD spectra are shown as dotted blue triangles. STD spectrum is the difference spectrum of the on-resonance spectrum from the reference (off-resonance) spectrum.

While STD NMR measures the differences in saturation transfer from magnetisation-saturated protein to the ligand, CPMG exploits the differences in T_2 relaxation rate between the protein-bound ligand and the unbound ligand in solution. CPMG involves in initial 90° pulse, followed by 180° pulses which result in spin-echoes, all at the same phase, and thus a more accurate determination of T_2 relaxation time in solution.¹¹¹ As T_2

relaxation rate increases with the size of the molecule,²¹⁸ a ligand bound to protein is expected to experience a faster T_2 relaxation rate than the unbound ligand. Thus, a spin-lock time is usually selected in CPMG experiments to ensure that at least 99% of the protein signal intensity is eliminated while the signal intensity of the ligand remains observable. This is crucial as, when a ligand is bound to protein, a further drop in ligand signal intensity at the specified spin-lock time (e.g. 400 ms) is expected since less unbound ligand will be available in the solution.¹¹² In competition CPMG experiments, a high-affinity ligand competes with a low-affinity ligand for binding to the protein, and thus a lesser amount of low-affinity ligand is expected to bind to the protein (i.e. more free ligand in the bulk solution). This results in an increase or restoration of the ligand signal intensity to the unbound state.

^{19}F NMR experiments of 20 μM 5-F-Trp SPSB2 (prepared by Dr Eleanor Leung, Medicinal Chemistry, Monash Institute of Pharmaceutical Sciences, Australia) in 50 mM sodium phosphate buffer, pH 7.4, and 50 mM NaCl were recorded at 30 °C in the presence and absence of 1 mM compound. ^{19}F NMR chemical shifts were referenced against 0.005% trifluoroethanol. All spectra were processed using an exponential window function with a line broadening of 40 Hz. 2D heteronuclear single quantum coherence (^1H , ^{15}N)-HSQC) spectra of SPSB2 in the absence and the presence of compounds were recorded using 100 μM ^{15}N -labelled SPSB2 dissolved in 10 mM sodium phosphate buffer, pH 7.0, 50 mM NaCl with 10% $^2\text{H}_2\text{O}$. The molar ratio of SPSB2 to the compound was 1:10. Spectra were acquired at 22 °C using a data matrix size of 128 (t_1) \times 8192 (t_2) and with 8 scans per t_1 increment. The spectral widths were 13.5 and 35.0 ppm for ^1H and ^{15}N , respectively. Both the ^1H and ^{15}N chemical shifts were referenced indirectly *via* the H_2O signal in ^1H , and the absolute frequency ratio in ^{15}N .²¹¹ All data processing was performed using the Bruker TopSpin 3.2 software.

3.2.2.1 Sample preparation

Each compound was dissolved at 200 μM in a 10 mM phosphate, 50 mM NaCl, pH 7.0, buffer containing 10% $^2\text{H}_2\text{O}$ (for spin lock), 1% deuterated DMSO, both with and without 10 μM of purified SPSB2 and prepared as 500 μL NMR sample. As for the competition screening, 100 μM of DINNN or the KEEKDINNNVKKKT peptide was added to the same concentration of compound and protein. As the NMR experiments were run at a

temperature of 283 K, sample temperature was allowed to equilibrate for 2 min prior to each NMR run. All runs were automated with IconNMR (version 4.7, Bruker).

3.2.2.2 STD Experiments

STD experiments were recorded with 5 s saturation time, a relaxation delay of 5 s and a sweep width of 13.5 ppm with the frequency of the on-resonance irradiation was set to -0.8 ppm and the off-resonance pulse was set at 33 ppm. The residual water signal was suppressed using excitation sculpting. 128 scans were recorded for each spectrum.

3.2.2.3 CPMG Relaxation Experiments

CPMG experiments were recorded with a spin-lock time of 600 ms to reduce or eliminate the signals of the protein and the bound ligands, without significantly affecting the signals of the unbound ligand. Typically, 32 scans were recorded for each spectrum.

3.2.3 Surface plasmon resonance (SPR) experiments

Immobilisation of murine SPSB2 protein on the CM5 chip was carried out according to the protocol described in **Section 2.3.4**.

3.2.3.1 Testing of the immobilised surface with a known analyte

Prior to investigating the binding affinity of the compounds, it is crucial to test the analyte binding capacity and the homogeneity of the immobilised surface by injecting a known analyte (in this case, the DINNN peptide). Hence, eight concentrations of DINNN peptide ranging from 0.08 μM (at a two-fold increase) to 10 μM in a running buffer containing 10 mM HEPES, 150 mM NaCl, 3 mM EDTA, 0.05% Tween 20 and 5% DMSO, pH 7.4, were injected onto the surface with a contact time of 20 s, a flow rate of 100 $\mu\text{L}/\text{min}$, and a dissociation time of 180 s.

3.2.3.2 Estimation of binding affinity of the NMR positive hits

The binding of the NMR-positive hits was tested using 400 μM as the highest concentration, in a 2-fold dilution series with four concentrations in total in a running buffer containing 10 mM HEPES, 150 mM NaCl, 3 mM EDTA, 0.05% Tween 20 and 5% DMSO, pH 7.4. Each sample was spun down to precipitate insoluble material and injected onto the surface with a contact time of 30 s, a flow rate of 60 $\mu\text{L}/\text{min}$, and a dissociation time of 180 s. No further regeneration step was carried out as the NMR-

positive hits were able to dissociate rapidly. The sensorgrams were further corrected for non-specific binding to the surface by subtracting the signals from the reference surface from those of the target protein surface. After subtracting the blank signals (when only the running buffer was injected), the corrected signal was fitted to a steady-state 1:1 interaction model and the K_D was estimated based on the input of calculated theoretical R_{max} of each analyte as shown in **Equation 3.1** and the percentage of the active surface of the immobilised protein.

$$R_{max} = \frac{MW_{analyte}}{MW_{ligand}} \times \text{Immobilisation amount} \times \text{stoichiometry ratio} \quad (3.1)$$

3.3 Results

3.3.1 Key interactions essential for SPSB2-iNOS binding

As described in **Section 1.3.2**, the binding interface between the SPSB2 and DINNNNN motif (as observed in SPSB2-VASA complex (PDB ID: 3EMW)⁵⁵) is mediated by a network of hydrogen bonds, i.e. between the amide side chain of Asn186 and Asn188 (VASA) and Arg68, Thr102, Tyr120, Val206 and Gly208 (SPSB2) (**Figure 3.2A**). In addition, the negatively charged carboxylic side chain of Asp184 (VASA) was also found to form an additional hydrogen bond to the phenolic side chain of Tyr120 (SPSB2). Although a hydrogen bond was also observed between the main chain of Asn189 (VASA) and the side chain of Pro70 (SPSB2), Asn189 was not conserved in iNOS as iNOS has a valine instead of asparagine (DINNNV versus DINNNNN). As Val and Asn have distinctively different side chain properties, i.e. hydrophobic versus polar side chains in Val and Asn, respectively, it is predicted that the folding of the peptide at the end of the DINNNN sequence may be different from iNOS. This suggests that the hydrogen bond interaction between Pro70 (SPSB2) and Asn189 (VASA) may not be as important in iNOS as in VASA.

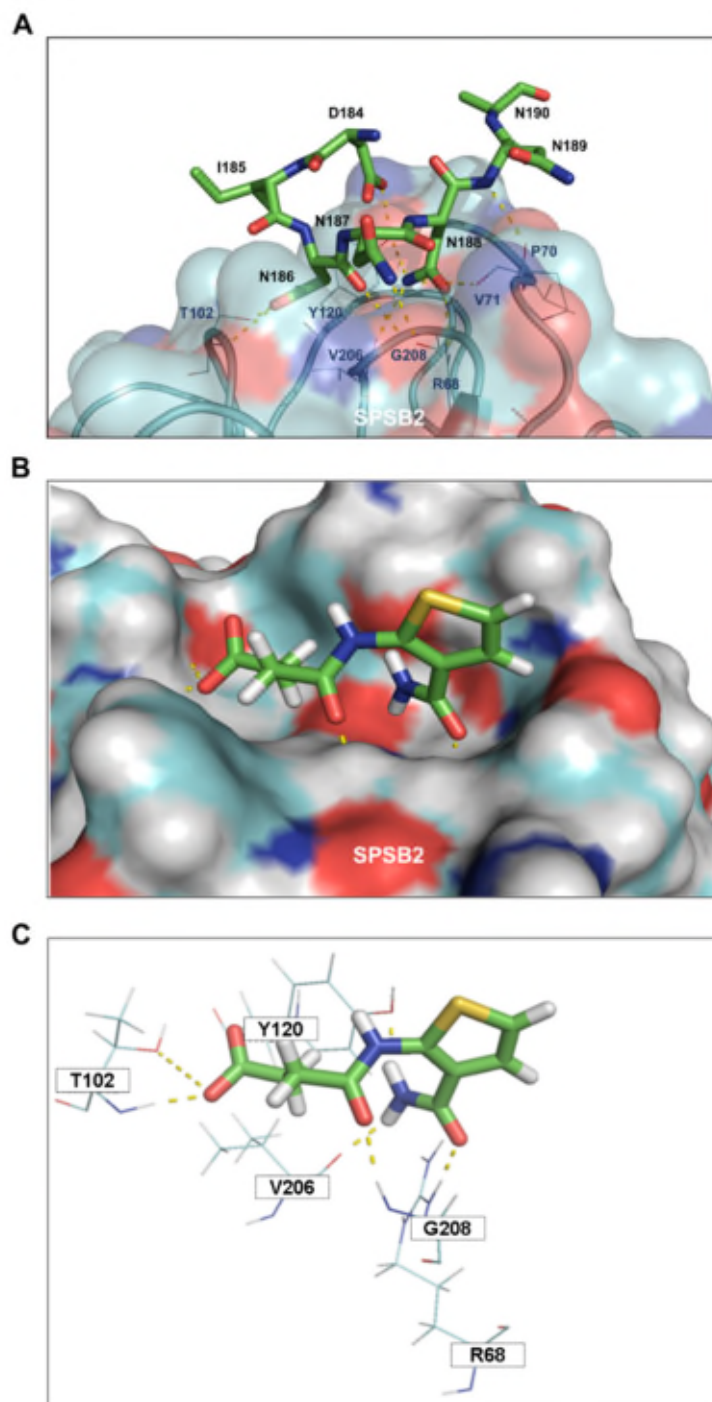


Figure 3.2. (A) Peptide-protein binding interface of the DINNNNN sequence of VASA peptide (stick) and the human SPSB2 (surface) (PDB ID: 3EMW).⁵⁵ Residues involved in the hydrogen bond (yellow dashes) interaction between SPSB2-DINNNNN are labelled. (B) Ligand-protein interactions between one of the *in silico* top scoring compound, STK441224 (stick) and the human SPSB2 protein (surface). (C) Residues in the iNOS binding site of SPSB2 making key hydrogen bonds (yellow dashes) with the compound are labelled and represented as lines.

3.3.2 13 potential hits were identified from *in silico* screening

Utilising the knowledge of key hydrogen bonds mediating the SPSB2-iNOS interaction, approximately 961,514 compounds (which include the parent compounds and their respective ionisation species, tautomers and stereoisomers) prepared by LigPrep (version 2.5, Schrödinger), were docked and analysed. Post-docking analysis revealed only 93 compounds docked to the iNOS binding site of SPSB2 showed binding modes in agreement with the pre-defined key hydrogen bonds criteria (**Figure 3.2C**). Upon visualisation of the individual ligand-receptor interactions of all 93 compounds with PyMOL (version 1.5.0.4, Schrödinger), the top 13 compounds (**Figure 3.3**) with ligand efficiency ≥ 0.30 were selected for further analysis by STD and CPMG NMR.

3.3.3 Two *in silico* hits gave positive responses in STD and CPMG

When all 13 compounds were tested with both STD and CPMG NMR, only two compounds (i.e. STK441224 and STK847123) were positive in both STD (**Figure 3.4**) and CPMG (**Figure 3.5**) and were able to compete with linear peptides Ac-DINNN-NH₂ or Ac-KEEKDINNNVKKKT-NH₂ for its binding site on SPSB2. Another three compounds, STK802097, STK068548 and STK692712, gave positive signals in STD but not CPMG (**Table 3.1**), suggesting that these compounds are probably very weak binders. STK847123 was found to compete with the linear peptide Ac-KEEKDINNNVKKKT-NH₂ but not the Ac-DINNN-NH₂ in its binding to the SPSB2 protein. This suggests that STK847123 may have bound to a second binding site adjacent to the DINNN binding site, which would have interfered with the 13-residue peptide binding on the SPSB2 but not Ac-DINNN-NH₂. Based on these observations, the three compounds with positive responses in both STD and CPMG were subjected to SPR to estimate their binding affinities for SPSB2.

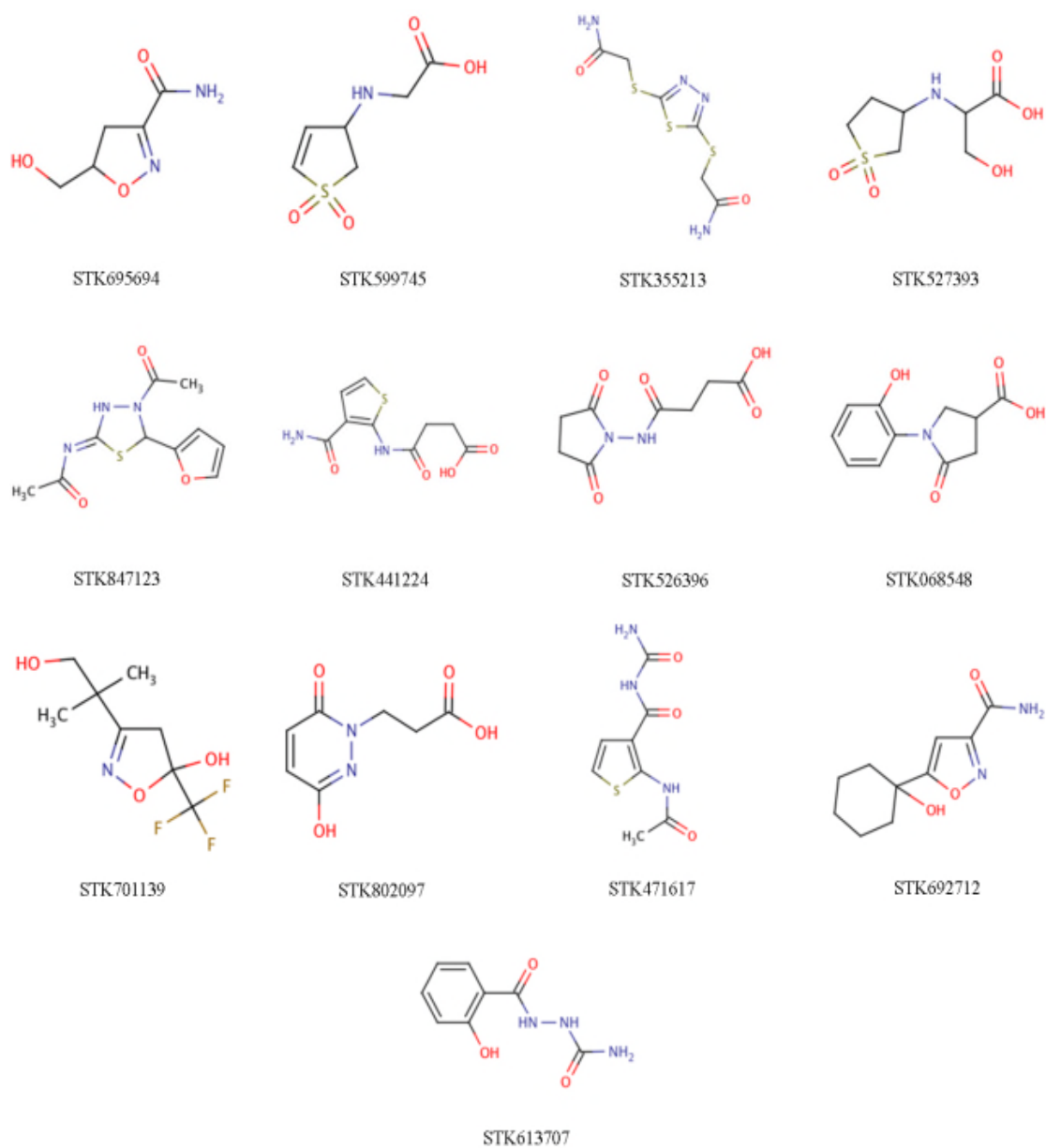


Figure 3.3. 13 compounds from the *in silico* screening of the Vitas-M Lab virtual lead-like compound library with LE > 0.3.

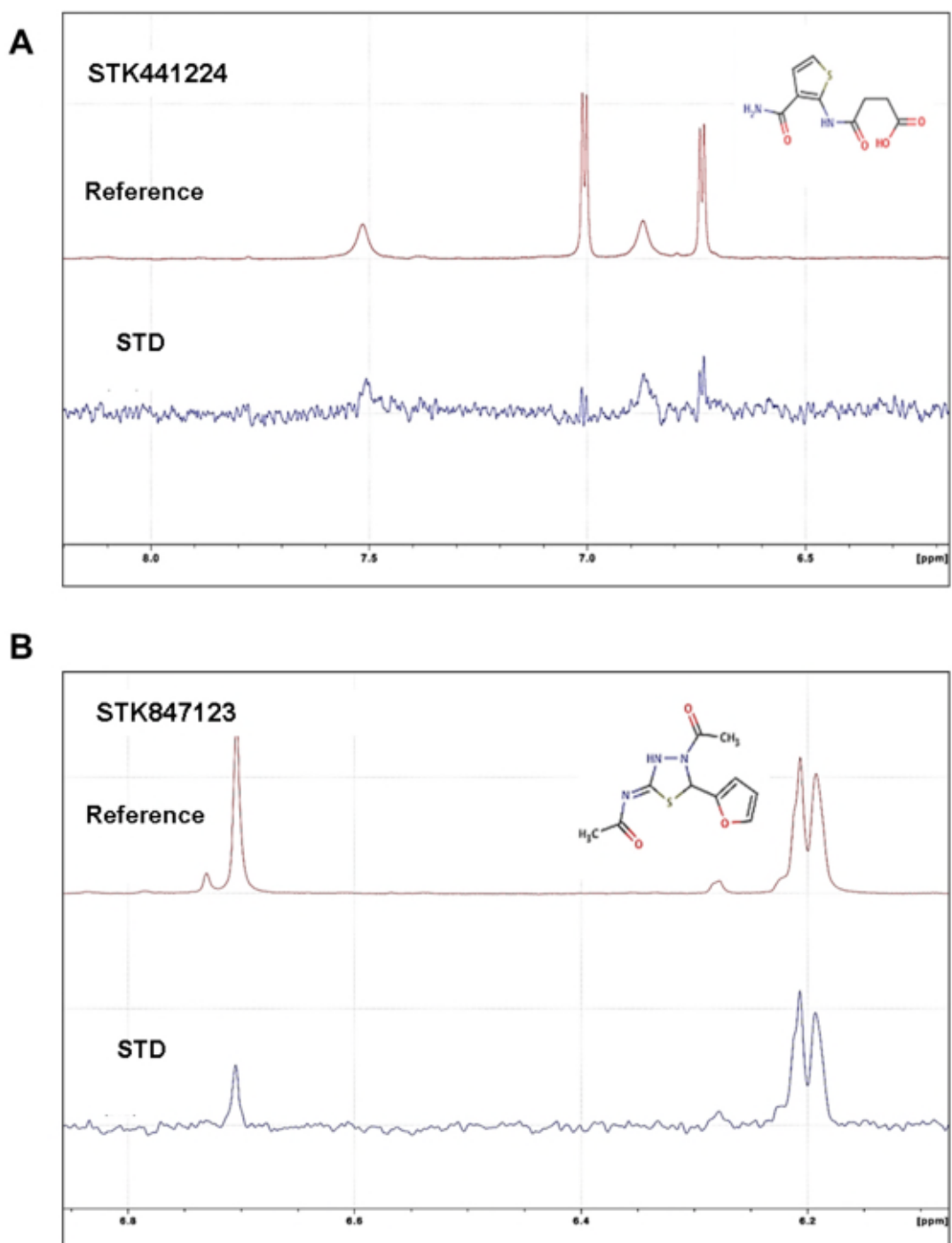


Figure 3.4. The off-resonance reference NMR spectrum (top) and STD spectrum (bottom) for (A) STK441224-SPSB2 and (B) STK847123-SPSB2 protein complexes. The positive signal intensity of a peak in the y-axis of STD spectra suggests that the specified proton is in close vicinity to the SPSB2 protein.

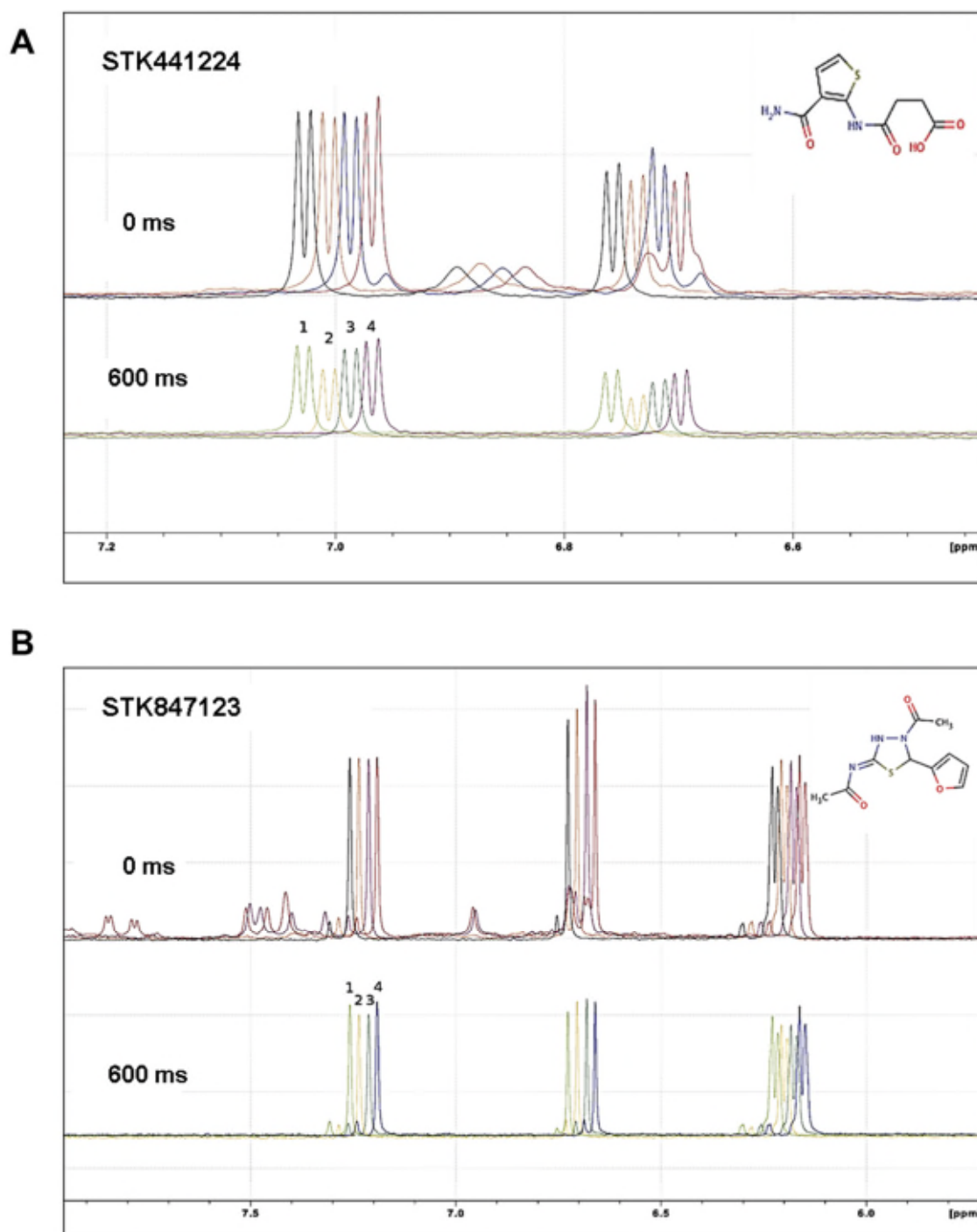


Figure 3.5. CPMG NMR spectra of the positive hits (A) STK441224 and (B) STK847123 at both 0 ms (top) and 600 ms (bottom) on (1) its own, (2) with SPSB2 protein, and (3) with SPSB2 protein plus competition with 5-residue linear peptide Ac-DINNN-NH₂ or (4) the 13-residue linear peptide Ac-KEEKDINNNVKKT-NH₂. A drop in peak intensity upon titration with SPSB2 suggests that the compounds bound to SPSB2. Restoration of the peak intensity to their unbound state upon titration with linear peptides, suggests that they bound to the iNOS binding site.

Table 3.1. Summary of the STD and CPMG NMR results of the 13 compounds in complex with the SPSB2 protein (in competition with Ac-DINNN-NH₂ or 13-residues linear peptide Ac-KEEKDINNNVKKKT-NH₂)

Compound	Experiments			
	NMR			
	STD + SPSB2	CPMG		
		+ SPSB2	+ SPSB2 + DINNN	+ SPSB2 + 13-residues
STK526396	X	X	X	X
STK802097	✓	X	X	X
STK613707	X	X	X	X
STK701139	X	X	X	X
STK695694	X	O	O	O
STK692712	✓	X	X	X
STK527393	X	X	X	X
STK471617	X	X	X	X
STK599745	X	X	X	X
STK355213	X	O	O	O
STK441224	✓	✓	✓	✓
STK068548	✓	X	X	X
STK847123	✓	✓	X	✓

O: CPMG signal was completely attenuated after 600 ms; X: Negative STD or CPMG results; ✓: Positive STD or CPMG results

3.3.4 The two potential hits bound at low millimolar affinities

To confirm that the surface of the SPSB2 is active prior to testing compounds by SPR, the SPSB2 chip was first injected with increasing concentrations of the linear peptide Ac-DINNN-NH₂. The maximum response, R_{\max} as estimated from the double-referenced subtracted sensorgrams fitted to 1:1 kinetic model was found to be 31% of the calculated R_{\max} based on the immobilised level of SPSB2 and the molecular masses of peptide and protein, suggesting that about 31% of the immobilised SPSB2 is active. When the STD and CPMG-positive hits were injected onto the pre-immobilised SPSB2 on the sensor chip of SPR (**Figure 3.6**), both compounds gave positive responses in SPR with fast on

and off binding, suggesting that these compounds bound weakly to SPSB2. The SPR sensorgrams, however, could not be fitted to the 1:1 interaction model with pre-determined R_{\max} based on 31% occupancy. When the SPR sensorgrams were fitted to the 1:1 interaction model without pre-determined R_{\max} , the K_D of STK441224 and STK847123 were estimated as 1.8 and 4.1 mM, respectively.

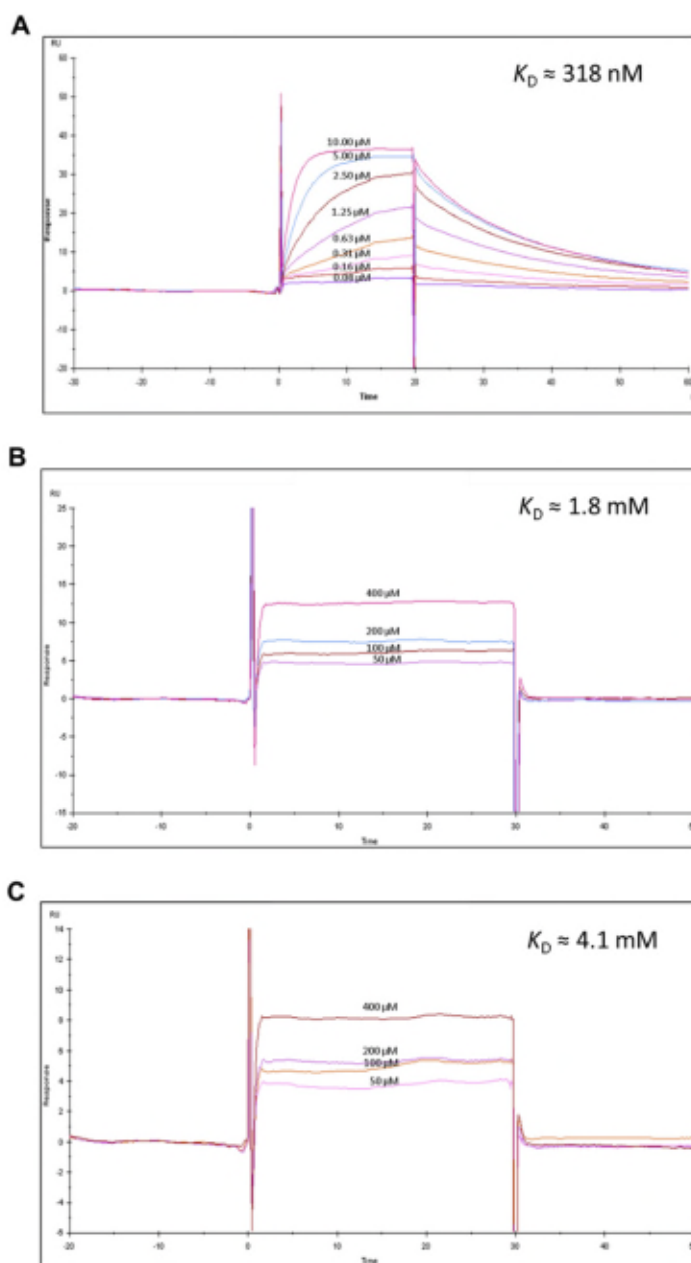


Figure 3.6. Blank-subtracted SPR sensorgrams of (A) Ac-DINNN-NH₂, (B) STK441224 and (C) STK847123 injected at increasing concentration to the SPSB2 protein on a CM5 sensor chip. The binding constant, K_D was determined *via* double-referenced subtracted sensorgrams fitted to 1:1 interaction model.

3.3.5 The potential hits bound weakly or promiscuously to SPSB2

To assess the binding specificity of these compounds for the iNOS binding site of SPSB2, both STK441224 and STK847123 were tested by ^{19}F NMR according to the protocol described in Leung *et al.*¹¹⁶ Neither compound showed any perturbation in any of the peak corresponding to 5-F-Trp207, a key Trp residue in the vicinity of the iNOS binding site (**Figure 3.7**). In contrast, STK441224 resulted in a small shift in the most downfield peak while STK847123 did not perturb any of the 5-F-Trp peaks. Other STD NMR positive hit STK692712 also did not perturb any of the 5-F-Trp peaks, while a similar shift to the most downfield 5-F-Trp peak as in STK441224 was observed in the presence of both STK802097 and STK068548.

When STK441224 was subjected to [^1H , ^{15}N]-HSQC experiments, a significant number of backbone amide proton peaks of the ^{15}N -labelled SPSB2 protein was perturbed in the presence of 1 and 3 mM STK441224 (**Figure 3.8A**). Minor shifts were also observed for backbone amide peaks of Thr102 and Arg68, suggesting that the compound was indeed bound to the iNOS binding site of SPSB2. Nevertheless, the observed shift was relatively small compared to other shifted peaks in the spectra, and resonances of other peaks in the iNOS binding site such as the indole side chain of Trp207 (^1H chemical shift = 10.2 ppm) were not significantly perturbed, suggesting that the compound bound weakly to the iNOS binding site of SPSB2. Most of the other shifted peaks were found to be the backbone amide peaks of positively charged residues such as Arg, His and Lys or its immediate neighbouring residue such as Gly87 (Arg86), Gly193 (Arg192), Gly83 (Arg82), Gly47 (His46), Gly196 (Arg197), Ser144 (Lys145), Ala90 (His89). Backbone amide of other residues spatially close to the Arg residues such as Gly176 and Thr177 (Arg192) and Met217 (Arg215) were also found to be perturbed.

In contrast, the presence of 1 mM STK847123 did not result in significant perturbation to any of the backbone amide peaks of ^{15}N -labelled SPSB2 protein (**Figure 3.8B**). This observation is consistent for a compound with an estimated K_D of 4.1 mM, as the predicted percentage of 100 μM protein bound with 1 mM concentration of the compound is expected to be less than 20%, and therefore significant chemical shift perturbations to the backbone amide of the ^{15}N -labelled protein are unlikely to be observed.

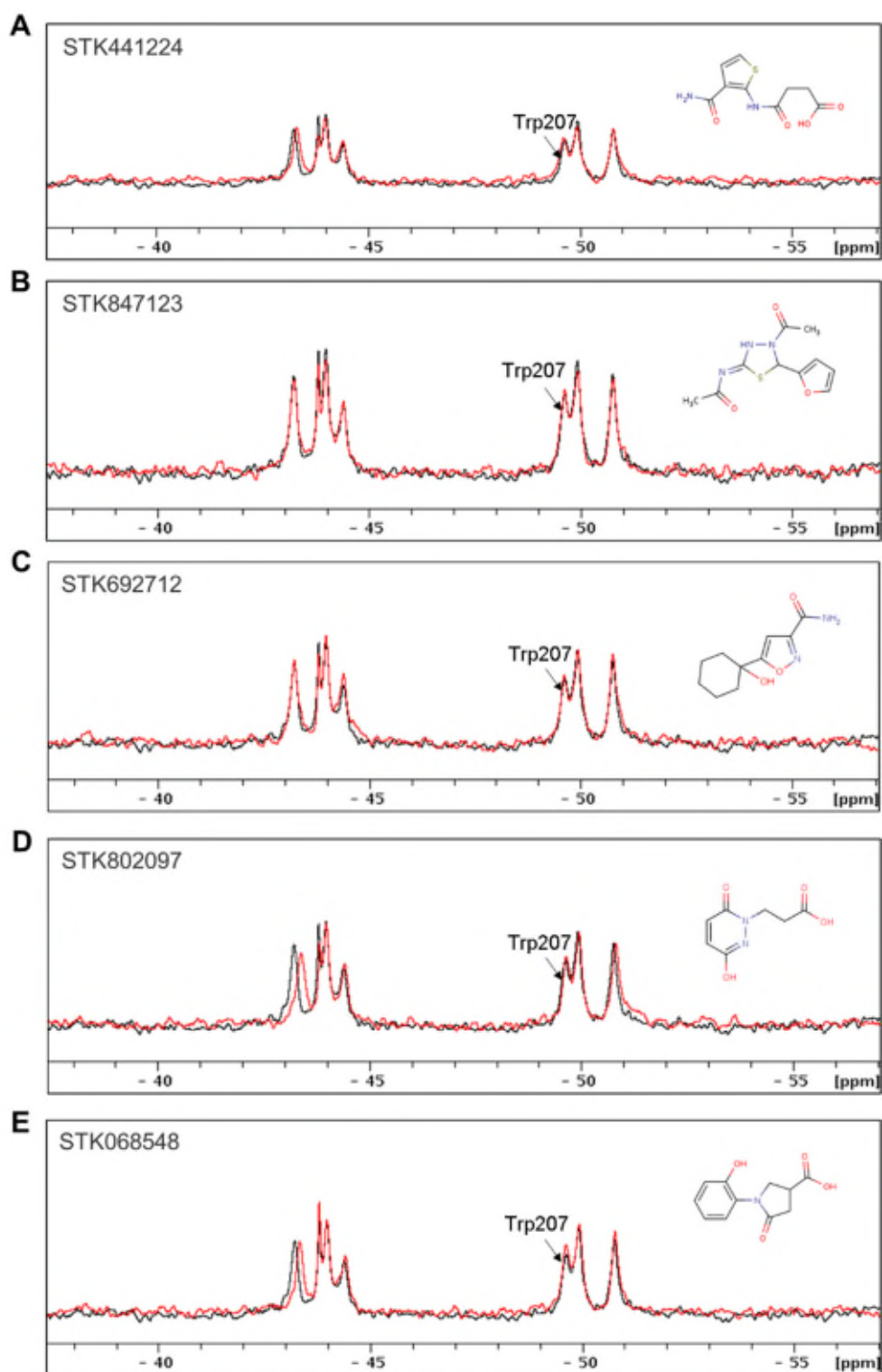


Figure 3.7. ^{19}F NMR spectra of 20 μM 5-F-Trp SPSB2 in the absence (black) and the presence (red) of 1 mM compounds (A) STK441224, (B) STK847123, (C) STK692712, (D) STK802097 and (E) STK068548 in 20 mM sodium phosphate buffer, pH 7.4, and 50 mM NaCl at 30 $^{\circ}\text{C}$. The resonance of the Trp residue closest to the iNOS peptide binding site, Trp207, is labelled.

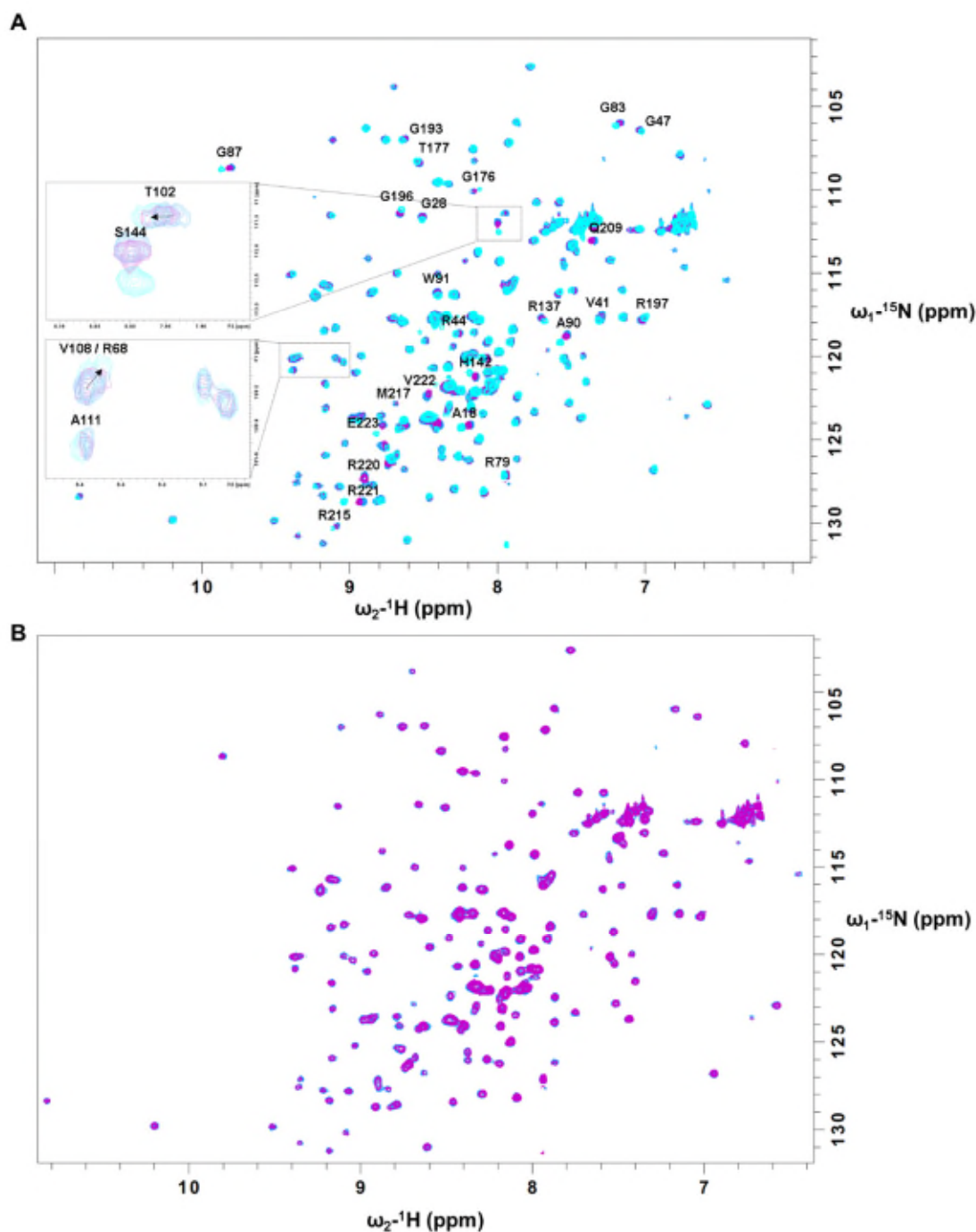


Figure 3.8. Overlays of $[\text{}^1\text{H}, \text{}^{15}\text{N}]$ -HSQC spectra of $100\ \mu\text{M}$ ^{15}N -labelled SPSB2 in the absence of ligand (blue) and the presence of (A) 1 mM STK441224 (purple) or 3 mM STK441224 (cyan) or (B) 1 mM STK847123 (purple) in 10 mM phosphate, pH 7, 50 mM NaCl at $22\ \text{ }^\circ\text{C}$. Backbone amide resonances of ^{15}N -labelled SPSB2 showing significant chemical shift perturbation in the presence of ligand are labelled in the spectra, with the perturbed resonances from residues in the iNOS binding site shown as expanded images in the spectra.

3.3.6 The iNOS binding site of SPSB2 is less druggable

To re-evaluate the druggability of the iNOS binding site of SPSB2 following the lack of success in the current *in silico* guided FBDD campaign (and other fragment screen conducted in parallel by other members in the group), the crystal structure of SPSB2 was subjected to computational prediction analysis, i.e. SiteMap²¹⁹ (Maestro, version 10.3, Schrödinger) and FTMap²²⁰ (<http://ftmap.bu.edu>) (**Figure 3.9**). The SiteMap analysis revealed that the estimated Dscore and SiteScore for all sites ranged from 0.51-0.56 and 0.54-0.64, respectively, which are way below the average values for a druggable site (Dscore = 1.11, SiteScore = 1.09).²²¹ Although FTMap revealed two druggable sites which were bound with at least 16 probe clusters, none of these sites is the iNOS binding site, suggesting that the iNOS binding site of SPSB2 is less druggable.

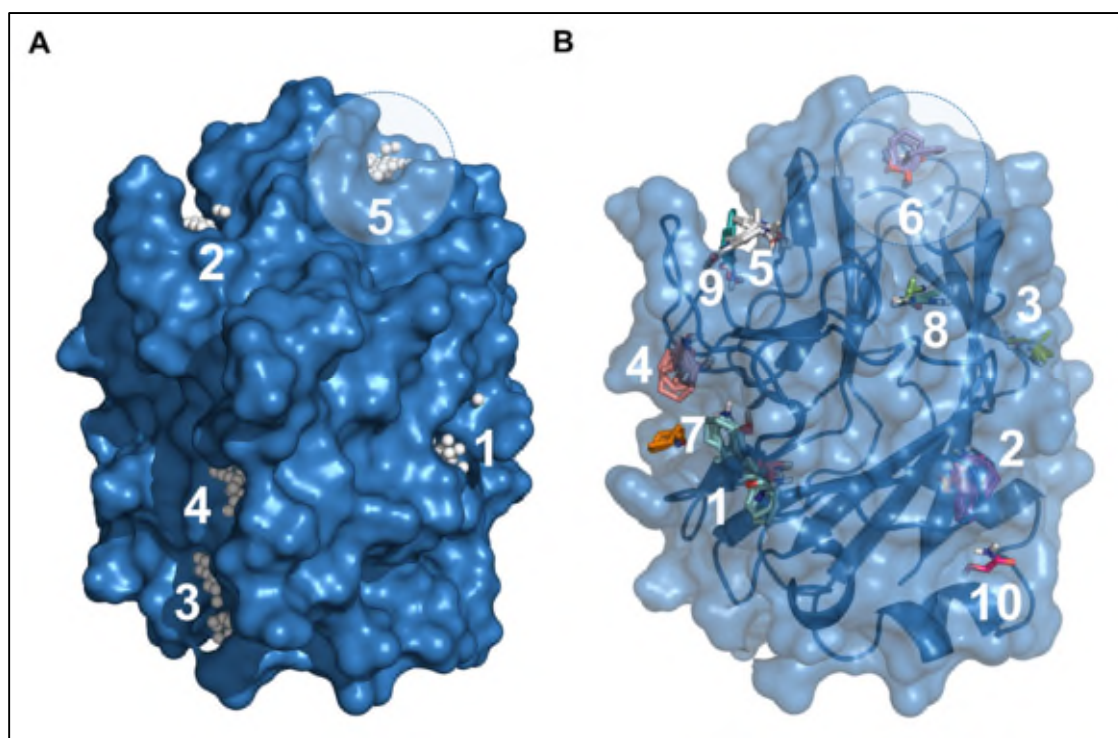


Figure 3.9. Crystal structure of SPSB2 (PDB ID: 3EMW) (blue) with possible binding sites as predicted by (A) SiteMap (white spheres) and (B) FTMap (sticks). The drugability of each site was ranked in sequence with 1 as the most druggable site and 5 (or 10 in B) as the least druggable site. In both A and B, the iNOS binding site was shown in a circle.

3.4 Discussion

Both ligand-based NMR (STD and CPMG) and SPR experiments suggest that STK441224 is the best hit of all 13 *in silico* top scoring compounds tested, with an estimated K_D of approximately 1.8 mM by SPR. STD spectra revealed that both amide (6.87 ppm, 7.50 ppm) and thiophene (6.72 ppm, 7.00 ppm) moieties of STK441224 were in close contact with SPSB2, as evidenced by positive intensities in the difference spectrum. In addition, CPMG experiments on STK441224 also revealed a significant decrease in the signal intensity of the thiophene peaks after 600 ms of spin-lock time in the presence of SPSB2. Further competition studies with the linear peptides Ac-DINNN-NH₂ and Ac-KEEKDINNNVKKK-NH₂ peptides by CPMG NMR revealed that the peak intensities of the thiophene moiety returned to the unbound state in the presence of these peptides suggesting that the compound is bound to the iNOS binding site of SPSB2.

However, no significant chemical shift perturbation to the peak corresponding to the 5-F-Trp207, one of the key residue in the vicinity of the iNOS binding site was observed when the compound was tested against the target-based ¹⁹F NMR experiments. Instead, a minor shift was observed in the most downfield 5-F-Trp peak suggesting that the compound was also bound to site(s) other than the iNOS binding site on SPSB2. Similar 5-F-Trp peak shifts were also observed for other STD-positive compounds with a carboxylic acid moiety such as STK802097 and STK068548, suggesting that small compounds with carboxylic acid moieties have a tendency to bind non-specifically to SPSB2. To further investigate this possibility, STK441224 was subjected to [¹H, ¹⁵N]-HSQC NMR experiments. Clearly, most of the backbone amide proton peaks of ¹⁵N-labelled SPSB2 perturbed in the presence of 1 and 3 mM STK441224 were from solvent-exposed positively charged residues of SPSB2, suggesting that the carboxylic group of the compound has a tendency to form salt bridges or hydrogen bonds with the side chains of positively charged residues, supporting the notion that the carboxylic acid of STK441224 contributed to its promiscuity in binding to SPSB2. Our data thus suggest that the binding of STK441224 to the iNOS binding site of SPSB2 would have been much weaker than the SPR estimated K_D of 1.8 mM, thus accounting for the lack of shift of the 5-F-Trp207 resonance by ¹⁹F NMR.

Despite the fact that STK441224 may have bound weakly to the iNOS binding site and is a promiscuous binder, it is still the most promising hit of all the analogues tested. Although it is not uncommon for a fragment hit with millimolar affinity in an FBDD campaign to be highly non-specific at this stage as it is usually small in size, the limited success of the current *in silico* guided approach, as well as the limited number of hits identified in a separate fragment screen carried out in parallel by other colleagues in the group, has prompted us to re-evaluate the suitability of the iNOS binding site on SPSB2 as a suitable site for binding small molecules, as opposed to peptidic ligands. Therefore, the druggability of the SPSB2-iNOS binding interface was assessed using two different computational prediction methods i.e. SiteMap²¹⁹ and FTMap.²²⁰ None of the estimated druggability score (Dscore) and SiteScore (SScore) as calculated by SiteMap for the top five most druggable sites on SPSB2 are higher than the average values observed for a set of 63 targets by Halgren²²¹ for either difficult (Dscore = 0.871, SScore = 0.995) or druggable (Dscore = 1.108, SScore = 1.091) sites. The estimated Dscore and SScore values of the five sites, which ranged from 0.51- 0.56 and 0.54-0.64, respectively, were lower than the average values for an undruggable site (Dscore = 0.631, SiteScore = 0.827), suggesting that the SPSB2 protein is highly undruggable. Although FTMap revealed that there are two main hot spots or druggable sites on SPSB2 that bound to 18 and 17 probe clusters, respectively, neither of these sites is in the SPSB2-iNOS binding interface. The iNOS binding site was only found to bind to eight probe clusters, which is just half of the expected minimum number of clusters required for a druggable target.²²² Clearly, both SiteMap and FTMap suggest that the iNOS binding site of SPSB2 (which is highly hydrophilic, shallow and small in size), is not a druggable site and therefore may not be suitable for a drug-like compound. In addition, the distance between the iNOS binding site and the nearest possible neighbouring binding site is larger than the size of a drug-like compound, eliminating the possibilities of improving the affinity of the compound *via* linking the binder of both sites. Hence, further elaboration of the fragment hit STK441224 was not attempted in the present study.

3.5 Conclusions

We attempted to discover a potential fragment inhibitor of SPSB2-iNOS interaction using *in silico*, NMR and SPR approaches. 13 compounds with ligand efficiency above 0.30 were shortlisted from the initial virtual screening of 961,514 compounds from a

commercial fragment library. STD and CPMG NMR experiments showed that two of the 13 compounds, i.e. STK441224 and STK847123, were able to bind to the SPSB2 protein as predicted *in silico*. However, only STK441224 was able to compete with the linear peptides Ac-DINNN-NH₂ and Ac-KEEKDINNNVKKKT-NH₂ peptides. As estimated by SPR experiments, compound STK441224 stood out as a more promising hit, with the K_D of approximately 1.8 mM. Nevertheless, ¹⁹F NMR and [¹H, ¹⁵N]-HSQC experiments revealed that STK441224 bound promiscuously to SPSB2 protein, presumably due to its carboxylic acid moiety. Further investigation into the druggability profile of SPSB2 by SiteMap and FTMap revealed that SPSB2-iNOS binding interface is not druggable, suggesting that targeting SPSB2-iNOS interaction with drug-like small molecule inhibitors is probably not the most suitable approach and therefore other ways to develop a more potent and specific novel class of inhibitor of SPSB2-iNOS interaction should be pursued. Subsequent chapters describe these alternative approaches.

CHAPTER 4

Disulphide-bridged cyclic peptide inhibitor of SPSB2-iNOS interaction

4.1 Declaration for Thesis Chapter 4

Declaration by candidate

In the case of **Chapter 4**, the nature and extent of my contribution to the work was the following:

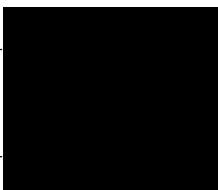
Nature of contribution	Extent of contribution (%)
Designed and performed the experiments, analysed the data and wrote the manuscript.	70

The following co-authors contributed to the work. If co-authors are students at Monash University, the extent of their contribution in percentage terms must be stated:

Name	Nature of contribution	Extent of contribution (%) for student co-authors only
Eleanor W.W. Leung	ITC, ¹⁹ F NMR, proteolysis assays	
Hiromasu Yagi	NMR	
Charles A. Galea	Plasma stability assay	
Sandeep Chhabra	NMR	
David K. Chalmers	Intellectual input	
Sandra E. Nicholson	BMDM cell lysate inhibition assay	
Philip E. Thompson	Intellectual input	
Raymond S. Norton	Intellectual input, manuscript preparation	

The undersigned hereby certify that the above declaration correctly reflects the nature and extent of the candidate's and co-authors' contributions to this work.

**Candidate's
Signature**

		Date 22/02/2016
--	---	---------------------------

**Main
Supervisor's
Signature**

		Date 22/02/2016
--	---	---------------------------

4.2 Introduction

Chapter 3 revealed limited success in the attempts to discover small molecule inhibitors of SPSB2-iNOS interaction using an *in silico* and NMR-guided FBDD approach, in which only two potential fragment hits were identified, one a promiscuous binder and the other a very weak binder with measured K_D of 1.8 and 4.1 mM, respectively. Further investigation with SiteMap and FTMap revealed that the iNOS binding site of SPSB2 is less druggable, suggesting that the iNOS binding site may not be suitable to be targeted with drug-like small molecule inhibitors.

In this Chapter, the design of cyclic peptide inhibitor of SPSB2-iNOS interaction, mimicking the crystal structure of the SPSB2-bound linear peptide DINNN is described (PDB ID: 3EMW),⁵⁵ based on the fact that the linear peptide readily adopts a Type-I β -turn conformation upon binding to SPSB2 and the distance between the *N*- and *C*-terminus of the linear peptide is less than 4 Å, suggesting the possibility of joining both ends together to form a cyclic peptide. Moreover, as described in **Chapter 1**, cyclisation was able to improve the potency and proteolytic stability of linear peptides.

Hence, in this Chapter, *in silico* models of cyclic peptide analogues, incorporating a different number of amino acid linkers between the *N*- and *C*-terminus of the linear peptide DINNN, were designed, followed by cyclisation *via* either a lactam bridge or a disulphide bridge between two additionally introduced Cys residues. The best *in silico* designed and energy minimised model, with lowest backbone RMSD to the crystal structure of DINNN and no violation of dihedral angles by Ramachandran plot, was synthesised and characterised by LC-MS and NMR experiments, and the NMR solution structure of the synthesised cyclic peptide was determined. Its ability to bind to the iNOS binding site of SPSB2 was investigated by ¹⁹F NMR and [¹H, ¹⁵N]-HSQC experiments and the binding affinity of the interaction was measured by SPR and ITC. Its ability to displace full-length iNOS from SPSB2 in macrophage cell lysates and its stability in three main digestive enzymes, pepsin, trypsin and α -chymotrypsin, human plasma, as well as in redox environment, were explored. As the results of this Chapter have been published in *Journal of Medicinal Chemistry*, they are presented in the format of a published article in the immediate section below.

A Potent Cyclic Peptide Targeting SPSB2 Protein as a Potential Anti-infective Agent

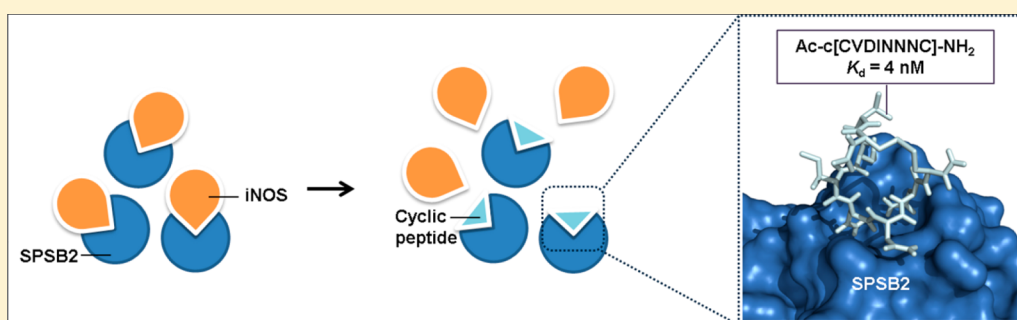
Beow Keat Yap,[†] Eleanor W. W. Leung,[†] Hiromasa Yagi,[†] Charles A. Galea,[†] Sandeep Chhabra,[†] David K. Chalmers,[†] Sandra E. Nicholson,^{‡,§} Philip E. Thompson,[†] and Raymond S. Norton^{*,†}

[†]Medicinal Chemistry, Monash Institute of Pharmaceutical Sciences, Monash University, Parkville 3052, Victoria, Australia

[‡]The Walter and Eliza Hall Institute of Medical Research, Parkville 3052, Victoria, Australia

[§]The Department of Medical Biology, University of Melbourne, Parkville, Victoria 3052, Australia

S Supporting Information



ABSTRACT: The protein SPSB2 mediates proteasomal degradation of inducible nitric oxide synthase (iNOS). Inhibitors of SPSB2–iNOS interaction may prolong the lifetime of iNOS and thereby enhance the killing of persistent pathogens. We have designed a cyclic peptide, Ac-c[CVDINNNC]-NH₂, containing the key sequence motif mediating the SPSB2–iNOS interaction, which binds to the iNOS binding site on SPSB2 with a K_d of 4.4 nM, as shown by SPR, [¹H,¹⁵N]-HSQC, and ¹⁹F NMR. An in vitro assay on macrophage cell lysates showed complete inhibition of SPSB2–iNOS interactions by the cyclic peptide. Furthermore, its solution structure closely matched (backbone rmsd 1.21 Å) that of the SPSB2-bound linear DINNN peptide. The designed peptide was resistant to degradation by the proteases pepsin, trypsin, and chymotrypsin and stable in human plasma. This cyclic peptide exemplifies potentially a new class of anti-infective agents that acts on the host innate response, thereby avoiding the development of pathogen resistance.

INTRODUCTION

Nitric oxide (NO), which is produced biosynthetically from L-arginine by inducible nitric oxide synthase (iNOS) in cells such as macrophages and dendritic cells, plays an important role in combating infections.¹ Several studies have reported that the expression of iNOS was significantly enhanced in animal models during infections such as salmonellosis,² tuberculosis,³ and leishmaniasis.⁴ In addition, iNOS knockout mice were found to succumb to infection by intracellular pathogens within 3–4 weeks.⁵ These observations indicate that iNOS and NO play an important role in host immunity.

Recently, Kuang et al.⁶ identified SPRY domain-containing SOCS (suppressor of cytokine signaling) box protein 2 (SPSB2) as a novel negative regulator that recruits an E3 ubiquitin ligase complex to polyubiquitinate iNOS, resulting in its proteasomal degradation. SPSB2-deficient macrophages showed prolonged iNOS expression, resulting in a corresponding increase in NO production and enhanced killing of *Leishmania major* parasites. It was also shown that a linear peptide from the disordered N-terminal region of iNOS, KEEKDINNNVKKKT, bound to SPSB2 with a K_d of 13 nM,

and that the most important residues mediating this interaction were DINNN, in particular the first, third, and fifth residues of this sequence motif. Structural studies by X-ray crystallography revealed that the SPRY domain of SPSB2 binds to Asp184, Asn186, and Asn188 of the DINNN sequence of the VASA peptide, the same motif as that in the N-terminal region of iNOS (where the corresponding residues are Asp23, Asn25, and Asn27).⁷ In SPSB2, Tyr120 of the SPRY domain was found to be critical for binding to the iNOS peptide,⁶ with Arg100, Gly101, Thr102, His103, Leu123, Leu124, Leu125, Ser126, Asn127, Ser128, Val206, and Trp207 also contributing to binding.⁶

In addition to SPSB2, SPSB1 and SPSB4 were also found to be important in the negative regulation of iNOS expression in macrophages.⁸ Both SPSB1 and SPSB4 bound to the same DINNN sequence in iNOS as SPSB2, suggesting that inhibitors that mimic the iNOS peptide and target the SPRY domain of the SPSB proteins would be advantageous in disrupting the

Received: April 17, 2014

Published: July 28, 2014

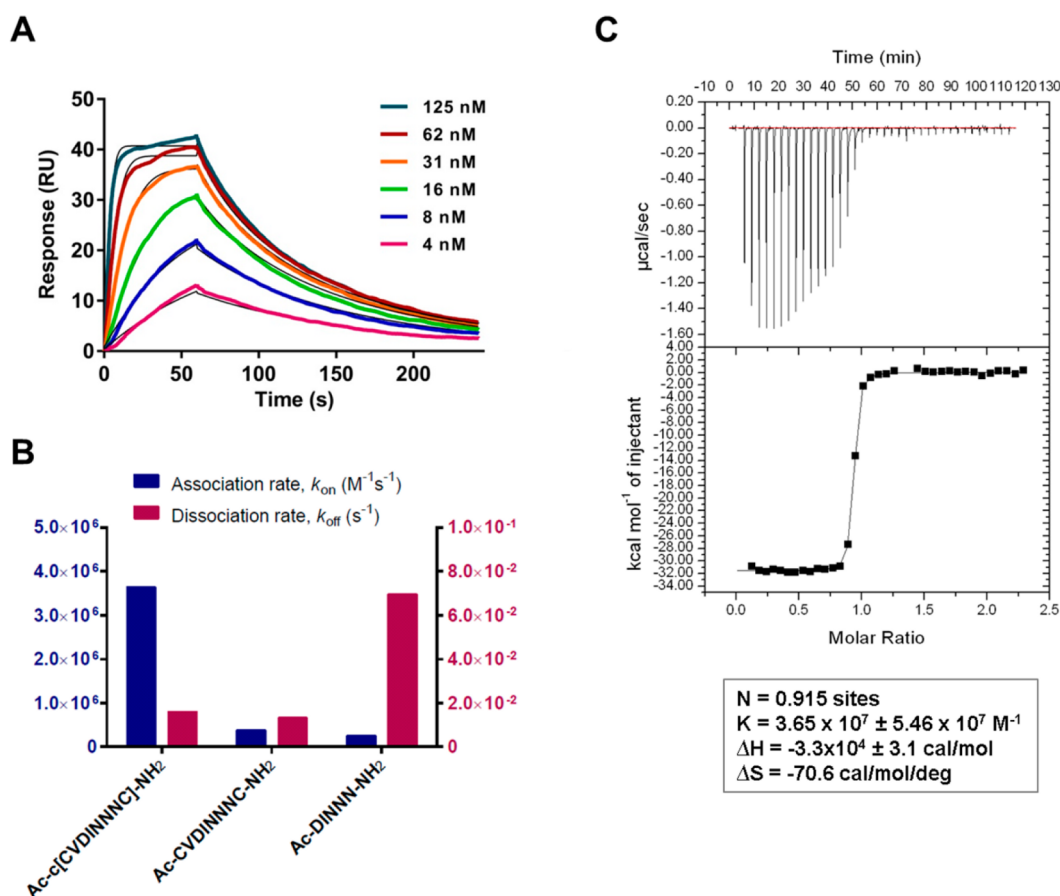


Figure 1. Ac-c[CVDINNNC]-NH₂ interacts with SPSB2. (A) SPR sensorgram of immobilized SPSB2 exposed to increasing concentrations of cyclic peptide Ac-c[CVDINNNC]-NH₂ in 10 mM HEPES, 150 mM NaCl, 3 mM EDTA, and 0.05% Tween 20, pH 7.4, at 25 °C. (B) k_{on} and k_{off} of the cyclic peptide Ac-c[CVDINNNC]-NH₂, its reduced counterpart, and the linear peptide Ac-DINNN-NH₂ estimated from the reference subtracted sensorgrams fitted to a steady state 1:1 interaction model. (C) ITC raw thermogram data (upper panel) and binding isotherm (lower panel) for the cyclic peptide in complex with SPSB2 protein in 50 mM HEPES, 50 mM NaCl, pH 7.4, at 25 °C. The data were fitted using a single-site binding model.

iNOS interaction with all of these SPSB proteins, thus prolonging iNOS expression in cells where iNOS is being produced in response to infection. As SPSB proteins were found to bind only to iNOS, but not endothelial NOS (eNOS) and neuronal NOS (nNOS),⁹ this strategy would limit any potential toxicity associated with excessive systemic NO.

Linear peptides with free carboxyl and amino terminals are likely to be unstable in vivo as they are susceptible to degradation by both endo- and exopeptidases. Moreover, they are generally unstructured and flexible in solution, rendering them entropically unfavorable for receptor binding and biological activity. Consistent with this, cyclic peptides have been found to be more resistant to enzymatic degradation and proteolytic digestion by proteases than their linear counterparts, with improved potency as well as high selectivity and binding affinity.¹⁰ In this study, we describe the design and synthesis of a cyclic peptide mimicking the SPSB2-bound conformation of the linear sequence DINNN. Structural analysis by NMR indicated that the solution structure of the designed peptide closely matched the bound state, and binding studies with SPR and ITC showed that it bound with high affinity to SPSB2. An inhibition assay with macrophage lysate confirmed that the cyclic peptide is a potent inhibitor of the SPSB2–iNOS interaction. The peptide was also found to be

highly stable against a range of proteolytic enzymes (pepsin, trypsin, and α -chymotrypsin) as well as in human plasma.

RESULTS AND DISCUSSION

Design of Cyclic Peptide Ac-c[CVDINNNC]-NH₂. Cyclic peptides were designed based on the SPSB2-bound conformation of DINNN,⁷ which is a Type I β -turn conformation with the distance between C ^{α} (i) and C ^{α} ($i + 3$) being <7 Å, the backbone NH($i + 3$) of Asn187 and CO(i) of Asp184 of the VASA peptide (PDB code 3EMW)⁷ forming an intramolecular hydrogen bond, and the $\phi(i + 1)$, $\psi(i + 1)$, $\phi(i + 2)$ and $\psi(i + 2)$ dihedral angles being -60° , -28° , -109° , and $+24^\circ$, respectively (Supporting Information, Figure S1A).¹¹ In addition, the distance between the amide nitrogen of the N-terminal and carbonyl carbon of the C-terminal of DINNN is <4 Å, suggesting the plausibility of joining the two ends together. The designed models were further optimized by insertion of several different linker residues and compared to the structure of the linear peptide bound to SPSB2 (Supporting Information, Table S1). Among the cyclic peptide models, a one-residue insertion between the N-terminal Cys and DINNN peptide sequence (i.e., CXDINNNC, X = different type of amino acid residues) gave the lowest backbone rmsd between the model peptides and the crystal structure of linear DINNN bound to SPSB2 (0.12–0.15 Å). When these models were

rigidly docked to SPSB2 with Glide SP (version 5.8, Schrödinger), it was found that all inserted X residues (depicted as "X2" in Supporting Information, Figure S1B) extended out of the binding pocket, suggesting that the nature of residue X would not influence binding of the cyclic peptide to SPSB2. As DINNN is highly polar and charged, a hydrophobic residue was included at this position in order to improve its overall hydrophobicity and drug-likeness. Thus, the cyclic peptide Ac-c[CVDINNNC]-NH₂ was synthesized. The LC-MS profiles of the synthesized and purified cyclic peptide are illustrated in Supporting Information, Figure S2. The purity of this peptide was ~95%, with only a single set of peaks observed by 1D ¹H NMR (Supporting Information, Figure S3), suggesting its suitability for structural and binding studies. The deconvoluted mass (*M_r* 932.90 Da) was also consistent with the theoretical mass (*M_r* 933.03 Da).

Interaction of Ac-c[CVDINNNC]-NH₂ with SPSB2. The cyclic peptide Ac-c[CVDINNNC]-NH₂ was found to bind tightly to immobilized SPSB2 by SPR analysis, with a *K_d* of 4.4 nM (Figure 1A). In contrast, the Ac-DINNN-NH₂ linear peptide containing the conserved binding motif of iNOS, bound more weakly to SPSB2, with a *K_d* of 318 nM (Table 1).

Table 1. Kinetics and Thermodynamics of the Interactions with SPSB2 of Ac-c[CVDINNNC]-NH₂, Ac-CVDINNNC-NH₂, and Ac-DINNN-NH₂^a

	cyclic peptide		linear peptides	
	Ac-c[CVDINNNC]-NH ₂	Ac-DINNN-NH ₂	Ac-DINNN-NH ₂	Ac-CVDINNNC-NH ₂
SPR				
<i>k_{on}</i> (× 10 ⁵ M ⁻¹ s ⁻¹)	36.3	2.2		3.7
<i>k_{off}</i> (× 10 ⁻² s ⁻¹)	1.6	7.0		1.3
<i>K_d</i> (nM)	4.4	318		35.1
ITC				
Δ <i>H</i> (kcal/mol)	-33.0	-13.8		ND
<i>T</i> Δ <i>S</i> (kcal/mol)	-21.1	-4.7		ND
Δ <i>G</i> (kcal/mol)	-11.9	-9.1		ND

^aND: Not determined.

The *K_d* of the reduced form of the cyclic peptide, i.e., linear Ac-CVDINNNC-NH₂, was 35 nM (Supporting Information, Figure S4). As depicted in Figure 1B, linear Ac-CVDINNNC-NH₂ bound to SPSB2 with *k_{on}* similar to Ac-DINNN-NH₂ when both sensorgrams were fitted to a 1:1 binding model (Supporting Information, Figure S4). In contrast, an approximately 5-fold lower *k_{off}* was observed in linear Ac-CVDINNNC-NH₂. Thus, linear Ac-CVDINNNC-NH₂ binds more tightly to SPSB2 than Ac-DINNN-NH₂, presumably because of additional interaction(s) of the three extra residues with SPSB2.

Comparison of the *k_{on}* and *k_{off}* values of the cyclic peptide and its reduced counterpart revealed that the cyclic peptide bound approximately 10-fold more rapidly to SPSB2 than its reduced form. This suggests that cyclization plays a key role in enhancing the association rate and ultimately improving the binding affinity of the linear peptide, presumably through preorganization of the cyclic peptide into the bound state. Consistent with this interpretation, both linear peptides Ac-DINNN-NH₂ and Ac-CVDINNNC-NH₂ bound to SPSB2 with slower *k_{on}* (2–4 × 10⁵ M⁻¹ s⁻¹) than the cyclic peptide (Table 1).

The thermodynamics of the interaction were also probed using isothermal titration calorimetry (ITC). In agreement with the SPR observations, the cyclic peptide bound with a 1:1 binding stoichiometry (Table 1, Figure 1C). The binding of both cyclic Ac-c[CVDINNNC]-NH₂ and linear Ac-DINNN-NH₂ to SPSB2 were mainly enthalpy-driven, with the enthalpy change, Δ*H*, approximately 9 kcal/mol more negative for the cyclic peptide, presumably because it participates in more hydrogen bonds and van der Waals interactions with SPSB2 than the linear peptide, consistent with the lower dissociation rate observed in SPR. Intriguingly, the ITC results also indicated that the cyclic peptide was entropically less favorable for binding than the linear peptide, with approximately 16 kcal/mol higher entropy penalty for the cyclic peptide binding to SPSB2.

Binding Site of Ac-c[CVDINNNC]-NH₂. Two complementary NMR studies were carried out to confirm that the cyclic peptide bound to the desired site on SPSB2. Leung et al. demonstrated that ¹⁹F NMR can rapidly identify ligands that target the iNOS binding site on 5-F-Trp-SPSB2.¹² SPSB2 has six Trp residues, two of which are solvent-exposed (Figure 2B); Trp207, which is one of the solvent-exposed Trp, has been identified as one of the key residues mediating the SPSB2–iNOS interactions by both NMR and X-ray crystallography studies.^{6,13} Indeed, the ¹⁹F NMR signal of Trp207 was shifted significantly downfield upon binding to the 13-residue linear peptide, Ac-KEEKDINNNVKKKT-NH₂.¹² Figure 2A shows that the Trp207 signal of 5-F-Trp-labeled SPSB2 shifted downfield from -49.6 to -47.2 ppm upon addition of cyclic peptide, confirming that the cyclic peptide bound to the iNOS binding site. The extent of the chemical shift change is ~0.5 ppm less than that reported for the 13-residue linear peptide,¹² suggesting that the cyclic peptide bound slightly differently to the iNOS binding site of SPSB2. The peak of the other solvent-exposed Trp (Trp131) was not significantly shifted, confirming that the cyclic peptide did not bind to site(s) in the vicinity of this residue. Although there was a minor shift in the peak immediately upfield of Trp131, this is likely due to secondary effects.¹²

To further verify the binding site of the cyclic peptide on SPSB2 by NMR, we recorded [¹H,¹⁵N]-HSQC spectra¹⁴ of ¹⁵N-labeled SPSB2 in the absence and presence of linear Ac-DINNN-NH₂ and cyclic Ac-c[CVDINNNC]-NH₂ peptides. In agreement with SPR and ITC, titration of the cyclic peptide Ac-c[CVDINNNC]-NH₂ to SPSB2 generated a set of chemical shift perturbations that were in slow exchange on the NMR time scale relative to the chemical shifts of the peptide-free form. A similar set of SPSB2 resonances was perturbed when linear Ac-DINNN-NH₂ was added, confirming that the cyclic peptide binds to the iNOS binding site (Figure 2C). Several minor differences were observed between the cyclic and the linear peptides; in the presence of the cyclic peptide, new resonances κ1–κ6 were observed, while in the presence of the linear peptide, a different set of resonances, λ1–λ5, appeared. This indicates that the backbone amides corresponding to these resonances interact slightly differently with the cyclic and linear peptides. Resonances κ1, κ4, and κ6 but not κ2, κ3, and κ5 were also observed in the [¹H,¹⁵N]-HSQC spectrum of SPSB2 in the presence of Ac-KEEKDINNNVKKKT-NH₂,⁶ suggesting that the cyclic peptide bound in a similar but not identical manner to the 13-residue iNOS peptide. This observation is consistent with the results from ¹⁹F NMR experiments.

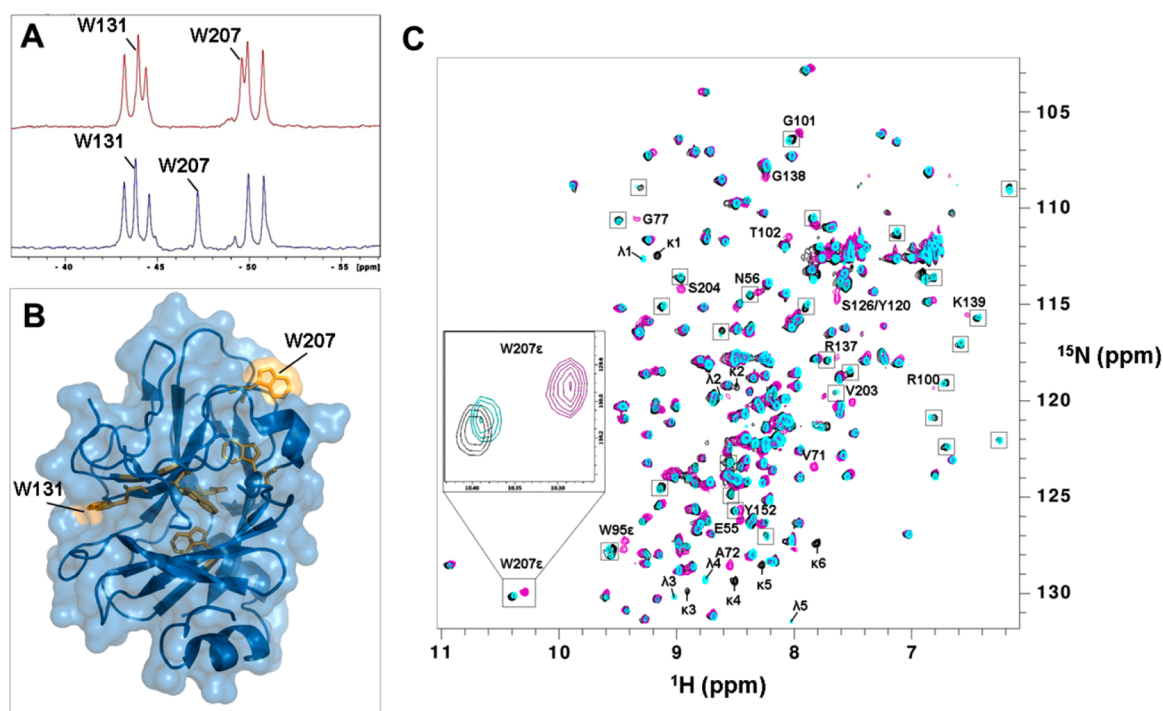


Figure 2. Ac-c[CVDINNNC]-NH₂ binds to the iNOS binding site on SPSB2. (A) ¹⁹F NMR spectra of 5-F-Trp SPSB2 in the absence (upper panel) and presence (lower panel) of cyclic peptide Ac-c[CVDINNNC]-NH₂ in 50 mM sodium phosphate buffer, pH 7.4, and 50 mM NaCl at 25 °C. The resonances of solvent-exposed Trp residues, W131 and W207, are labeled. (B) Distribution of Trp amino acid residues (stick in yellow) in the crystal structure of murine SPSB2 (PDB code 3EK9). Trp residues are shown in yellow sticks and the solvent-exposed Trp residues, W131 and W207, are labeled. (C) [¹H,¹⁵N]-HSQC spectra of ¹⁵N-labeled SPSB2 in the absence (purple) and presence of the cyclic peptide Ac-c[CVDINNNC]-NH₂ (black) and the linear peptide Ac-DINNN-NH₂ (cyan). The perturbed backbone amide and indole Trp207 resonances (inset) in the presence of peptides are labeled. Among the perturbed resonances, the resonances perturbed in the same manner by both the cyclic and the linear peptides are boxed. Resonances perturbed differently between the cyclic and the linear peptide are labeled as κ1–κ6 and λ1–λ5, respectively.

Structure of Cyclic Peptide Ac-c[CVDINNNC]-NH₂. To characterize the role of cyclization in improving the association rate of the linear peptide to SPSB2, the solution structure of the cyclic peptide was solved using NMR spectroscopy. Seventy-five distance restraints, which include 41 intraresidue, 23 sequential, and 11 medium-to-long-range NOEs, were generated (Table 2) from a 2D NOESY experiment (400 ms

Table 2. NMR Structural Statistics for the Final 20 Structures of Cyclic Peptide Ac-c[CVDINNNC]-NH₂ in Aqueous Solution

NMR Distance and Dihedral Constraints	
distance constraints	
total NOEs	75
intraresidue	41
inter-residue	
sequential ($ i - j = 1$)	23
medium ($1 < i - j \leq 5$)	9
long ($ i - j > 5$)	2
hydrogen bond	1
total dihedral angle restraints	
Φ	4
Ψ	1
χ ₁	1
Structure Statistics	
average pairwise rmsd (Å)	
all heavy atoms	0.86 ± 0.15
backbone heavy atoms (N, C ^α , C')	0.42 ± 0.13

mixing time). These restraints, together with six dihedral angle restraints, a disulfide bond constraint between the N- and C-terminal cysteine residues, and a hydrogen bond restraint between the backbone amide of Asn5 (NH) and Asp3 (CO) (Supporting Information, Figure S5), were used to determine the solution structure of the cyclic peptide. A final ensemble of 20 structures with a pairwise backbone rmsd of 0.42 ± 0.13 Å was generated (Figure 3A). The structure has a hydrogen bond between the NH(*i* + 2) of Asn5 and CO(*i*) of Asp3, with mean φ and ψ dihedral angles for Ile4 of -76° and 69° , respectively, suggesting that the cyclic peptide adopts a γ -turn-like conformation in solution.¹¹ The backbone rmsd of the DINNN sequence of the closest-to-average structure of the cyclic peptide to the crystal structure of the linear peptide bound to SPSB2 is 1.21 Å (Figure 3B), thus validating our structure-based design process. The backbone DINNN motif of the solution structure aligned well with the in silico modeled structure of Ac-c[CVDINNNC]-NH₂ (Supporting Information, Figure S6A), suggesting that the DINNN conformation changed little upon binding to SPSB2, and supporting our hypothesis that cyclization contributes to preorganization of the cyclic peptide into the bound state. Intriguingly, the linker residues Cys1, Val2, and Cys8 of the solution structure were significantly different from the in silico modeled SPSB2-bound conformation, suggesting that these residues adopted a different conformation upon binding to SPSB2. When the in silico model of the SPSB2-bound cyclic peptide was rigidly docked into SPSB2 with Glide SP (version 5.8, Schrödinger), a hydrogen bond interaction between the NH of Cys8 and the CO of Pro70 of SPSB2 was observed (Supporting Information,

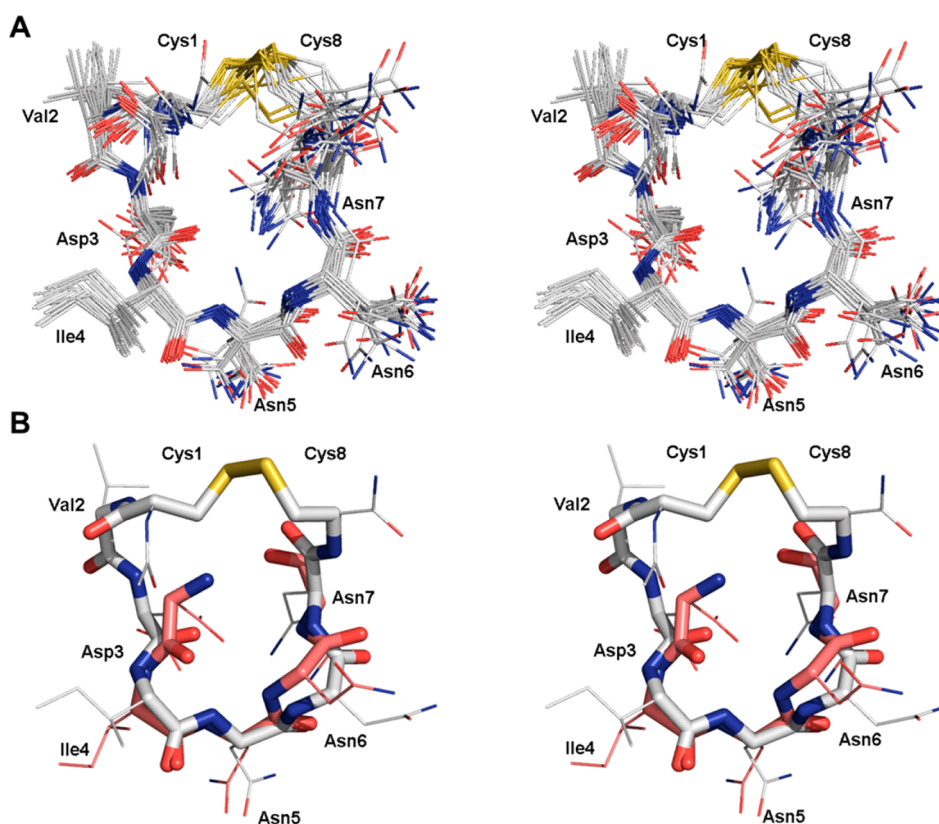


Figure 3. Stereo views of solution structure of the cyclic peptide Ac-c[CVDINNNC]-NH₂ determined by NMR spectroscopy. (A) Final ensemble of 20 structures satisfying the NMR restraints with pairwise rmsd for backbone heavy atoms (N, C^α, C^β) of the ensemble of 0.42 ± 0.13 Å. (B) Superposition of the representative structure of the peptide (with lowest CYANA target function value) on the crystal structure of the DINNN peptide bound to SPSB2 (backbone rmsd of 1.21 Å).

Figure S6B), as well as an interaction between the backbone CO of Cys8 and the side chain of Ala72 of SPSB2, suggesting that Cys8 contributed to binding of the cyclic peptide to SPSB2.

Displacement of Full-Length iNOS by Cyclic Peptide.

To investigate whether the cyclic peptide was able to displace the binding of full-length iNOS from SPSB2 protein in a more physiological setting, a GST-based pull-down assay was performed using lipopolysaccharide (LPS) and interferon- γ -stimulated macrophages as a source of full-length iNOS. Bone marrow-derived macrophages (BMDM) were generated from wild-type mice and incubated overnight with LPS and IFN- γ prior to cell lysis. Western blotting with anti-iNOS antibodies revealed that the interaction of SPSB2 with full-length iNOS was completely inhibited in cell lysates in the presence of the cyclic peptide (Figure 4, upper panel). Reprobe with anti-GST antibodies confirmed that equivalent amounts of the GST proteins were present (Figure 4, lower panel).

Peptide Stability. The susceptibility of the cyclic peptide to proteolysis by three important digestive enzymes, pepsin, trypsin, and α -chymotrypsin, and its stability in human plasma were investigated. The cyclic peptide Ac-c[CVDINNNC]-NH₂ did not show any degradation upon incubation with pepsin, trypsin, and α -chymotrypsin at 37 °C for 24–96 h (Figure 5A–C), presumably because of the lack of sequence-specific cleavage sites for these enzymes. In contrast, the linear peptide Ac-KEEKDINNNVKKKT-NH₂ was digested by pepsin after 2 h incubation at 37 °C (data not shown). Figure 5D shows that

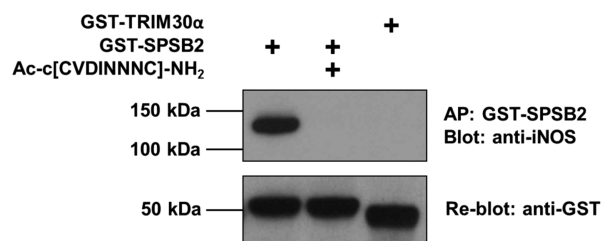


Figure 4. Ac-c[CVDINNNC]-NH₂ is able to displace full-length iNOS in cell lysates. Cell lysates from LPS/IFN- γ -stimulated BMDM were incubated with GST-TRIM30 α -B30.2 domain (as a negative control) or GST-SPSB2-SPRY domain in the presence (+) or absence of cyclic peptide Ac-c[CVDINNNC]-NH₂. GST-fusion proteins were recovered via affinity purification (AP) using glutathione–Sepharose and the interaction with iNOS analyzed by Western blotting with anti-iNOS antibody (upper panel). Equivalent protein loading was confirmed by stripping and reprobing the membrane with anti-GST antibody (lower panel).

the cyclic peptide is also stable in human plasma, with approximately 83% of peptide remaining after 24 h.

The stability of the cyclic peptide in the cytoplasm of macrophages is also relevant. While the cytoplasm of most cells is reducing, it is worth noting that disulfide bridges can form in the cytoplasm under oxidative stress,¹⁵ for example, during infection, due to the generation of excessive reactive oxygen species such as hydrogen peroxide by NADPH oxidase. In fact, the ratio of the most abundant redox couple in the cytoplasm, the glutathione disulfide–glutathione couple (GSH/GSSG)¹⁶ was found to decrease by approximately 3-fold upon exposure

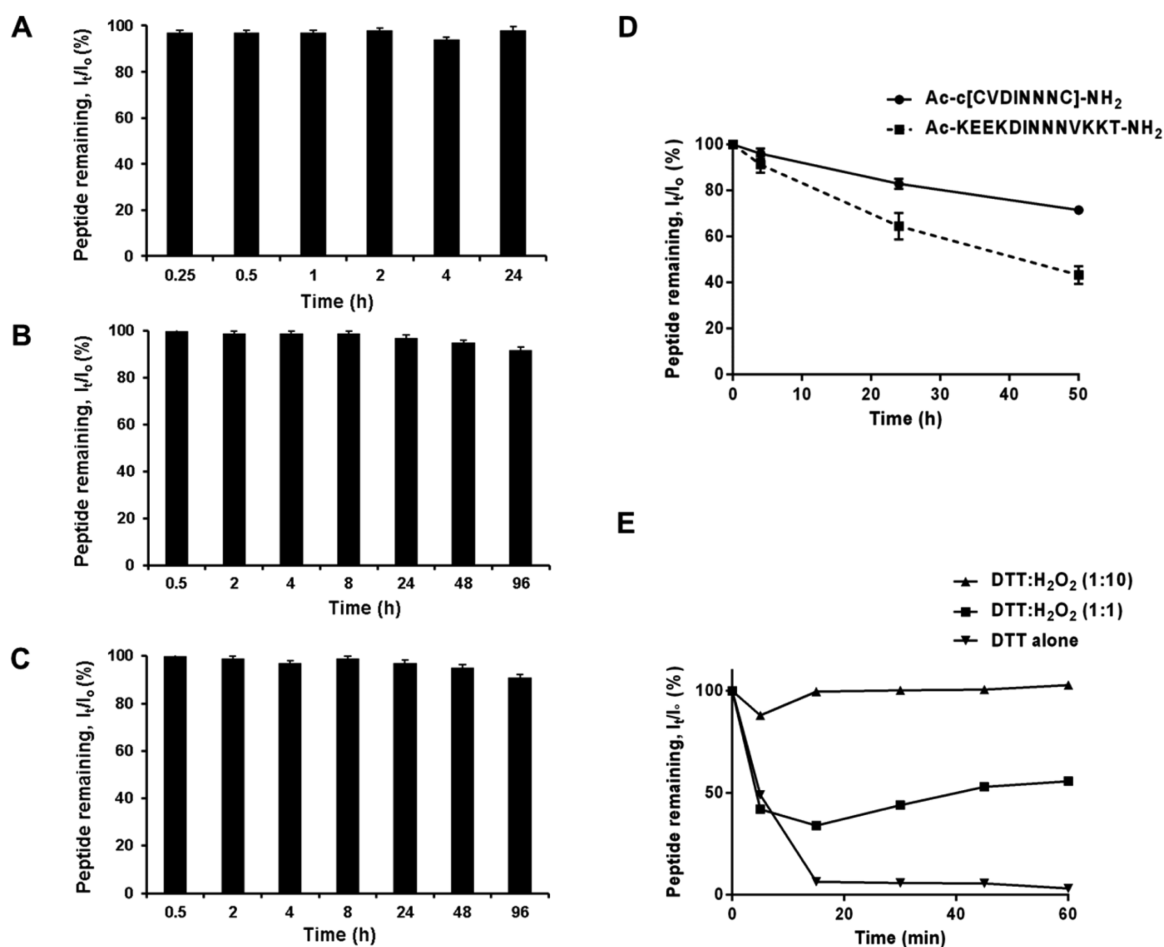


Figure 5. Ac-c[CVDINNNC]-NH₂ is resistant to the proteases pepsin, trypsin, and α -chymotrypsin and is stable in human plasma and in oxidative environment. Stability of Ac-c[CVDINNNC]-NH₂ after treatment with (A) pepsin, (B) trypsin, and (C) α -chymotrypsin at 37 °C for 24–96 h, as determined by LC-MS. I_0 and I_t represent peak area at times 0 and t , respectively. (D) The stability of cyclic peptide Ac-c[CVDINNNC]-NH₂ and linear peptide Ac-KEEKDINNNVKKK-NH₂ in human plasma at 37 °C for 50 h as determined by RP-HPLC, where I_0 and I_t represent peak height at times 0 and t , respectively. Data were collected from three separate experiments ($n = 3$) on human plasma samples for each peptide and are indicated as mean \pm standard error of the mean. The cyclic peptide is more stable than the 13-residue linear peptide Ac-KEEKDINNNVKKK-NH₂, with significant difference in stability between cyclic and linear peptides observed after 24 h. (E) Effect of different redox environment on the stability of cyclic peptide Ac-c[CVDINNNC]-NH₂ as determined by incubation of the cyclic peptide in 10 mM Tris, pH 7.4, at 37 °C, in the presence of 1 mM DTT as reducing agent, and different concentrations of H₂O₂ as pro-oxidant to simulate different redox environments: 1 mM DTT in the absence of H₂O₂ was used to simulate the physiological environment of the cytoplasm which is reducing, while 1–10 mM H₂O₂ (1:1–1:10 ratios of DTT: H₂O₂) was used to mimic the oxidative environment of the cytoplasm. The cyclic peptide is susceptible to reduction in reducing conditions but is likely to be stable in an oxidizing environment, a condition likely to be observed during infection-induced acute oxidative stress in macrophages.

to the oxidant hydrogen peroxide, which subsequently resulted in an increase in disulfide formation in proteins in the cytoplasm.¹⁷ To investigate the effect of different redox environments on the cyclic peptide, it was incubated in vitro in 10 mM Tris buffer, pH 7.4, at 37 °C in the presence of different ratios of reducing agent, 1 mM dithiothreitol (DTT), and oxidant, hydrogen peroxide (H₂O₂) (1:1 to 1:10) (Figure 5E). The 1–10 mM concentrations of H₂O₂ were used to simulate the oxidative environment in the cytoplasm because these levels of H₂O₂ have been reported during acute oxidative burst in phagocytes.¹⁸ As expected, in the absence of H₂O₂, the cyclic peptide was significantly reduced after 15 min of incubation. However, addition of 1 mM H₂O₂ to the sample (1:1 ratio of DTT: H₂O₂) significantly improved the stability of the cyclic peptide, with approximately 55% cyclic peptide remaining after 1 h incubation. When H₂O₂ was in excess to DTT (10 mM H₂O₂; 1:10 ratio of DTT: H₂O₂), no significant

changes to the amount of cyclic peptide were observed after 1 h. This suggests that the cyclic peptide is unlikely to be stable in the reducing environment of cytoplasm but may be stabilized during oxidative stress when the production of oxidants such as ROS species exceeds the reducing capacity of the glutathione (GSH/GSSG) and thioredoxin (Trx_{red}/Trx_{ox}) redox couple in the cytoplasm. Thus, it is possible that the cyclic peptide may remain oxidized throughout the infection phase and be able to function in stimulated macrophages, although further work is warranted to assess this.

CONCLUSION

We have designed and synthesized a cyclic peptide Ac-c[CVDINNNC]-NH₂ based on the DINNN peptide sequence motif. The cyclic peptide adopts a similar conformation in solution to that of the linear peptide bound to SPSB2, and ¹⁹F and [¹H,¹⁵N]-HSQC NMR confirmed that the cyclic peptide

bound to SPSB2 at the iNOS binding site. Compared with a linear peptide containing the key binding motif (DINNN), which has a K_d of 318 nM, the cyclic peptide has substantially higher affinity for the target protein, as well as enhanced resistance to degradation by proteases and in human plasma. Moreover, the cyclic peptide completely attenuated the interaction between full-length iNOS and SPSB2 in BMDM lysates. These data confirm that the cyclic peptide is a potent inhibitor of SPSB2–iNOS interactions and thus potentially a new class of anti-infective that would not be susceptible to the development of microbial resistance.

EXPERIMENTAL PROCEDURES

In Silico Design of Cyclic Peptide Mimicking SPSB2–DINNN Interactions. The 3D structure of the SPSB2-bound DINNN peptide was obtained from the crystal structure of the SPSB2–DINNN complex (PDB code 3EMW).⁷ Using the Biopolymer module of SYBYL-X (version 2.0, Tripos), the monomer(s) of DINNN were mutated, deleted, or built to yield different peptide sequences for cyclization. Peptides of different length and containing disulfide bridges were designed. Hydrogen atoms were added to all residues in the peptide.

The preliminary designed cyclic peptides were subjected to energy minimization to correct the modeled bond lengths and angles and to remove any steric clashes resulting from the modeling. The Ramachandran plot¹⁹ (Maestro version 9.3, Schrödinger) was inspected to ensure that the backbone ϕ and ψ angles were within the allowed regions. The optimized models were finally fitted to the backbone of the 3D structure of the DINNN peptide, and the rmsd between the models and the original DINNN peptide was calculated. One of the cyclic peptides with the lowest rmsd, Ac-c[CVDINNNC]-NH₂, was selected for synthesis.

Cyclic Peptide Ac-c[CVDINNNC]-NH₂ Synthesis and Purification. The linear peptide Ac-CVDINNNC-NH₂ was synthesized on-resin (solid-phase peptide synthesis) using an automated Peptide Synthesizer 3 (PS3) via Fmoc chemistry.²⁰ It was assembled via the coupling of 0.3 mmol (3 equiv) of Fmoc-protected amino acids to 0.1 mmol Rink Amide AM resin (0.47 mmol/g loading). Coupling reactions between the C-terminal residue and the resin, and between subsequent amino acid residues, were carried out for 50 min per coupling cycle under the activation of 0.3 mmol (3 equiv) *O*-(1*H*-6-chlorobenzotriazole-1-yl)-1,1,3,3-tetramethyluronium hexafluorophosphate (HCTU) and 0.6 mmol (6 equiv) DIPEA. Double coupling was carried out to couple the second Asn to the first Asn as well as the third Asn to the second Asn as single coupling resulted in deletion of one Asn from the peptide sequence.

The Fmoc protecting group was removed after each coupling cycle (except in double coupling where Fmoc was removed only after the second coupling) with 20% piperidine in DMF. *N*-Acetylation was carried out with 10 equiv acetic anhydride and 15 equiv DIPEA in DMF for 3 h. The linear peptide was cleaved from the resin with a solution containing 92.5% TFA and scavengers 2.5% TIPS, 2.5% dimethoxybenzene (DMB), and 2.5% 3,6-dioxo-1,8-octanedithiol (DODT). After cleavage, the peptides were precipitated with cold diethyl ether twice and dissolved in a 1:1 water:acetonitrile mixture prior to lyophilization. All reactions were carried out at room temperature. Cyclization was carried out in solution with 0.1 M ammonium bicarbonate, pH 8.0, for 24 h at a peptide concentration of 0.5 mM. The crude peptide was purified by reverse-phase high performance liquid chromatography (RP-HPLC) on a Phenomenex Luna C18 (2) column (100 Å, 5 μ m, 100 mm \times 10 mm) using a gradient of 20–50% B (A, 99.9% H₂O, 0.1% TFA; B, 80% ACN, 19.9% H₂O, 0.1% TFA) over 30–60 min. The purity and molecular mass of the synthesized and cyclized peptide were confirmed with liquid chromatography–mass spectroscopy (LC-MS) on a Shimadzu LCMS2020 instrument, incorporating a Phenomenex Luna C8 column (100 Å, 3 μ m, 100 \times 2 mm) using a linear gradient of 100% H₂O

(0.05% TFA) for 4 min, followed by 0–60% ACN (0.05% TFA) in water over 10 min at a flow rate of 0.2 mL/min.

SPSB2 Protein Expression and Purification. The glutathione S-transferase-tagged SPSB2 (GST-SPSB2) expression construct has been described previously.²¹ GST-SPSB2 was expressed in *Escherichia coli* strain BL21 (DE3); cells were grown in 10 mL of LB-ampicillin (LBA) medium at 37 °C until the OD₆₀₀ reached 0.6–0.8. Then 1 mL of this preculture was used to inoculate 1 L of LBA growth medium (or M9 minimal media containing ¹⁵NH₄Cl as the sole source of nitrogen for ¹⁵N-labeled SPSB2 protein) and allowed to grow at 37 °C. Protein expression was induced by adding 1 mM isopropyl β -D-1-thiogalactopyranoside (IPTG) at OD₆₀₀ = 0.6–0.8 and incubating at room temperature overnight. Cell pellets were resuspended on ice in a 20 mM Tris, 150 mM NaCl, pH 8.0 (TN) buffer containing Roche's cOmplete, Mini Protease Inhibitor Cocktail and Novagen's BugBuster Master Mix, for 30 min. Soluble proteins were isolated by centrifugation at 18000 rpm for 20 min at 4 °C. GST-SPSB2 proteins were purified using a glutathione–Sepharose gravity-flow chromatography column, followed by overnight thrombin cleavage with 1 mM of thrombin in 50 mM Tris, 2.5 mM CaCl₂, 2 mM β -mercaptoethanol, pH 7.5 (thrombin cleavage buffer) at 4 °C. SPSB2 and GST were separated by size-exclusion chromatography (Superdex 75 10/300 GL) using an ÄKTA FPLC. Purified SPSB2 fractions were pooled and evaluated by sodium dodecyl sulfate polyacrylamide gel electrophoresis (SDS-PAGE). The protein concentration was determined via protein absorbance at 280 nm with a NanoDrop spectrophotometer. 5-F-Trp labeled SPSB2 (5-F-Trp SPSB2) was prepared as described previously by Leung et al.¹²

Surface Plasmon Resonance. SPR experiments were performed at 25 °C on a Biacore T200. Immobilization was carried out via standard amine coupling method on a CM5 sensor chip with a flow rate of 10 μ L/min and a running buffer of 10 mM HEPES, 150 mM NaCl, 3 mM EDTA, and 0.05% Tween 20, pH 7.4. Both the target (SPSB2 protein) and reference (blank) flow cells were activated for 7 min using a mixture of 0.2 M 1-ethyl-3-(3-(dimethylamino)propyl)-carbodiimide (EDC) and 0.05 M *N*-hydroxysuccinimide (NHS). This was followed by an immediate injection of 150 μ L of 100 μ g/mL of SPSB2 protein, dissolved in 10 mM of sodium acetate, pH 5.5, in the target flow cell. Finally, 150 μ L of 1 M ethanolamine-HCl, pH 8.5, was injected into both target and reference flow cells to deactivate any remaining activated carboxyl groups on the surface.

The binding of both the linear peptide Ac-DINNN-NH₂ (GL Biochem Ltd.) and the cyclic peptide was investigated in a running buffer containing 10 mM HEPES, 150 mM NaCl, 3 mM EDTA, and 0.05% Tween 20, pH 7.4. Each peptide was injected onto the surface with contact time of 30–60 s, flow rate of 100 μ L/min, and dissociation time of 120–600 s. No further regeneration step was carried out as all peptides were able to dissociate completely after 600 s. The sensorgrams were further corrected for nonspecific binding to the surface by subtracting the signals of the reference surface from those of the target protein surface. The corrected signal was then fitted to a steady state 1:1 interaction model with Biacore T200 Evaluation Software (version 2.0), and the binding affinity, K_d , association rate, k_{on} , and dissociation rate, k_{off} were estimated.

Isothermal Titration Calorimetry. ITC experiments were performed at 25 °C on an ITC200 (MicroCal Inc.). Both peptides and SPSB2 protein were prepared in 50 mM HEPES, 50 mM NaCl, pH 7.4. Solutions of 50 μ M SPSB2 in the cell were titrated by injection of a total of 290 μ L of 500 μ M peptide. Data analysis was performed using the evaluation software Origin version 7.0 (MicroCal Inc.). Parameters were derived from a nonlinear least-squares fit to the data, using the “one set of sites” model.

NMR Spectroscopy. All NMR experiments were recorded on a Bruker Avance 600 MHz spectrometer, equipped with a 5 mm TCI cryoprobe. 2D heteronuclear single quantum coherence ([¹⁵N,¹H]-HSQC) spectra of SPSB2 in the absence and the presence of cyclic peptide Ac-c[CVDINNNC]-NH₂ and linear peptide Ac-DINNN-NH₂ were recorded using 100 μ M ¹⁵N-labeled SPSB2 dissolved in 10 mM sodium phosphate buffer pH 7.0, 50 mM NaCl with 10% ²H₂O. The molar ratio of SPSB2 to peptide was 1:1. Spectra were acquired at 22

$^{\circ}\text{C}$ using a data matrix size of $128 (t_1) \times 8192 (t_2)$ and with 8 scans per t_1 increment. The spectral widths were 13.5 and 35.0 ppm for ^1H and ^{15}N , respectively. Both the ^1H and ^{15}N chemical shifts were referenced indirectly via the H_2O signal in ^1H , and the absolute frequency ratio in ^{15}N .²² All spectra were processed and analyzed using Bruker TopSpin (version 3.2).

^{19}F NMR spectra of 50 μM 5-F-Trp SPSB2 in 50 mM sodium phosphate buffer, pH 7.4, and 50 mM NaCl were recorded at 30 $^{\circ}\text{C}$ in the presence and absence of 250 μM Ac-c[CVDINNNC]- NH_2 . ^{19}F NMR chemical shifts were referenced against 0.005% trifluoroethanol. Exponential window function with a line-broadening of 40 Hz was used to process all spectra.

For structure calculations of Ac-c[CVDINNNC]- NH_2 , a 1.4 mM cyclic peptide was dissolved in 10 mM phosphate buffer at pH 4.8, 50 mM NaCl with 10% $^2\text{H}_2\text{O}$. Homonuclear 2D spectra were recorded at 10 $^{\circ}\text{C}$ for backbone and side chain proton resonances assignments. A 2D total correlation spectroscopy (TOCSY) spectrum was acquired using the DIPSI-2 pulse sequence²³ with excitation sculpting for water suppression²⁴ and a mixing time of 70 ms. 2D NOESY spectra were collected at different mixing times (70, 200, 300, and 400 ms) to analyze the time-dependence of NOE intensities. For carbon and nitrogen chemical shift assignments, [$^1\text{H}, ^{13}\text{C}$]-HSQC (256 \times 2048, 32 scans) and [$^1\text{H}, ^{15}\text{N}$]-SOFAST HMQC (64 \times 2048, 400 scans) spectra were acquired in 10 mM phosphate buffer at pH 4.8, 50 mM NaCl with 10% $^2\text{H}_2\text{O}$ at 10 $^{\circ}\text{C}$. For all these spectra, a sine-bell squared window function was used for processing. All spectra were processed using Bruker TopSpin (version 3.2) and analyzed using CcpNmr-Analysis (version 2.1.5). The chemical shift assignments are summarized in Supporting Information, Table S2.

For determination of potential amide backbone hydrogen bonding of the cyclic peptide, a series of 1D ^1H spectra was acquired at 10, 12, 15, 20, and 25 $^{\circ}\text{C}$, and the amide resonance temperature coefficients were determined from the slope of the linear least-squares fits to the data (Supporting Information, Figure S5). A series of 1D ^1H spectra was also recorded at different time intervals after dissolving freeze-dried material in $^2\text{H}_2\text{O}$ at pH 4.8 at 10 $^{\circ}\text{C}$ to monitor the amide exchange rate. For φ angle determination, $^3J_{\text{NH-H}\alpha}$ coupling constants were measured from both 2D double quantum filtered correlated spectroscopy (DQF-COSY) spectra and 1D ^1H spectra at 10 $^{\circ}\text{C}$, processed with an exponential window function (LB = -2 Hz).

The solution structures of the cyclic peptide were calculated using the program CYANA (version 3.0)²⁵ in which distance restraints were calculated based on the volume of each assigned peak in the NOESY spectra at 400 ms mixing time. The cyclic peptide backbone torsion angle restraints (φ and ψ angles) were predicted from the NMR chemical shift assignments using TALOS-N.²⁶ For side chain torsion angle restraints (χ_1 angles), only residue(s) with NMR parameters ($^3J_{\text{AF}2}$, $^3J_{\text{AF}3}$, $\text{NOE}_{\text{AF}2}$, $\text{NOE}_{\text{AF}3}$, $\text{NOE}_{\text{NH}\beta 2}$, $\text{NOE}_{\text{NH}\beta 3}$) consistent with one of the three classes of side chain rotamers, g^+g^+ , g^+t^+ , and t^+g^+ , as described by Wagner et al. were included for calculations.²⁷ A disulfide bond constraint was also added between the two cysteine residues. Hydrogen bond constraints were included only if consistent acceptors were observed in >50% of the calculated structures and supported by low temperature coefficient (magnitude <4.6 ppb/K).²⁸ The 20 structures that satisfy all experimental distance restraints and torsion angle restraints without steric overlap between all nonbonded atom pairs, i.e., lowest CYANA target function, were selected and assessed using MOLMOL (version 2K.1).²⁹ The structural statistics are summarized in Table 2. Structural figures were prepared using PyMOL (version 1.5.0.4).

Cell Lysate Inhibition Assays. Murine bone marrow macrophages (BMDM)s were derived by culture of whole bone marrow in Dulbecco's Modified Eagle's Medium (DMEM) supplemented with 100 U/mL penicillin, 0.1 mg/mL streptomycin, 10% fetal bovine serum (FBS), and 20% L-cell conditioned medium as a source of macrophage colony stimulating factor (M-CSF).³⁰ Cells were cultured for 5 days prior to replating and incubation with 10 ng/mL murine interferon-gamma ($\text{IFN-}\gamma$) and 20 ng/mL *Salmonella Minnesota*-derived lipopolysaccharide (LPS) overnight at 37 $^{\circ}\text{C}$. Cells were lysed in kinase assay lysis buffer³¹ containing Roche's cOmplete, Mini

Protease Inhibitor Cocktail and 1 mM phenylmethylsulfonyl fluoride on ice for 30 min. The cell lysates were incubated with 10 $\mu\text{g}/\text{mL}$ recombinantly expressed GST-tagged TRIM30 α -B30.2 domain (as a negative control), or GST-tagged SPSB2-SPRY domain, in the absence and presence of 10 μM cyclic peptide for 2 h. The SPSB2-iNOS protein complexes were recovered from the cell lysate via incubation with glutathione-Sepharose 4B beads (GE Healthcare) for 1 h. Proteins were separated by SDS-PAGE under reducing conditions and electrophoretically transferred to nitrocellulose membranes (Millipore). Membranes were blocked overnight in 10 wt %/vol skim milk and incubated with mouse monoclonal anti-iNOS primary antibody (BD Biosciences) for 2 h. Antibody binding was visualized with peroxidase-conjugated sheep anti-mouse Ig antibody (GE Healthcare) and the ECL system (Millipore). To reblot, the membrane was first stripped of antibodies in 0.1 M Gly, pH 2.9, followed by incubation with mouse monoclonal anti-GST primary antibody for 2 h. Antibody binding was visualized with peroxidase-conjugated sheep anti-mouse Ig antibody (GE Healthcare) and the ECL system (GE Healthcare).

Proteolysis Assays. Proteolysis assays were performed at a 200:1 substrate (peptide)/enzyme ratio with pepsin, trypsin, and α -chymotrypsin. For all assays, peptides were incubated with enzyme at 37 $^{\circ}\text{C}$ for up to 96 h in the presence of trypsin/ α -chymotrypsin and for 24 h in the presence of pepsin. As a positive control to ensure that active enzyme was present, bovine serum albumin was used as substrate in place of Ac-c[CVDINNNC]- NH_2 . All digestion assay data were analyzed by LC-MS (0–60% ACN gradient, 10 min). Trypsin (EC 3.4.21.4, Sigma) and α -chymotrypsin (EC 3.4.21.1, Sigma) stocks were prepared in 20 mM Tris, 5 mM EDTA (pH 8), and pepsin (EC 3.4.23.1, Sigma) stocks were prepared in 30 mM NaCl (pH 2). The trypsin and α -chymotrypsin reactions were quenched with 0.1% TFA, and the pepsin reactions were quenched with 50% 1 M NaOH.

Plasma Stability Assay. Both cyclic peptide Ac-c[CVDINNNC]- NH_2 and the linear 13-residue peptide Ac-KEEKDINNNVKKKT- NH_2 were incubated in human plasma at 37 $^{\circ}\text{C}$ at a final peptide concentration of 50 μM . At each time point (0, 4, 24, and 50 h), the plasma proteins were precipitated with 8% trichloroacetic acid (TCA) at 2:1 (v/v) ratio of sample:TCA and incubated on ice for 15 min before being spun down at 14000 rpm for 5 min. The supernatants were then collected and analyzed by RP-HPLC on an Agilent 1260 Infinity HPLC system fitted with an Agilent Poroshell 120 SB-C18 column (4.6 mm \times 100 mm, 2.7 μm) using a linear gradient of 5–100% buffer B [100% ACN (0.1% TFA)] in buffer A [100% water (0.1% TFA)] at 35 $^{\circ}\text{C}$ over 10 min at a flow rate of 1 mL/min.

Redox Stability Assay. Cyclic peptide Ac-c[CVDINNNC]- NH_2 was incubated in 10 mM Tris, pH 7.4, at 37 $^{\circ}\text{C}$ at a final peptide concentration of 0.5 mg/mL for 1 h in the presence of 1 mM DTT and 1 mM or 10 mM H_2O_2 (1:1 and 1:10 ratio of DTT: H_2O_2 , respectively). At 5, 15, 30, 45, and 60 min, 30 μL samples were collected and analyzed immediately by RP-HPLC on an Agilent 1260 Infinity HPLC system fitted with an Agilent Poroshell 120 SB-C18 column (4.6 mm \times 100 mm, 2.7 μm) using a linear gradient of 5–100% buffer B [100% ACN (0.1% TFA)] in buffer A [100% water (0.1% TFA)] at 35 $^{\circ}\text{C}$ over 10 min at a flow rate of 1 mL/min. As the peptide reduction by DTT can be very rapid, the initial time point of each sample was determined prior to adding 1% (v/v) 100 mM stock DTT to the sample. The height of the cyclic peptide peak at 254 nm at each time point was recorded, and % peptide remaining was determined. The identity of the peaks was confirmed by LC-MS.

■ ASSOCIATED CONTENT

● Supporting Information

Additional tables listing the rmsd of designed cyclic peptide analogues and chemical shift assignments of the cyclic peptide. Also included are figures illustrating the crystal structure of SPSB2-bound DINNN peptide, and in silico models of the designed cyclic peptide analogues, LC-MS profiles of the synthesized cyclic peptide, ^1H NMR spectra of the solution structure of the cyclic peptide, SPR and ITC data for both

native linear peptide and the reduced form of the cyclic peptide, the least-squares fits of amide resonance shift with temperature, the overlay of in silico model and solution structure of the cyclic peptide, and the rigid docking results of the in silico model of the cyclic peptide. This material is available free of charge via the Internet at <http://pubs.acs.org>.

AUTHOR INFORMATION

Corresponding Author

*Phone: +613 9903 9167. Fax: +613 9903 9582. E-mail: ray.norton@monash.edu.

Notes

The authors declare no competing financial interest.

ACKNOWLEDGMENTS

We thank Prof. Jonathan Baell, A/Prof. Martin Scanlon, and Dr. Mark Mulcair for helpful discussions, and Dr. David Shackelford for providing human plasma from the Australian Red Cross Blood Service. B.K.Y. is the recipient of an Academic Staff Training Scheme Fellowship of Universiti Sains Malaysia. R.S.N. and S.E.N. acknowledge fellowship support from the National Health and Medical Research Council of Australia. This study was supported by the Australian National Health Medical Research Council (NHMRC) grants 1022693 and 1016647, as well as an NHMRC IRISS grant 361646 and a Victorian State Government Operational Infrastructure Scheme grant.

ABBREVIATIONS USED

SPSB2, SPRY-domain of SOCS box protein 2; ITC, isothermal titration calorimetry; DIPEA, *N,N*-diisopropylethylamine; K_d , affinity constant; k_{on} , equilibrium association rate; k_{off} , equilibrium dissociation rate; HEPES, 2-[4-(2-hydroxyethyl)-piperazin-1-yl]ethanesulfonic acid

REFERENCES

- Chakravorty, D.; Hensel, M. Inducible nitric oxide synthase and control of intracellular bacterial pathogens. *Microbes Infect.* **2003**, *5*, 621–627.
- Khan, S. A.; Strijbos, P. J.; Everest, P.; Moss, D.; Stratford, R.; Mastroeni, P.; Allen, J.; Servos, S.; Charles, I. G.; Dougan, G.; Maskell, D. J. Early responses to *Salmonella typhimurium* infection in mice occur at focal lesions in infected organs. *Microb. Pathog.* **2001**, *30*, 29–38.
- Chan, E. D.; Chan, J.; Schluger, N. W. What is the role of nitric oxide in murine and human host defense against tuberculosis? Current knowledge. *Am. J. Respir. Cell Mol. Biol.* **2001**, *25*, 606–612.
- Stenger, S.; Donhauser, N.; Thüring, H.; Rölinghoff, M.; Bogdan, C. Reactivation of latent leishmaniasis by inhibition of inducible nitric oxide synthase. *J. Exp. Med.* **1996**, *183*, 1501–1514.
- Scharton-Kersten, T. M.; Yap, G.; Magram, J.; Sher, A. Inducible nitric oxide is essential for host control of persistent but not acute infection with the intracellular pathogen *Toxoplasma gondii*. *J. Exp. Med.* **1997**, *185*, 1261–1274.
- Kuang, Z.; Lewis, R. S.; Curtis, J. M.; Zhan, Y.; Saunders, B. M.; Babon, J. J.; Kolesnik, T. B.; Low, A.; Masters, S. L.; Willson, T. A.; Kedzierski, L.; Yao, S.; Handman, E.; Norton, R. S.; Nicholson, S. E. The SPRY domain-containing SOCS box protein SPSB2 targets iNOS for proteasomal degradation. *J. Cell Biol.* **2010**, *190*, 129–141.
- Filippakopoulos, P.; Low, A.; Sharpe, T. D.; Uppenberg, J.; Yao, S.; Kuang, Z.; Savitsky, P.; Lewis, R. S.; Nicholson, S. E.; Norton, R. S.; Bullock, A. N. Structural basis for Par-4 recognition by the SPRY domain- and SOCS box-containing proteins SPSB1, SPSB2, and SPSB4. *J. Mol. Biol.* **2010**, *401*, 389–402.

- (a) Lewis, R. S.; Kolesnik, T. B.; Kuang, Z.; D’Cruz, A. A.; Blewitt, M. E.; Masters, S. L.; Low, A.; Willson, T.; Norton, R. S.; Nicholson, S. E. TLR regulation of SPSB1 controls inducible nitric oxide synthase induction. *J. Immunol.* **2011**, *187*, 3798–3805. (b) Nishiya, T.; Matsumoto, K.; Maekawa, S.; Kajita, E.; Horinouchi, T.; Fujimuro, M.; Ogasawara, K.; Uehara, T.; Miwa, S. Regulation of inducible nitric-oxide synthase by the SPRY domain- and SOCS box-containing proteins. *J. Biol. Chem.* **2011**, *286*, 9009–9019.
- (9) Matsumoto, K.; Nishiya, T.; Maekawa, S.; Horinouchi, T.; Ogasawara, K.; Uehara, T.; Miwa, S. The ECS(SPSB) E3 ubiquitin ligase is the master regulator of the lifetime of inducible nitric-oxide synthase. *Biochem. Biophys. Res. Commun.* **2011**, *409*, 46–51.
- (10) (a) Camerino, M. A.; Chalmers, D. K.; Thompson, P. E. Computer-assisted design of cyclic peptides and peptidomimetics. *Chim. Oggi* **2008**, *26*, 46–51. (b) Fletcher, J. M.; Hughes, R. A. Modified low molecular weight cyclic peptides as mimetics of BDNF with improved potency, proteolytic stability and transmembrane passage in vitro. *Bioorg. Med. Chem.* **2009**, *17*, 2695–2702. (c) Hess, S.; Linde, Y.; Ovadia, O.; Safrai, E.; Shalev, D. E.; Swed, A.; Halbfinger, E.; Lapidot, T.; Winkler, I.; Gabinet, Y.; Faier, A.; Yarden, D.; Xiang, Z.; Portillo, F. P.; Haskell-Luevano, C.; Gilon, C.; Hoffman, A. Backbone cyclic peptidomimetic melanocortin-4 receptor agonist as a novel orally administered drug lead for treating obesity. *J. Med. Chem.* **2008**, *51*, 1026–1034. (d) Byk, G.; Halle, D.; Zeltser, I.; Bitan, G.; Selinger, Z.; Gilon, C. Synthesis and biological activity of NK-1 selective, N-backbone cyclic analogs of the C-terminal hexapeptide of substance P. *J. Med. Chem.* **1996**, *39*, 3174–3178. (e) Hayouka, Z.; Hurevich, M.; Levin, A.; Benyamini, H.; Iosub, A.; Maes, M.; Shalev, D. E.; Loyter, A.; Gilon, C.; Friedler, A. Cyclic peptide inhibitors of HIV-1 integrase derived from the LEDGF/p75 protein. *Bioorg. Med. Chem.* **2010**, *18*, 8388–8395. (f) Piserchio, A.; Salinas, G. D.; Li, T.; Marshall, J.; Spaller, M. R.; Mierke, D. F. Targeting specific PDZ domains of PSD-95: structural basis for enhanced affinity and enzymatic stability of a cyclic peptide. *Chem. Biol.* **2004**, *11*, 469–473.
- (11) Richardson, J. S. The anatomy and taxonomy of protein structure. *Adv. Protein Chem.* **1981**, *34*, 167–339.
- (12) Leung, E. W. W.; Yagi, H.; Harjani, J. R.; Mulcair, M. D.; Scanlon, M. J.; Baell, J. B.; Norton, R. S. ¹⁹F NMR as a probe of ligand interaction with the iNOS binding site of SPRY-domain containing SOCS box protein 2. *Chem. Biol. Drug Des.* **2014**, DOI: 10.1111/cbdd.12355.
- (13) Kuang, Z.; Yao, S.; Xu, Y.; Lewis, R. S.; Low, A.; Masters, S. L.; Willson, T. A.; Kolesnik, T. B.; Nicholson, S. E.; Garrett, T. J. P.; Norton, R. S. SPRY domain-containing SOCS box protein 2: crystal structure and residues critical for protein binding. *J. Mol. Biol.* **2009**, *386*, 662–674.
- (14) Bodenhausen, G.; Ruben, D. J. Natural abundance nitrogen-15 NMR by enhanced heteronuclear spectroscopy. *Chem. Phys. Lett.* **1980**, *69*, 185–189.
- (15) Wouters, M. A.; Fan, S. W.; Haworth, N. L. Disulfides as redox switches: from molecular mechanisms to functional significance. *Antioxid. Redox Signaling* **2010**, *12*, 53–91.
- (16) Schafer, F. Q.; Buettner, G. R. Redox environment of the cell as viewed through the redox state of the glutathione disulfide/glutathione couple. *Free Radical Biol. Med.* **2001**, *30*, 1191–1212.
- (17) Cumming, R. C.; Andon, N. L.; Haynes, P. A.; Park, M.; Fischer, W. H.; Schubert, D. Protein disulfide bond formation in the cytoplasm during oxidative stress. *J. Biol. Chem.* **2004**, *279*, 21749–21758.
- (18) Hampton, M. B.; Kettle, A. J.; Winterbourn, C. C. Inside the neutrophil phagosome: oxidants, myeloperoxidase, and bacterial killing. *Blood* **1998**, *92*, 3007–3017.
- (19) Ramachandran, G. N.; Ramakrishnan, C.; Sasisekharan, V. Stereochemistry of polypeptide chain configurations. *J. Mol. Biol.* **1963**, *7*, 95–99.
- (20) Atherton, E.; Logan, C. J.; Sheppard, R. C. Peptide synthesis. Part 2. Procedures for solid-phase synthesis using *N*_α-fluorenylmethoxycarbonylamino acids on polyamide supports. Synthesis of substance P and of acyl carrier protein 65–74 decapeptide. *J. Chem. Soc., Perkin. Trans. 1* **1981**, 538–546.

(21) Yao, S.; Masters, S. L.; Zhang, J. G.; Palmer, K. R.; Babon, J. J.; Nicola, N. A.; Nicholson, S. E.; Norton, R. S. Backbone ^1H , ^{13}C and ^{15}N assignments of the 25 kDa SPRY domain-containing SOCS box protein 2 (SSB-2). *J. Biomol. NMR* **2005**, *31*, 69–70.

(22) Wishart, D. S.; Bigam, C. G.; Yao, J.; Abildgaard, F.; Dyson, H. J.; Oldfield, E.; Markley, J. L.; Sykes, B. D. ^1H , ^{13}C and ^{15}N chemical shift referencing in biomolecular NMR. *J. Biomol. NMR* **1995**, *6*, 135–140.

(23) Shaka, A. J.; Lee, C. J.; Pines, A. Iterative schemes for bilinear operators; application to spin decoupling. *J. Magn. Reson. (1969)* **1988**, *77*, 274–293.

(24) Hwang, T. L.; Shaka, A. J. Water suppression that works. Excitation sculpting using arbitrary wave-forms and pulsed-field gradients. *J. Magn. Reson. A* **1995**, *112*, 275–279.

(25) Güntert, P. Automated NMR structure calculation with CYANA. *Methods Mol. Biol.* **2004**, *278*, 353–378.

(26) Shen, Y.; Bax, A. Protein backbone and sidechain torsion angles predicted from NMR chemical shifts using artificial neural networks. *J. Biomol. NMR* **2013**, *56*, 227–241.

(27) Wagner, G.; Braun, W.; Havel, T. F.; Schaumann, T.; Go, N.; Wüthrich, K. Protein structures in solution by nuclear magnetic resonance and distance geometry. The polypeptide fold of the basic pancreatic trypsin inhibitor determined using two different algorithms, DISGEO and DISMAN. *J. Mol. Biol.* **1987**, *196*, 611–639.

(28) Baxter, N. J.; Williamson, M. P. Temperature dependence of ^1H chemical shifts in proteins. *J. Biomol. NMR* **1997**, *9*, 359–369.

(29) Koradi, R.; Billeter, M.; Wüthrich, K. MOLMOL: a program for display and analysis of macromolecular structures. *J. Mol. Graph.* **1996**, *14* (51–55), 29–32.

(30) Wormald, S.; Zhang, J. G.; Krebs, D. L.; Mielke, L. A.; Silver, J.; Alexander, W. S.; Speed, T. P.; Nicola, N. A.; Hilton, D. J. The comparative roles of suppressor of cytokine signaling-1 and -3 in the inhibition and desensitization of cytokine signaling. *J. Biol. Chem.* **2006**, *281*, 11135–11143.

(31) Nicholson, S. E.; Novak, U.; Ziegler, S. F.; Layton, J. E. Distinct regions of the granulocyte colony-stimulating factor receptor are required for tyrosine phosphorylation of the signaling molecules JAK2, Stat3, and p42, p44MAPK. *Blood* **1995**, *86*, 3698–3704.

SUPPORTING INFORMATION

A Potent Cyclic Peptide Targeting SPSB2 Protein as a Potential Anti-infective Agent

Beow Keat Yap,[†] Eleanor W. W. Leung,[†] Hiromasa Yagi,[†] Charles A. Galea,[†] Sandeep Chhabra,[†] David K. Chalmers,[†] Sandra E. Nicholson,^{‡,‡} Philip E. Thompson,[†] and Raymond S. Norton^{*,†}

[†]Medicinal Chemistry, Monash Institute of Pharmaceutical Sciences, Monash University, Parkville 3052, Victoria, Australia

[‡]The Walter and Eliza Hall Institute of Medical Research, Parkville 3052, Victoria, Australia

[‡]The Department of Medical Biology, University of Melbourne, Parkville, Victoria 3052, Australia

Table S1. Modeled cyclic peptides with different length of linkers and their respective rmsd to the crystal structure of linear DINNN-containing peptide bound to SPSB2 (PDB code 3EMW). The backbone rmsd values are shown for the DINNN sequence of each peptide to the corresponding sequence in crystal structure. Side chain replacement of the second residue of CADINNNC with all but proline and cysteine residues did not yield significant difference in backbone rmsd values.

Cyclization Method	Number of linker residue(s)^	Example of Modeled Cyclic Peptide Sequence	Backbone rmsd (Å)
<i>N</i> -terminal to <i>C</i> -terminal cyclisation	0	DINNN	0.79*
	1	ADINNN	0.56*
	2	ADINNNA	0.71
	3	ADINNNAA	0.57*
	4	AADINNNAA	0.53
	5	AADINNNAAA	0.30
Disulfide bridge formation between thiol groups of cysteines	2	CDINNNC	0.47
	3	CADINNNC	0.13
		CIDINNNC	0.12
		CVDINNNC	0.12
		CLDINNNC	0.12
		CFDINNNC	0.12
		CWDINNNC	0.14
		CYDINNNC	0.12
		CMDINNNC	0.13
		CGDINNNC	0.12
		CRDINNNC	0.15
		CHDINNNC	0.12
		CKDINNNC	0.13
		CDDINNNC	0.12
		CEDINNNC	0.13
		CNDINNNC	0.13
	CQDINNNC	0.13	
	CSDINNNC	0.12	
CTDINNNC	0.12		
3	CDINNNAC	0.66	
4	CADINNNAC	0.37	
5	CADINNNAAC	0.20	
5	CAADINNNAC	0.36*	

* disallowed region in Ramachandran Plot

Table S2. Chemical shifts of cyclic peptide Ac-c[CVDINNNC]-NH₂ in 10 mM phosphate buffer, 50 mM NaCl, pH 4.8 at 10 °C

Residues	N	HN	H ^α	C ^α	H ^β	C ^β	Others
	ppm						
Cys1	126.2	8.51	4.62	56.2	3.14, 3.14	41.5	*CH ₃ 24.3; *H 2.03
Val2	125.4	8.66	4.20	62.7	2.16	32.4	H ^γ 0.95, 0.96; C ^γ 17.6, 20.2
Asp3	124.8	8.22	4.71	54.4	2.75, 2.63	42.1	
Ile4	116.5	8.55	4.16	62.7	1.92	38.7	H ^{γ1} 1.44, 1.23; H ^{γ2} 0.94; H ^δ 0.91; C ^{γ1} 27.3; C ^{γ2} 21.1; C ^δ 13.5
Asn5	119.5	8.42	4.78	53.6	2.77, 2.88	38.5	H ^δ 7.82, 7.00; N ^δ 113.8
Asn6	116.9	8.35	4.67	53.9	2.76, 3.00	38.5	H ^δ 7.75, 6.95; N ^δ 113.4
Asn7	123.4	8.57	4.75	53.7	2.80, 2.86	38.1	H ^δ 7.75, 7.03; N ^δ 113.6
Cys8	119.4	8.46	4.68	55.6	3.02, 3.31	40.8	[#] H ^δ 7.31, 7.70; [#] N ^δ 108.8

*N-terminal acetyl group, [#]C-terminal amide group

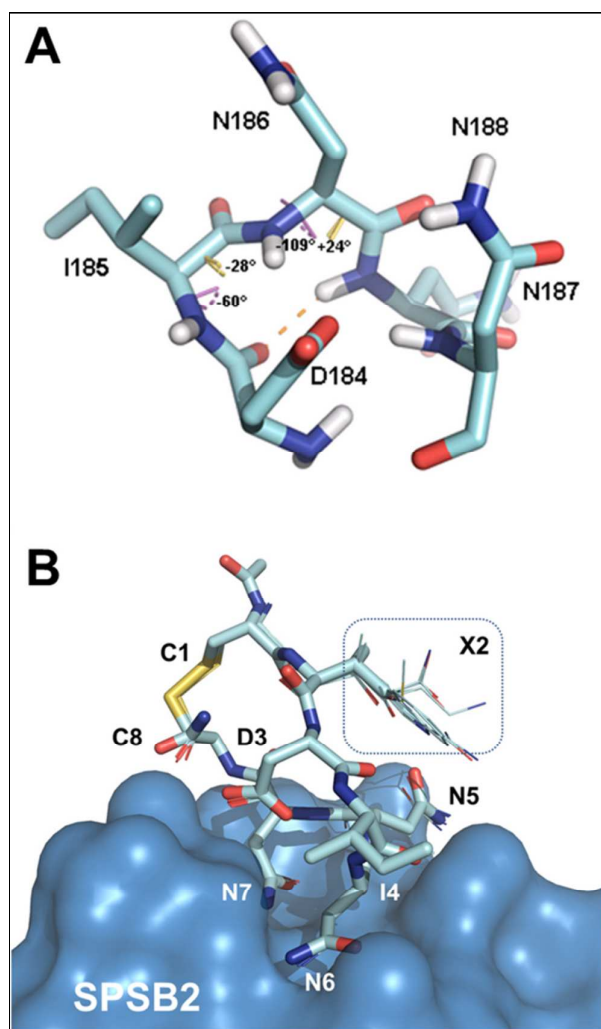


Figure S1. (A) Crystal structure of the DINNN peptide bound to SPSB2 (PDB code 3EMW) with intra-molecular hydrogen bond between the backbone NH($i+3$) of Asn187 and CO(i) of Asp184 dotted in orange. The dihedral angles, ϕ and ψ , are indicated in magenta and yellow, respectively. (B) Rigid body docking of the *in silico* models of CXDINNNC to SPSB2 (X = Ala, Ile, Val, Leu, Phe, Trp, Tyr, Met, Gly, Arg, His, Lys, Asp, Glu, Asn, Gln, Ser or Thr) showed that the identity of residue X neither affects the overall structure of the cyclic peptide nor interferes with the binding of the cyclic peptide to SPSB2 as these residues all extended out of the binding pocket.

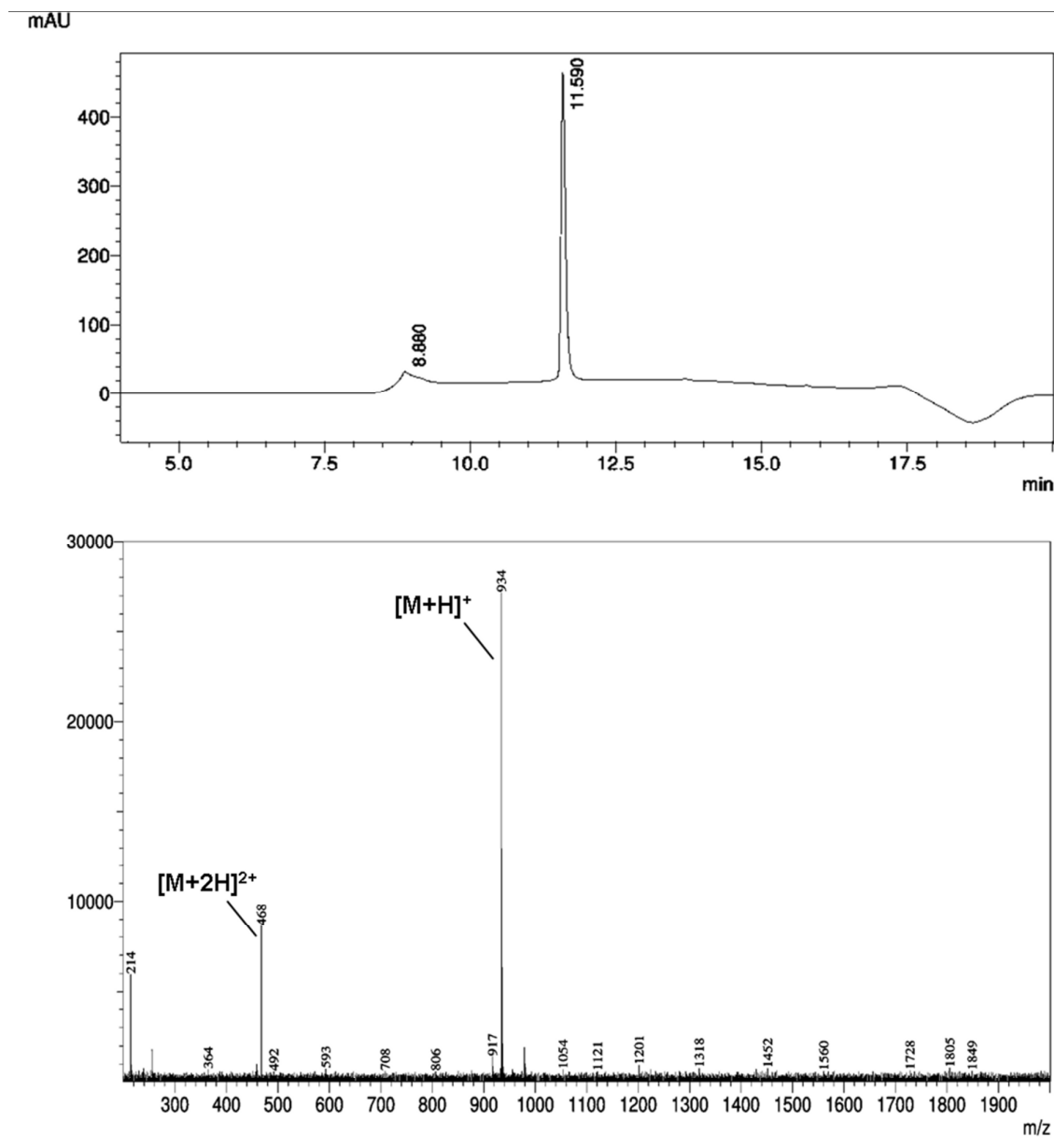


Figure S2. Liquid-chromatography (upper panel) and mass-spectroscopy (lower panel) profiles of the synthesized and purified cyclic peptide Ac-c[CVDINNNC]-NH₂. Purity is ~95%, based on the peak area in the chromatogram

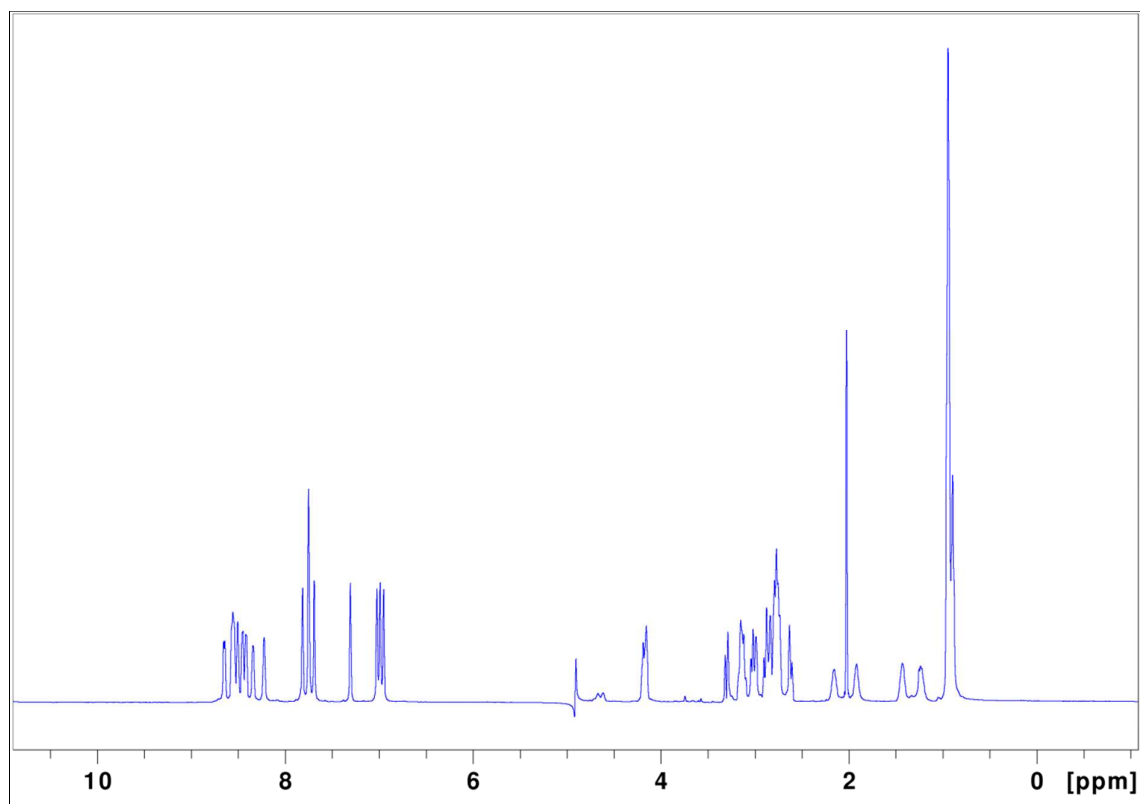


Figure S3. 1D ¹H spectrum of Ac-c[CVDINNNC]-NH₂ in 10 mM sodium phosphate buffer, 50 mM NaCl, pH 4.8, acquired at 10 °C on a 600 MHz spectrometer

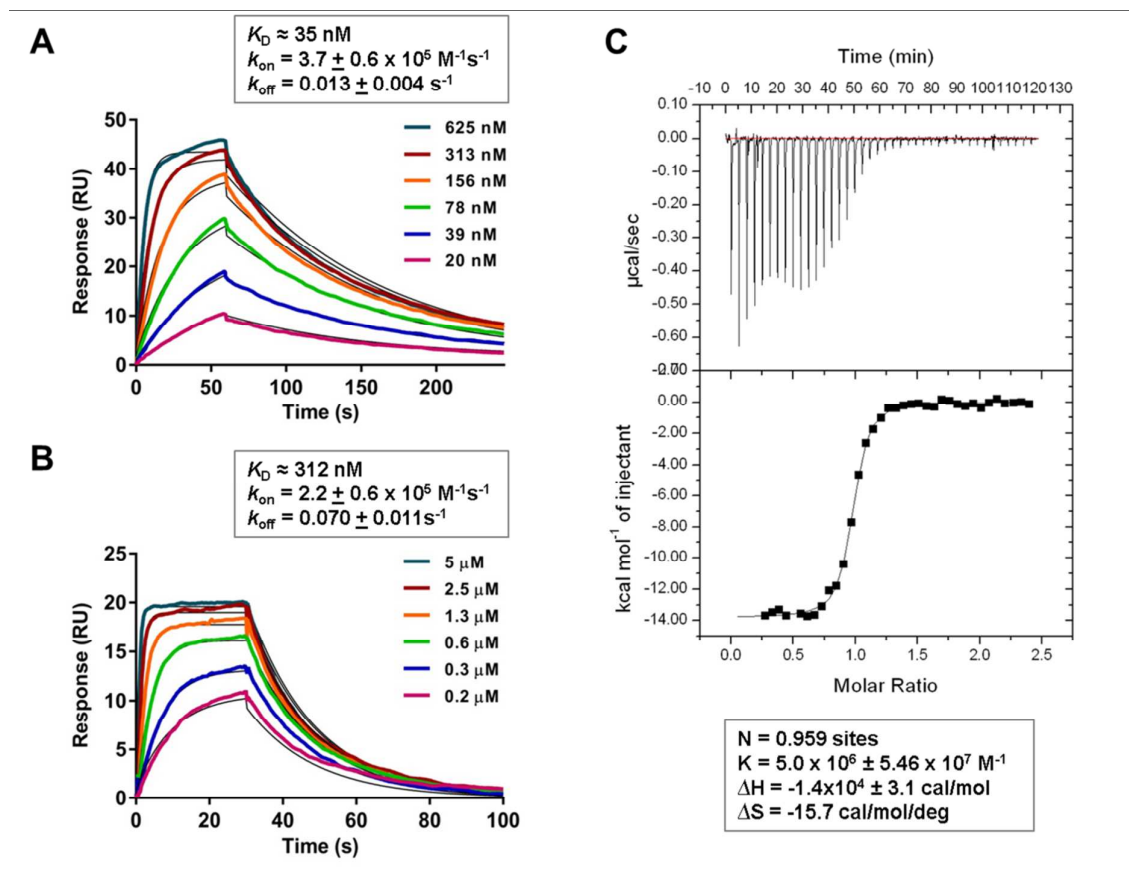


Figure S4. SPR sensorgrams of immobilized SPSB2 exposed to increasing concentrations of (A) reduced form of the cyclic peptide, Ac-CVDINNNC-NH₂, and (B) Ac-DINNN-NH₂. (C) ITC binding curves of Ac-DINNN-NH₂ in complex with SPSB2 protein. Repeating the SPR experiment in (A) with 1 mM DTT in the running buffer, to ensure that the peptide remained fully reduced, yielded the same results.

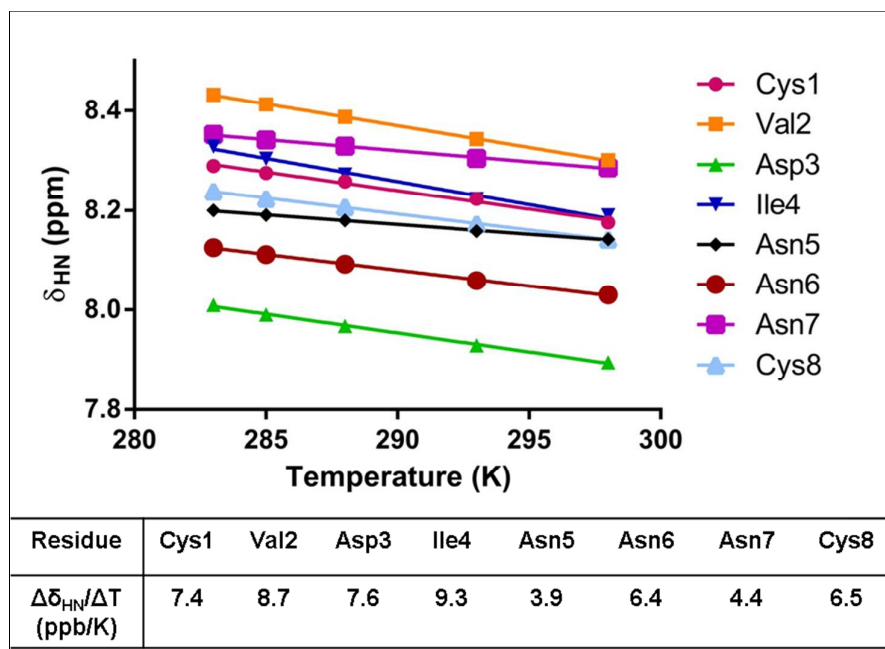


Figure S5. Temperature dependence of backbone amide chemical shifts of Ac-c[CVDINNNC]-NH₂. (Top) Plots of amide proton (δ_{HN}) over a range of temperatures. (Bottom) Temperature coefficients ($\Delta\delta_{\text{HN}}/\Delta T$) of backbone amide resonances. The values are determined from the slope of the linear least-squares fits to the data in the top panel.

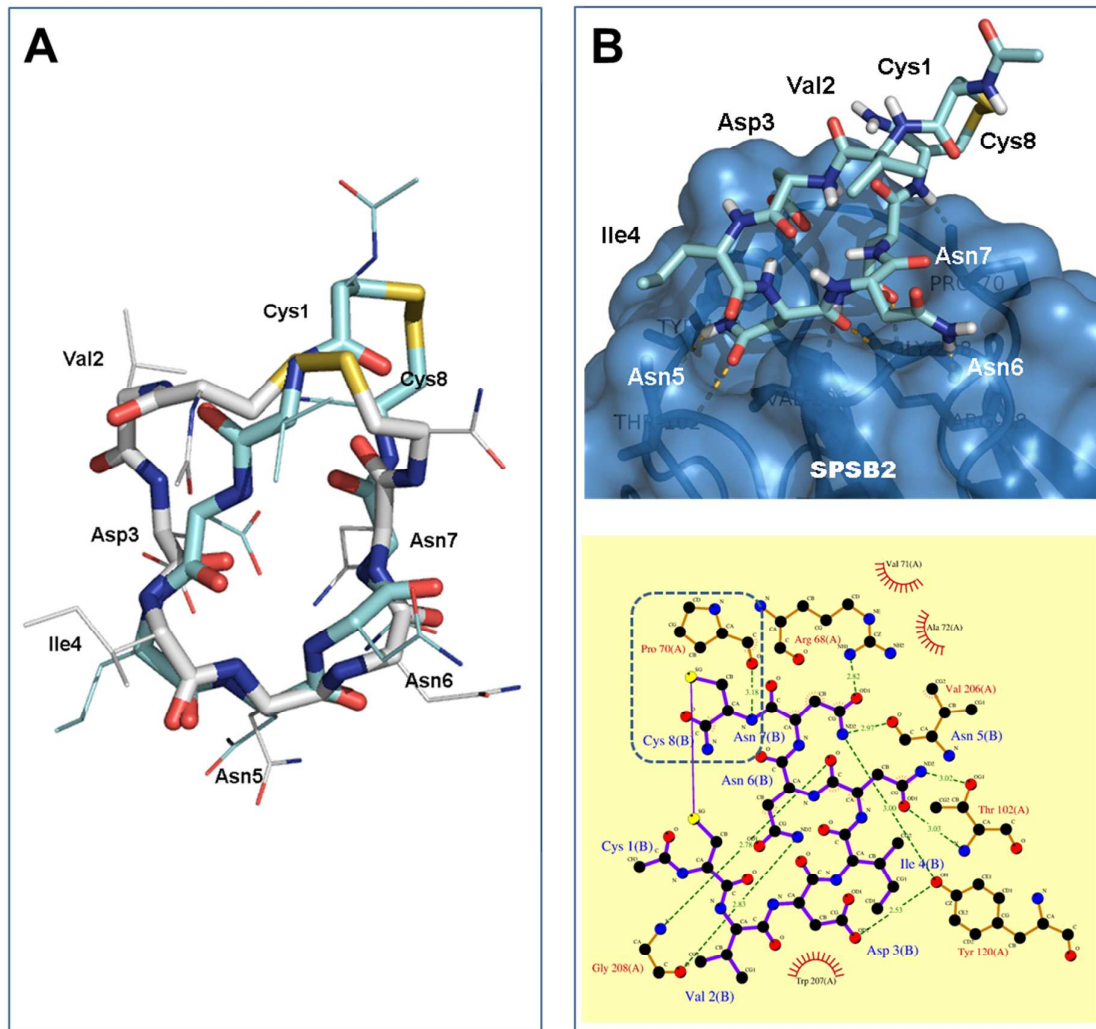


Figure S6. (A) Overlay of *in silico* modelled structure (cyan) and the NMR-determined solution structure (white) of Ac-c[CVDINNNC]-NH₂. The two structures are well-aligned over the backbone DINNN motif, with rmsd of 1.23 Å. Significant differences in the conformation of residues Cys1, Val2 and Cys8 between the solution structure (unbound conformation) and *in silico* model (predicted bound conformation) suggests that these residues adopted different conformations upon binding to SPSB2. (B) Rigid body docking of *in silico* SPSB2-bound model of Ac-c[CVDINNNC]-NH₂ with Glide SP (version 5.8, Schrödinger) (**upper panel**). Cyclic peptide-SPSB2 interactions were generated by LIGPLOT v4.0 (**bottom panel**) with hydrogen bond dotted in green and hydrophobic interactions in red. SPSB2 residues that are involved in hydrogen bonds with the peptides are colored in brown while those involved in hydrophobic interactions are shown as red eye-lashes and labelled as chain A. Cyclic peptide residues are represented in purple and labelled as chain B. A hydrogen bond interaction was observed between the backbone NH of residue Cys8 of the cyclic peptide and backbone CO of residue Pro70 of SPSB2 (rectangular box), with an additional interaction was observed involving the backbone CO of residue Cys8 of the cyclic peptide and the side chain of Ala72 of SPSB2.

CHAPTER 5

Redox-stable cyclic peptide inhibitors of SPSB2-iNOS interaction

5.1 Declaration for Thesis Chapter 5

Declaration by candidate

In the case of **Chapter 5**, the nature and extent of my contribution to the work was the following:

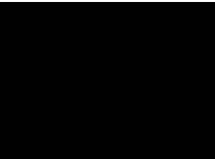
Nature of contribution	Extent of contribution (%)
Designed and performed the experiments, analysed the data and wrote the manuscript.	80

The following co-authors contributed to the work. If co-authors are students at Monash University, the extent of their contribution in percentage terms must be stated:

Name	Nature of contribution	Extent of contribution (%) for student co-authors only
Jitendra R. Harjani	Synthesis of cystathionine building block	
Eleanor W.W. Leung	¹⁹ F NMR	
Sandra E. Nicholson	BMDM cell lysate inhibition assay	
Martin J. Scanlon	Intellectual input	
David K. Chalmers	Intellectual input	
Philip E. Thompson	Intellectual input	
Jonathan B. Baell	Intellectual input	
Raymond S. Norton	Intellectual input, manuscript preparation	

The undersigned hereby certify that the above declaration correctly reflects the nature and extent of the candidate's and co-authors' contributions to this work.

**Candidate's
Signature**

	Date 22/02/2016
---	---------------------------

**Main
Supervisor's
Signature**

	Date 22/02/2016
---	---------------------------

5.2 Introduction

Chapter 4 revealed a potent disulphide-bridged cyclic peptide inhibitor of SPSB2-iNOS interaction with the peptide sequence of Ac-c[CVDINNNC]-NH₂, and a measured K_D of 4 nM by SPR, an approximate 80-fold improvement in affinity compared to the linear peptide Ac-DINNN-NH₂ ($K_D \approx 318$ nM). Cyclisation was found to improve association of the peptide to SPSB2 by ~10-fold, presumably due to pre-organisation of the cyclic peptide into the bound conformation in solution, supported by the close resemblance between the NMR solution structure of the disulphide-bridged cyclic peptide and the crystal structure of the linear DINNN peptide bound to SPSB2, with a backbone RMSD of 1.21 Å. The cyclic peptide was also found to bind specifically to the iNOS binding site of SPSB2, as evidenced by ¹⁹F NMR and [¹H, ¹⁵N]-HSQC, and was able to displace full-length iNOS from interacting with SPSB2 in macrophage cell lysates. In addition, it was also found to be stable in pepsin, trypsin, α-chymotrypsin and in human plasma. The cyclic peptide, which is cyclised through a disulphide bond between the two Cys residues at the *N*- and *C*-terminus of the peptide, however, is highly reduction-sensitive, as it was completely reduced after 15 min of incubation in a reaction mixture containing 1 mM dithiothreitol (DTT).

Thus, in this Chapter, the design of redox-stable cyclic peptide inhibitors of SPSB2-iNOS interaction is described. In contrast to the use of an amino acid linker in the design of cyclic peptide analogues in **Chapter 4**, *in silico* models of redox-stable cyclic peptide analogues were designed *via* incorporation of a different number of unusual amino acid linkers between the *N*- and *C*-terminus of the linear peptide DINNN, followed by cyclisation *via* a lactam bridge. Together with the cystathionine analogue of the disulphide bridge cyclic peptide (where the disulphide bond was replaced with a thioether bridge), the best *in silico* designed and energy minimised lactam bridge-cyclised model, with lowest backbone RMSD to the crystal structure of DINNN and no violation of dihedral angles in a Ramachandran plot, were synthesised and characterised by LC-MS and NMR experiments. Their abilities to bind to the iNOS binding site of SPSB2 were determined by ¹⁹F NMR and the binding affinities of the interactions were measured by SPR. Their abilities to displace full-length iNOS from SPSB2 in macrophage cell lysates were also investigated, and their stabilities in redox environment were explored. As the findings from this Chapter have been recently published in *FEBS Letters*, they are presented in the format of a published article in the immediate section below.

Redox-stable cyclic peptide inhibitors of the SPSB2–iNOS interaction

Beow Keat Yap¹, Jitendra R. Harjani¹, Eleanor W. W. Leung¹, Sandra E. Nicholson^{2,3}, Martin J. Scanlon¹, David K. Chalmers¹, Philip E. Thompson¹, Jonathan B. Baell¹ and Raymond S. Norton¹

1 Medicinal Chemistry, Monash Institute of Pharmaceutical Sciences, Monash University, Parkville, Vic., Australia

2 The Walter and Eliza Hall Institute of Medical Research, Parkville, Vic., Australia

3 The Department of Medical Biology, University of Melbourne, Parkville, Vic., Australia

Correspondence

R. S. Norton, Medicinal Chemistry, Monash Institute of Pharmaceutical Sciences, Monash University, Parkville 3052, Victoria, Australia

Fax: +61 3 9903 9582

Tel: +61 3 9903 9167

E-mail: ray.norton@monash.edu

(Received 5 February 2016, revised 18 February 2016, accepted 22 February 2016, available online 6 March 2016)

doi:10.1002/1873-3468.12115

Edited by Barry Halliwell

SPSB2 mediates the proteasomal degradation of iNOS. Inhibitors of SPSB2–iNOS interaction are expected to prolong iNOS lifetime and thereby enhance killing of persistent pathogens. Here, we describe the synthesis and characterization of two redox-stable cyclized peptides containing the DINNN motif required for SPSB2 binding. Both analogues bind with low nanomolar affinity to the iNOS binding site on SPSB, as determined by SPR and ¹⁹F NMR, and efficiently displace full-length iNOS from binding to SPSB2 in macrophage cell lysates. These peptides provide a foundation for future development of redox-stable, potent ligands for SPSB proteins as a potential novel class of anti-infectives.

Keywords: anti-infective; cyclic peptide; inducible nitric oxide synthase; redox-stable; SPRY domain of the SOCS-box protein 2

SPSB2 protein plays a key role in modulating the lifetime of iNOS in macrophages during infection [1]. It acts as a negative regulator that recruits an E3 ubiquitin ligase complex that polyubiquitinates iNOS and thereby mediates its proteasomal degradation [1]. SPSB2-deficient macrophages exhibit prolonged iNOS expression, NO production and ultimately enhanced killing of persistent pathogens such as *Leishmania major* parasites and *Mycobacterium tuberculosis*, suggesting that inhibitors of the SPSB2–iNOS interaction have potential as a new class of anti-infectives [1].

Kuang *et al.* [1] showed that a linear peptide from the disordered N-terminal region of iNOS, KEEK-DINNNVKKKT, bound to SPSB2 with a K_D of 13 nM, and that the most important residues mediating this interaction were DINNN, in particular the first, third and fifth residues of this sequence motif. In addition, structural studies by X-ray crystallography revealed that the SPRY domain of SPSB2 binds to Asp184, Asn186 and Asn188 of the DINNN sequence of the VASA peptide, the same motif as in the N-terminal region of iNOS (where the corresponding residues are Asp23, Asn25

Abbreviations

SPSB2, SPRY domain of the SOCS-box protein 2; iNOS, inducible nitric oxide synthase; SPR, surface plasmon resonance; NMR, nuclear magnetic resonance; NO, nitric oxide; k_{on} , association rate; k_{off} , dissociation rate; K_D , binding constant; DTT, dithiothreitol; SPPS, solid-phase peptide synthesis; LC-MS, liquid chromatography–mass spectroscopy; GST, glutathione *S*-transferase; TCEP.HCl, tris(2-carboxyethyl)phosphine hydrochloride; H₂O₂, hydrogen peroxide; HPLC, high-performance liquid chromatography; HCTU, *O*-(1H-6-chlorobenzotriazole-1-yl)-1,1,3,3-tetramethyluronium hexafluorophosphate; DIPEA, *N,N*-diisopropylethylamine; DMF, dimethylformamide; DCM, dichloromethane; HSQC, heteronuclear single quantum coherence; TFA, trifluoroacetic acid; TIPS, triisopropylsilane; DODT, 3,6-dioxa-1,8-octanedithiol; HFIP, hexafluoro-2-propanol; MeCN, acetonitrile; BMDM, bone marrow-derived macrophage; IFN- γ , interferon-gamma; LPS, lipopolysaccharide; SDS/PAGE, sodium dodecyl sulphate polyacrylamide gel electrophoresis.

and Asn27) [2]. Further binding studies by surface plasmon resonance (SPR) experiments revealed the linear DINNN peptide bound to SPSB2 with a K_D of 318 nM [3], suggesting that the flanking residues of the DINNN sequence in the N-terminal region of iNOS contributed to its low nanomolar binding affinity to SPSB2.

Recently, we established that cyclization of the linear peptide *via* a disulphide bridge in the cyclic peptide Ac-c[CVDINNNC]-NH₂ (CP0) improved its binding to SPSB2 by approximately 70-fold, with a K_D by SPR of approximately 4 nM [3]. Comparison of the kinetic profiles of the binding to SPSB2 of DINNN linear peptide, the disulphide-bridged cyclic peptide and its reduced counterpart revealed that cyclization improved k_{on} of the peptide to SPSB2 by approximately 10-fold, presumably through preorganization of the cyclic peptide into a conformation resembling the bound state. Both ¹⁹F NMR and [¹H,¹⁵N]-HSQC NMR experiments confirmed the cyclic peptide bound to the iNOS binding site on SPSB2. In addition, the cyclic peptide was found to be stable in human plasma and resistant to proteolysis by trypsin, α -chymotrypsin and pepsin. Not surprisingly, however, the disulphide-bridged cyclic peptide was also found to be reductively labile, with the disulphide bond being reduced completely after 15-min treatment with 1 mM DTT at 37 °C in Tris buffer, pH 7.4. While disulphide bridges can form in the cytoplasm under oxidative stress [4], for example during infection, cyclic peptide analogues that are stable to the normally reducing intracellular conditions are likely to be more effective.

There have been reports of disulphide replacements with thioethers [5–8], dicarba bridges [9,10] and diselenides [11] to generate redox-stable analogues without significantly compromising the binding affinity or activity of the parent peptide. However, it cannot be assumed *a priori* that replacement of a disulphide with a thioether will necessarily return biologically active compounds and each example needs to be investigated in a context- and sequence-specific manner. Similarly, previous work by Muttenthaler *et al.* [7] found that the head-to-tail lactam-bridge-cyclized analogue of oxytocin exhibited significant improvement in plasma stability, although little or no detectable binding or functional activity was observed, suggesting that careful design of the cyclic peptide for optimal binding to its target is crucial.

In this study, we describe the design and synthesis of a cystathionine analogue (CP1) of the disulphide-bridged cyclic peptide CP0 [3] and a lactam-bridge analogue between the N- and C termini of a peptide incorporating the DINNN linear motif, CP2 (Fig. 1). Both analogues were synthesized by SPPS [6] and their

identity and purity were characterized by both LC-MS and NMR studies (Figs S1–S6). The effect of replacing the disulphide bond with a thioether bridge or a lactam bridge on the binding of the analogues to SPSB2 was determined by both SPR and ¹⁹F NMR experiments. Their ability to inhibit the interaction of full-length iNOS with SPSB2 in macrophage lysates was also determined. To determine the stability of these analogues, redox assays were carried out in both reducing and oxidizing environments.

Materials and methods

Synthesis of cyclic peptide analogues CP1 and CP2

The cystathionine analogue CP1 was synthesized on resin using an automated Peptide Synthesizer 3 (PS3™) *via* Fmoc chemistry essentially as described by Dekan *et al.* [6] and Yap *et al.* [3]. About 0.3 mmol (3 equiv) of the first residue Fmoc-Cys(S-Stbu)-OH was coupled to 0.1 mmol Rink Amide AM Resin (0.47 mmol·g⁻¹ loading) for 50 min per coupling cycle under the activation of 0.3 mmol (3 equiv) HCTU and 0.6 mmol (6 equiv) DIPEA in dimethylformamide. Subsequent residues were assembled on resin using similar conditions as above (with double coupling used to couple the second Asn to the first Asn as well as the third Asn to the second Asn). The *tert*-butyldimethylsilyl (OTBDMS) derivative of the homoserine (Hse) residue [6] at the N terminus was converted to its Cl-homoalanine analogue with 10 equiv triphenylphosphine dichloride in DCM for 6 h, while the *tert*-butylthio side chain of Cys residue at the C terminus was reduced with 10% (w/v) DTT and 2.5% (v/v) DIPEA in dimethylformamide overnight. The resin was washed 6 times with dimethylformamide, followed by 3 times with dimethylformamide:H₂O (3 : 2) prior to cyclization in 0.1 M NaHCO₃ in dimethylformamide:H₂O (3 : 2) for 72 h. After washing with dimethylformamide:H₂O extensively (to remove NaCl), followed by washing 3 times with dimethylformamide, the Fmoc protecting group at the N terminus was removed with 20% (v/v) piperidine in dimethylformamide for 30 min. N-acetylation was then carried out with 10 equiv acetic anhydride and 15 equiv DIPEA in dimethylformamide for 3 h. The crude cyclic peptide was cleaved from the resin with a solution containing 92.5% (v/v) TFA and scavengers containing 2.5% (v/v) TIPS, 2.5% (v/v) dimethoxybenzene and 2.5% (v/v) DODT. After cleavage, the cyclic peptide was precipitated with cold diethyl ether twice and dissolved in a 1 : 1 water:acetonitrile (H₂O: MeCN) mixture prior to lyophilization. All reactions were carried out at room temperature.

Synthesis of analogue CP2 was carried out according to Scheme S1. About 0.1 mmol (1 equiv) of the first residue Fmoc- β -alanine-OH was loaded to 0.2 mmol of preswelled

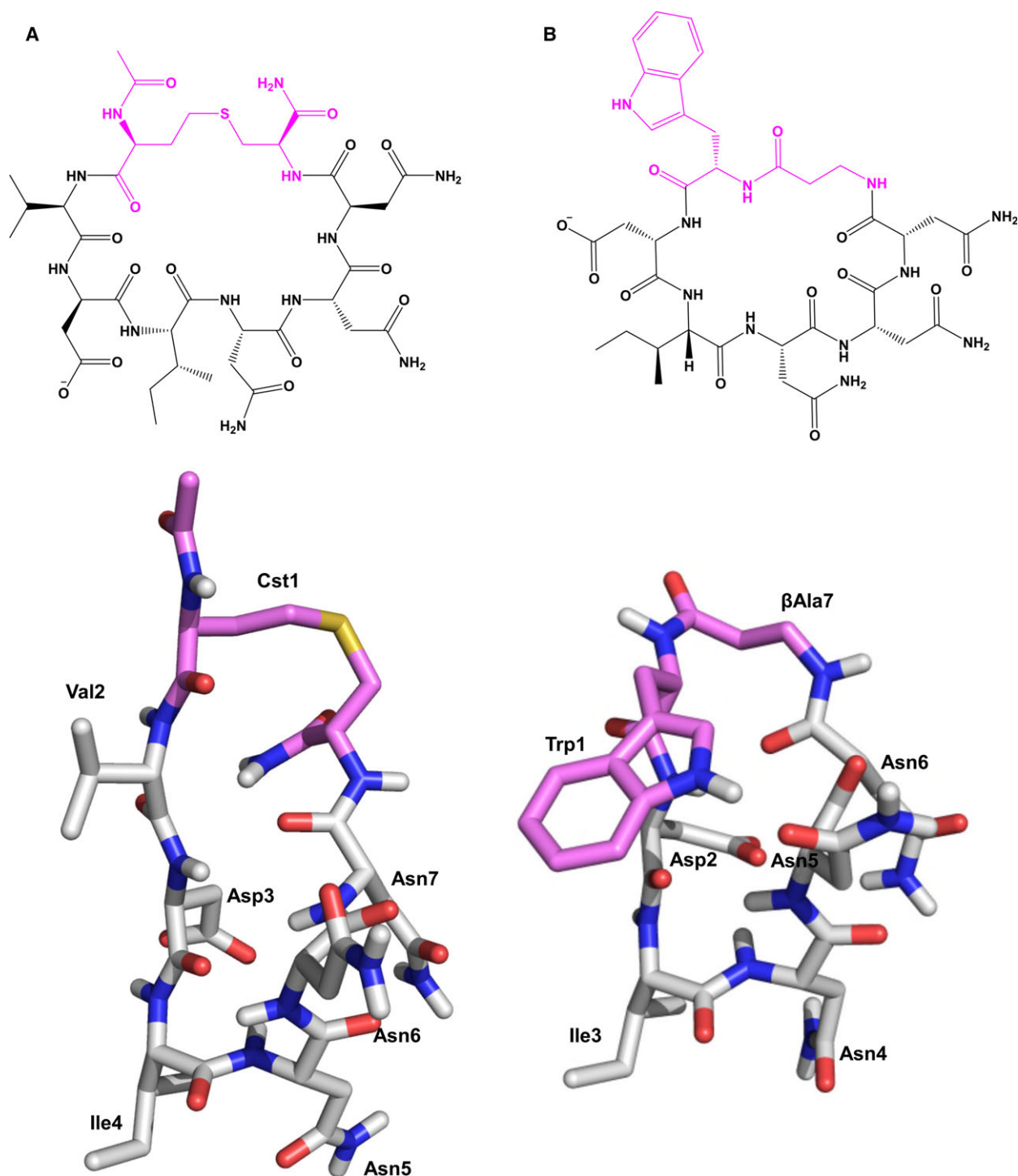


Fig. 1. Chemical structures (upper panel) and *in silico* models (bottom panel) of cyclic peptide analogues. (A) CP1, the cystathionine analogue of Ac-c[CVDINNNC]-NH₂ and (B) CP2, the lactam-bridge-cyclized peptide c[WDINNNβA]. The linker joining the N- and C termini of DINNN linear peptide is highlighted in purple.

2-chlorotrityl resin (1.2 mmol·g⁻¹ loading) for 1 h in 5 equiv DIPEA in DCM. The resin was further reacted with 0.8 mL·g⁻¹ resin of methanol for 30 min to cap remaining

uncoupled resin. After washing the resin 3 times each with DCM and dimethylformamide, the resin was subjected to SPPS, in which subsequent amino acid residues were assem-

bled on the resin under the activation of 0.3 mmol (3 equiv) HCTU and 0.6 mmol (6 equiv) DIPEA in dimethylformamide. Double coupling was used to couple the second Asn to the first Asn as well as the third Asn to the second Asn. The Fmoc protecting group at the N terminus was removed with 20% (v/v) piperidine in dimethylformamide for 30 min. The resin was then washed 3 times each with dimethylformamide, methanol and diethyl ether and dried under vacuum. Cleavage of the side chain-protected linear peptide from the resin was carried out with 30% (v/v) HFIP in DCM for 30 min twice and the cleaved peptide was pooled and dried under a stream of nitrogen (N_2) gas. The cleaved peptide was redissolved in $H_2O:MeCN$ (1 : 9) and lyophilized. Cyclization was carried out in solution at a concentration of $0.5\text{ mg}\cdot\text{mL}^{-1}$ overnight with 3 equiv of HCTU and 6 equiv of DIPEA in dimethylformamide. The crude cyclic peptide was dried under vacuum and the side chain protecting groups were cleaved from the cyclic peptide with a cleavage cocktail solution containing 95% (v/v) TFA and scavengers 2.5% (v/v) TIPS and 2.5% (v/v) DODT. After cleavage, the cyclic peptide was precipitated with cold diethyl ether twice and dissolved in a $H_2O:MeCN$ (1 : 1) mixture prior to lyophilization. All reactions were carried out at room temperature.

The crude peptides CP1 and CP2 were purified by reverse-phase HPLC on a Phenomenex[®] Luna C18 (2) column (100 Å, 5 µm, 100 × 10 mm) using a gradient of 20–50% B (A: 99.9% H_2O , 0.1% TFA; B: 80% MeCN, 19.9% H_2O , 0.1% TFA) over 30–60 min. The purity and molecular mass of the synthesized cyclic peptides were confirmed with LC-MS on a Shimadzu LCMS2020 instrument (Shimadzu Corporation, Kyoto, Japan), incorporating a Phenomenex[®] Luna C8 column (100 Å, 3 µm, 100 × 2 mm, Phenomenex, Torrance, CA, USA) using a linear gradient of 100% H_2O (0.05% TFA) for 4 min, followed by 0–60% MeCN (0.05% TFA) in water over 10 min at a flow rate of $0.2\text{ mL}\cdot\text{min}^{-1}$.

SPSB2 protein expression and purification

The expression and purification of SPSB2 were carried out as described previously [3]. The protein concentration was determined *via* absorbance at 280 nm with a NanoDrop[®] spectrophotometer (Thermo Scientific, Wilmington, DE, USA). 5-F-Trp-labelled SPSB2 (5-F-Trp SPSB2) was prepared as described by Leung *et al.* [12].

NMR spectroscopy

To determine NMR assignments for both CP1 and CP2, the cyclic peptides were dissolved in water at pH 4.8 with 10% 2H_2O . All NMR experiments were recorded on a Bruker Avance 600 MHz spectrometer, equipped with a 5-mm TCI cryoprobe. Homonuclear 2D spectra were recorded at 10 and 25 °C for CP1 and CP2, respectively, where the peaks are best resolved (Figs S7–S8). A 2D TOCSY spec-

trum was acquired using the DIPSI-2 pulse sequence [13] with excitation sculpting for water suppression [14], a spin-lock time of 70 ms and a relaxation delay of 1.3 s. 2D ROESY spectra [15,16] with WATERGATE [17,18] for water suppression were collected with a 300 ms mixing time and relaxation delay of 3 s. 2D DQF-COSY spectra [19] were acquired with a relaxation delay of 1.3 s. For carbon and nitrogen chemical shift assignments, $[^1H,^{13}C]$ -HSQC (256 × 2048) and $[^1H,^{15}N]$ -SOFAST HMQC (64 × 2048) spectra [20] were acquired. For all these spectra, a sine-bell squared window function was used for processing. All spectra were processed using BRUKER TOPSPIN (version 3.2, Bruker Corporation, Billerica, MA, USA) and analysed using CCPNMR-ANALYSIS (version 2.1.5, University of Cambridge, Cambridge, UK). 1H chemical shifts were referenced to 3-trimethylsilyl-1-propanesulfonic acid sodium sulfate (DSS), while ^{13}C and ^{15}N chemical shifts were referenced indirectly through their gyromagnetic ratios [21]. The chemical shift assignments are summarized in Figs S3 and S6 and accessible at the BioMag ResBank (BMRB) website (CP1, BMRB ID: 26676; CP2, BMRB ID: 26677). ^{19}F NMR experiments of 50 µM 5-F-Trp SPSB2 in 50 mM sodium phosphate buffer, pH 7.4 and 50 mM NaCl were recorded at 30 °C in the presence and absence of 75 µM peptide. ^{19}F NMR chemical shifts were referenced against 0.005% trifluoroethanol. All spectra were processed using an exponential window function with line broadening of 40 Hz.

Surface plasmon resonance

SPR experiments were carried out at 25 °C on a Biacore[™] T200 (GE Healthcare Life Sciences, Pittsburgh, PA, USA). Immobilization was carried out *via* standard amine coupling on a CM5 sensor chip as described in Yap *et al.* [3]. The binding of all cyclic peptides, CP0, CP1, CP1_{ox} and CP2 was investigated in 10 mM HEPES, 150 mM NaCl, 3 mM EDTA and 0.05% (v/v) Tween 20, pH 7.4. The cyclic peptides were injected onto the surface with a contact time of 60–100 s, flow rate of $100\text{ }\mu\text{L}\cdot\text{min}^{-1}$ and dissociation time of 600 s. The double-referenced sensorgrams were fitted to a steady-state 1 : 1 binding model with BIACORE T200 EVALUATION software (version 2.0, GE Healthcare Life Sciences) and K_D , k_{on} and k_{off} were estimated. Differences between the K_D of each analogue were determined using one-way ANOVA and Tukey's multiple comparison test in GRAPHPAD PRISM (version 6.05, GraphPad Software, Inc., La Jolla, CA, USA). Cyclic peptide concentrations were determined using a Direct Detect[®] spectrometer (Merck Millipore, Darmstadt, Germany).

Redox stability assays

For reduction assays, cyclic peptides CP0 (synthesized according to method described by Yap *et al.* [3]), CP1 and

CP2 were incubated in 0.1 M ammonium bicarbonate, pH 7.4, at 37 °C at a final peptide concentration of 0.5 mg·mL⁻¹ for 30 min in the presence of 5 mM TCEP.HCl. At time 0 and 30 min, 30 µL samples were collected and 5 µL aliquots were injected and analysed immediately by LC-MS. For oxidation experiments, both CP1 and CP2 were incubated in 0.1 M ammonium bicarbonate, pH 7.4, at 37 °C at a final peptide concentration of 0.5 mg·mL⁻¹ for 5 h in the presence of 10 mM H₂O₂. At time 0, 20 min, 1 h, 3 h and 5 h, 30 µL samples were collected and 5 µL aliquots were injected and analysed immediately by LC-MS. In both experiments, LC-MS analyses were carried out on a Shimadzu LCMS2020 instrument incorporating a Phenomenex[®] Luna C8 column (100 Å, 3 µm, 100 × 2 mm) and using a linear gradient of 100% H₂O (0.05% TFA) for 4 min, followed by 0–60% MeCN (0.05% TFA) in water over 10 min at a flow rate of 0.2 mL·min⁻¹.

Cell lysate assays

Murine BMDM cells were derived by culture of whole bone marrow of C57BL/6 mice in Dulbecco's modified Eagle's medium supplemented with 100 U·mL⁻¹ penicillin, 0.1 mg·mL⁻¹ streptomycin, 10% (v/v) foetal bovine serum and 20% (v/v) L-cell conditioned medium as a source of macrophage colony-stimulating factor [22]. Cells were cultured for 5 days prior to replating and incubation with 10 ng·mL⁻¹ murine interferon-gamma (IFN-γ) and 20 ng·mL⁻¹ *Salmonella minnesota*-derived lipopolysaccharide (LPS) overnight at 37 °C. Cells were lysed in kinase assay lysis buffer [23] containing Roche's cOmplete Protease Inhibitor Cocktail and 1 mM phenylmethylsulfonyl fluoride on ice for 30 min. The cell lysates were incubated with 2.5 µg·mL⁻¹ recombinantly expressed GST (as a negative control), or GST-tagged SPSB2-SPRY domain, in the absence and presence of 10 µM cyclic peptide for 2 h. The SPSB2-iNOS protein complexes were recovered from the cell lysate *via* incubation with glutathione-Sepharose 4B beads (GE Healthcare Life Sciences) for 1 h. Proteins were separated by SDS/PAGE under reducing conditions and electrophoretically transferred to nitrocellulose membranes (Merck Millipore, Darmstadt, Germany). Membranes were blocked overnight in 10% (w/v) skim milk and incubated with mouse monoclonal anti-iNOS or anti-GST primary antibodies (BD Biosciences, Franklin Lakes, NJ, USA) for 2 h. Antibody binding was visualized with peroxidase-conjugated sheep anti-mouse Ig antibody (GE Healthcare Life Sciences) and the ECL system (GE Healthcare Life Sciences).

Results and Discussion

Two redox-stable cyclic peptides containing the DINNN motif required for SPSB2 binding were designed and synthesized, one with a thioether bridge,

CP1, and the other with a lactam bridge between the N- and C termini of the DINNN linear motif, CP2. In the design of CP2, different numbers of β-Ala and L-Ala residues were incorporated between the N- and C termini of the DINNN sequence in order to determine the effect of different linker lengths on the overall conformation of the cyclic peptide models. Models were generated with the Biopolymer module of SYBYL[®]-X (version 2.0, Tripos International, St. Louis, MO, USA) and energy minimized with restraints using MAESTRO (version 10.3, Schrödinger, New York, NY, USA). This study showed that the cyclic peptide sequence c[ADINNNβA] could be accommodated within the binding site with a backbone root-mean-square deviation (RMSD) of 0.22 Å to the crystal structure of the DINNN linear peptide bound to SPSB2 and with no violation of dihedral angles in the Ramachandran plot [24] (Fig. S9). Substitution of the Ala residue of c[ADINNNβA] with other amino acid residues did not cause significant changes in the overall conformation of the models, with the backbone RMSD between the models and the crystal structure of SPSB2-bound DINNN linear peptide remaining in the range 0.22–0.34 Å. Furthermore, rigid docking of these models with SPSB2 using GLIDE SP (version 5.8, Schrödinger) suggested no steric clashes between the iNOS binding site of SPSB2 and the side chains of 19 other common amino acid residues replacing Ala in c[ADINNNβA], indicating that the nature of this residue is not essential. To enable easier quantification of this analogue for further studies and to improve its overall hydrophobicity, an analogue with Trp was selected for synthesis. The cyclic peptide c[WDINNNβA] (CP2) (Fig. 1B) was selected over analogues containing Tyr and Phe in place of Trp because CP2 had an additional hydrogen bond between the Trp indole NH and the side chain amide of the second Asn of the cyclic peptide c[WDINNNβA] (Fig. S10). CP2 was therefore synthesized by SPPS, and its identity and purity were confirmed by LC-MS and NMR.

The binding of cyclic peptide analogues CP1 and CP2 to SPSB2 was investigated by SPR and ¹⁹F NMR. SPR experiments on CP1 and CP2 (Fig. 2) revealed a ~ 5-fold ($P < 0.05$) and ~ 3-fold ($P > 0.05$) decrease in binding affinity to SPSB2 in CP1 ($K_D \approx 31$ nM) and CP2 ($K_D \approx 21$ nM), respectively, compared to CP0 ($K_D \approx 6$ nM). ¹⁹F NMR experiments were carried out on 5-F-Trp SPSB2 as described by Leung *et al.* [12] The ¹⁹F resonance corresponding to Trp207, a key residue in the iNOS binding site of SPSB2, is expected to be shifted significantly downfield when the peptide is bound in the correct pose in the iNOS binding site. Consistent with our previous observations [3], addition of CP0

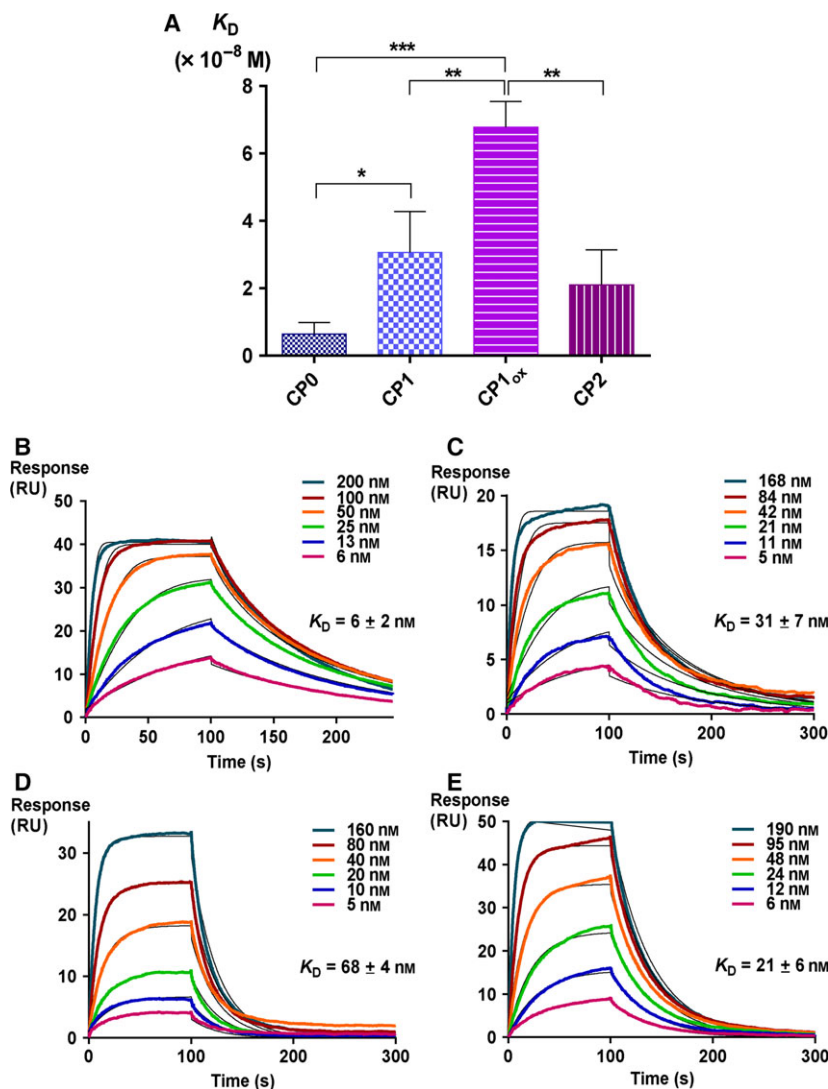


Fig. 2. Cyclic peptide analogues CP1, CP1_{ox} and CP2 bind to the iNOS binding site of SPSB2 with low nanomolar affinities. (A) The binding constant, K_D , of CP0, CP1, CP1_{ox} and CP2 measured from double-referenced subtracted SPR sensorgrams fitted to a steady-state 1 : 1 interaction model from three independent runs ($n = 3$), indicated as mean \pm standard error of the mean. The statistical significance difference between the calculated K_D of each cyclic peptide as determined using one-way ANOVA and Tukey's multiple comparison test in GraphPad Prism (version 6.05) was represented by * $P < 0.05$, ** $P < 0.01$ and *** $P < 0.001$. Representative SPR sensorgrams of immobilized SPSB2 exposed to increasing concentrations of (B) CP0, (C) CP1, (D) CP1_{ox} and (E) CP2 in 10 mM HEPES, 150 mM NaCl, 3 mM EDTA and 0.05% Tween 20, pH 7.4 at 25 °C. The data were fitted using a single-site binding model.

caused a significant downfield shift of the ^{19}F resonance from Trp207 (Fig. 3A). Smaller shifts were also observed in three other ^{19}F resonances (at -43 to -45 ppm), as observed by Leung *et al.* [12] Addition of 1.5 molar excess of CP1 or CP2 to the protein caused a significant 2.4 ppm downfield shift of the ^{19}F resonance from Trp207, implying that these analogues also bind to the iNOS binding site of SPSB2. Minor shifts were also observed in the three ^{19}F resonances at -43 to -45 ppm, although the extent of the shift of the most downfield resonance is smaller than the corresponding

shift in the presence of CP0. Intriguingly, the Trp207 peak of SPSB2 in the presence of CP2 is 0.2 ppm further downfield and broader than in the presence of CP0 or CP1, suggesting that there may be some conformational averaging in the vicinity of Trp207 in the complex between CP2 and 5-F-Trp SPSB2. A slightly faster k_{off} as measured by SPR, for the interaction between CP2 and SPSB2 ($k_{\text{off}} \approx 0.04 \text{ s}^{-1}$) compared to CP0- or CP1-SPSB2 ($k_{\text{off}} \approx 0.02 \text{ s}^{-1}$) (Table 1) supports this notion, although further work would be required to confirm this correlation.

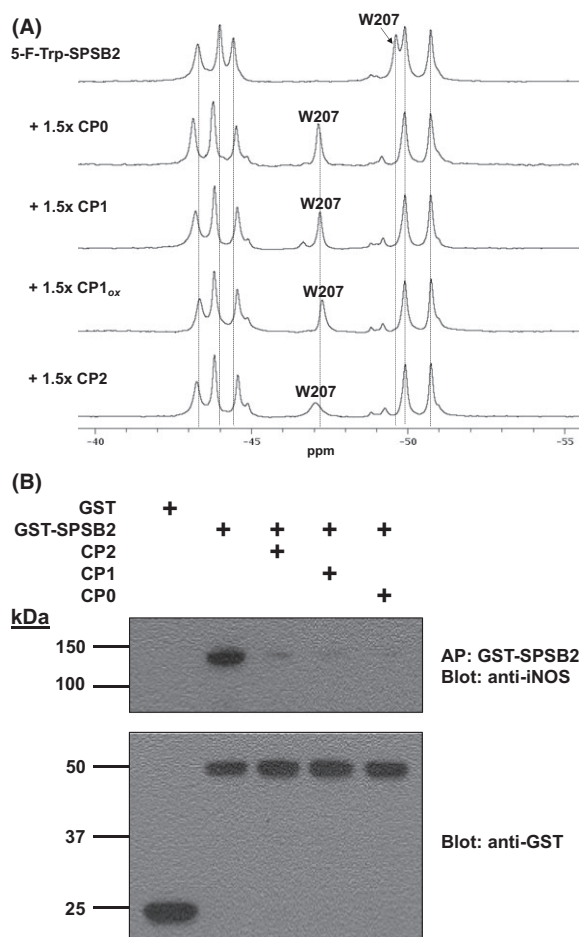


Fig. 3. CP1 and CP2 bind to the iNOS binding site of SPSB2 and are able to compete with full-length iNOS for binding to SPSB2 in macrophage cell lysate. (A) ^{19}F NMR spectra of 5-F-Trp SPSB2 in the absence (most upper panel) and presence of 1.5-fold cyclic peptide Ac-c[CVDINNNC]-NH₂ (CP0), its cystathionine analogue, CP1, and its oxidized product, CP1_{ox} and lactam-bridge-cyclized peptide analogue, CP2, in 50 mM sodium phosphate buffer, pH 7.4 and 50 mM NaCl at 30 °C. The resonance of the Trp residue closest to the iNOS peptide binding site, Trp207, is labelled. (B) Cell lysates from LPS/IFN- γ -stimulated BMDM were incubated with GST (as a negative control) or GST-SPSB2-SPRY domain in the presence (+) or absence of cyclic peptides CP0–CP2. GST-fusion proteins were recovered by affinity purification (AP) using glutathione–Sepharose and the interaction with iNOS was analysed by western blotting with either anti-iNOS antibody (upper panel) or anti-GST antibody (lower panel).

The ability of the cyclic peptide analogues to compete with full-length iNOS for binding to SPSB2 in a more physiological setting was also investigated. A GST-based affinity purification assay was carried out on murine BMDM cell lysates. GST-SPSB2-SPRY domain, with and without the cyclic peptide analogues, was added to the cell lysates containing endogenous iNOS (induced in response to LPS and IFN- γ) and

Table 1. The binding kinetics (K_D , k_{on} and k_{off}) \pm standard error of the mean (SEM) of the cyclic peptide CP0–CP2 estimated from the reference-subtracted SPR sensorgrams fitted to a steady-state 1 : 1 interaction model.

Cyclic peptide	K_D (nM)	k_{on} ($\times 10^6 \text{ M}^{-1}\cdot\text{s}^{-1}$)	k_{off} (s^{-1})
CP0	6 ± 2	3.37 ± 0.54	0.020 ± 0.003
CP1	31 ± 7	1.07 ± 0.62	0.024 ± 0.008
CP2	21 ± 6	2.63 ± 1.16	0.043 ± 0.001

recovered using glutathione–Sepharose beads. Western blotting with anti-iNOS antibodies indicated that both CP1 and CP2 (at 10 μM peptide concentration) were able to compete with full-length iNOS for binding to the SPSB2 protein (Fig. 3B), as was observed for the disulphide-bridged cyclic peptide CP0, although the extent of inhibition is slightly stronger for CP1 than CP2. Similar inhibition was also observed for the 13-residue linear peptide from the disordered N-terminal region of iNOS ($K_D \approx 13 \text{ nM}$) at 1–10 μM peptide concentration [1].

The stabilities of the cyclic peptide analogues CP1 and CP2 in both reducing and oxidizing environments were also investigated. When both CP1 and CP2 were incubated in 0.1 M ammonium bicarbonate buffer, pH 7.4 and 5 mM TCEP.HCl at 37 °C for 30 min, no significant changes were observed in the concentrations of the cyclic peptide in the reactions mixture (as estimated from the \log_{10} peak area of the HPLC peak at 214 nm) after 30 min in reducing buffer, indicating that both analogues were resistant to reduction under these conditions (Fig. 4A). In contrast, the disulphide-bridged cyclic peptide Ac-c[CVDINNNC]-NH₂ (CP0) was completely reduced to Ac-CVDINNNC-NH₂ (CP0_{red}) under the same conditions and a peak with a mass increase of + 2 Da from 933 to 935 Da was observed in the LC-MS (Fig. S11), consistent with the previous observation by Yap *et al.* [3] While it was expected that both CP1 and CP2 would be reductively stable, it was possible that CP1 might be susceptible to oxidation as it is known that thioether bridges can be oxidized to sulfoxides [5,6]. Thus, both CP1 and CP2 were incubated in 0.1 M ammonium bicarbonate buffer, pH 7.4, at 37 °C for 5 h in the presence of 10 mM H₂O₂, a level that has been reported during acute oxidative bursts in phagocytes [25]. More than 50% of an oxidized peak (CP1_{ox}) with an additional mass of + 16 Da relative to CP1 was observed after 5 h of incubation in the oxidizing buffer (Fig. S12), while no oxidation of CP2 was observed in the same environment (Fig. 4B), indicating that CP2 is more stable to oxidation than CP1 under these conditions. To assess the ability of oxidized CP1 to bind to SPSB2, CP1_{ox}

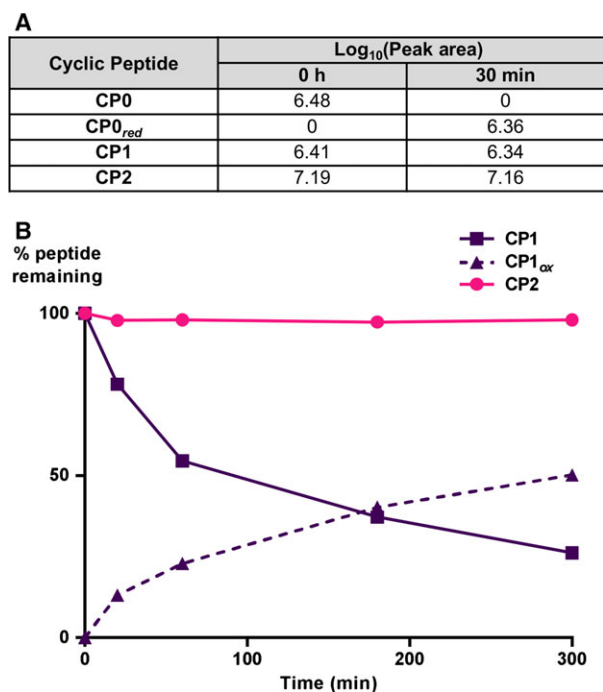


Fig. 4. Redox stability of cyclic peptide analogues. (A) Amount of cyclic peptide remaining based on the log₁₀ peak area determined by HPLC after treatment with 5 mM TCEP.HCl in degassed 0.1 M ammonium bicarbonate buffer, pH 7.4 at 37 °C (B) % cyclic peptides remaining after treatment with 10 mM H₂O₂ in 0.1 M ammonium bicarbonate buffer, pH 7.4 at 37 °C.

was purified and the binding to SPSB2 was measured. SPR revealed a ~2-fold drop in CP1_{ox} binding affinity to SPSB2 ($P < 0.01$) compared to CP1, with measured K_D of 68 nM (Fig. 2D), and ¹⁹F NMR experiments confirmed its binding to the iNOS binding site on the SPSB2 protein (Fig. 3A).

Conclusions

In summary, we have generated two cyclic peptide analogues that are reduction-resistant, with CP2 being more oxidatively stable than CP1. Both cyclic peptide analogues, as well as the oxidized product of the cystathionine analogue were able to bind to the iNOS binding site of SPSB2 with reasonably strong affinities, with the K_D of the most potent analogue, CP2 (21 nM) being comparable to that reported for the 13-residue iNOS linear peptide. Both CP1 and CP2 were also able to compete with full-length iNOS for binding to SPSB2 in macrophage cell lysates. As it is important to know if these cyclic peptide analogues also have similar effects in whole cells, our current efforts are focused on their delivery to the cytoplasm of macrophages. This study thus provides a foundation for the future development

of a redox-stable, potent drug candidate targeting SPSB proteins as a potential novel class of anti-infectives.

Acknowledgements

BKY is the recipient of the Academic Staff Training Scheme Fellowship of Universiti Sains Malaysia. RSN and JBB acknowledge fellowship support from the National Health and Medical Research Council of Australia. This study was supported in part by the Australian National Health Medical Research Council (NHMRC) (Grants 1022693 and 1016647), as well as an NHMRC IRISS grant 361646 and a Victorian State Government Operational Infrastructure Scheme grant. The authors declare no competing financial interest.

Author contributions

BKY, EWWL, JRH and SEN designed and performed the experiments, and analysed the data. BKY and RSN wrote the manuscript with input from JBB, MJS, DKC and PET.

References

- Kuang Z, Lewis RS, Curtis JM, Zhan Y, Saunders BM, Babon JJ, Kolesnik TB, Low A, Masters SL, Willson TA *et al.* (2010) The SPRY domain-containing SOCS box protein SPSB2 targets iNOS for proteasomal degradation. *J Cell Biol* **190**, 129–141.
- Filippakopoulos P, Low A, Sharpe TD, Uppenberg J, Yao S, Kuang Z, Savitsky P, Lewis RS, Nicholson SE, Norton RS *et al.* (2010) Structural basis for Par-4 recognition by the SPRY domain- and SOCS box-containing proteins SPSB1, SPSB2, and SPSB4. *J Mol Biol* **401**, 389–402.
- Yap BK, Leung EW, Yagi H, Galea CA, Chhabra S, Chalmers DK, Nicholson SE, Thompson PE and Norton RS (2014) A potent cyclic peptide targeting SPSB2 protein as a potential anti-infective agent. *J Med Chem* **57**, 7006–7015.
- Wouters MA, Fan SW and Haworth NL (2010) Disulfides as redox switches: from molecular mechanisms to functional significance. *Antioxid Redox Signal* **12**, 53–91.
- Knerer PJ, Tzekou A, Ricklin D, Qu H, Chen H, van der Donk WA and Lambris JD (2011) Synthesis and activity of thioether-containing analogues of the complement inhibitor compstatin. *ACS Chem Biol* **6**, 753–760.
- Dekan Z, Vetter I, Daly NL, Craik DJ, Lewis RJ and Alewood PF (2011) α -Conotoxin ImI incorporating stable cystathionine bridges maintains full potency and identical three-dimensional structure. *J Am Chem Soc* **133**, 15866–15869.

- 7 Muttenthaler M, Andersson A, de Araujo AD, Dekan Z, Lewis RJ and Alewood PF (2010) Modulating oxytocin activity and plasma stability by disulfide bond engineering. *J Med Chem* **53**, 8585–8596.
- 8 Pulka-Ziach K, Pavet V, Chekkat N, Estieu-Gionnet K, Rohac R, Lechner MC, Smulski CR, Zeder-Lutz G, Altschuh D, Gronemeyer H *et al.* (2015) Thioether analogues of disulfide-bridged cyclic peptides targeting death receptor 5: conformational analysis, dimerisation and consequences for receptor activation. *ChemBioChem* **16**, 293–301.
- 9 van Lierop BJ, Robinson SD, Kompella SN, Belgi A, McArthur JR, Hung A, MacRaid CA, Adams DJ, Norton RS and Robinson AJ (2013) Dicarba α -conotoxin Vc1.1 analogues with differential selectivity for nicotinic acetylcholine and GABAB receptors. *ACS Chem Biol* **8**, 1815–1821.
- 10 MacRaid CA, Illesinghe J, van Lierop BJ, Townsend AL, Chebib M, Livett BG, Robinson AJ and Norton RS (2009) Structure and activity of (2,8)-dicarba-(3,12)-cystino α -ImI, an α -conotoxin containing a nonreducible cystine analogue. *J Med Chem* **52**, 755–762.
- 11 Armishaw CJ, Daly NL, Nevin ST, Adams DJ, Craik DJ and Alewood PF (2006) α -selenoconotoxins, a new class of potent $\alpha 7$ neuronal nicotinic receptor antagonists. *J Biol Chem* **281**, 14136–14143.
- 12 Leung EW, Yagi H, Harjani JR, Mulcair MD, Scanlon MJ, Baell JB and Norton RS (2014) ^{19}F NMR as a probe of ligand interactions with the iNOS binding site of SPRY domain-containing SOCS box protein 2. *Chem Biol Drug Des* **84**, 616–625.
- 13 Shaka AJ, Lee CJ and Pines A (1988) Iterative schemes for bilinear operators; application to spin decoupling. *J Magn Reson (1969)* **77**, 274–293.
- 14 Hwang TL and Shaka AJ (1995) Water suppression that works. Excitation sculpting using arbitrary waveforms and pulsed-field gradients. *J Magn Reson, Series A* **112**, 275–279.
- 15 Bax A and Davis DG (1985) Practical aspects of two-dimensional transverse NOE spectroscopy. *J Magn Reson (1969)* **63**, 207–213.
- 16 Hwang TL and Shaka AJ (1992) Cross relaxation without TOCSY: transverse rotating-frame Overhauser effect spectroscopy. *J Am Chem Soc* **114**, 3157–3159.
- 17 Piotto M, Saudek V and Sklenar V (1992) Gradient-tailored excitation for single-quantum NMR spectroscopy of aqueous solutions. *J Biomol NMR* **2**, 661–665.
- 18 Sklenar V, Piotto M, Leppik R and Saudek V (1993) Gradient-tailored water suppression for ^1H - ^{15}N HSQC experiments optimized to retain full sensitivity. *J Magn Reson, Series A* **102**, 241–245.
- 19 Derome AE and Williamson MP (1990) Rapid-pulsing artifacts in double-quantum-filtered COSY. *J Magn Reson (1969)* **88**, 177–185.
- 20 Schanda P and Brutscher B (2005) Very fast two-dimensional NMR spectroscopy for real-time investigation of dynamic events in proteins on the time scale of seconds. *J Am Chem Soc* **127**, 8014–8015.
- 21 Wishart DS, Bigam CG, Yao J, Abildgaard F, Dyson HJ, Oldfield E, Markley JL and Sykes BD (1995) ^1H , ^{13}C and ^{15}N chemical shift referencing in biomolecular NMR. *J Biomol NMR* **6**, 135–140.
- 22 Wormald S, Zhang JG, Krebs DL, Mielke LA, Silver J, Alexander WS, Speed TP, Nicola NA and Hilton DJ (2006) The comparative roles of suppressor of cytokine signaling-1 and -3 in the inhibition and desensitization of cytokine signaling. *J Biol Chem* **281**, 11135–11143.
- 23 Nicholson SE, Novak U, Ziegler SF and Layton JE (1995) Distinct regions of the granulocyte colony-stimulating factor receptor are required for tyrosine phosphorylation of the signaling molecules JAK2, Stat3, and p42, p44MAPK. *Blood* **86**, 3698–3704.
- 24 Ramachandran GN, Ramakrishnan C and Sasisekharan V (1963) Stereochemistry of polypeptide chain configurations. *J Mol Biol* **7**, 95–99.
- 25 Hampton MB, Kettle AJ and Winterbourn CC (1998) Inside the neutrophil phagosome: oxidants, myeloperoxidase, and bacterial killing. *Blood* **92**, 3007–3017.

Supporting information

Additional Supporting Information may be found online in the supporting information tab for this article:

Scheme S1. Synthesis of lactam-bridge cyclic peptide CP2.

Fig. S1. LC-MS chromatogram and 1D ^1H NMR spectrum of purified CP1.

Fig. S2. 2D NMR spectra of CP1.

Fig. S3. ^1H , ^{13}C and ^{15}N chemical shifts of CP1.

Fig. S4. LC-MS chromatogram and 1D ^1H NMR spectrum of purified CP2.

Fig. S5. 2D NMR spectra of CP2.

Fig. S6. ^1H , ^{13}C and ^{15}N chemical shifts of CP2.

Fig. S7. Temperature-dependence experiments of CP1.

Fig. S8. Temperature-dependence experiments of CP2.

Fig. S9. Rigid docking studies of *in silico* models of c[ADINNN β A] and its analogues on the iNOS binding site of SPSB2.

Fig. S10. *In silico* models of three aromatic analogues of c[ADINNN β A].

Fig. S11. LC-MS profiles of CP0 at time 0 and 30 min postincubation in TCEP.HCl-containing reaction mixture.

Fig. S12. LC-MS profiles of CP1 at time 0 and 5 h postincubation in H_2O_2 -containing reaction mixture.

SUPPORTING INFORMATION

Redox-Stable Cyclic Peptide Inhibitors of the SPSB2-iNOS Interaction

Beow Keat Yap¹, Jitendra R. Harjani¹, Eleanor W.W. Leung¹, Sandra E. Nicholson^{2,3}, Martin J. Scanlon¹, David K. Chalmers¹, Philip E. Thompson¹, Jonathan B. Baell¹ and Raymond S. Norton¹

¹ Medicinal Chemistry, Monash Institute of Pharmaceutical Sciences, Monash University, Parkville 3052, Victoria, Australia

² The Walter and Eliza Hall Institute of Medical Research, Parkville 3052, Victoria, Australia

³ The Department of Medical Biology, University of Melbourne, Parkville, Victoria 3052, Australia

Correspondence

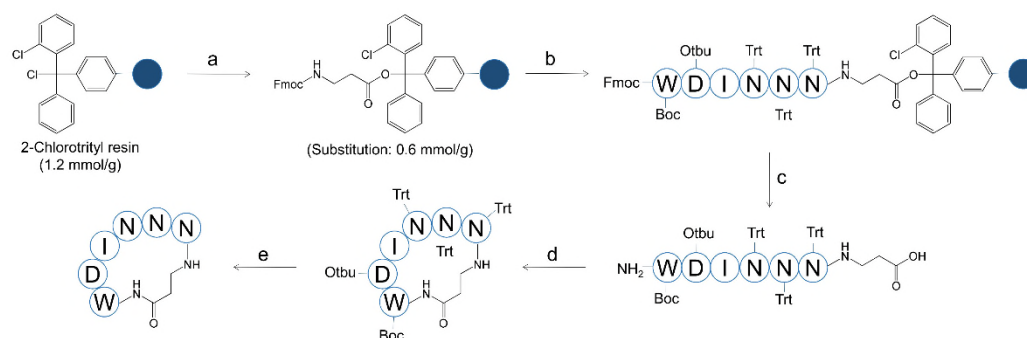
R. S. Norton, Medicinal Chemistry, Monash Institute of Pharmaceutical Sciences, Monash University, Parkville 3052, Victoria, Australia

Fax: +61 3 9903 9582

Tel.: +61 3 9903 9167

E-mail: ray.norton@monash.edu

Scheme S1. Synthesis of lactam-bridge cyclic peptide CP2



^aReagents and conditions: (a) Fmoc-β-Ala-OH (1 equiv), DIPEA (5 equiv), DMF, 60 min; (b) SPPS; (c) 20% (v/v) piperidine, DMF, 30 min; 30% (v/v) HFIP, DCM, 30 min, twice; (d) HCTU (3 equiv), DIPEA (6 equiv), DMF, 16 h; (e) 95% (v/v) TFA, 2.5% (v/v) TIPS, 2.5% (v/v) DODT, 2 h

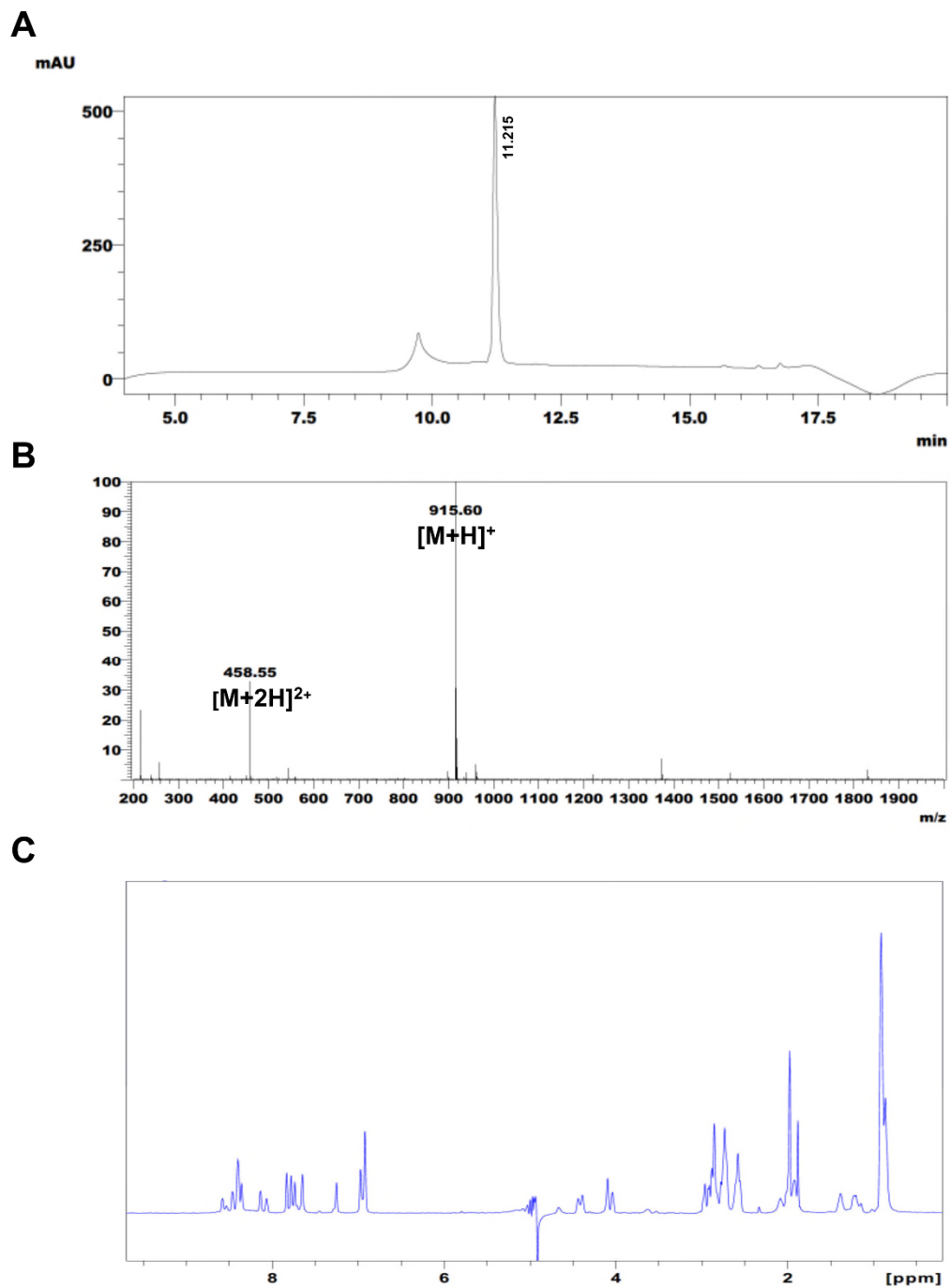


Fig. S1. (A) Liquid-chromatography and (B) mass-spectroscopy profiles of the purified cystathionine analogue of Ac-c[CVDINNNC]-NH₂ (CP1). Purity is ~95%, based on the peak area in the chromatogram. (C) 1D ¹H NMR spectrum of CP1 in water, pH 4.8, acquired at 10 °C on a 600 MHz spectrometer.

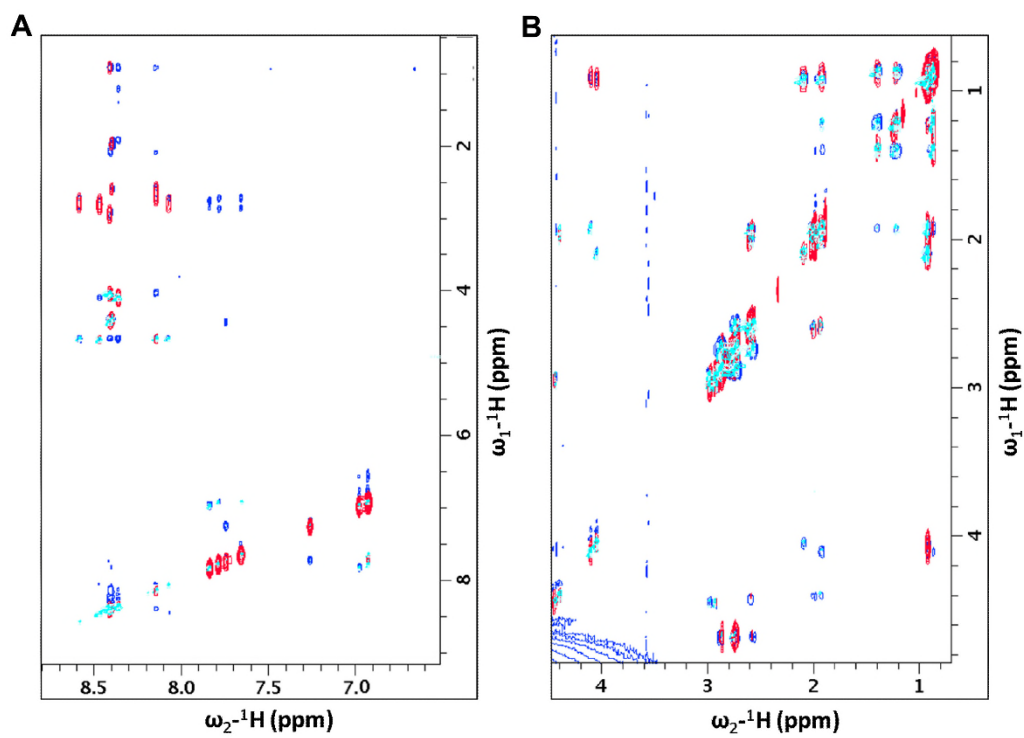
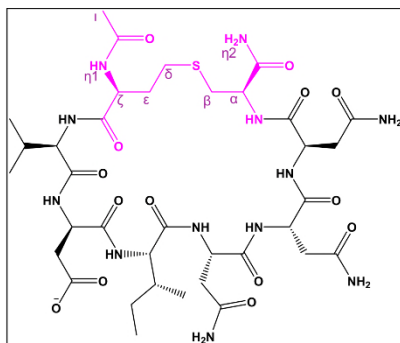


Fig. S2. Overlay of (A) aromatic and (B) aliphatic regions of 2D [$^1\text{H},^1\text{H}$]-TOCSY (red), [$^1\text{H},^1\text{H}$]-ROESY (blue) and [$^1\text{H},^1\text{H}$]-DQF-COSY (cyan) spectra of CP1 in water, pH 4.8, acquired at 10 °C on a 600 MHz spectrometer.



Residue	N	HN	H ^α	C ^α	H ^β	C ^β	Others
	ppm						
Cst1	120.5	8.44	4.47	53.1	2.94, 3.01	32.0	H ^{δ*} 2.63, H ^{ε1} 2.03, H ^{ε2} 1.96, H ^ζ 4.43, H ^{η1} 8.42, H ^{η2a} 7.28, H ^{η2b} 7.76, H ^ι 2.01, C ^δ 27.4, C ^ε 30.7, C ^ζ 52.9, C ^ι 21.5, N ^{η1} 126.7, N ^{η2} 109.4
Val2	122.1	8.43	4.07	60.4	2.12	29.8	H ^{γ1} 0.96, H ^{γ2} 0.94, C ^{γ1} 18.4, C ^{γ2} 17.7
Asp3	122.1	8.17	4.70	50.9	2.60, 2.76	39.3	
Ile4	121.6	8.39	4.13	59.8	1.95	35.6	H ^{γ1a} 1.24, H ^{γ1b} 1.42, H ^{γ2} 0.93, H ^{δ1} 0.90, C ^{γ1} 24.5, C ^{γ2} 14.9, C ^{δ1} 10.9
Asn5	119.6	8.49	4.70	50.9	2.79, 2.89	36.0	H ^{δ1} 7.00, H ^{δ2} 7.85, N ^δ 114.4
Asn6	117.0	8.10	4.70	50.9	2.75, 2.91	35.5	H ^{δ1} 6.95, H ^{δ2} 7.68, N ^δ 113.0
Asn7	118.3	8.61	4.70	50.9	2.76, 2.90	36.6	H ^{δ1} 6.95, H ^{δ2} 7.81, N ^δ 113.7

Fig. S3. (Top) Chemical structure of CP1 with linker residues between *N*- and *C*-terminus of DINNN linear peptide highlighted in purple. **(Bottom)** Chemical shifts of CP1 in water, pH 4.8, at 10 °C on a 600 MHz spectrometer. The atom designation of residue Cst1 is based on the chemical structure shown in the top panel.

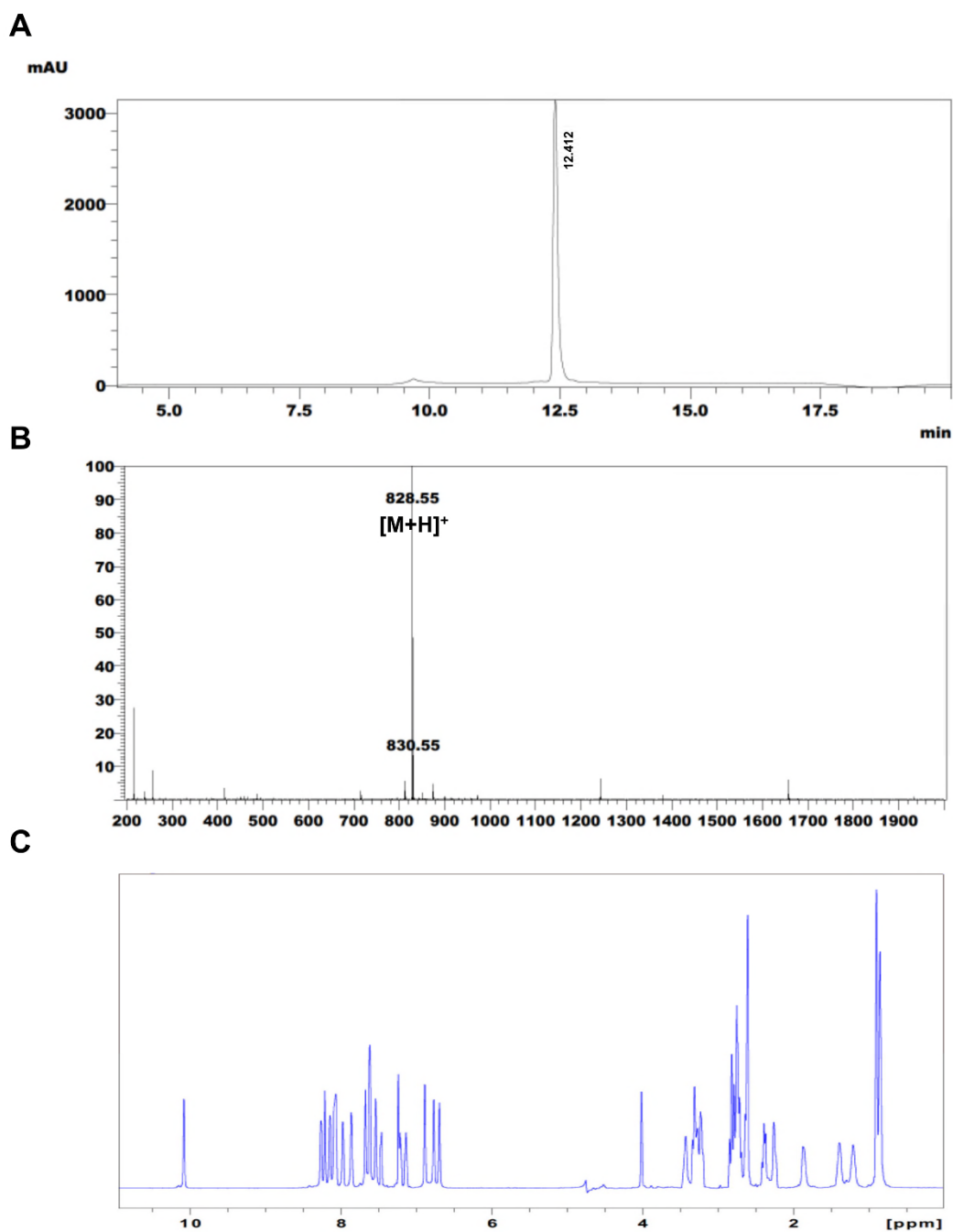


Fig. S4. (A) Liquid-chromatography and (B) mass-spectrometry profiles of the purified lactam-bridged cyclic peptide (CP2). Purity is ~95%, based on the peak area in the chromatogram. (C) 1D 1H spectrum of CP2 in water, pH 4.8, acquired at 25 °C on a 600 MHz spectrometer.

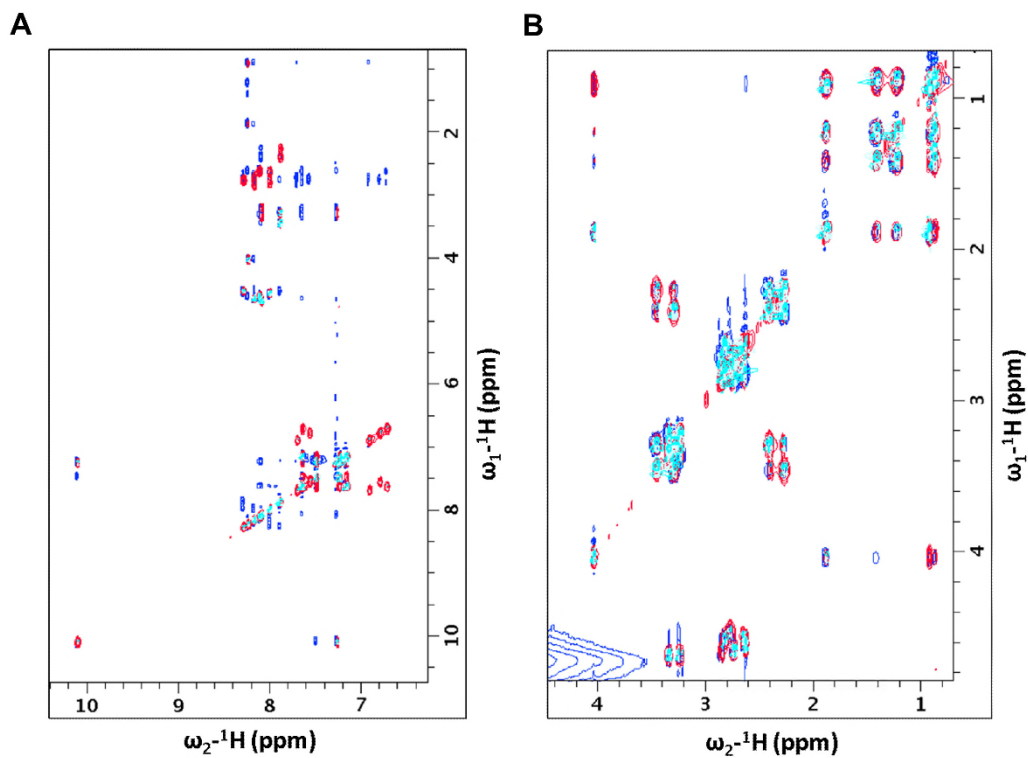
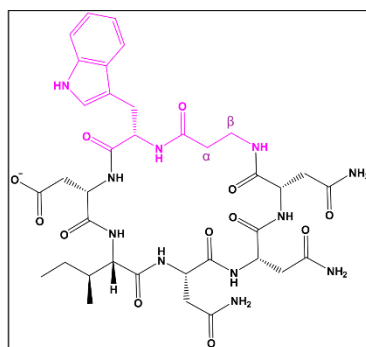


Fig. S5. Overlay of (A) aromatic and (B) aliphatic regions of 2D [$^1\text{H},^1\text{H}$]-TOCSY (red), [$^1\text{H},^1\text{H}$]-ROESY (blue) and [$^1\text{H},^1\text{H}$]-DQF-COSY (cyan) spectra of CP2 in water, pH 4.8, acquired at 25 °C on a 600 MHz spectrometer.



Residue:	N	HN	H ^α	C ^α	H ^β	C ^β	Others
ppm							
Trp1	125.7	8.11	4.70	55.2	3.26, 3.36	26.5	H ^{δ1} 7.28, H ^{ε1} 10.12, H ^{ε3} 7.66, H ^{ζ2} 7.51, H ^{ζ3} 7.19, H ^{η2} 7.26, C ^{δ1} 124.5, C ^{ε3} 118.4, C ^{ζ2} 112.0, C ^{ζ3} 119.4, C ^{η2} 122.1, N ^{ε1} 129.2
Asp2	119.5	8.13	4.65	50.8	2.65	39.0	
Ile3	119.8	8.25	4.06	60.3	1.91	35.8	H ^{γ1a} 1.25, H ^{γ1b} 1.44, H ^{γ2} 0.93, H ^{δ1} 0.90, C ^{γ1} 24.9, C ^{γ2} 14.8, C ^{δ1} 10.9
Asn4	118.2	8.19	4.68	51.2	2.76, 2.87	35.9	H ^{δ1} 6.93, H ^{δ2} 7.72, N ^δ 113.7
Asn5	115.7	8.01	4.60	51.0	2.67, 2.84	35.8	H ^{δ1} 6.74, H ^{δ2} 7.66, N ^δ 113.2
Asn6	117.6	8.30	4.56	51.4	2.66, 2.80	35.9	H ^{δ1} 6.81, H ^{δ2} 7.58, N ^δ 112.6
Bal7	116.7	7.90	2.29, 2.43	35.0	3.32, 3.48	35.9	

Fig. S6. (Top) Chemical structure of CP2 with linker residues between *N*- and *C*-terminus of DINNN linear peptide highlighted in purple. **(Bottom)** Chemical shifts of CP2 in water, pH 4.8, at 25 °C on a 600 MHz spectrometer. The atom designation of residue Bal7 is based on the chemical structure shown in the top panel.

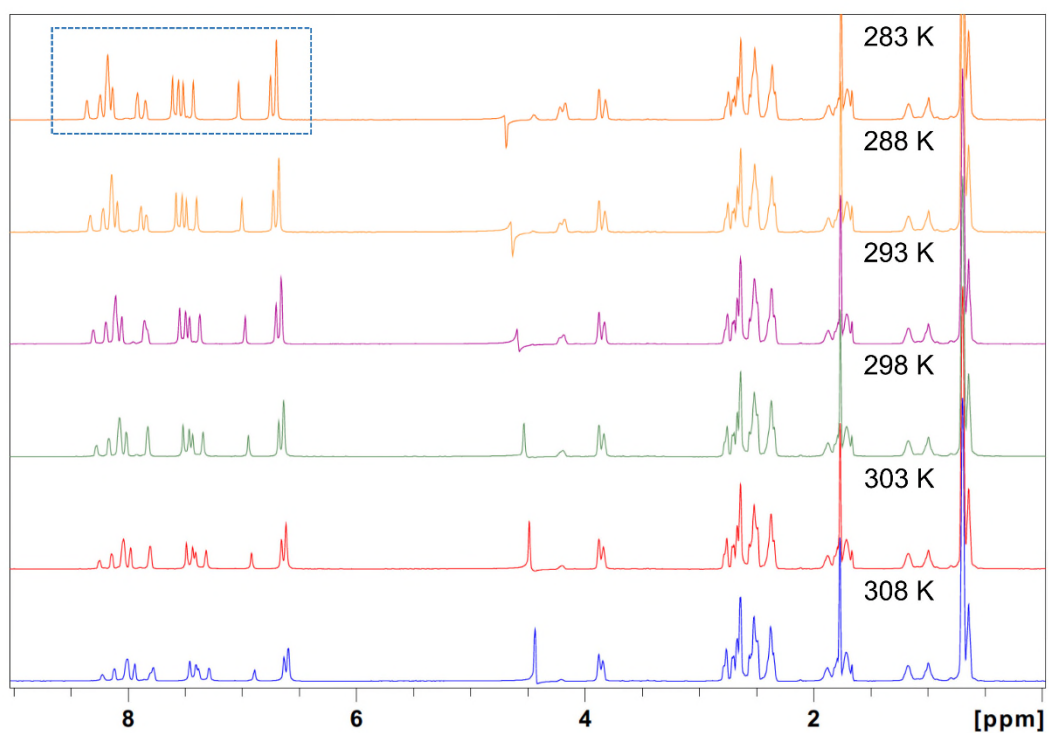


Fig. S7. Temperature-dependence experiments of 700 μM CP1 in 90% $^1\text{H}_2\text{O}$, 10% $^2\text{H}_2\text{O}$, pH 4.8. As an increase in temperature did not improve backbone amide peak resolution (in dotted blue rectangular box) but peak broadening occurred, 2D NMR experiments were recorded at 283 K.

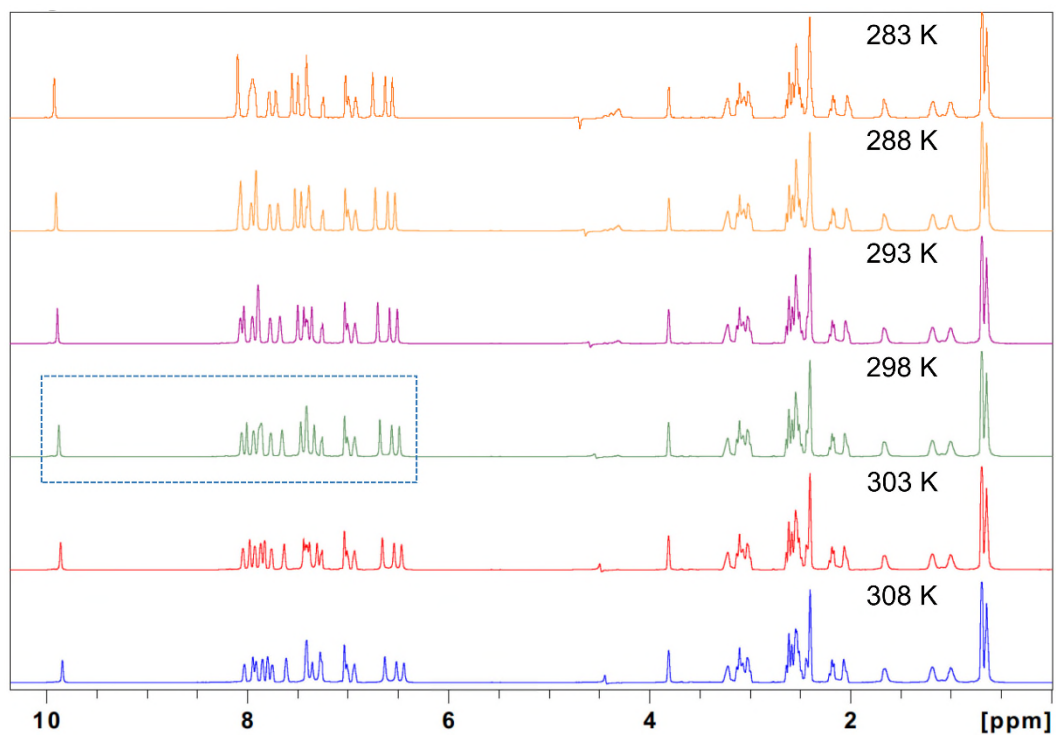


Fig. S8. Temperature-dependence experiments of 1.9 mM CP2 in 90% $^1\text{H}_2\text{O}$, 10% $^2\text{H}_2\text{O}$, pH 4.8 at 283 K to 308 K. As the backbone amide peaks (in dotted blue rectangular box) were better resolved at ≥ 298 K, 2D NMR experiments were recorded at 298 K.

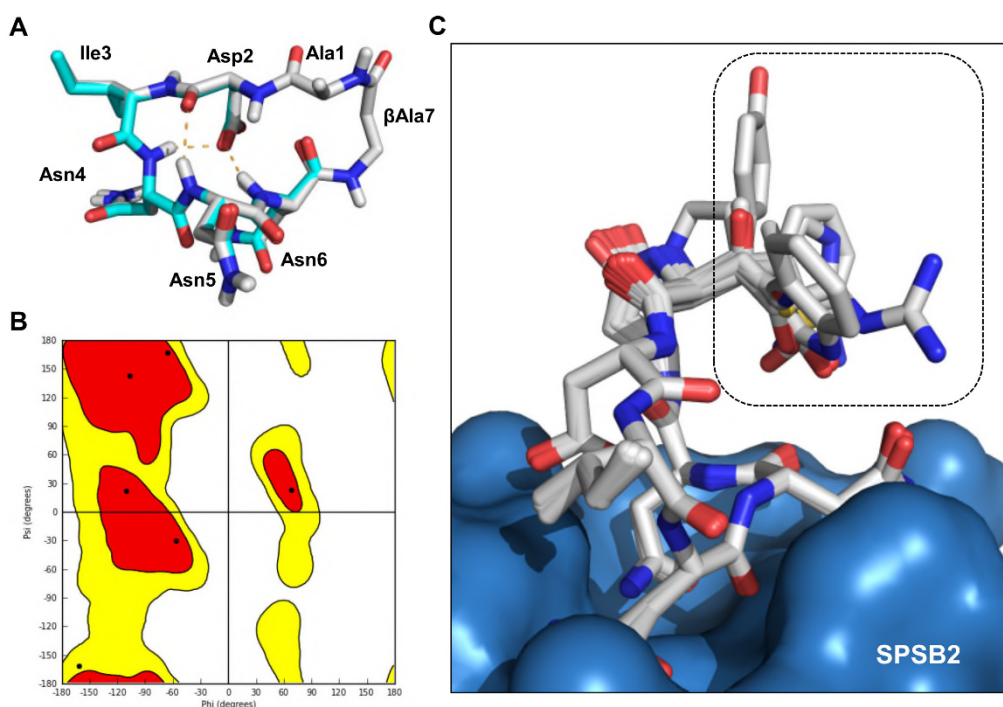


Fig. S9. (A) Overlay of DINNN linear peptide (cyan) and *in silico* model of c[ADINNN β A] (white) with intramolecular hydrogen bonds represented by orange dashes. RMSD between the backbone DINNN of the two peptides is approximately 0.22 Å. (B) Ramachandran Plot of the *in silico* model c[ADINNN β A] suggests no significant problem in the dihedral angles of the modeled amino acid residues. (C) Rigid docking on SPSB2 protein of c[ADINNN β A] analogue with Ala substituted by 19 other amino acid residues revealed no steric clashes between the substituted side chains (rectangular dashed box) and the iNOS binding site of SPSB2.

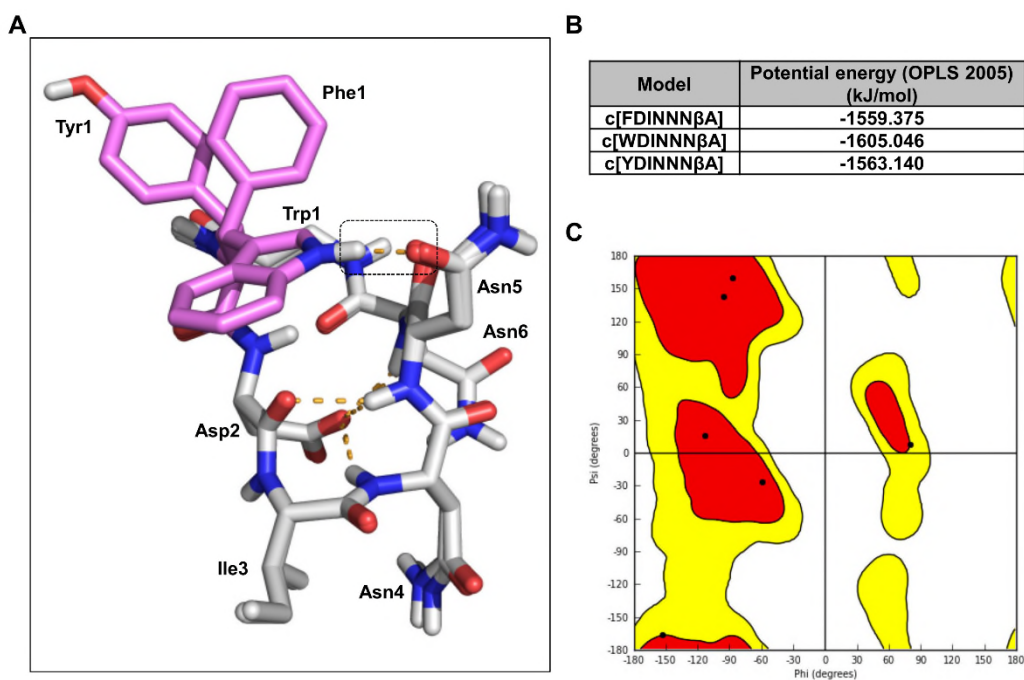


Fig. S10. (A) Overlay of three aromatic analogues of c[ADINNNβA] with the residue replacing Ala in pink and the hydrogen bond between the indole NH of Trp1 and carbonyl oxygen of the amide side chain of Asn5 highlighted in a rectangular dashed box. (B) Potential energy of each analogue as predicted by OPLS 2005 force field. (C) Ramachandran plot of the cyclic peptide analogue c[WDINNNβA] (CP2) suggests no significant problem in the dihedral angles of the modeled amino acid residues.

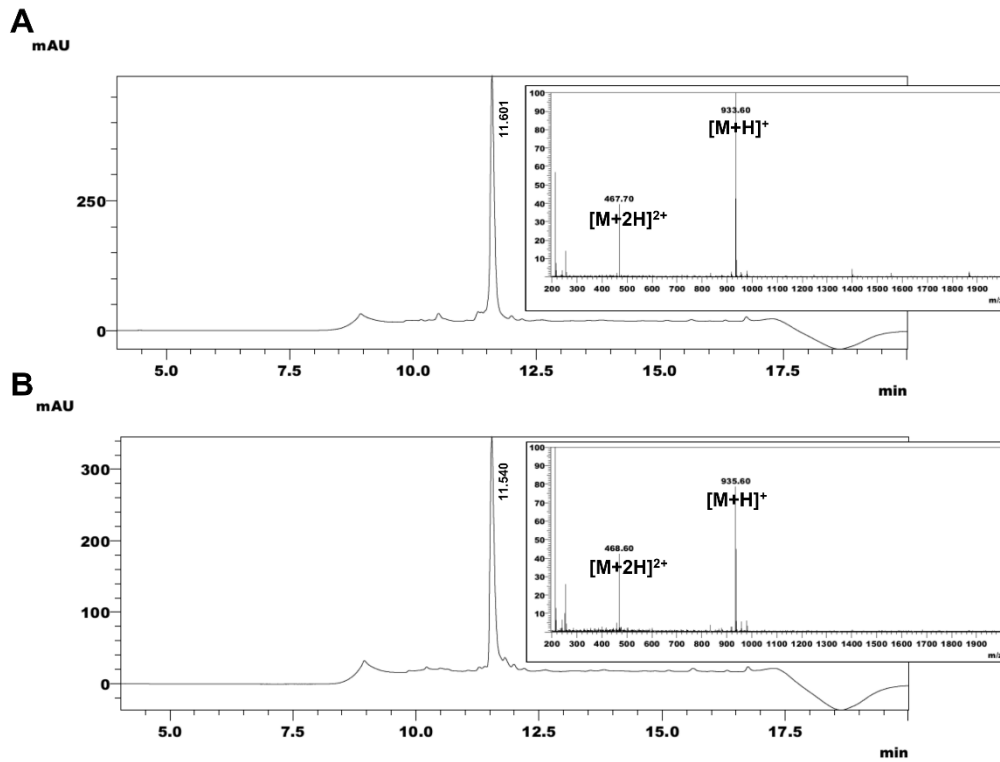


Fig. S11. Liquid-chromatography mass-spectroscopy profiles of CP0 at (A) 0 and (B) 30 min post-incubation with degassed 0.1 M ammonium bicarbonate, pH 7.4, and 5 mM TCEP.HCl. An additional mass of +2 Da was observed in the reduced analogue of CP0 (CP0_{red}).

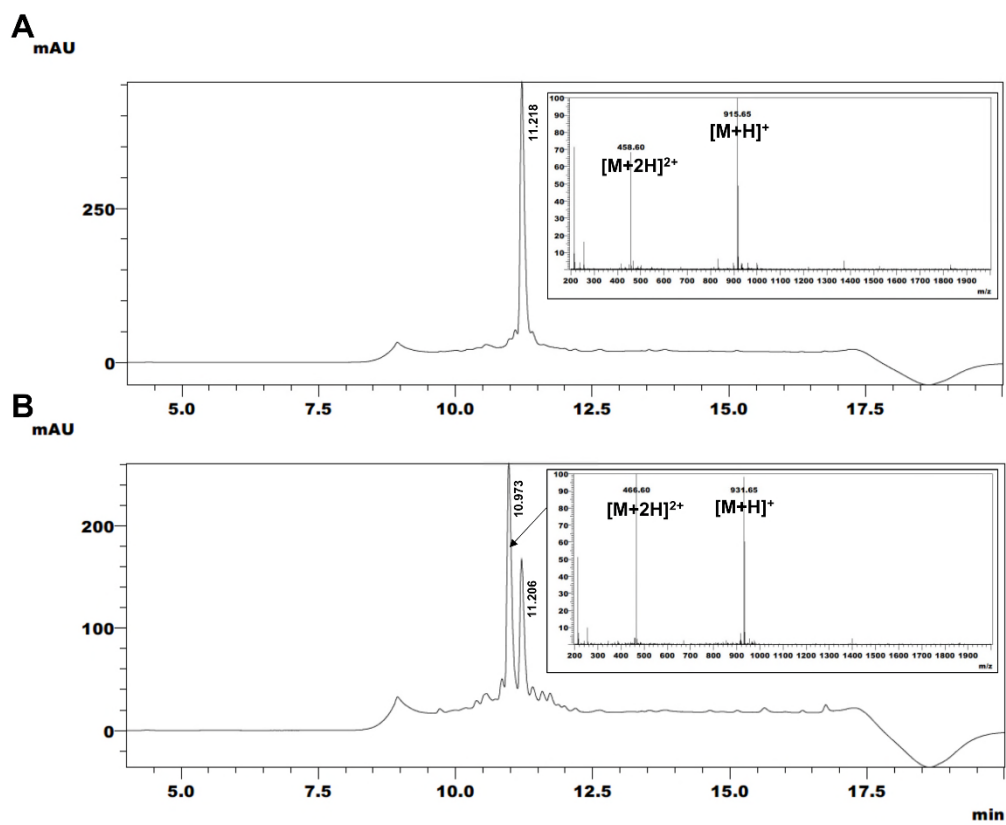


Fig. S12. Liquid-chromatography mass-spectrometry profiles of CP1 at (A) 0 and (B) 5 h post-incubation with 0.1 M ammonium bicarbonate, pH 7.4, and 10 mM H₂O₂. An additional mass of +16 Da was observed in the oxidized analogue of CP1 ($CP1_{ox}$).

CHAPTER 6

Cyclic peptidomimetics targeting SPSB2 as potential anti-infectives agents

6.1 Declaration for Thesis Chapter 6

Declaration by candidate

In the case of **Chapter 6**, the nature and extent of my contribution to the work was the following:

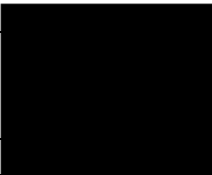
Nature of contribution	Extent of contribution (%)
Designed and performed the experiments, analysed the data and wrote the manuscript.	40

The following co-authors contributed to the work. If co-authors are students at Monash University, the extent of their contribution in percentage terms must be stated:

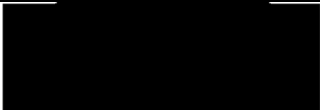
Name	Nature of contribution	Extent of contribution (%) for student co-authors only
Jitendra R. Harjani	Synthesis of mimetic building blocks, manuscript preparation	
Eleanor W.W. Leung	¹⁹ F NMR, ITC	
Andrew Lucke	Molecular dynamics simulations	
Sandra E. Nicholson	BMDM cell lysate inhibition assay	
Martin J. Scanlon	Intellectual input	
David K. Chalmers	Intellectual input	
Philip E. Thompson	Intellectual input	
Raymond S. Norton	Intellectual input, manuscript preparation	
Jonathan B. Baell	Intellectual input, manuscript preparation	

The undersigned hereby certify that the above declaration correctly reflects the nature and extent of the candidate's and co-authors' contributions to this work.

**Candidate's
Signature**

	Date 22/02/2016
---	---------------------------

**Main
Supervisor's
Signature**

	Date 22/02/2016
---	---------------------------

6.2 Introduction

Chapter 5 revealed two potent redox-stable cyclic peptide inhibitors of SPSB2-iNOS interaction, one containing a thioether bridge (**CP1**) and the other a lactam bridge (**CP2**) with the peptide sequence of c[WDINNN β A], and SPR measured K_D values of 31 and 21 nM, respectively, i.e. approximately 10 to 15-fold better affinities than the linear peptide Ac-DINNN-NH₂ ($K_D \approx 318$ nM). The cyclic peptide analogues were also found to bind specifically to the iNOS binding site of SPSB2, as evidenced by ¹⁹F NMR, and were able to displace full-length iNOS from interacting with SPSB2 in macrophage cell lysates. In addition, both **CP1** and **CP2** were found to be stable in reducing condition, with **CP2** more oxidatively stable than **CP1**. Although **CP1** was found to form sulphoxide analogue after 5 h incubation in an oxidising environment, the sulphoxide analogue was able to maintain its binding to the iNOS binding site of SPSB2 and displace full-length iNOS from SPSB2 in macrophage cell lysate, albeit with a 2-fold weaker affinity compared to **CP1** ($K_D \approx 68$ nM).

In this Chapter, an alternative approach to generating redox-stable inhibitors of the SPSB2-iNOS interaction is described. Briefly, an interactive *de novo* design approach was used to design four cyclic peptidomimetic analogues, mimicking the crystal structure of the SPSB2-bound linear peptide DINNN (PDB ID: 3EMW).⁵⁵ In contrast to the use of amino acid linkers (**Chapter 4**) or unusual amino acid linkers (**Chapter 5**) in the design of cyclic peptide analogues, *in silico* models of redox-stable cyclic peptidomimetic analogues were designed *via* incorporation of different organic scaffolds between the *N*- and *C*-terminus of the linear peptide DINNN. Four mimetic building blocks were retrosynthetically designed and synthesised prior to incorporation into SPPS using the Fmoc chemistry. The purity and identity of the mimetics were characterised by LC-MS and NMR experiments. Their abilities to bind to the iNOS binding site of SPSB2 were determined by ¹⁹F NMR and the binding affinities of the interactions were measured by SPR and ITC. To explore the dynamics of the interaction between the most potent mimetic analogue and the iNOS binding site of SPSB2, a 1 μ s MD simulation was performed on the *in silico* model of the mimetic/SPSB2 complex. The ability of the mimetics to displace full-length iNOS from SPSB2 in macrophage cell lysates was also investigated. The results of this Chapter are presented in the format of an online published article of *Journal of Medicinal Chemistry* in the immediate section below.

Design, Synthesis, and Characterization of Cyclic Peptidomimetics of the Inducible Nitric Oxide Synthase Binding Epitope That Disrupt the Protein–Protein Interaction Involving SPRY Domain-Containing Suppressor of Cytokine Signaling Box Protein (SPSB) 2 and Inducible Nitric Oxide Synthase

Jitendra R. Harjani,[†] Beow Keat Yap,[†] Eleanor W. W. Leung,[†] Andrew Lucke,[†] Sandra E. Nicholson,^{‡,§} Martin J. Scanlon,[†] David K. Chalmers,[†] Philip E. Thompson,[†] Raymond S. Norton,^{*,†} and Jonathan B. Baell^{*,†}

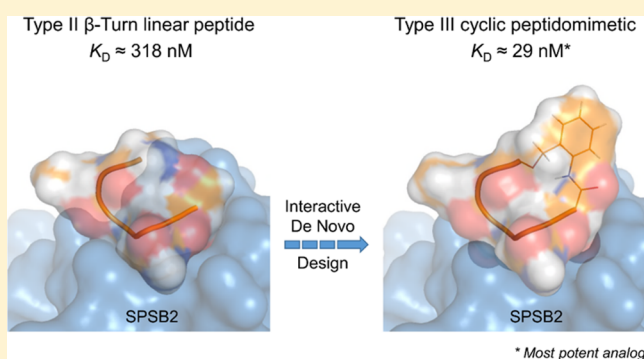
[†]Medicinal Chemistry, Monash Institute of Pharmaceutical Sciences, Monash University, Parkville, Victoria 3052, Australia

[‡]The Walter and Eliza Hall Institute of Medical Research, Parkville, Victoria 3052, Australia

[§]The Department of Medical Biology, University of Melbourne, Parkville, Victoria 3052, Australia

Supporting Information

ABSTRACT: SPRY domain-containing suppressor of cytokine signaling box protein (SPSB) 2-deficient macrophages have been found to exhibit prolonged expression of inducible nitric oxide synthase (iNOS) and enhanced killing of persistent pathogens, suggesting that inhibitors of the SPSB2–iNOS interaction have potential as novel anti-infectives. In this study, we describe the design, synthesis, and characterization of cyclic peptidomimetic inhibitors of the SPSB2–iNOS interaction constrained by organic linkers to improve stability and druggability. SPR, ITC, and ¹⁹F NMR analyses revealed that the most potent cyclic peptidomimetic bound to the iNOS binding site of SPSB2 with low nanomolar affinity (K_D 29 nM), a 10-fold improvement over that of the linear peptide DINNN (K_D 318 nM), and showed strong inhibition of SPSB2–iNOS interaction in macrophage cell lysates. This study exemplifies a novel approach to cyclize a Type II β -turn linear peptide and provides a foundation for future development of this group of inhibitors as new anti-infectives.



INTRODUCTION

The SPRY domain-containing SOCS box protein 2 (SPSB2) modulates the lifespan of inducible nitric oxide synthase (iNOS) in macrophages during infection by mediating the proteasomal degradation of this enzyme.¹ It has been shown that the reduction of intracellular SPSB2 results in prolonged iNOS expression and enhanced nitric oxide (NO) production, which ultimately improves the killing of persistent pathogens. This suggests the potential of SPSB2–iNOS inhibitors as a new class of anti-infectives. X-ray crystallographic studies showed that the SPRY domain of SPSB2 binds to Asp184, Asn186, and Asn188 within the DINNN sequence of VASA, which correspond to Asp23, Asn25, and Asn27 in the N-terminal region of iNOS.^{1,2}

The binding affinity, K_D , of the 5-residue linear peptide sequence (DINNN), as determined by SPR, was only 318 nM,³ about 25 times weaker than that of the 13-residue linear peptide sequence (KEEKDINNNVKKKT) of the N-terminal region of iNOS (K_D by isothermal titration calorimetry (ITC) \approx 13 nM),¹ suggesting that the flanking residues of the DINNN linear

peptide contributed to the low nanomolar binding between the N-terminal region of iNOS and SPSB2. Recently, we showed that the *N*-acetylated cyclic peptide c[CVDINNNC]-NH₂ had significant improvement in binding to SPSB2 (K_D by SPR: 4.4 nM) when compared to its linear counterpart.³ The disulfide-bridged cyclic peptide was also found to be stable in human plasma and was stable against trypsin, α -chymotrypsin, and pepsin, but the presence of a disulfide bridge in this peptide rendered it susceptible to reduction in the cytoplasm, with a consequent loss of the gain in affinity afforded by cyclization.

In this study, we describe a set of organic linkers that were designed in silico to optimally link the N- and C-termini of the DINNN linear peptide. The organic linkers offer several advantages over amino acid linkers, including tunability of size, shape, and length, in addition to resistance to proteolysis. Careful design of the organic linker imparts structural rigidity to the

Received: March 15, 2016

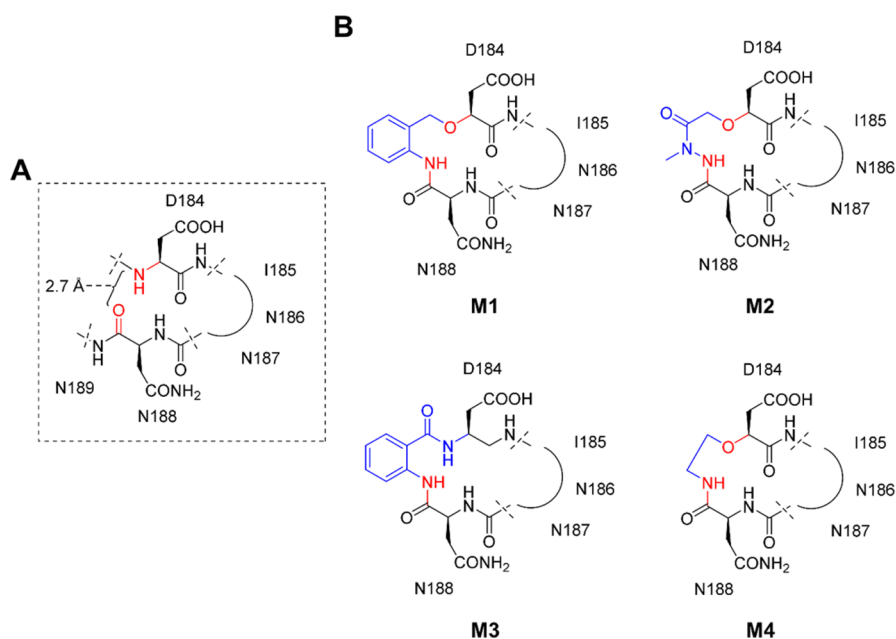


Figure 1. Rational design of mimetics **M1–M4**. (A) SPSB2-bound DINNN linear peptide (PDB ID: 3EMW) showing the N–O distance of 2.7 Å. (B) Type III mimetic analogues **M1–M4** were designed in silico, incorporating benzyl, hydrazide, anthranilamide, or ethyl functional group, respectively, as optimal scaffold (blue) joining the two ends (red) together.

conformation without interfering with the ability of the cyclic peptidomimetic to bind to the protein. Organic linkers offer good redox stability when compared to the disulfide-based cyclic peptide.³ We describe the details of our design and synthesis of the building blocks that enabled us to synthesize the cyclic peptidomimetics using Fmoc chemistry. The interaction of these cyclic peptidomimetics with SPSB2 was characterized using SPR, ITC, and ¹⁹F NMR experiments, and their ability to displace full-length iNOS from its complex with SPSB2 in a macrophage cell lysate was confirmed. A comparison of the binding properties presents an opportunity to understand how the structurally different portions in these cyclic peptidomimetics contribute to their binding affinities.

RESULTS AND DISCUSSION

Design of Cyclic Peptidomimetics M1–M4. The design of the cyclic peptidomimetics was based on a technique called interactive de novo design,⁴ which we developed and that furnishes type III mimetics,⁵ where the peptide backbone is replaced by suitable organic scaffolds. In brief, the method is based on identifying the vectors in a binding epitope that we wish to match and replacing them with an organic scaffold mimetic. Although there are computational approaches to such problems, we have great success adopting an interactive approach, where the medicinal chemist interactively builds scaffolds that are both synthetically accessible and conformationally appropriate. We have applied this approach successfully to disparate, discontinuous binding epitopes where three vectors are matched in an organic scaffold. In the current problem, which relates more to the design of a molecular paperclip to furnish cyclic peptidomimetics, we proposed to target just two vectors. Although relatively distant residues are readily spanned, it is convenient to focus on constrictions, and in this context, observation of the DINNNNN heptapeptide revealed that the Asp184 amide NH was relatively close to the Asn188 C=O at only 2.685 Å (Figure 1A). Furthermore, the C α –N bond vector relationship with that of the Asn188 amide group was deemed

suitable for mimetic design with the intention of keeping the DINNN sequence for binding to SPSB2.

The crystal structure of SPSB2-VASA peptide at 1.8 Å resolution (Protein Databank ID: 3EMW)² was loaded into SYBYL-X (version 2.0, Tripos) in order to undertake the mimetic design. All unnecessary residues were stripped, and the Asn188 carboxamide group was flipped in silico to give an amide that moved closer to the Asp184 nitrogen atom. A variety of scaffolds was then built interactively and joined with Asp184. A preferred type III peptidomimetic is identified as **M1** (Figure 1B). In building this scaffold and prior to minimization, it was expected that the torsion angles 1, 2, 3, and 4 of around 180, 45, –45, and –80°, respectively, had acceptably low strain energies. Furthermore, the ethereal oxygen atom was deliberately chosen to facilitate synthesis and interact favorably with the anilide NH. This minimization led to a barely perceptible change in the designed conformation, with a final N–O distance of 2.01 Å.

In this approach, initial identification of a suitably synthetically versatile and conformationally appropriate scaffold is always deceptively difficult, but it becomes progressively easier once an initial scaffold has been identified. Hence, it is relatively easy to envisage that replacement of the **M1** phenyl ring with an N-methylated *cisoid* amide bond would also furnish an appropriate scaffold. The resulting acylhydrazide peptidomimetic **M2** (Figure 1B) uses the same ethereal oxygen linkage as part of the Asp184 incorporation. However, it contrasts with **M1** in that it contains polar groups in the mimetic region rather than the hydrophobic phenyl ring. Although it was not known if one might be preferred over the other, it is nevertheless a convenient matching pair to have. In both cases, there is the opportunity of derivatizing the mimetic scaffold without any conformational interference. For **M1**, this would be through the addition of other groups on the phenyl ring, whereas for **M2**, it would be the extension of the N-methyl group. In neither scaffold does an appropriate side chain conformation have to be designed; rather, this is inherited from Asp184.

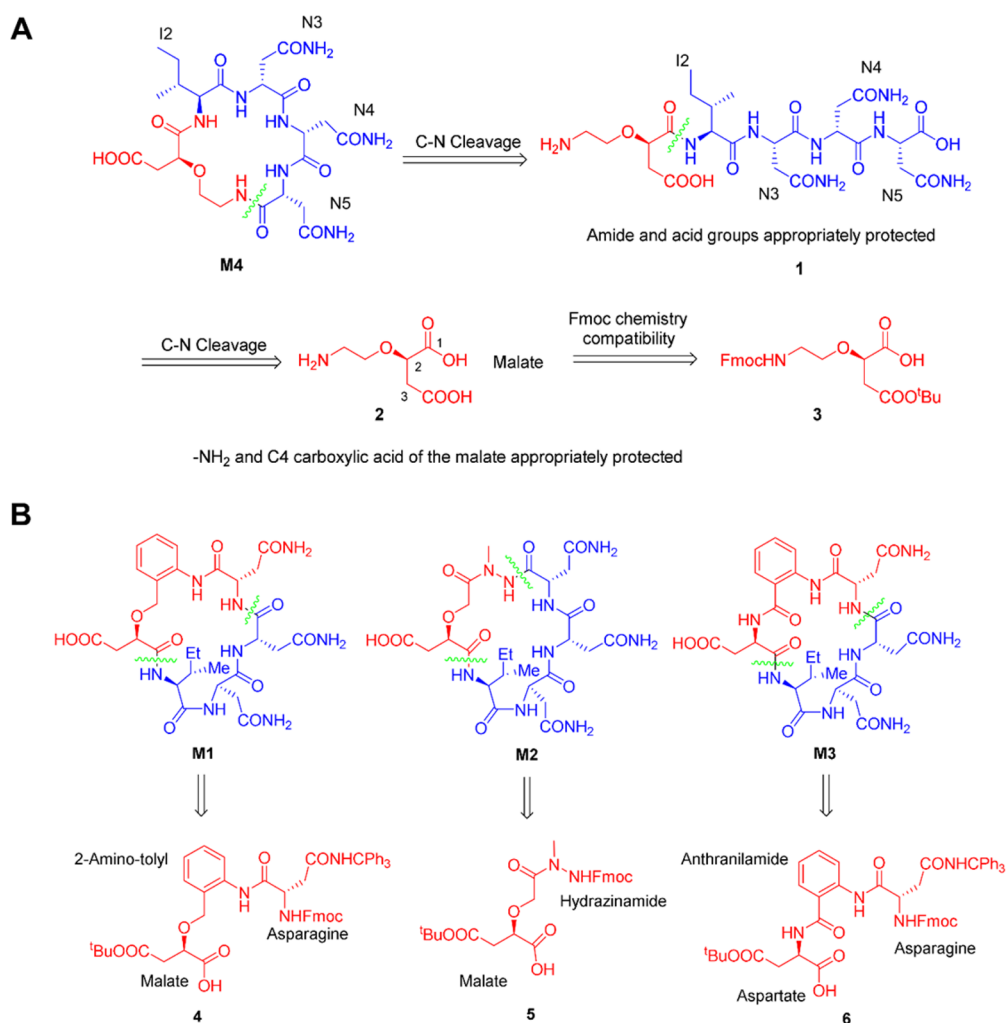


Figure 2. Retrosynthesis approach to the synthesis of cyclic peptidomimetics **M1**–**M4**. (A) Cleavage of both N- and C-terminus of INNN motif (blue) at the C–N bond (green jagged lines) from the designed ethylene-based peptidomimetic **M4** followed by suitable –NH₂ and C4 carboxylic acid protection resulted in mimetic building block **3** (red). (B) A similar retrosynthesis approach was used to design mimetic building blocks **4**–**6** from mimetics **M1**–**M3**, respectively.

To explore further the effect of linker rigidity on the designed conformation and binding to SPSB2, the methylene-oxy group in **M1** was substituted with an amide bond as a more rigid alternative scaffold, as shown in **M3**. We hypothesized that the benzyl group in **M1** may also be easily replaced with a more flexible aliphatic ethylene linker as in **M4**. Hence, **M3** relates indirectly to the principles of interactive de novo design, whereas **M4** diverges completely from these principles. Nonetheless, energy minimization of in silico models of both **M3** and **M4** did not result in significant changes to the overall conformation of the mimetics compared to the crystal structure of SPSB2–DINNN, although **M4** was connected by a linker with one covalent bond less than those of **M1**–**M3**. On the basis of these considerations, peptidomimetics **M1**–**M4** were selected for synthesis (Figure S1).

Synthesis of Building Blocks Required for the Synthesis of **M1–**M4**.** The principle used in designing the synthesis of the cyclic peptidomimetics is illustrated with an example of an ethylene-based peptidomimetic **M4**. In cyclic peptidomimetic **M4** (Figure 2A), only amino acid residues designated here as I2, N3, N4, and N5 (or the INNN motif) were connected to each other via peptide backbone. Thus, disconnection at an amide C–N bond that connects the INNN motif to the rest of the cyclic

molecule, i.e., at the C-terminus of N5, will lead to linear structure **1**, which may be cyclized to **M4** by a peptide coupling strategy involving the free terminal –NH₂ and –COOH groups. This strategy requires that all other groups (such as –CONH₂ and –COOH) in **1** that might potentially participate in the coupling reaction or suffer from side reactions during the coupling conditions be suitably protected. A further disconnection of the INNN motif from the rest of the linear chain at an amide C–N bond at the N-terminus of I2 results in **2**, which is an amino dicarboxylic acid that required protection of the malate C4 carboxylic acid group for the desired regioselective coupling. Further protection at the –NH₂ group in **2** as –NHFmoc and at the C4 carboxylate of malate as a *tert*-butyl ester results in target molecule **3**, which is compatible with standard Fmoc peptide chemistry and therefore should be a good precursor for the synthesis of appropriately protected **1**. The advantage of this approach would be that except for **3** all other precursors and reagents required for this synthesis of appropriately protected **1** are commercially available. In addition to this, well-optimized peptide coupling, deprotection, and peptide cleavage and cyclization strategies commonly used in solid-phase Fmoc peptide chemistry can be used in the synthesis of **M4**.

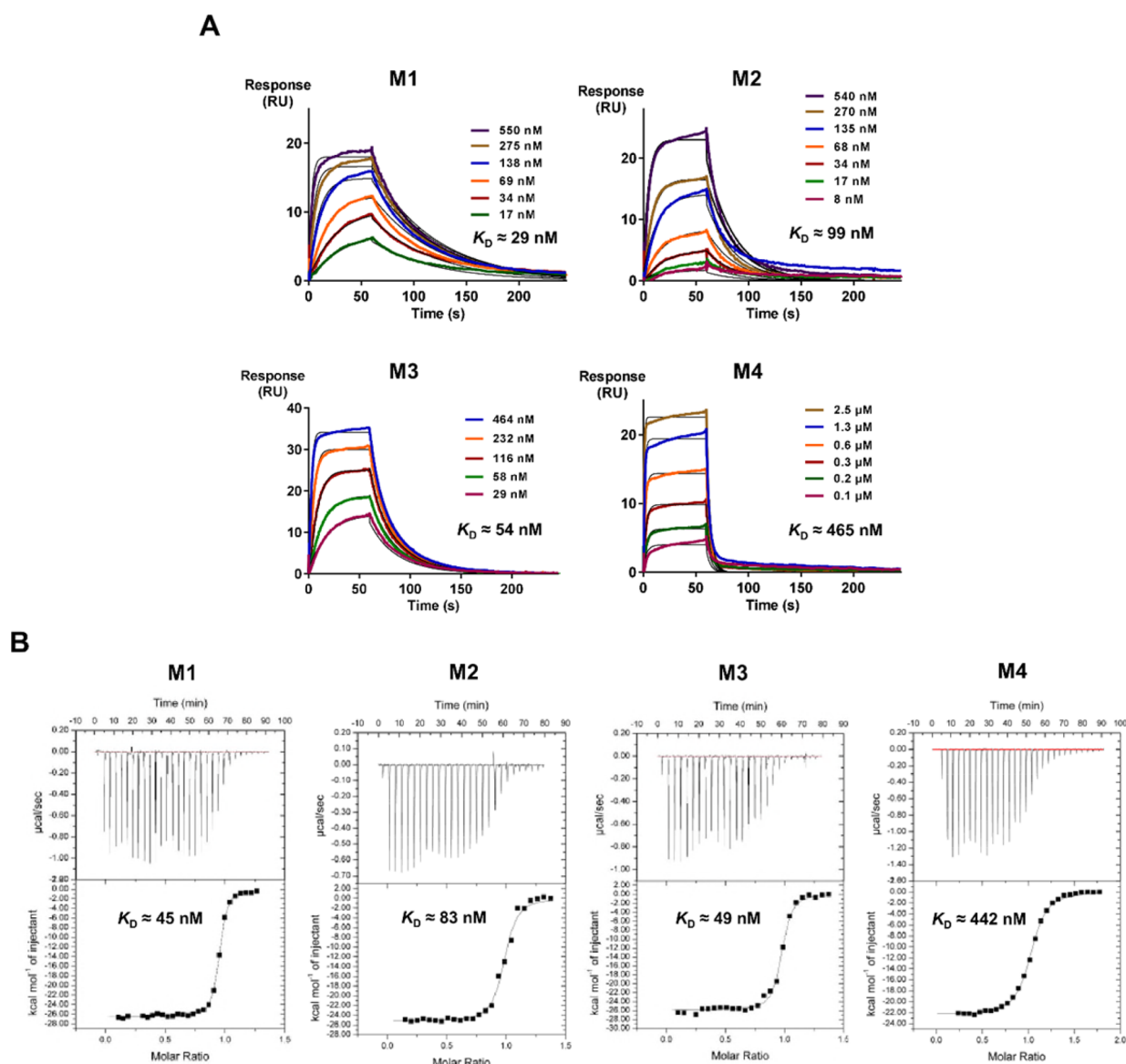


Figure 3. Peptidomimetics M1–M3 bind to SPSB2 with low nanomolar affinity. Representative SPR sensorgrams of immobilized SPSB2 exposed to increasing concentrations of mimetics (A) M1–M4 in 10 mM HEPES, 150 mM NaCl, 3 mM EDTA, and 0.05% Tween 20, pH 7.4, at 25 °C. Data were fitted using a single-site binding model. (B) Calorimetric titration of M1–M4 with SPSB2. ITC experiments were performed at 25 °C in 50 mM phosphate, pH 7.4, and 150 mM NaCl.

Applying similar principles of retrosynthesis to cyclic peptidomimetics M1–M3, we arrive at building blocks such as 4–6 (Figure 2B). Structurally fragmenting 4–6 further leads to simple chemical structures such as *N*-methylhydrazine, malate, anthranilamide, aspartate, and asparagine. The simplicity of these fragments also suggests that inexpensive, commercially available precursors may be useful for the synthesis of peptidomimetic building blocks 4–6, which should provide access to cyclic peptidomimetics M1–M3, respectively (Figure 2B). The synthesis of building blocks 4–6 relied on the synthesis of the malate diester precursor with C1 as $-\text{COOBn}$ and C4 as $-\text{COO}t\text{-Bu}$ (numbering sequence identified in 2). The synthesis of this diester resulted in racemization at the chiral C-atom of the malate. We decided to carry through the racemic malate diester using it in the synthesis of 4–6 that were racemic at the malate, knowing that the final step in the purification of peptides generally involves purification of the peptide by separation using HPLC. We were expecting that isoforms of M1, M2, and M4

might be separated from their attempted synthesis. Detailed descriptions of synthesis procedures used for the synthesis of building blocks 3–6 are provided in the Supporting Information.

Synthesis and Characterization of Peptidomimetics M1–M4 by LC-MS and NMR. Utilizing the synthesized building blocks, linear peptidomimetics M1–M4 were assembled on-resin (solid-phase peptide synthesis) using an automated Peptide Synthesizer 3 (PS3) and Fmoc chemistry (Figure S1).⁶ Following cyclization in solution, all side-chain-protected groups were removed with TFA in the presence of scavengers. The cyclized peptidomimetics were purified by reverse-phase high-performance liquid chromatography (RP-HPLC), and their identity and purity were determined by LC-MS and NMR experiments.

The analysis of crude M1 by LC-MS indicated two closely eluted peaks, i.e., P1 and P2, that had the same observed m/z and therefore the same deconvoluted mass (Figure S2A). After separation by RP-HPLC, P1 and P2 were characterized by 1D

Table 1. Kinetics (K_D , k_{on} , and k_{off}) \pm Standard Error of the Mean (s.e.m.) and Thermodynamics of the Interactions with SPSB2 of Cyclic Peptidomimetics M1–M4 Estimated from the Double Reference-Subtracted SPR Sensorgrams Fitted to a Steady-State 1:1 Interaction Model and the ITC Experiments, Respectively

mimetic	SPR			ITC		
	K_D (nM)	k_{on} ($\times 10^5$ M $^{-1}$ s $^{-1}$)	k_{off} ($\times 10^{-2}$ s $^{-1}$)	K_D (nM) ^b	ΔH (kcal/mol) ^c	$T\Delta S$ (kcal/mol) ^d
M1	29 \pm 7	8.6 \pm 2.2	2.0 \pm 0.3	45	–26	–16.5
M2	99 \pm 21	11.9 \pm 8.6	8.0 \pm 4.0	83	–24	–15.7
M3	54 \pm 7	11.0 \pm 2.1	6.0 \pm 1.5	49	–22	–11.8
M4	465 \pm 43 ^a	4.7	26.0	442	–23	–14.6

^a K_D was estimated on the basis of both steady-state affinity and kinetic steady state 1:1 interaction models from three independent experiments. ^bAll titrations were performed in 50 mM phosphate, pH 7.4, and 150 mM NaCl using MicroCal ITC₂₀₀. ^c K_D and ΔH were determined from the analysis of ITC data using a 1:1 binding model in the Origin software package. ^dEntropies were calculated using the relationships $\Delta G^\circ = RT \ln K_D$ and $\Delta G^\circ = \Delta H - T\Delta S$.

and 2D NMR. The chemical shift and integration of signals in 1D NMR of both P1 and P2 indicated that they were likely isomers of M1. Both P1 and P2 exhibited similar groups of spin systems in 2D [$^1H, ^1H$]-TOCSY experiments,⁷ and the backbone amide resonances of both P1 and P2 were able to be sequentially assigned using 2D [$^1H, ^1H$]-ROESY⁸ and [$^1H, ^1H$] DQF-COSY⁹ experiments (Table S1). To investigate the identity of these isomers, NOE peaks observed in the 2D ROESY NMR for P1 and P2 were compared with the distances between atoms in the designed in silico SPSB2-bound model derived from the crystal structure of SPSB2–DINNN linear peptide (PDB ID: 3EMW).² In principle, atoms separated through space by a distance of less than 5 Å can be observed as NOE peaks in 2D [$^1H, ^1H$]-NOESY or ROESY experiments. The inter-residue NOEs between assigned peaks in the 2D [$^1H, ^1H$]-ROESY spectra of both P1 and P2 in water at pH 4.8 acquired at a 300 ms mixing time at 10 °C were compared to each other. A strong NOE cross-peak between resonances at 4.22 and 4.50 ppm (H^α and H^{1b}) and a weaker NOE cross-peak between resonances at 4.22 and 4.61 ppm (H^α and H^{1a}) was apparent in the 2D [$^1H, ^1H$]-ROESY spectra of P1 (Figure S3A). However, similar NOE cross-peaks between H^α and H^{1*} were not observed in the 2D [$^1H, ^1H$]-ROESY spectra of P2 (Figure S3B). When the distances between the H^α and H^{1*} in SPSB2-M1, i.e., the bound model of mimetic M1, were measured (Figure S3C), we observed that H^α and H^{1*} were spatially separated by 2.4–3.5 Å. This model suggested that one strong and one weak inter-residue NOE cross-peaks are expected in the 2D [$^1H, ^1H$]-ROESY spectra of M1, indicating that P1 is the originally designed mimetic represented as M1 (Figure 1). Because the racemic malate was used for the synthesis of M1, we assumed that perhaps P2 may be the epimer of the designed M1, although future work is warranted to confirm its identity.

A similar observation was made for the crude product obtained when the synthesis of M2 was attempted. Two peaks were observed in this case and designated P3 and P4. When the purified products corresponding to peaks P3 and P4 of mimetic M2 were analyzed by NMR, we observed that the number of proton resonances in the backbone amide region of 1H NMR spectra of both P3 and P4 was more than the expected number of amide resonances of the designed mimetic, which could be due to conformational isomerism of the peptidomimetic or impurities from either a deletion peptide or organic impurities that coelute with P3 and/or P4 during the purification. To investigate the possible origin of the additional amide resonances, we conducted a variable-temperature NMR study on both P3 and P4. An increase in the temperature from 10 to 30 °C resulted in broadening of 10 out of 12 resonances in the backbone amide

region of the 1H NMR spectra of P3, with sharpening of 2 of the existing resonances observed after 25 °C (Figure S4A, left), suggesting that some amide protons may be involved in conformational exchange whereas others were rapidly exchanged with the solvent at high temperature. 2D [$^1H, ^1H$]-TOCSY experiments on P3, however, revealed three spin systems with an $A_3MPT(B_3)X$ -like pattern, a common pattern of the spin system for an Ile. In addition, 9 backbone amide proton peaks were observed, which is more than twice the expected number of amide resonances for M2 (Figure S4B, left), suggesting that P3 may not be designed peptidomimetic M2. In contrast, we were able to sequentially assign the resonances of P4 via 2D [$^1H, ^1H$]-ROESY and [$^1H, ^1H$]-DQF-COSY NMR experiments (Table S2), confirming it to be designed mimetic M2. In addition, the variable-temperature NMR experiments on peak P4 indicated that the number of broadened peaks in the amide region with the increase in temperature matches the expected number of the amide resonances for M2 (Figure S4A, right). Notably, three of the resonances (as shown in the 2D [$^1H, ^1H$]-TOCSY experiment) belong to spin systems with an AMX pattern, i.e., Asn3, Asn4, and Asn5, whereas another resonance belongs to the spin system with the $A_3MPT(B_3)X$ pattern, i.e., Ile (Figure S4B, right), consistent with that of designed mimetic M2. The presence of other temperature-resistant proton resonances in the NMR spectra of P4 (including possible aromatic peaks between 7 and 8 ppm) suggests that the purified P4 peak also contains some coeluting organic impurities from purification.

Syntheses of mimetics M3 and M4 yielded single products. This was indicated by a single peak in the UV trace with a matching m/z in their LC-MS profiles (Figure S2C,D). In addition, all backbone amide proton resonances observed for purified mimetics M3 and M4 (Figure S5C,D) could be sequentially assigned via [$^1H, ^1H$]-ROESY and [$^1H, ^1H$] DQF-COSY with the number and characteristics of the spin systems observed by [$^1H, ^1H$]-TOCSY matching the predicted spin systems for each mimetic (Tables S3 and S4). These observations thus confirmed the identity of the products as designed mimetics M3 and M4.

SPR Analysis of M1–M4 Binding to SPSB2. The binding of M1–M4 to SPSB2 was analyzed by SPR (Figure 3A). K_D values for M1–M4 ranged from 29 to 465 nM (Table 1), with M1 bound more tightly to SPSB2 than M2 ($p < 0.05$) and M4 ($p < 0.01$), and comparable to M3 ($p > 0.05$). Consistent with the observations made for *N*-acetylated cyclic peptide c-[CVDINNNC]-NH₂, M1–M3 demonstrated a faster association rate ($1\text{--}2 \times 10^6$ M $^{-1}$ s $^{-1}$) than that of the linear peptide, presumably by offering more rigid binding conformations.³ These observations suggest that cyclization of DINNN via the

organic linkers improved their binding affinity for SPSB2. The off rates were found to be modestly different from each other, with the slowest off rate being that of **M1**, followed by those of **M3** and **M2**. **M4**, however, did not show improvement in affinity for SPSB2 when compared with the linear peptide DINNN with a K_D of approximately 465 nM and a k_{off} of 0.3 s^{-1} . This indicates that the structural characteristics of the linker are crucial in determining how these cyclic peptidomimetics interact with SPSB2. The peptidomimetics corresponding to peaks P2 and P3 of **M1** and **M2**, respectively, were also found to bind to SPSB2, although their binding affinity as determined by SPR was approximately two to three times lower than that of P1 and P4 from the respective syntheses (Figure S6).

ITC Analysis of M1–M4 Binding to SPSB2. To investigate further the thermodynamics of these interactions, ITC titration curves were obtained for the binding of **M1–M4** to SPSB2 (Figure 3C). In all four cases, the binding of peptidomimetic to SPSB2 was an exothermic event, with negative peaks ($\Delta H < 0$) following each injection. Table 1 summarizes the thermodynamic parameters obtained during this study. The binding stoichiometry was close to 1:1 in all cases. Both **M1** and **M3** bound to SPSB2 with stronger affinities, with K_D values of 45 and 49 nM, respectively. **M2** had a K_D of 83 nM, and the weakest binder, **M4**, had a K_D of ~ 442 nM. All K_D values measured by ITC match with those of SPR except for mimetic **M1**, where an approximately 1.5-fold lower K_D value was observed by SPR.

Although both **M1** and **M3** showed similar K_D values by ITC, the enthalpy change associated with the binding of **M1** to SPSB2 (-26 kcal/mol at 25°C) was about 4 kcal mol^{-1} higher in magnitude than that for **M3**. The observed enthalpy change in **M1** upon binding to SPSB2 was also the highest in magnitude of the four cyclic peptidomimetics investigated. In general, the enthalpy changes associated with the binding of these peptidomimetics were significantly larger in magnitude than those observed for small molecules (typically about $-15 \text{ kcal mol}^{-1}$).¹⁰ One plausible explanation for this might be an extensive hydrogen bonding network predicted to form between these peptidomimetics and SPSB2.

¹⁹F NMR Analysis of the Interaction of SPSB2 with M1–M4. Owing to the high sensitivity of ¹⁹F chemical shifts to changes in their local environment, we utilized ¹⁹F NMR to probe ligand binding to SPSB2. Our previous study successfully established a fluorine-labeling scheme for SPSB2 whereby all six Trp residues in SPSB2 were replaced with 5-fluorotryptophan (5-F-Trp) using a Trp auxotroph *Escherichia coli* strain. These six Trp residues were well-resolved in the ¹⁹F NMR spectrum and were assigned by utilizing site-directed mutagenesis. Four of the Trp residues were unambiguously assigned to Trp 48, Trp131, Trp133, and Trp207, and the remaining two Trp residues were unassigned because mutating these residues affected the structure of the protein. We have shown previously that ligands targeting the iNOS-binding site of SPSB2 induce significant chemical shift perturbations of the 5-F-Trp indole resonances of SPSB2, particularly the ¹⁹F resonance of Trp207.¹¹ Peptides containing the DINNN sequence typically cause a downfield shift of about 3 ppm of the ¹⁹F resonance of Trp207. As shown in Figure 4, the binding of **M1** and **M2** to 5-F-Trp-SPSB2 caused a similar downfield shift of the Trp207 resonance to that caused by Ac-c-[CVDINNNC]-NH₂, although the chemical shift changes were slightly larger and the peak widths were broader for **M1** and **M2** (Figure 4). Although the spectral perturbations for **M1** and **M2** were relatively similar, a sharper Trp207 resonance was observed with **M1** than with **M2**. The resonance at -44.5 ppm

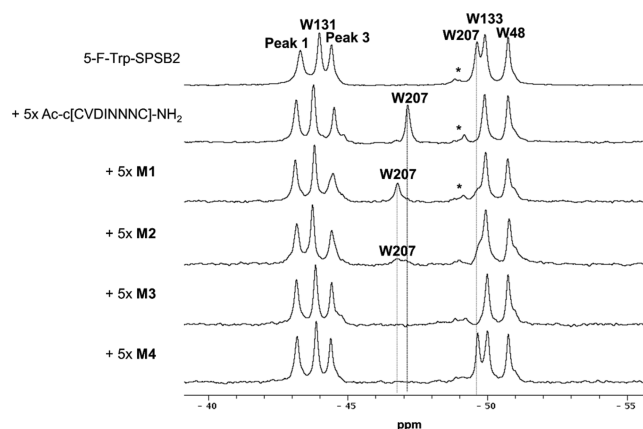


Figure 4. ¹⁹F NMR spectra of 5-F-Trp-SPSB2 in the absence and presence of peptidomimetics **M1–M4**. Cyclized CVDINNNC was used as a control for comparison. In each experiment, $50 \mu\text{M}$ 5-F-Trp-SPSB2 in the presence of cyclic peptide or peptidomimetic at SPSB2–peptide/peptidomimetic molar ratio of 1:5 was used. ¹⁹F NMR spectra were recorded at 30°C in 50 mM phosphate, $\text{pH } 7.0$, 50 mM NaCl, 2 mM DTT, 2 mM EDTA, 0.02% sodium azide at 564 MHz on a Bruker Avance 600 MHz spectrometer equipped with a cryoprobe tuned to ¹⁹F. The peak marked by asterisks (*) was attributed to denatured protein.

was also perturbed but only by **M1**, **M2**, and the control peptide, Ac-c-[CVDINNNC]-NH₂. Although this resonance (peak 3) was unassigned, it is likely that it originated from Trp95 and that its adjacent shoulder peaks are minor conformers. According to the crystal structure, Trp95 is approximately 6 \AA away from Trp207; hence, it is likely to be more affected by peptidomimetic/peptide binding than Trp91, which is about 18 \AA from Trp207. In the presence of **M3**, the Trp207 resonance broadened beyond detection, suggesting that the complex with **M3** samples multiple conformations. In contrast, mimetic **M4** (with expected bound occupancy of 99.8% at $K_D \approx 442 \text{ nM}$) did not perturb the chemical shift of Trp207 resonance but rather caused some sharpening of this resonance (25% increase in peak height), suggesting that **M4** may bind to SPSB2 in such a way that Trp207 is not perturbed in the same way as with the control cyclic peptide and other mimetics. In some instances, the presence of mimetic, e.g., **M1–M3**, caused the appearance of minor peaks.

Simulation of M1 Bound to SPSB2. To understand further the observed binding dynamics of the most potent peptidomimetic **M1** by ¹⁹F NMR, a $1 \mu\text{s}$ MD simulation was performed of the modeled SPSB2-bound **M1** on the crystal structure of SPSB2 protein (Protein Databank ID: 3EMW).² Throughout the simulation, the protein backbone rmsd was 2.7 \AA relative to that of the initial structure. In addition, mimetic **M1** remains closely bound to the iNOS binding site on SPSB2, where the side chain of **M1**-N4 is located above the side chain of Trp207 of SPSB2, with an average distance between side chain nitrogens of 5.1 \AA . Further analysis of hydrogen bonding interactions revealed seven persistent hydrogen bonds with occupancy of $>25\%$ between SPSB2 and **M1** (Table S5). The hydrogen bonding present during simulation was consistent with that inferred from the binding of VASA peptide to SPSB2,² with key hydrogen bonds observed between the equivalent amide side chain (NH) of residue N5 of mimetic **M1** (**M1**-N5) and the backbone carbonyl group of Val206 of SPSB2 as well as between the carbonyl side chain of **M1**-N5 and NH side chain of Arg68 of SPSB2 (Figure 5). Furthermore, residue **M1**-N3 made a side chain donor interaction with the side chain of Thr102, side chain

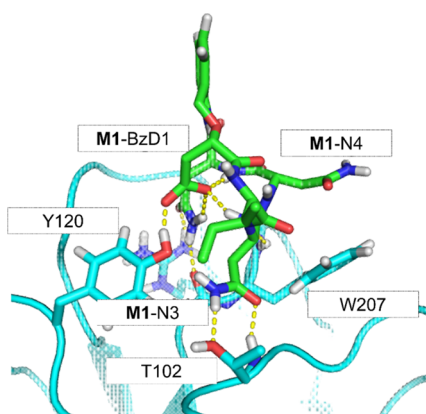


Figure 5. Peptidomimetic **M1** maintained its bound conformation on SPSB2. The final frame of 1 μ s molecular dynamics simulation of SPSB2-M1 complex with peptidomimetic **M1** (green, sticks) and SPSB2 protein (cyan, ribbon). Side chains of residues in SPSB2 making hydrogen bonds (yellow, dotted lines) with **M1** are represented as sticks (cyan).

acceptor interaction with the backbone of Thr102, and backbone acceptor interaction with the main chain of Gly208 of SPSB2.

The side chain of **M1**-BzD1 was also found to accept hydrogen bonds from the Tyr120 side chain and the backbone NH of Gln73. Nevertheless, the hydrogen bond between the side chain of **M1**-BzD1 and Tyr120 of SPSB2 was not maintained throughout the simulation because the hydrogen bond breaks and forms during the simulation coincident with the side chain of Tyr120 adopting a transient second orientation away from the side chain of **M1**-BzD1. Furthermore, the distance between the side chain nitrogens of Trp207 and **M1**-N4 was found to fluctuate between 3.1 and 10.3 Å throughout the simulations. These observations suggest that although mimetic **M1** is bound to the SPSB2 protein it did not lock the iNOS binding site of SPSB2 into a single bound conformation, which is consistent with the observation of a broader ^{19}F resonance for Trp207 in the presence of **M1** compared with the disulfide-bridged cyclic peptide.

Displacement of Full-Length iNOS from SPSB2 in Macrophage Cell Lysates by M1–M4. The ability of these cyclic peptidomimetics to inhibit the interaction between full-length iNOS and SPSB2 in a complex cellular lysate was investigated. **M1–M4** were incubated in lysates from bone-marrow-derived macrophages (BMDM) stimulated with LPS and IFN- γ . Recombinantly expressed GST-tagged SPSB2 protein was used to pull down iNOS from the macrophage cell lysate. As shown in the Western blots with anti-iNOS antibodies in Figure 6, affinity purification with GST-SPSB2 in the presence of peptidomimetics resulted in a significant reduction in the amount of iNOS pulled down, suggesting that all peptidomimetics were competing with full-length iNOS for binding to the SPSB2 protein in the macrophage cell lysate. Mimetic **M1** was found to give the strongest reduction, followed by mimetics **M3**, **M2**, and **M4**, consistent with the observations by both SPR and ITC.

To elucidate the effect of structural differences of the organic scaffold used for cyclization of peptidomimetics on their ability to bind to SPSB2, the results of SPR, ITC, and ^{19}F NMR experiments were compared. The SPR and ITC assays showed low nanomolar binding affinities for all cyclic peptidomimetics on SPSB2 except **M4**, with **M1** showing the strongest affinity to SPSB2 ($K_D \approx 29\text{--}45$ nM), followed by **M3** ($K_D \approx 49\text{--}54$ nM),

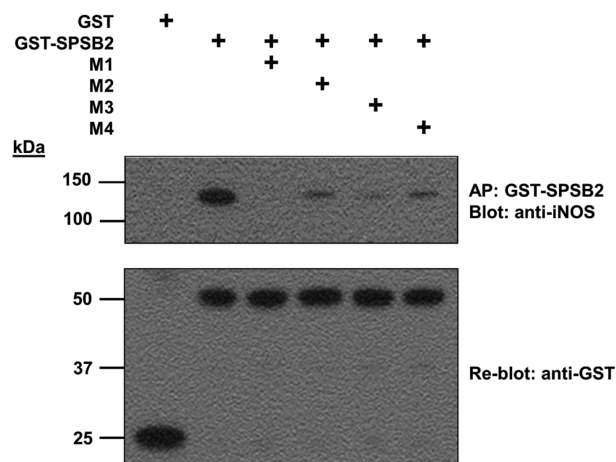


Figure 6. Peptidomimetics **M1–M4** displaced full-length iNOS from interacting with SPSB2 protein in macrophage cell lysates. Cell lysates from LPS/IFN- γ -stimulated BMDM were incubated with GST-SPSB2-SPRY domain or GST-protein (as a negative control) in the absence and presence (+) of **M1–M4**. Affinity purification (AP) via glutathione-Sepharose was used to recover GST fusion proteins, and the interaction with iNOS was analyzed by Western blotting with anti-iNOS antibody (upper panel). Equivalent protein loading was confirmed by stripping and reprobing the membrane with anti-GST antibody (lower panel).

M2 ($K_D \approx 83\text{--}99$ nM), and **M4** ($K_D \approx 442\text{--}465$ nM). Mimetic **M4**, which has a covalent bond shorter than those of the other mimetics, did not show any improvement over the linear peptide DINNN, presumably because of its suboptimal conformation for binding to SPSB2, as supported by a k_{off} 4-fold faster than that of the linear peptide DINNN ($k_{\text{off}} \approx 0.07$ s $^{-1}$).³ In contrast, **M2** and **M3** showed off rates similar to that of the linear peptide, whereas **M1** gave the slowest off rate, comparable to the observed k_{off} for the disulfide-bridged cyclic peptide ($k_{\text{off}} = 0.02$ s $^{-1}$).³

M1–M3 perturbed the 5-F-Trp207 resonance of SPSB2, indicating that these mimetics bound to the iNOS binding site of SPSB2 in a pose similar to those of the cyclic peptide Ac-c[CVDINNNC]-NH $_2$, although significant differences in peak line width were evident. A sharper 5-F-Trp207 resonance was observed in the presence of **M1**; molecular dynamic simulations of this complex revealed that **M1** maintained its bound conformation on SPSB2 throughout the 1 μ s simulations, with seven persistent hydrogen bonds observed between **M1** and key residues in the iNOS binding site of SPSB2, consistent with its slow off rate and strong binding enthalpies according to SPR and ITC. Intriguingly, the ^{19}F resonance of 5-F-Trp207 was not perturbed in the presence of mimetic **M4**. A slight sharpening of the peak was observed, suggesting that **M4** may have adopted a different binding conformation on SPSB2, locking the iNOS binding site of SPSB2, in the unbound state. When mimetic **M4** was incubated with macrophage cell lysates, a significant reduction in the amount of iNOS pulled down by GST-tagged SPSB2 from the cell lysates was observed, confirming that **M4** was still bound to the iNOS binding site of SPSB2 although the reduction was smaller than those caused by **M1** and **M3**, consistent with their higher binding affinities by SPR and ITC.

Although cyclic peptides of this size tend to have much better bioavailability than larger peptides,¹² cellular permeability can still be problematic, especially for molecules with low overall lipophilicity.¹³ However, because macrophages are an important target for our mimetics and these cells can ingest particles of diameter 0.5–10 μm ,¹⁴ the next step in progression of these

molecules will be to couple them to polymers that favor uptake by macrophages. Preliminary results on peptidomimetic analogue **M1** show some uptake by murine BMDMs even in the absence of polymeric carriers, but there is considerable scope for enhancement of this process.

Given a positive outcome of design and synthesis in this study, it is worth mentioning, as we have described in detail elsewhere,^{4d,e} that this approach of designing peptidomimetics is quite different from those involved in design of scaffolds to replace secondary structures such as β -turns of which successful reports first emerged more than 35 years ago.¹⁵ Our method is applicable to any binding epitope, whether continuous or discontinuous, and because there is a wealth of structural knowledge around biologically active peptides in current databases, we believe that this approach has broad applicability. In our hands, it is routinely successful yet appears to be seldom reported by others. With respect to its application reported herein, our results provide a foundation for future development of cyclic peptidomimetics targeting SPSB2 protein as potential novel class of anti-infectives.

CONCLUSIONS

To design new inhibitors of the SPSB2–iNOS interaction, we performed interactive de novo design using the crystal structure of the linear peptide DINNN bound to SPSB2. This led to designed cyclic peptidomimetics **M1** and **M2** and partners **M3** and **M4**, which incorporate organic scaffolds between the N- and C-termini of the DINNN sequence. Four building blocks were synthesized for incorporation into solid-phase peptide synthesis by Fmoc chemistry. These building blocks were used for the synthesis of **M1–M4**. Synthesis and further characterization of the final purified products by LC-MS and 2D NMR confirmed the identity of designed mimetics **M1–M4**. The most potent cyclic peptidomimetic inhibitor identified in this study, **M1**, bound strongly to SPSB2 ($K_D = 29$ nM) and inhibited full-length iNOS from interacting with SPSB2 in macrophage cell lysate. Although **M1** is less potent than a previously identified disulfide-bridged cyclic peptide, it is smaller in size and is redox-stable, suggesting that it has a greater potential to be developed into a new class of anti-infective drugs. Because antibiotic resistance continues to be a significant public health problem, newer anti-infectives that have a different mode of action, such as the ones discussed in this work, would be of interest to a broad research community.

EXPERIMENTAL PROCEDURES

Synthesis and Purification of **M1–M4.** All reactions were carried out at room temperature. The linear peptidomimetics required for the synthesis of **M1–M4** were synthesized on-resin (solid-phase peptide synthesis) using an automated Peptide Synthesizer 3 (PS3) and Fmoc chemistry.⁶ Peptidomimetic building blocks 3–6 (0.1 mmol, 1 equiv, synthesized according to methods outlined in the Supporting Information) were loaded on 0.2 mmol of 2-chlorotrityl chloride resin (1.2 mequiv/g substitution) followed by chain assembly via the coupling of 0.3 mmol (3 equiv) of Fmoc-protected amino acids to resin-bound 3–6 (Figure S1). The coupling reactions between the C-terminal residue and the resin and those involving subsequent amino acid residues were carried out using a mixture of 0.3 mmol (3 equiv) of HCTU and 0.6 mmol (6 equiv) of DIPEA over 50 min. Double couplings were carried out to couple the second Asn to the first Asn as well as the third Asn to the second Asn because single coupling was found to result in substantial deletion(s) of Asn from the peptide sequence. The Fmoc protecting group was removed with 20% (v/v) piperidine in DMF after each coupling/double coupling cycle was

completed. In each case, the side-chain-protected linear peptidomimetic was cleaved from the resin using 30% hexafluoroisopropanol (HFIP) in DCM. The N- and C-termini were coupled (cyclization) in solution at a peptidomimetic concentration of 0.5 mM over 24 h using 3 equiv of HCTU and 6 equiv of DIPEA in DMF. The protecting groups (Tr for amide and *tert*-butyl ester for carboxylic acid) were removed with a solution containing 95% (v/v) TFA, 2.5% (v/v) triisopropylsilane (TIPS), and 2.5% (v/v) 3,6-dioxa-1,8-octanedithiol (DODT), the latter two being the scavengers. After cleavage, the peptidomimetics were precipitated with cold diethyl ether twice and dissolved in a 1:1 mixture of water (H₂O) and acetonitrile (MeCN) prior to lyophilization. Crude peptidomimetics **M2–M4** were purified by RP-HPLC on a Phenomenex Luna C18 (2) column (100 Å, 5 μ m, 100 \times 10 mm) using a gradient of 5–40% B (A: 99.9% H₂O, 0.1% TFA; B: 80% MeCN, 19.9% H₂O, 0.1% TFA) over 35–70 min. For the crude product obtained during the synthesis of peptidomimetic **M1**, peaks P1 and P2 in the UV trace of LC-MS shown in Figure S2A were separated using the same column but at a gradient of 20–60% B over 40 min (A: 10 mM ammonium acetate pH 3.8; B: 50% 10 mM ammonium acetate pH 3.8, 50% MeCN). Under these conditions, peak P2 was found to elute faster than P1.

Purity of Peptide Building Blocks and Mimetics **M1–M4.** To establish the purity of 3–6, low-resolution mass spectrometry analyses were performed with an Agilent 6100 Series Single Quad LC/MS coupled with an Agilent 1200 Series HPLC, 1200 Series G1311A quaternary pump, 1200 series G1329A thermostated autosampler, and 1200 series G1314B variable wavelength detector. The conditions for liquid chromatography were: RP-HPLC analysis fitted with a Phenomenex Luna C8(2) 5 μ m (50 \times 4.6 mm²) 100 Å column; column temperature, 30 °C; injection volume, 5 μ L; solvent, 99.9% acetonitrile, 0.1% formic acid; gradient, 5–100% of solvent over 10 min; detection, 254 nm. The conditions for mass spectrometry were as follows: quadrupole ion source; ion mode, multimode-ES; drying gas temp, 300 °C; vaporizer temperature, 200 °C; capillary voltage, 2000 V (positive), 4000 V (negative); scan range, 100–1000 *m/z*; step size, 0.1 *s*; acquisition time, 10 min. The purity of 3–6 was >95%.

For **M1–M4**, the purity and molecular mass of the synthesized cyclic peptidomimetic were confirmed by LC-MS on a Shimadzu LCMS2020 instrument, incorporating a Phenomenex Luna C8 column (100 Å, 3 μ m, 100 \times 2 mm), using a linear gradient of 100% H₂O (0.05% TFA) for 4 min, followed by 0–60% MeCN (0.05% TFA) in water over 10 min at a flow rate of 0.2 mL/min. The purity of **M1–M4** was >95%.

SPSB2 Protein Expression and Purification. The GST-tagged SPSB2 (GST-SPSB2) expression construct has been described previously.¹⁶ The SPSB2 and 5-F-Trp labeled SPSB2 (5-F-Trp SPSB2) were both prepared as described previously.¹¹

NMR Spectroscopy. All NMR experiments were recorded on a Bruker Avance 600 MHz spectrometer, equipped with a 5 mm TCI cryoprobe. For chemical shift assignments of **M1–M4**, the cyclic peptidomimetic was dissolved in water at pH 4.7–4.8 with 10% ²H₂O. Homonuclear 2D NMR spectra were recorded at a temperature that allowed for the optimal resolution of the backbone amide peaks, which was 10 °C for **M1–M3** and 25 °C for **M4**. ¹H chemical shifts were referenced to DSS, whereas ¹³C and ¹⁵N chemical shifts were referenced indirectly through their gyromagnetic ratios.¹⁷ The 2D TOCSY spectrum (2048 \times 300) was acquired using the DIPSI-2 pulse sequence^{7a} with excitation sculpting for water suppression,¹⁸ a relaxation delay of 1.3 s, and a spin-lock time of 70 ms. ROESY spectra (2048 \times 300)⁸ with WATERGATE for water suppression¹⁹ were acquired with a 300 ms spin-lock time and a relaxation delay of 3 s. DQF-COSY spectra (2048 \times 300)⁹ were acquired in 99.9% ²H₂O, with a relaxation delay of 1.3 s. For carbon and nitrogen chemical shift assignments, [¹H,¹³C]-HSQC (2048 \times 256) and [¹H,¹⁵N]-SOFAST HMQC (2048 \times 64) spectra²⁰ were acquired at pH 4.8 using 99.9% ²H₂O and 90% ¹H₂O/10% ²H₂O, respectively. Spectra were processed with a sine-bell squared window function using Bruker TopSpin (Version 3.2) and analyzed using CcpNmr-Analysis (version 2.1.5). The chemical shift assignments of **M1–M4** are summarized as Tables S1–S4, respectively.

Surface Plasmon Resonance. SPR experiments were performed at 25 °C on a Biacore T200. SPSB2 immobilization was carried out via the

standard amine coupling method on a CMS sensor chip using a running buffer of 10 mM HEPES, 150 mM NaCl, 3 mM EDTA, and 0.05% Tween 20 at pH 7.4, as described previously.³ The binding of **M1–M4** was investigated using the same running buffer. Each peptidomimetic was injected onto the surface with a contact time of 60–100 s, flow rate of 100 $\mu\text{L}/\text{min}$, and dissociation time of 200–300 s. The sensorgrams were double-corrected for nonspecific binding to the surface by subtracting (1) the signals on the reference surface from that of the target protein surface and (2) the signals of the blank sample (no mimetics) from that of the mimetic containing samples. The corrected signal was fitted to a steady-state 1:1 interaction model with Biacore T200 Evaluation Software (version 2.0) and the binding affinity, K_D , association rate, k_{on} , and dissociation rate, k_{off} , were determined. Differences between the K_D of each analogue were evaluated using one-way ANOVA and multiple Tukey's comparison tests with GraphPad Prism (version 6.05).

Isothermal Titration Calorimetry. ITC measurements were acquired at 25 °C using a MicroCal ITC₂₀₀ instrument. A solution of 50 μM SPSB2 was prepared in 50 mM phosphate, pH 7.4, and 150 mM NaCl using a PD-10 column (GE Healthcare). Solutions of **M1–M4** were prepared as 5 mM stocks in the same buffer. In each ITC experiment, the sample cell was filled with 300 μL of SPSB2 solution, and the syringe was filled with 40 μL of the peptidomimetic solution. During the experiment, the SPSB2 solution was stirred at 1000 rpm. The titration was initiated with the first injection of 0.2 μL , followed by a series of 29 periodic injections (1 μL each). The data were analyzed using the evaluation software Origin 7 (MicroCal Inc.). Thermodynamic parameters were derived from a nonlinear least-squares fit to the data, using the "one set of sites" model.

¹⁹F NMR Spectroscopy. ¹⁹F NMR studies of **M1–M4** binding to 5-F-Trp-SPSB2 were performed as described previously.¹¹ Experiments were conducted at 30 °C in 50 mM phosphate buffer, pH 7.0, 50 mM NaCl, 2 mM DTT, 2 mM EDTA, and 0.02% sodium azide at 564 MHz on a Bruker Avance 600 MHz spectrometer equipped with a cryogenic probe tuned to ¹⁹F. Chemical shifts were referenced against 0.005% trifluoroethanol as an internal reference. NMR experiments were conducted with 50 μM 5-F-Trp-SPSB2 and a 5-fold molar excess of peptidomimetic (**M1–M4**). All spectra were processed using an exponential window function with a line-broadening of 40 Hz.

Molecular Dynamics Simulations. Molecular dynamics (MD) simulations were performed with GROMACS 5.0.6²¹ using the GROMOS 54a7 force field.²² The starting model of **M1** bound to SPSB2 was built using the complex of the 20-residue VASA peptide (Protein Databank ID: 3EMW) as a template. The protein was prepared using Maestro (Schrödinger, version 10.3); missing atoms were added and protonation states of ionizable residues adjusted to pH 7.0. All hydrogens and added atoms were subjected to restrained minimization with default settings. **M1** was constructed from VASA peptide residues Asp184–Asn188, which were modified by removing the N-terminus nitrogen and replacing it with an ether linkage to a 2-oxyphenylamine group. An amide bond was created from the phenylamine nitrogen to the C-terminus of Asn188. Finally, the SPSB2 protein–**M1** complex was minimized. ATB²³ was used to generate topology information for residue BzD1, which was added to the GROMOS force field files. The topology file for the mimetic **M1** was built from the topology file for the linear peptide H-BzD1-I2-N3-N4-N5-OH (created using the GROMACS program 2gmx) through removing the terminal atoms and adding the appropriate bonds and angles.

MD simulations were performed on a SPSB2–**M1** complex solvated with SPC water model containing 150 mM NaCl. Periodic boundary conditions were used with a dodecahedral cell. Simulations were performed using the particle mesh Ewald method.²⁴ van der Waals and short-range Ewald cut-offs were set to 0.9 nm, bonds to hydrogen atoms were constrained with the LINCS algorithm, temperature coupling was controlled via the v-rescale method²⁵ at 300 K, and pressure was controlled via Parrinello–Rahman isotropic coupling²⁶ at 1 bar. Following an initial minimization, 200 ps of NVT ensemble simulation for equilibration was performed with position restraints on the heavy atoms of SPSB2 and **M1** using a 2 fs time step. Similarly, 200 ps of NPT ensemble simulation was performed with constraints. Finally, to achieve

a NPT production simulation time of 1 μs , a time step of 5 fs with HMR²⁷ to slow high-frequency motions was utilized.

Cell Lysate Inhibition Assay. The cell lysate inhibition assay was performed on murine BMDM extracted and cultured according to the protocol described previously.²⁸ Cell lysates were incubated with 2.5 $\mu\text{g}/\text{mL}$ recombinantly expressed GST protein (as a negative control) or GST-tagged SPSB2–SPRY domain, both in the absence and presence of 10 μM cyclic peptidomimetics **M1–M4** for 2 h, followed by another 1 h of incubation with glutathione Sepharose 4B beads (GE Healthcare) to pull down the SPSB2–iNOS protein complex from the cell lysate. Proteins were separated by SDS-PAGE under reducing conditions and electrophoretically transferred to nitrocellulose membranes (Millipore). The membranes were blocked overnight in 10% (w/v) skim milk prior to incubation with mouse monoclonal anti-iNOS primary antibody (BD Biosciences) for 2 h. This was followed by another 1 h of incubation with peroxidase-conjugated sheep anti-mouse Ig antibody (GE Healthcare). Antibody binding was visualized with the ECL system (GE Healthcare) after extensive washing with phosphate-buffered saline and 0.1% Tween 20 (2 h, with a change of buffer every 20 min). To confirm equivalent protein loading, the membrane was reblotted with mouse monoclonal anti-GST primary antibody for 2 h after stripping off the anti-iNOS and peroxidase-conjugated sheep anti-mouse Ig antibodies in 0.1 M Gly, pH 2.9. The anti-GST antibody binding was visualized with peroxidase-conjugated sheep anti-mouse Ig antibody (GE Healthcare) and the ECL system (GE Healthcare).

■ ASSOCIATED CONTENT

📄 Supporting Information

The Supporting Information is available free of charge on the ACS Publications website at DOI: [10.1021/acs.jmedchem.6b00386](https://doi.org/10.1021/acs.jmedchem.6b00386).

Schematic representation and detailed description of methods used for the synthesis and characterization of the building blocks required for the synthesis of peptidomimetics **M1–M4**, schematic summary of methods used for the synthesis of peptidomimetics **M1–M4**, HPLC profiles of the crude peptidomimetics **M1–M4**, H NMR and HPLC profiles of purified peptidomimetics **M1–M4** and chemical shift assignments for peptides **M1–M4** (PDF)

■ AUTHOR INFORMATION

Corresponding Authors

*Phone: +613 9903 9167. Fax: +613 9903 9582. E-mail: Ray.Norton@monash.edu.

*Phone +613 9903 9044. Fax: +613 9903 9581. E-mail: Jonathan.Baell@monash.edu.

Author Contributions

J.R.H. and B.K.Y. contributed equally to this work.

Notes

The authors declare no competing financial interest.

■ ACKNOWLEDGMENTS

We thank Kade Roberts for helpful discussions. B.K.Y. is the recipient of an Academic Staff Training Scheme Fellowship of Universiti Sains Malaysia. R.S.N. and J.B.B. acknowledge Fellowship support from the National Health and Medical Research Council of Australia (NHMRC). This study was supported by NHMRC research grants 1016647 and 1022693, as well as NHMRC Independent Research Institute Infrastructure Support (IRIIS) grant 361646 and a Victorian State Government Operational Infrastructure Scheme grant.

■ ABBREVIATIONS USED

SPSB2, SPRY-domain-containing suppressor of cytokine signaling box protein 2; iNOS, inducible nitric oxide synthase; K_D , binding affinity; ITC, isothermal titration calorimetry; SPR, surface plasmon resonance; RP-HPLC, reverse-phase high-performance liquid chromatography; k_{off} , dissociation rate; BMDM, bone-marrow-derived macrophages; IFN- γ , interferon gamma; HCTU, *O*-(1*H*-6-chlorobenzotriazole-1-yl)-1,1,3,3-tetramethyluronium hexafluorophosphate; DIPEA, *N,N*-diisopropylethylamine; HFIP, hexafluoroisopropanol; DODT, 3,6-dioxal-1,8-octanedithiol; MeCN, acetonitrile; DSS, 3-trimethylsilyl-1-propanesulfonic acid sodium sulfate; TOCSY, total correlation spectroscopy; DQF-COSY, double-quantum filtered correlation spectroscopy; DIPSI, decoupling in the presence of scalar interactions; WATERGATE, water suppression by gradient tailored excitation; SOFAST, band-selective optimized flip-angle short transient; HEPES, 4-(2-hydroxyethyl)-1-piperazineethanesulfonic acid; ATB, automated topology builder; LINCOS, linear constraint solver; HMR, hydrogen mass repartitioning; k_{on} , association rate; ECL, electrochemiluminescence

■ REFERENCES

- (1) Kuang, Z.; Lewis, R. S.; Curtis, J. M.; Zhan, Y.; Saunders, B. M.; Babon, J. J.; Kolesnik, T. B.; Low, A.; Masters, S. L.; Willson, T. A.; Kedzierski, L.; Yao, S.; Handman, E.; Norton, R. S.; Nicholson, S. E. The SPRY domain-containing SOCS box protein SPSB2 targets iNOS for proteasomal degradation. *J. Cell Biol.* **2010**, *190*, 129–141.
- (2) Filippakopoulos, P.; Low, A.; Sharpe, T. D.; Uppenberg, J.; Yao, S.; Kuang, Z.; Savitsky, P.; Lewis, R. S.; Nicholson, S. E.; Norton, R. S.; Bullock, A. N. Structural basis for Par-4 recognition by the SPRY domain- and SOCS box-containing proteins SPSB1, SPSB2, and SPSB4. *J. Mol. Biol.* **2010**, *401*, 389–402.
- (3) Yap, B. K.; Leung, E. W.; Yagi, H.; Galea, C. A.; Chhabra, S.; Chalmers, D. K.; Nicholson, S. E.; Thompson, P. E.; Norton, R. S. A potent cyclic peptide targeting SPSB2 protein as a potential anti-infective agent. *J. Med. Chem.* **2014**, *57*, 7006–7015.
- (4) (a) Andersson, A.; Baell, J. B.; Duggan, P. J.; Graham, J. E.; Lewis, R. J.; Lumsden, N. G.; Tranberg, C. E.; Tuck, K. L.; Yang, A. ω -conotoxin GVIA mimetics based on an anthranilamide core: effect of variation in ammonium side chain lengths and incorporation of fluorine. *Bioorg. Med. Chem.* **2009**, *17*, 6659–6670. (b) Baell, J. B.; Duggan, P. J.; Forsyth, S. A.; Lewis, R. J.; Phei Lok, Y.; Schroeder, C. I. Synthesis and biological evaluation of nonpeptide mimetics of ω -conotoxin GVIA. *Bioorg. Med. Chem.* **2004**, *12*, 4025–4037. (c) Baell, J. B.; Duggan, P. J.; Forsyth, S. A.; Lewis, R. J.; Lok, Y. P.; Schroeder, C. I.; Shepherd, N. E. Synthesis and biological evaluation of anthranilamide-based non-peptide mimetics of ω -conotoxin GVIA. *Tetrahedron* **2006**, *62*, 7284–7292. (d) Baell, J. B.; Forsyth, S. A.; Gable, R. W.; Norton, R. S.; Mulder, R. J. Design and synthesis of type-III mimetics of ω -conotoxin GVIA. *J. Comput.-Aided Mol. Des.* **2001**, *15*, 1119–1136. (e) Baell, J. B.; Harvey, A. J.; Norton, R. S. Design and synthesis of type-III mimetics of ShK toxin. *J. Comput.-Aided Mol. Des.* **2002**, *16*, 245–262. (f) Brady, R. M.; Baell, J. B.; Norton, R. S. Strategies for the development of conotoxins as new therapeutic leads. *Mar. Drugs* **2013**, *11*, 2293–2313. (g) Brady, R. M.; Hatzis, E.; Connor, T.; Street, I. P.; Baell, J. B.; Lessene, G. Synthesis of conformationally constrained benzoylureas as BH3-mimetics. *Org. Biomol. Chem.* **2012**, *10*, 5230–5237. (h) Brady, R. M.; Zhang, M.; Gable, R.; Norton, R. S.; Baell, J. B. *De novo* design and synthesis of a μ -conotoxin KIIIA peptidomimetic. *Bioorg. Med. Chem. Lett.* **2013**, *23*, 4892–4895. (i) Harvey, A. J.; Gable, R. W.; Baell, J. B. A three-residue, continuous binding epitope peptidomimetic of ShK toxin as a Kv1.3 inhibitor. *Bioorg. Med. Chem. Lett.* **2005**, *15*, 3193–3196. (j) Tranberg, C. E.; Yang, A.; Vetter, I.; McArthur, J. R.; Baell, J. B.; Lewis, R. J.; Tuck, K. L.; Duggan, P. J. ω -Conotoxin GVIA mimetics that bind and inhibit neuronal Ca(v)2.2 ion channels. *Mar. Drugs* **2012**, *10*, 2349–2368.
- (5) Ripka, A. S.; Rich, D. H. Peptidomimetic design. *Curr. Opin. Chem. Biol.* **1998**, *2*, 441–452.
- (6) Atherton, E.; Logan, C. J.; Sheppard, R. C. Peptide synthesis. Part 2. Procedures for solid-phase synthesis using *N*^α-fluorenylmethoxycarbonylamino-acids on polyamide supports. Synthesis of substance P and of acyl carrier protein 65–74 decapeptide. *J. Chem. Soc., Perkin Trans. 1* **1981**, 538–546.
- (7) (a) Shaka, A. J.; Lee, C. J.; Pines, A. Iterative schemes for bilinear operators; application to spin decoupling. *J. Magn. Reson. (1969-1992)* **1988**, *77*, 274–293. (b) Braunschweiler, L.; Ernst, R. R. Coherence transfer by isotropic mixing: Application to proton correlation spectroscopy. *J. Magn. Reson. (1969-1992)* **1983**, *53*, 521–528.
- (8) (a) Bax, A.; Davis, D. G. Practical aspects of two-dimensional transverse NOE spectroscopy. *J. Magn. Reson. (1969-1992)* **1985**, *63*, 207–213. (b) Hwang, T. L.; Shaka, A. J. Cross relaxation without TOCSY: transverse rotating-frame Overhauser effect spectroscopy. *J. Am. Chem. Soc.* **1992**, *114*, 3157–3159.
- (9) Derome, A. E.; Williamson, M. P. Rapid-pulsing artifacts in double-quantum-filtered COSY. *J. Magn. Reson. (1969-1992)* **1990**, *88*, 177–185.
- (10) Klebe, G. Applying thermodynamic profiling in lead finding and optimization. *Nat. Rev. Drug Discovery* **2015**, *14*, 95–110.
- (11) Leung, E. W.; Yagi, H.; Harjani, J. R.; Mulcair, M. D.; Scanlon, M. J.; Baell, J. B.; Norton, R. S. ¹⁹F NMR as a probe of ligand interactions with the iNOS binding site of SPRY domain-containing SOCS box protein 2. *Chem. Biol. Drug Des.* **2014**, *84*, 616–625.
- (12) Bock, J. E.; Gavenonis, J.; Kritzer, J. A. Getting in shape: controlling peptide bioactivity and bioavailability using conformational constraints. *ACS Chem. Biol.* **2013**, *8*, 488–499.
- (13) Hewitt, W. M.; Leung, S. S. F.; Pye, C. R.; Ponkey, A. R.; Bednarek, M.; Jacobson, M. P.; Lokey, R. S. Cell-permeable cyclic peptides from synthetic libraries inspired by natural products. *J. Am. Chem. Soc.* **2015**, *137*, 715–721.
- (14) Makino, K.; Yamamoto, N.; Higuchi, K.; Harada, N.; Ohshima, H.; Terada, H. Phagocytic uptake of polystyrene microspheres by alveolar macrophages: effects of the size and surface properties of the microspheres. *Colloids Surf., B* **2003**, *27*, 33–39.
- (15) Ball, J. B.; Alewood, P. F. Conformational constraints: nonpeptide β -turn mimics. *J. Mol. Recognit.* **1990**, *3*, 55–64.
- (16) Yao, S.; Masters, S. L.; Zhang, J. G.; Palmer, K. R.; Babon, J. J.; Nicola, N. A.; Nicholson, S. E.; Norton, R. S. Backbone ¹H, ¹³C and ¹⁵N assignments of the 25 kDa SPRY domain-containing SOCS box protein 2 (SSB-2). *J. Biomol. NMR* **2005**, *31*, 69–70.
- (17) Wishart, D. S.; Bigam, C. G.; Yao, J.; Abildgaard, F.; Dyson, H. J.; Oldfield, E.; Markley, J. L.; Sykes, B. D. ¹H, ¹³C and ¹⁵N chemical shift referencing in biomolecular NMR. *J. Biomol. NMR* **1995**, *6*, 135–140.
- (18) Hwang, T. L.; Shaka, A. J. Water suppression that works. Excitation sculpting using arbitrary wave-forms and pulsed-field gradients. *J. Magn. Reson., Ser. A* **1995**, *112*, 275–279.
- (19) (a) Piotto, M.; Saudek, V.; Sklenar, V. Gradient-tailored excitation for single-quantum NMR spectroscopy of aqueous solutions. *J. Biomol. NMR* **1992**, *2*, 661–665. (b) Sklenar, V.; Piotto, M.; Leppik, R.; Saudek, V. Gradient-tailored water suppression for ¹H-¹⁵N HSQC experiments optimized to retain full sensitivity. *J. Magn. Reson., Ser. A* **1993**, *102*, 241–245.
- (20) Schanda, P.; Kupče, E.; Brutscher, B. SOFAST-HMQC experiments for recording two-dimensional heteronuclear correlation spectra of proteins within a few seconds. *J. Biomol. NMR* **2005**, *33*, 199–211.
- (21) Pronk, S.; Pall, S.; Schulz, R.; Larsson, P.; Bjelkmar, P.; Apostolov, R.; Shirts, M. R.; Smith, J. C.; Kasson, P. M.; van der Spoel, D.; Hess, B.; Lindahl, E. GROMACS 4.5: a high-throughput and highly parallel open source molecular simulation toolkit. *Bioinformatics* **2013**, *29*, 845–854.
- (22) Schmid, N.; Eichenberger, A. P.; Choutko, A.; Riniker, S.; Winger, M.; Mark, A. E.; van Gunsteren, W. F. Definition and testing of the GROMOS force-field versions 54A7 and 54B7. *Eur. Biophys. J.* **2011**, *40*, 843–856.
- (23) Malde, A. K.; Zuo, L.; Breeze, M.; Stroet, M.; Poger, D.; Nair, P. C.; Oostenbrink, C.; Mark, A. E. An automated force field topology

builder (ATB) and repository: version 1.0. *J. Chem. Theory Comput.* **2011**, *7*, 4026–4037.

(24) Essmann, U.; Perera, L.; Berkowitz, M. L.; Darden, T.; Lee, H.; Pedersen, L. G. A smooth particle mesh Ewald method. *J. Chem. Phys.* **1995**, *103*, 8577–8593.

(25) Bussi, G.; Donadio, D.; Parrinello, M. Canonical sampling through velocity rescaling. *J. Chem. Phys.* **2007**, *126*, 014101.

(26) Parrinello, M.; Rahman, A. Polymorphic transitions in single crystals: A new molecular dynamics method. *J. Appl. Phys.* **1981**, *52*, 7182–7190.

(27) Feenstra, K. A.; Hess, B.; Berendsen, H. J. C. Improving efficiency of large time-scale molecular dynamics simulations of hydrogen-rich systems. *J. Comput. Chem.* **1999**, *20*, 786–798.

(28) (a) Wormald, S.; Zhang, J. G.; Krebs, D. L.; Mielke, L. A.; Silver, J.; Alexander, W. S.; Speed, T. P.; Nicola, N. A.; Hilton, D. J. The comparative roles of suppressor of cytokine signaling-1 and -3 in the inhibition and desensitization of cytokine signaling. *J. Biol. Chem.* **2006**, *281*, 11135–11143. (b) Nicholson, S. E.; Novak, U.; Ziegler, S. F.; Layton, J. E. Distinct regions of the granulocyte colony-stimulating factor receptor are required for tyrosine phosphorylation of the signaling molecules JAK2, Stat3, and p42, p44MAPK. *Blood* **1995**, *86*, 3698–3704.

Supporting Information - 1

Design, Synthesis, and Characterization of Cyclic Peptidomimetics of the Inducible Nitric Oxide Synthase Binding Epitope That Disrupt the Protein-Protein Interaction Involving SPRY Domain-Containing Suppressor of Cytokine Signaling Box Protein (SPSB) 2 and Inducible Nitric Oxide Synthase

Jitendra R. Harjani,^{†§} Beow Keat Yap,^{†§} Eleanor W. W. Leung,[†] Andrew Lucke,[†] Sandra E. Nicholson,^{‡‡} Martin J. Scanlon,[†] David K. Chalmers,[†] Philip E. Thompson,[†] Raymond S. Norton,^{†*} Jonathan B. Baell^{†*}

[†] Medicinal Chemistry, Monash Institute of Pharmaceutical Sciences, Monash University, Parkville, Victoria 3052, Australia

[‡]The Walter and Eliza Hall Institute of Medical Research, Parkville, Victoria 3052, Australia

^{‡‡}The Department of Medical Biology, University of Melbourne, Parkville, Victoria 3052, Australia

[§]These authors contributed equally

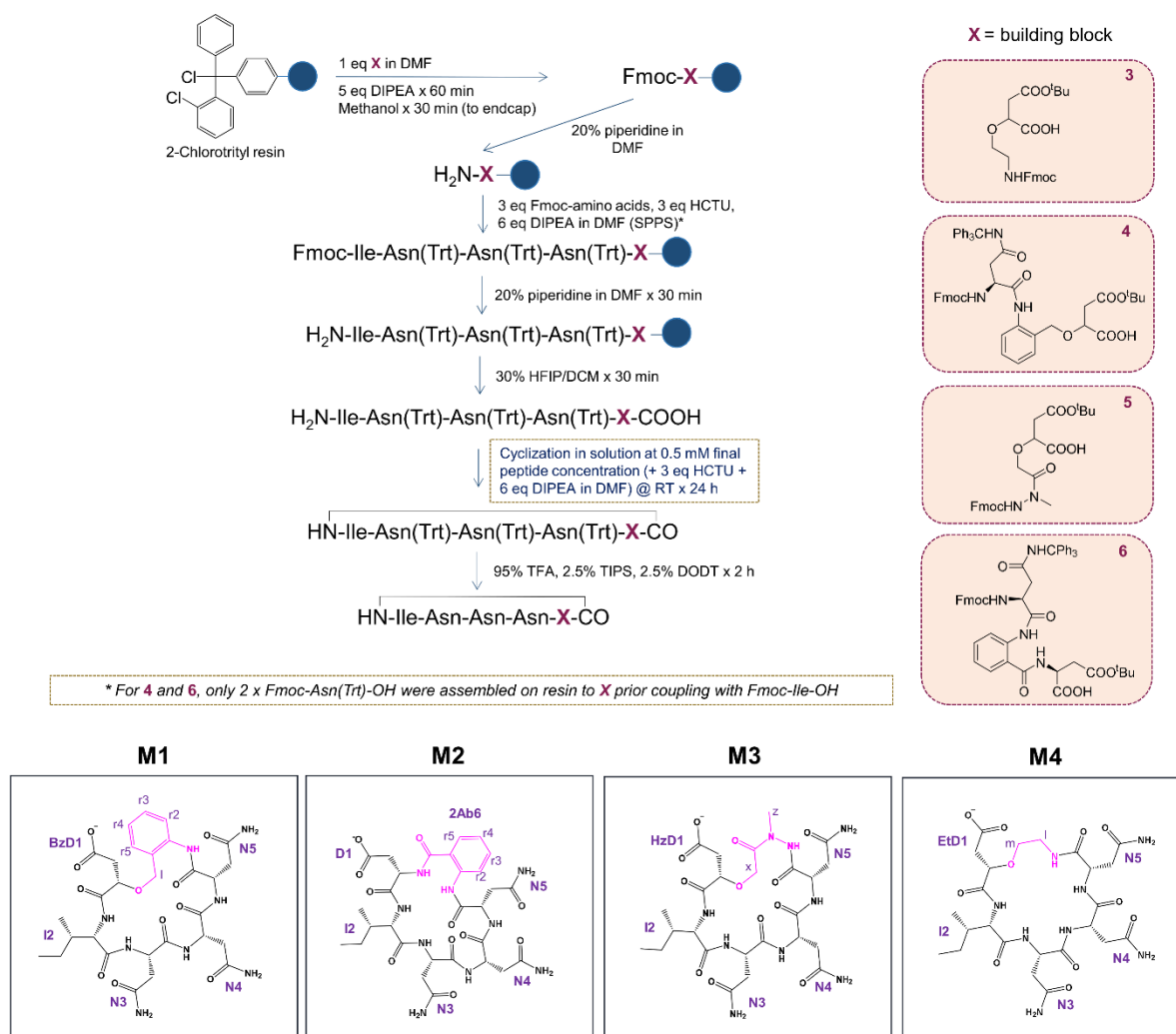


Figure S1. Synthetic pathway used in the assembly of mimetic building block **3**, **4**, **5** and **6** (box in pink) on solid phase peptide synthesis with Fmoc-chemistry to generate peptidomimetic **M4**, **M1**, **M2** and **M3**, respectively. Structure of each peptidomimetic is shown in the bottom panel with linker residue (purple) connecting the *N*- and *C*-termini of peptide DINNN and the atom designations of the organic linker used are labelled.

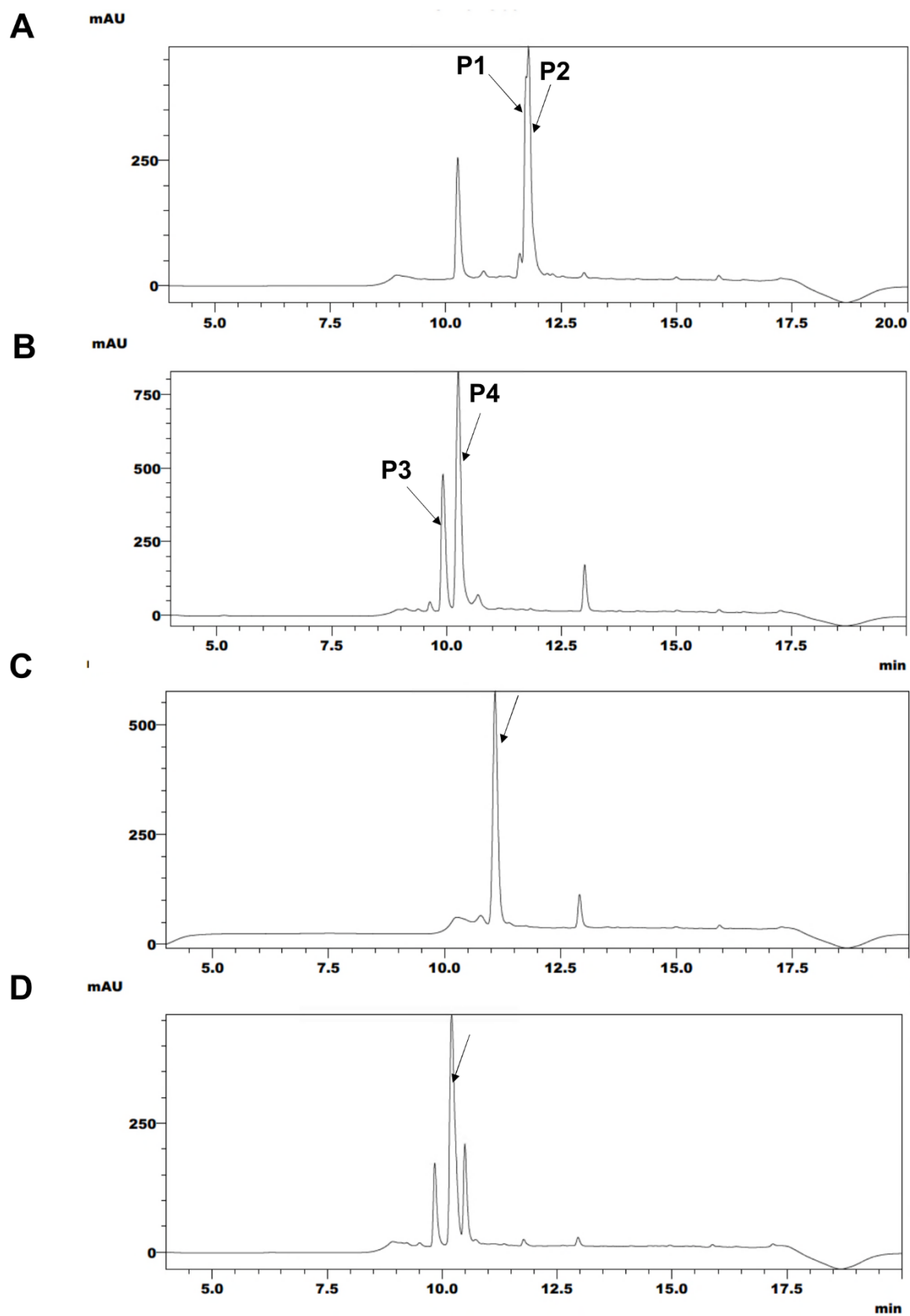


Figure S2. HPLC profiles of the crude cyclic peptidomimetic (A) **M1**, (B) **M2**, (C) **M3** and (D) **M4**. The peaks in the UV trace for which the observed m/z in the MS matched the calculated m/z are highlighted with arrows.

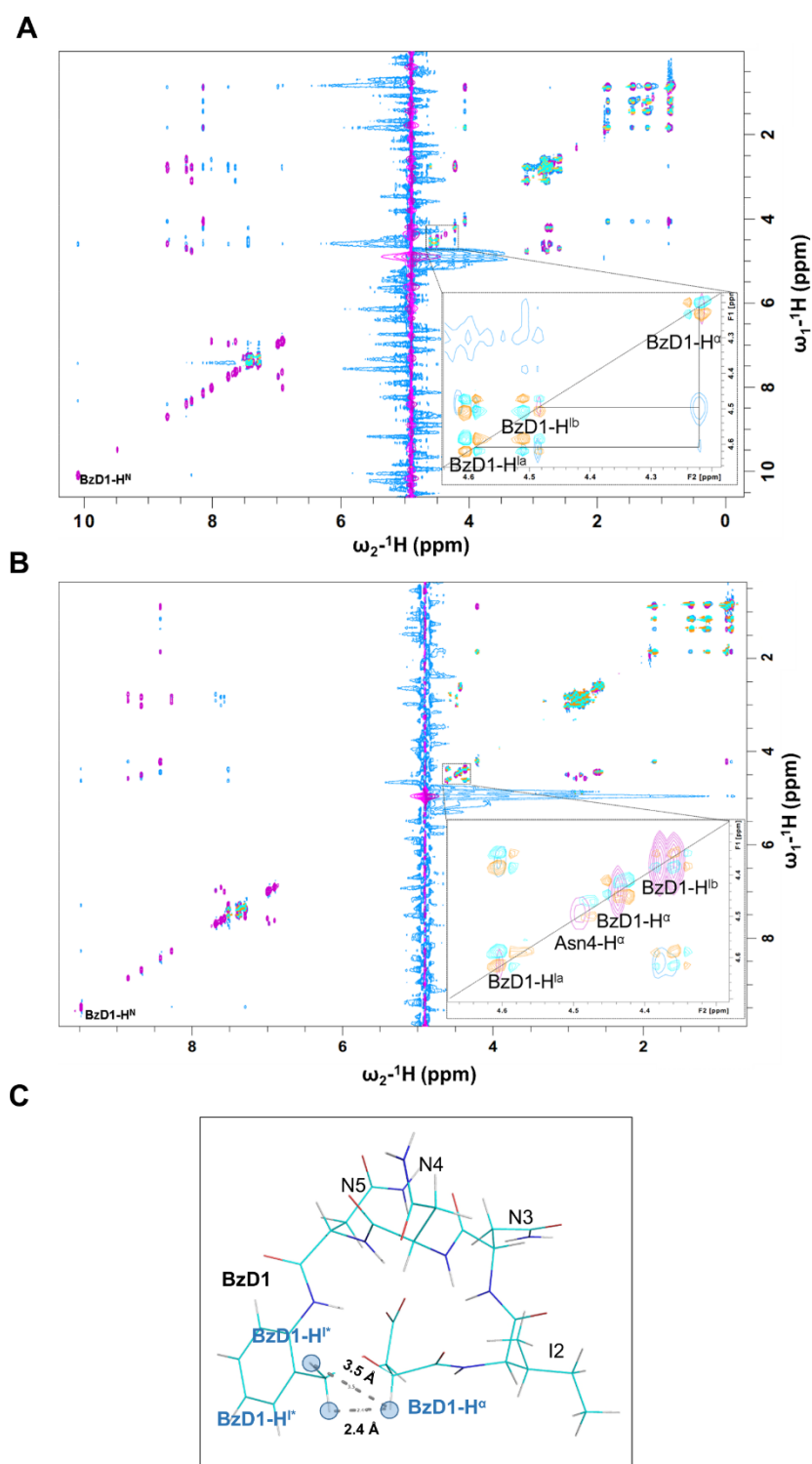


Figure S3. (A) Overlay of 2D [^1H , ^1H] TOCSY (purple) and [^1H , ^1H] ROESY (blue) spectra of the purified product corresponding to peak P1 of peptidomimetic **M1**, in 90% $^1\text{H}_2\text{O}$ and 10% $^2\text{H}_2\text{O}$, pH 4.8 at 10 °C and 2D [^1H , ^1H] DQF-COSY (cyan/brown) spectra in 99.9% $^2\text{H}_2\text{O}$. (B) Overlay of 2D [^1H , ^1H] TOCSY (purple) and [^1H , ^1H] ROESY (blue) spectra of the purified product corresponding to peak P2 of peptidomimetic **M1** in 90% $^1\text{H}_2\text{O}$ and 10% $^2\text{H}_2\text{O}$, pH 4.8 at 10 °C, and 2D [^1H , ^1H] DQF-COSY (cyan/brown) spectra in 99.9% $^2\text{H}_2\text{O}$. (C) *In silico* SPSB2-peptidomimetic **M1** bound model derived from the crystal structure of SPSB2-DINNN linear peptide (PDB: 3EMW) with distances between H^α and H^1 of residue BzD1 shown with grey dotted lines.

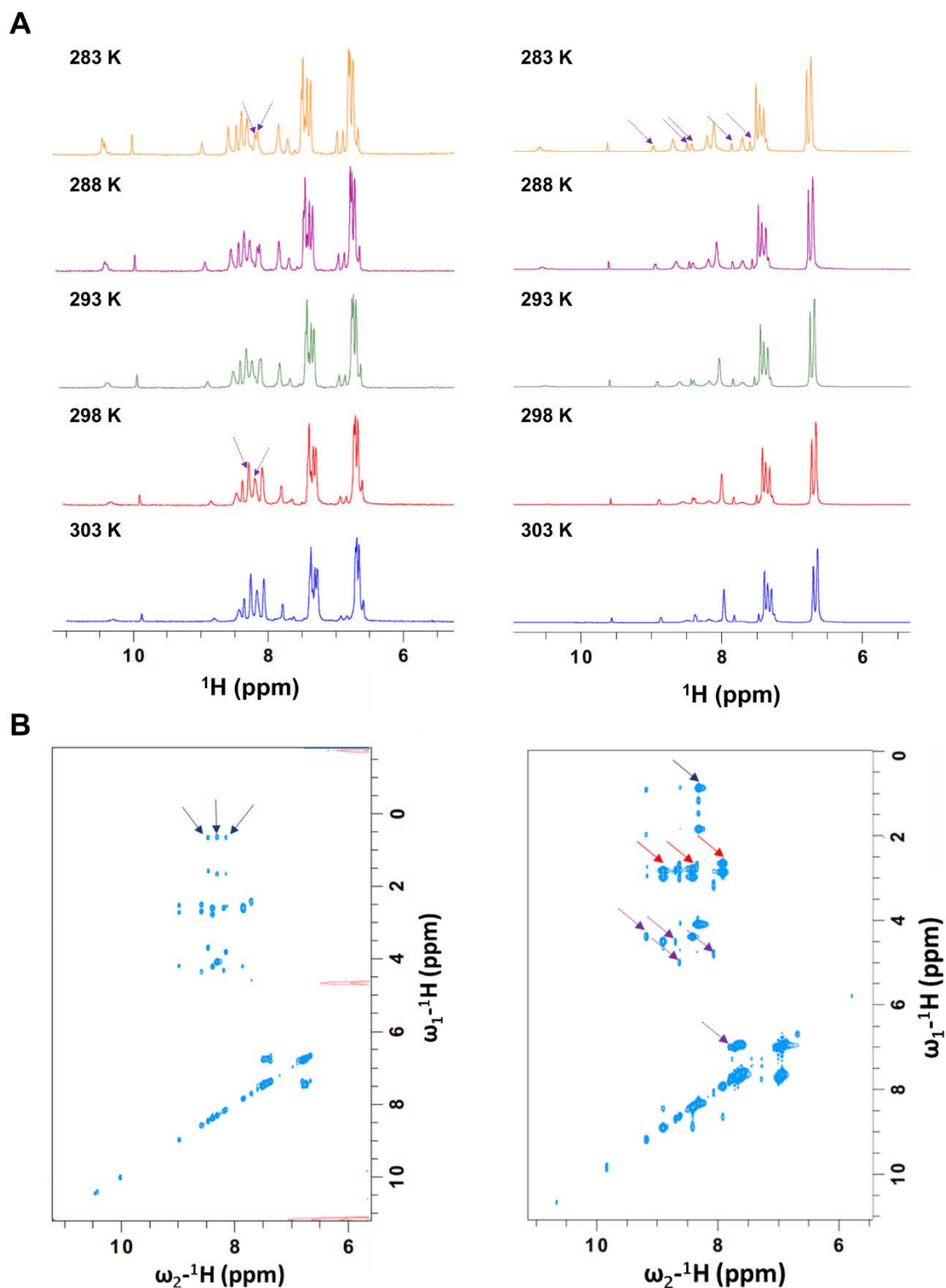


Figure S4. (A) The proton resonances in the backbone and side chain amide regions of ^1H NMR spectra of the purified product corresponding to P3 (left) and P4 (right) of peptidomimetic **M2**, acquired at 600 MHz with temperatures increasing from 10 to 30 $^\circ\text{C}$ in 90% $^1\text{H}_2\text{O}$, 10% $^2\text{H}_2\text{O}$, pH 4.7. Resonances showing peak sharpening (in P3) or no changes in peak intensity (in P4) when temperature increases are labelled in dotted purple arrows. (B) Amide region of 2D $[\text{^1H}, \text{^1H}]$ -TOCSY spectra of the product corresponding to P3 (left) and P4 (right) of peptidomimetic **M2**, acquired at 10 $^\circ\text{C}$ in 90% $^1\text{H}_2\text{O}$, 10% $^2\text{H}_2\text{O}$, pH 4.7, with the spin system exhibiting $\text{A}_3\text{MPT}(\text{B}_3)\text{X}$ or AMX patterns highlighted in solid dark blue arrow and solid dark red arrows, respectively.

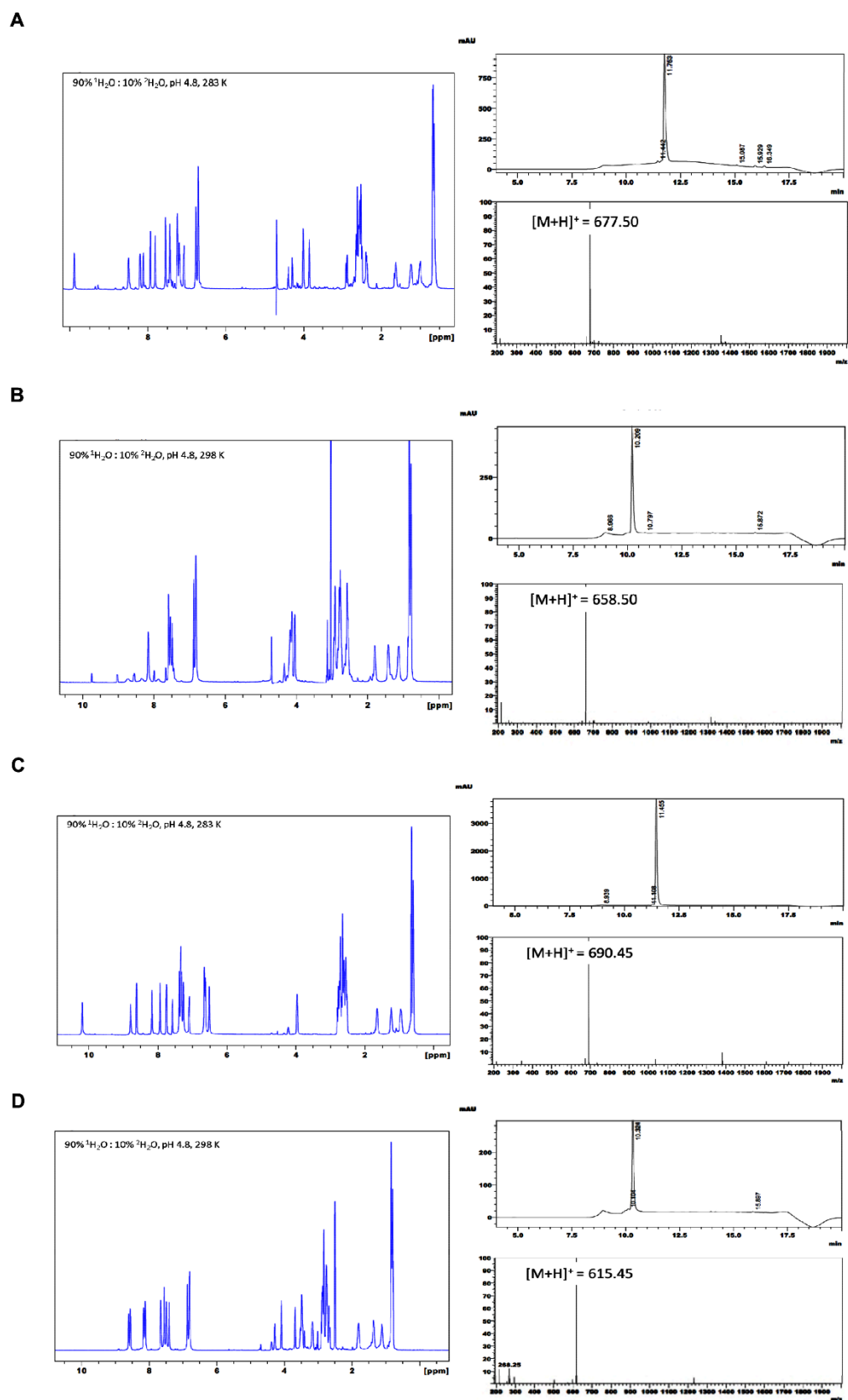


Figure S5. ^1H NMR (left) and LC-MS (right) profiles of purified cyclic peptidomimetics (A) **M1** (P1), (B) **M2** (P4), (C) **M3** and (D) **M4**.

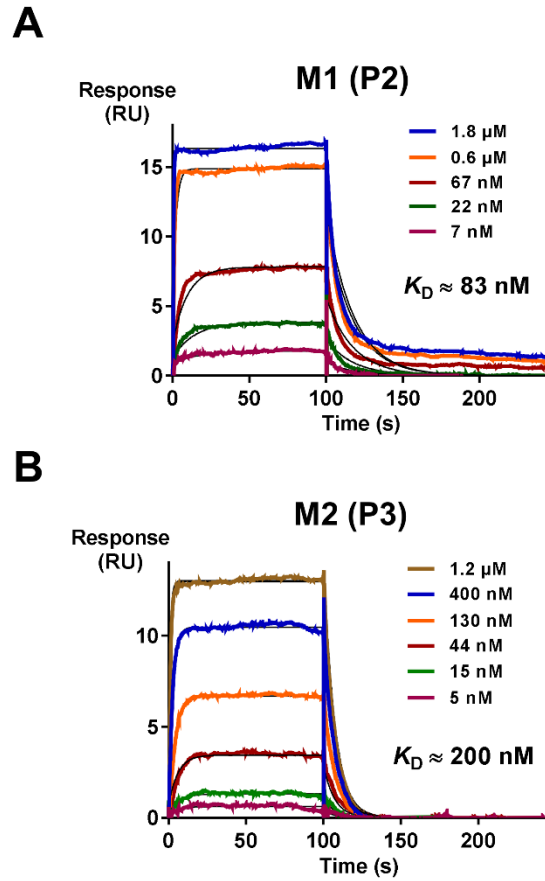


Figure S6. Representative SPR sensorgrams of immobilized SPSB2 exposed to increasing concentrations of mimetic (A) **M1** (P2) and (B) **M2** (P3) in 10 mM HEPES, 150 mM NaCl, 3 mM EDTA and 0.05% Tween 20, pH 7.4 at 25 °C. Data were fitted using a single-site binding model.

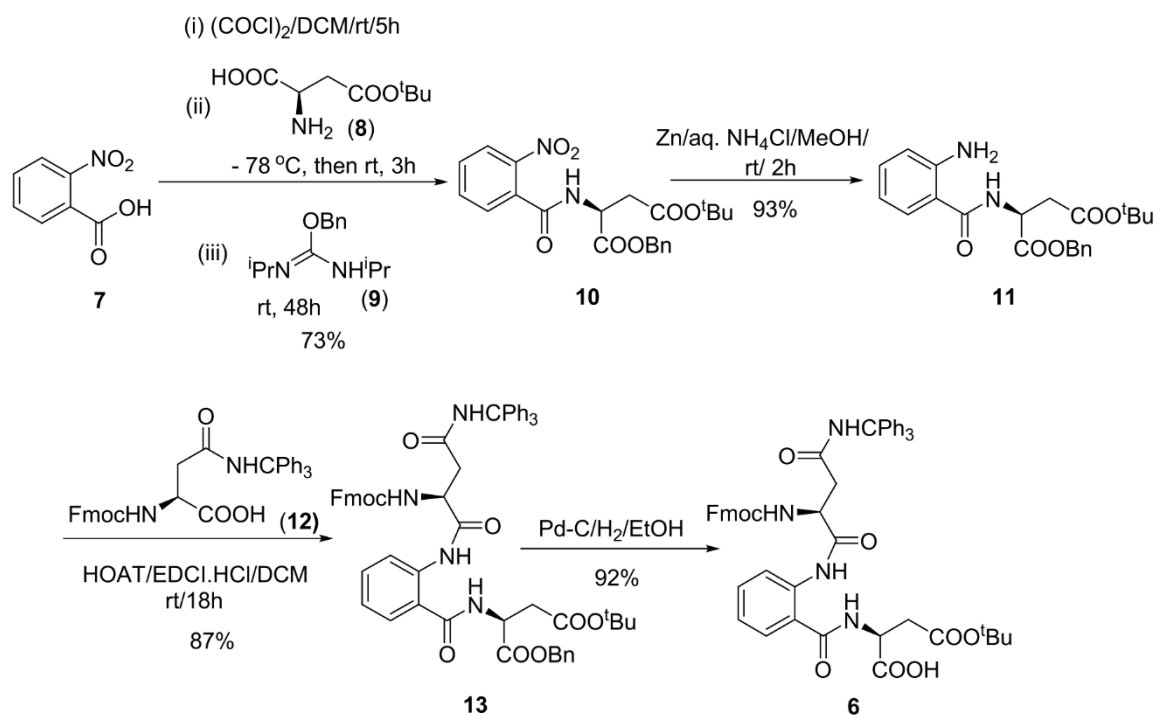


Figure S7. Synthesis of building block **6** required for the synthesis of anthranilamide-based cyclic peptidomimetic **M3**. Details of the synthesis are outlined below.

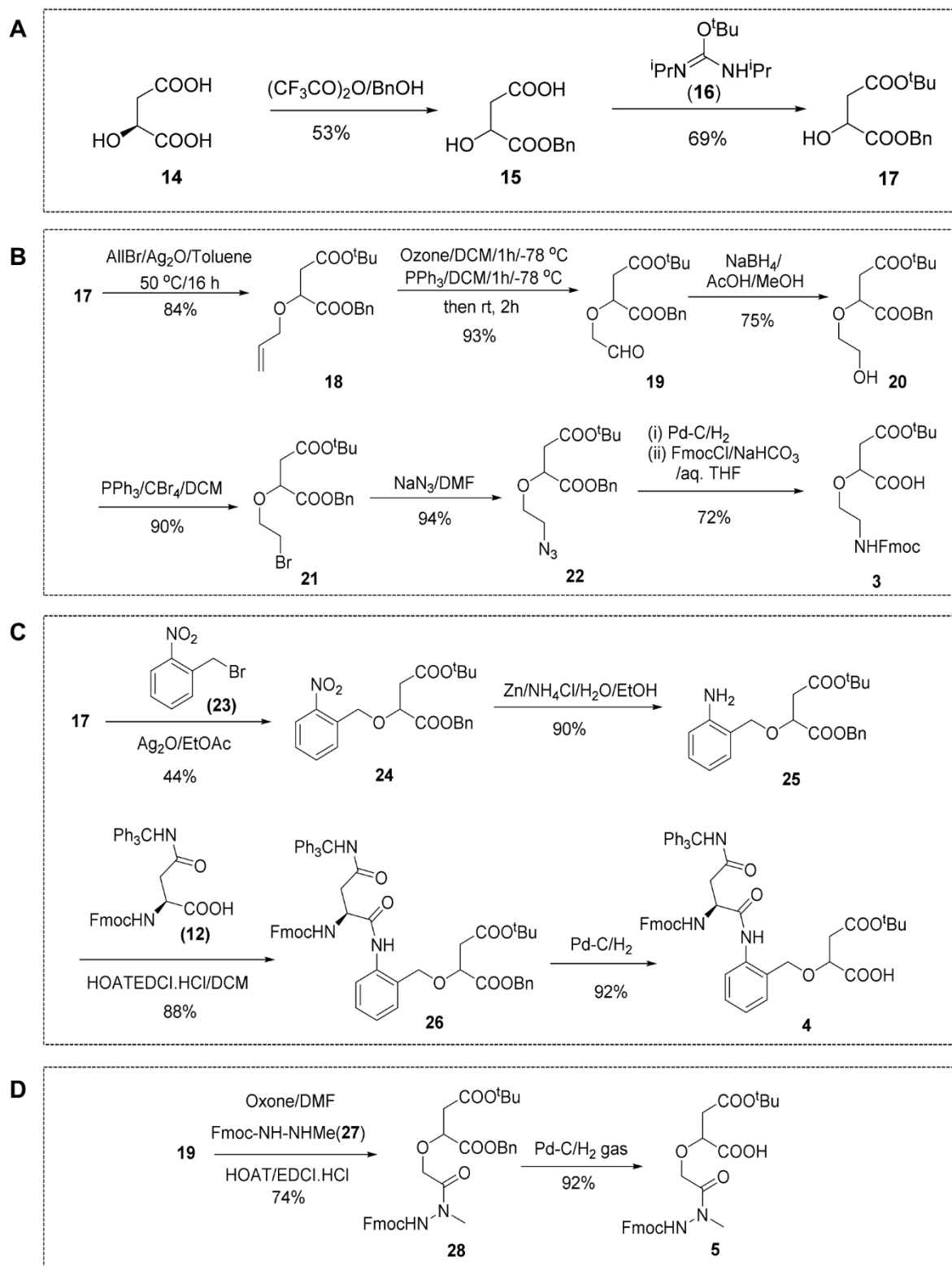


Figure S8. Synthetic schemes for the synthesis of (A) mixed malate **17**, a key intermediate to the synthesis of mimetic building block (B) **3**, (C) **4** and (D) **5**. Details of each of the syntheses are outlined below.

Table S1. The chemical shifts of **M1** (both P1 and P2) in water, pH 4.8 at 10 °C recorded at 600 MHz. The atom designation of residue BzD1 is based on the structure shown in **Figure S1**.

Residue	N	HN	H ^α	C ^α	H ^β	C ^β	Others
P1	ppm						
BzD1	125.5	10.13	4.26	75.3	2.75, 2.80	40.6	H ^{1a} 4.54, H ^{1b} 4.64, H ² 7.48, H ³ 7.44, H ⁴ 7.32, H ⁵ 7.48, C ¹ 69.1, C ² 130.7, C ³ 129.6, C ⁴ 126.8, C ⁵ 125.3
Ile2	118.1	8.18	4.10	59.9	1.87	35.7	H ^{γ1a} 1.25, H ^{γ1b} 1.49, H ^{γ2} 0.92, H ^{δ1} 0.89, C ^{γ1} 25.1, C ^{γ2} 14.5, C ^{δ1} 10.5
Asn3	119.6	8.74	4.64	51.9	2.77, 2.88	35.9	H ^{δ1} 7.01, H ^{δ2} 7.79, N ^δ 114.0
Asn4	116.3	8.44	4.74	50.9	2.63, 2.87	36.0	H ^{δ1} 6.95, H ^{δ2} 8.05, N ^δ 115.6
Asn5	117.9	8.36	4.81	51.5	2.82, 3.14	35.3	H ^{δ1} 6.95, H ^{δ2} 7.68, N ^δ 113.0
P2	ppm						
BzD1	126.6	9.51	4.47	77.0	2.62, 2.66	41.1	H ^{1a} 4.41, H ^{1b} 4.65, H ² 7.33, H ³ 7.41, H ⁴ 7.40, H ⁵ 7.55, C ¹ 67.5, C ² 126.7, C ³ 129.3, C ⁴ 127.7, C ⁵ 129.1
Ile2	121.6	8.46	4.25	59.0	1.89	36.2	H ^{γ1a} 1.18, H ^{γ1b} 1.40, H ^{γ2} 0.92, H ^{δ1} 0.87, C ^{γ1} 24.3, C ^{γ2} 14.7, C ^{δ1} 10.5
Asn3	120.5	8.88	4.61	51.0	2.80, 2.94	35.4	H ^{δ1} 7.01, H ^{δ2} 7.72, N ^δ 113.4
Asn4	114.4	8.71	4.53	51.5	2.85, 3.04	35.2	H ^{δ1} 6.94, H ^{δ2} 7.65, N ^δ 113.5
Asn5	116.4	8.31	4.92	51.0	2.86, 2.96	35.8	H ^{δ1} 7.03, H ^{δ2} 7.60, N ^δ 112.8

Table S2. The chemical shifts of mimetic **M2** (P4) in water, pH 4.7 at 10 °C recorded at 600 MHz. The atom designation of residue HzD1 is based on the structure shown in **Figure S1**.

Residue	N	HN	H ^α	C ^α	H ^β	C ^β	Others
	ppm						
HzD1	117.9	10.83	4.22	79.2	2.68, 2.66	40.8	H ^{x1} 3.93, H ^{x2} 4.23, H ^z 3.12, C ^{x1} 67.4, C ^z 35.2
Ile2	120.4	8.35	4.13	59.1	1.87	35.5	H ^{γ1a} 1.20, H ^{γ1b} 1.50, H ^{γ2} 0.90, H ^{δ1} 0.86, C ^{γ1} 24.9, C ^{γ2} 14.6, C ^{δ1} 10.0
Asn3	121.5	8.94	4.53	51.2	2.85, 3.01	35.3	H ^{δ1} 7.04, H ^{δ2} 7.76, N ^δ 113.7
Asn4	113.0	8.45	4.42	51.9	2.83, 3.01	35.3	H ^{δ1} 6.98, H ^{δ2} 7.71, N ^δ 113.4
Asn5	114.6	7.95	4.94	48.3	2.69, 2.88	35.6	H ^{δ1} 6.97, H ^{δ2} 7.65, N ^δ 112.1

Table S3. The chemical shifts of peptidomimetic **M3** in water, pH 4.7 at 10 °C recorded at 600 MHz. The atom designation of residue 2Ab6 is based on the chemical structure shown in **Figure S1**.

Residue	N	HN	H ^α	C ^α	H ^β	C ^β	Others
	ppm						
Asp1	124.9	8.93	4.83	52.3	2.83, 2.91	38.7	
Ile2	119.5	8.23	4.23	58.7	1.89	35.1	H ^{γ1a} 1.19, H ^{γ1b} 1.48, H ^{γ2} 0.89, H ^{δ1} 0.85, C ^{γ1} 24.7, C ^{γ2} 14.6, C ^{δ1} 9.8
Asn3	123.9	9.18	4.45	51.9	2.78, 2.98	35.1	H ^{δ1} 6.97, H ^{δ2} 7.71, N ^δ 113.4
Asn4	111.5	8.53	4.57	51.7	2.88, 2.98	35.3	H ^{δ1} 6.84, H ^{δ2} 7.65, N ^δ 113.2
Asn5	116.9	8.00	4.97	51.0	2.77, 3.02	36.3	H ^{δ1} 6.94, H ^{δ2} 7.59, N ^δ 112.7
2Ab6	126.7	10.48					H ^{r2} 7.78, H ^{r3} 7.60, H ^{r4} 7.34, H ^{r5} 7.57, C ^{r2} 123.1, C ^{r3} 132.2, C ^{r4} 125.8, C ^{r5} 128.4

Table S4. The chemical shifts of peptidomimetic **M4** in water, pH 4.7 at 25 °C recorded at 600 MHz. The atom designation of residue EtD1 is based on the chemical structure shown in **Figure S1**.

Residue	N	HN	H ^α	C ^α	H ^β	C ^β	Others
	ppm						
EtD1	115.0	7.75	4.37	77.3	2.59	40.3	H ^{1a} 3.58, H ^{1b} 3.78, H ^{ma} 3.26, H ^{mb} 3.56, C ¹ 68.5, C ^m 39.4
Ile2	121.6	8.21	4.18	59.0	1.90	36.3	H ^{γ1a} 1.20, H ^{γ1b} 1.45, H ^{γ2} 0.92, H ^{δ1} 0.89, C ^{γ1} 24.7, C ^{γ2} 14.7, C ^{δ1} 10.6
Asn3	120.3	8.65	4.65	50.6	2.82, 2.93	35.8	H ^{δ1} 6.96, H ^{δ2} 7.64, N ^δ 113.2
Asn4	114.8	8.70	4.47	51.9	2.84, 2.98	35.0	H ^{δ1} 6.91, H ^{δ2} 7.58, N ^δ 113.0
Asn5	116.7	8.25	4.70	50.8	2.76, 2.95	35.9	H ^{δ1} 6.89, H ^{δ2} 7.50, N ^δ 112.6

Table S5. Intramolecular and intermolecular hydrogen bonds between SPSB2 and cyclic peptidomimetic **M1** with occupancy of >25 % during a 1 μs molecular dynamics simulation of the complex

Donor	Acceptor	% Occupancy
Hydrogen bonds between SPSB2 and M1		
M1 -N5-Side	V206-Main	51
R68-Side	M1 -N5-Side	40
M1 -N3-Side	T102-Side	35
Y120-Side	M1 -BzD1-Side	31
Q73-Main	M1 -BzD1-Side	30
G208-Main	M1 -N3-Main	30
T102-Main	M1 -N3-Side	27
Intramolecular hydrogen bonds of M1		
M1 -N5-Side	M1 -BzD1-Side	52
M1 -N3-Main	M1 -BzD1-Side	34

Materials and methods used in the synthesis of mimetic building blocks 3, 4, 5 and 6

The following chemicals were procured from commercial suppliers: 2-nitrobenzoic acid (Sigma Aldrich, 95%), oxalyl chloride (Alfa Aesar, 98%), *L*-aspartic acid- β -*tert*-butylester (Chem Impex, 99%), benzyl alcohol (BnOH, Alfa Aesar, 99%), copper(I)chloride (Sigma Aldrich, 97%), zinc dust (Sigma Aldrich, 10 μ m, 98%), *N,N'*-diisopropylcarbodiimide (DIC, Oakwood Chemical, > 99%), ammonium chloride (Merck Millipore, ACS reagent grade), *N*^α-Fmoc-*N*^γ-trityl-*L*-asparagine (Chem Impex, 99%), 1-hydroxy-7-azabenzotriazole (HOAT, AK Scientific, 99%), 1-(3-dimethylaminopropyl)-3-ethylcarbodiimide hydrochloride (EDC_i.HCl, AK Scientific, 99%), Pd-C (10% loading, wetted with ca. 53% water, AK Scientific), *tert*-butyl alcohol (Bu^tOH, Alfa Aesar, ACS reagent, 99%), L-malic acid (Chem Impex, 99%), trifluoroacetic anhydride (Oakwood Chemical, 99%), allyl bromide (Sigma Aldrich, reagent grade, 97%), potassium peroxymonosulfate (Oxone®, monopersulfate compound, Sigma Aldrich), silver(I)oxide (Ag₂O, Merck Millipore, > 99%), triphenylphosphine (PPh₃, Sigma Aldrich, reagent plus, 99%), sodium borohydride (NaBH₄, Alfa Aesar, 98%), glacial acetic acid (AcOH, Merck Millipore, ACS reagent, 100%), carbon tetrabromide (CBr₄, Alfa Aesar, 98%), sodium azide (NaN₃, Alfa Aesar, 99%), sodium chloride (NaCl, Merck Millipore, ACS reagent, > 99%), sodium hydrogen carbonate (NaHCO₃, Merck Millipore, ACS reagent), fluorenylmethoxycarbonyl chloride (FmocCl, Oakwood Chemical, 97%), Di-*tert*-butyl dicarbonate (Boc₂O, AK Scientific, 99%), trifluoroacetic acid (TFA, Alfa Aesar, 99%), 2-nitrobenzyl bromide (AK Scientific, 98%), methyl hydrazine (Sigma Aldrich, 98%), hydrogen (Air Liquide, > 99%), anhydrous magnesium sulfate (MgSO₄, Merck Millipore, ACS reagent grade) and 37% hydrochloric acid (HCl, Merck Millipore, ACS reagent grade). Isoreas **9**¹ and **16**² were synthesized using procedures described in the literature. Their yield and characterization data were consistent with those reported in the literature.^{1,2} Analytical grade solvents dichloromethane (DCM), Chloroform (CHCl₃), diethyl ether (Et₂O), methanol (MeOH), ethyl acetate (EtOAc), ethanol (EtOH), tetrahydrofuran (THF), dimethyl formamide (DMF) and hexanes, supplied by Merck were used during synthetic manipulations, workups and separations. Analytical TLC was performed on silica gel 60/F254 pre-coated aluminium sheets (0.25 mm, Merck). Celite® S (Sigma Aldrich) was used as a filter aid. Flash chromatography was carried out with the SiliaFlash® P 60 (SiliCycle, 40–64 μ m, 230–400 mesh).

NMR

¹H and ¹³C NMR spectra were recorded at 400.13 and 100.62 MHz respectively, on a Bruker Avance III Nanobay spectrometer with a BACS 60 sample changer. The NMR solvents were purchased from Cambridge Isotope Laboratories. Chemical shifts (δ , ppm) are reported relative to the solvent peak (CDCl₃): 7.26 [¹H] or 77.16 [¹³C]; DMSO *d*₆: 2.50 [¹H] or 39.52 [¹³C]). Proton resonances are annotated as: chemical shift (δ), multiplicity (s, singlet; d, doublet; m, multiplet), coupling constant (*J*, Hz), and the number of protons.

LCMS

Low resolution mass spectrometry analyses were performed with an Agilent 6100 Series Single Quad LC/MS coupled with an Agilent 1200 Series HPLC, 1200 Series G1311A quaternary pump, 1200 series G1329A thermostated autosampler and 1200 series G1314B variable wavelength detector. The conditions for liquid chromatography were: reverse phase HPLC analysis fitted with a Phenomenex Luna C8(2) 5 μ m (50 x 4.6 mm) 100 Å column; column temperature: 30 °C; injection volume: 5 μ L; solvent: 99.9% acetonitrile, 0.1% formic acid; gradient: 5–100% of solvent over 10 min; detection: 254 nm. The conditions for mass spectrometry were: quadrupole ion source; ion mode: multimode-ES; drying gas temp: 300 °C; vaporizer temperature: 200 °C; capillary voltage: 2000 V (positive), 4000 V (negative); scan range: 100-1000 m/z; step size: 0.1 sec; acquisition time: 10 min. In case of **23**, 5 min acquisition time was used.

HRMS

High resolution MS was performed with an Agilent 6224 TOF LC/MS coupled to an Agilent 1290 Infinity LC. All data were acquired and reference mass corrected via a dual-spray electrospray ionisation (ESI) source. Each scan or data point on the total ion chromatogram (TIC) is an average of 13,700 transients, producing a spectrum every second. Mass spectra were created by averaging the scans across each peak and subtracting the background from the first 10 s of the TIC. Acquisition was performed using the Agilent Mass Hunter Data Acquisition software ver. B.05.00 Build 5.0.5042.2 and analysis was performed using Mass Hunter Qualitative Analysis ver. B.05.00 Build 5.0.519.13. Acquisition parameters: mode, ESI; drying gas flow, 11 L/min; nebuliser pressure, 45 psi; drying gas temperature, 325 °C; voltages: capillary, 4000 V; fragmentor, 160 V; skimmer, 65 V; octapole RF, 750 V; scan range, 100–1500 m/z; positive ion mode internal reference ions, m/z 121.050873 and 922.009798. LC conditions: Agilent Zorbax SB-C18 Rapid Resolution HT (2.1 x 50 mm, 1.8 mm column), 30 °C; sample

(5 μ L) was eluted using a binary gradient (solvent A: 0.1% aq. HCO₂H; solvent B: 0.1% HCO₂H in CH₃CN; 5–100% B [3.5 min], 0.5 mL/min).

Synthesis and characterization of mimetic building blocks 3, 4, 5 and 6

Synthesis of mimetic building block 6

The synthesis of the building block **6**, required for synthesis of the anthranilamide-based cyclic peptidomimetic **D** used 2-nitrobenzoic acid as the synthetic equivalent for the anthranilamide core (**Figure S7**).³ 2-Nitrobenzoic acid **7** was activated as an acid chloride using oxalyl chloride in DCM in the presence of catalytic DMF as a promoter.^{3b} At low temperatures, the nitrobenzoyl chloride was treated with triethylamine and then with the half ester of aspartic acid **8** to obtain the corresponding benzamide derivative. After the usual workup, the benzamide derivative of the half aspartate ester was subjected to esterification with the *N,N'*-diisopropyl-*O*-benzyl isourea **9** to obtain the nitrobenzamide derivative of the aspartate mixed diester **10**.^{1,4} This three-step continuous process of amide synthesis and esterification provided efficient access to **10** starting with 2-nitrobenzoic acid. The nitro group in **10** was then reduced with zinc and ammonium chloride in aqueous MeOH to generate the corresponding anthranilamide **11**.⁵ The selectivity of this zinc-mediated method towards the reduction of –NO₂ group over the –COOBn group is evident from the excellent yields of anthranilamide **11** isolated from this reaction. The amide coupling of Fmoc-*N*-trityl-*L*-asparagine, **12** with **11**, mediated by HOAT and EDCi.HCl at room temperature furnished the anilide derivative **13** in good yields.⁶ The Pd-C-mediated hydrogenolysis of the benzyl ester group in **13** under hydrogen atmosphere provided neutral conditions, leaving the Fmoc and trityl protection groups unaffected in **6**.

Synthesis of 10: DMF (50 μ L) was added to the suspension of 2-nitrobenzoic acid (2.505 g, 15 mmol) in dry DCM (100 mL), and maintained under nitrogen atmosphere at -40 °C. This was followed by the dropwise addition of oxalyl chloride (1.905 g, 15 mmol) while provisions were made to compensate for the buildup of excess pressure caused by the evolution of the gaseous by-products (such as CO, CO₂ and HCl). The reaction mixture was slowly allowed to reach room temperature, at which point gas evolution became more apparent. As the solution became clear (in about 3 h), the gas evolution subsided and the reaction was complete. DCM (100 mL) was added to the resultant benzoyl chloride solution and it was cooled to -78 °C. This was followed by dropwise addition of triethylamine (3.03 g, 30 mmol) followed by a portion-wise addition of *L*-aspartic acid- β -*tert*-butylester (2.835 g, 15 mmol) while still maintaining the reaction mixture at -78 °C. The solution was once again allowed to slowly reach room temperature. Stirring was continued at room temperature for 2 h. Water (150 mL) was added to the reaction mixture and it was stirred vigorously to separate the ionic triethylammonium salts from the benzamide in the DCM layer. The DCM layer was separated, dried over anhydrous MgSO₄ and evaporated under reduced pressure to obtain a light yellow solid that was treated with a solution of *N,N'*-diisopropyl-*O*-benzylisourea **9** (3.744 g, 16 mmol) in DCM (100 mL). This reaction mixture was stirred for 48 h at room temperature. After assuring the completion of the esterification reaction by TLC, the reaction mixture was filtered through Celite® (10 g) and washed with DCM (3 \times 10 mL). The filtrate and washings were combined and evaporated under reduced pressure to obtain the crude product. Pure **10** was separated from the crude product by column chromatography (20% EtOAc in hexanes). Yield: 73%, 4.691 g.

1-Benzyl 4-(*tert*-butyl) (2-nitrobenzoyl)-*L*-aspartate **10**: Light yellow viscous liquid. $[\alpha]_D^{20} = -9.6^\circ$ ($c = 1$, CHCl₃). IR (neat) ν_{\max} 851, 901, 955, 1046, 1076, 1117, 1148, 1192, 1213, 1256, 1287, 1346, 1366, 1412, 1454, 1476, 1499, 1528, 1576, 1613, 1649, 1655, 1670, 1724, 2980, 3291 cm⁻¹. ¹H NMR (400 MHz, DMSO *d*₆): $\delta = 9.27$ – 9.25 (d, $J = 7.6$ Hz, 1H), 8.06 – 8.04 (d, $J = 8.0$ Hz, 1H), 7.82 – 7.78 (m, 1H), 7.73 – 7.69 (m, 1H), 7.51 – 7.49 (dd, $J = 7.6$, 1.2 Hz, 1H), 7.40 – 7.31 (m, 5H), 5.21 – 5.14 (AB of benzyl, $J = 14.6$, 12.6 Hz, 2H), 4.84 – 4.79 (X of ABX, dd, $J = 14.8$, 7.2 Hz, 1H), 2.88 – 2.69 (AB of ABX, $J = 16.4$, 7.2 , 6.4 Hz, 2H), 1.39 (s, 9 H) ppm. ¹³C NMR (101 MHz, DMSO *d*₆): $\delta = 170.09$, 168.86 , 165.36 , 146.92 , 135.76 , 133.62 , 131.68 , 131.03 , 129.03 , 128.42 , 128.11 , 127.89 , 124.15 , 80.63 , 66.43 , 49.25 , 36.51 , 27.63 ppm. LCMS (EI+): m/z 451.1 (MNa)⁺, $t_R = 6.61$ min (100%). HRMS (EI): calcd. for C₂₂H₂₄N₂O₇Na [M+Na]⁺: m/z 451.1476; Found: m/z 451.1478.

Synthesis of 11: A clear solution of **10** (4.28 g, 10 mmol) in MeOH (100 mL) was obtained by heating the mixture to 40 °C while being stirred. Zinc (6.50 g, 100 mmol) was added to the resultant solution. The heating was discontinued to allow the solution to reach room temperature. An aqueous solution of NH₄Cl (5.35 g, 100 mmol)

was added drop wise into the suspension of zinc in the methanolic solution of **10**. The solution was stirred at room temperature for 2 h and then monitored by TLC. Once the conversion was verified, the solution was filtered and the residual zinc was washed with MeOH (2×15 mL). The filtrate and washings were combined and evaporated under reduced pressure to obtain a nearly dry residual mass that was treated with water (100 mL) and DCM (100 mL). The product was extracted into the DCM layer. The DCM layer was separated, dried over anhydrous MgSO₄ and evaporated under reduced pressure. Pure **11** was separated from the crude product by column chromatography (20% EtOAc in hexanes). Yield 93%, 3.706 g.

1-Benzyl 4-(*tert*-butyl) (2-aminobenzoyl)-*L*-aspartate **11**: Colorless viscous liquid. $[\alpha]_D^{20} = +18.8^\circ$ ($c = 1$, CHCl₃). IR (neat): ν_{\max} 847, 901, 953, 1030, 1150, 1190, 1211, 1252, 1293, 1327, 1346, 1366, 1393, 1410, 1452, 1483, 1501, 1508, 1561, 1584, 1613, 1642, 1647, 1719, 2932, 2976, 3356, 3458 cm⁻¹. ¹H NMR (400 MHz, DMSO *d*₆): $\delta = 8.64$ – 8.62 (d, $J = 8.0$ Hz, 1H), 7.49 – 7.47 (d, $J = 8.0$ Hz, 1H), 7.36 – 7.30 (m, 5H), 7.18 – 7.14 (m, 1H), 6.72 – 6.70 (d, $J = 8.4$, 1H), 6.54 – 6.50 (m, 1H), 6.40 (bs, 2H), 5.15 (s, 2H), 4.87 – 4.82 (X of ABX, $J = 14.6$, 7.4 Hz, 1H), 2.90 – 2.69 (AB of ABX, $J = 16.0$, 8.0, 6.4 Hz, 2H), 1.37 (s, 9H) ppm. ¹³C NMR (101 MHz, DMSO *d*₆): $\delta = 170.95$, 169.24, 168.82, 149.85, 135.91, 132.13, 128.38, 128.29, 128.01, 127.70, 116.41, 114.49, 113.65, 80.39, 66.17, 49.13, 36.82, 27.64 ppm. LCMS (EI+): m/z 421.1 (MNa)⁺, $t_R = 6.69$ min (100%). HRMS (EI): calcd. for C₂₂H₂₇N₂O₅ [M+H]⁺: m/z 399.1914; Found: m/z 399.1913.

Synthesis of 13: To a solution of **11** (2.790 g, 7 mmol) in DCM (100 mL), *N*⁹-Fmoc-*N*⁷-trityl-*L*-asparagine **12** (4.178 g, 7 mmol), HOAT (1.047 g, 7.7 mmol) and EDCi.HCl (1.478 g, 7.7 mmol) were added. The resulting solution was stirred at room temperature for 16 h. After verifying the completion of the reaction by TLC, water (100 mL) was added to the reaction mixture and the resultant solution was stirred vigorously. The DCM layer was separated, dried over anhydrous MgSO₄ and evaporated under reduced pressure. Pure **13** was separated from the crude product by column chromatography (50% EtOAc in hexanes). Yield 87 %, 5.950 g.

1-Benzyl 4-(*tert*-butyl) (2-((*S*)-2-(((9*H*-fluoren-9-yl)methoxy)carbonyl)amino)-4-oxo-4-(tritylamino)butanamido)benzoyl)-*L*-aspartate **13**: White solid. MP: 101–103 °C. $[\alpha]_D^{20} = -30.4^\circ$ ($c = 1$, THF). IR (neat): ν_{\max} 843, 903, 1001, 1036, 1080, 1148, 1209, 1244, 1290, 1366, 1393, 1447, 1489, 1495, 1505, 1586, 1651, 1682, 1715, 1723 cm⁻¹. ¹H NMR (400 MHz, DMSO *d*₆): $\delta = 9.21$ – 9.19 (d, $J = 8.0$ Hz, 1H), 8.69 (s, 1H), 8.60 – 8.58 (d, $J = 8.4$ Hz, 1H), 8.11 – 8.09 (d, $J = 7.6$ Hz, 1H), 7.90 – 7.88 (d, $J = 7.6$ Hz, 2H), 7.82 – 7.81 (d, $J = 6.8$ Hz, 2H), 7.75 – 7.74 (d, $J = 7.6$ Hz, 1H), 7.60 – 7.56 (m, 2H), 7.43 – 7.36 (m, 3H), 7.29 – 7.16 (m, 21H), 5.13 – 5.06 (AB of benzyl, $J = 18.0$, 12.4 Hz, 2H), 4.94 – 4.88 (dd, $J = 14.4$, 7.6 Hz, 1H), 4.53 – 4.49 (dd, $J = 5.6$, 9.2 Hz, 1H), 4.42 – 4.36 (dd, $J = 13.6$, 7.6 Hz, 1H), 4.30 – 4.19 (m, 2H), 2.89 – 2.69 (m, 4H), 1.26 (m, 9H) ppm. ¹³C NMR (101 MHz, DMSO): $\delta = 170.54$, 170.31, 169.01, 168.99, 168.17, 155.99, 144.73, 144.10, 143.56, 140.82, 140.71, 139.03, 135.66, 132.64, 128.61, 128.36, 128.06, 127.78, 127.69, 127.62, 127.45, 127.06, 126.38, 125.52, 125.16, 122.87, 120.17, 120.13, 120.09, 119.58, 80.48, 69.51, 66.46, 66.30, 53.91, 49.28, 46.79, 38.34, 36.46, 27.51 ppm. LCMS (EI+): m/z 999.2 (MNa)⁺, $t_R = 7.79$ min (100%). HRMS (EI): calcd. for C₆₀H₅₇N₄O₉ [M+H]⁺: m/z 977.4120; Found: m/z 977.4126.

Synthesis of 6: Pd-C (of 10% loading with 53% moisture content; 0.293 g) was added to the solution of **13** (2.931 g, 3 mmol) in EtOH (200 mL). The solution was initially purged with hydrogen gas and then maintained under hydrogen atmosphere for 48 h at room temperature while being stirred. Once the completion of the reaction was ensured by TLC, the ethanolic solution was filtered through Celite® (20 g) and washed with EtOH (3×20 mL). The filtrate and washings were combined and evaporated under reduced pressure to produce the crude product which was analytically pure. Yield: 92%, 2.448 g.

(*S*)-2-(2-((*S*)-2-(((9*H*-fluoren-9-yl)methoxy)carbonyl)amino)-4-oxo-4-(tritylamino)butanami do)benzamido)-4-(*tert*-butoxy)-4-oxobutanoic acid **6**: White solid. MP: 158–160 °C. $[\alpha]_D^{20} = -20.8^\circ$ ($c = 1$, THF). IR (neat): ν_{\max} 669, 696, 737, 756, 843, 901, 1001, 1034, 1148, 1246, 1275, 1366, 1445, 1506, 1586, 1651, 1682, 1717 cm⁻¹. ¹H NMR (400 MHz, DMSO *d*₆): $\delta = 8.98$ – 8.96 (d, $J = 8.0$ Hz, 1H), 8.69 (s, 1H), 8.59 – 8.57 (d, $J = 8.4$ Hz, 1H), 8.14 – 8.12 (d, $J = 7.2$ Hz, 1H), 7.91 – 7.88 (dd, $J = 7.6$, 2.8 Hz, 2H), 7.84 – 7.80 (m, 2H), 7.76 – 7.74 (d, $J = 7.2$ Hz, 1H), 7.58 – 7.54 (m, 1H), 7.43 – 7.37 (m, 2H), 7.29 – 7.14 (m, 20H), 4.85 – 4.79 (dd, $J = 14.4$, 8.0 Hz, 1H), 4.51 – 4.47 (dd, $J = 9.2$, 5.6 Hz, 1H), 4.36 – 4.16 (m, 3H), 2.83 – 2.63 (m, 4H), 1.26 (s, 9H) ppm. ¹³C NMR (101 MHz, DMSO *d*₆): $\delta = 172.16$, 170.57, 169.38, 168.93, 167.85, 156.00, 144.72, 144.07, 143.56, 140.80, 140.68, 139.06, 132.44, 128.59, 128.27, 127.70, 127.62, 127.44, 127.10, 126.37, 125.54, 125.19, 122.83, 120.12, 120.09, 120.05, 119.77, 80.15, 69.49, 66.31, 54.05, 49.45, 46.74, 38.37, 36.89, 27.55 ppm. LCMS (EI-): m/z 885.3 (M-H)⁻, $t_R = 7.25$ min (96%). HRMS (EI): calcd. for C₅₃H₅₁N₄O₉ [M+H]⁺: m/z 887.3651; found: m/z 887.3634.

Synthesis of mixed malate ester required for synthesis of mimetic building block 3, 4 and 5

Selective activation of the carboxylic acid group at C1 of L-malic acid **14** was achieved using trifluoroacetic anhydride, which resulted in formation of the C1 benzyl monoester of L-malic acid upon treatment with benzyl alcohol (**Figure S8A**).⁷ The malic acid half ester **15** was further esterified with *N,N'*-diisopropyl-*O*-*tert*-butylisourea **16** to produce the mixed malate ester **17**.⁸ The mixed malate **17**, with two orthogonal protecting groups at the two carboxylic acid functional groups, was critical in allowing for the generation of the free –COOH at the desired position, under neutral hydrogenolytic conditions, in the last step of the synthesis of the peptidomimetic building blocks **3**, **4** and **5**. The *tert*-butyl ester group on the other –COOH group of the malate **17** was not only required to keep the peptidomimetic building-blocks **3**, **4** and **5** compatible with the Fmoc solid phase peptide synthesis chemistries, but also helped prevent the participation of the free –COOH group in the reactions used for the synthesis of **3**, **4** and **5**. Although the literature claims that the stereochemistry at the chiral malate *C*-atom remains unchanged,^{8a,9} optical rotation measurements, however, indicate that the conversion of **14** to **15** leads to racemisation of the malate. Although racemisation was unexpected and undesirable, it was not likely to pose a significant problem in achieving our overall goal of synthesizing **B**, **C** and **E**. Bearing in mind that RP-HPLC purifications are commonly employed in peptide purifications as a final step, the synthesis of **3**, **4** and **5** that were racemic at malate, was attempted starting with racemic malate diester **17**.

Synthesis of 15: L-Malic acid (10.00 g, 74.63 mmol) was placed in a round bottom flask (RBF) that was cooled under ice. Trifluoroacetic anhydride (47.04 g, 224 mmol) was added dropwise into the RBF and maintained under nitrogen atmosphere. The solution was stirred at 0 °C for 3 h, by which time the *L*-malic acid dissolved in trifluoroacetic anhydride generating a clear solution. While continuing to maintain the solution at 0 °C, trifluoroacetic anhydride was evaporated under reduced pressure generating a viscous liquid that eventually solidified. Benzyl alcohol (24.19 g, 224 mmol) was added to the residual mass and the resulting solution was slowly warmed up to room temperature while being stirred. The reaction mixture was stirred at room temperature for 16 h. A 15% aqueous solution of Na₂CO₃ (200 mL) was added to the reaction mixture resulting in a clear basic solution whose pH was adjusted to 7 by gradually adding 6N aq. HCl. This caused the separation of benzyl alcohol from the aq. solution. Benzyl alcohol was removed from the aqueous solution using EtOAc (3×75 mL) for extractions. The aqueous layer was acidified further to pH 2 with 6N aq. HCl, causing the separation of monobenzyl ester of malate. The aqueous layer was saturated with sodium chloride and the product was extracted from the aqueous layer with EtOAc (3×75 mL). The EtOAc layers were combined, dried over anhydrous MgSO₄ and evaporated under reduced pressure to yield the malate monoester **15**. Yield: 53%, 8.860 g.

4-(Benzyloxy)-3-hydroxy-4-oxobutanoic acid **15**: Colorless viscous liquid. IR (neat): ν_{\max} 822, 909, 949, 1001, 1028, 1040, 1101, 1169, 1262, 1400, 1454, 1649, 1709, 3034 cm⁻¹. ¹H NMR (400 MHz, CDCl₃) δ = 7.39–7.32 (m, 5H), 5.23 (s, 2H), 4.56–4.53 (*X* of ABX, *J* = 6.4, 4.4 Hz, 1H), 2.95–2.81 (*AB* of ABX, *J* = 16.6, 6.2, 4.2 Hz, 2H) ppm. ¹³C NMR (101 MHz, CDCl₃): δ = 175.75, 173.17, 134.95, 128.82, 128.58, 68.04, 67.23, 38.48 ppm. LCMS (EI-): *m/z* 223.1 (M-H)⁻, *t_R* = 5.28 min (100%). HRMS (EI): calcd. for C₁₁H₁₂O₅Na [M+Na]⁺: *m/z* 247.0577; found: *m/z* 247.0574.

Synthesis of 17: A solution of monobenzyl ester of malate **15** (4.480 g, 20 mmol) in DCM (100 mL) was treated with *N,N'*-diisopropyl-*O*-*tert*-butylisourea **16** (16.00 g, 80 mmol). This solution was stirred at room temperature for 4 d. The reaction mixture was filtered through Celite® (20 g) and washed with DCM (3×20 mL). The filtrate and washings were combined and evaporated under reduced pressure to obtain the crude product. Pure **17** was separated from the crude product using column chromatography (10% EtOAc in hexanes). Yield: 69 %, 3.864 g.

1-Benzyl 4-(*tert*-butyl) 2-hydroxysuccinate **17**: Colorless viscous liquid. IR (neat): 841, 912, 953, 1001, 1028, 1044, 1100, 1148, 1188, 1213, 1254, 1366, 1393, 1454, 1724, 2976, 3484 cm⁻¹. ¹H NMR (400 MHz, CDCl₃): δ = 7.38–7.33 (m, 5H), 5.27–5.19 (*AB* of benzyl, *J* = 17.2, 12.0 Hz, 2H), 4.48–4.44 (*X* of ABX, *J* = 10.0, 5.2 Hz, 1H), 3.26–3.25 (d, *J* = 5.6 Hz, 1H), 2.81–2.71 (*AB* of ABX, *J* = 16.4, 5.6, 4.4 Hz, 2H), 1.42 (s, 9H) ppm. ¹³C NMR (101 MHz, CDCl₃): δ = 173.57, 169.80, 135.26, 128.78, 128.70, 128.53, 81.79, 67.68, 67.64, 39.78, 28.14 ppm. LCMS (EI+): *m/z* 303.1 (MNa)⁺, *t_R* = 6.45 min (97%). HRMS (EI) calcd. for C₁₅H₂₀O₅Na[M+Na]⁺: *m/z* 303.1203; found: *m/z* 303.1202.

Synthesis of mimetic building block 3

The *O*-allyl ether of the mixed malate **18** was obtained using silver (I) oxide-mediated etherification of **17** using allyl bromide (**Figure S8B**).¹⁰ The *O*-allylated malate **18** was subjected to ozonolysis at -78 °C followed by a reductive workup with triphenylphosphine to obtain the aldehyde **19**.¹¹ The aldehyde **19** was subjected to a borohydride reduction to generate the primary alcohol **20**, which was then subjected to the Appel reaction to obtain the bromo derivative of the mixed malate **21**.¹² A nucleophilic substitution reaction involving the alkyl bromide **21** and sodium azide in DMF results in the formation of the azide derivative **22**.¹³ The azide functionalized diester **22** was subjected to a Pd-C/H₂-mediated reduction, which was expected to reduce the azide group and cause hydrogenolysis of the -COOBn group, resulting in the formation of the amino acid.¹⁴ In a continuing reaction, the amino acid was subjected to Fmoc protection using standard Fmoc-Cl and NaHCO₃ in aq. THF, resulting in formation of the Fmoc-protected amino acid **3**.

Synthesis of 18: A solution of the mixed malate ester **17** (3.360 g, 12 mmol) in toluene (75 mL) was treated with Ag₂O (5.561 g, 24 mmol) and allyl bromide (7.260 g, 60 mmol). The reaction mixture was heated to 50 °C for 16 h, at which stage the conversion appeared to be completed by TLC. The solution was cooled to room temperature, filtered through Celite® (20 g) and washed with toluene (3×20 mL). The filtrate and washings were combined and evaporated under reduced pressure to yield the crude product, from which pure **18** was separated by column chromatography (5% EtOAc in hexanes). Yield: 84%, 3.226 g.

1-Benzyl 4-(*tert*-butyl) 2-(allyloxy)succinate **18**: Colorless liquid. IR (neat): ν_{\max} 843, 922, 992, 1028, 1069, 1125, 1148, 1213, 1258, 1269, 1366, 1393, 1456, 1499, 1728, 2978 cm⁻¹. ¹H NMR (400 MHz, CDCl₃) δ = 7.36–7.33 (m, 5H), 5.93–5.83 (ddt, J = 5.6, 10.4, 17.3 Hz, 1H), 5.28–5.15 (m, 4H), 4.35–4.32 (*X* of ABX, J = 8.0, 4.8 Hz, 1H), 4.23–4.19 (dd, J = 12.4, 5.6 Hz, 1H), 4.03–3.98 (dd, J = 12.4, 6.0, 1H), 2.75–2.63 (*AB* of ABX, J = 16.0, 8.0, 5.0 Hz, 2H), 1.43 (s, 9H) ppm. ¹³C NMR (101 MHz, CDCl₃) δ = 171.58, 169.28, 135.60, 134.03, 128.74, 128.54, 128.42, 118.03, 81.37, 74.80, 72.19, 66.93, 39.28, 28.14 ppm. LCMS (EI+): m/z 343.1 (MNa)⁺, t_R = 6.92 min (97%). HRMS (EI): calcd. for C₁₈H₂₄O₅Na [M+Na]⁺: m/z 343.1516; found: m/z 343.1516.

Synthesis of 19: A solution of *O*-allyl malate diester **18** (2.560 g, 8 mmol) in DCM (80 mL) was cooled to -78 °C. Ozone was bubbled through this cold solution until a persistent blue color was apparent in the DCM solution for at least 5 min. Nitrogen was bubbled through the solution to purge excess unreacted ozone resulting in a significant bleaching of the blue color. This was followed by the addition of triphenylphosphine (4.197 g, 16 mmol) in small portions into the DCM solution of ozonide, while stirring and maintaining the temperature at -78 °C. The solution was slowly warmed to room temperature and stirring was continued for 2 h. The reaction mixture was evaporated under reduced pressure and dry loaded onto the silica column. The aldehyde **19** was separated from PPh₃ and PPh₃O using column chromatography (50% EtOAc in hexanes). Yield: 93%, 2.396 g.

1-Benzyl 4-(*tert*-butyl) 2-(2-oxoethoxy)succinate **19**: Colorless liquid. IR (neat): ν_{\max} 843, 918, 949, 1001, 1028, 1148, 1213, 1256, 1271, 1366, 1393, 1454, 1499, 1726, 2932, 2978, 3447 cm⁻¹. ¹H NMR (400 MHz, CDCl₃): δ = 9.72–9.71 (t, J = 1.0 Hz, 1H), 7.39–7.32 (m, 5H), 5.23–5.15 (*AB* of benzyl, 18.8, 12.0 Hz, 2H), 4.39–4.36 (*X* of ABX, J = 7.8, 4.6 Hz, 1H), 4.32–4.27 (dd, J = 17.6, 1.2 Hz, 1H), 4.17–4.12 (dd, J = 17.6, 1.2 Hz, 1H), 2.85–2.72 (*AB* of ABX, J = 16.4, 7.8, 4.8 Hz, 2H), 1.43 (s, 9H) ppm. ¹³C NMR (101 MHz, CDCl₃) δ = 200.41, 170.76, 169.05, 135.22, 128.82, 128.74, 128.54, 81.73, 76.40, 76.39, 67.32, 38.95, 28.13 ppm. LCMS (EI+): m/z 280.2 (M-C₂H₂O)⁺, t_R = 4.56 min (92%). HRMS (EI): calcd. for C₁₇H₂₃O₆ [M+H]⁺: m/z 323.1489; found: m/z 323.1484.

Synthesis of 20: A solution of aldehyde **19** (2.256 g, 7 mmol) in MeOH (50 mL) was treated with glacial acetic acid (4.200 g, 70 mmol) while being maintained in an ice bath. Sodium borohydride (0.371 g, 9.8 mmol) was added in small portions to this solution over a 10 min period while ensuring that the provisions were made for venting the excess pressure built-up caused by the release of hydrogen gas. The solution was continually stirred and maintained at 0 °C during the addition of sodium borohydride. The reaction mixture was stirred at room temperature for 3 h after which the solvent was evaporated under reduced pressure until it was nearly dry. Aqueous Na₂CO₃ (10 mL of 10% solution) and brine (20 mL) were added to the residual mass and the product was extracted with DCM (3×30 mL). The DCM layers were combined, dried over anhydrous MgSO₄ and evaporated under reduced pressure to yield the crude product. Pure **20** was separated from the crude product using column chromatography (20% EtOAc in hexanes). Yield: 75%, 1.701 g.

1-Benzyl 4-(*tert*-butyl) 2-(2-hydroxyethoxy)succinate **20**: Colorless viscous liquid. ν_{\max} 843, 891, 918, 953, 1001,

1053, 1130, 1150, 1213, 1258, 1368, 1393, 1454, 1499, 1724, 2934, 2978 cm^{-1} . ^1H NMR (400 MHz, CDCl_3) δ = 7.39–7.32 (m, 5H), 5.23–5.15 (AB of benzyl, 17.8, 12.2 Hz, 2H), 4.41–4.38 (X of ABX, J = 9.4, 3.8 Hz, 1H), 3.82–3.78 (m, 1H), 3.72–3.63 (m, 3H), 3.06–3.03 (t, J = 6.0, 1H), 2.79–2.62 (AB of ABX, J = 16.4, 9.2, 3.6 Hz, 2H), 1.44 (s, 9H) ppm. ^{13}C NMR (101 MHz, CDCl_3) δ = 171.89, 169.91, 135.37, 128.82, 128.70, 128.50, 81.88, 75.65, 73.19, 67.27, 61.87, 38.99, 28.15 ppm. LCMS (EI+): m/z 347.1 (MNa) $^+$, t_R = 6.24 min (93%). HRMS (EI): calcd. for $\text{C}_{17}\text{H}_{24}\text{O}_6\text{Na}$ [M+Na] $^+$: m/z 347.1465; found: m/z 347.1463.

Synthesis of 21: A solution of primary alcohol **20** (1.620 g, 5 mmol) in DCM (20 mL) was treated with triphenylphosphine (1.442 g, 5.5 mmol) and the resultant mixture was cooled to -20 $^\circ\text{C}$. A solution of CBR_4 (1.821 g, 5.5 mmol) in DCM (20 mL) was added dropwise into the cold solution of **20** and PPh_3 in DCM. The reaction mixture was gradually warmed to room temperature and the stirring was continued for 3 h, at which point the conversion appeared to be complete by TLC. The reaction mixture was evaporated under reduced pressure to yield the crude product. Pure **21** was separated from the crude product by column chromatography (15% EtOAc in hexanes). Yield: 90%, 1.742 g.

1-Benzyl 4-(*tert*-butyl) 2-(2-bromoethoxy)succinate **21**: Colorless liquid. IR (neat): ν_{max} 843, 916, 953, 1001, 1017, 1030, 1046, 1067, 1121, 1150, 1213, 1258, 1275, 1366, 1393, 1422, 1454, 1499, 1726, 2976 cm^{-1} . ^1H NMR (400 MHz, CDCl_3) δ = 7.38–7.33 (m, 5H), 5.23–5.15 (AB of benzyl, 18.4, 12.4 Hz, 2H), 4.37–4.34 (X of ABX, J = 8.4, 4.4 Hz, 1H), 4.07–4.01 (dt, J = 10.4, 6.2 Hz, 1H), 3.79–3.73 (dt, J = 10.4, 6.4 Hz, 1H), 3.46–3.43 (td, J = 6.5, 1.1 Hz, 2H), 2.78–2.64 (AB of ABX, J = 16.0, 8.4, 4.4 Hz, 2H), 1.43 (s, 9H). ^{13}C NMR (101 MHz, CDCl_3) δ = 171.20, 169.18, 135.41, 128.79, 128.64, 128.48, 81.56, 75.99, 71.27, 67.14, 39.07, 29.88, 28.16 ppm. LCMS (EI+): m/z 411.0 (MNa) $^+$, t_R = 7.04 min (100%). HRMS (EI): calcd. for $\text{C}_{17}\text{H}_{23}\text{BrO}_5\text{Na}$ [M+Na] $^+$: m/z 409.0621; found: m/z 409.0622.

Synthesis of 22: Sodium azide (0.390 g, 6 mmol) was added to the solution of alkyl bromide **21** (1.162 g, 3 mmol) in DMF (10 mL). The solution was heated at 50 $^\circ\text{C}$ for 24 h. At this point the conversion appeared to be complete by TLC. DMF was evaporated under reduced pressure to obtain a nearly dry residual mass that was treated with water (30 mL). Et_2O (3×30 mL) was used for extracting the product from the aqueous layer. The ethereal extracts were combined, dried over anhydrous MgSO_4 and evaporated under reduced pressure to yield the crude product. Pure **22** was separated from the crude product by column chromatography (15% EtOAc in hexanes). Yield: 94%, 0.984 g.

1-Benzyl 4-(*tert*-butyl) 2-(2-azidoethoxy)succinate **22**: Colorless liquid. IR (neat): ν_{max} 843, 918, 953, 993, 1030, 1065, 1128, 1150, 1213, 1258, 1275, 1366, 1393, 1454, 1476, 1499, 1726, 2099, 2932, 2978 cm^{-1} . ^1H NMR (400 MHz, CDCl_3) δ = 7.38–7.31 (m, 5H), 5.24–5.15 (AB of benzyl, J = 18.8, 12.4 Hz, 2H), 4.35–4.32 (X of ABX, J = 8.2, 4.6 Hz, 1H), 3.94–3.89 (ddd, J = 9.9, 6.0, 3.6 Hz, 1H), 3.66–3.61 (ddd, J = 10.4, 7.0, 3.6 Hz, 1H), 3.45–3.39 (ddd, J = 10.4, 6.8, 3.6 Hz, 1H), 3.36–3.30 (ddd, J = 9.6, 6.0, 3.6 Hz, 1H), 2.79–2.65 (AB of ABX, J = 16.4, 8.4, 4.4 Hz, 2H), 1.44 (s, 9H). ^{13}C NMR (101 MHz, CDCl_3) δ = 171.20, 169.19, 135.46, 128.78, 128.63, 128.48, 81.54, 76.05, 70.29, 67.11, 50.78, 39.07, 28.13 ppm. HRMS (EI): calcd. for $\text{C}_{17}\text{H}_{23}\text{N}_3\text{O}_5\text{Na}$ [M+Na] $^+$: m/z 372.1530; found: m/z 372.1530.

Synthesis of 3: Pd-C (of 10% loading with 53% moisture content; 0.052 g) was added to the solution of **22** (0.524 g, 1.5 mmol) in EtOH (20 mL). The solution was initially purged with hydrogen gas and then maintained under hydrogen atmosphere for 18 h at room temperature while being constantly stirred. Once the completion of the reaction was ensured by TLC, the ethanolic solution was filtered through Celite® (10 g) and washed with EtOH (3×10 mL). The filtrate and washings were combined and evaporated under reduced pressure to obtain a viscous oily mass that was treated with water (15 mL) and NaHCO_3 (0.504 g, 6 mmol). This solution was treated dropwise with a solution of FmocCl in THF (0.388 g, 1.5 mmol in 15 mL). The solution was stirred vigorously at room temperature for 16 h. The reaction mixture was evaporated under reduced pressure to remove most of the THF. Aqueous 1N HCl was added to the residual mass until the aqueous solution was verified to be acidic. Et_2O (3×20 mL) was used for extracting the product from the aqueous solution. The ethereal extracts were combined, dried over anhydrous MgSO_4 and evaporated under reduced pressure to yield the crude product. Pure **3** was separated from the crude product by column chromatography (50% EtOAc and 1% AcOH in hexanes). Traces of acetic acid from the product were removed by repeated co-evaporation with acetonitrile followed by DCM. Yield: 72%, 0.491 g.

2-(2-(((9*H*-fluoren-9-yl)methoxy)carbonyl)amino)ethoxy)-4-(*tert*-butoxy)-4-oxobutanoic acid **3**: Colorless viscous oil. IR (neat): ν_{max} 841, 912, 965, 1032, 1130, 1148, 1248, 1366, 1449, 1478, 1522, 1711, 2878, 2936,

2978, 3347 cm^{-1} . ^1H NMR (400 MHz, DMSO d_6) δ = 7.90–7.88 (d, J = 7.6 Hz, 2H), 7.69–7.67 (d, J = 7.6 Hz, 2H), 7.43–7.39 (m, 2H), 7.34–7.30 (m, 2H), 7.25–7.22 (t, J = 5.6 Hz, 1H), 4.28–4.18 (m, 3H), 4.14–4.10 (dd, J = 8.4, 4.8 Hz, 1H), 3.62–3.57 (m, 1H), 3.43–3.34 (m, 1H), 3.15–3.11 (dd, J = 11.8, 5.8 Hz, 2H), 2.67–2.62 (dd, J = 15.6, 4.8 Hz, 1H), 2.52–2.46 (m, 1H), 1.38 (s, 9H) ppm. ^{13}C NMR (101 MHz, DMSO d_6) δ = 172.44, 169.01, 156.12, 143.90, 140.74, 127.62, 127.07, 125.18, 120.13, 80.34, 75.08, 68.78, 65.42, 46.71, 38.60, 27.66 ppm. LCMS (EI+): m/z 478.1 (MNa) $^+$, t_R = 6.59 min (97%). HRMS (EI) calcd. for $\text{C}_{25}\text{H}_{29}\text{NO}_7\text{Na}$ [M+Na] $^+$: m/z 478.1836; found: m/z 478.1836.

Synthesis of mimetic building block 4

The mixed malate ester **17** was also a synthetic equivalent used for the synthesis of building block **4** (Figure S8C). A silver(I)oxide-mediated *O*-benzylation of the mixed malate with 2-nitrobenzyl bromide resulted in formation of the 2-nitrobenzyl ether of the mixed malate **24**.¹⁵ A zinc-mediated selective reduction of the nitro group in **24** resulted in formation of the corresponding aniline **25**, leaving other reducible groups such as the benzyl ether and ester unaffected.⁵ The HOAT/EDCI.HCl-mediated coupling of the aniline **25** with Fmoc-*N*-trityl-*L*-asparagine, **12** resulted in the formation of the anilide derivative **26**.⁶ A Pd-C-mediated selective hydrogenolysis of **26** offered neutral conditions for the formation of the carboxylic acid **4**, which was required in the synthesis of the benzyl-based cyclic peptidomimetic **B**.

Synthesis of 24: A solution of mixed malate ester **17** (3.360 g, 12 mmol) in EtOAc (100 mL) was treated with Ag_2O (5.562 g, 24 mmol) and 2-nitrobenzyl bromide **23** (2.592 g, 12 mmol). The reaction mixture was stirred at room temperature for 48 h while it was periodically sonicated, after which the mixed malate **17** appeared to be consumed. The formation of multiple products was evident by TLC. The solution was filtered through Celite® (15 g) and washed with EtOAc (3×20 mL). The filtrate and washings were combined and evaporated under reduced pressure to yield the crude product. Pure **24** was separated from the crude product by column chromatography (10% EtOAc in hexanes). Yield: 44%, 2.191 g.

1-Benzyl 4-(*tert*-butyl) 2-((2-nitrobenzyl)oxy)succinate **24**: Light yellow solid. MP: 69–71 °C. IR (neat): ν_{max} 808, 843, 858, 893, 912, 920, 941, 957, 970, 988, 1009, 1038, 1053, 1073, 1115, 1146, 1177, 1186, 1200, 1211, 1235, 1260, 1271, 1300, 1337, 1368, 1393, 1400, 1452, 1497, 1524, 1576, 1613, 1701, 1724, 1746 cm^{-1} . ^1H NMR (400 MHz, CDCl_3) δ = 8.09–8.06 (dd, J = 8.2, 1.0 Hz, 1H), 7.87–7.85 (d, J = 8.0 Hz, 1H), 7.64–7.59 (m, 1H), 7.45–7.40 (m, 1H), 7.37–7.33 (m, 5H), 5.25–5.14 (m, 3H), 4.98–4.94 (d, J = 14.8 Hz, 1H), 4.52–4.49 (X of ABX, J = 7.6, 4.8 Hz, 1H), 2.86–2.75 (AB of ABX, J = 16.0, 7.6, 5.2 Hz, 2H), 1.42 (s, 9H) ppm. ^{13}C NMR (101 MHz, CDCl_3) δ = 171.05, 169.09, 146.92, 135.39, 134.61, 133.87, 128.95, 128.78, 128.64, 128.50, 128.11, 124.72, 81.57, 76.02, 69.68, 67.21, 39.22, 28.13 ppm. LCMS (EI+): m/z 438.2 (MNa) $^+$, t_R = 7.14 min (93%). HRMS (EI): calcd. for $\text{C}_{22}\text{H}_{25}\text{NO}_7\text{Na}$ [M+Na] $^+$: m/z 438.1523; found: m/z 438.1522.

Synthesis of 25: *O*-Benzyl malate **24** (1.038 g, 2.5 mmol), zinc (1.625 g, 25 mmol) and NH_4Cl (1.338 g, 25 mmol) were used in the procedure outlined for the synthesis of **11**. Analytically pure **25** was separated from the crude product using column chromatography (15% EtOAc in hexanes). Yield: 90%, 0.867 g.

1-Benzyl 4-(*tert*-butyl) 2-((2-aminobenzyl)oxy)succinate **25**: White solid. MP: 71–73 °C. IR (neat): ν_{max} 843, 866, 887, 901, 914, 932, 986, 1020, 1032, 1074, 1121, 1152, 1188, 1209, 1223, 1269, 1314, 1368, 1395, 1404, 1435, 1458, 1495, 1578, 1607, 1634, 1723, 2974, 3036, 3364, 3462 cm^{-1} . ^1H NMR (400 MHz, CDCl_3) δ = 7.40–7.33 (m, 5H), 7.14–7.10 (m, 1H), 7.03–7.01 (dd, J = 7.6, 1.6 Hz, 1H), 6.67–6.64 (m, 2H), 5.24–5.16 (AB of benzyl, J = 16.8, 12.4 Hz, 2H), 4.70–4.68 (d, J = 10.0 Hz, 1H), 4.48–4.46 (d, J = 10.0 Hz, 1H), 4.42–4.39 (X of ABX, J = 8.4, 4.0 Hz, 1H), 2.77–2.64 (AB of ABX, J = 16.2, 8.6, 4.4 Hz, 2H), 1.42 (s, 9H) ppm. ^{13}C NMR (101 MHz, CDCl_3) δ = 171.97, 169.42, 147.05, 135.35, 130.79, 129.96, 128.82, 128.72, 128.58, 121.13, 117.65, 115.83, 81.56, 74.49, 72.32, 67.24, 39.08, 28.15 ppm. LCMS (EI+): m/z 408.2 (MNa) $^+$, t_R = 6.80 min (100%). HRMS (EI): calcd. for $\text{C}_{22}\text{H}_{28}\text{NO}_5$ [M+H] $^+$: m/z 386.1962; found: m/z 386.1954.

Synthesis of 26: Aryl amine **25** (0.771 g, 2 mmol), *N* $^\alpha$ -Fmoc-*N* $^\gamma$ -trityl-*L*-asparagine **12** (1.193 g, 2 mmol), HOAT (0.299 g, 2.2 mmol) and EDCI.HCl (0.422 g, 2.2 mmol) were used in the procedure outlined for the synthesis of **13**. Analytically pure **26** was separated from the crude product using column chromatography (35% EtOAc in hexanes). Yield: 88%, 1.696 g.

1-Benzyl 4-(*tert*-butyl) 2-((2-((*S*)-2-(((9*H*-fluoren-9-yl)methoxy)carbonyl)amino)-4-oxo-4-(tritylamino)butanamido)benzyl)oxy)succinate **26**: White solid. MP: 92–94 °C. $[\alpha]_D^{20} = -5.4$ ($c = 1$, THF). IR (neat): ν_{\max} 843, 941, 1034, 1078, 1105, 1150, 1213, 1244, 1290, 1366, 1449, 1489, 1514, 1591, 1682, 1723 cm^{-1} . ^1H NMR (400 MHz, DMSO d_6) $\delta = 9.47$ – 9.46 (d, $J = 3.6$ Hz, 1H), 8.65 – 8.63 (d, $J = 6.4$ Hz, 1H), 7.90 – 7.88 (d, $J = 7.2$ Hz, 2H), 7.82 – 7.71 (m, 3H), 7.63 – 7.60 (m, 1H), 7.43 – 7.13 (m, 27H), 5.14 – 5.05 (m, 2H), 4.63 – 4.21 (m, 7H), 2.84 – 2.56 (m, 4H), 1.28 (s, 9H) ppm. ^{13}C NMR (101 MHz, DMSO d_6) $\delta = 170.86$, 170.39 , 170.36 , 168.83 , 168.80 , 168.62 , 168.59 , 155.87 , 144.74 , 144.71 , 143.79 , 143.74 , 140.73 , 135.89 , 135.58 , 130.02 , 129.98 , 128.72 , 128.60 , 128.40 , 128.15 , 128.11 , 128.10 , 128.03 , 128.00 , 127.67 , 127.43 , 127.09 , 126.36 , 125.30 , 125.22 , 124.72 , 123.87 , 123.80 , 120.15 , 80.52 , 74.49 , 74.36 , 69.49 , 68.99 , 68.90 , 66.26 , 65.91 , 54.93 , 52.59 , 46.68 , 38.34 , 27.54 ppm. LCMS (EI+): m/z 986.3 (MNa)⁺, $t_R = 8.00$ min (100%). HRMS (EI) calcd. for $\text{C}_{60}\text{H}_{58}\text{N}_3\text{O}_9$ [M+H]⁺: m/z 964.4168; found: m/z 964.4161.

Synthesis of 4: Pd-C (of 10% loading with 53% moisture content; 0.096 g) and **26** (0.964 g, 1 mmol) were used in the procedure outlined for the synthesis of **6**. The reaction was completed in 18 h. The crude product was analytically pure and did not require purification. Yield: 92%, 0.804 g.

2-((2-((*S*)-2-(((9*H*-fluoren-9-yl)methoxy)carbonyl)amino)-4-oxo-4-(tritylamino)butanamido) benzyl)oxy)-4-(*tert*-butoxy)-4-oxobutanoic acid **4**: White solid. MP: 118–120 °C. $[\alpha]_D^{20} = -4.7^\circ$ ($c = 1$, CHCl_3). IR (neat): ν_{\max} 843, 901, 934, 968, 1003, 1034, 1074, 1105, 1152, 1250, 1290, 1314, 1366, 1393, 1449, 1491, 1522, 1591, 1618, 1684, 1721 cm^{-1} . ^1H NMR (400 MHz, DMSO d_6) $\delta = 9.58$ (s, 1H), 8.71 – 8.66 (m, 1H), 7.90 – 7.88 (d, $J = 7.6$ Hz, 2H), 7.78 – 7.67 (m, 3H), 7.43 – 7.12 (m, 22H), 4.65 – 4.61 (dd, 11.8 , 5.4 Hz, 1H), 4.58 – 4.53 (m, 1H), 4.40 – 4.34 (m, 2H), 4.30 – 4.17 (m, 3H), 2.82 – 2.52 (m, 4H), 1.32 – 1.31 (m, 9H) ppm. ^{13}C NMR (101 MHz, DMSO d_6) $\delta = 172.97$, 172.81 , 170.52 , 170.34 , 169.05 , 168.98 , 168.91 , 168.69 , 155.80 , 144.74 , 143.81 , 143.74 , 140.71 , 136.22 , 129.62 , 129.53 , 128.61 , 128.08 , 127.64 , 127.41 , 127.08 , 126.33 , 125.32 , 125.23 , 124.37 , 123.26 , 120.12 , 80.25 , 74.83 , 74.72 , 69.49 , 69.47 , 69.02 , 68.97 , 65.90 , 52.71 , 46.68 , 38.67 , 27.60 ppm. LCMS (EI+) m/z 896.2 (MNa)⁺, $t_R = 7.59$ and 7.73 min (95%, diastereomers). HRMS (EI) calcd. for $\text{C}_{53}\text{H}_{52}\text{N}_3\text{O}_9$ [M+H]⁺: m/z 874.3698; found: m/z 874.3689.

Synthesis of mimetic building block 5

The aldehyde **19** provided a convenient access to the synthesis of the peptide building block **5** that was required for the synthesis of hydrazine-based peptidomimetic **C** (**Figure S8D**). Oxone®, which is known to oxidize aldehydes to carboxylic acids, was used for the oxidation of **19** in DMF.¹⁶ The crude acid from this oxidation step was carried through to a HOAT/EDCI.HCl-mediated amide coupling with Fmoc-protected *N*-methylhydrazine **27**, resulting in the formation of hydrazinamide **28**.^{6,17} In the final step, **28** was debenzylated under neutral hydrogenolytic conditions to yield the carboxylic acid **5**, the peptide building block required for the synthesis of a hydrazine-based cyclic peptidomimetic **C**.^{14b,c}

Synthesis of 27: NaHCO_3 (2.87 g, 34.13 mmol) was added to the solution of Boc_2O (4.96 g, 22.75 mmol) in chloroform (70 mL). Methyl hydrazine (1.38 g, 30 mmol) was added dropwise into this solution while it was stirred vigorously at room temperature for 6 h after which the reaction mixture was filtered and evaporated under reduced pressure over a rotary evaporator and then under high vacuum to remove any un-reacted methyl hydrazine. The resultant product was treated with THF (60 mL), water (60 mL) and NaHCO_3 (3.82 g, 45.5 mmol). A solution of FmocCl (5.89 g, 22.75 mmol) in THF (40 mL) was added dropwise into the mixture of the crude product-aqueous THF- NaHCO_3 mixture. The reaction mixture was stirred at the room temperature for 16 h and then evaporated under reduced pressure to yield a gummy residue. Water (100 mL) and DCM (100 mL) were added to this residual mass to extract the crude product into the DCM layer. The DCM layer was separated, dried over anhydrous MgSO_4 , concentrated over a rotary evaporator (about 50 mL) and treated with CF_3COOH (13.00 g, 114 mmol). This solution was stirred at room temperature for 16 h, after which the reaction mixture was evaporated under reduced pressure to yield a viscous material. Aqueous saturated NaHCO_3 (200 mL) was added to this residue and DCM (3×80 mL) was used to extract the product. The DCM layers were combined, dried over anhydrous MgSO_4 and concentrated (to about 50 mL) under reduced pressure. Hexanes (200 mL) were added into this DCM solution resulting in the precipitation of the desired Fmoc protected methyl hydrazine **27**, which was filtered and dried under reduced pressure. Yield: 82%, 5.004 g.

(9*H*-fluoren-9-yl)methyl 2-methylhydrazine-1-carboxylate **27**: White solid. MP: 138–140 °C. IR (neat): ν_{\max} 799, 845, 953, 1026, 1144, 1179, 1204, 1269, 1400, 1449, 1541, 1670, 1744 cm^{-1} . ^1H NMR (400 MHz, DMSO d_6) $\delta =$

10.12 (bs, 2H), 7.91–7.89 (d, $J = 7.2$ Hz, 2H), 7.71–7.69 (d, $J = 7.2$, 2H), 7.44–7.41 (m, 2H), 7.36–7.32 (m, 2H), 4.52–4.51 (d, $J = 6.4$ Hz, 2H), 4.30–4.27 (t, $J = 6.4$ Hz, 1H), 2.64 (bs, 3H) ppm. ^{13}C NMR (101 MHz, DMSO d_6) $\delta = 155.37, 143.42, 140.80, 127.74, 127.12, 125.07, 120.20, 66.58, 46.47, 36.44$ ppm. LCMS (EI+) m/z 179.2 ($\text{M-C}_2\text{H}_5\text{N}_2\text{O}_2$) $^+$, $t_{\text{R}} = 5.65$ min (100%). HRMS (EI) calcd. for $\text{C}_{16}\text{H}_{17}\text{N}_2\text{O}_2$ $[\text{M}+\text{H}]^+$: m/z 269.1285; found: m/z 269.1286.

Synthesis of 28: Oxone® (3.074 g, 10 mmol) was added to a solution of aldehyde **19** (1.610 g, 5 mmol) in DMF (25 mL). The resultant mixture was stirred for 16 h at room temperature, after which DMF was evaporated under reduced pressure to obtain a nearly dry residual material. DCM (50 mL) was added to this residue, which was then filtered and washed with DCM (20 mL). The filtrate and washings were combined and treated with **27** (1.342 g, 5 mmol), HOAT (0.748 g, 5.5 mmol) and EDCi.HCl (1.056 g, 5.5 mmol). The reaction mixture was stirred at room temperature for 16 h, after which water (50 mL) was added to this solution and the product was extracted into the DCM layer. The DCM layer was dried using anhydrous MgSO_4 , concentrated (to about 30 mL) and treated with hexanes (150 mL) to precipitate the product **28** that was separated from the solution by filtration and dried under reduced pressure. The hydrazinamide **28** isolated by this method was of good analytical purity. Yield: 74%, 2.176 g.

1-Benzyl 4-(*tert*-butyl) 2-(2-(2-(((9*H*-fluoren-9-yl)methoxy)carbonyl)-1-methylhydrazinyl)-2-oxoethoxy)succinate **28**: White solid. MP: 116–118 °C. IR (neat): ν_{max} 845, 860, 959, 1015, 1038, 1103, 1152, 1231, 1252, 1292, 1368, 1393, 1451, 1478, 1528, 1663, 1724, 1738, 2976, 3262 cm^{-1} . ^1H NMR (400 MHz, DMSO d_6) $\delta = 9.76$ (s, 1H), 7.90–7.88 (d, $J = 7.2$ Hz, 2H), 7.67–7.66 (m, 2H), 7.43–7.32 (m, 9H), 5.16–5.09 (m, 2H), 4.52–3.95 (m, 6H), 2.89 (s, 3H), 2.71–2.69 (d, $J = 6.0$ Hz, 2H), 1.34 (s, 9H) ppm. ^{13}C NMR (101 MHz, DMSO d_6) $\delta = 170.28, 168.56, 155.24, 143.46, 140.85, 135.72, 128.42, 128.08, 127.86, 127.73, 127.10, 125.02, 120.20, 80.53, 74.93, 67.17, 66.18, 65.99, 46.67, 38.50, 34.75, 27.60$ ppm. LCMS (EI+): m/z 611.3 (MNa^+), $t_{\text{R}} = 7.06$ min (100 %). HRMS (EI): calcd. for $\text{C}_{33}\text{H}_{37}\text{N}_2\text{O}_8$ $[\text{M}+\text{H}]^+$: m/z 589.2544; found: m/z 589.2543.

Synthesis of 5: Pd-C (of 10% loading with 53% moisture content; 0.118 g) and **28** (1.176 g, 2 mmol) were used in the procedure outlined for the synthesis of **6**. The reaction was completed in 18 h. The crude product was analytically pure and did not require any purification. Yield: 92%, 0.916 g.

2-(2-(2-(((9*H*-fluoren-9-yl)methoxy)carbonyl)-1-methylhydrazinyl)-2-oxoethoxy)-4-(*tert*-butoxy)-4-oxobutanoic acid **5**: White solid. MP: 71–73 °C. IR (neat): ν_{max} 841, 955, 1005, 1042, 1076, 1107, 1146, 1244, 1290, 1366, 1393, 1425, 1449, 1642, 1721, 2982 cm^{-1} . ^1H NMR (400 MHz, DMSO d_6) $\delta = 9.80$ (s, 1H), 7.91–7.89 (d, $J = 7.2$ Hz, 2H), 7.69–7.67 (m, 2H), 7.44–7.41 (m, 2H), 7.36–7.33 (m, 2H), 4.53 (bs, 2H), 4.31–4.14 (m, 4H), 2.91 (bs, 3H), 2.69–2.58 (m, 2H), 1.38 (s, 9H) ppm. ^{13}C NMR (101 MHz, DMSO d_6) $\delta = 172.03, 170.84, 168.86, 155.21, 143.49, 140.86, 127.75, 127.12, 125.03, 120.21, 80.33, 75.28, 67.23, 66.18, 46.68, 38.62, 34.81, 27.67$ ppm. LCMS (EI+) m/z 521.2 (MNa^+), $t_{\text{R}} = 6.51$ min (93%). HRMS (EI): calcd. for $\text{C}_{26}\text{H}_{30}\text{N}_2\text{O}_8\text{Na}$ $[\text{M}+\text{Na}]^+$: m/z 521.1894; found: m/z 521.1893.

List of References:

- (1) Pícha, J.; Buděšínský, M.; Hančlová, I.; Šanda, M.; Fiedler, P.; Vaněk, V.; Jiráček, J., Efficient synthesis of phosphonodepsipeptides derived from norleucine. *Tetrahedron* **2009**, *65*, 6090-6103.
- (2) Tietze, L. F.; Brasche, G.; Grube, A.; Bohnke, N.; Stadler, C., Synthesis of novel spinosyn A analogues by Pd-mediated transformations. *Chemistry* **2007**, *13*, 8543-8563.
- (3) (a) Clark, A. S.; Deans, B.; Stevens, M. F.; Tisdale, M. J.; Wheelhouse, R. T.; Denny, B. J.; Hartley, J. A., Antitumor imidazotetrazines. 32. Synthesis of novel imidazotetrazinones and related bicyclic heterocycles to probe the mode of action of the antitumor drug temozolomide. *J. Med. Chem.* **1995**, *38*, 1493-1504; (b) Ramesh, V. V.; Kale, S. S.; Kotmale, A. S.; Gawade, R. L.; Puranik, V. G.; Rajamohanam, P. R.; Sanjayan, G. J., Carboxamide versus sulfonamide in peptide backbone folding: a case study with a hetero foldamer. *Org. Lett.* **2013**, *15*, 1504-1507.
- (4) Kuebelbeck, A.; Larbig, G.; Mier, W.; Beijer, B.; Haberkorn, U. Conjugates of ϵ -polylysine with carboxyl group-carrying compounds and further conjugation for use in drug and contrast agent targeting of kidney. WO 2011009539 A1 20110127, 2011.
- (5) (a) Wurtz, N. R.; Priestley, E. S.; Cheney, D. L.; Glunz, P. W.; Zhang, X.; Ladziata, V.; Parkhurst, B.; Mueller, L. Preparation of macrocyclic amino acid derivatives as factor VIIa inhibitors useful as anticoagulants. WO 2008079836 A2 20080703, 2008; (b) Tsukinoki, T.; Tsuzuki, H., Organic reaction in water. Part 5. Novel synthesis of anilines by zinc metal-mediated chemoselective reduction of nitroarenes. *Green Chem.* **2001**, *3*, 37-38.
- (6) Carpino, L. A., 1-Hydroxy-7-azabenzotriazole. An efficient peptide coupling additive. *J. Am. Chem. Soc.* **1993**, *115*, 4397-4398.
- (7) (a) Schobert, R.; Jagusch, C., An efficient synthesis of carlosic acid and other 5-carboxymethyltetronates from malates. *Synthesis* **2005**, *2005*, 2421-2425; (b) Shin, I.; Lee, M.; Lee, J.; Jung, M.; Lee, W.; Yoon, J., Synthesis of optically active phthaloyl D-aminoxy acids from L-amino acids or L-hydroxy acids as building blocks for the preparation of aminoxy peptides. *J. Org. Chem.* **2000**, *65*, 7667-7675.
- (8) (a) Allais, F.; Martinet, S.; Ducrot, P.-H., Straightforward total synthesis of 2-O-Feruloyl-l-malate, 2-O-Sinapoyl-l-malate and 2-O-5-Hydroxyferuloyl-l-malate. *Synthesis* **2009**, *2009*, 3571-3578; (b) Liao, X.; Pearson, N. D.; Pendrak, I.; Sano, M. Preparation of cephalosporins as antibacterial compounds. WO 2013052568 A1 20130411, 2013.
- (9) Kotoku, M.; Maeba, T.; Seki, N.; Hirashima, S.; Fujioka, S.; Obika, S.; Yamanaka, H.; Yokota, M.; Sakai, T.; Hirata, K.; Maeda, K.; Shiozaki, M.; Shinagawa, Y.; Ikenogami, T.; Doi, S.; Oka, T.; Matsuo, T.; Suwa, Y.; Ito, K.; Noji, S.; Hara, Y. Preparation of isoxazoles and their use as ROR- γ antagonists and pharmaceuticals. WO 2014065413 A1, 2014.
- (10) (a) Dahlgren, A.; Johansson, P.-O.; Kvarnström, I.; Musil, D.; Nilsson, I.; Samuelsson, B., Novel morpholinone-based d-Phe-Pro-Arg mimics as potential thrombin inhibitors: Design, synthesis, and x-ray crystal structure of an enzyme inhibitor complex. *Bioorg. Med. Chem.* **2002**, *10*, 1829-1839; (b) Pihko, P. M.; Rissa, T. K.; Aksela, R., Enantiospecific synthesis of isomers of AES, a new environmentally friendly chelating agent. *Tetrahedron* **2004**, *60*, 10949-10954.
- (11) Florence, G. J.; Morris, J. C.; Murray, R. G.; Osler, J. D.; Reddy, V. R.; Smith, T. K., Synthesis and stereochemical assignment of (+)-chamuvarinin. *Org. Lett.* **2011**, *13*, 514-517.
- (12) (a) Appel, R., Tertiary phosphane/tetrachloromethane, a versatile reagent for chlorination, dehydration, and P ~~and~~ *Angew. Chem. Int. Edit.* **1975**, *14*, 801-811; (b) Beckwith Athelstan, L. J.; Zimmerman, J., Cyclization of the 3-tert-butylhex-5-enyl radical: a test of transition-state structure. *J. Org. Chem.* **1991**, *56*, 5791-5796.
- (13) Luehr, G. W.; Sundaram, A.; Jaishankar, P.; Bhakta, C.; Druzgala, P. Preparation of pyrazole and triazole based compounds as therapeutic agonists of peroxisome proliferator activated receptor- α . WO 2010071813 A1 20100624, 2010.
- (14) (a) Lin, H. J.; Adak, A. K.; Reddy, L. V.; Wu, S. H.; Lin, C. C., Total synthesis of an immunomodulatory phosphoglycolipid from thermophilic bacteria. *Chemistry* **2013**, *19*, 7989-

- 7998; (b) Greene, T. W.; Wuts, P. G. M., *Protective groups in organic synthesis*. Wiley: New York, 1991; (c) Kocienski, P. J., *Protecting groups*. Thieme: Stuttgart, 1994.
- (15) Gmeiner, P.; Junge, D., Regioselective transformation of malic acid: A practical method for the construction of enantiomerically pure indolizidines. *J. Org. Chem.* **1995**, *60*, 3910-3915.
- (16) (a) Borhan, B.; Travis, B. R.; Schomaker, J. M. Catalytic osmium-assisted oxidative cleavage of olefins using peroxymonosulfuric acid and salts thereof. US 20030149299 A1 20030807, 2003; (b) Travis, B. R.; Sivakumar, M.; Hollist, G. O.; Borhan, B., Facile oxidation of aldehydes to acids and esters with Oxone. *Org. Lett.* **2003**, *5*, 1031-1034.
- (17) (a) Chung, J. U.; Jung, K.-Y.; Jeong, M.-W.; Jung, H.-K.; La, H.-J. Novel hexahydropyrazinotriazinedione compounds of reverse turn mimetics and their preparation and use thereof. WO 2009051397 A2 200904, 2009; (b) Moon, S. H.; Chung, J. U.; Lee, S. C.; Eguchi, M.; Kahn, M.; Jeong, K. W.; Nguyen, C.; Lee, S. J. Reverse-turn mimetics for use as therapeutic and diagnostic agents. US 20070043052 A1 20070222, 2007.

Supporting Information - 2

Design, Synthesis, and Characterization of Cyclic Peptidomimetics of the Inducible Nitric Oxide Synthase Binding Epitope That Disrupts the Protein-Protein Interaction Involving SPRY Domain-Containing Suppressor of Cytokine Signaling Box Protein (SPSB) 2 and Inducible Nitric Oxide Synthase

Jitendra R. Harjani,^{†§} Beow Keat Yap,^{†§} Eleanor W. W. Leung,[†] Andrew Lucke,[†] Sandra E. Nicholson,^{‡¥} Martin J. Scanlon,[†] David K. Chalmers,[†] Philip E. Thompson,[†] Raymond S. Norton,^{†*} Jonathan B. Baell^{†*}

[†] Medicinal Chemistry, Monash Institute of Pharmaceutical Sciences, Monash University, Parkville, Victoria 3052, Australia

[‡]The Walter and Eliza Hall Institute of Medical Research, Parkville, Victoria 3052, Australia

[¥]The Department of Medical Biology, University of Melbourne, Parkville, Victoria 3052, Australia

[§]These authors contributed equally

Page number	Contents
6	¹ H NMR spectrum of 1-benzyl 4-(<i>tert</i> -butyl) (2-nitrobenzoyl)- <i>L</i> -aspartate 10
7	¹³ C NMR spectrum of 1-benzyl 4-(<i>tert</i> -butyl) (2-nitrobenzoyl)- <i>L</i> -aspartate 10
8	HRMS report of 1-benzyl 4-(<i>tert</i> -butyl) (2-nitrobenzoyl)- <i>L</i> -aspartate 10
9	¹ H NMR spectrum of 1-benzyl 4-(<i>tert</i> -butyl) (2-aminobenzoyl)- <i>L</i> -aspartate 11
10	¹³ C NMR spectrum of 1-benzyl 4-(<i>tert</i> -butyl) (2-aminobenzoyl)- <i>L</i> -aspartate 11
11	HRMS report of 1-benzyl 4-(<i>tert</i> -butyl) (2-aminobenzoyl)- <i>L</i> -aspartate 11
12	¹ H NMR spectrum of 1-benzyl 4-(<i>tert</i> -butyl) (2-((<i>S</i>)-2-(((9 <i>H</i> -fluoren-9-yl)methoxy)carbonyl)amino)-4-oxo-4-(tritylamino)butanamido)benzoyl)- <i>L</i> -aspartate 13
13	¹³ C NMR spectrum 1-benzyl 4-(<i>tert</i> -butyl) (2-((<i>S</i>)-2-(((9 <i>H</i> -fluoren-9-yl)methoxy)carbonyl)amino)-4-oxo-4-(tritylamino)butanamido)benzoyl)- <i>L</i> -aspartate 13
14	HRMS report of 1-benzyl 4-(<i>tert</i> -butyl) (2-((<i>S</i>)-2-(((9 <i>H</i> -fluoren-9-yl)methoxy)carbonyl)amino)-4-oxo-4-(tritylamino)butanamido)benzoyl)- <i>L</i> -aspartate 13
15	¹ H NMR spectrum of (<i>S</i>)-2-(2-((<i>S</i>)-2-(((9 <i>H</i> -fluoren-9-yl)methoxy)carbonyl)amino)-4-oxo-4-(tritylamino)butanamido)benzamido)-4-(<i>tert</i> -butoxy)-4-oxobutanoic acid 6
16	¹³ C NMR spectrum of (<i>S</i>)-2-(2-((<i>S</i>)-2-(((9 <i>H</i> -fluoren-9-yl)methoxy)carbonyl)amino)-4-oxo-4-(tritylamino)butanamido)benzamido)-4-(<i>tert</i> -butoxy)-4-oxobutanoic acid 6
17	HRMS report of (<i>S</i>)-2-(2-((<i>S</i>)-2-(((9 <i>H</i> -fluoren-9-yl)methoxy)carbonyl)amino)-4-oxo-4-(tritylamino)butanamido)benzamido)-4-(<i>tert</i> -butoxy)-4-oxobutanoic acid 6

18	¹ H NMR spectrum of 4-(benzyloxy)-3-hydroxy-4-oxobutanoic acid 15
19	¹³ C NMR spectrum of 4-(benzyloxy)-3-hydroxy-4-oxobutanoic acid 15
20	HRMS report of 4-(benzyloxy)-3-hydroxy-4-oxobutanoic acid 15
21	¹ H NMR spectrum of 1-benzyl 4-(<i>tert</i> -butyl) 2-hydroxysuccinate 17
22	¹³ C NMR spectrum of 1-benzyl 4-(<i>tert</i> -butyl) 2-hydroxysuccinate 17
23	HRMS report of 1-benzyl 4-(<i>tert</i> -butyl) 2-hydroxysuccinate 17
24	¹ H NMR spectrum of 1-benzyl 4-(<i>tert</i> -butyl) 2-(allyloxy)succinate 18
25	¹³ C NMR spectrum of 1-benzyl 4-(<i>tert</i> -butyl) 2-(allyloxy)succinate 18
26	HRMS report of 1-benzyl 4-(<i>tert</i> -butyl) 2-(allyloxy)succinate 18
27	¹ H NMR spectrum of 1-benzyl 4-(<i>tert</i> -butyl) 2-(2-oxoethoxy)succinate 19
28	¹³ C NMR spectrum of 1-benzyl 4-(<i>tert</i> -butyl) 2-(2-oxoethoxy)succinate 19
29	HRMS report of 1-benzyl 4-(<i>tert</i> -butyl) 2-(2-oxoethoxy)succinate 19
30	¹ H NMR spectrum of 1-benzyl 4-(<i>tert</i> -butyl) 2-(2-hydroxyethoxy)succinate 20
31	NMR spectrum of 1-benzyl 4-(<i>tert</i> -butyl) 2-(2-hydroxyethoxy)succinate 20
32	HRMS report of 1-benzyl 4-(<i>tert</i> -butyl) 2-(2-hydroxyethoxy)succinate 20
33	NMR spectrum of 1-benzyl 4-(<i>tert</i> -butyl) 2-(2-bromoethoxy)succinate 21
34	¹³ C NMR spectrum of 1-benzyl 4-(<i>tert</i> -butyl) 2-(2-bromoethoxy)succinate 21

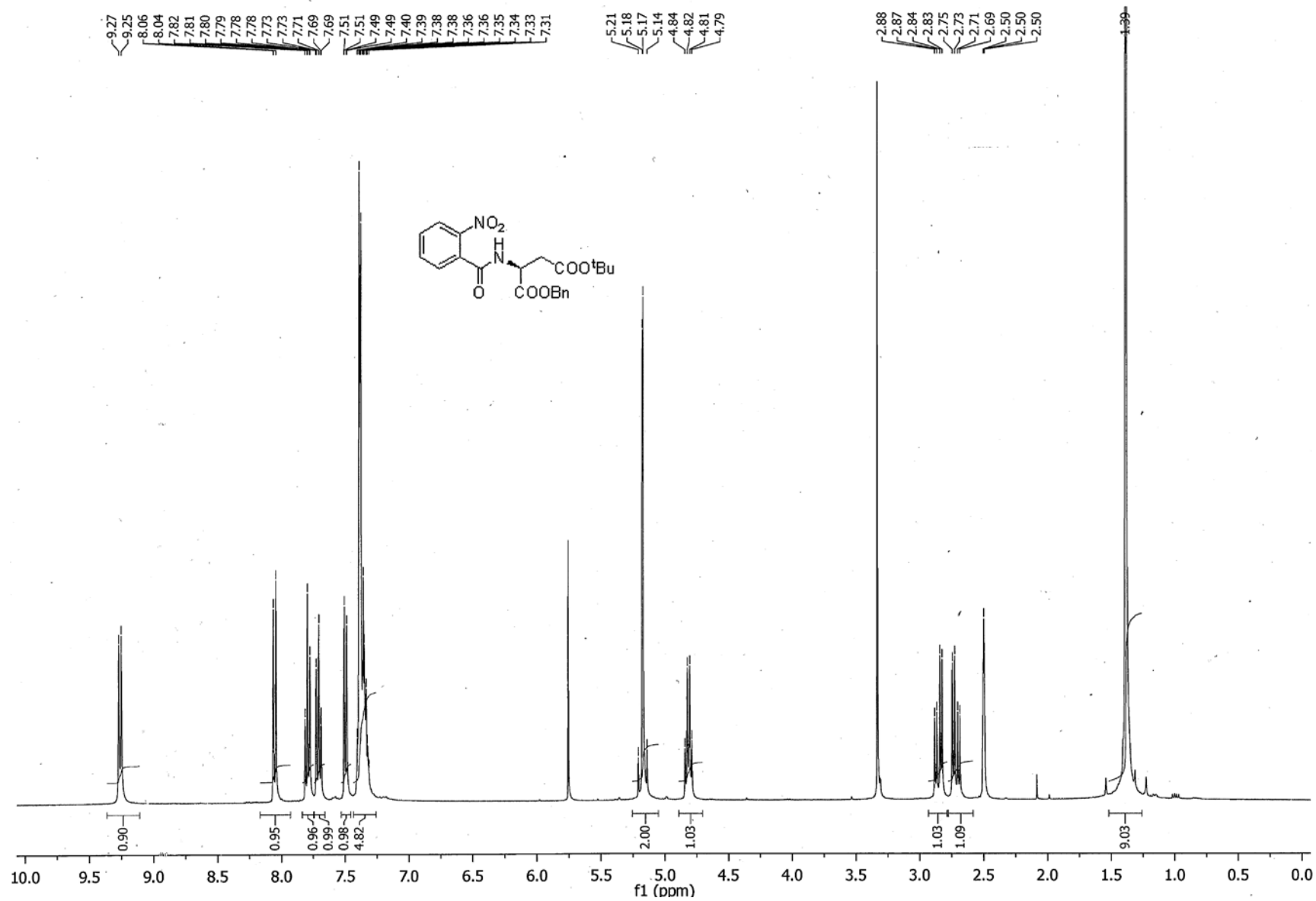
- 35 HRMS report of 1-benzyl 4-(*tert*-butyl) 2-(2-bromoethoxy)succinate **21**
- 36 ¹H NMR spectrum of 1-benzyl 4-(*tert*-butyl) 2-(2-azidoethoxy)succinate **22**
- 37 ¹³C NMR spectrum of 1-benzyl 4-(*tert*-butyl) 2-(2-azidoethoxy)succinate **22**
- 38 HRMS report of 1-benzyl 4-(*tert*-butyl) 2-(2-azidoethoxy)succinate **22**
- 39 ¹H NMR spectrum of 2-(2-(((9*H*-fluoren-9-yl)methoxy)carbonyl)amino)ethoxy)-4-(*tert*-butoxy)-4-oxobutanoic acid **3**
- 40 ¹³C NMR spectrum of 2-(2-(((9*H*-fluoren-9-yl)methoxy)carbonyl)amino)ethoxy)-4-(*tert*-butoxy)-4-oxobutanoic acid **3**
- 41 HRMS report of 2-(2-(((9*H*-fluoren-9-yl)methoxy)carbonyl)amino)ethoxy)-4-(*tert*-butoxy)-4-oxobutanoic acid **3**
- 42 ¹H NMR spectrum of ¹H NMR spectrum of 1-benzyl 4-(*tert*-butyl) 2-((2-nitrobenzyl)oxy)succinate **24**
- 43 ¹³C NMR spectrum of ¹³C NMR spectrum of 1-benzyl 4-(*tert*-butyl) 2-((2-nitrobenzyl)oxy)succinate **24**
- 44 HRMS report of 1-benzyl 4-(*tert*-butyl) 2-((2-nitrobenzyl)oxy)succinate **24**
- 45 ¹H NMR spectrum of 1-benzyl 4-(*tert*-butyl) 2-((2-aminobenzyl)oxy)succinate **25**
- 46 ¹³C NMR spectrum of 1-benzyl 4-(*tert*-butyl) 2-((2-aminobenzyl)oxy)succinate **25**
- 47 HRMS report of 1-benzyl 4-(*tert*-butyl) 2-((2-aminobenzyl)oxy)succinate **25**
- 48 ¹H NMR spectrum of 1-benzyl 4-(*tert*-butyl) 2-((2-((*S*)-2-(((9*H*-fluoren-9-yl)methoxy)carbonyl)amino)-4-oxo-4-(tritylamino)butanamido)benzyl)oxy)succinate **26**
- 49 ¹³C NMR spectrum of 1-benzyl 4-(*tert*-butyl) 2-((2-((*S*)-2-(((9*H*-fluoren-9-yl)methoxy)carbonyl)amino)-4-oxo-4-(tritylamino)butanamido)benzyl)oxy)succinate **26**

50

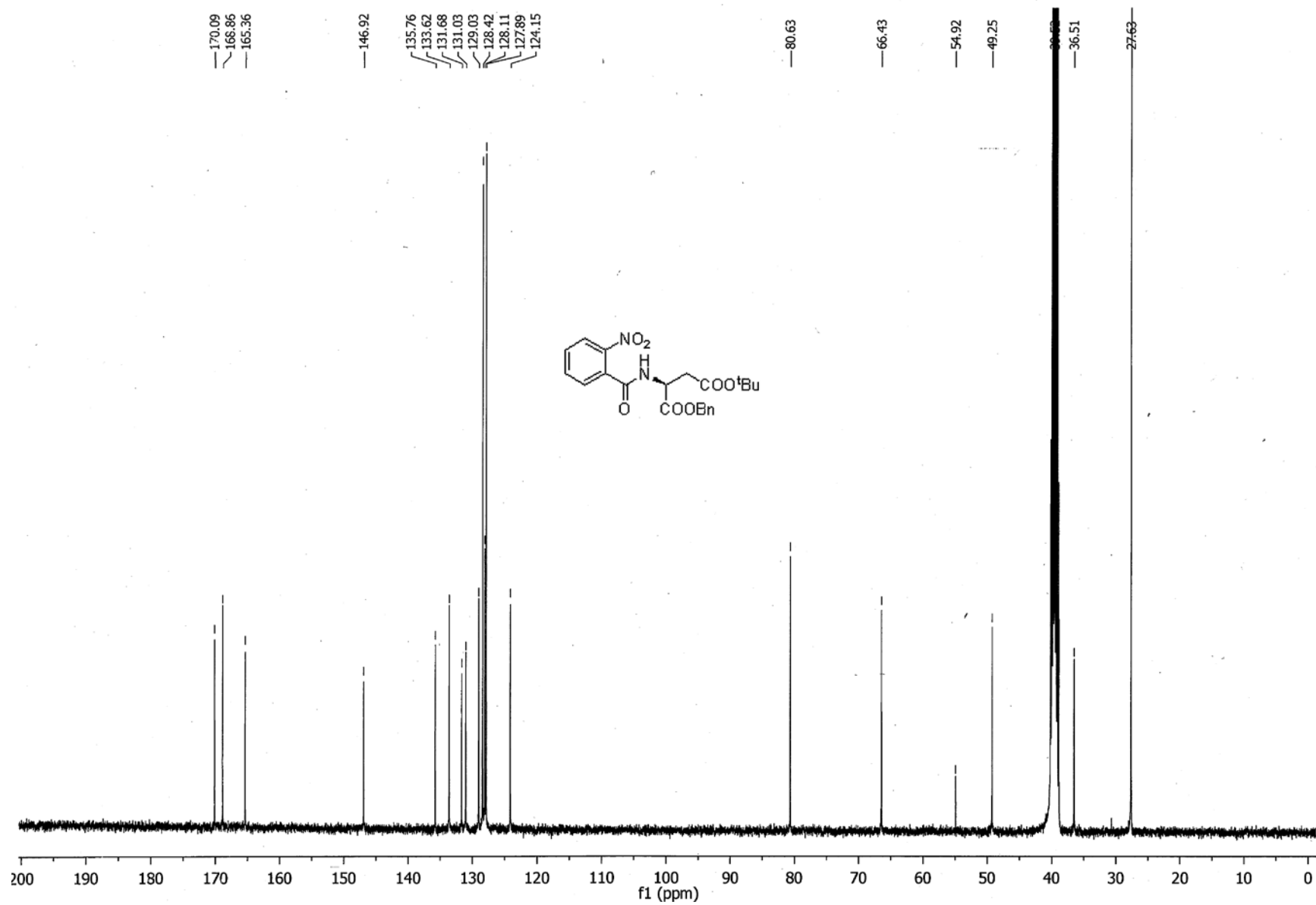
- HRMS report of 1-benzyl 4-(*tert*-butyl) 2-((2-((*S*)-2-(((9*H*-fluoren-9-yl)methoxy)carbonyl)amino)-4-oxo-4-(tritylamino)butanamido)benzyl)oxy)succinate **26**
- 51 ¹H NMR spectrum of 2-((2-((*S*)-2-(((9*H*-fluoren-9-yl)methoxy)carbonyl)amino)-4-oxo-4-(tritylamino)butanamido)benzyl)oxy)-4-(*tert*-butoxy)-4-oxobutanoic acid **4**
- 52 ¹³C NMR spectrum of 2-((2-((*S*)-2-(((9*H*-fluoren-9-yl)methoxy)carbonyl)amino)-4-oxo-4-(tritylamino)butanamido)benzyl)oxy)-4-(*tert*-butoxy)-4-oxobutanoic acid **4**
- 53 HRMS report of 2-((2-((*S*)-2-(((9*H*-fluoren-9-yl)methoxy)carbonyl)amino)-4-oxo-4-(tritylamino)butanamido)benzyl)oxy)-4-(*tert*-butoxy)-4-oxobutanoic acid **4**
- 54 ¹H NMR spectrum of (9*H*-fluoren-9-yl)methyl 2-methylhydrazine-1-carboxylate **27**
- 55 ¹³C NMR spectrum of (9*H*-fluoren-9-yl)methyl 2-methylhydrazine-1-carboxylate **27**
- 56 HRMS report of (9*H*-fluoren-9-yl)methyl 2-methylhydrazine-1-carboxylate **27**
- 57 ¹H NMR spectrum of 1-benzyl 4-(*tert*-butyl) 2-(2-(2-(((9*H*-fluoren-9-yl)methoxy)carbonyl)-1-methylhydrazinyl)-2-oxoethoxy)succinate **28**
- 58 ¹³C NMR spectrum of 1-benzyl 4-(*tert*-butyl) 2-(2-(2-(((9*H*-fluoren-9-yl)methoxy)carbonyl)-1-methylhydrazinyl)-2-oxoethoxy)succinate **28**
- 59 HRMS report of 1-benzyl 4-(*tert*-butyl) 2-(2-(2-(((9*H*-fluoren-9-yl)methoxy)carbonyl)-1-methylhydrazinyl)-2-oxoethoxy)succinate **28**
- 60 ¹H NMR spectrum of 2-(2-(2-(((9*H*-fluoren-9-yl)methoxy)carbonyl)-1-methylhydrazinyl)-2-oxoethoxy)-4-(*tert*-butoxy)-4-oxobutanoic acid **5**
- 61 ¹³C NMR spectrum of 2-(2-(2-(((9*H*-fluoren-9-yl)methoxy)carbonyl)-1-methylhydrazinyl)-2-oxoethoxy)-4-(*tert*-butoxy)-4-oxobutanoic acid **5**

62

HRMS report of 2-(2-(2-(((9*H*-fluoren-9-yl)methoxy)carbonyl)-1-methylhydrazinyl)-2-oxoethoxy)-4-(*tert*-butoxy)-4-oxobutanoic acid **5**



¹H NMR spectrum of 1-benzyl 4-(*tert*-butyl) (2-nitrobenzoyl)-*L*-aspartate **10**



¹³C NMR spectrum of 1-benzyl 4-(*tert*-butyl) (2-nitrobenzoyl)-*L*-aspartate **10**

Qualitative Compound Report

Data File	JRH-314-168-01.d	Sample Name	JRH-314-168-01
Sample Type	Sample	Position	P1-A1
Instrument Name	Instrument 1	User Name	Dr Jason Dang
Acq Method	Monash_Direct_Low_Frag_No_Formic.m	Acquired Time	11/4/2014 11:25:25 AM
IRM Calibration Status	XXXXXXXXXX	DA Method	Monash_Accuracy.m
Comment			

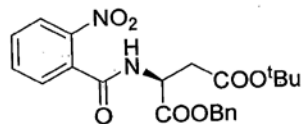
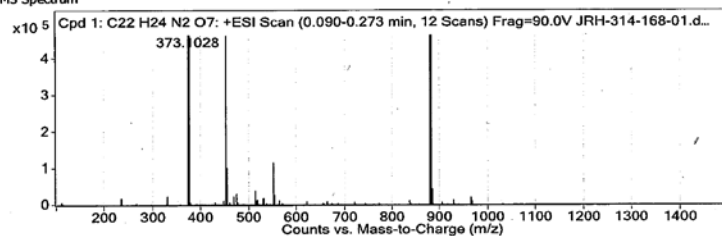
Sample Group		Info.	
Formula	C22H24N2O7	Acquisition SW	6200 series TOF/6500 series
		Version	Q-TOF B.05.01 (B5125.1)

Compound Table

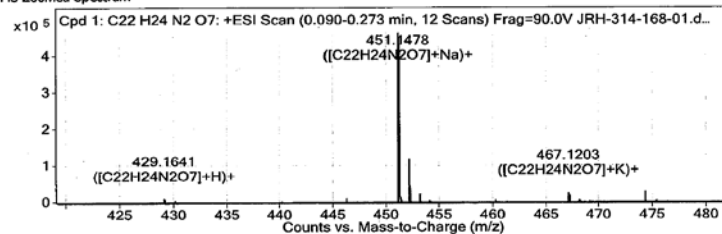
Compound Label	RT	Mass	Abund	Formula	Tgt Mass	Diff (ppm)	MFG Formula	DB Formula
Cpd 1: C22 H24 N2 O7	0.14	428.1583	465346	C22 H24 N2 O7	428.1584	-0.02	C22 H24 N2 O7	C22 H24 N2 O7

Compound Label	m/z	RT	Algorithm	Mass
Cpd 1: C22 H24 N2 O7	451.1478	0.14	Find By Formula	428.1583

MS Spectrum



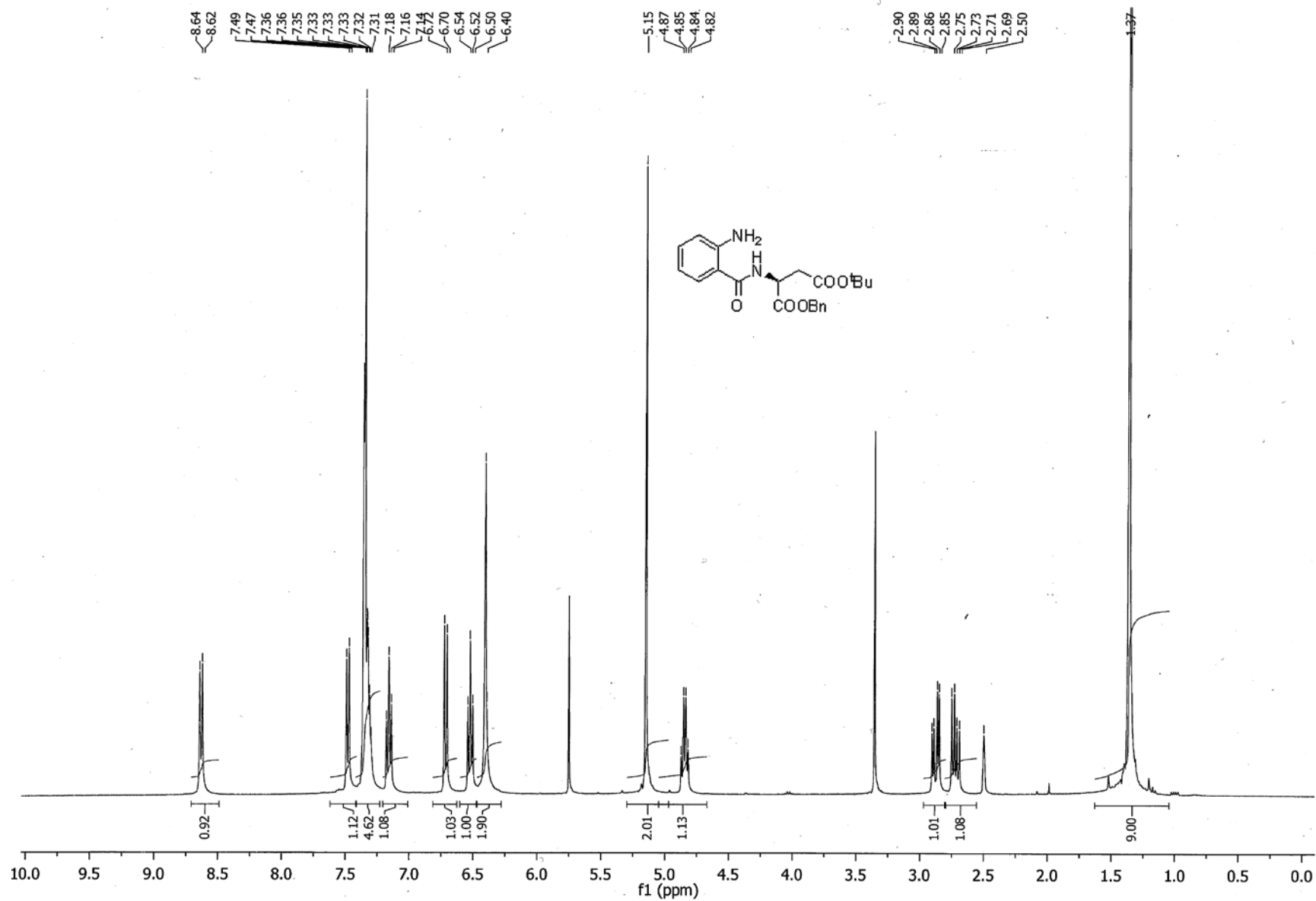
MS Zoomed Spectrum



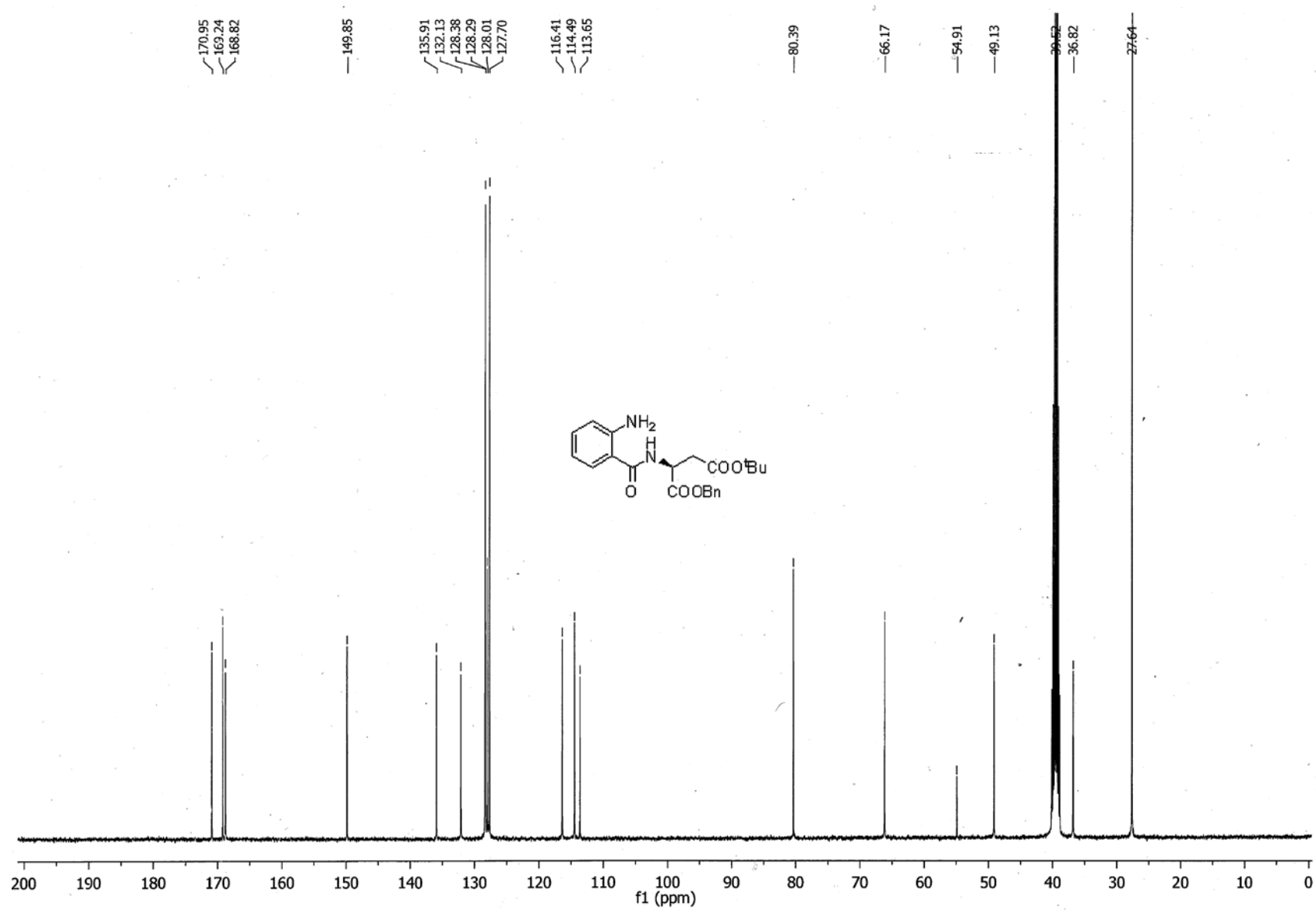
MS Spectrum Peak List

m/z	Calc m/z	Diff(ppm)	z	Abund	Formula	Ion
429.1641	429.1656	3.53	1	7111.62	C22H24N2O7	(M+H)+
451.1478	451.1476	-0.42	1	465345.71	C22H24N2O7	(M+Na)+
467.1203	467.1215	2.52	1	23462.33	C22H24N2O7	(M+K)+

--- End Of Report ---



¹H NMR spectrum of 1-benzyl 4-(*tert*-butyl) (2-aminobenzoyl)-*L*-aspartate **11**



¹³C NMR spectrum of 1-benzyl 4-(*tert*-butyl) (2-aminobenzoyl)-*L*-aspartate **11**

Qualitative Compound Report

Data File	JRH-314-172-01.d	Sample Name	JRH-314-172-01
Sample Type	Sample	Position	P1-A2
Instrument Name	Instrument 1	User Name	Dr Jason Dang
Acq Method	Monash_Direct_Low_Frag_No_Formic.m	Acquired Time	11/4/2014 11:28:42 AM
IRM Calibration Status	XXXXXXXXXX	DA Method	Monash_Accuracy.m
Comment			

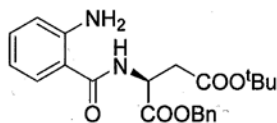
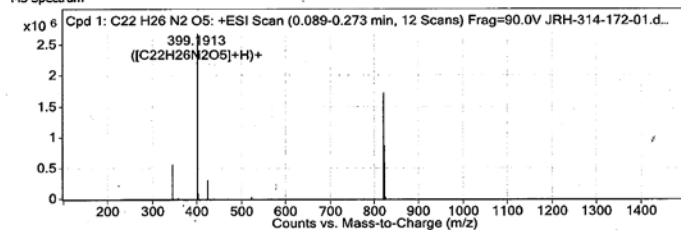
Sample Group	C22H26N2O5	Info.	
Formula		Acquisition SW	6200 series TOF/6500 series
		Version	Q-TOF B.05.01 (B5125.1)

Compound Table

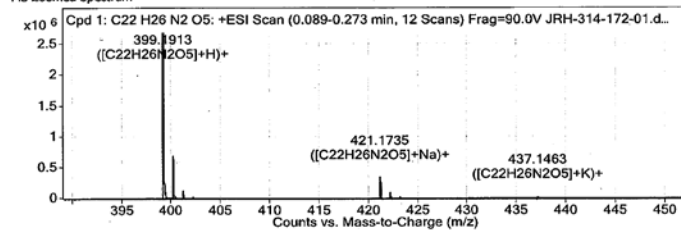
Compound Label	RT	Mass	Abund	Formula	Tgt Mass	Diff (ppm)	MFG Formula	DB Formula
Cpd 1: C22 H26 N2 O5	0.173	398.1841	2719495	C22 H26 N2 O5	398.1842	-0.14	C22 H26 N2 O5	C22 H26 N2 O5

Compound Label	m/z	RT	Algorithm	Mass
Cpd 1: C22 H26 N2 O5	399.1913	0.173	Find By Formula	398.1841

MS Spectrum



MS Zoomed Spectrum

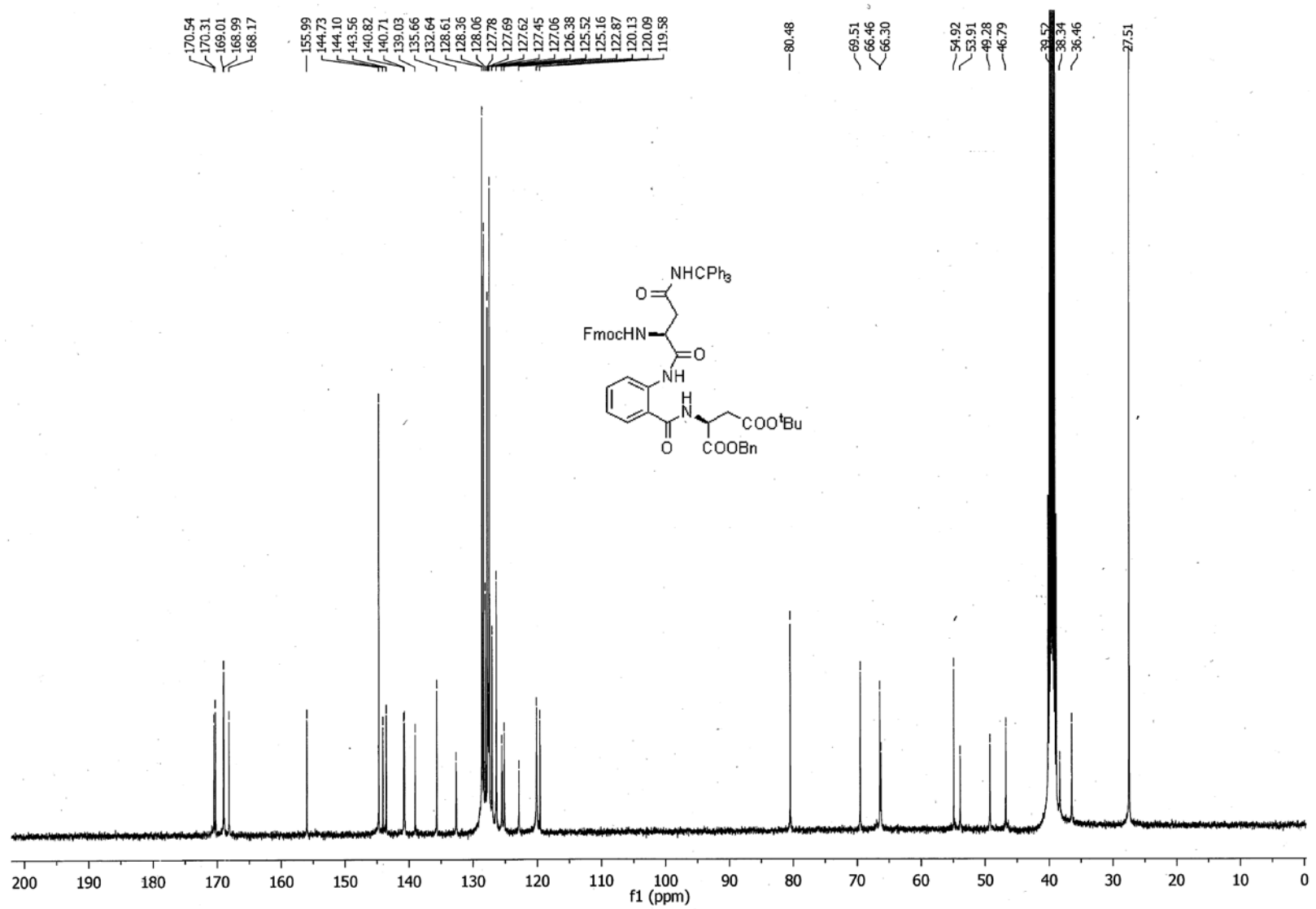


MS Spectrum Peak List

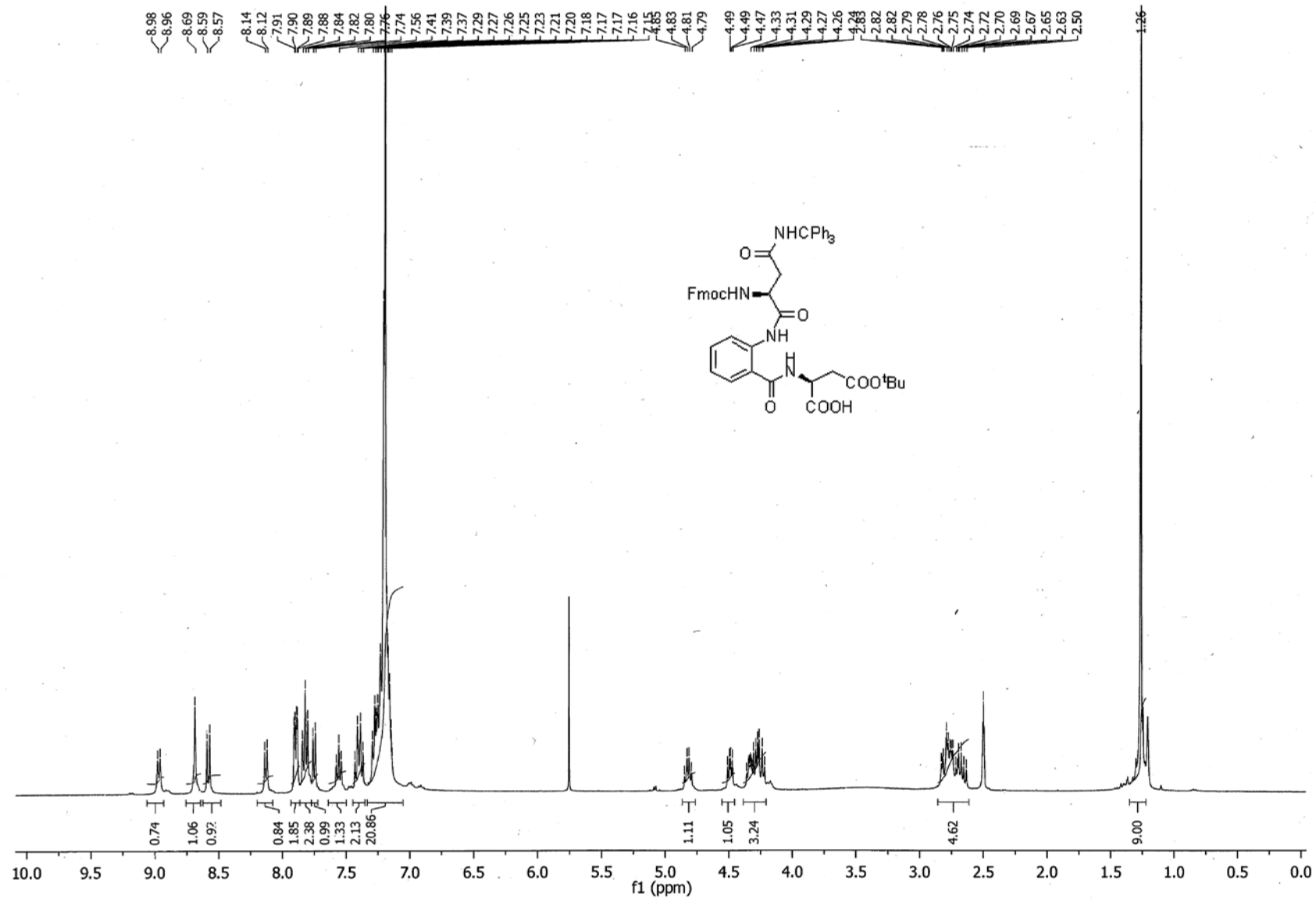
m/z	Calc m/z	Diff (ppm)	z	Abund	Formula	Ion
399.1913	399.1914	0.38	1	2719495.4	C22H26N2O5	(M+H)+
421.1735	421.1734	-0.28	1	325439.65	C22H26N2O5	(M+Na)+
437.1463	437.1473	2.44	1	15033.47	C22H26N2O5	(M+K)+

--- End Of Report ---

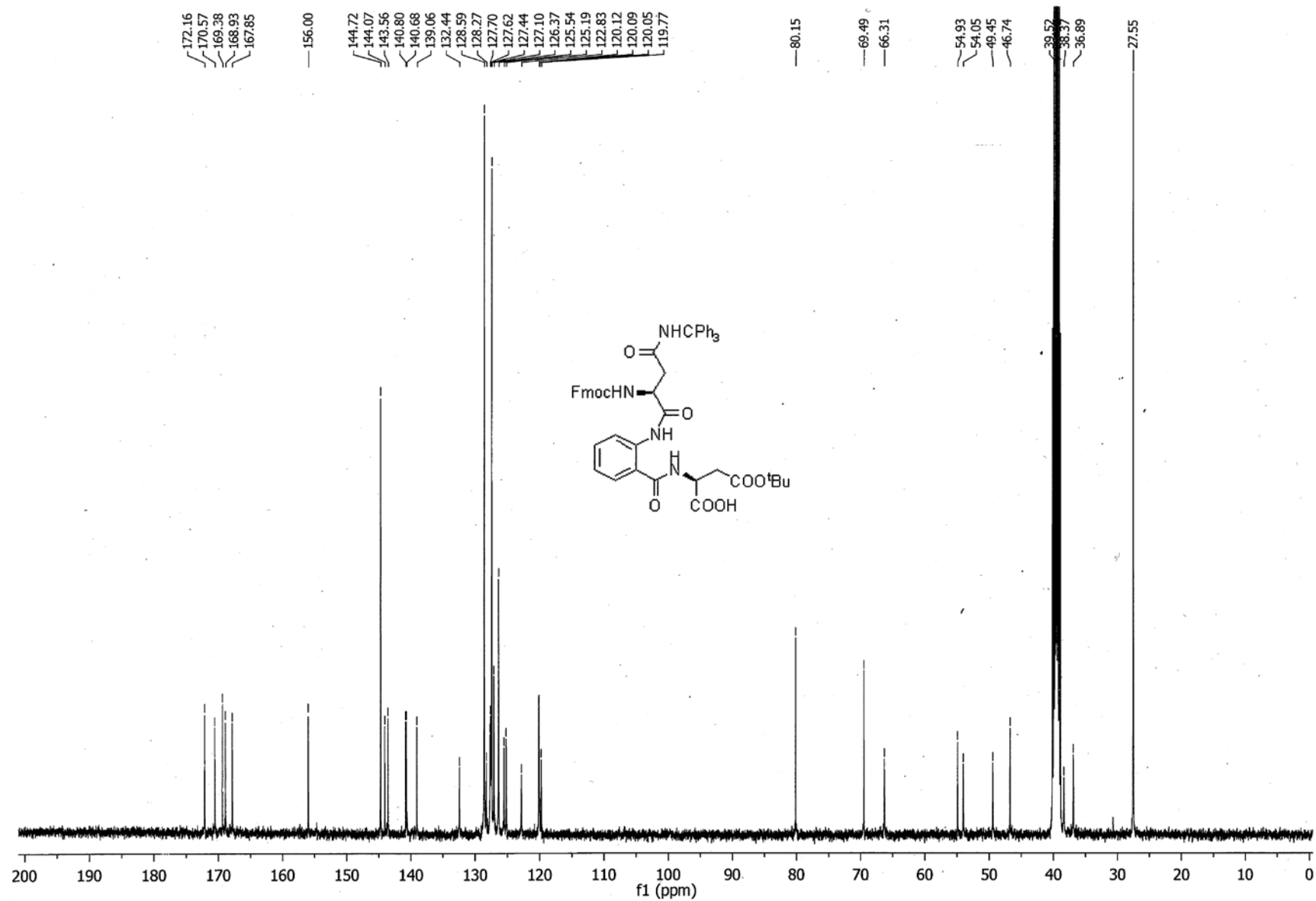
HRMS report of 1-benzyl 4-(*tert*-butyl) (2-aminobenzoyl)-*L*-aspartate 11



¹³C NMR spectrum 1-benzyl 4-(*tert*-butyl) (2-((*S*)-2-(((9*H*-fluoren-9-yl)methoxy)carbonyl)amino)-4-oxo-4-(tritylamino)butanamido)benzoyl)-*L*-aspartate **13**



¹H NMR spectrum of (S)-2-(2-(((S)-2-(((9H-fluoren-9-yl)methoxy)carbonyl)amino)-4-oxo-4-(tritylamino)butanamido)benzamido)-4-(tert-butoxy)-4-oxobutanoic acid **6**



^{13}C NMR spectrum of (S)-2-(2-((S)-2-(((9H-fluoren-9-yl)methoxy)carbonyl)amino)-4-oxo-4-(tritylamino)butanamido)benzamido)-4-(tert-butoxy)-4-oxobutanoic acid **6**

Qualitative Compound Report

Data File	JRH-314-180-01.d	Sample Name	JRH-314-180-01
Sample Type	Sample	Position	P1-A4
Instrument Name	Instrument 1	User Name	Dr Jason Dang
Acq Method	Monash_Direct_Low_Frag_No_Formic.m	Acquired Time	11/4/2014 11:35:10 AM
IRM Calibration Status	XXXXXXXXXX	DA Method	Monash_Accuracy.m
Comment			

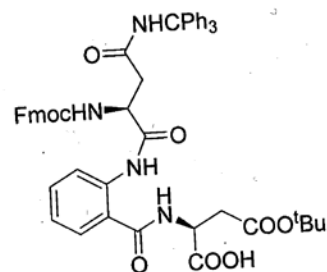
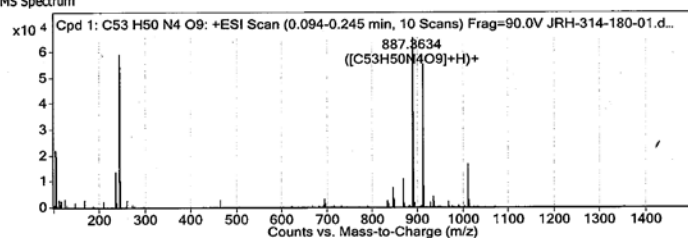
Sample Group	Info.		
Formula	C53H50N4O9	Acquisition SW	6200 series TOF/6500 series
		Version	Q-TOF B.05.01 (B5125.1)

Compound Table

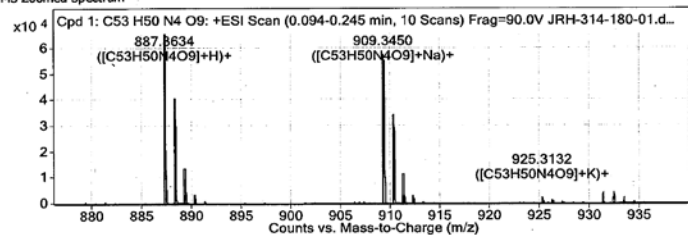
Compound Label	RT	Mass	Abund	Formula	Tgt Mass	Diff (ppm)	MFG Formula	DB Formula
Cpd 1: C53 H50 N4 O9	0.128	886.3557	67530	C53 H50 N4 O9	886.3578	-2.39	C53 H50 N4 O9	C53 H50 N4 O9

Compound Label	m/z	RT	Algorithm	Mass
Cpd 1: C53 H50 N4 O9	887.8634	0.128	Find By Formula	886.3557

MS Spectrum



MS Zoomed Spectrum

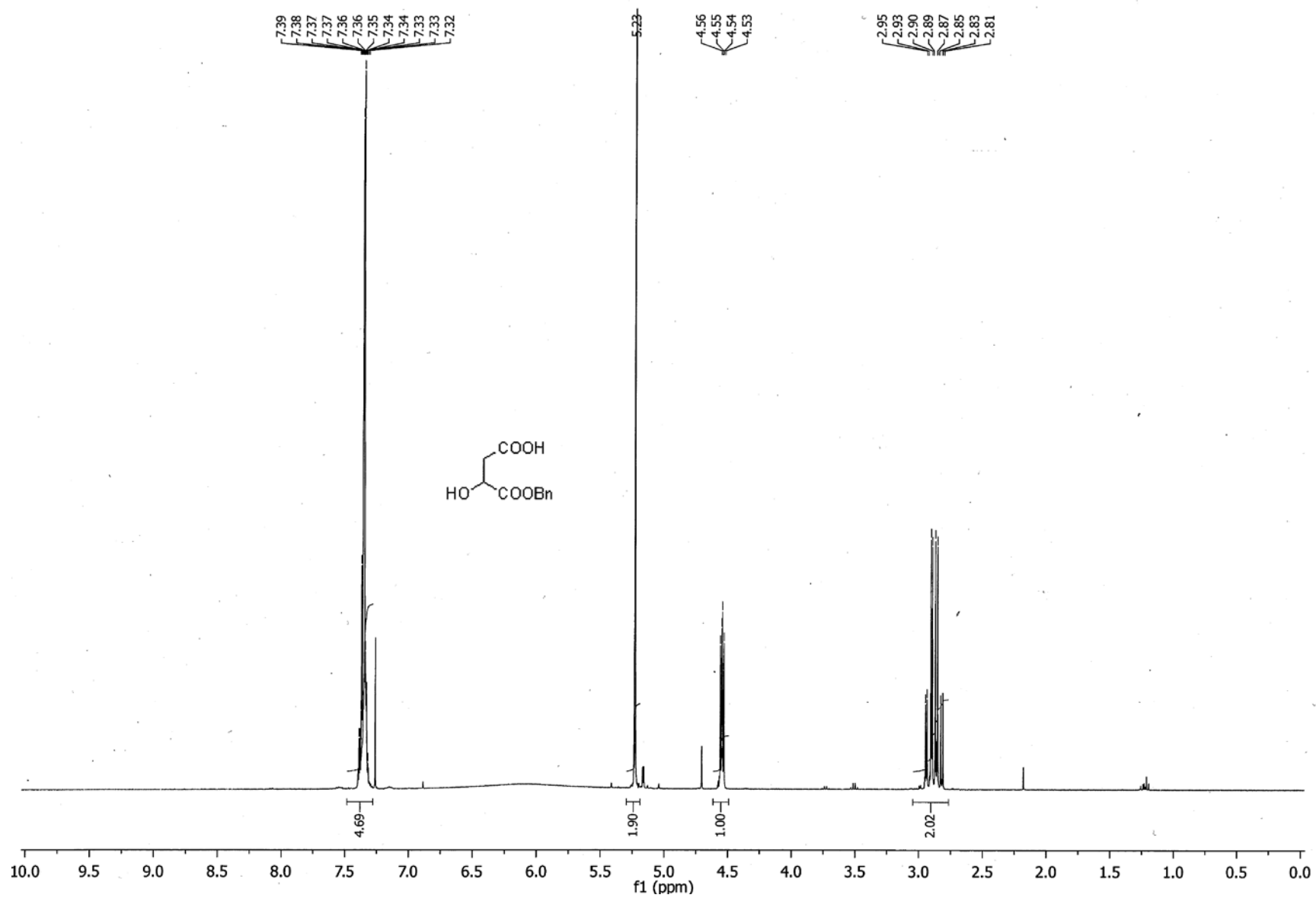


MS Spectrum Peak List

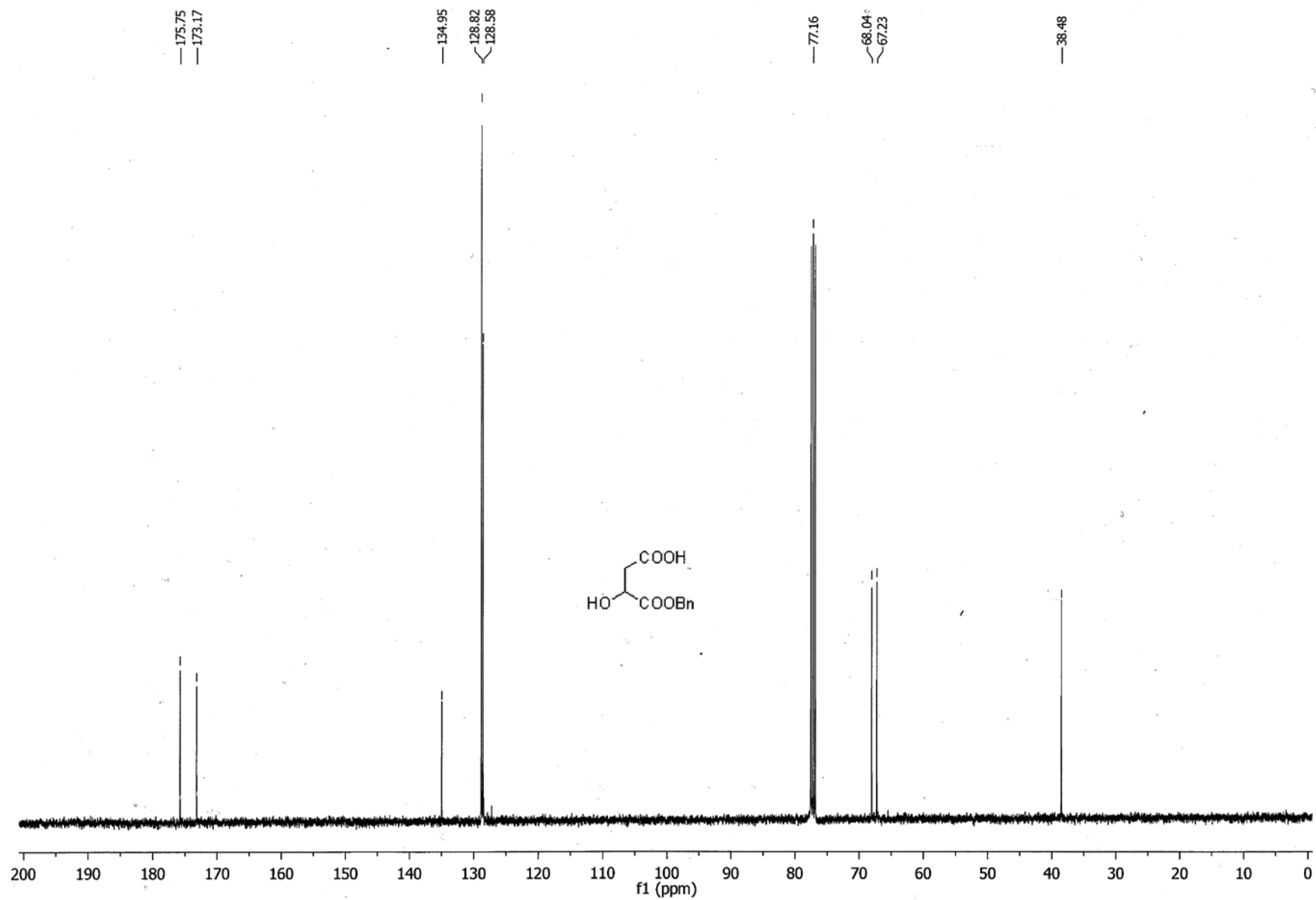
m/z	Calc m/z	Diff(ppm)	z	Abund	Formula	Ion
887.3634	887.3651	1.87	1	67529.67	C53H50N4O9	(M+H)+
909.345	909.347	2.16	1	57293.38	C53H50N4O9	(M+Na)+
925.3132	925.3209	8.41	1	1866.03	C53H50N4O9	(M+K)+

--- End Of Report ---

HRMS report of (S)-2-(2-(((S)-2-(((9H-fluoren-9-yl)methoxy)carbonyl)amino)-4-oxo-4-(tritylamino)butanamido)benzamido)-4-(tert-butoxy)-4-oxobutanoic acid **6**



¹H NMR spectrum of 4-(benzyloxy)-3-hydroxy-4-oxobutanoic acid **15**



¹³C NMR spectrum of 4-(benzyloxy)-3-hydroxy-4-oxobutanoic acid **15**

Qualitative Compound Report

Data File	JRH-255-178-01.d	Sample Name	JRH-255-178-01
Sample Type	Sample	Position	P1-A5
Instrument Name	Instrument 1	User Name	Dr Jason Dang
Acq Method	Monash_Direct_Low_Frag_No_Formic.m	Acquired Time	11/4/2014 11:38:27 AM
IRM Calibration Status	XXXXXXXXXX	DA Method	Monash_Accuracy.m
Comment			

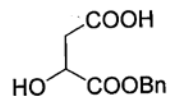
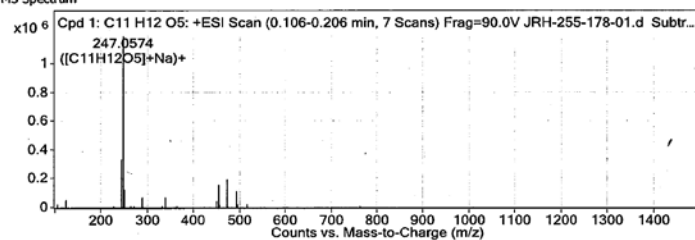
Sample Group		Info.	
Formula	C11H12O5	Acquisition SW	6200 series TOF/6500 series
		Version	Q-TOF B.05.01 (B5125.1)

Compound Table

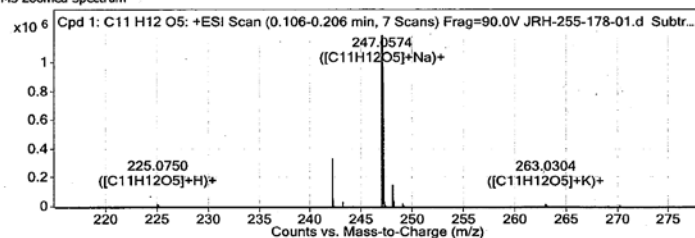
Compound Label	RT	Mass	Abund	Formula	Tgt Mass	Diff (ppm)	MFG Formula	DB Formula
Cpd 1: C11 H12 O5	0.123	224.0682	1197698	C11 H12 O5	224.0685	-1.44	C11 H12 O5	C11 H12 O5

Compound Label	m/z	RT	Algorithm	Mass
Cpd 1: C11 H12 O5	247.0574	0.123	Find By Formula	224.0682

MS Spectrum



MS Zoomed Spectrum

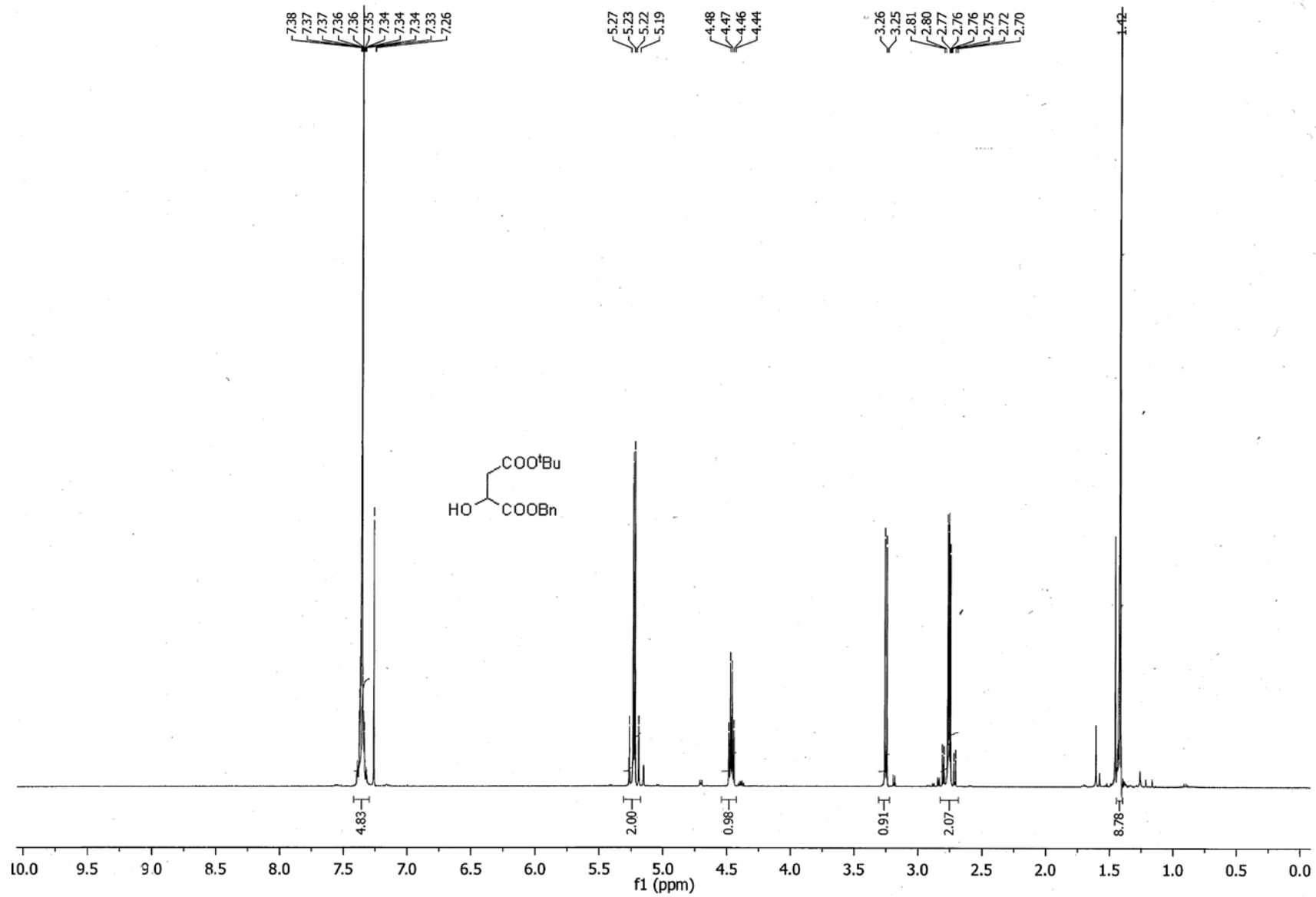


MS Spectrum Peak List

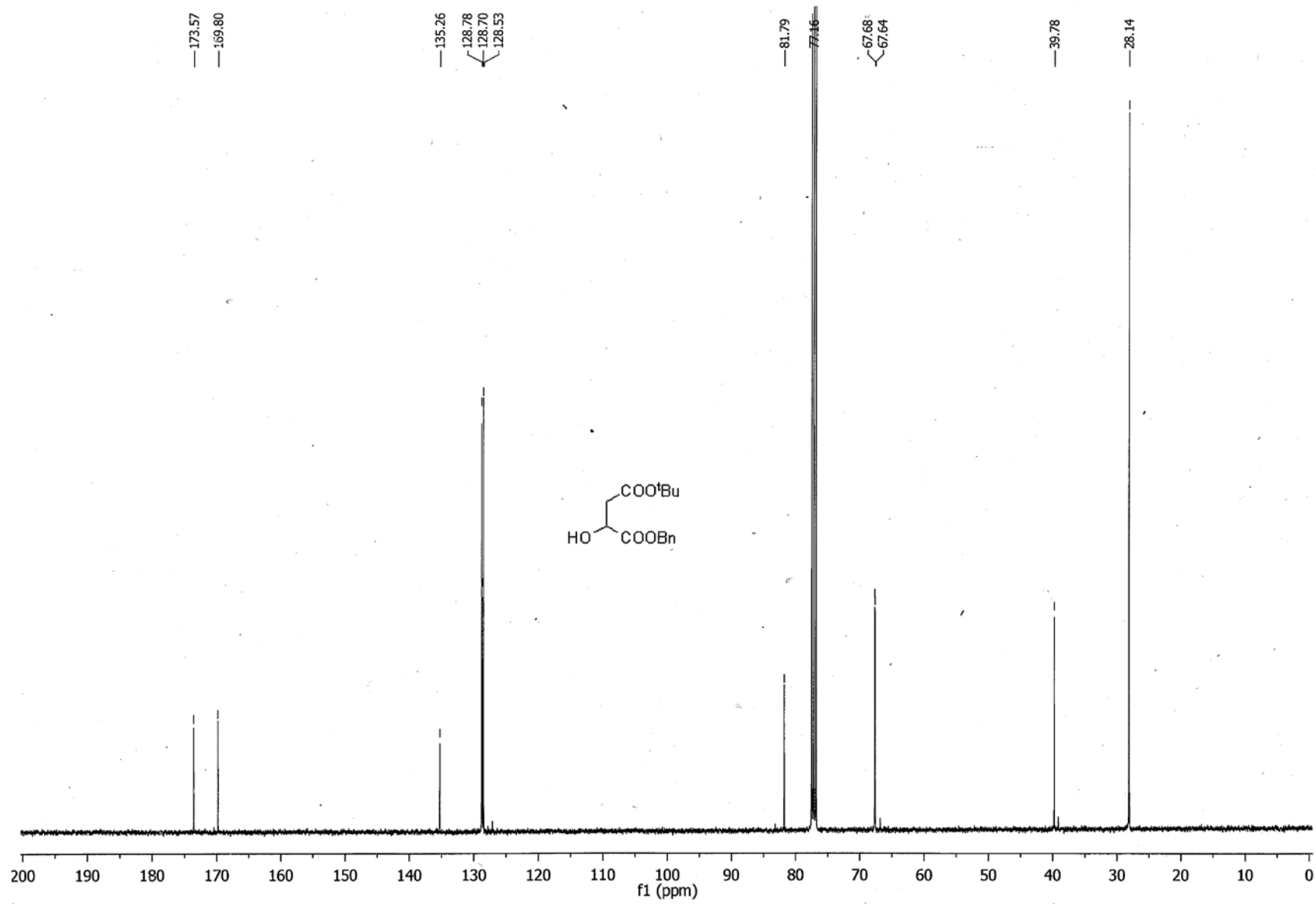
m/z	Calc m/z	Diff (ppm)	z	Abund	Formula	Ion
225.075	225.0757	3.31	1	14143.8	C11H12O5	(M+H)+
247.0574	247.0577	1.18	1	1197697.94	C11H12O5	(M+Na)+
263.0304	263.0316	4.57	1	11214.11	C11H12O5	(M+K)+

--- End Of Report ---

HRMS report of 4-(benzyloxy)-3-hydroxy-4-oxobutanoic acid 15



¹H NMR spectrum of 1-benzyl 4-(*tert*-butyl) 2-hydroxysuccinate 17



¹³C NMR spectrum of 1-benzyl 4-(*tert*-butyl) 2-hydroxysuccinate **17**

Qualitative Compound Report

Data File	JRH-255-204-01.d	Sample Name	JRH-255-204-01
Sample Type	Sample	Position	P1-A6
Instrument Name	Instrument 1	User Name	Dr Jason Dang
Acq Method	Monash_Direct_Low_Frag_No_Formic.m	Acquired Time	11/4/2014 11:41:44 AM
IRM Calibration Status	XXXXXXXXXX	DA Method	Monash_Accuracy.m
Comment			

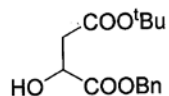
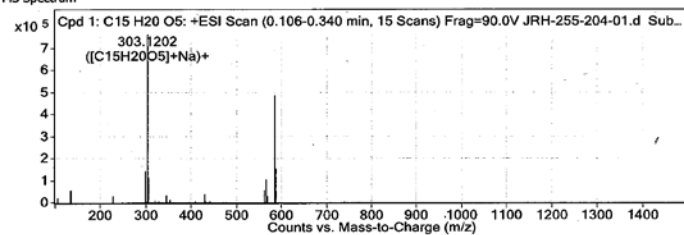
Sample Group	C15H20O5	Info.	6200 series TOF/6500 series
Formula		Acquisition SW Version	Q-TOF B.05.01 (B5125.1)

Compound Table

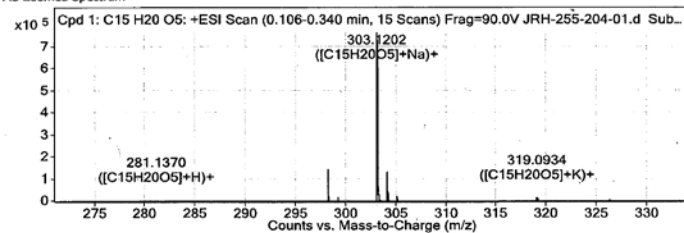
Compound Label	RT	Mass	Abund	Formula	Tgt Mass	Diff (ppm)	MFG Formula	DB Formula
Cpd 1: C15 H20 O5	0.139	280.131	776817	C15 H20 O5	280.1311	-0.43	C15 H20 O5	C15 H20 O5

Compound Label	m/z	RT	Algorithm	Mass
Cpd 1: C15 H20 O5	303.1202	0.139	Find By Formula	280.131

MS Spectrum



MS Zoomed Spectrum

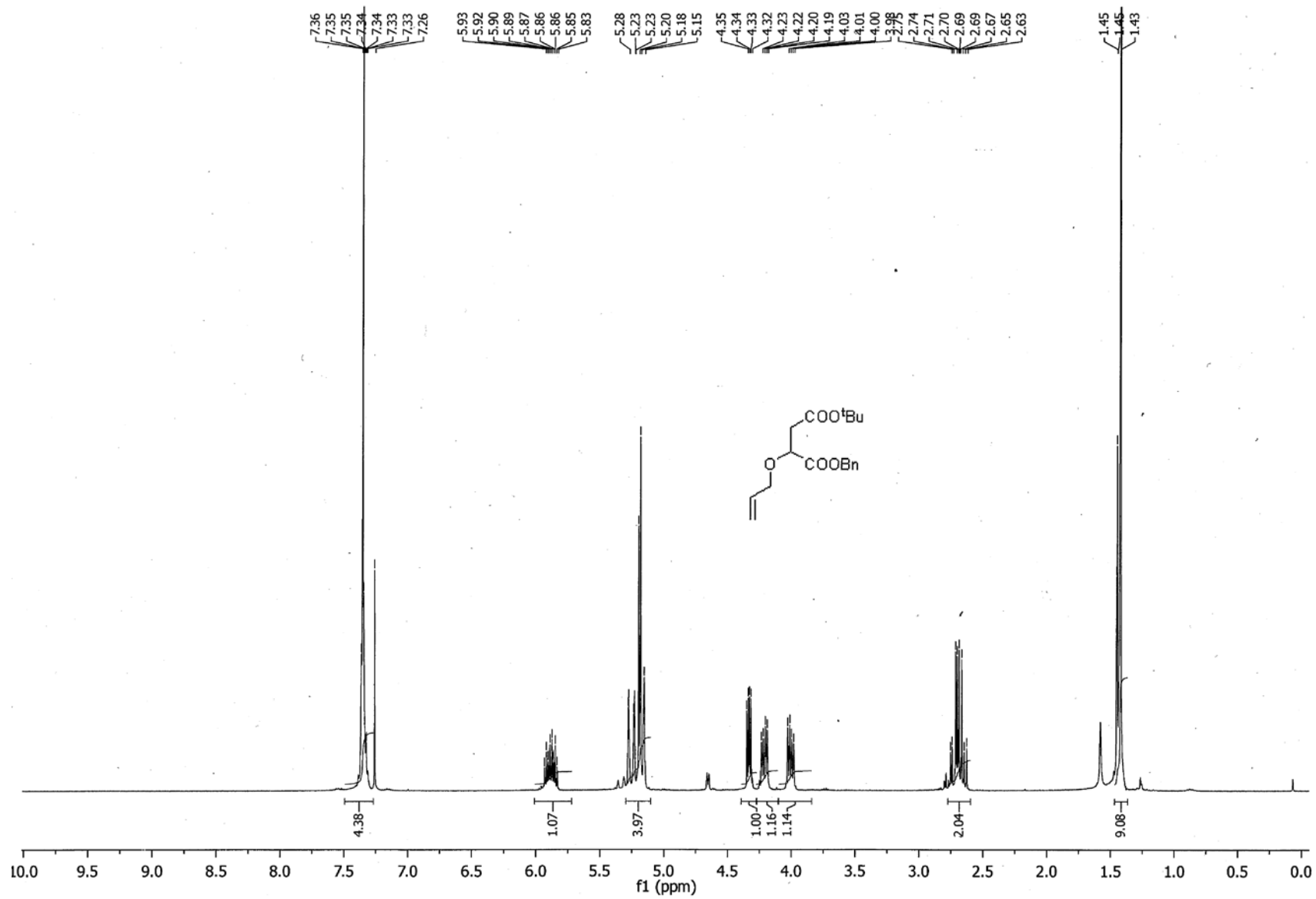


MS Spectrum Peak List

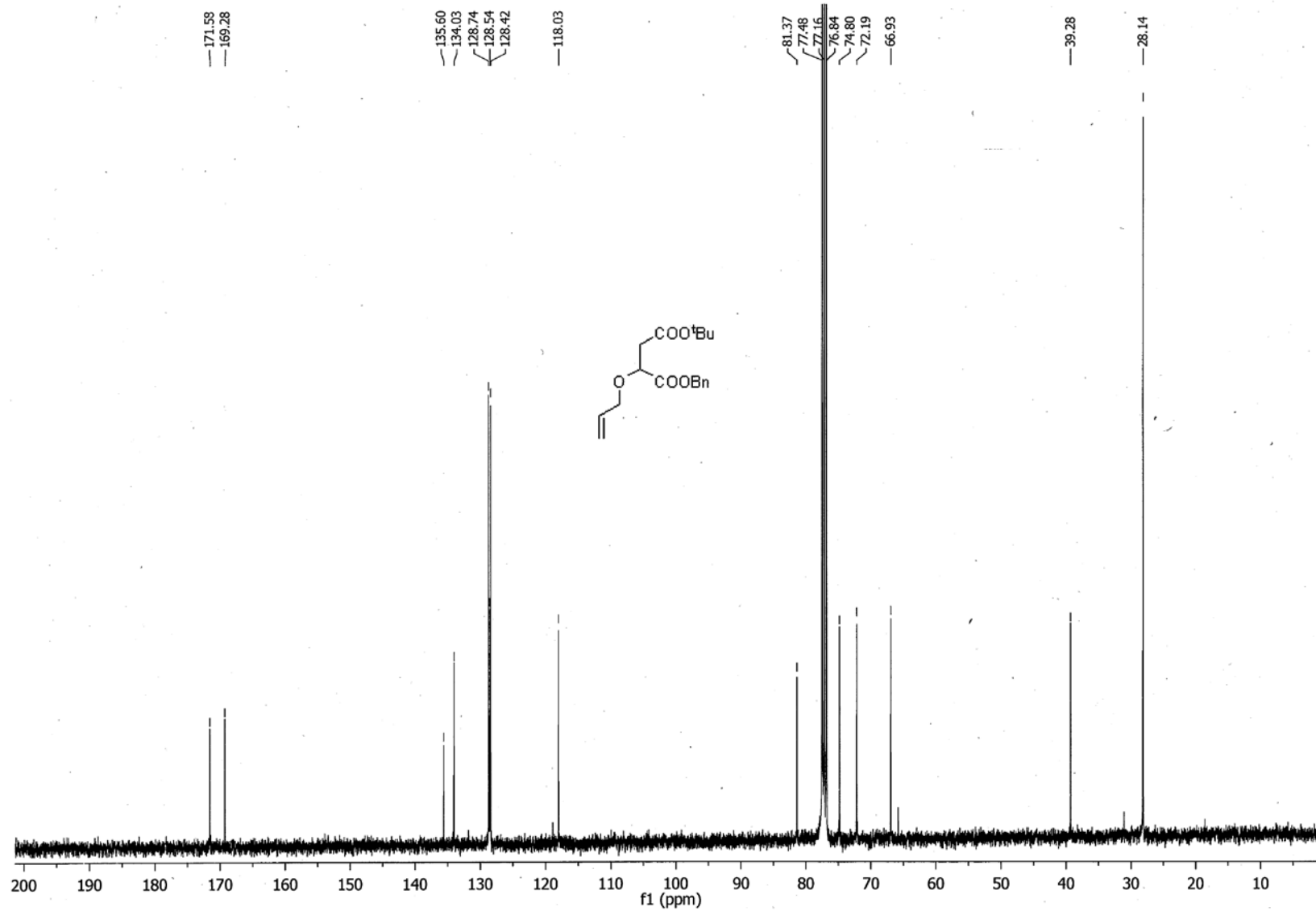
m/z	Calc m/z	Diff (ppm)	z	Abund	Formula	Ion
281.137	281.1384	4.64	1	1327.76	C15H20O5	(M+H)+
303.1202	303.1203	0.31	1	776817.09	C15H20O5	(M+Na)+
319.0934	319.0942	2.69	1	11446.59	C15H20O5	(M+K)+

--- End Of Report ---

HRMS report of 1-benzyl 4-(*tert*-butyl) 2-hydroxysuccinate **17**



¹H NMR spectrum of 1-benzyl 4-(*tert*-butyl) 2-(allyloxy)succinate **18**



¹³C NMR spectrum of 1-benzyl 4-(*tert*-butyl) 2-(allyloxy)succinate **18**

Qualitative Compound Report

Data File	JRH-314-062-01.d	Sample Name	JRH-314-062-01
Sample Type	Sample	Position	P1-A7
Instrument Name	Instrument 1	User Name	Dr Jason Dang
Acq Method	Monash_Direct_Low_Frag_No_Formic.m	Acquired Time	11/4/2014 11:45:00 AM
IRM Calibration Status		DA Method	Monash_Accuracy.m
Comment			

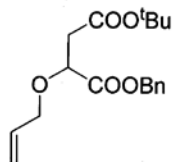
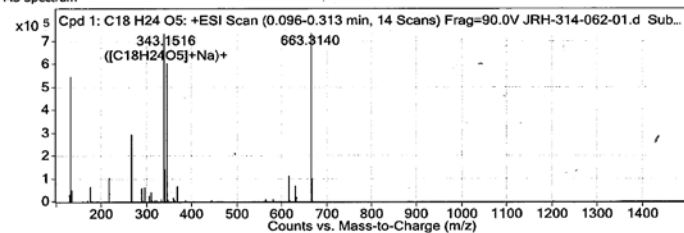
Sample Group	Info.	6200 series TOF/6500 series
Formula	Acquisition SW	Q-TOF B.05.01 (B5125.1)
	Version	

Compound Table

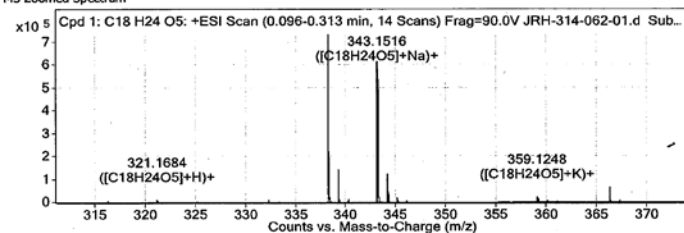
Compound Label	RT	Mass	Abund	Formula	Tgt Mass	Diff (ppm)	MFG Formula	DB Formula
Cpd 1: C18 H24 O5	0.129	320.1623	610446	C18 H24 O5	320.1624	-0.26	C18 H24 O5	C18 H24 O5

Compound Label	m/z	RT	Algorithm	Mass
Cpd 1: C18 H24 O5	343.1516	0.129	Find By Formula	320.1623

MS Spectrum



MS Zoomed Spectrum

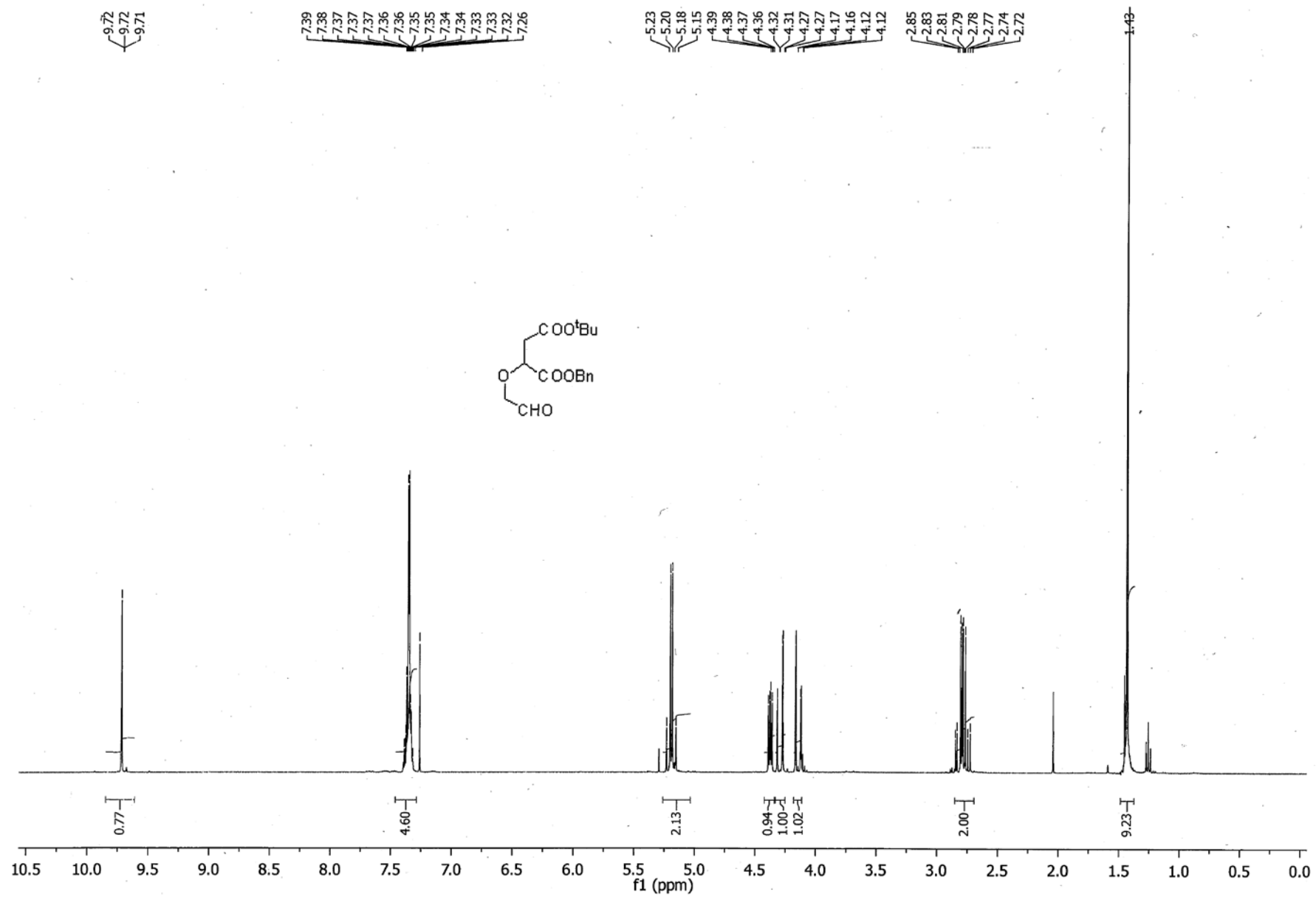


MS Spectrum Peak List

m/z	Calc m/z	Diff(ppm)	z	Abund	Formula	Ion
321.1684	321.1697	4.05	1	6788.71	C18H24O5	(M+H)+
343.1516	343.1516	0.03	1	610446.46	C18H24O5	(M+Na)+
359.1248	359.1255	1.96	1	19124.84	C18H24O5	(M+K)+

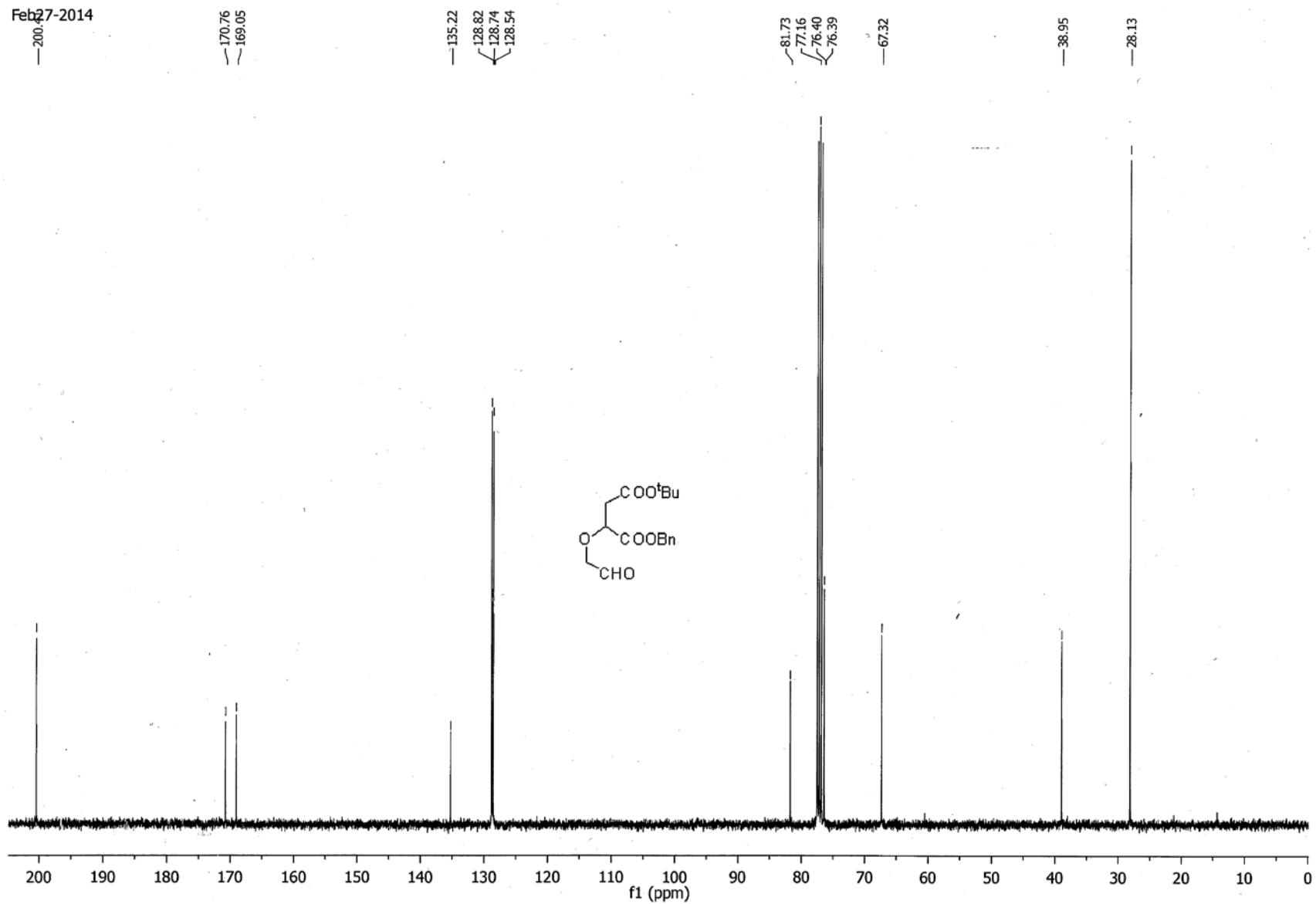
--- End Of Report ---

HRMS report of 1-benzyl 4-(*tert*-butyl) 2-(allyloxy)succinate **18**



¹H NMR spectrum of 1-benzyl 4-(*tert*-butyl) 2-(2-oxoethoxy)succinate **19**

Feb 27-2014



^{13}C NMR spectrum of 1-benzyl 4-(*tert*-butyl) 2-(2-oxoethoxy)succinate **19**

Qualitative Compound Report

Data File	JRH-314-066-01.d	Sample Name	JRH-314-066-01
Sample Type	Sample	Position	P1-A8
Instrument Name	Instrument 1	User Name	Dr Jason Dang
Acq Method	Monash_Direct.m	Acquired Time	08-Dec-14 1:45:12 PM
IRM Calibration Status		DA Method	Monash_Accuracy.m
Comment			

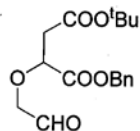
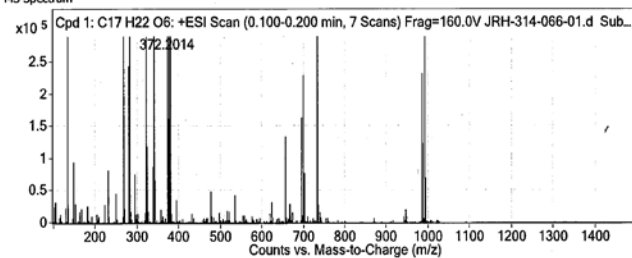
Sample Group		Info.	
Formula	C17H22O6	Acquisition SW Version	6200 series TOF/6500 series Q-TOF B.05.01 (B5125.1)

Compound Table

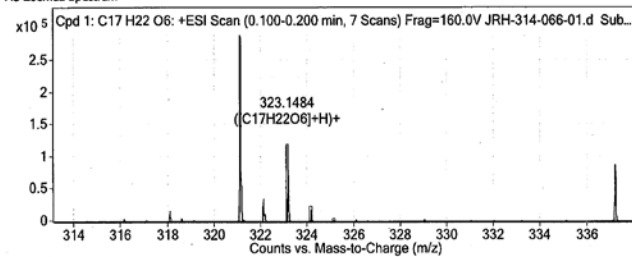
Compound Label	RT	Mass	Abund	Formula	Tgt Mass	Diff (ppm)	MFG Formula	DB Formula
Cpd 1: C17 H22 O6	0.134	322.1409	118945	C17 H22 O6	322.1416	-2.29	C17 H22 O6	C17 H22 O6

Compound Label	m/z	RT	Algorithm	Mass
Cpd 1: C17 H22 O6	323.1484	0.134	Find By Formula	322.1409

MS Spectrum



MS Zoomed Spectrum

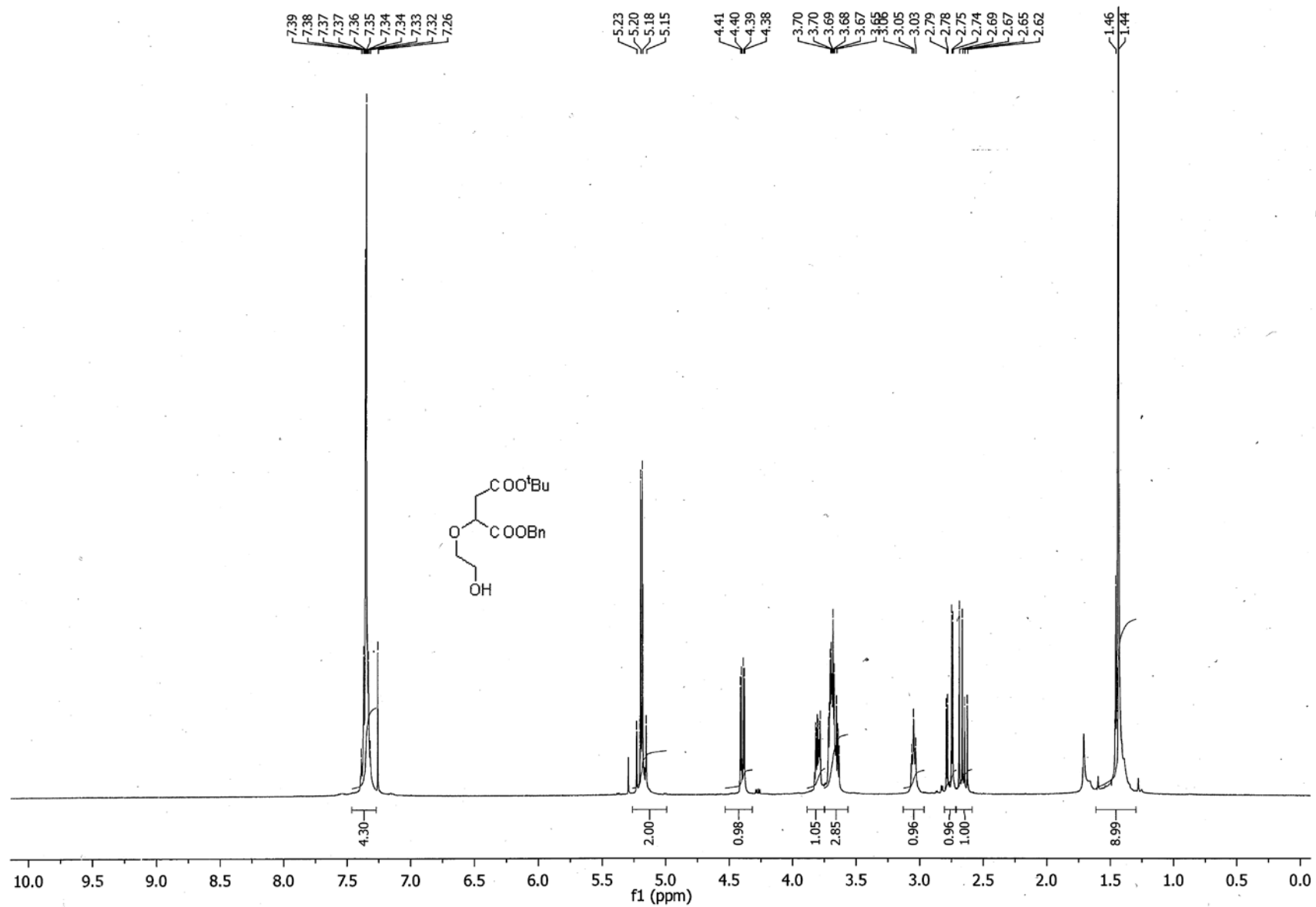


MS Spectrum Peak List

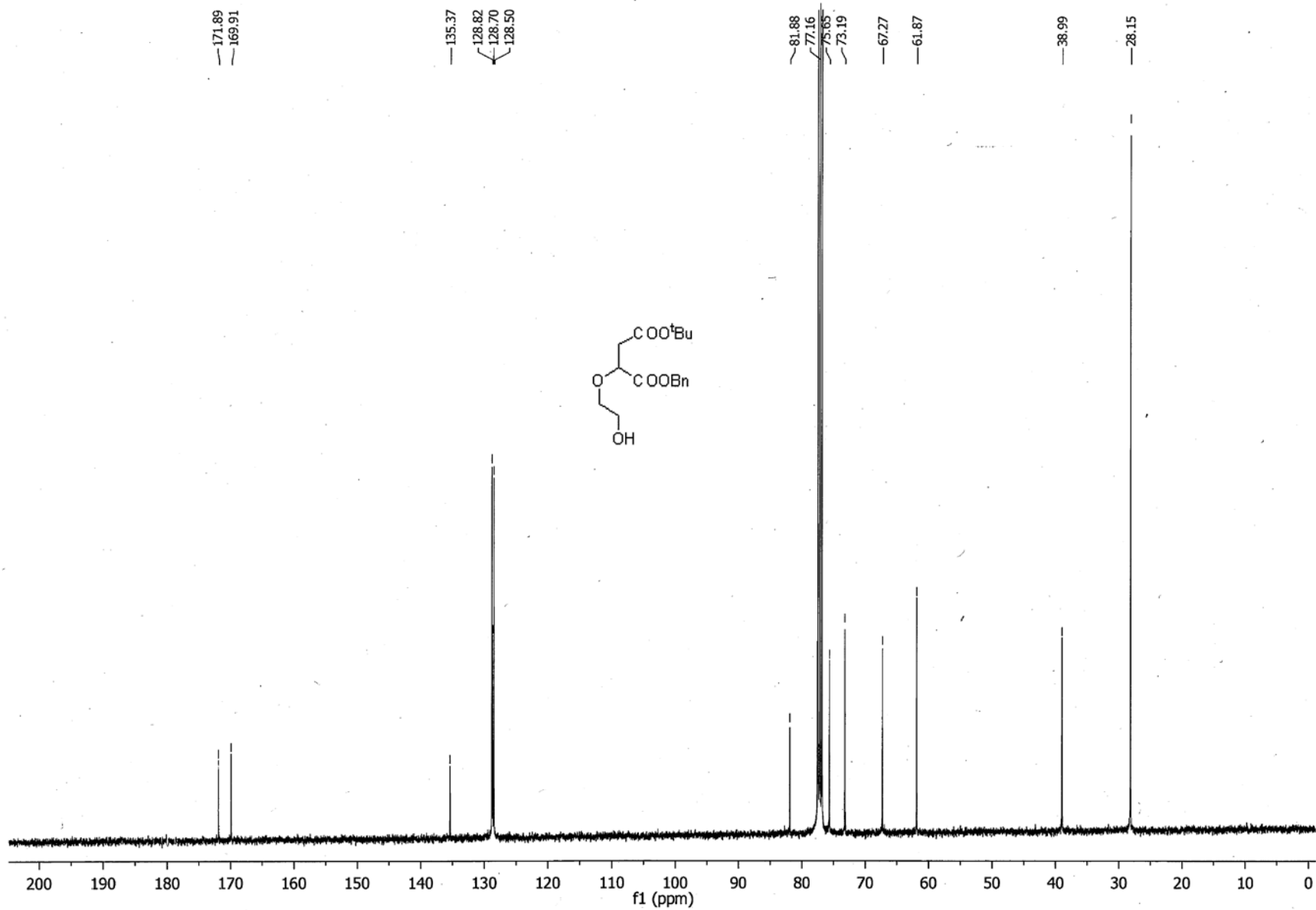
m/z	Calc m/z	Diff(ppm)	z	Abund	Formula	Ion
323.1484	323.1489	1.72	1	118945.14	C17H22O6	(M+H)+
324.1511	324.1523	3.8	1	18304.83	C17H22O6	(M+H)+
372.2014				4876456.76		

--- End Of Report ---

HRMS report of 1-benzyl 4-(*tert*-butyl) 2-(2-oxoethoxy)succinate **19**



¹H NMR spectrum of 1-benzyl 4-(*tert*-butyl) 2-(2-hydroxyethoxy)succinate **20**



¹³C NMR spectrum of 1-benzyl 4-(*tert*-butyl) 2-(2-hydroxyethoxy)succinate **20**

Qualitative Compound Report

Data File	JRH-314-184-01.d	Sample Name	JRH-314-184-01
Sample Type	Sample	Position	P1-A9
Instrument Name	Instrument 1	User Name	Dr Jason Dang
Acq Method	Monash_Direct_Low_Frag_No_Formic.m	Acquired Time	11/4/2014 11:51:31 AM
IRM Calibration Status	XXXXXXXXXX	DA Method	Monash_Accuracy.m
Comment			

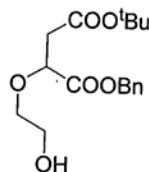
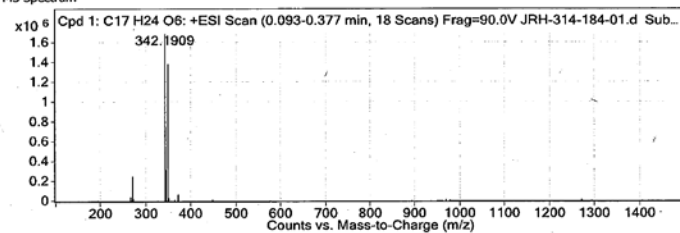
Sample Group	Info.	
Formula	Acquisition SW	6200 series TOF/6500 series
C17H24O6	Version	Q-TOF B.05.01 (85125.1)

Compound Table

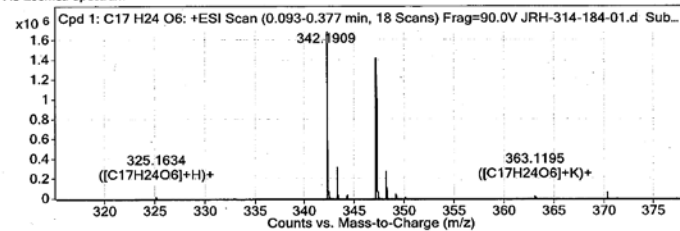
Compound Label	RT	Mass	Abund	Formula	Tgt Mass	Diff (ppm)	MFG Formula	DB Formula
Cpd 1: C17 H24 O6	0.143	324.1571	1415467	C17 H24 O6	324.1573	-0.46	C17 H24 O6	C17 H24 O6

Compound Label	m/z	RT	Algorithm	Mass
Cpd 1: C17 H24 O6	347.1463	0.143	Find By Formula	324.1571

MS Spectrum



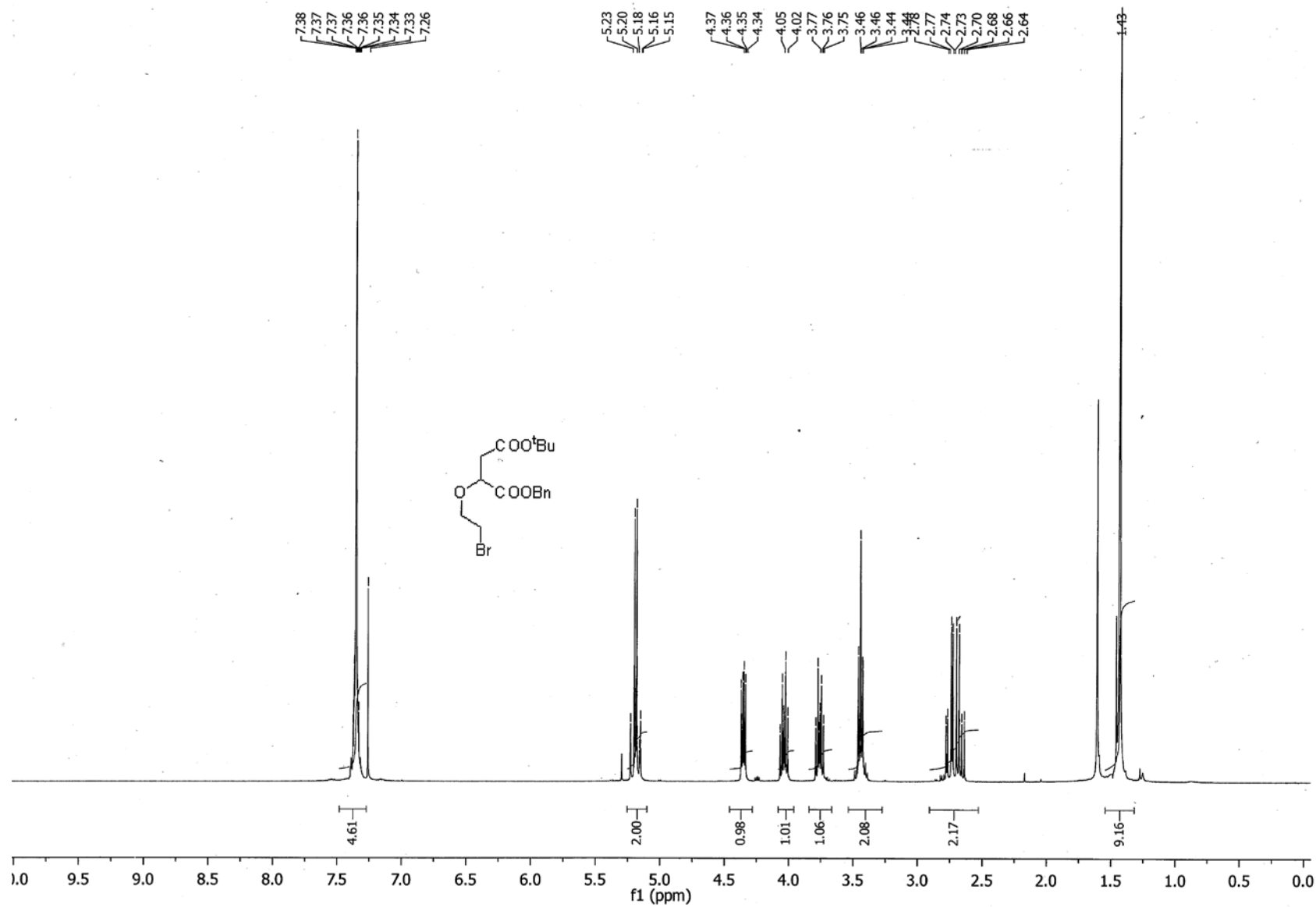
MS Zoomed Spectrum



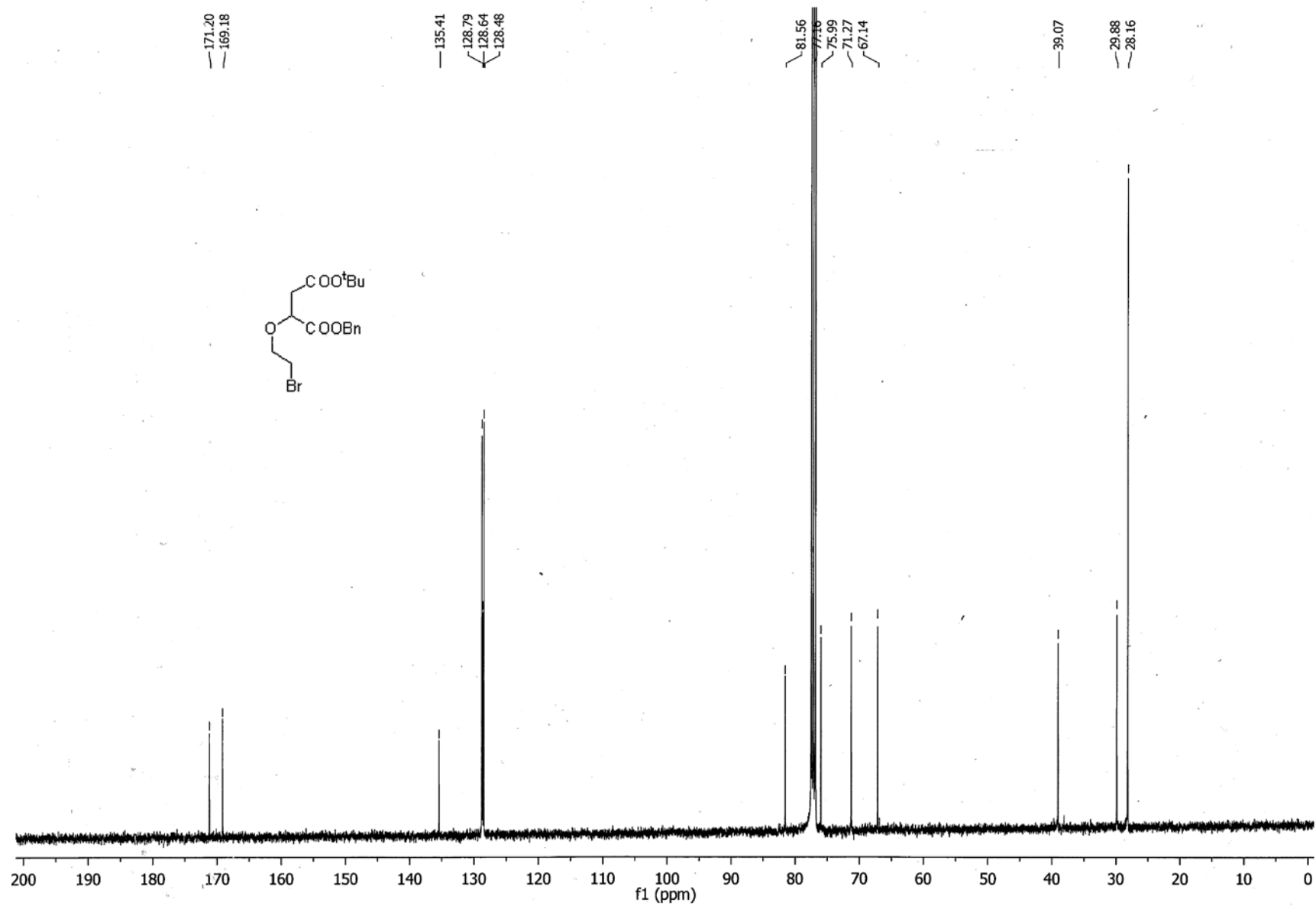
MS Spectrum Peak List

m/z	Calc m/z	Diff(ppm)	z	Abund	Formula	Ion
325.1634	325.1646	3.69	1	6535.92	C17H24O6	(M+H)+
347.1463	347.1465	0.49	1	1415467.21	C17H24O6	(M+Na)+
363.1195	363.1204	2.57	1	17415.74	C17H24O6	(M+K)+

--- End Of Report ---



¹H NMR spectrum of 1-benzyl 4-(*tert*-butyl) 2-(2-bromoethoxy)succinate **21**



¹³C NMR spectrum of 1-benzyl 4-(*tert*-butyl) 2-(2-bromoethoxy)succinate **21**

Qualitative Compound Report

Data File	JRH-314-188-01.d	Sample Name	JRH-314-188-01
Sample Type	Sample	Position	P1-B1
Instrument Name	Instrument 1	User Name	Dr. Jason Dang
Acq Method	Monash_Direct_Low_Frag_No_Formic.m	Acquired Time	11/4/2014 11:54:47 AM
IRM Calibration Status		DA Method	Monash_Accuracy.m
Comment			

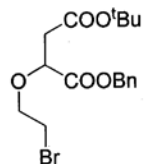
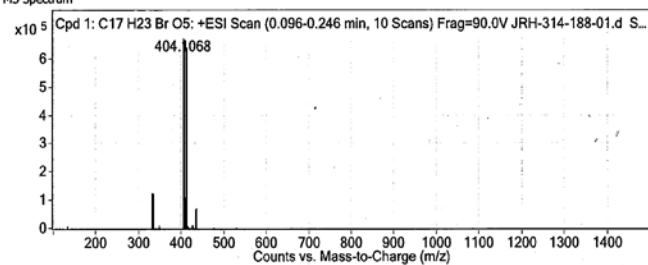
Sample Group		Info.	
Formula	C17H23BrO5	Acquisition SW	6200 series TOF/6500 series
		Version	Q-TOF B.05.01 (B5125.1)

Compound Table

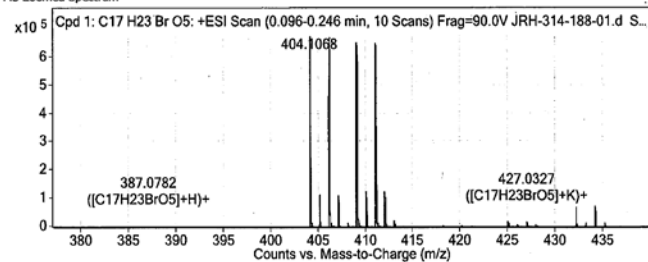
Compound Label	RT	Mass	Abund	Formula	Tgt Mass	Diff (ppm)	MFG Formula	DB Formula
Cpd 1: C17H23BrO5	0.129	386.0729	648366	C17H23BrO5	386.0729	-0.09	C17H23BrO5	C17H23BrO5

Compound Label	m/z	RT	Algorithm	Mass
Cpd 1: C17H23BrO5	411.0604	0.129	Find By Formula	386.0729

MS Spectrum



MS Zoomed Spectrum

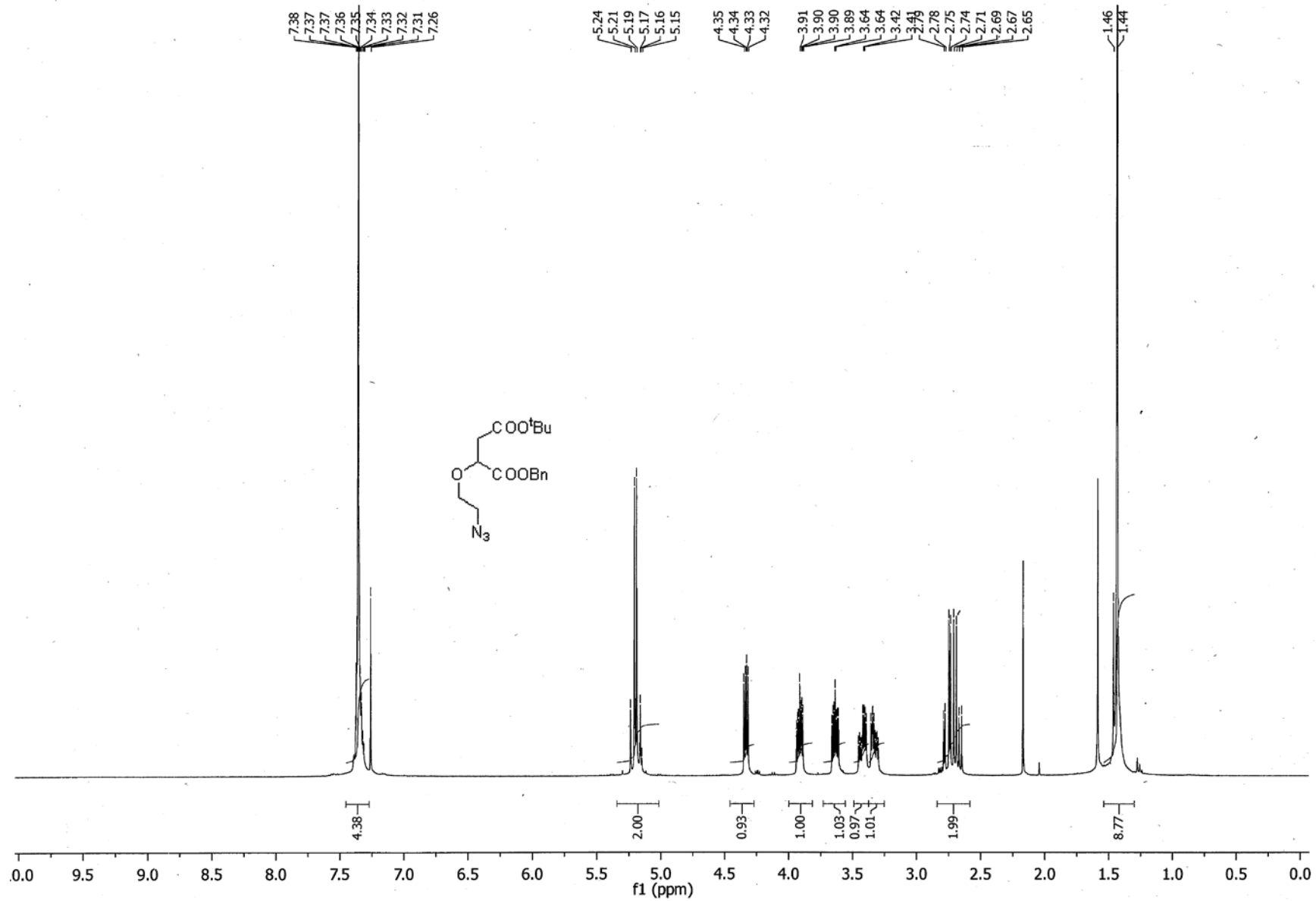


MS Spectrum Peak List

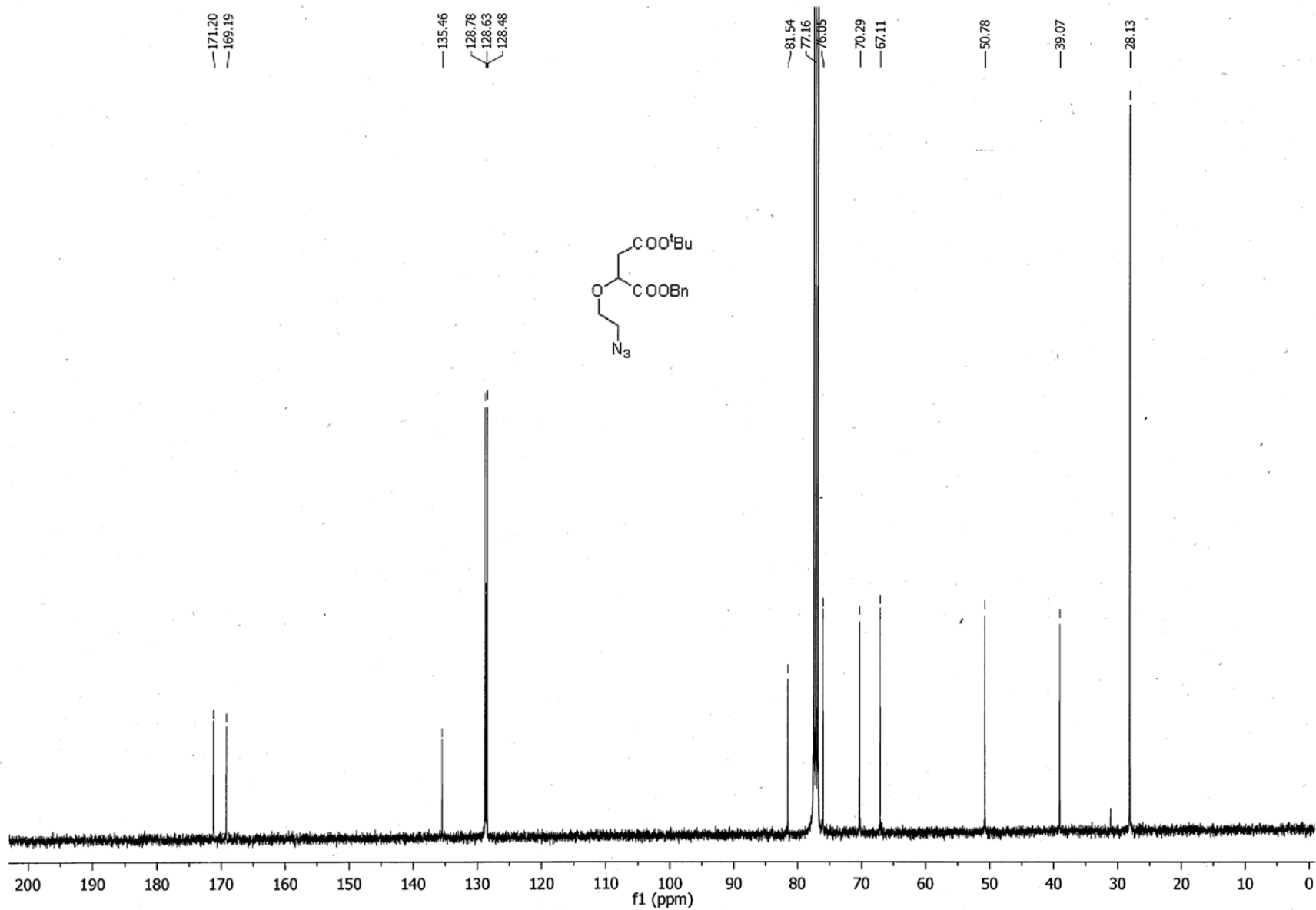
m/z	Calc m/z	Diff(ppm)	z	Abund	Formula	Ion
387.0782	387.0802	5.12	1	1704.81	C17H23BrO5	(M+H)+
409.0622	409.0621	-0.3	1	648342.63	C17H23BrO5	(M+Na)+
425.0346	425.036	3.49	1	13513.38	C17H23BrO5	(M+K)+

--- End Of Report ---

HRMS report of 1-benzyl 4-(*tert*-butyl) 2-(2-bromoethoxy)succinate **21**



¹H NMR spectrum of 1-benzyl 4-(*tert*-butyl) 2-(2-azidoethoxy)succinate **22**



¹³C NMR spectrum of 1-benzyl 4-(*tert*-butyl) 2-(2-azidoethoxy)succinate **22**

Qualitative Compound Report

Data File	JRH-314-192-01.d	Sample Name	JRH-314-192-01
Sample Type	Sample	Position	P1-B2
Instrument Name	Instrument 1	User Name	Dr Jason Dang
Acq Method	Monash_Direct_Low_Frag_No_Formic.m	Acquired Time	11/9/2014 11:58:04 AM
IRM Calibration Status	XXXXXXXXXX	DA Method	Monash_Accuracy.m
Comment			

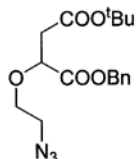
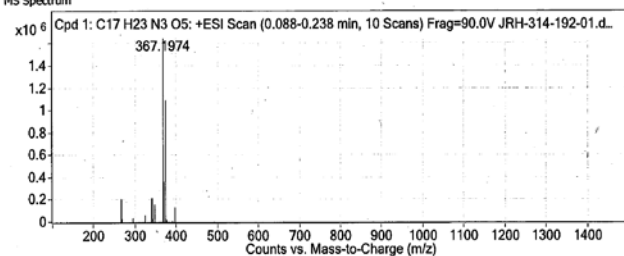
Sample Group		Info.	
Formula	C17H23N3O5	Acquisition SW Version	6200 series TOF/6500 series Q-TOF B.05.01 (B5125.1)

Compound Table

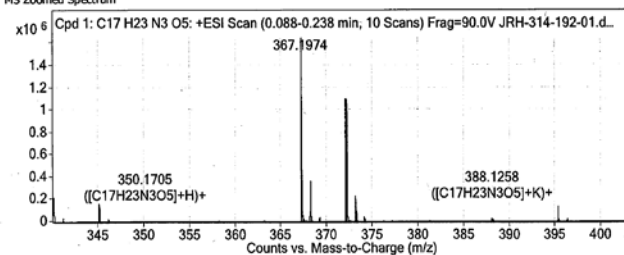
Compound Label	RT	Mass	Abund	Formula	Tgt Mass	Diff (ppm)	MFG Formula	DB Formula
Cpd 1: C17 H23 N3 O5	0.121	349.1637	1091639	C17 H23 N3 O5	349.1638	-0.12	C17 H23 N3 O5	C17 H23 N3 O5

Compound Label	m/z	RT	Algorithm	Mass
Cpd 1: C17 H23 N3 O5	372.153	0.121	Find By Formula	349.1637

MS Spectrum



MS Zoomed Spectrum

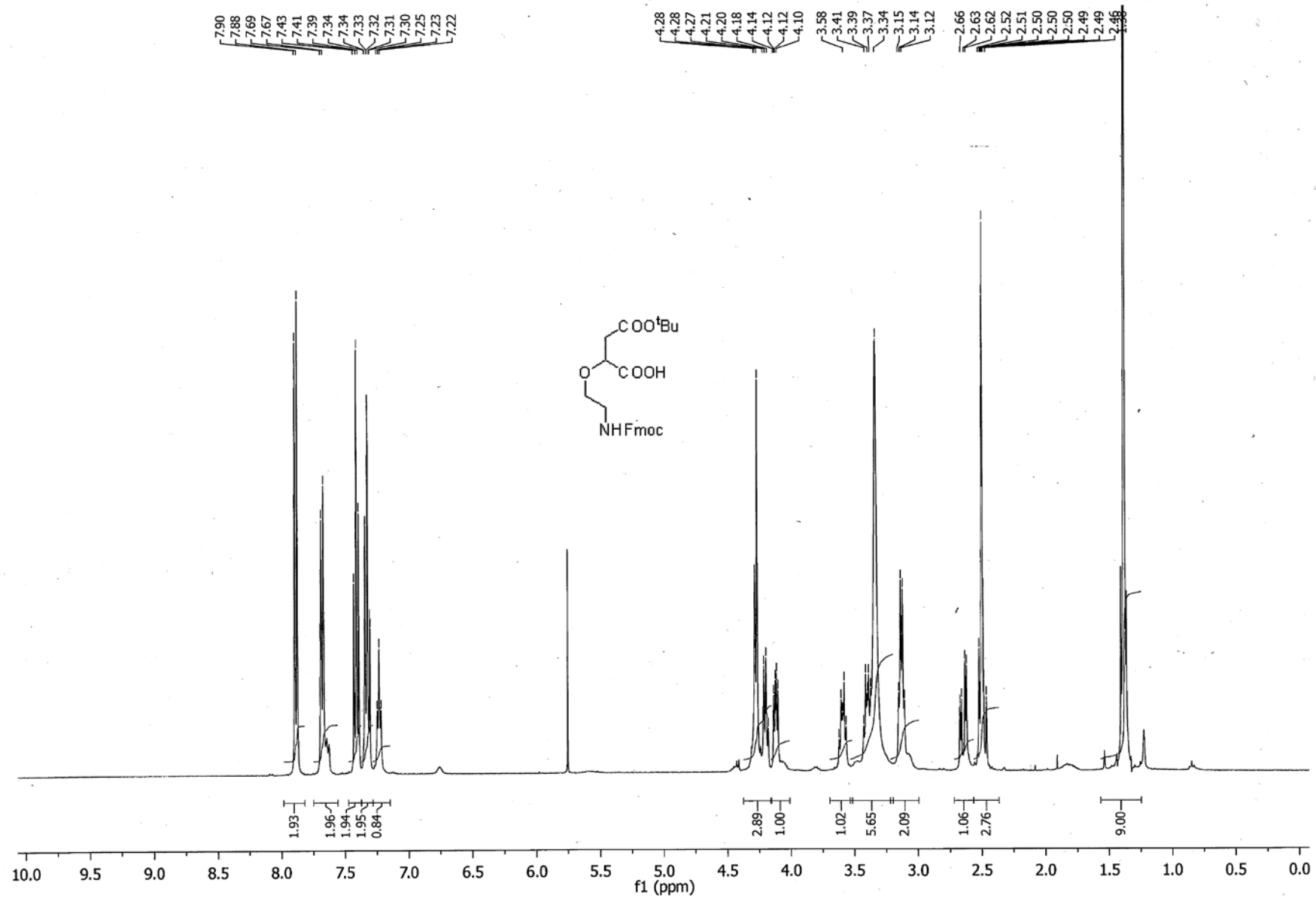


MS Spectrum Peak List

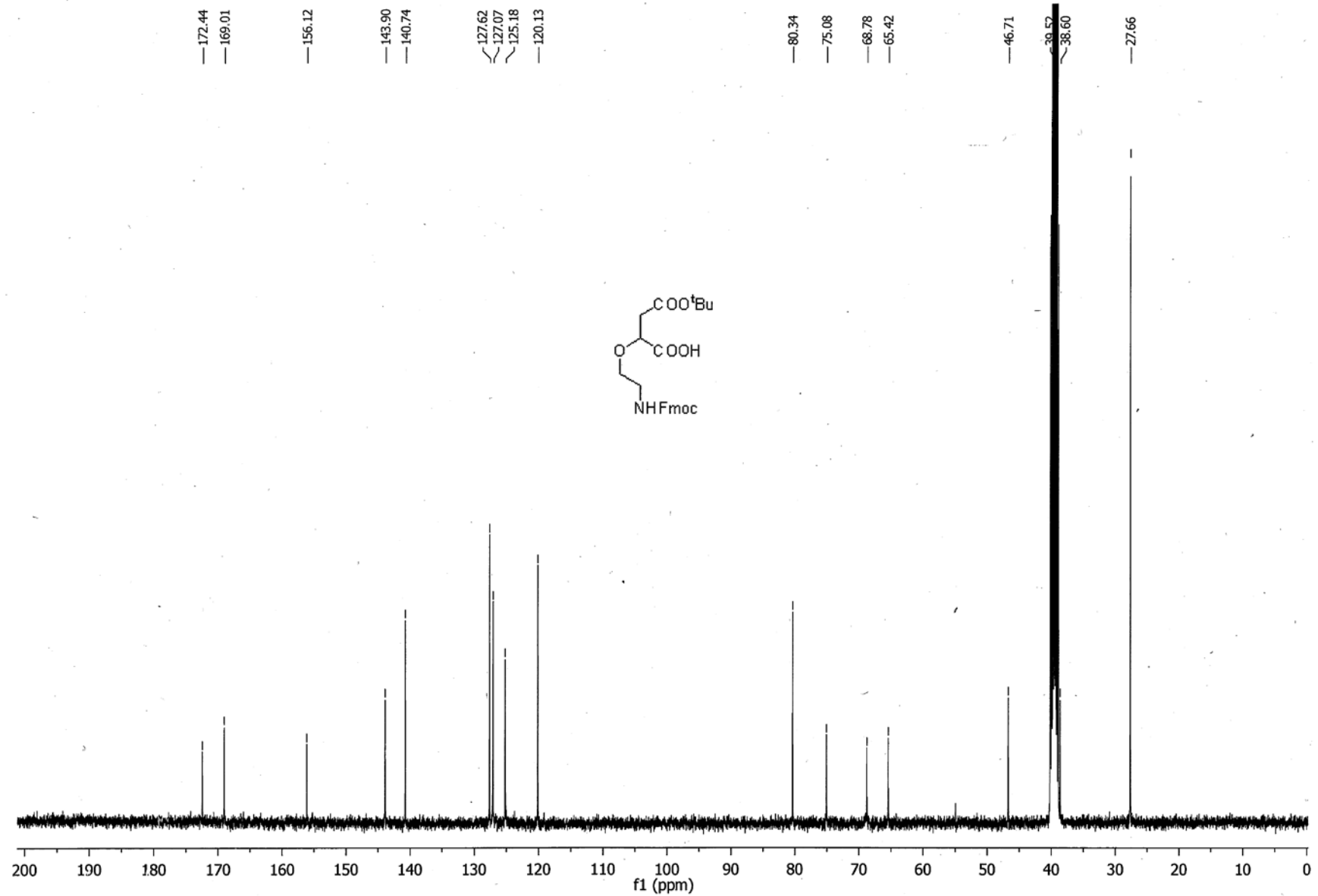
m/z	Calc m/z	Diff(ppm)	z	Abund	Formula	Ion
350.1705	350.171	1.43	1	2142.25	C17H23N3O5	(M+H)+
372.153	372.153	0.05	1	1091638.63	C17H23N3O5	(M+Na)+
388.1258	388.1269	2.91	1	19509.73	C17H23N3O5	(M+K)+

--- End Of Report ---

HRMS report of 1-benzyl 4-(*tert*-butyl) 2-(2-azidoethoxy)succinate **22**



¹H NMR spectrum of 2-(2-(((9H-fluoren-9-yl)methoxy)carbonyl)amino)ethoxy)-4-(tert-butoxy)-4-oxobutanoic acid **3**



¹³C NMR spectrum of 2-(2-(((9H-fluoren-9-yl)methoxy)carbonyl)amino)ethoxy)-4-(tert-butoxy)-4-oxobutanoic acid **3**

Qualitative Compound Report

Data File	JRH-314-196-01.d	Sample Name	JRH-314-196-01
Sample Type	Sample	Position	P1-B3
Instrument Name	Instrument 1	User Name	Dr Jason Dang
Acq Method	Monash_Direct_Low_Frag_No_Formic.m	Acquired Time	11/4/2014 12:01:21 PM
IRM Calibration Status	XXXXXXXXXX	DA Method	Monash_Accuracy.m
Comment			

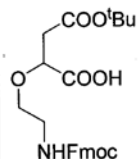
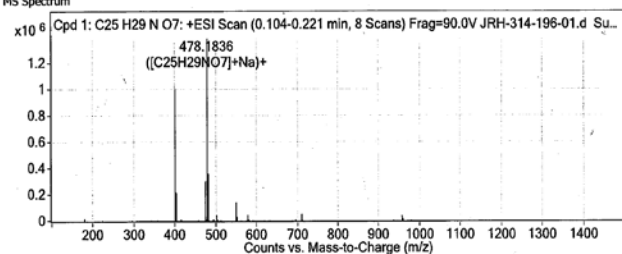
Sample Group	Info.	6200 series TOF/6500 series	
Formula	C25H29NO7	Acquisition SW Version	Q-TOF B.05.01 (B5125.1)

Compound Table

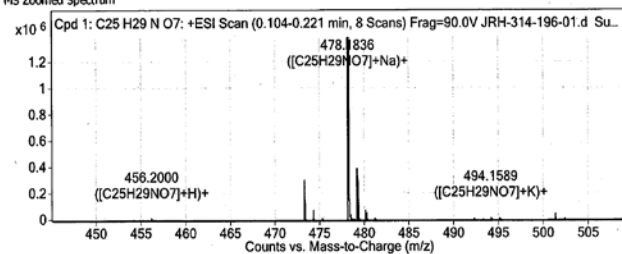
Compound Label	RT	Mass	Abund	Formula	Tgt Mass	Diff (ppm)	MFG Formula	DB Formula
Cpd 1: C25 H29 N O7	0.121	455.1944	1386720	C25 H29 N O7	455.1944	-0.03	C25 H29 N O7	C25 H29 N O7

Compound Label	m/z	RT	Algorithm	Mass
Cpd 1: C25 H29 N O7	478.1836	0.121	Find By Formula	455.1944

MS Spectrum



MS Zoomed Spectrum

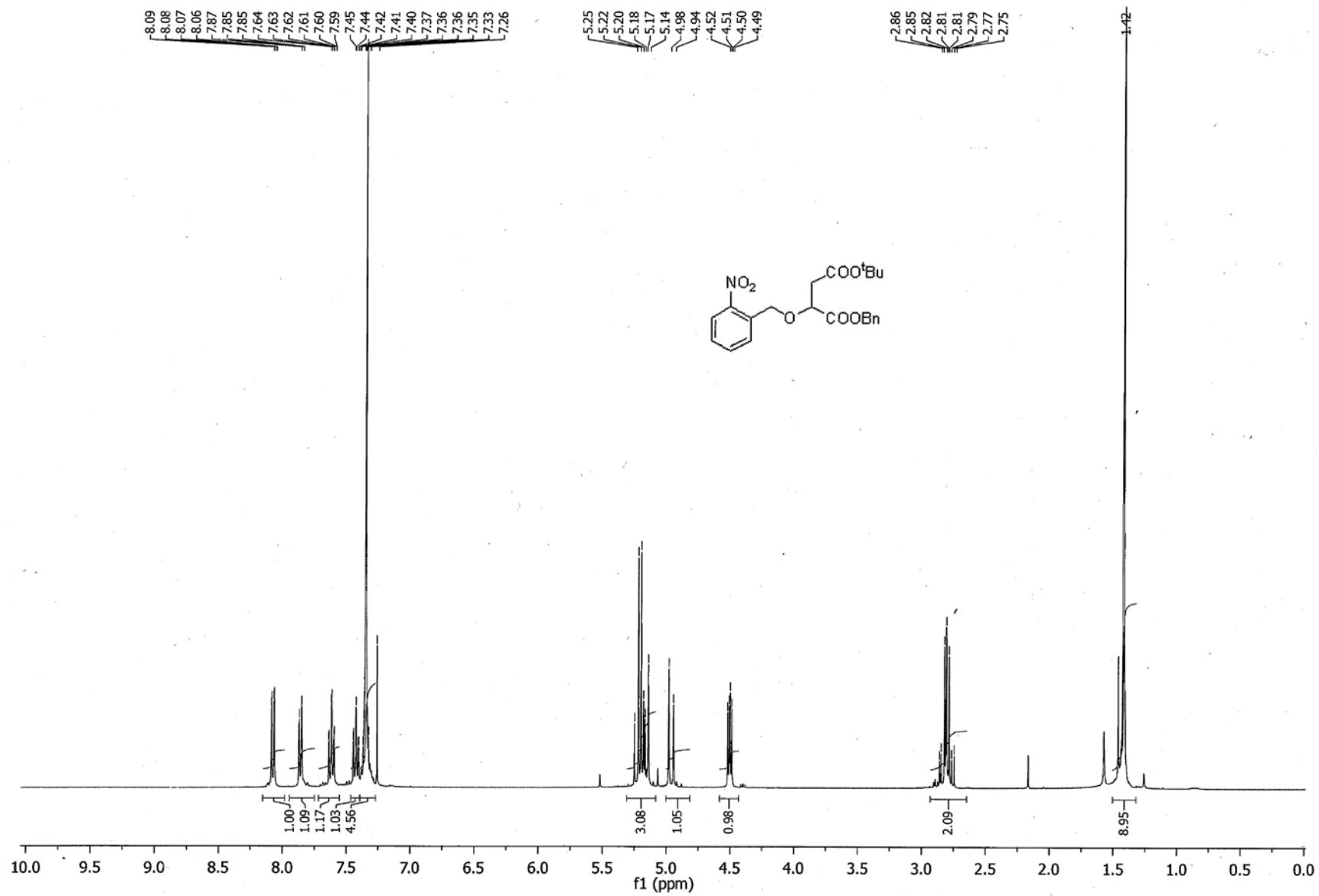


MS Spectrum Peak List

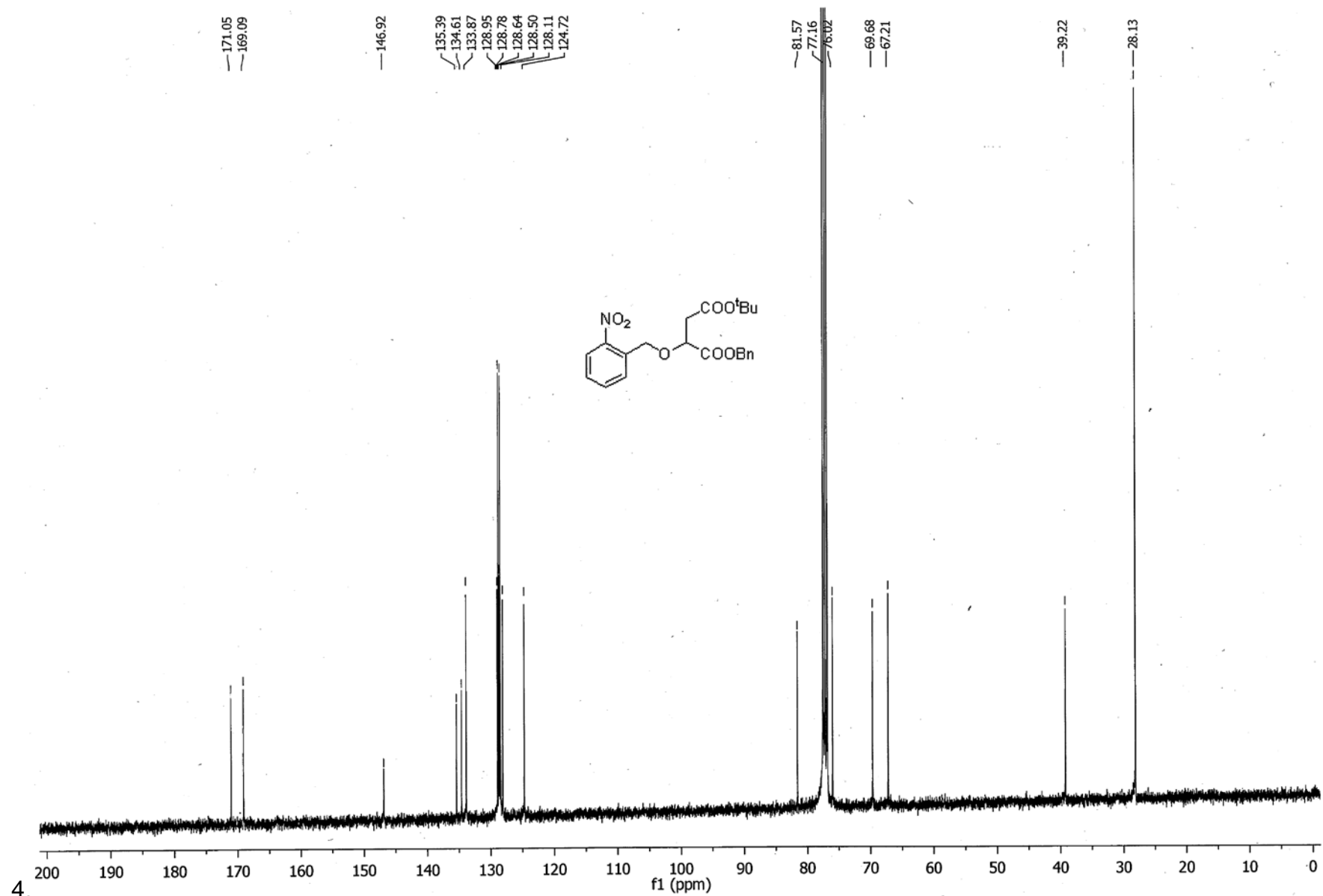
m/z	Calc m/z	Diff(ppm)	z	Abund	Formula	Ion
456.2	456.2017	3.67	1	10622.52	C25H29NO7	(M+H)+
478.1836	478.1836	0.07	1	1386720.13	C25H29NO7	(M+Na)+
494.1589	494.1576	-2.65	1	15603.68	C25H29NO7	(M+K)+

--- End Of Report ---

HRMS report of 2-(2-(((9H-fluoren-9-yl)methoxy)carbonyl)amino)ethoxy)-4-(*tert*-butoxy)-4-oxobutanoic acid **3**



¹H NMR spectrum of ¹H NMR spectrum of 1-benzyl 4-(*tert*-butyl) 2-((2-nitrobenzyl)oxy)succinate **24**



4 ¹³C NMR spectrum of 1-benzyl 4-(*tert*-butyl) 2-((2-nitrobenzyl)oxy)succinate **24**

Qualitative Compound Report

Data File	JRH-314-086-01.d	Sample Name	JRH-314-086-01
Sample Type	Sample	Position	P1-B4
Instrument Name	Instrument 1	User Name	Dr Jason Dang
Acq Method	Monash_Direct_Low_Frag_No_Formic.m	Acquired Time	11/4/2014 12:04:36 PM
IRM Calibration Status	XXXXXXXXXX	DA Method	Monash_Accuracy.m
Comment			

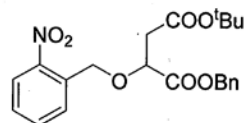
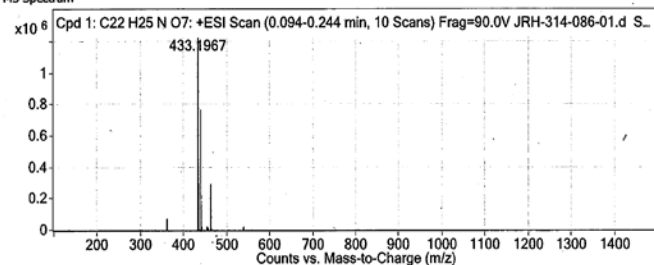
Sample Group		Info.	
Formula	C22H25NO7	Acquisition SW	6200 series TOF/6500 series
		Version	Q-TOF B.05.01 (B5125.1)

Compound Table

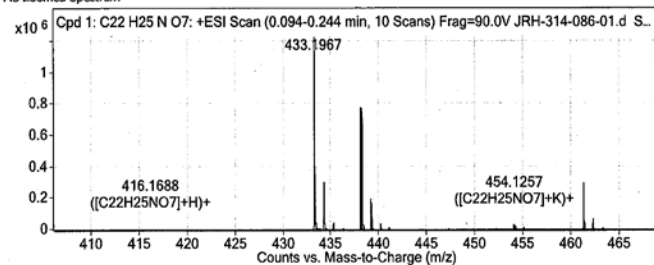
Compound Label	RT	Mass	Abund	Formula	Tgt Mass	Diff (ppm)	MFG Formula	DB Formula
Cpd 1: C22 H25 N O7	0.128	415.1629	772040	C22 H25 N O7	415.1631	-0.55	C22 H25 N O7	C22 H25 N O7

Compound Label	m/z	RT	Algorithm	Mass
Cpd 1: C22 H25 N O7	438.1522	0.128	Find By Formula	415.1629

MS Spectrum



MS Zoomed Spectrum

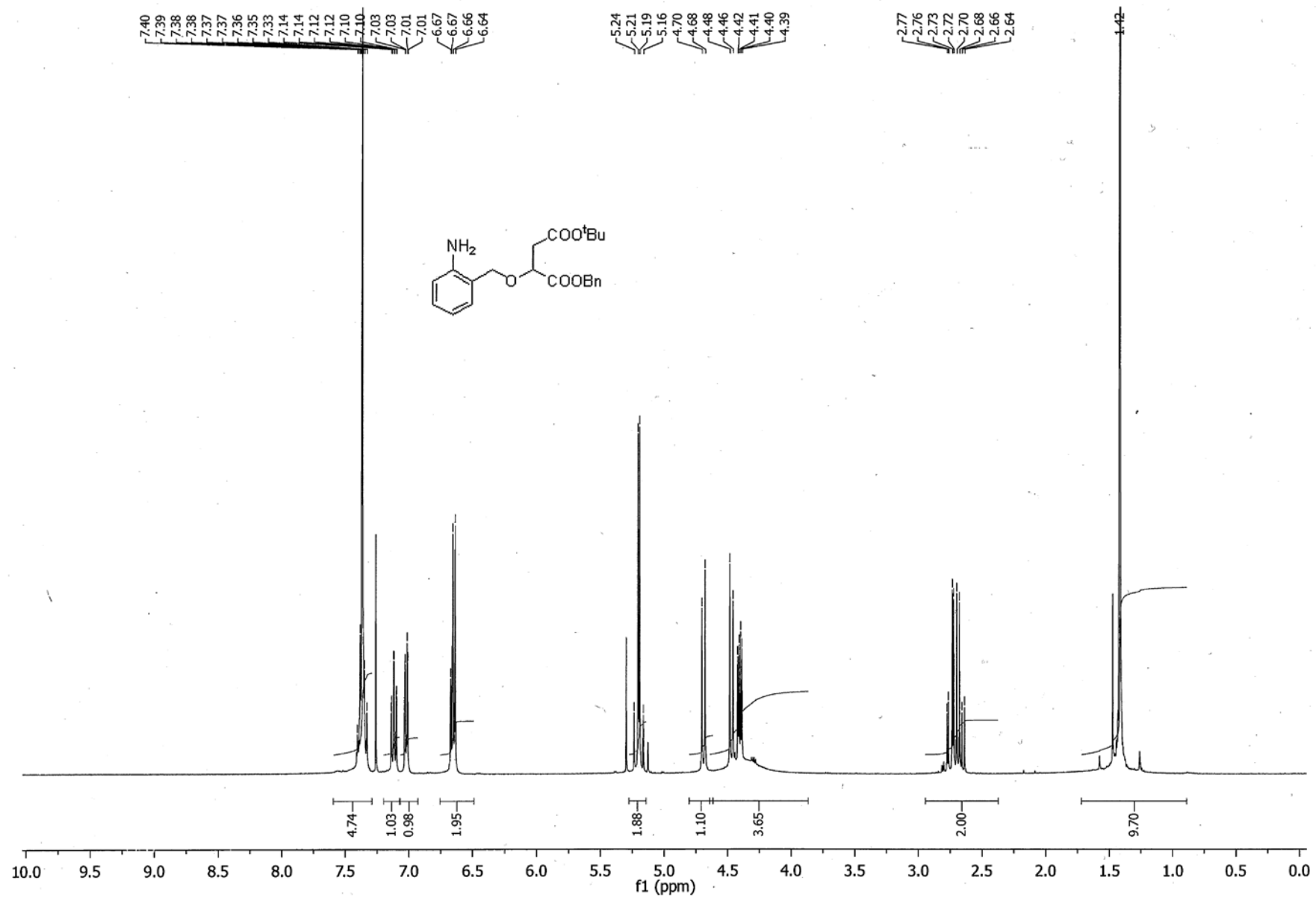


MS Spectrum Peak List

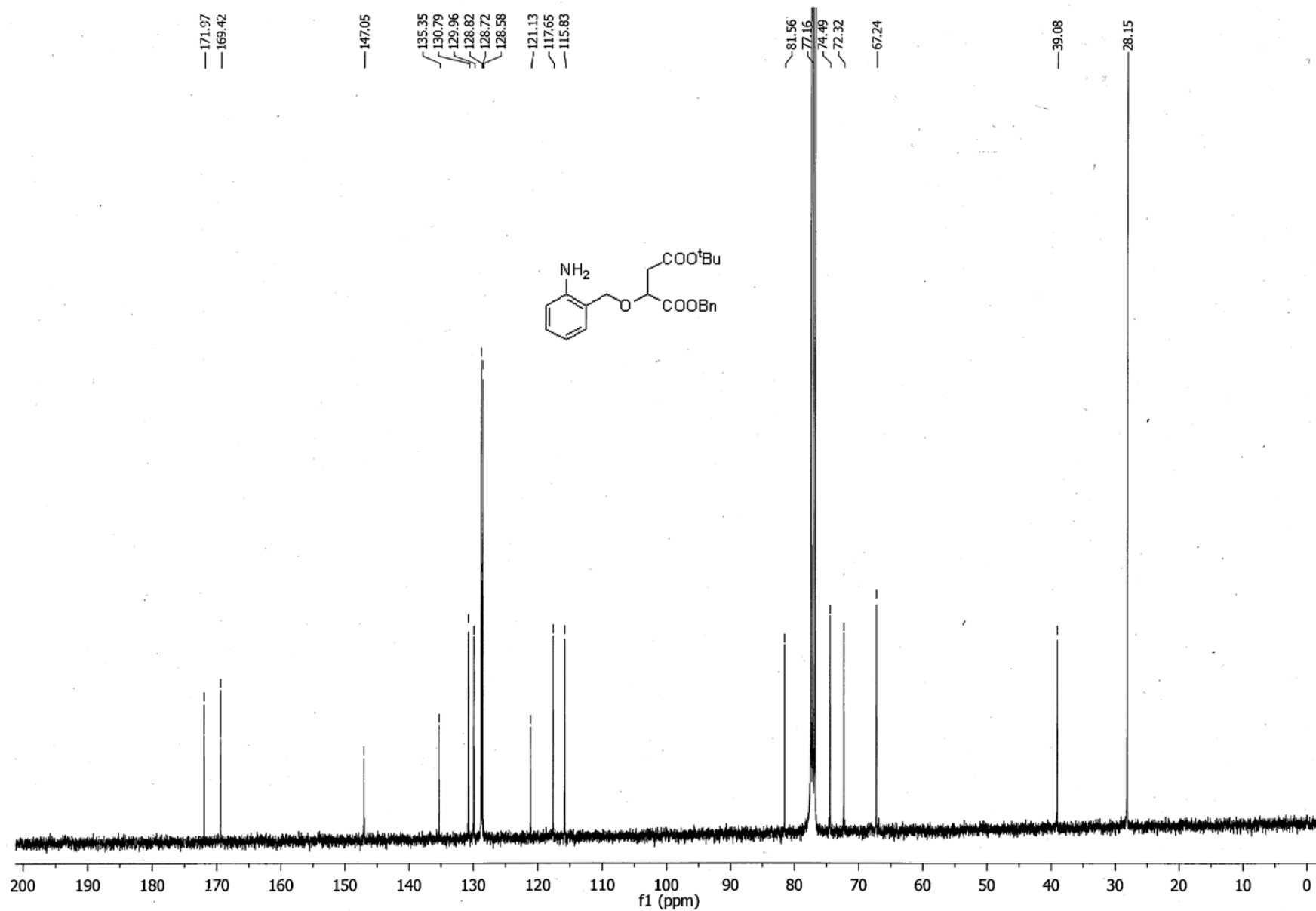
m/z	Calc m/z	Diff(ppm)	z	Abund	Formula	Ion
416.1688	416.1704	3.83	1	1623.26	C22H25NO7	(M+H)+
438.1522	438.1523	0.37	1	772040.15	C22H25NO7	(M+Na)+
454.1257	454.1263	1.22	1	23200.07	C22H25NO7	(M+K)+

--- End Of Report ---

HRMS report of 1-benzyl 4-(tert-butyl) 2-((2-nitrobenzyl)oxy)succinate **24**



¹H NMR spectrum of 1-benzyl 4-(*tert*-butyl) 2-((2-aminobenzyl)oxy)succinate **25**



¹³C NMR spectrum of 1-benzyl 4-(tert-butyl) 2-((2-aminobenzyl)oxy)succinate **25**

Qualitative Compound Report

Data File	JRH-314-090-01.d	Sample Name	JRH-314-090-01
Sample Type	Sample	Position	P1-B5
Instrument Name	Instrument 1	User Name	Dr Jason Dang
Acq Method	Monash_Direct_Low_Frag_No_Formic.m	Acquired Time	11/4/2014 12:07:55 PM
IRM Calibration Status	XXXXXXXXXX	DA Method	Monash_Accuracy.m
Comment			

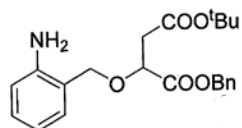
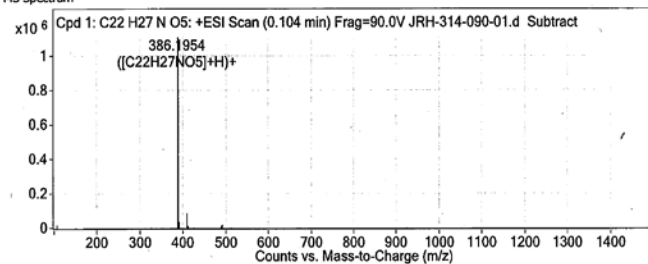
Sample Group	C22H27NO5	Info.	6200 series TOF/6500 series
Formula		Acquisition SW Version	Q-TOF B.05.01 (B5125.1)

Compound Table

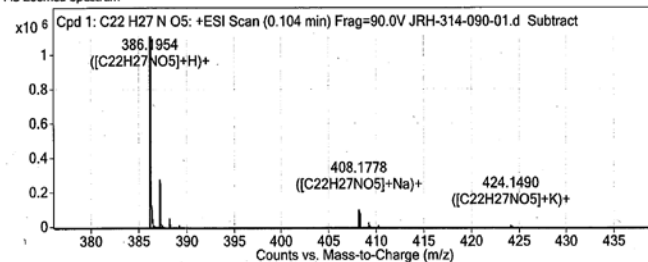
Compound Label	RT	Mass	Abund	Formula	Tgt Mass	Diff (ppm)	MFG Formula	DB Formula
Cpd 1: C22 H27 N O5	0.104	385.1883	1122617	C22 H27 N O5	385.1889	-1.59	C22 H27 N O5	C22 H27 N O5

Compound Label	m/z	RT	Algorithm	Mass
Cpd 1: C22 H27 N O5	386.1954	0.104	Find By Formula	385.1883

MS Spectrum



MS Zoomed Spectrum



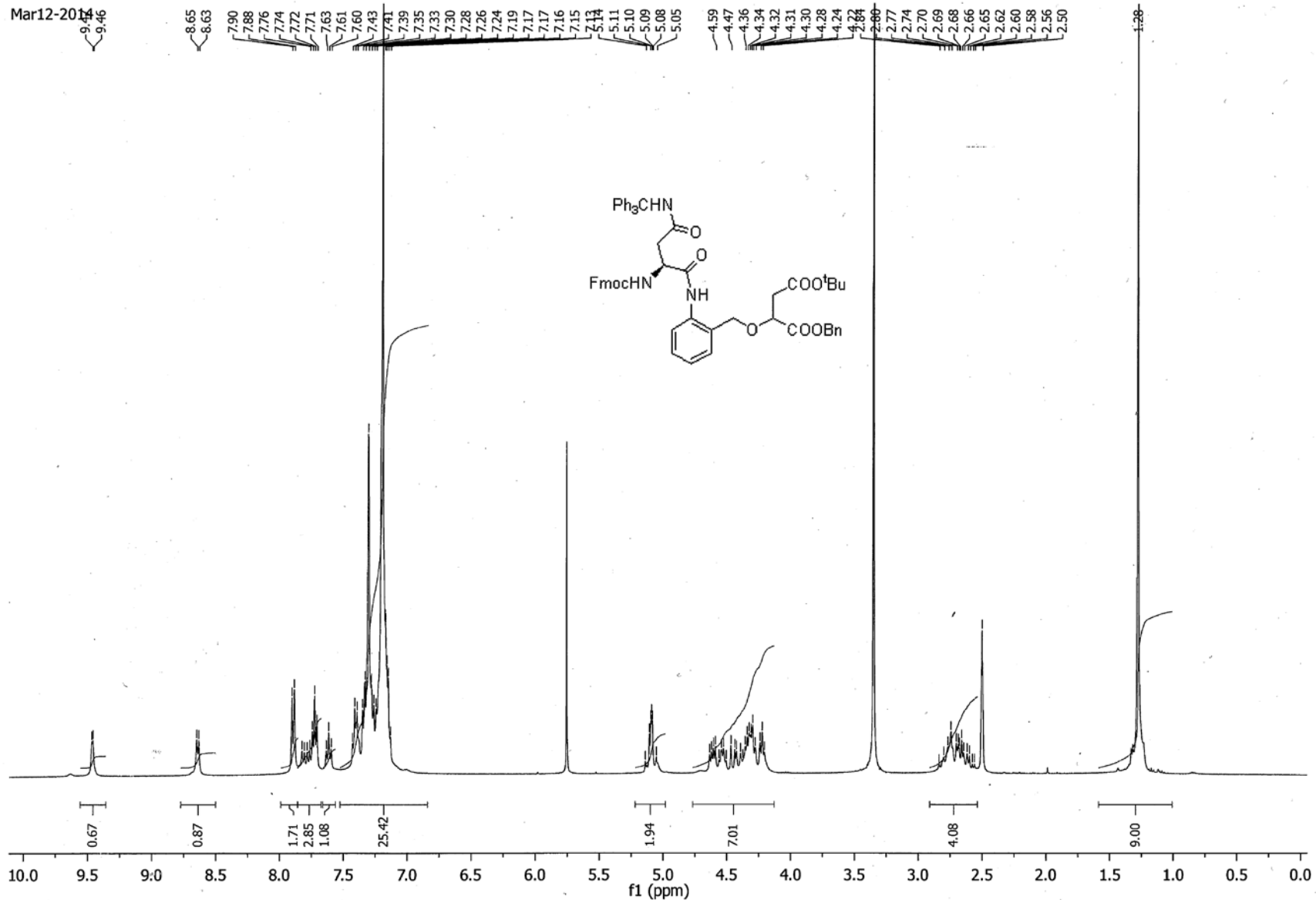
MS Spectrum Peak List

m/z	Calc m/z	Diff(ppm)	z	Abund	Formula	Ion
386.1954	386.1962	1.97	1	1122617.07	C22H27NO5	(M+H)+
408.1778	408.1781	0.9	1	95323.28	C22H27NO5	(M+Na)+
424.149	424.1521	7.31	1	5944.52	C22H27NO5	(M+K)+

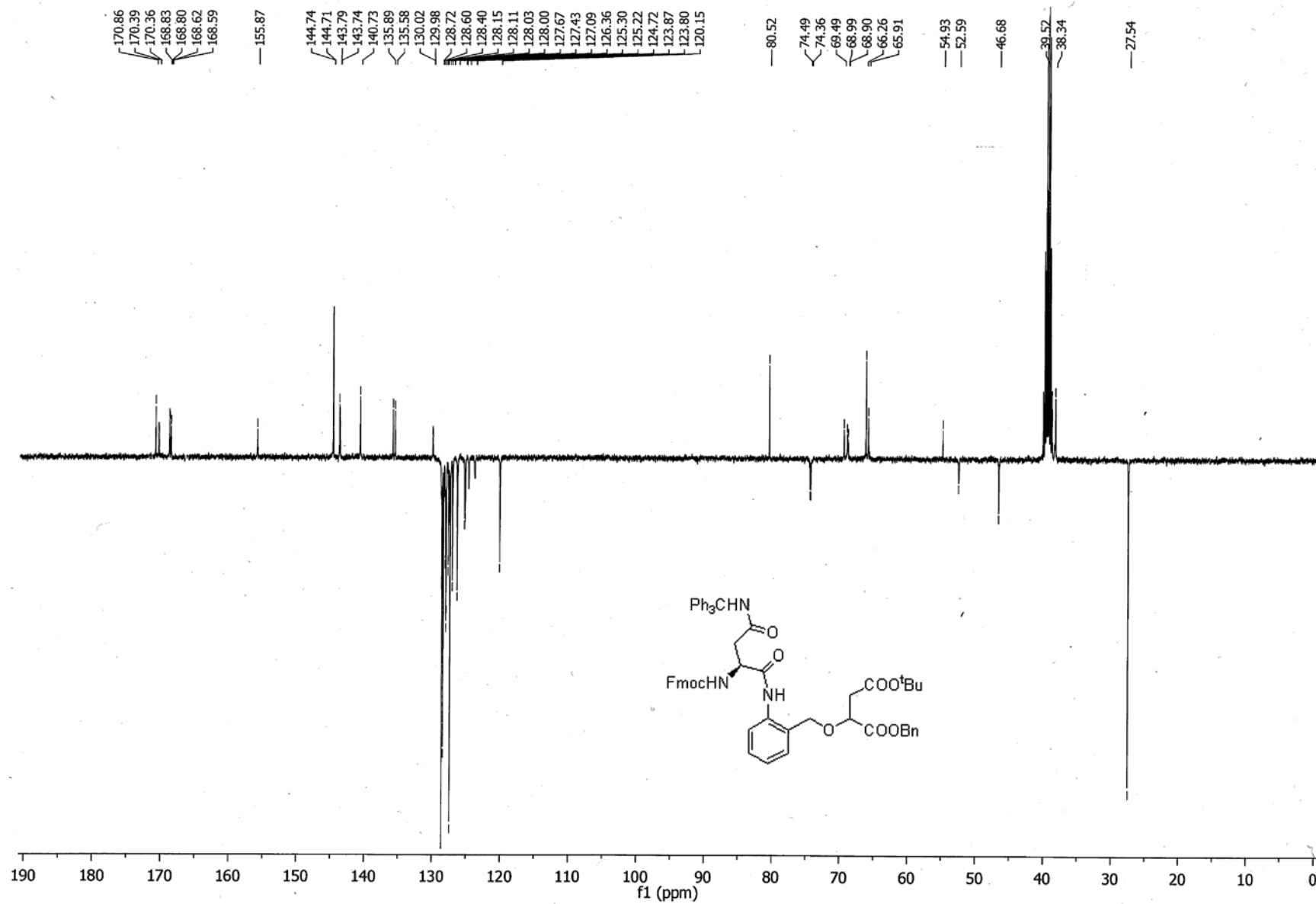
--- End Of Report ---

HRMS report of 1-benzyl 4-(*tert*-butyl) 2-((2-aminobenzyl)oxy)succinate **25**

Mar12-2014



^1H NMR spectrum of 1-benzyl 4-(*tert*-butyl) 2-((2-(((*S*)-2-(((9*H*-fluoren-9-yl)methoxy)carbonyl)amino)-4-oxo-4-(tritylamino)butanamido)benzyl)oxy)succinate **26**



^{13}C NMR spectrum of 1-benzyl 4-(*tert*-butyl) 2-((2-((*S*)-2-(((9*H*-fluoren-9-yl)methoxy)carbonyl)amino)-4-oxo-4-(tritylamino)butanamido)benzyl)oxy)succinate **26**

Qualitative Compound Report

Data File	JRH-314-094-01.d	Sample Name	JRH-314-094-01
Sample Type	Sample	Position	P1-B6
Instrument Name	Instrument 1	User Name	Dr Jason Dang
Acq Method	Monash_Direct_Low_Frag_No_Formic.m	Acquired Time	11/4/2014 12:11:13 PM
IRM Calibration Status	XXXXXXXXXX	DA Method	Monash_Accuracy.m
Comment			

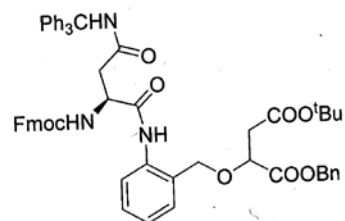
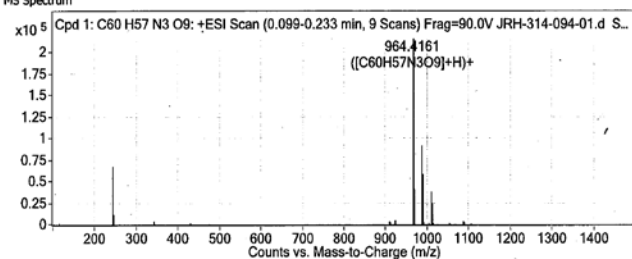
Sample Group	Info.	
Formula	C60H57N3O9	6200 series TOF/6500 series
	Acquisition SW Version	Q-TOF B.05.01 (B5125.1)

Compound Table

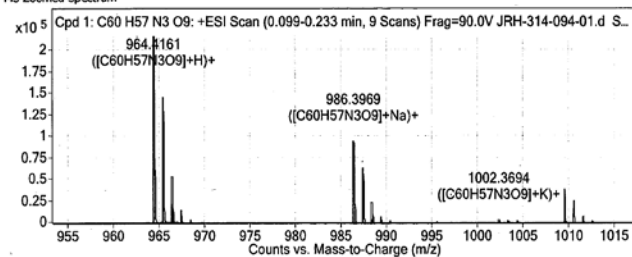
Compound Label	RT	Mass	Abund	Formula	Tgt Mass	Diff (ppm)	MFG Formula	DB Formula
Cpd 1: C60 H57 N3 O9	0.116	963.4081	216341	C60 H57 N3 O9	963.4095	-1.39	C60 H57 N3 O9	C60 H57 N3 O9

Compound Label	m/z	RT	Algorithm	Mass
Cpd 1: C60 H57 N3 O9	964.4161	0.116	Find By Formula	963.4081

MS Spectrum



MS Zoomed Spectrum



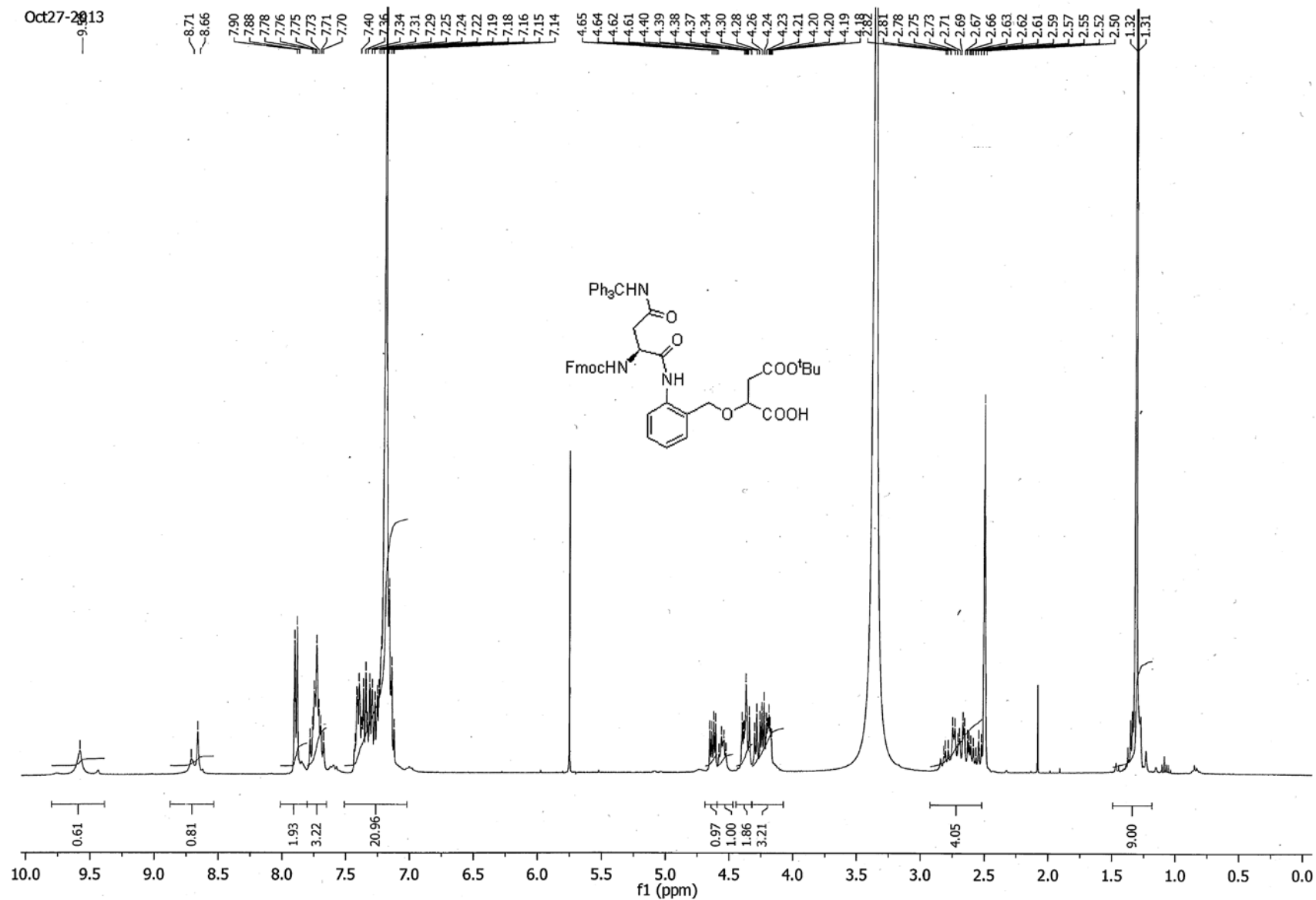
MS Spectrum Peak List

m/z	Calc m/z	Diff (ppm)	z	Abund	Formula	Ion
964.4161	964.4168	0.7	1	216340.87	C60H57N3O9	(M+H)+
986.3969	986.3987	1.78	1	93701.51	C60H57N3O9	(M+Na)+
1002.3694	1002.3726	3.27	1	2215.41	C60H57N3O9	(M+K)+

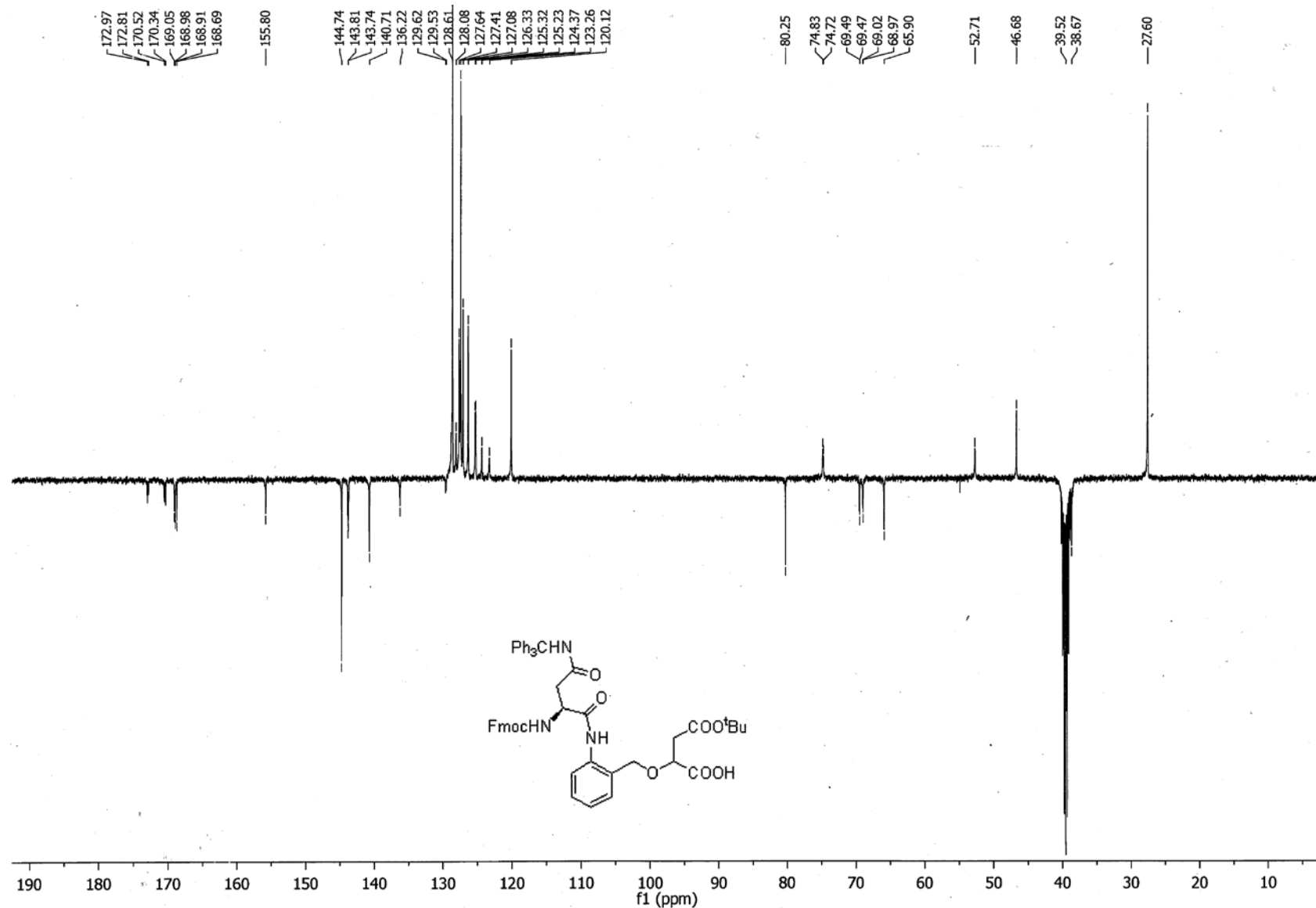
--- End Of Report ---

HRMS report of 1-benzyl 4-(*tert*-butyl) 2-((2-((*S*)-2-(((9*H*-fluoren-9-yl)methoxy)carbonyl)amino)-4-oxo-4-(tritylamino)butanamido)benzyl)oxy)succinate **26**

Oct27-2013



^1H NMR spectrum of 2-((2-((S)-2-(((9H-fluoren-9-yl)methoxy)carbonyl)amino)-4-oxo-4-(tritylamino)butanamido)benzyl)oxy)-4-(tert-butoxy)-4-oxobutanoic acid **4**



^{13}C NMR spectrum of 2-((2-((S)-2-(((9H-fluoren-9-yl)methoxy)carbonyl)amino)-4-oxo-4-(tritylamino)butanamido)benzyl)oxy)-4-(tert-butoxy)-4-oxobutanoic acid **4**

Qualitative Compound Report

Data File	JRH-314-098.d	Sample Name	JRH-314-098
Sample Type	Sample	Position	P1-B7
Instrument Name	Instrument 1	User Name	Dr Jason Dang
Acq Method	Monash_Direct_Low_Frag_No_Formic.m	Acquired Time	11/4/2014 12:14:28 PM
IRM Calibration Status		DA Method	Monash_Accuracy.m
Comment			

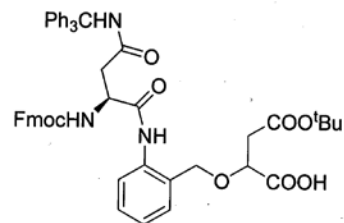
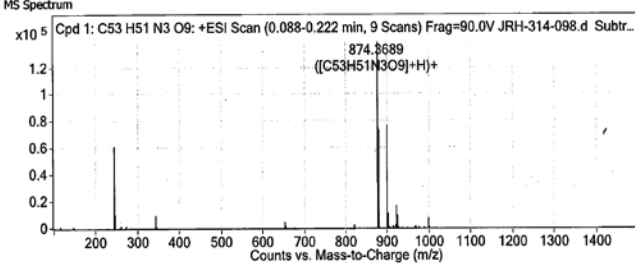
Sample Group	Info.	6200 series TOF/6500 series
Formula	Acquisition SW Version	Q-TOF B.05.01 (85125.1)

Compound Table

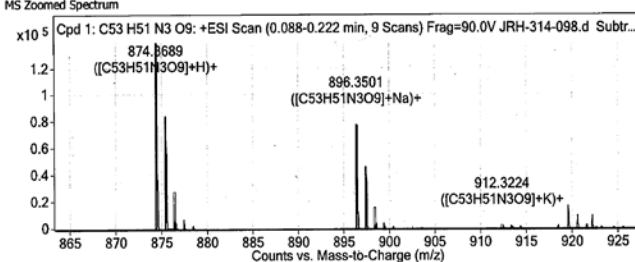
Compound Label	RT	Mass	Abund	Formula	Tgt Mass	Diff (ppm)	MFG Formula	DB Formula
Cpd 1: C53 H51 N3 O9	0.122	873.361	141153	C53 H51 N3 O9	873.3625	-1.79	C53 H51 N3 O9	C53 H51 N3 O9

Compound Label	m/z	RT	Algorithm	Mass
Cpd 1: C53 H51 N3 O9	874.3689	0.122	Find By Formula	873.361

MS Spectrum



MS Zoomed Spectrum

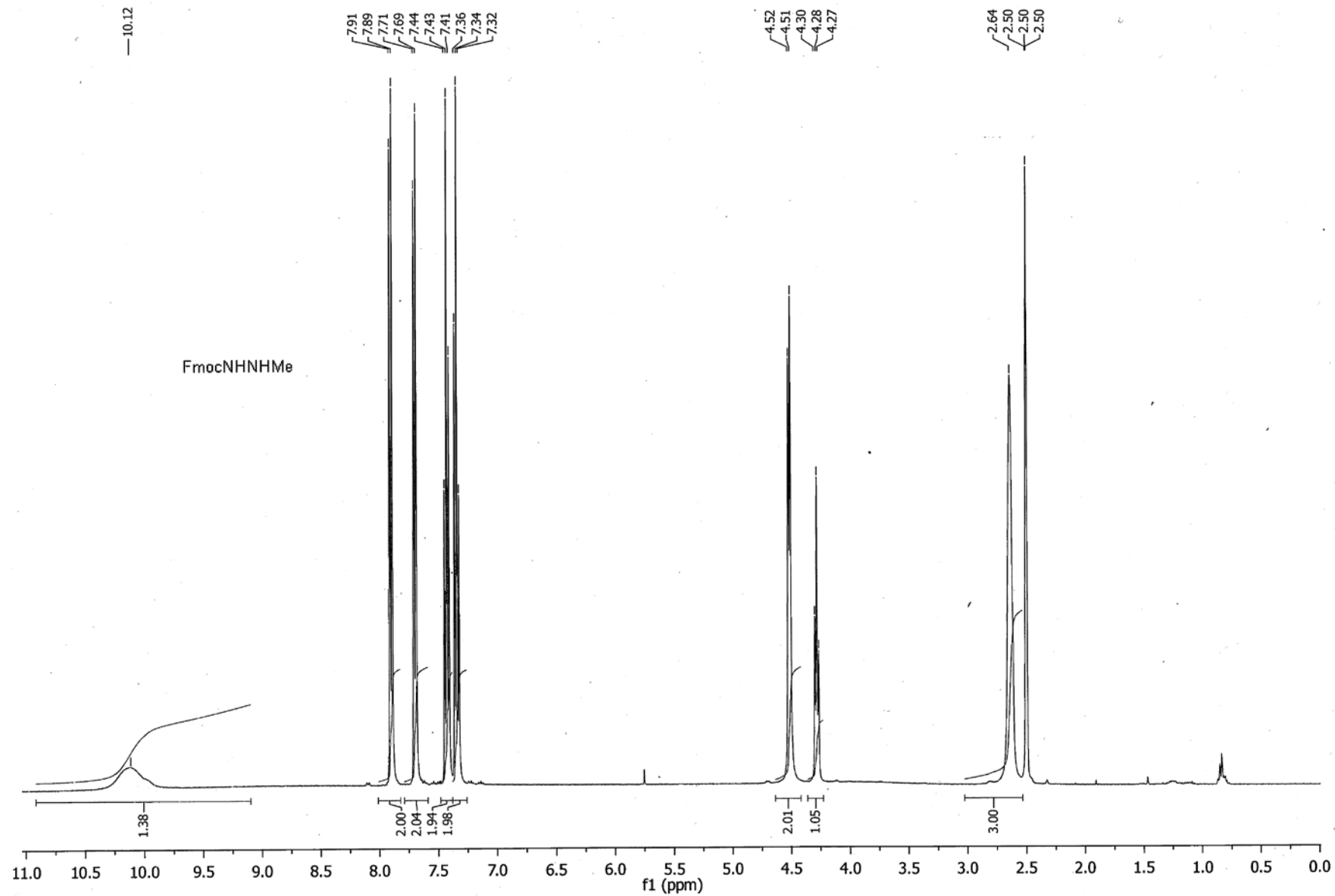


MS Spectrum Peak List

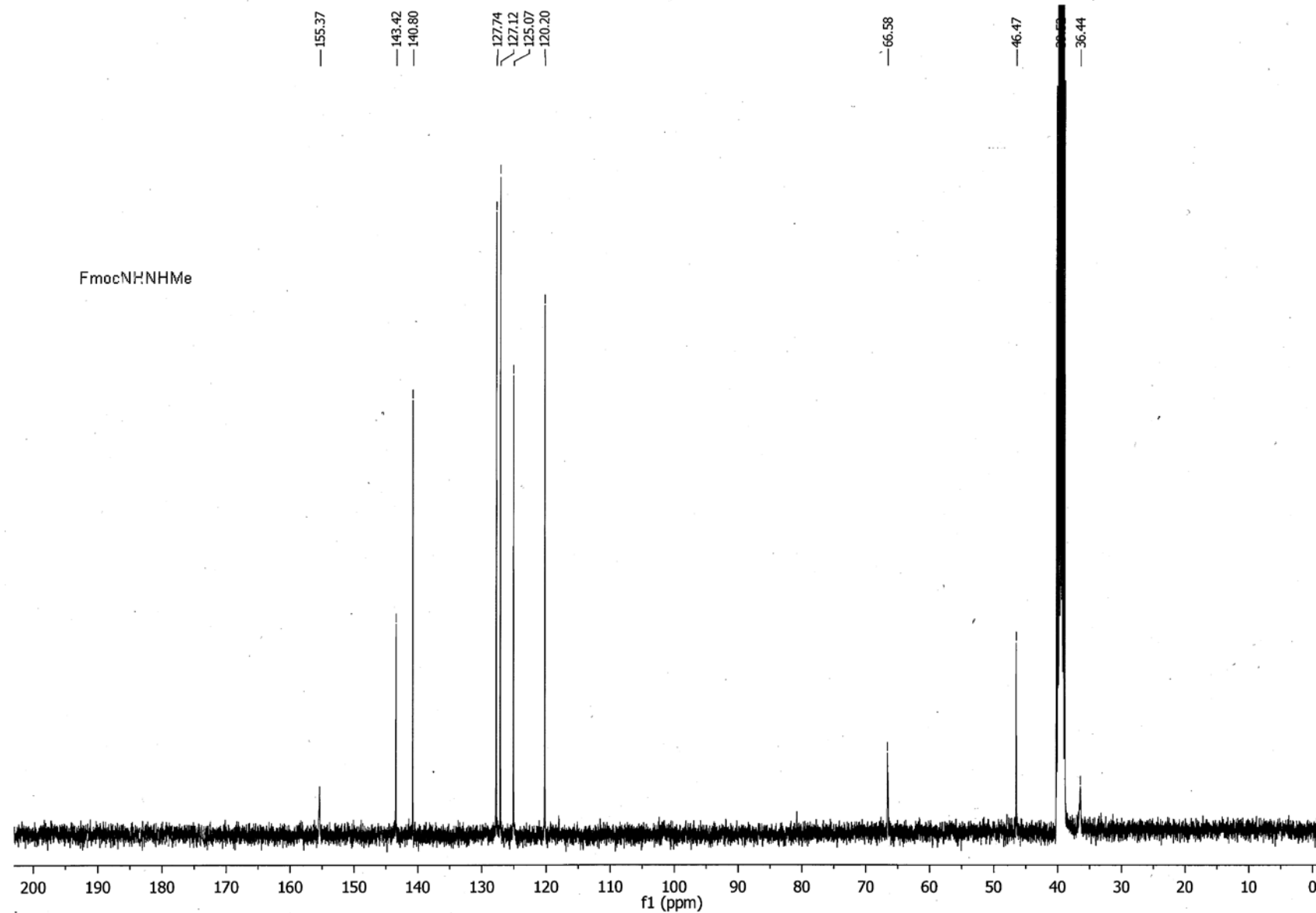
m/z	Calc m/z	Diff(ppm)	z	Abund	Formula	Ion
874.3689	874.3698	1.08	1	141152.74	C53H51N3O9	(M+H)+
896.3501	896.3518	1.81	1	77711.16	C53H51N3O9	(M+Na)+
912.3224	912.3257	3.61	1	1985.47	C53H51N3O9	(M+K)+

--- End Of Report ---

HRMS report of 2-((2-((S)-2-(((9H-fluoren-9-yl)methoxy)carbonyl)amino)-4-oxo-4-(tritylamino)butanamido)benzyl)oxy)-4-(tert-butoxy)-4-oxobutanoic acid **4**



¹H NMR spectrum of (9*H*-fluoren-9-yl)methyl 2-methylhydrazine-1-carboxylate **27**



^{13}C NMR spectrum of (9*H*-fluoren-9-yl)methyl 2-methylhydrazine-1-carboxylate **27**

Qualitative Compound Report

Data File	JRH-255-162-02.d	Sample Name	JRH-255-162-02
Sample Type	Sample	Position	P1-A9
Instrument Name	Instrument 1	User Name	Dr Jason Dang
Acq Method	Monash_Direct.m	Acquired Time	08-Dec-14 1:48:29 PM
IRM Calibration Status		DA Method	Monash_Accuracy.m
Comment			

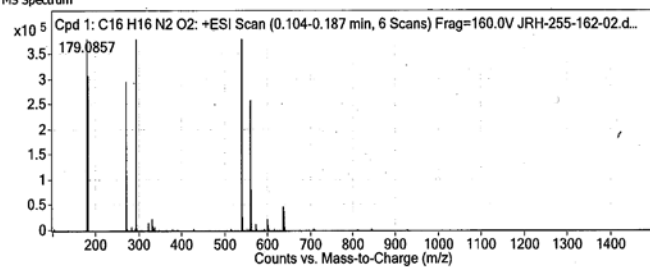
Sample Group		Info.	
Formula	C16H16N2O2	Acquisition SW Version	6200 series TOF/6500 series Q-TOF B.05.01 (B5125.1)

Compound Table

Compound Label	RT	Mass	Abund	Formula	Tgt Mass	Diff (ppm)	MFG Formula	DB Formula
Cpd 1: C16 H16 N2 O2	0.12	268.1214	388014	C16 H16 N2 O2	268.1212	0.65	C16 H16 N2 O2	C16 H16 N2 O2

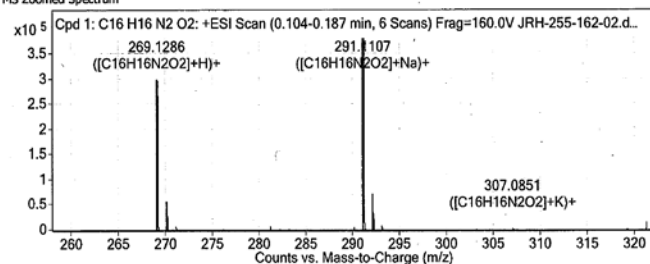
Compound Label	m/z	RT	Algorithm	Mass
Cpd 1: C16 H16 N2 O2	291.1107	0.12	Find By Formula	268.1214

MS Spectrum



Fmoc-NH-NHMe

MS Zoomed Spectrum

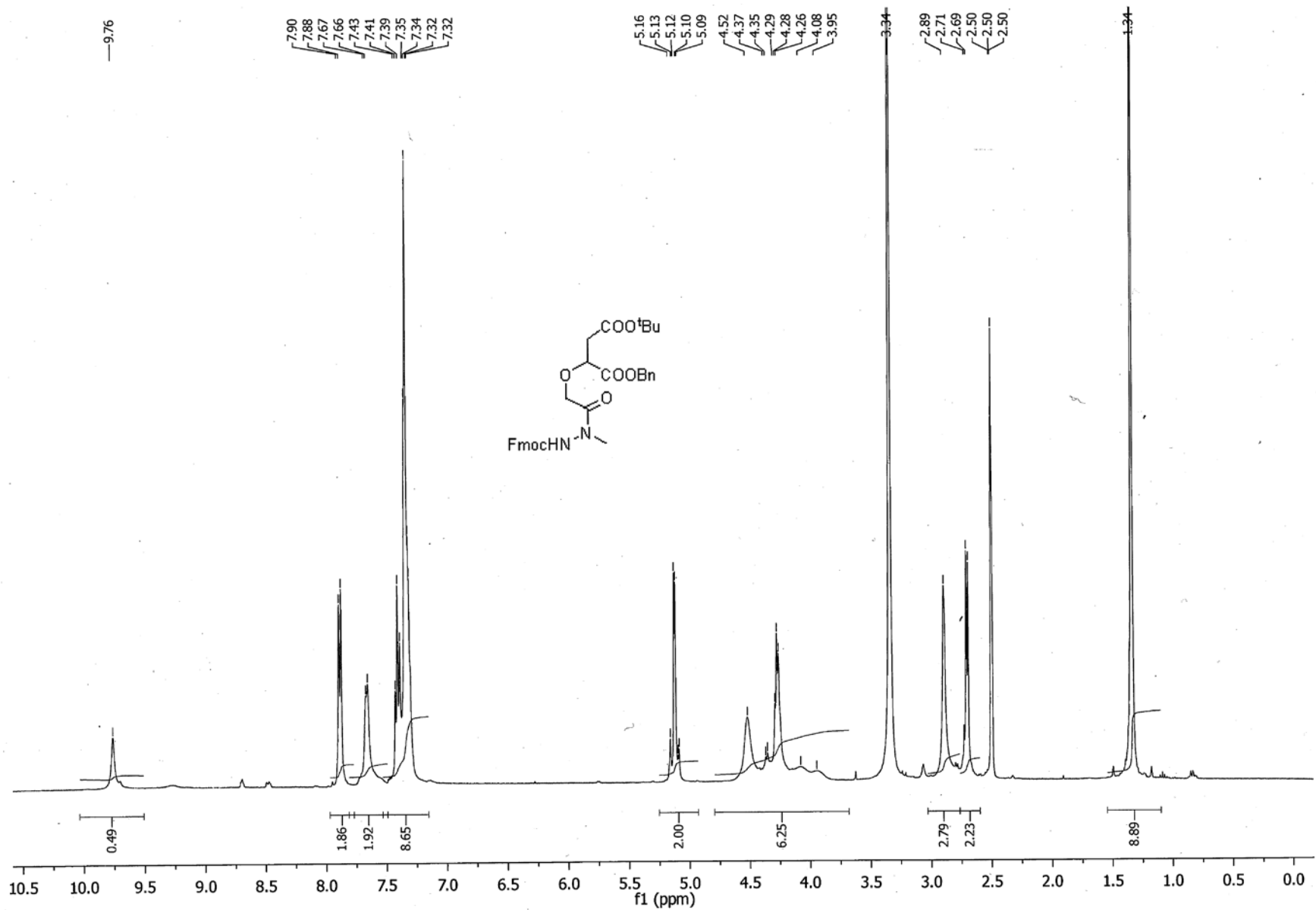


MS Spectrum Peak List

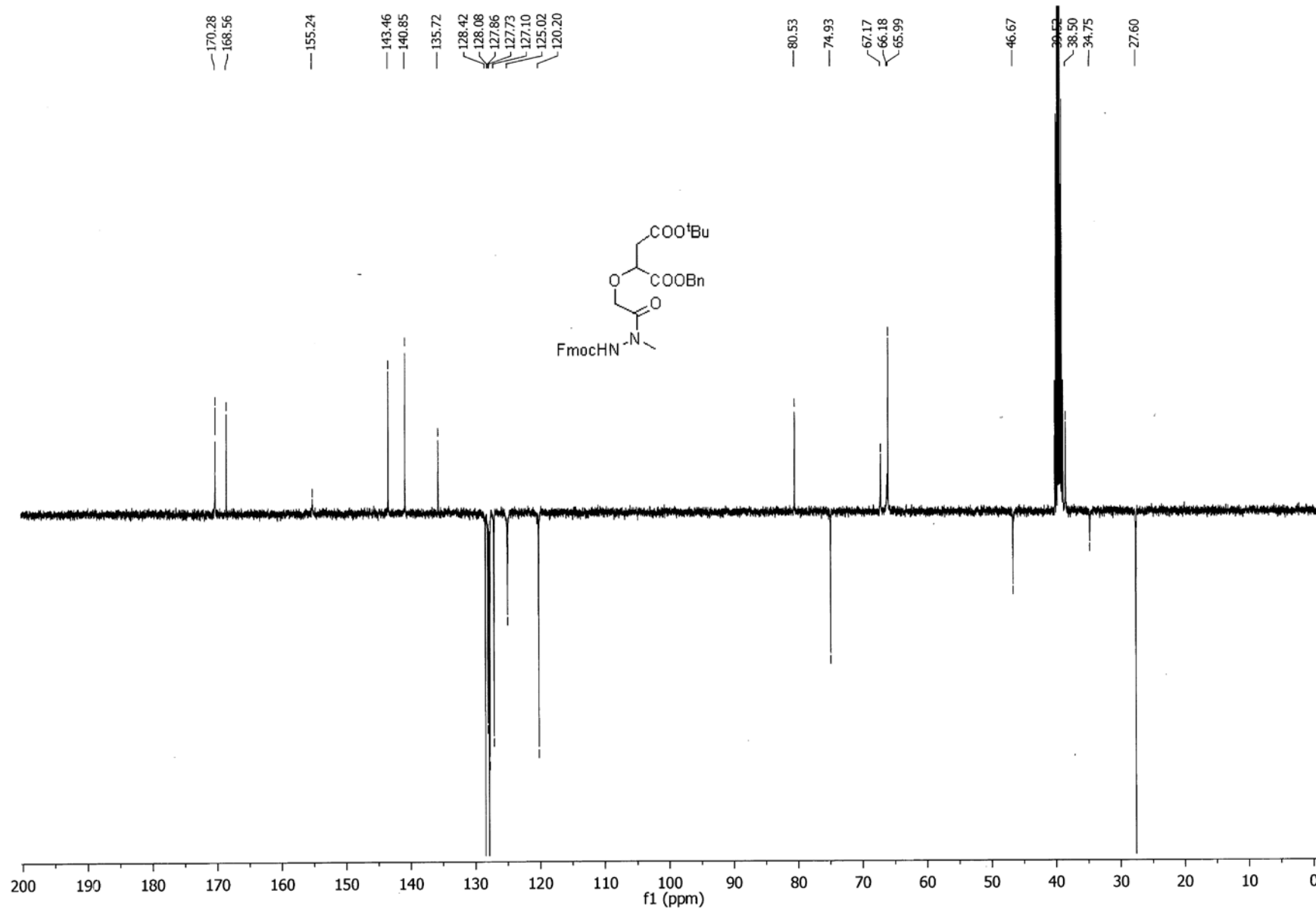
m/z	Calc m/z	Diff(ppm)	z	Abund	Formula	Ion
269.1286	269.1285	-0.64	1	296227.41	C16H16N2O2	(M+H)+
291.1107	291.1104	-1.2	1	388013.98	C16H16N2O2	(M+Na)+
307.0851	307.0843	-2.65	1	1081.68	C16H16N2O2	(M+K)+

--- End Of Report ---

HRMS report of (9H-fluoren-9-yl)methyl 2-methylhydrazine-1-carboxylate **27**



¹H NMR spectrum of 1-benzyl 4-(*tert*-butyl) 2-(2-(2-(((9*H*-fluoren-9-yl)methoxy)carbonyl)-1-methylhydrazinyl)-2-oxoethoxy)succinate **28**



¹³C NMR spectrum of 1-benzyl 4-(*tert*-butyl) 2-(2-(2-(((9*H*-fluoren-9-yl)methoxy)carbonyl)-1-methylhydrazinyl)-2-oxoethoxy)succinate **28**

Qualitative Compound Report

Data File	JRH-314-074-01.d	Sample Name	JRH-314-074-01
Sample Type	Sample	Position	P1-B8
Instrument Name	Instrument 1	User Name	Dr Jason Dang
Acq Method	Monash_Direct_Low_Frag_No_Formic.m	Acquired Time	11/4/2014 12:17:47 PM
IRM Calibration Status	XXXXXXXXXX	DA Method	Monash_Accuracy.m
Comment			

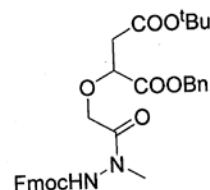
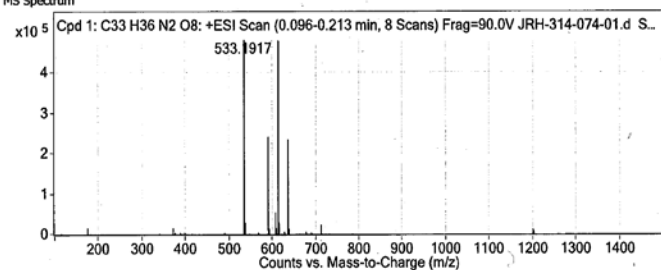
Sample Group		Info.	
Formula	C33H36N2O8	Acquisition SW Version	6200 series TOF/6500 series Q-TOF B.05.01 (B5125.1)

Compound Table

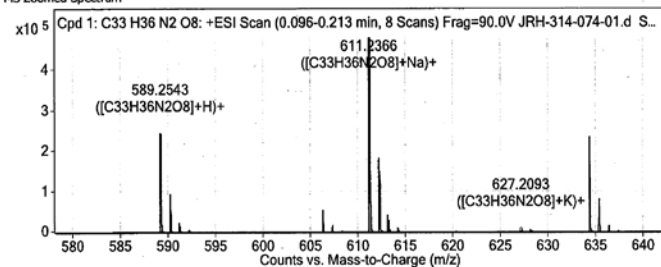
Compound Label	RT	Mass	Abund	Formula	Tgt Mass	Diff (ppm)	MFG Formula	DB Formula
Cpd 1: C33 H36 N2 O8	0.112	588.2471	482638	C33 H36 N2 O8	588.2472	-0.08	C33 H36 N2 O8	C33 H36 N2 O8

Compound Label	m/z	RT	Algorithm	Mass
Cpd 1: C33 H36 N2 O8	611.2366	0.112	Find By Formula	588.2471

MS Spectrum



MS Zoomed Spectrum

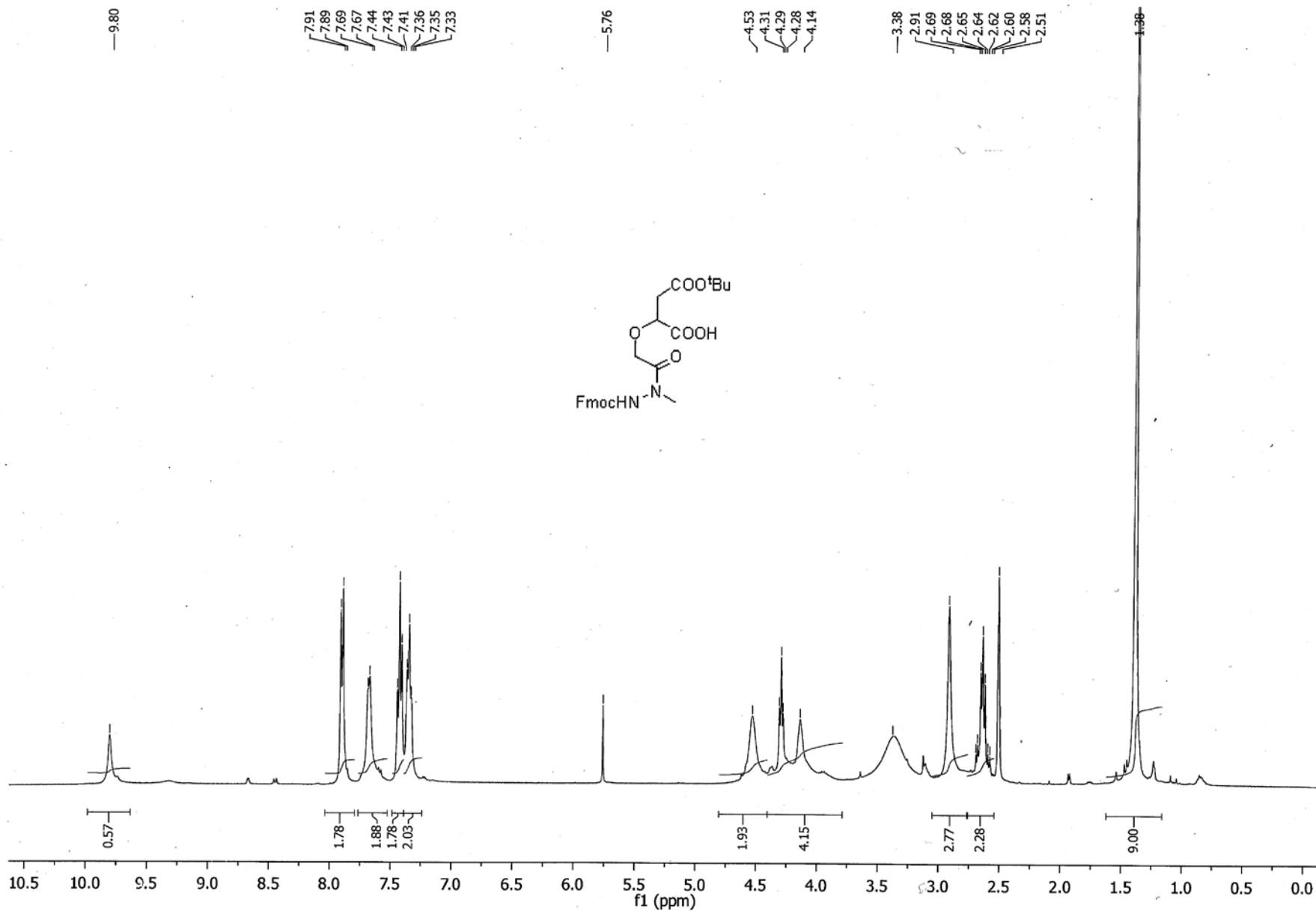


MS Spectrum Peak List

m/z	Calc m/z	Diff(ppm)	z	Abund	Formula	Ion
589.2543	589.2544	0.18	1	243140.77	C33H36N2O8	(M+H)+
611.2366	611.2364	-0.35	1	482637.57	C33H36N2O8	(M+Na)+
627.2093	627.2103	1.59	1	7171.57	C33H36N2O8	(M+K)+

-- End Of Report --

HRMS report of 1-benzyl 4-(*tert*-butyl) 2-(2-(2-(((9*H*-fluoren-9-yl)methoxy)carbonyl)-1-methylhydrazinyl)-2-oxoethoxy)succinate **28**



¹H NMR spectrum of 2-(2-(2-(((9H-fluoren-9-yl)methoxy)carbonyl)-1-methylhydrazinyl)-2-oxoethoxy)-4-(tert-butoxy)-4-oxobutanoic acid **5**

Qualitative Compound Report

Data File	JRH-314-078-01.d	Sample Name	JRH-314-078-01
Sample Type	Sample	Position	P1-B9
Instrument Name	Instrument 1	User Name	Dr Jason Dang
Acq Method	Monash_Direct_Low_Frag_No_Formic.m	Acquired Time	11/4/2014 12:21:02 PM
IRM Calibration Status	XXXXXXXXXX	DA Method	Monash_Accuracy.m
Comment			

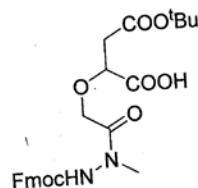
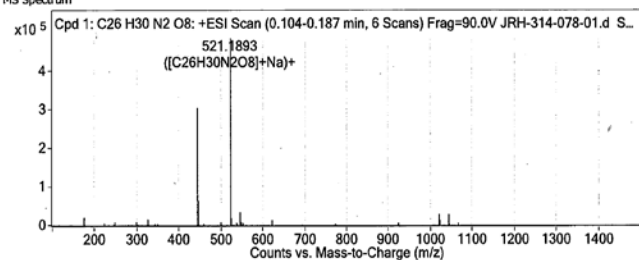
Sample Group		Info.	
Formula	C26H30N2O8	Acquisition SW Version	6200 series TOF/6500 series Q-TOF B.05.01 (B5125.1)

Compound Table

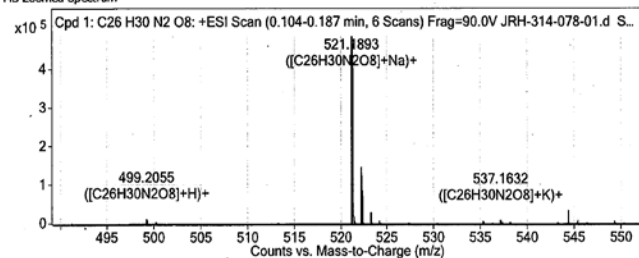
Compound Label	RT	Mass	Abund	Formula	Tgt Mass	Diff (ppm)	MFG Formula	DB Formula
Cpd 1: C26 H30 N2 O8	0.121	498.1999	487245	C26 H30 N2 O8	498.2002	-0.66	C26 H30 N2 O8	C26 H30 N2 O8

Compound Label	m/z	RT	Algorithm	Mass
Cpd 1: C26 H30 N2 O8	521.1893	0.121	Find By Formula	498.1999

MS Spectrum



MS Zoomed Spectrum



MS Spectrum Peak List

m/z	Calc m/z	Diff(ppm)	z	Abund	Formula	Ion
499.2055	499.2075	4.02	1	10598.63	C26H30N2O8	(M+H)+
521.1893	521.1894	0.27	1	487244.93	C26H30N2O8	(M+Na)+
537.1632	537.1634	0.41	1	6314.52	C26H30N2O8	(M+K)+

--- End Of Report ---

HRMS report of 2-(2-(2-(((9H-fluoren-9-yl)methoxy)carbonyl)-1-methylhydrazinyl)-2-oxoethoxy)-4-(tert-butoxy)-4-oxobutanoic acid **5**

CHAPTER 7

Design, synthesis and characterisation of cyclic peptide analogues for macrophage targeting

7.1 Introduction

Two highly redox-stable cyclic peptide analogues of the disulphide-bridged cyclic peptide (**Chapter 4**), one with a thioether bridge (**CP1**) and the other with a lactam bridge (**CP2**), were shown to bind to SPSB2 with low nanomolar affinities ($K_D \approx 21\text{-}31$ nM) (**Chapter 5**). Three of the four cyclic peptidomimetic utilising organic moieties as scaffolds for cyclisation also demonstrated nanomolar binding affinities to the iNOS binding site of SPSB2 (K_D 29-99 nM), with mimetic **M1** showing the strongest affinity to SPSB2 (**Chapter 6**). As cyclic peptide **CP2** has more sites for derivatisation than mimetic **M1**, and with its ease of synthesis, **CP2** was selected as template for the design of analogues for macrophage-targeted delivery studies in this Chapter.

As described in **Chapter 1**, both mannose and MGL receptors are abundantly expressed on the surface of tissue macrophages, suggesting that mannose or GalNAc-containing glycopolymers have the potential to selectively target macrophages. Based on these observations, both mannose and GalNAc glycopolymers (with reduction-sensitive linker dithiophenol maleimide²²³) were designed, synthesised and conjugated to the cyclic peptide. The uptake profiles of the glycopolymer-conjugated cyclic peptides by macrophages were explored. Both mannose and MGL receptors with a cytoplasmic di-aromatic Y-F motif, however, were reported to be internalised into the macrophage or dendritic cells *via* clathrin-dependent or receptor-mediated endocytosis and transported along the endosomal-lysosomal pathway.^{164, 165} This suggests that a mechanism to facilitate the endosomal escape of the endocytosed mannose- or GalNAc-conjugated cyclic peptide to the cytoplasm (where the target protein is) will be required. Thus, the role of oligohistidine in assisting the endosomal escape of both glycopolymer-conjugated and unconjugated cyclic peptide to the cytoplasm of the macrophages was also explored. As previous work by Lo and Wang¹⁹³ found an up to 7000-fold improvement in gene transfection efficiency when a Tat-peptide was covalently fused with 10 histidine residues compared to Tat peptide alone, a 10-residue oligohistidine was selected for conjugation to the cyclic peptide analogues in this study.

Hence, in this Chapter, the design and synthesis of four analogues of **CP2** consisting of non-oligohistidine (**CP3**, **CP4**) (**Figure 7.1**) and oligohistidine-conjugated analogues (**CP5**, **CP6**) are described. Two of the analogues (**CP4**, **CP6**) were fluorophore-labelled

with rhodamine B isothiocyanate (RBITC) for cell-tracking by confocal laser scanning microscope. The effect of these modifications on their binding to the iNOS binding site of SPSB2 was determined by both SPR and ^{19}F NMR. The role of mannose and GalNAc glycopolymers (**CP7-CP10**) in conferring selective uptake of the RBITC-conjugated cyclic peptide by macrophages was also explored and the distribution of oligohistidine and non-oligohistidine-conjugated cyclic peptides in the macrophages was compared.

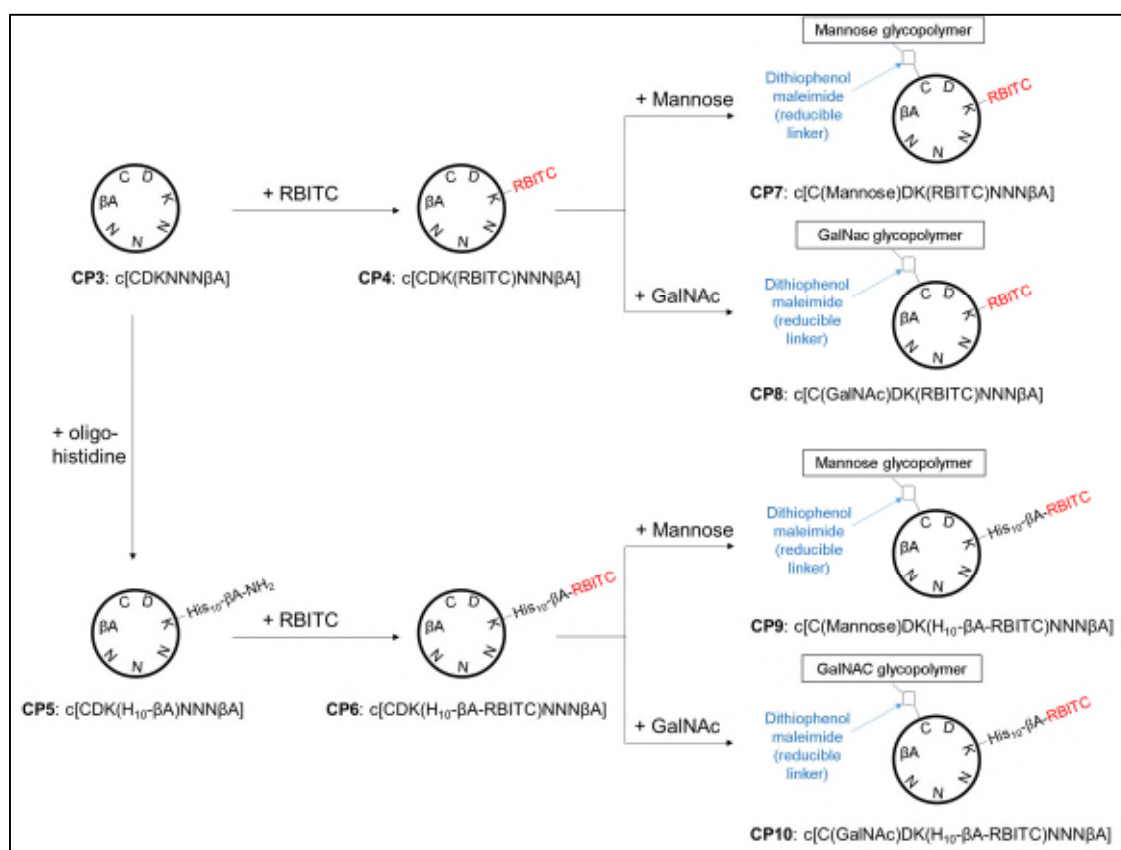


Figure 7.1. Summary of cyclic peptide analogues of **CP2** generated in this Chapter, with one unconjugated analogue (**CP3**), six fluorophore (RBITC)-labelled analogues (**CP4**, **CP6-CP10**), four oligohistidine-conjugated analogues (**CP5-CP6**, **CP9-CP10**), two mannose glycopolymer-conjugated analogues (**CP7**, **CP9**) and two GalNAc-glycopolymer-conjugated analogues (**CP8**, **CP10**).

7.2 Materials and methods

In silico design of analogues for macrophage-targeted delivery studies, LC-MS characterisation of the purified cyclic peptide analogues, SPSB2 protein expression and purification and the set-up of SPR experiments for binding experiments were carried out according to methods described in **Chapter 2**.

7.2.1 Synthesis and purification of cyclic peptide analogues CP3-CP6

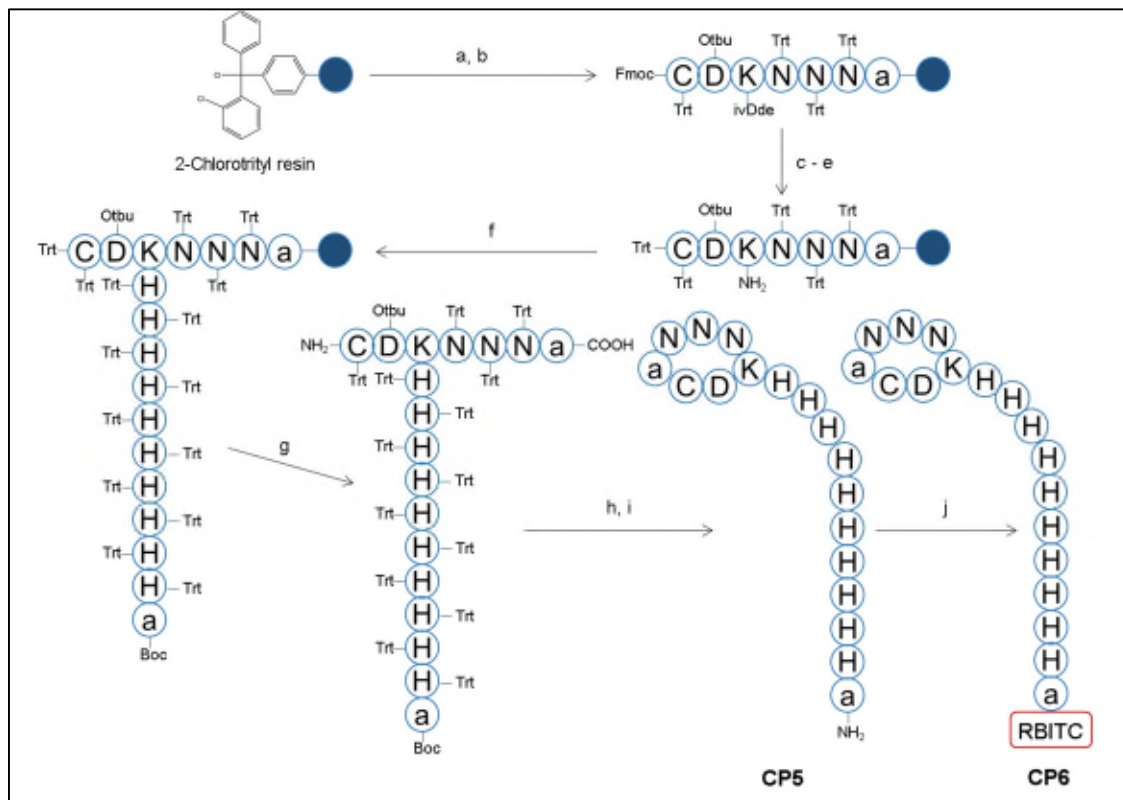
Synthesis and purification of cyclic peptide analogue **CP3** were carried out according to methods described in **Section 2.3.3.2** and **2.3.3.3**, respectively. Further reaction of purified cyclic peptide analogue **CP3** with RBITC (3 eq) in basic condition (i.e. 2.5% (v/v) DIPEA in DMF) under constant shaking overnight in the dark yielded disulphide-linked dimer of cyclic peptide analogue **CP4**. After three cycles of precipitation with cold diethyl ether, the crude **CP4** dimer was lyophilised in the MeCN:H₂O (1:1) mixture. Crude **CP4** dimer powder was redissolved in MeCN:Buffer A (1:3) mixture and incubated with a 10-fold excess of TCEP.HCl for 30 min prior purification by RP-HPLC on a C18(2) column using a gradient of 35-75% B (A: 99.9% H₂O, 0.1% TFA; B: 80% MeCN, 19.9% H₂O, 0.1% TFA) over 20 min.

Synthesis of the cyclic peptide analogue **CP5** was performed according to **Scheme 7.1**. As for **CP3**, side-chain protected linear peptide CDKNNNβA was first assembled on resin by SPPS. The Fmoc protecting group at the *N*-terminus of the linear peptide on resin was then substituted by a base-stable trityl (Trt) protecting group *via* treatment with 20% (v/v) piperidine in DMF (2 x 5 min), followed by reaction with trityl chloride (TrCl) and DIPEA in DCM overnight. The *N*-terminus tritylation step is essential to prevent the release of free *N*-terminus amine during subsequent use of 4% (v/v) hydrazine hydrate in DCM (4 x 15 min) in the removal of 1-(4,4-Dimethyl-2,6-dioxocyclohexylidene)-3-methylbutyl (ivDde) side chain protecting group of Lys residue for further chain elongation by SPPS.

Following the complete assembly of the side chain and *N*-terminus protected linear peptide CDK(H₁₀βA)NNNβA by SPPS (with the last amino acid coupled to the resin as Boc-β-Ala-OH), the crude peptide was cleaved off the resin with cleavage cocktail containing 3% (v/v) TFA and 5% (v/v) TIPS in DCM for 2 h. This cleavage condition also removed the Trt protecting group at the *N*-terminus of the peptide, resulting in single primary amine and single carboxylic acid for overnight cyclisation with HCTU and DIPEA in DMF. After cyclisation, all side chain protecting groups (including the *N*^α-Boc protecting group) were removed by reaction with a cleavage cocktail solution containing 95% (v/v) TFA and scavengers 2.5% (v/v) TIPS, 2.5% (v/v) DODT for 2 h. The crude cyclic peptide was recovered by precipitation with cold diethyl ether and lyophilised in MeCN:H₂O mixture. Purification was carried out by RP-HPLC on the

C18(2) column using a gradient of 5-50% B (A: 99.9% H₂O, 0.1% TFA; B: 80% MeCN, 19.9% H₂O, 0.1% TFA) over 45 min.

Scheme 7.1. Synthesis of oligohistidine-conjugated cyclic peptide analogue **CP5** and its RBITC-conjugated derivative **CP6**



^a Reagents and conditions: (a) Fmoc-β-Ala-OH (1 eq), DIPEA (5 eq), DMF, 60 min; (b) SPPS; (c) 20% (v/v) piperidine, DMF, 5 min, twice; (d) TrCl (3.5 eq), DIPEA (6 eq), DCM, 16 h; (e) 4% (v/v) hydrazine hydrate, DCM, 15 min, 4 times; (f) SPPS; (g) 3% (v/v) TFA, 5% (v/v) TIPS, DCM, 2 h; (h) HCTU (3 eq), DIPEA (6 eq), DMF, 16 h; (i) 95% (v/v) TFA, 2.5% (v/v) TIPS, 2.5% (v/v) DODT, 2 h; (j) RBITC (2 eq), DMF:0.1 M Na₂CO₃, pH 9, (1:1), 16 h, RT, dark

Initial attempts to conjugate RBITC to purified **CP5** to yield cyclic peptide analogue **CP6** using the same protocol as described for **CP4** did not give the desired result. Precipitation was observed in the reaction mixture containing 2.5% (v/v) DIPEA in DMF, resulted in negligible desired product, presumably the complete deprotonation of His side chains of **CP5** in the strong basic environment resulted in its propensity to form aggregates. A further conjugation attempt of RBITC to **CP5** in DMF:0.1 M Na₂CO₃, pH 9, buffer (1:1) in the dark at room temperature overnight (**Scheme 7.1**) gave the desired

product **CP6**. After lyophilisation, the crude **CP6** powder was redissolved in MeCN:Buffer A (1:3) and incubated with a 10-fold excess TCEP.HCl for 30 min prior to purification by RP-HPLC on the C18(2) column using a gradient of 25-75% B (A: 99.9% H₂O, 0.1% TFA; B: 80% MeCN, 19.9% H₂O, 0.1% TFA) over 25 min. The LC-MS chromatograms of the purified **CP3-CP6** are shown in **Figure 7.2**.

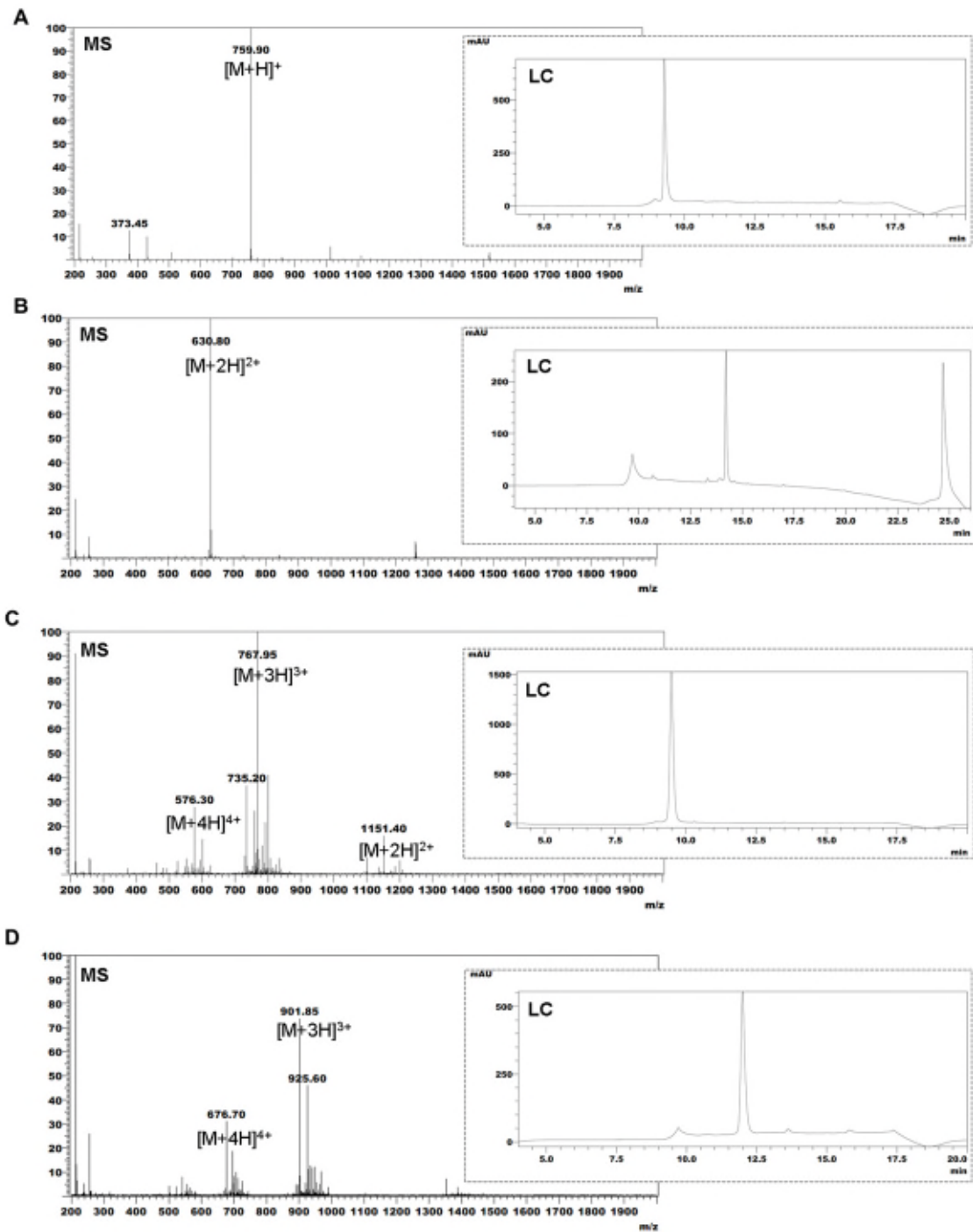


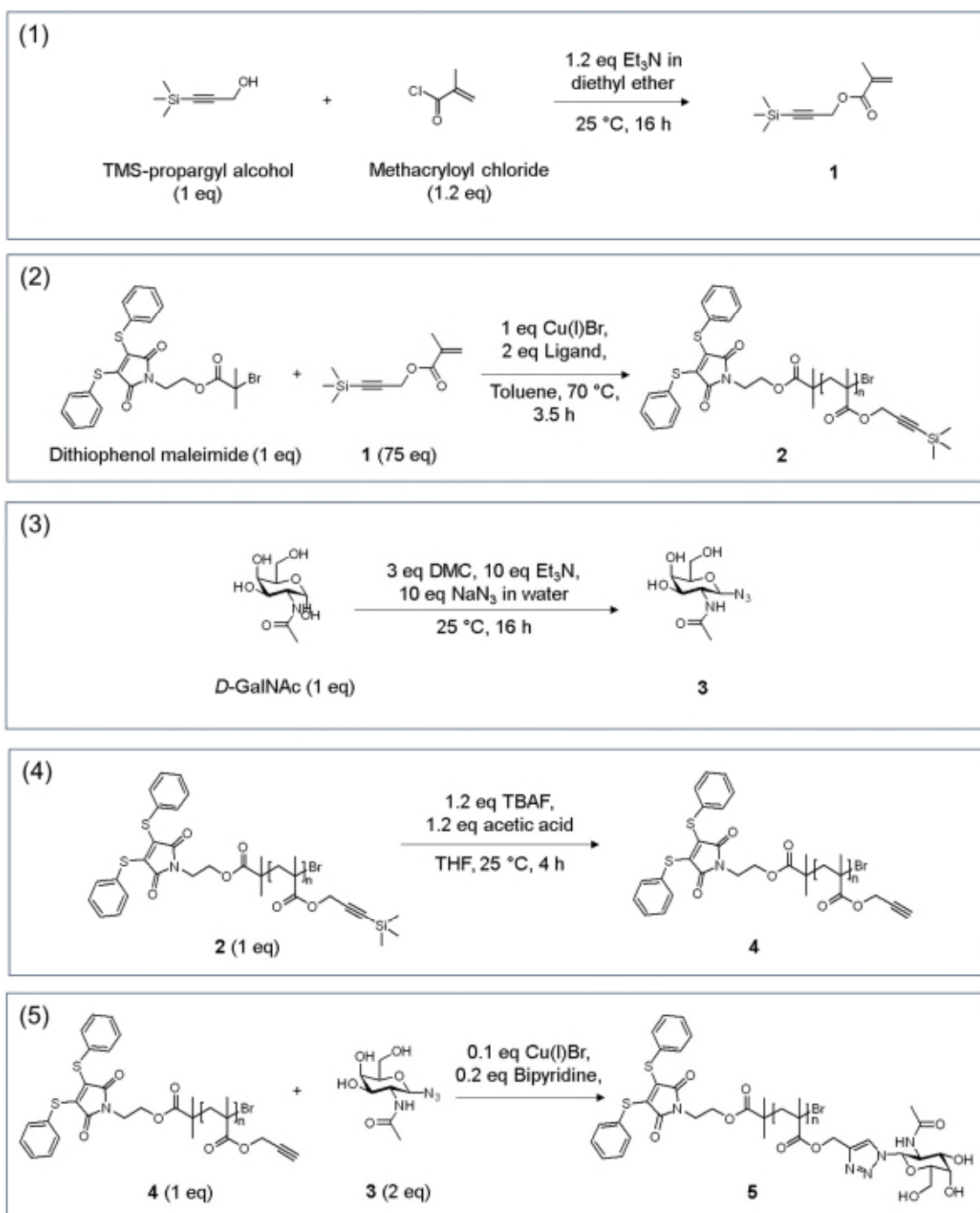
Figure 7.2. LC-MS profiles of the purified (A) **CP3** (c[CDKNNNβA]), (B) **CP4** (c[CDK(RBITC)NNNβA]), (C) **CP5** (c[CDK(H₁₀βA)NNNβA]) and (D) **CP6** (c[CDK(H₁₀βA-RBITC)NNNβA]) analogues. Purity is ~95%, based on the peak area in the chromatogram. The deconvoluted mass of **CP5** is +98 Da relative to the theoretical mass, presumably due to phosphate (H₃PO₄⁻) salt formation with the imidazole ring of the His residue.

7.2.2 Synthesis and purification of GalNAc and mannose glycopolymers

Synthesis of GalNAc glycopolymer was carried out in 5 steps (**Scheme 7.2**). Detailed method and characterisation of intermediates from each step and the final product **5** by ¹H NMR are illustrated in **Section 7.2.2.1-7.2.2.4 (Figure 7.3-7.7)**.

7.2.2.1 Synthesis of TMS-protected methacrylate monomer **1**

In a round bottom flask, TMS-propargyl alcohol (5 g, 40 mmol) was dissolved in approximately 50 mL diethyl ether. Triethylamine (7.1 mL, 50 mmol) was then added to the flask immersed in an ice water bath under constant stirring. After attaching a separating funnel onto the round bottom flask, the mixture was degassed by bubbling with nitrogen for 10 min. Methacryloyl chloride (4.4 mL, 50 mmol) and 25 mL diethyl ether were then added to the closed separating funnel, mixed and degassed by nitrogen bubbling for 10 min. The methacryloyl chloride mixture was then added dropwise into the round bottom flask in an ice water bath and left stirring overnight at room temperature. The white precipitates (presumably triethylamine hydrochloride salts) were removed from the reaction mixture by filtration under vacuum and the organic filtrate was washed with distilled water, dried with MgSO₄ and concentrated by rotavap. The monomer **1** was further purified by flash chromatography on silica using a gradient of 0-2% B (A: petroleum ether; B: diethyl ether) over 120 min to give a final yield of 4.7 g (~60% yield). The purity of the monomer **1** was characterised by ¹H NMR in CDCl₃ as illustrated in **Figure 7.3**.

Scheme 7.2. Synthesis scheme of GalNAc glycopolymer **5**

^a Reagents and conditions: (1) synthesis of trimethylsilyl (TMS)-protected methacrylate monomer **1**; (2) Polymerisation of **1** with dithiophenol maleimide initiator (a generous gift from Dr Paul Wilson, Department of Chemistry, University of Warwick, UK) using the atom transfer radical polymerisation (ATRP) technique²²⁴ to yield TMS-protected dithiophenol maleimide polymethacrylate polymer **2** with *N*-ethyl-2-pyridyl methanimine as ligand; (3) synthesis of β -D-GalNAc sugar azide monomer **3**; (4) removal of TMS protecting group from polymer **2**; and (5) Cu(I)-catalysed azide/alkyne

cycloaddition (CuAAC) “click” reaction²²⁵ between the TMS-protected polymer **4** with sugar azide **3** to yield GalNAc glycopolymer as the final product **5**.

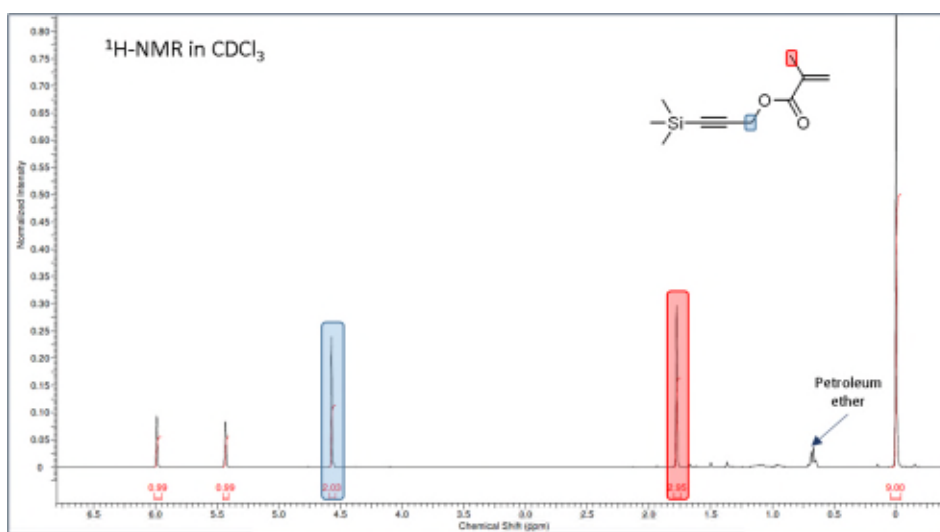


Figure 7.3. ¹H NMR of the purified TMS-protected methacrylate monomer **1** in CDCl₃.

7.2.2.2 Polymerisation of TMS-protected methacrylate monomer **1** with dithiophenol maleimide initiator via atom transfer radical polymerisation (ATRP) approach

In an oven-dried Schlenk tube, copper (I) bromide (15 mg, 10 μmol) was added and degassed with nitrogen for 30 min. In a separate vial, *N*-ethyl-2-pyridylmethanimine ligand (27 mg, 20 μmol), dithiophenol maleimide initiator (52 mg, 10 μmol), monomer **1** (1.5 g, 7.6 mmol) and toluene (1.5 g) were added, mixed and degassed by bubbling with nitrogen gas for 30 min. The ligand/initiator/monomer mixture was then cannulated (*t* = 0) into the Cu(I)Br catalyst-containing Schlenk tube immersed in a hot oil bath at 70 °C under positive inert (nitrogen) environment and constant stirring. At zero time and at 3.5 h, a sample was taken, passed through a short basic alumina column and eluted with deuterated chloroform CDCl₃, and subjected to ¹H NMR (**Figure 7.4**). At 3.5 h, approximately 89% conversion was achieved. Thus, after this time point, the Schlenk tube containing the reaction mixture was removed from the hot oil bath, diluted with toluene (~5 mL) and blown with compressed gas for ~ 1 h to terminate the reaction. To remove the catalyst, the reaction mixture was passed through a short basic alumina column and the polymer was recovered *via* elution with chloroform, concentration with rotavap, re-dissolution in minimal tetrahydrofuran (THF) and precipitation into methanol. The purified TMS-protected dithiophenol maleimide-polymethacrylate

polymer **2** was redissolved in CDCl_3 for ^1H NMR or DMF for gel permeation chromatography (GPC) analysis (**Figure 7.5**).

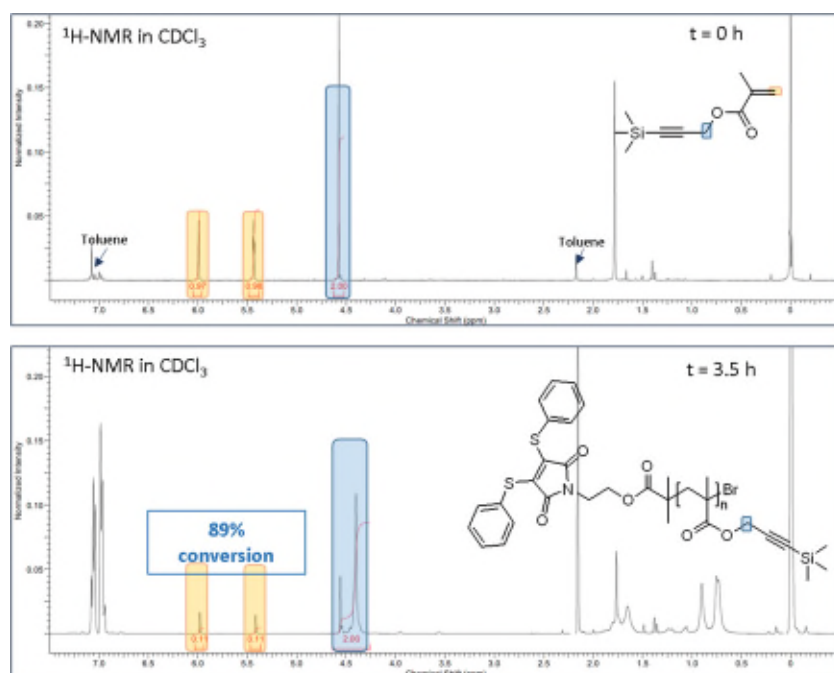


Figure 7.4. *In situ* monitoring of polymerisation reaction between the dithiophenol maleimide initiator and TMS-protected methacrylate monomer **1** by ^1H NMR in CDCl_3 .

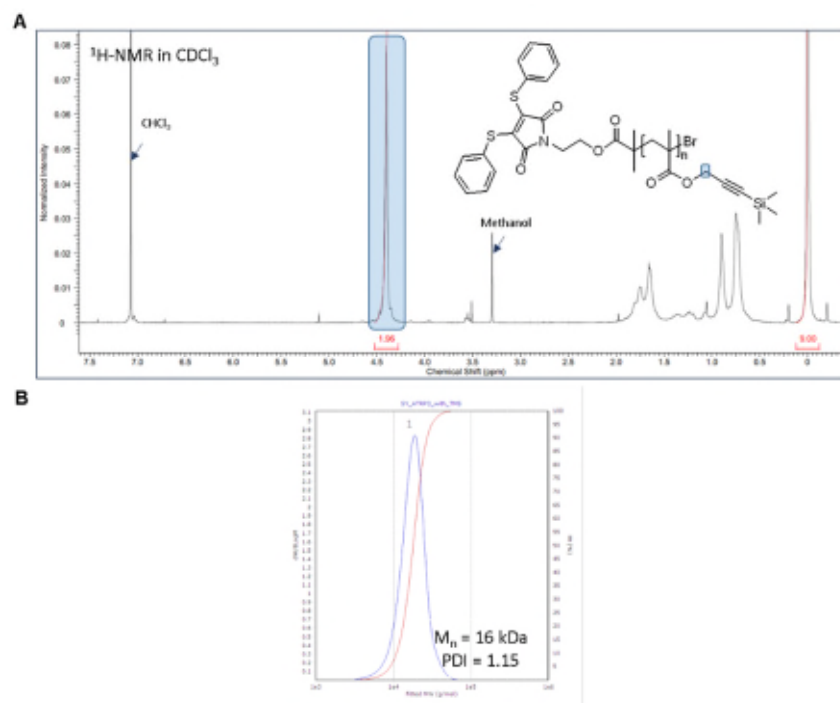


Figure 7.5. (A) ^1H NMR of the purified TMS-protected dithiophenol maleimide-polymethacrylate polymer **2** in CDCl_3 . (B) GPC analysis of **2** in DMF, with M_n = number-average molecular weight, PDI = polydispersity index.

7.2.2.3 Synthesis of β -D-GalNAc sugar azide monomer **3**

D-GalNAc sugar (3 g, 13.6 mol), 2-chloro-1,3-dimethylimidazolium (6.9 g, 40.7 mol), triethylamine (13.7 g, 135.6 mol), sodium azide (8.8 g, 135.6 mol) and water were added to a canonical flask and stirred overnight at ambient temperature. The sugar azide **3** was recovered from the reaction mixture *via* precipitation with DCM followed by filtration under vacuum, re-dissolution in absolute ethanol and incubation with activated Amberlite® IR 120 ion-exchange resin overnight. Following filtration and concentration by rotavap, the final purified product **3** was diluted in $^2\text{H}_2\text{O}$ for ^1H NMR (**Figure 7.6**).

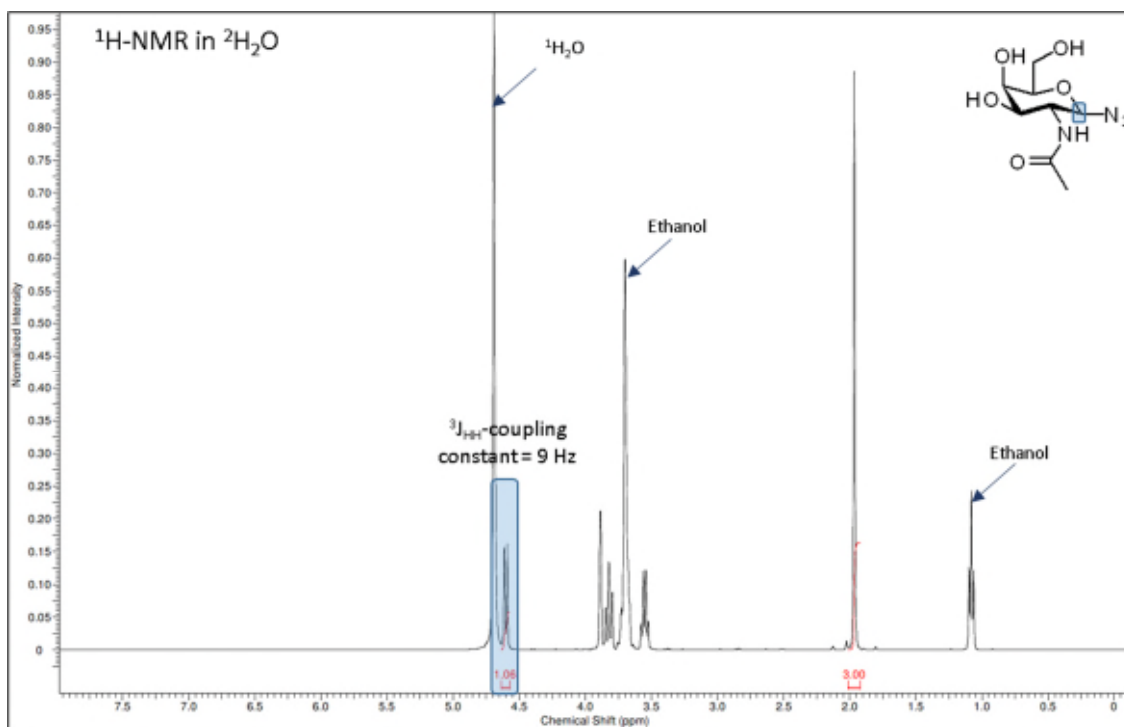


Figure 7.6. ^1H NMR of the purified β -D-GalNAc-Azide, **3** in $^2\text{H}_2\text{O}$. A $^3J_{\text{HH}}$ -coupling constant of 9 Hz confirms the β -configuration of the anomeric proton (highlighted in blue).

7.2.2.4 Conjugation of β -D-GalNAc sugar azide monomer and dithiophenol maleimide-polymethacrylate polymer via “click reaction” to give the GalNAc glycopolymer **5**

Prior to conjugation between the sugar azide monomer and the polymer, the TMS-protection group of **2** was first removed. Briefly, TMS-protected dithiophenol maleimide-polymethacrylate polymer **2** (450 mg, 2.3 mmol), acetic acid (165 mg, 2.8 mmol) and THF (40 mL) were added to a round bottom flask, mixed and degassed *via* bubbling with

nitrogen gas for 20 min under constant stirring. Tetra-n-butylammonium fluoride, TBAF (2.75 mL, 2.8 mmol) was then injected into the flask pre-immersed in an ice-water bath and allowed to stir for 20 min followed by another 4 h at room temperature. The reaction mixture was then passed through a basic alumina column (to remove the acetic acid), followed by a silica column (to remove TBAF) and the TMS-deprotected polymer **4** was eluted with chloroform and concentrated by rotavap.

To conjugate the sugar azide monomer **3** with the TMS-deprotected polymer **4**, Cu(I)Br (16 mg, 0.1 mmol) was first added to an oven-dried Schlenk tube, and degassed with nitrogen for 30 min. In a separate vial, TMS-deprotected polymer **4** (140 mg, 1.1 mmol), β -D-GalNAc sugar azide **3** (570 mg, 1.4 mmol), 2,2'-bipyridine ligand (35 mg, 0.2 mmol) and DMSO (5 mL) were added, mixed and degassed by bubbling with nitrogen gas for 30 min. The ligand/sugar azide/polymer mixtures were then cannulated into the Cu(I)Br catalyst containing Schlenk tube under positive inert (nitrogen) environment and constant stirring at room temperature for 40 h. The GalNAc glycopolymer **5** were recovered from the reaction mixture *via* precipitation with THF, re-dissolution in distilled water, incubation with copper-chelating resin (Cuprisorb[®]) for 1 h, filtration and extensive dialysis against distilled water (molecular mass cut-off of the dialysis tubing 3.5 kDa) with two changes of water per day for three consecutive days. The purified final product **5** was lyophilised and redissolved in ²H₂O for ¹H NMR or DMF for GPC analysis (**Figure 7.7**).

Synthesis of the mannose glycopolymer was carried out by Joji Tanaka (Department of Chemistry, University of Warwick, UK). Briefly, the synthesis involved two key reactions: polymerisation of dithiophenol maleimide with polyethylene glycol-acrylate (PEGA) copolymer *via* single-electron transfer living radical polymerisation (SET-LRP)²²³ to yield a dithiophenol maleimide-PEGA copolymer, followed by copolymerisation with β -mannose-acrylamide (β -ManAm) glycomonomer *via* aqueous SET-LRP²²⁶ to yield the mannose glycopolymer, **6** as the final product. Both glycopolymers showed narrow dispersity by GPC analysis in DMF, with a polydispersity index of 1.29.

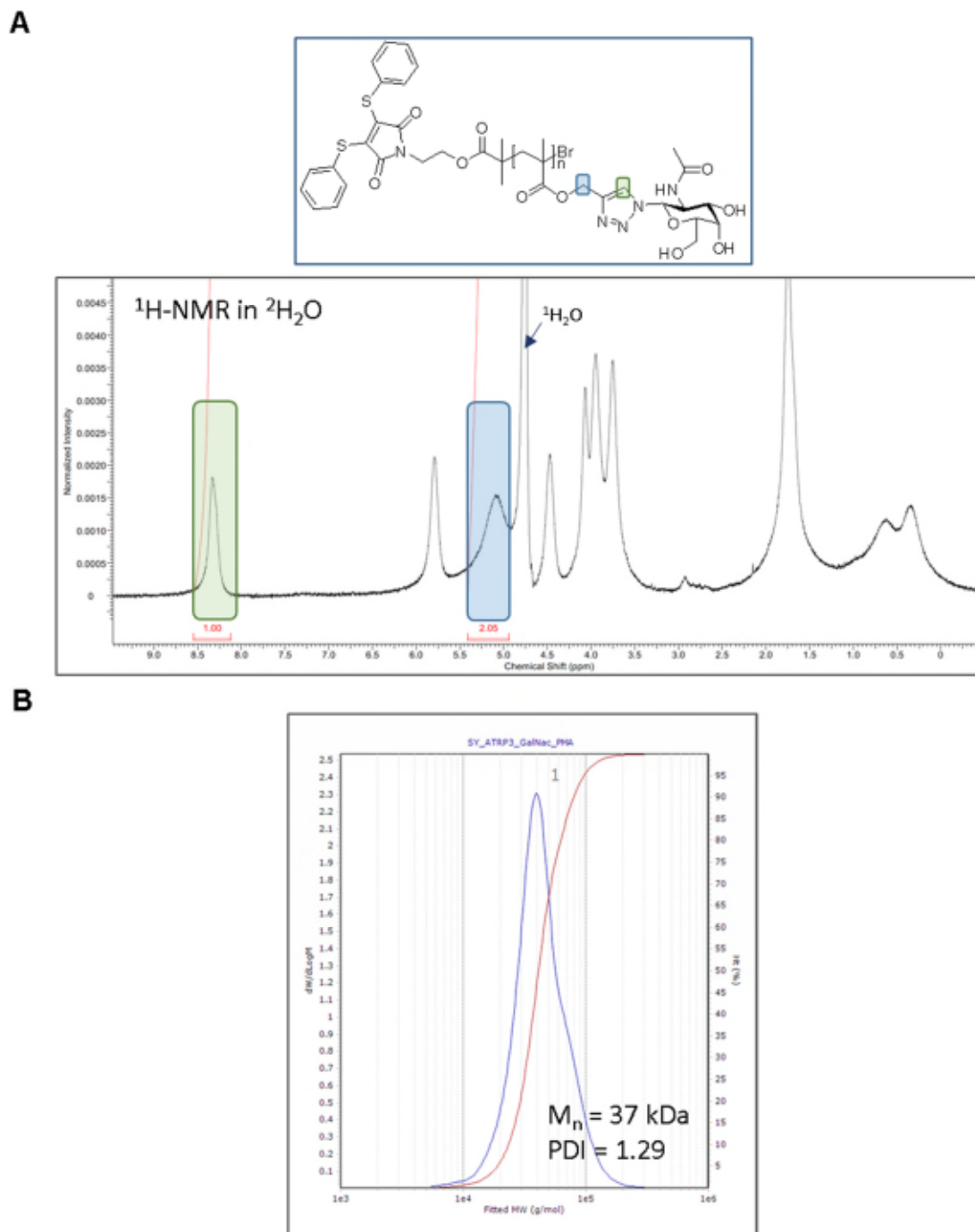


Figure 7.7. (A) ^1H NMR of the purified GalNAc glycopolymer, **5** in $^2\text{H}_2\text{O}$. (B) GPC analysis of **5** in DMF, with M_n = number-average molecular weight, PDI = polydispersity index.

7.2.3 Mannose and GalNAc glycopolymers conjugation to the cyclic peptides

To obtain mannose glycopolymer-conjugated cyclic peptide analogue **CP7**, cyclic peptide **CP4** (1 eq), reducing agent TCEP.HCl (3 eq) and mannose glycopolymer, **5** (3 eq) were dissolved in degassed 10 mM phosphate buffer, pH 7.0, 50 mM NaCl, mixed thoroughly and allowed to shake overnight at room temperature at a final cyclic peptide concentration of 0.25 mg/mL. The reaction mixture was then dialysed against distilled water (molecular mass cut-off of the dialysis tubing 6.5 kDa) to remove unreacted **CP4**, TCEP.HCl, phosphate buffer, NaCl and the released thiophenol from the glycopolymer. As the unconjugated mannose-glycopolymers will not interfere with the imaging of **CP7** uptake by macrophages *via* confocal laser scanning microscope, no further purification steps were carried out to separate **CP7** from the unconjugated mannose glycopolymer. The same approach was used to generate the GalNAc glycopolymer-conjugated cyclic peptide analogue **CP8** from **CP4**. The HPLC chromatograms of **CP7** and **CP8** (in mixture with unconjugated glycopolymers) are illustrated in **Figure 7.8** and **Figure 7.9**, respectively.

For oligohistidine-based mannose and GalNAc glycopolymer-conjugated cyclic peptide analogues **CP9** and **CP10**, respectively, a similar conjugation protocol to that for **CP7** and **CP8** was used except that the final cyclic peptide (**CP6**) concentration used for conjugation was 1 mg/mL and an additional purification step with nickel-charged chelating Sepharose resin was carried out to retain the oligohistidine-conjugated cyclic peptide analogues. Glycopolymer-attached oligohistidine-conjugated cyclic peptide analogues (**CP9**, **CP10**) were recovered by elution with 500 mM imidazole in 50 mM phosphate, pH 7.4, and 300 mM NaCl followed by dialysis against distilled water (molecular mass cut-off of the dialysis tubing 6.5 kDa). The HPLC chromatograms of the final product of **CP9** and **CP10** are illustrated in **Figure 7.10** and **Figure 7.11**, respectively.

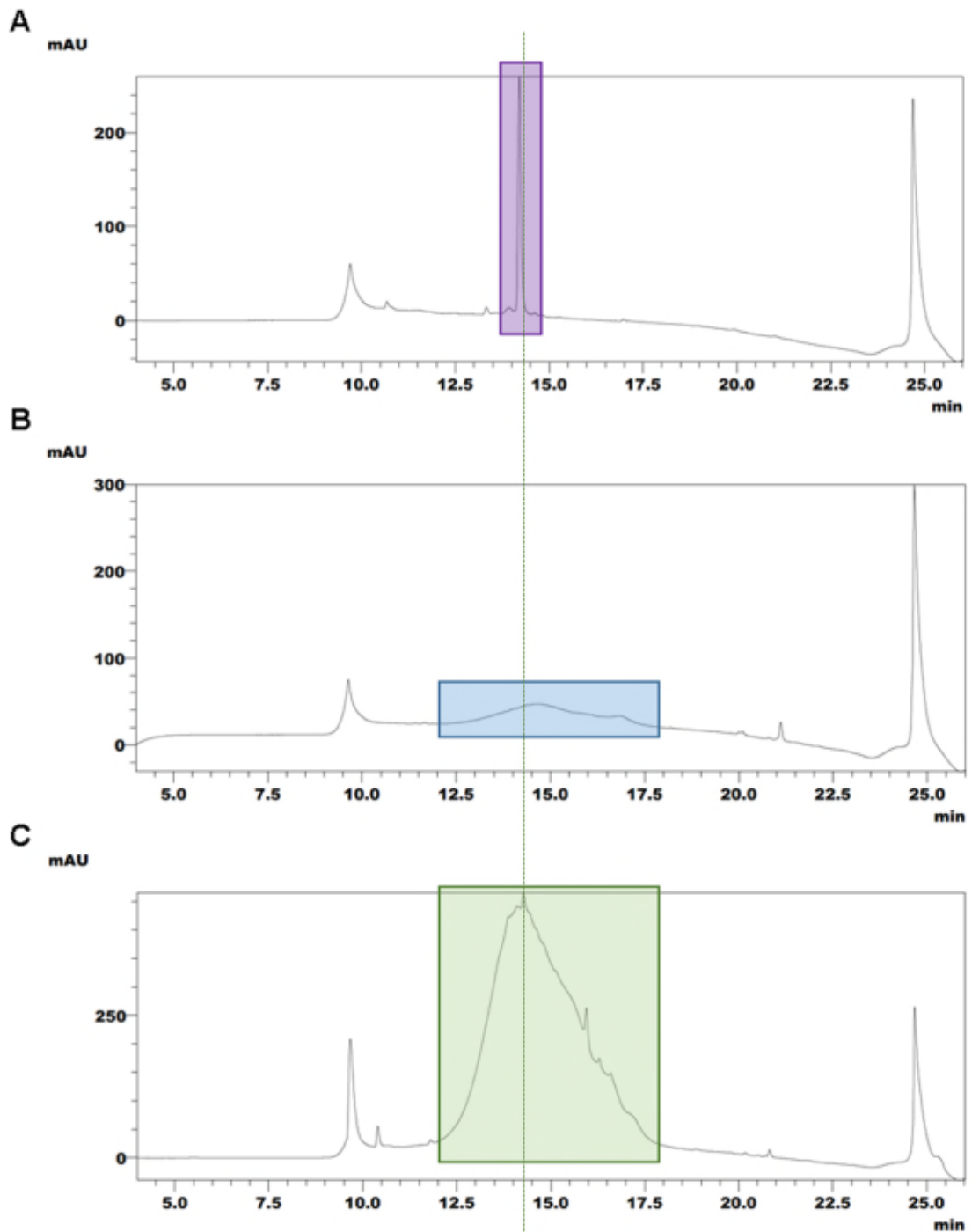


Figure 7.8. Liquid chromatography profiles of (A) **CP4** (c[CDK(RBITC)NNNβA]), (B) mannose glycopolymer and (C) **CP7** (c[C(Mannose)DK(RBITC)NNNβA]) and mannose glycopolymer mixture, with the corresponding peak highlighted in boxes. A minor shift in retention time was observed upon conjugation (green dotted line).

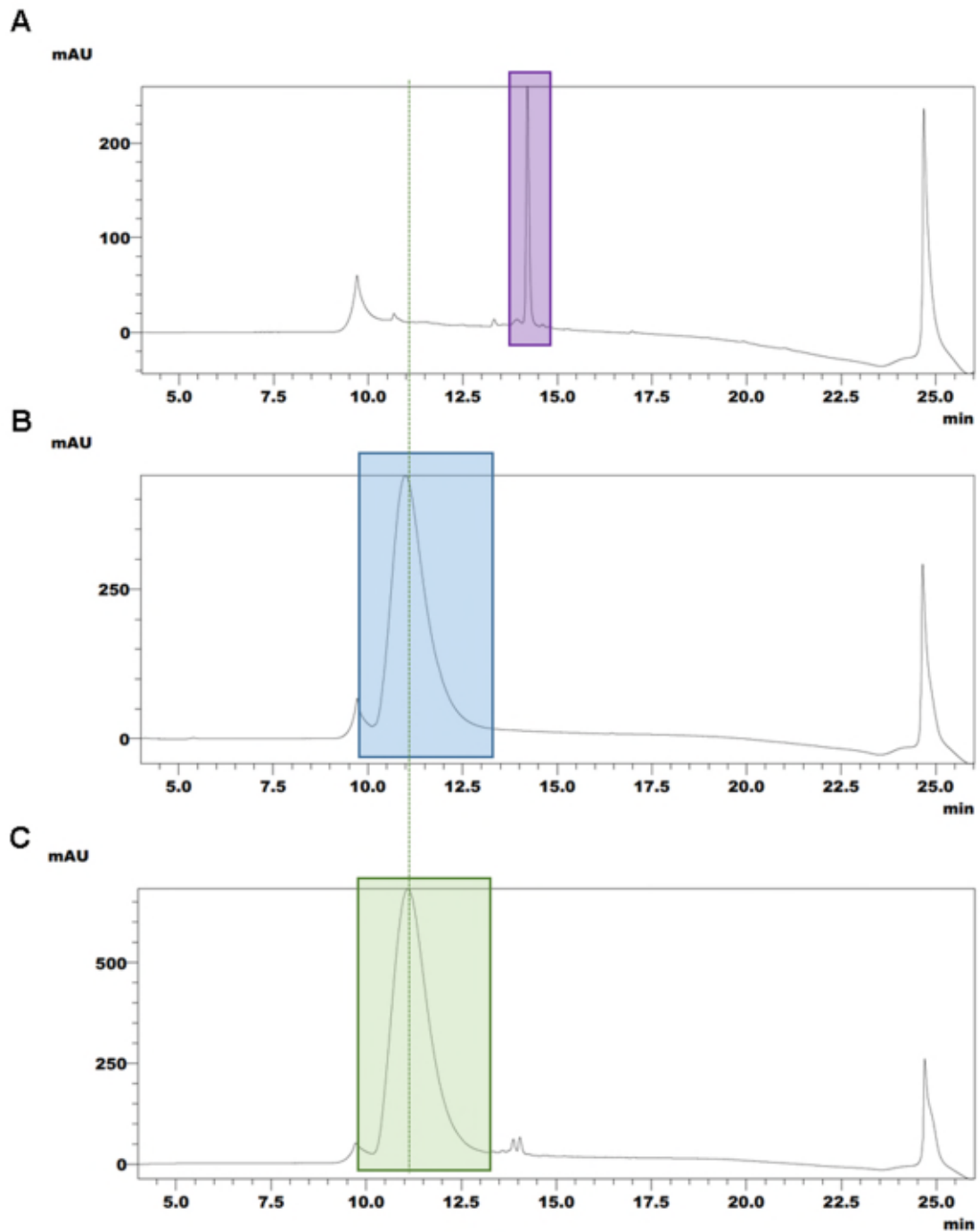


Figure 7.9. Liquid chromatography profiles of (A) **CP4** (c[CDK(RBITC)NNN β A]), (B) GalNAc glycopolymer and (C) **CP8** c[C(GalNAc)DK(RBITC)NNN β A]) and GalNAc glycopolymer mixture, with the corresponding peak highlighted in boxes. A minor shift in retention time was observed upon conjugation (green dotted line).

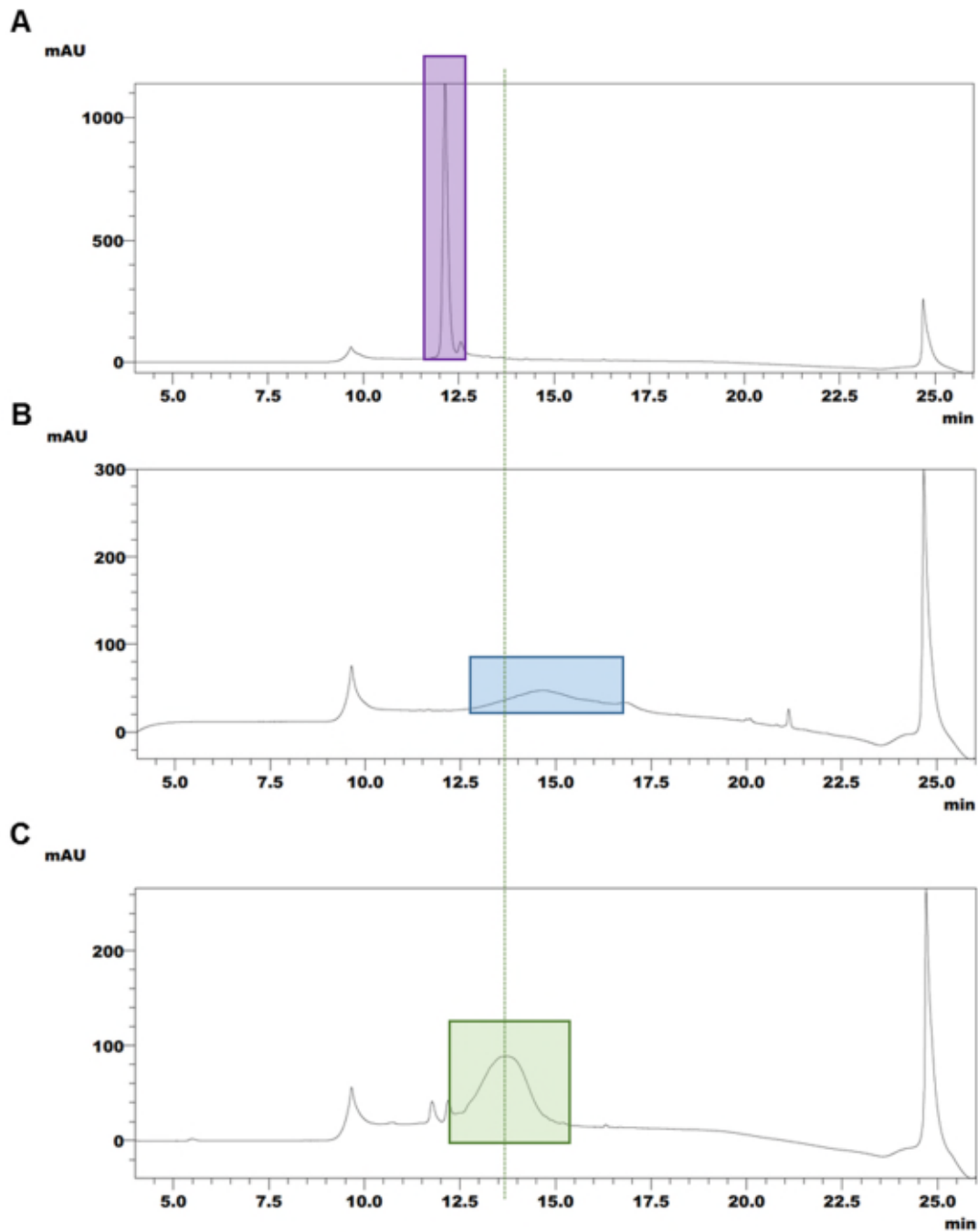


Figure 7.10. Liquid chromatography profiles of (A) **CP6** (c[CDK(H₁₀βA-RBITC)NNNβA]), (B) Mannose glycopolymer and (C) **CP9** (c[C(Mannose)DK(H₁₀βA-RBITC)NNNβA]), with the corresponding peak highlighted in boxes. A small shift in retention time was observed upon conjugation (green dotted line).

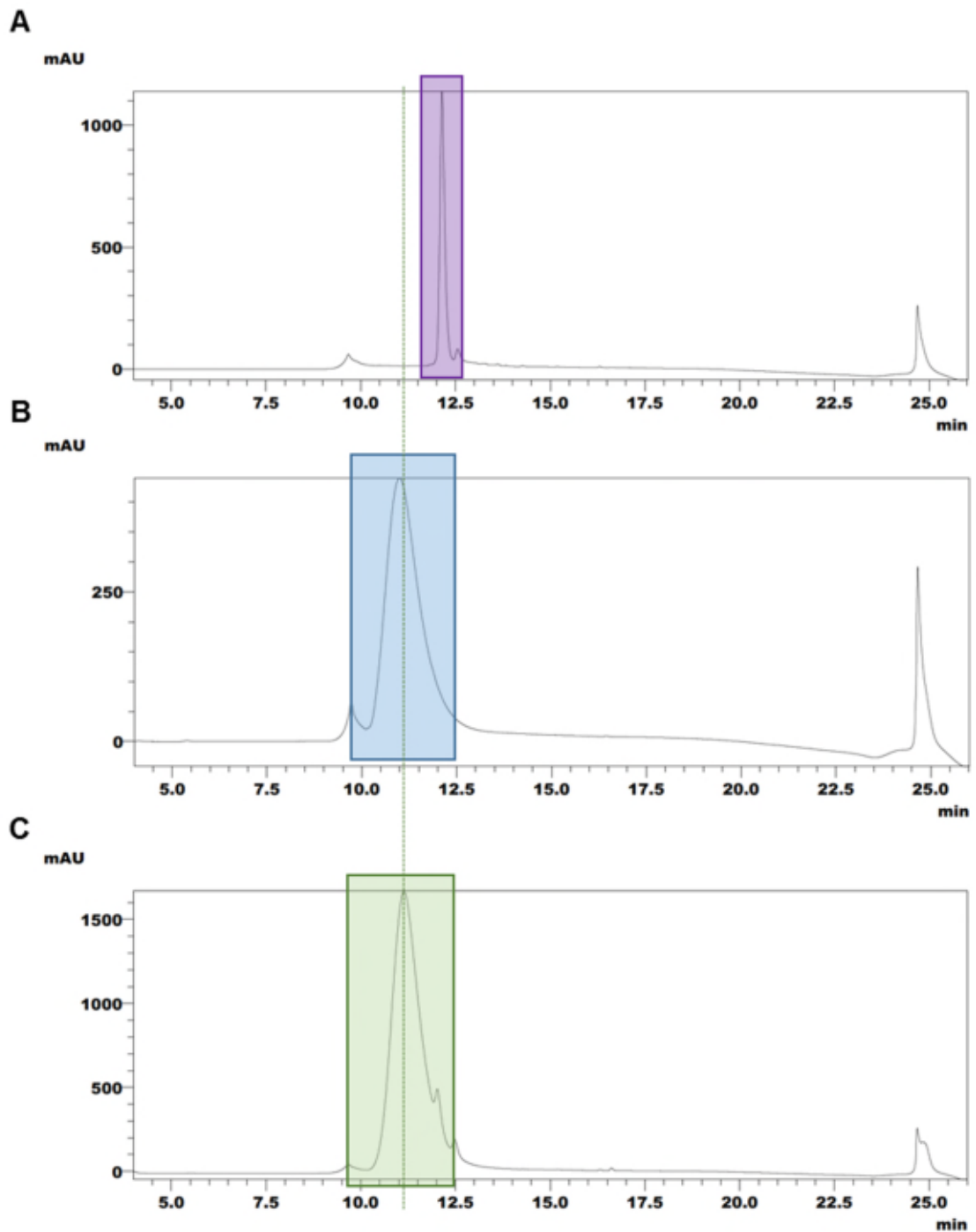


Figure 7.11. Liquid chromatography profiles of (A) **CP6** (c[CDK(H₁₀βA-RBITC)NNNβA]), (B) GalNAc glycopolymer and (C) **CP10** (c[C(GalNAc)DK(H₁₀βA-RBITC)NNNβA]), with the corresponding peak highlighted in boxes. A minor shift in retention time was observed upon conjugation (green dotted line).

7.2.4 Cells

Murine BMDMs were extracted and cultured according to the protocol described in **Section 2.3.6** prior to re-plating into μ -Slide 8 well glass bottom Ibidi chambers in phenol red-free DMEM media containing supplements at approximate cell densities of 5,000-10,000 cells/well for imaging. HEK293 cells (a generous gift from Dr Nicholas Veldhuis, Monash Institute of Pharmaceutical Sciences, Australia) were plated in μ -Slide 8 well glass bottom Ibidi chambers in DMEM media containing 10% (v/v) FBS, penicillin and streptomycin at 37 °C and 5% CO₂. The supplements-containing media were replaced with serum-free DMEM media before incubating with cyclic peptides for imaging.

7.2.5 Confocal laser scanning microscopy

Adherent cells in each well of the Ibidi chambers were incubated with 100 nM cyclic peptide analogues **CP4**, **CP6**, **CP7** or **CP8** for 3, 6, 9 and 18 h at 37 °C in the presence of 5% CO₂. Organelle-specific dyes such as NucBlue[®] Live ReadyProbes[®] (25 μ L, Thermo Fisher) and LysoTracker[®] Green DND-26 (100 nM, Thermo Fisher) for nucleus and late endosome/lysosome, respectively, were added to each well 2 h before imaging for counterstaining. After incubation, wells were washed 3 times with fresh HBSS buffer, pH 7.4, prior imaging using Leica SP8 confocal microscope fitted with sensitive HyD detectors and 12 kHz resonant scanner. All confocal images were taken by Cameron Nowell (Monash Institute of Pharmaceutical Sciences, Australia). All images were processed using Fiji.²²⁷

7.3 Results

7.3.1 Design of analogues for macrophage-targeted delivery studies

As described in **Chapter 5**, the cyclic peptide **CP2** (c[WDINNN β A]) bound to SPSB2 with $K_D \approx 21$ nM and showed high redox stability. Rigid docking of **CP2** onto the iNOS binding site of human SPSB2 (**Figure 7.12A**) suggested that the side chains of both Trp1 and Ile3 were not directly involved in interaction with the binding site as they were both pointing out of the binding site. In contrast, hydrogen bonds were observed between Asp2 (**CP2**) and Tyr120 (SPSB2), Asn4 (**CP2**) and Thr102 (SPSB2), Asn5 (**CP2**) and Gly208 (SPSB2), and Asn6 (**CP2**) and both Arg68 and Val206 (SPSB2), suggesting that only Trp1 and Ile3 can potentially be mutated to other amino acid residues without affecting

the cyclic peptide binding to SPSB2. For selective derivatisation, Trp1 and Ile3 were thus mutated to Cys1 and Lys3, respectively, to yield the first analogue **CP3** (**Figure 7.12B**). When the side chain of Lys3 was derivatised with a fluorophore dye, RBITC, the resulting analogue **CP4** showed no significant steric clashes between the dye moiety and the protein (**Figure 7.12C**). Similarly, the introduction of oligohistidine moiety at the Lys3 position, (**CP5**, **CP6**) as shown in **Figure 7.12D** did not interfere with the binding of the cyclic peptides on the iNOS binding site of SPSB2. Based on these observations, analogues **CP3**, **CP4**, **CP5** and **CP6** were synthesised.

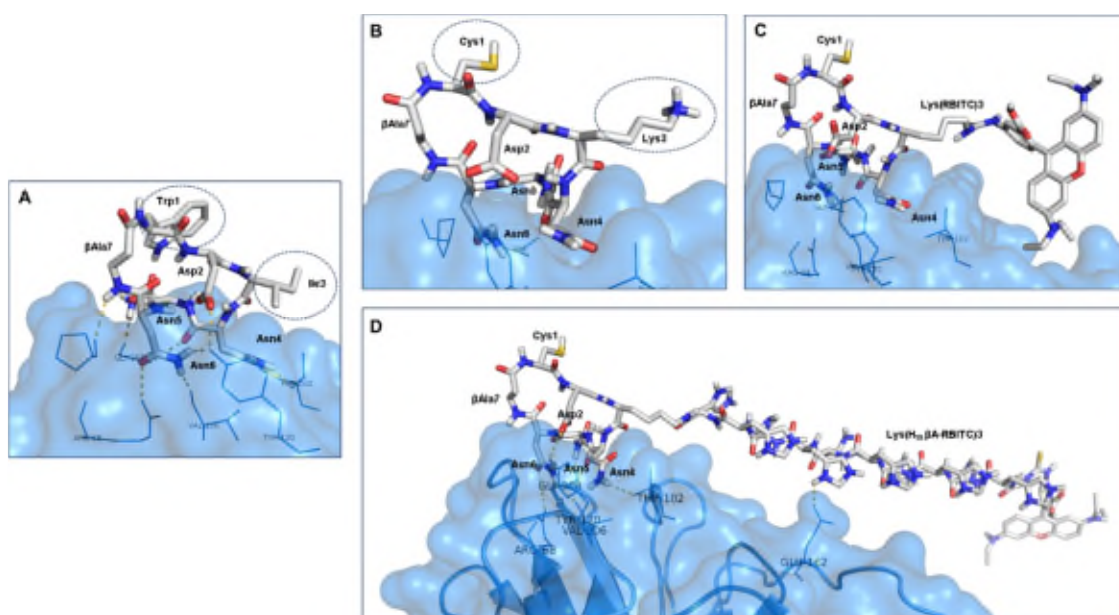


Figure 7.12. The design of analogues for macrophage-targeted delivery studies. (A) Rigid docking of **CP2** on the iNOS binding site of SPSB2 suggested that the side chains of Trp1 and Ile3 were pointing out of the binding site. Mutation of Trp1 with Cys1, and Ile3 with (B) Lys3 (**CP3**), (C) Lys(RBITC)3 (**CP4**) or (D) Lys(H₁₀-βA-RBITC)3 (**CP6**) revealed no significant steric clashes between the substituted moieties and the SPSB2 protein.

7.3.2 CP4, CP5 and CP6 bound to SPSB2 at low nanomolar affinities

When the binding of the synthesised and purified analogues **CP3**, **CP4**, **CP5** and **CP6** to SPSB2 was tested by SPR, an approximately 4-fold drop in affinity was observed for **CP3** compared to **CP2** ($K_D \approx 21$ nM) with measured K_D from 1:1 kinetic model of approximately 89 nM (**Figure 7.13**). On the other hand, **CP4** showed approximately 22-fold and 5-fold improvement over **CP3** and **CP2**, respectively, in its binding to SPSB2

with an estimated K_D of 4 nM (1:1 kinetic model). Although both **CP5** and **CP6** also demonstrated strong binding affinity to SPSB2, with approximate K_D of 17 and 5 nM, respectively, when fitted using a single site 1:1 kinetic model, the fits on the sensorgram were poor with the calculated chi-square values of 2 and 5, respectively (**Figure 7.13C-D, upper panels**), suggesting that the binding kinetics of these analogues on SPSB2 may not be just a simple 1:1. When the same sensorgrams were re-fitted using a steady-state affinity model, modest reductions in binding affinity to SPSB2 were observed, with estimated K_D from steady-state affinity models of 51 and 33 nM, respectively.

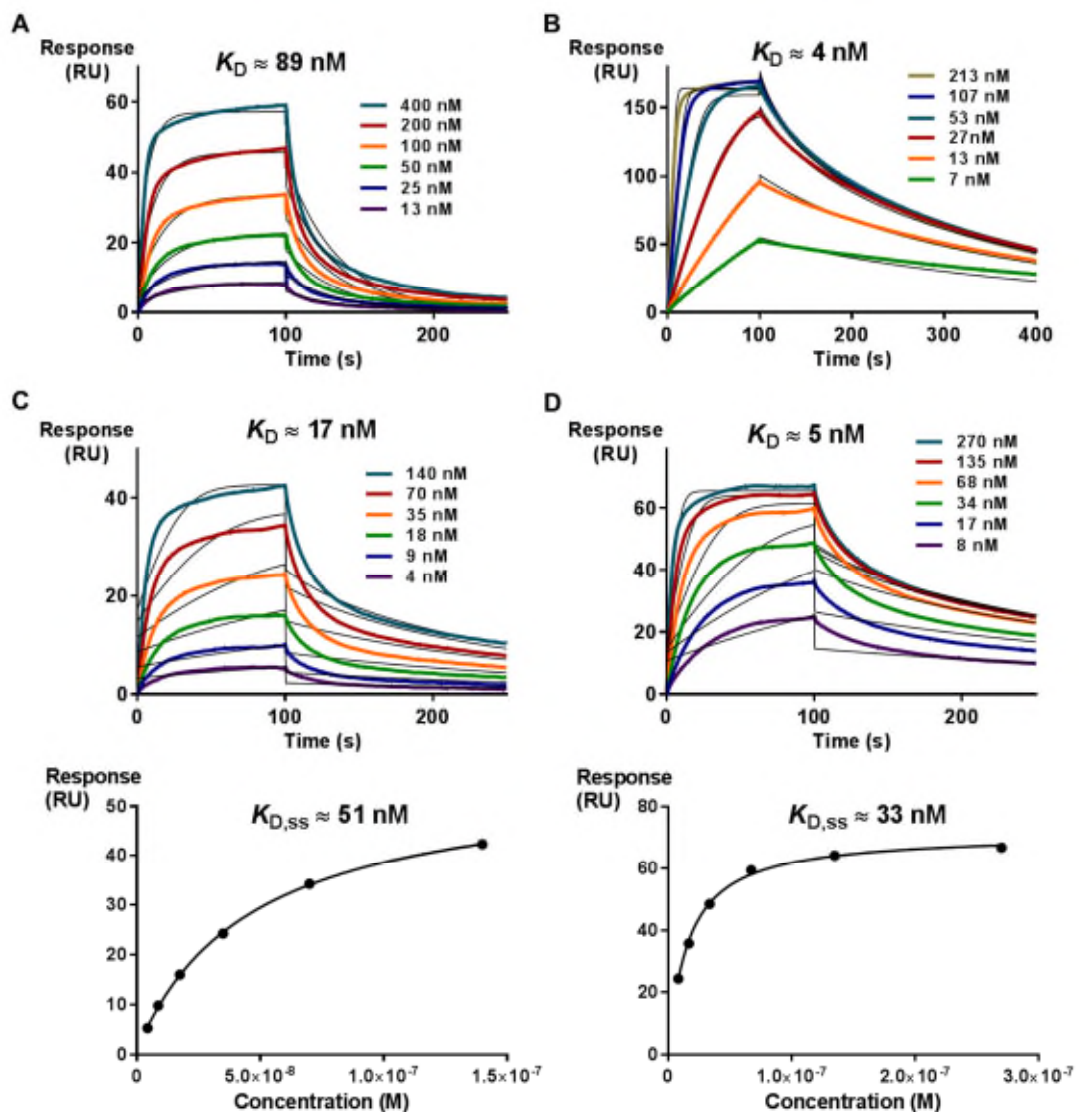


Figure 7.13. Cyclic peptide analogues CP4, CP5 and CP6 bound to SPSB2 at low nanomolar affinities. Representative SPR sensorgrams of immobilised SPSB2 exposed to increasing concentrations of (A) CP3, (B) CP4, (C) CP5 and (D) CP6 in 10 mM

HEPES, 150 mM NaCl, 3 mM EDTA, 0.1 mM TCEP.HCl and 0.05% Tween 20, pH 7.4, at 25 °C. The binding constant, K_D was measured from double-referenced subtracted SPR sensorgrams fitted to a single-site kinetic model. For **CP5** and **CP6**, the steady state binding constant, $K_{D,ss}$ was also measured using a steady-state affinity model (bottom panels).

7.3.3 CP4, CP5 and CP6 bound to the iNOS binding site of SPSB2

To investigate the binding site of the analogues on SPSB2, ^{19}F NMR experiments were carried out on 5-F-Trp SPSB2 according to the protocol by Leung *et al.*¹¹⁶ Typically, when a ligand is bound to the iNOS binding site of SPSB2, a significant ~ 3 ppm downfield shift of the ^{19}F resonance of Trp207 is observed (see example for **CP2** in **Figure 7.14**).

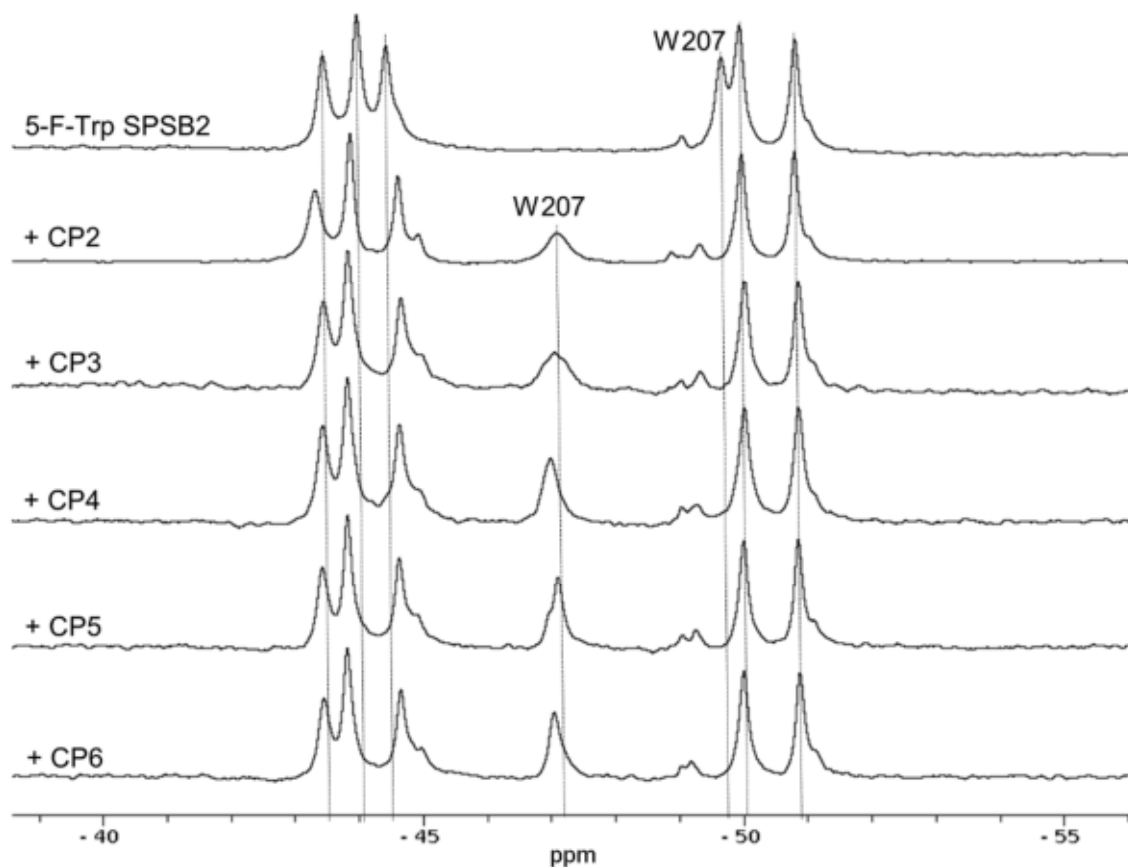


Figure 7.14. Cyclic peptide analogues CP4, CP5 and CP6 bound to the iNOS binding site of SPSB2. ^{19}F NMR spectra of 5-F-Trp SPSB2 in the absence (most upper panel) and the presence of 3-fold cyclic peptide **CP2** and its analogues, **CP3**, **CP4**, **CP5** and

CP6 in 50 mM sodium phosphate buffer, pH 7.4, and 50 mM NaCl at 30 °C. The resonance of the Trp residue closest to the iNOS peptide binding site, W207, is labelled.

When **CP3**, **CP4**, **CP5** and **CP6** were added to the 5-F-Trp SPSB2, significant (2.5 ppm) downfield shifts of the peak corresponding to 5-F-Trp207 were observed (**Figure 7.14**), suggesting that all analogues were bound to the iNOS binding site of SPSB2. The shifted peaks in the presence of **CP4**, **CP5** and **CP6** were much sharper than **CP2** and **CP3**, suggesting that **CP4**, **CP5** and **CP6** were able to stabilise the bound conformation of the iNOS binding site of SPSB2. A slight shoulder in the shifted peak of 5-F-Trp207, however, was observed in the presence of **CP5** suggesting the possibilities of more than one binding species, presumably from different imidazole phosphate salt species of **CP5** (**Figure 7.2C**). The three most downfield peaks (i.e. between -43 and -45 ppm) were also found to be slightly shifted to a similar extent by all analogues, presumably due to secondary effect as previously reported.^{116, 228}

7.3.4 Mannose and GalNAc glycopolymers helped target CP4 to BMDM cells

¹⁹F NMR and SPR showed that **CP4** was able to bind to the iNOS binding site of SPSB2 and at low nanomolar affinity, respectively. Thus, to investigate the role of glycopolymers in targeting cyclic peptide to macrophages, mannose or GalNAc was conjugated to **CP4**. When **CP4**, as well as the mannose and GalNAc-conjugated analogues (i.e. **CP7** and **CP8**, respectively), were incubated with BMDM cells for 3 h, imaging studies by confocal laser scanning microscope revealed that **CP4**, **CP7** and **CP8** were taken up by the macrophages after 3 h of incubation with bright yellow-orange spots (merged colour from red RBITC-conjugated cyclic peptide and green LysoTracker[®] counterstain dyes) observed inside the cells. When the experiments were repeated using human embryonic kidney (HEK293) cells, only **CP4** was internalised into the cells (**Figure 7.15A**), while **CP7** and **CP8** were not observed in the HEK293 cells. Similar results were observed when the cells were incubated with the cyclic peptide analogues for 18 h (**Figure 7.15B**). These observations suggest that both mannose and GalNAc did play some roles in conferring selectivity to the uptake of the rhodamine-conjugated cyclic peptide analogues by macrophages from the non-phagocytes such as HEK cells. The exact mechanism of the uptake of the glycopolymer-conjugated analogues by

macrophages (e.g. *via* receptor-mediated endocytosis or phagocytosis), however, remains to be investigated.

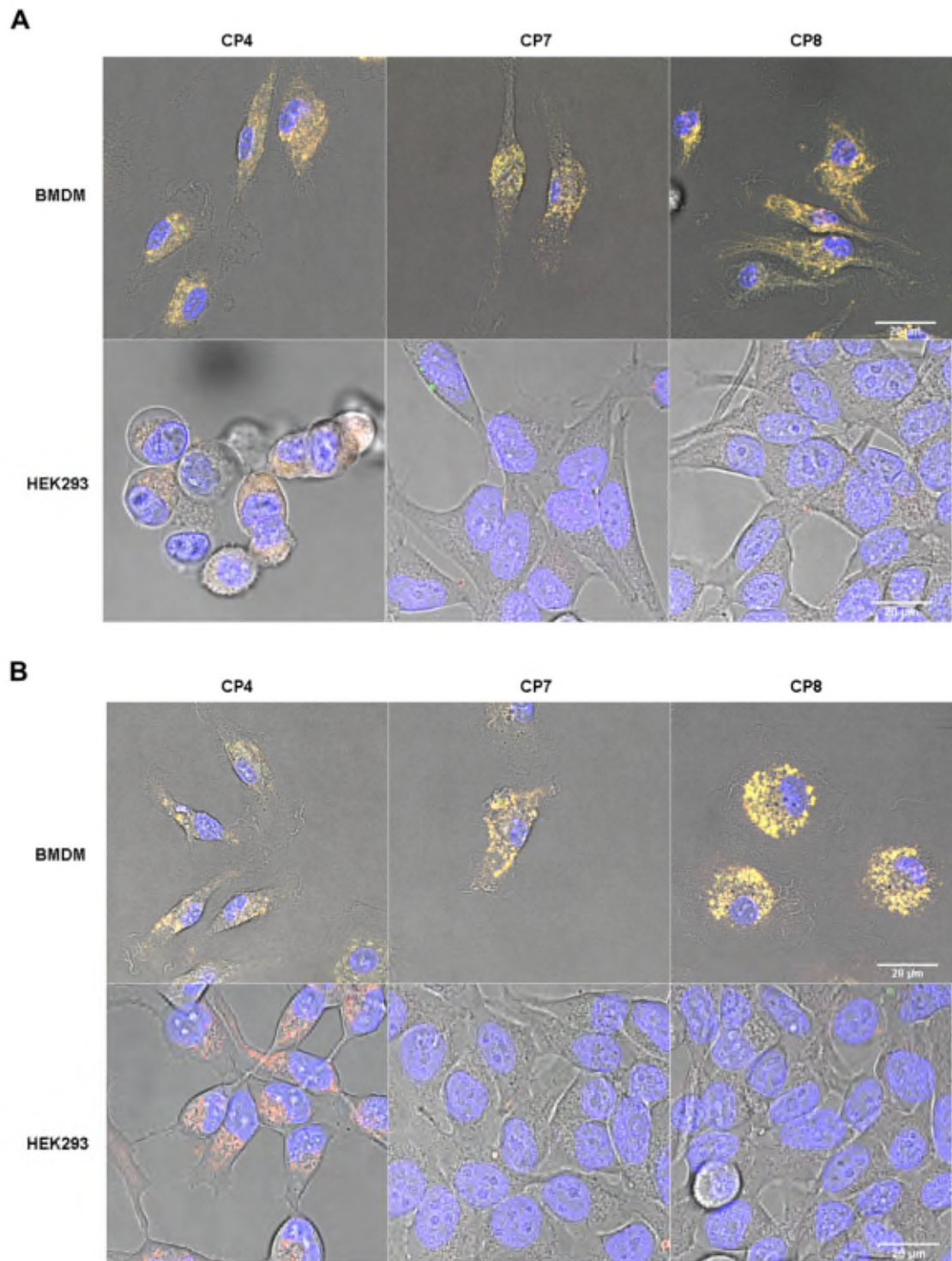


Figure 7.15. Both mannose and GalNAc glycopolymers improved selective uptake of CP4 by BMDM cells. Representative confocal microscopy merged images of cyclic peptide analogues **CP4**, **CP7** and **CP8** (red) and the counterstaining lysosome/endosome

(LysoTracker[®] Green DND-26, green) and nucleus (NucBlue Live, blue) dyes at **(A)** 3 h and **(B)** 18 h of incubation with either the BMDM cells (upper panel) or the HEK293 cells (bottom panel). Scale bars 20 μm .

7.3.5 Oligohistidine facilitates the endosomal escape of CP4 into cytoplasm

When both **CP4** and oligohistidine-conjugated analogue, **CP6** were incubated with macrophages for 3 h, no significant difference between the uptake of **CP4** and **CP6** was observed. Both **CP4** and **CP6** were found to co-localise with counterstain compartment dyes such as LysoTracker[®] Green DND-26 but not the nucleus dye (NucBlue Live) suggesting that both cyclic peptide analogues ended up mostly in the lysosomes or late endosomes (**Figure 7.16A**). Similar observations were made when these analogues were incubated for 6 h with the macrophages. A more diffuse distribution of **CP6**, however, was observed in the macrophages after 9 and 18 h of incubation (compared to a highly punctate distribution of **CP4** during the same period of incubation time), suggesting that **CP6** could have escaped from endosomes or lysosomes into the cytoplasm after 9 h of incubation (**Figure 7.16B**). Further investigation into each channel of the image revealed that the same diffuse distribution of LysoTracker[®] Green in the cells as **CP6** was observed (**Figure 7.17A**). In addition, dark vacuoles were observed in some of these cells, suggesting that they were in necrotic or apoptotic states (**Figure 7.17B**). No signs of endosomal/lysosomal escape and cell necrosis or apoptosis, however, were observed for BMDM cells incubated with the non-oligohistidine-conjugated cyclic peptide **CP4** or mannose or GalNAc-conjugated oligohistidine-based cyclic peptide analogues, **CP9** and **CP10** (**Figure 7.18**).

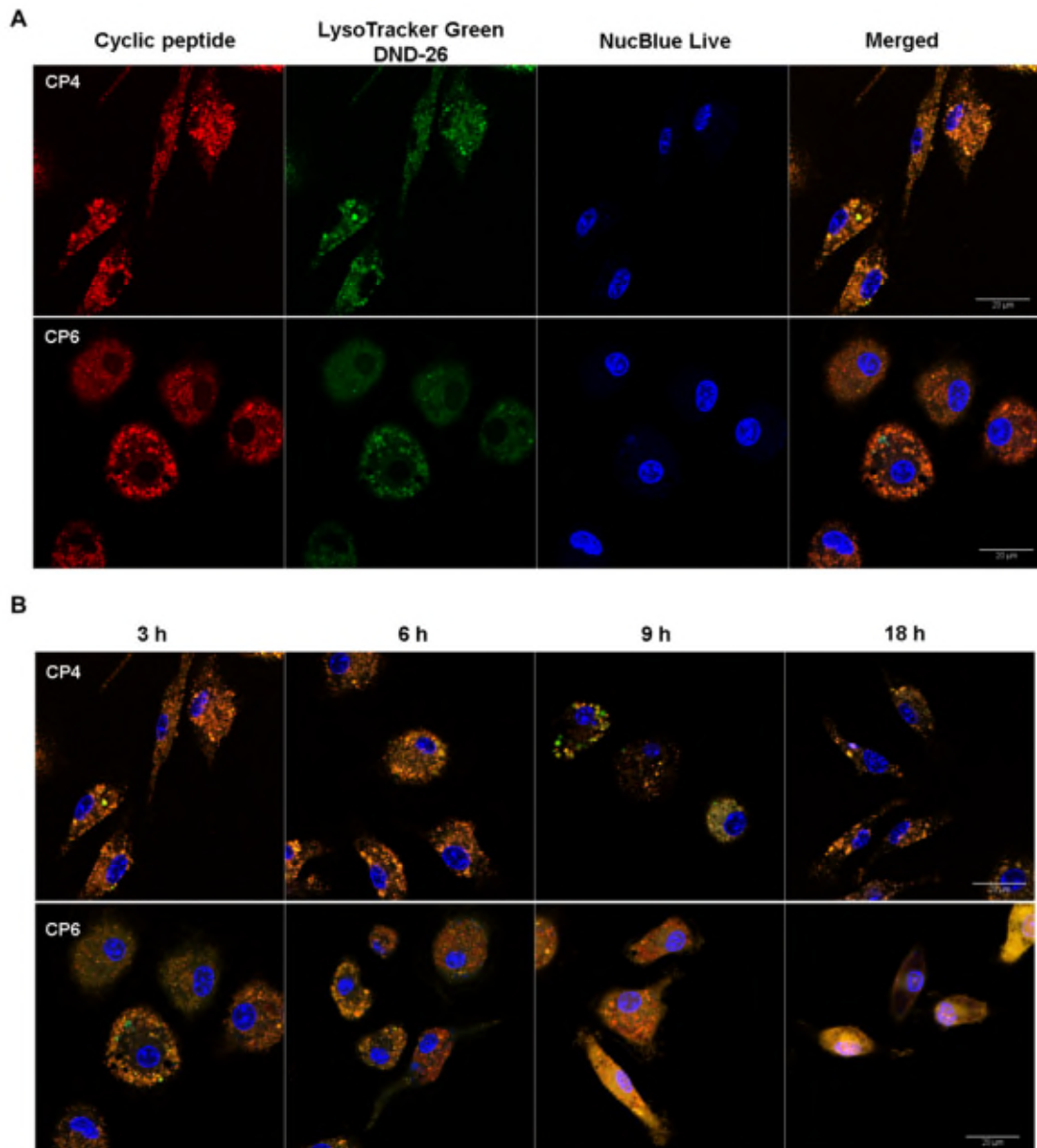


Figure 7.16. Oligohistidine facilitated the endosomal/lysosomal escape of CP4 to the cytoplasm in macrophages. (A) Representative confocal microscopy images of cyclic peptides **CP4** (red, upper panel) and **CP6** (red, bottom panel), and counterstaining lysosome/endosome dye (green), nucleus dye (blue) and the overlap image (most right). All images were taken after 3 h incubation of the cyclic peptides in the culture of BMDM cells in phenol red-free DMEM media with supplements at 37 °C and 5% CO₂ followed by 3 times post-washing with fresh HBSS buffer, pH 7.4. (B) Representative confocal microscopy merged images of cyclic peptide analogues **CP4** (upper panel) and **CP6** (bottom panel) and the counterstaining lysosome/endosome and nucleus dyes at 3, 6, 9 and 18 h of incubation with the BMDM cells. Scale bars 20 μm.

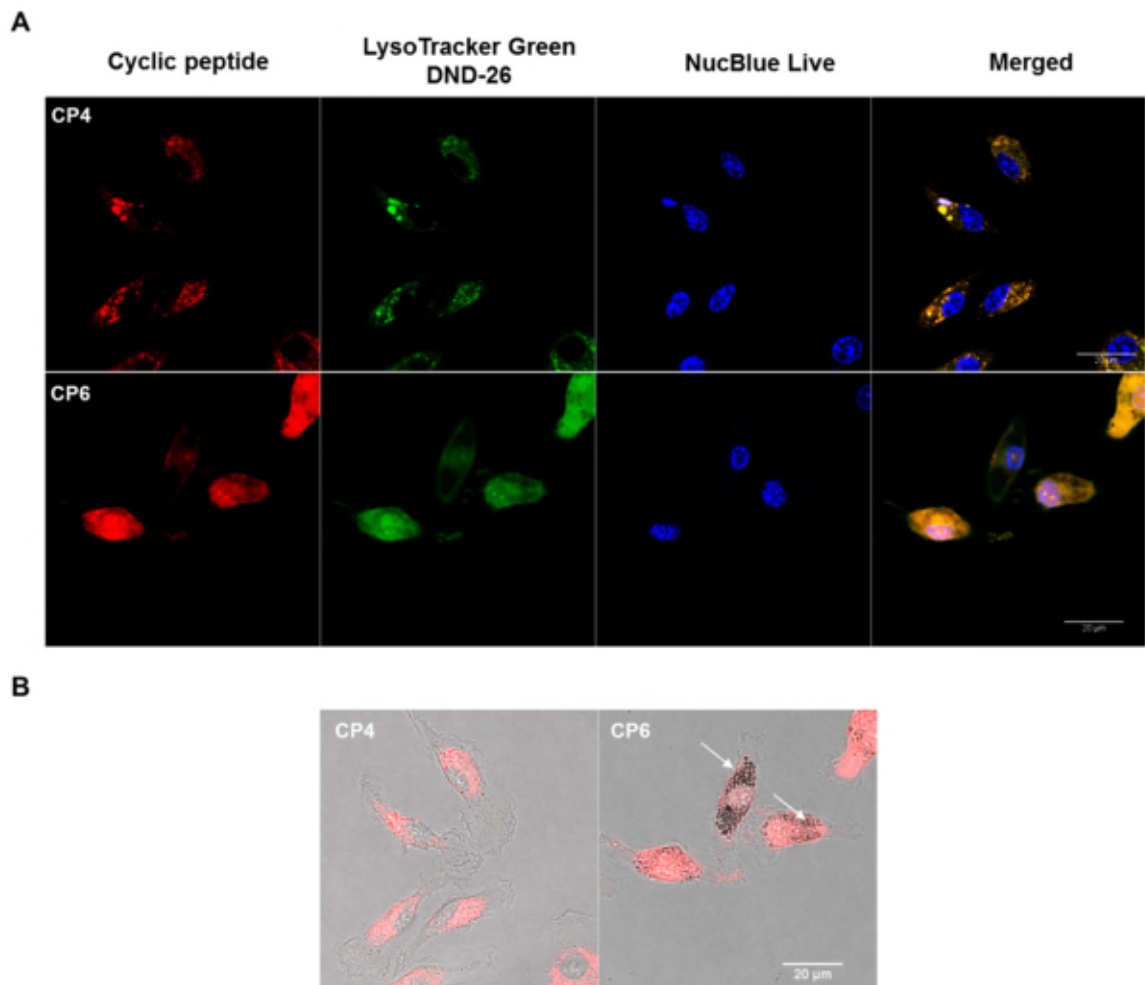


Figure 7.17. (A) Representative confocal microscopy images of cyclic peptides **CP4** (red, upper panel) and **CP6** (red, bottom panel) and counterstaining lysosome/endosome dye (green), nucleus dye (blue) and the overlap image (most right). All images were taken after 18 h incubation of the cyclic peptides in the culture of BMDM cells in phenol red-free DMEM media with supplements at 37 °C and 5% CO₂ followed by 3 times post-washing with fresh HBSS buffer, pH 7.4. (B) The confocal microscopy images of the macrophage cell morphology revealed signs of necrotic or apoptotic states (arrow) in some of the macrophages incubated with **CP6** but not **CP4** after 18 h of incubation. Scale bars 20 μm.

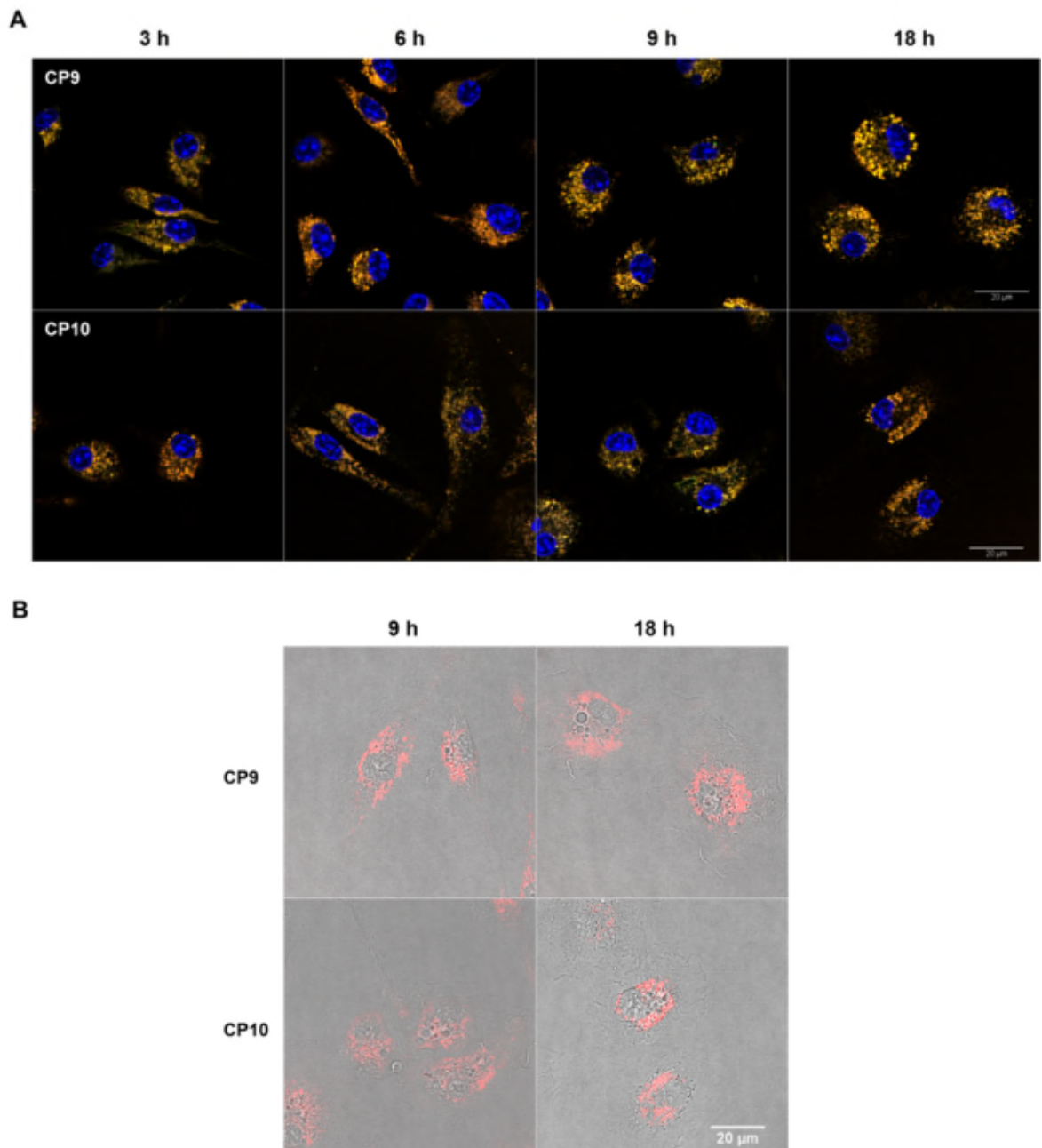


Figure 7.18. (A) Representative confocal microscopy merged images of cyclic peptide analogues, **CP9** and **CP10** and the counterstaining lysosome/endosome and nucleus dyes at 3, 6, 9 and 18 h of incubation with the macrophages. (B) The confocal microscopy images of the macrophage cell morphology revealed no signs of necrotic or apoptotic in the macrophages incubated with either **CP9** or **CP10** after 9 and 18 h of incubation. Scale bars 20 μm .

7.4 Discussion

In the present study, two possible derivatisation sites for the redox-stable cyclic peptide analogue **CP2** were identified. The first and third residues of **CP2** with the peptide sequence of c[WDINNN β A] were found to be amenable to derivatisation, consistent with the observations from *in silico* modelling. To illustrate, when both Trp and Ile were replaced with Cys and Lys, respectively, followed by conjugation of the primary amine of the Lys side chain with either a large lipophilic dye such as RBITC or a 10 histidine-containing moiety, the binding affinity to SPSB2 was not significantly affected, with only a modest 1 to 2-fold drop in affinity for the oligohistidine-conjugated analogues, **CP5** and **CP6** when tested by SPR. In contrast, the RBITC-conjugated analogue **CP4** demonstrated a 5-fold improvement in its binding affinity to SPSB2. All three analogues also showed a much slower dissociation rate than **CP2**, as evidenced by a gradual decline in the SPR response after the peptide was washed out and a sharper shifted peak corresponding to the 5-F-Trp207 of SPSB2 in ^{19}F NMR experiments. The unconjugated analogue **CP3**, with the sequence c[CDKNNN β A], however, demonstrated a 4-fold decrease in its binding affinity to SPSB2, with a slightly broader shifted 5-F-Trp207 peak compared to **CP4-CP6**. These observations clearly suggest that although the third residue of **CP2** is amenable to derivatisation, it favours a bulky or lipophilic moiety such as oligohistidine and RBITC in place of the Ile side chain.

To investigate the role of mannose and GalNAc in macrophage targeting, the most potent RBITC-conjugated analogue **CP4** was conjugated to either mannose or GalNAc glycopolymer *via* the thiol side chain of Cys1 in **CP4** and the reversible thiol-reactive dithiophenol maleimide moiety of the glycopolymers. The use of dithiophenol maleimide as a linker for the cyclic peptide-glycopolymer conjugate was inspired by the recent finding by Collins *et al.*,²²³ who demonstrated the successful release and reformation of native oxytocin from the oxytocin-polymer conjugate coupled through the same dithiophenol maleimide moiety when a physiological concentration of glutathione (GSH) of 6 mM was added to the oxytocin-polymer conjugate solution. As such, it is anticipated that cyclic peptide **CP4** (or other related analogues such as **CP6**) would be released from the glycopolymer conjugate when exposed to the reducing environment in the cytoplasm of the macrophage cell.

When the cyclic peptide-glycopolymer conjugates were incubated with both BMDM and HEK293 cells, confocal imaging showed that both mannose and GalNAc glycopolymer-conjugated cyclic peptides **CP7** and **CP8** were selectively taken up by the macrophages but not the HEK cells. In contrast, the unconjugated analogue **CP4** was taken up by both the macrophages and the HEK cells. These observations suggest that both glycopolymers played some roles in targeting the cyclic peptide to macrophages. It is hypothesised that the lack of uptake of glycopolymer-conjugated cyclic peptides by the HEK cells could be due to: (1) the large size of the glycopolymers (14-38 kDa) for mannose and GalNAc glycopolymers, respectively, compared to only 1.2 kDa for **CP4**, rendering the glycopolymer-conjugated cyclic peptides practically impossible to be taken up just by passive diffusion across the cell membrane of the HEK cells. Although **CP4** also violates the Lipinski's rule of five²¹⁶ (a common guideline used to predict the membrane permeability of a compound by passive diffusion), the high lipophilicity of the rhodamine B moiety in **CP4** could have contributed to its uptake by the HEK cells. A similar observation has been reported for non-polar cyclosporin A with a similar molecular mass of 1203 Da.^{229, 230} (2) Secondly, HEK cells are non-phagocytic cells, and therefore are not able to internalise the glycopolymer-conjugated cyclic peptides *via* phagocytosis like phagocytic cells such as macrophages can. Macrophages have been reported to possess the ability to take up any particles with a diameter from 0.5 to 10 μm .²³¹ (3) Lastly, HEK cells do not have mannose or MGL receptors on the cell surface to mediate the internalisation of the glycopolymer-conjugated cyclic peptides into the cell. These observations are in agreement with the previous findings by Fernandez *et al.*,²³² who also found that the FITC-conjugated, mannosylated BSA was readily taken up by monocyte-derived macrophages but not HEK cells. Although both glycopolymers were shown to help target the rhodamine-based cyclic peptide to macrophages, it is, however, still unclear at this point (1) if the uptake of the glycopolymer-conjugated cyclic peptides by the macrophages is through phagocytosis or receptor-mediated endocytosis or both, and (2) if there is any selectivity in their uptake between different phagocytic cells. Thus, more work to investigate the uptake mechanism and its selectivity is warranted.

We also attempted to investigate if a 10-residue oligohistidine was able to facilitate endosomal escape of the cyclic peptide into the cytoplasm of macrophages, where SPSB2 is known to be expressed. When the oligohistidine-based analogue **CP6** was incubated

with the BMDM, some signs of cyclic peptide escape from endosome/lysosome to the cytoplasm was observed after 9 and 18 h of incubation by confocal imaging, with some distinctive hazy, less punctate fluorescence being observed, consistent with the previous observations by Potocky *et al.*²³³ Similarly, the same diffuse distribution of LysoTracker[®] Green as **CP6** was also observed in these cells. Protonation of oligohistidine in the acidic environment of the late endosomes/lysosomes could have resulted in the “proton sponge effect”, causing the endosome or lysosome membrane to become leaky,^{166, 234} thus enabling release of the protonated oligohistidine-conjugated cyclic peptide into the cytoplasm. The subsequent release of protons from the protonated-oligohistidine in the cytoplasm (due to differences in pH) transiently lowers the pH of the cytoplasm and ultimately resulted in the co-staining of cytoplasm with the LysoTracker[®] Green. Further investigation into the morphology of the cells revealed that some of these cells were necrotic or apoptotic (as evidenced by dark vacuoles in the cell),²³⁵ suggesting that cytosolic acidification must have taken place and triggered cell apoptosis or necrosis events.²³⁶ Comparison with the same type of cells incubated with the non-oligohistidine-conjugated cyclic peptide **CP4** for the same period of time revealed no signs of cell necrosis or apoptosis. No signs of endosomal/lysosomal escape or cell necrosis or apoptosis, however, were observed for BMDM cells incubated with the mannose or GalNAc-conjugated oligohistidine-based cyclic peptide analogues **CP9** and **CP10**, suggesting that the large moiety of mannose or GalNAc glycopolymer would have either disrupted the oligohistidine’s ability to destabilise the endosomal/lysosomal membrane of the macrophage or affected the transport of the glycopolymer-conjugated cyclic peptide across the leaky membrane of endosome to the cytoplasm of the cells. The exact mechanism of this disruption, however, remains to be confirmed.

7.5 Conclusions

In summary, eight analogues of the redox-stable, potent cyclic peptide **CP2**, were generated. Substitution of the side chain of Ile3 of **CP2** with highly bulky or lipophilic groups such as oligohistidine and rhodamine B did not significantly affect their binding to the iNOS binding site of SPSB2. The present findings also demonstrated that Trp1 of **CP2** can be mutated to Cys1 and be further conjugated to glycopolymers for macrophage-targeted delivery studies. Both mannose and GalNAc glycopolymers were also shown to facilitate selective targeting of rhodamine-based cyclic peptide **CP4** to macrophages.

Although oligohistidine-based cyclic peptide **CP6** was found to escape endosomes/lysosomes after 9 and 18 h of incubation with macrophage, simultaneous cell necrosis was observed in some of the cells, suggesting the need for other safer endosomal escape machinery or mechanism in the future. In addition, the lack of endosomal escape for glycopolymer-conjugated oligohistidine-based cyclic peptides suggests the need for a linker joining the glycopolymer and cyclic peptide that is cleavable in acidic environments in endosomes or lysosomes.

CHAPTER 8

Conclusions and future work

The work in this thesis has successfully identified a number of potent inhibitors of the SPSB2-iNOS interaction. Although initial attempts to discover small molecule inhibitors of SPSB2-iNOS interaction *via in silico* and NMR-guided FBDD did not result in promising lead compounds (as only two potential fragment hits were identified, one of which bound promiscuously to SPSB2, and the other very weakly), the poor outcome led us to reinvestigate the druggability of the iNOS binding site on SPSB2 by SiteMap and FTMap. Clearly, the iNOS binding site was found to be less suitable for binding by drug-like small molecule inhibitors, which ultimately led us to opt for alternative strategies to target the iNOS binding site of SPSB2.

The shift in direction was indeed a rewarding one. Using rational design, a highly potent disulphide-bridged cyclic peptide inhibitor of SPSB2-iNOS interaction with the sequence Ac-c[CVDINNNC]-NH₂ (**CP0**) and a K_D of 4-6 nM was generated, in which the Val residue of the cyclic peptide was found to be highly amenable to derivatisation. To illustrate, replacement of Val with Lys (**Figure AI.1, Appendix I**) or N^α-methylated Val (**Figure AI.3, Appendix I**) did not significantly affect their binding to SPSB2, with measured K_D values of 6 and 3 nM, respectively. The cyclic peptide **CP0** was also found to be highly stable against pepsin, trypsin and α -chymotrypsin, as well as in human plasma. The cyclic peptide, however, is reduction sensitive, suggesting that it may be less effective in the reducing environment of the cytoplasm of macrophages.

To improve redox stability, two cyclic peptides **CP1** and **CP2**, and four cyclic peptidomimetics **M1**, **M2**, **M3** and **M4** were generated. Three analogues **CP1**, **CP2** and **M1** were able to produce at least an order of magnitude improvement in affinities to the iNOS binding site of SPSB2 compared to the linear peptide DINNN, with K_D values ranging from 21 to 31 nM. Although they have 3 to 5-fold weaker affinities for SPSB2 than the disulphide-bridged cyclic peptide, they were able to maintain their ability to displace full-length iNOS from SPSB2 in macrophage cell lysates. As **CP2** is more redox-stable than **CP1**, has more sites for derivatisation than **M1**, and is much easier to synthesise, **CP2** (c[WDINNN β A]) was used as a template to generate analogues for macrophage targeting.

To investigate possible sites for derivatisation in **CP2** for macrophage targeting and endosomal escape with glycopolymers and oligohistidine, respectively, eight analogues

of **CP2** were generated (**CP3-CP10**). SPR and ^{19}F NMR results confirmed that residues Trp1 and Ile3 can be replaced with Cys1 and Lys3, respectively, without significantly affecting their binding to SPSB2, although substitution at the Lys3 position favours bulky, non-polar derivatives such as rhodamine B and oligohistidine moieties. Similar observation was observed when the same position (i.e. between the Asp and the first Asn residue in the sequence) was replaced by a bulky, non-polar acridone (Acd) moiety in mimetic **M1**, in which no significant changes in affinity was observed upon substitution ($K_D \approx 34$ nM versus K_D of 29 nM in **M1** by SPR) (**Figure AI.7, Appendix I**). Similarly, Trp1, the first amino acid residue of **CP2**, preceding the Asp residue, was also found to allow substitution by 5-hydroxytryptophan and Acd (**Figure AI.5-AI.6, Appendix I**) with SPR-measured K_D values of 8-10 nM (**CP2**, $K_D \approx 21$ nM). These observations suggest that the first and third positions of **CP2** can be substituted without compromising their binding to SPSB2.

Preliminary cell uptake results shown in **Chapter 7** suggest that both mannose and GalNAc glycopolymers are able to help confer selectivity in the uptake of RBITC-conjugated cyclic peptide **CP4** by macrophages, although the exact mechanism involved in their uptake by BMDMs (i.e. *via* receptor-mediated endocytosis or phagocytosis) remains to be investigated. While the determination of the mechanism of uptake may not be crucial in this study, it can be conveniently carried out *via* the addition of a competitive receptor-specific endocytosis inhibitor to cultures of macrophages prior to incubation with the cyclic peptides. This may include mannose receptor inhibitors such as mannan, *D*-mannose, EDTA or soluble mannose binding lectin,²³⁷ or the MGL receptor inhibitors such as asialofetuin²³⁸ or GalNAc- α -O-methyl glycoside.²³⁹ To distinguish phagocytosis from receptor-mediated endocytosis, highly selective phagocytosis inhibitors such as cytochalasin D, staurosporine or cerulenine can be used.²⁴⁰

Oligohistidine was also found to facilitate the endosomal escape of cyclic peptide **CP6** into the cytoplasm of BMDMs, although a coincident cell apoptosis or necrosis was observed. This finding suggests that a less invasive approach for endosomal escape (as described in **Chapter 1**) may be needed in the future. In addition, mannose or GalNAc-conjugated oligohistidine-coupled cyclic peptides (**CP9**, **CP10**) did not show signs of endosomal escape, suggesting that the large glycopolymers, with an average molecular mass of 14 to 38 kDa may have either interfered with the ability of the oligohistidine to

disrupt the endosomal membrane, or the glycopolymer-conjugated cyclic peptides may be too large to penetrate through the leaky membrane of endosomes to the cytoplasm of the macrophages. Either way, this observation clearly suggests the need for a linker connecting the cyclic peptide and the glycopolymer that is cleavable in the endosome for efficient delivery of the cyclic peptide into the cytoplasm of macrophages. Such a linker may include a peptide sequence that acts as a substrate for cleavage by endosome or lysosome-specific proteases such as cathepsin D and cathepsin E,²⁴¹ or an acid-sensitive linker such as maleic acid amide.²⁴²

One possible limitation of this study is the sole use of confocal imaging to detect the endosomal escape of the cyclic peptide into the cytoplasm of macrophages. Furthermore, it is not known if the endosomal escape efficiency of the oligohistidine-conjugated cyclic peptide can be translated to its whole-cell inhibition ability. Thus, other approaches to monitoring the downstream effect of the cyclic peptide escape from the endosome into the cytoplasm should be used to complement the confocal imaging. This may include macrophage inhibition assays, in which changes in the level of iNOS in the cell upon inhibition by cyclic peptides are monitored (e.g. by Western Blots). In addition to the macrophage inhibition assays, cell viability assays such as MTT assays²⁴³ should also be carried out to assess cytotoxicity effect of other selected endosomal escape agent in the future.

A mechanical approach could also be used to deliver the cyclic peptide and peptidomimetic inhibitors into macrophages, without involving endocytosis, thereby avoiding the problem of endosomal escape. An example of this includes the electroporation technique, which involves the application of an external electrical field to transiently create nanoscale pores in the plasma membrane²⁴⁴ and thus increase the permeability of the cell membrane. Electroporation has been shown to effectively deliver siRNA into bone marrow-derived macrophages without causing cell toxicity or altering the macrophage biology.²⁴⁵ Recently, electroporation delivery has also been found to significantly increase the bioavailability of a cyclic-penetrating peptide-peptide nucleic acid conjugates in macrophages and thus improved the killing of *Salmonella enterica* serovar *Typhimurium* LT2 inside macrophages by up to a factor of 9 compared to experiments without electroporation.²⁴⁶ Although it is not known if this approach may be applied therapeutically to deliver the compounds into macrophages in real patients, it may

offer a quick answer to the current remaining question in this thesis: will the potent cyclic peptide and peptidomimetic inhibitors of SPSB2-iNOS interaction generated in this thesis be able to act as anti-infectives? If this approach is as powerful as it claims, the inhibitor-containing macrophages (upon electroporation) can then be infected with pathogens such as *M. tuberculosis* or *L. major* parasites and the mean number of pathogens per infected cell in the absence and the presence of the inhibitor after a specified time can then be evaluated and compared. The role of this class of inhibitors as anti-infective agents can then be confirmed.

In summary, the findings from the studies presented in this thesis not only provide various potent and stable cyclic peptide and peptidomimetic inhibitors of SPSB2-iNOS interaction but also demonstrate the potential of this class of analogue to be targeted to macrophages and delivered into the cell cytoplasm. This study thus provides an important platform for future development of these inhibitors into a new class of anti-infective drugs.

CHAPTER 9

References

- (1) WHO. (2014) Antimicrobial resistance: global report on surveillance, pp 1-257.
- (2) Reardon, S. (2014) Antibiotic resistance sweeping developing world, *Nature* 509, 141-142.
- (3) Llor, C., and Bjerrum, L. (2014) Antimicrobial resistance: risk associated with antibiotic overuse and initiatives to reduce the problem, *Ther. Adv. Drug Saf.* 5, 229-241.
- (4) Rice, L. B. (2008) Federal funding for the study of antimicrobial resistance in nosocomial pathogens: no ESKAPE, *J. Infect. Dis.* 197, 1079-1081.
- (5) Yong, D., Toleman, M. A., Giske, C. G., Cho, H. S., Sundman, K., Lee, K., and Walsh, T. R. (2009) Characterization of a new metallo- β -lactamase gene, bla(NDM-1), and a novel erythromycin esterase gene carried on a unique genetic structure in *Klebsiella pneumoniae* sequence type 14 from India, *Antimicrob. Agents Chemother.* 53, 5046-5054.
- (6) Johnson, A. P., and Woodford, N. (2013) Global spread of antibiotic resistance: the example of New Delhi metallo- β -lactamase (NDM)-mediated carbapenem resistance, *J. Med. Microbiol.* 62, 499-513.
- (7) Liu, Y. Y., Wang, Y., Walsh, T. R., Yi, L. X., Zhang, R., Spencer, J., Doi, Y., Tian, G., Dong, B., Huang, X., Yu, L. F., Gu, D., Ren, H., Chen, X., Lv, L., He, D., Zhou, H., Liang, Z., Liu, J. H., and Shen, J. (2016) Emergence of plasmid-mediated colistin resistance mechanism MCR-1 in animals and human beings in China: a microbiological and molecular biological study, *Lancet Infect. Dis.* 16, 161-168.
- (8) Hasman, H., Hammerum, A. M., Hansen, F., Hendriksen, R. S., Olesen, B., Agerso, Y., Zankari, E., Leekitcharoenphon, P., Stegger, M., Kaas, R. S., Cavaco, L. M., Hansen, D. S., Aarestrup, F. M., and Skov, R. L. (2015) Detection of mcr-1 encoding plasmid-mediated colistin-resistant *Escherichia coli* isolates from human bloodstream infection and imported chicken meat, Denmark 2015, *Euro Surveill.* 20.
- (9) Falagas, M. E., and Kasiakou, S. K. (2005) Colistin: the revival of polymyxins for the management of multidrug-resistant gram-negative bacterial infections, *Clin. Infect. Dis.* 40, 1333-1341.

- (10) Telenti, A., Imboden, P., Marchesi, F., Matter, L., Schopfer, K., Bodmer, T., Lowrie, D., Colston, M. J., and Cole, S. Detection of rifampicin-resistance mutations in *Mycobacterium tuberculosis*, *The Lancet* 341, 647-651.
- (11) Zhang, Y., Heym, B., Allen, B., Young, D., and Cole, S. (1992) The catalase-peroxidase gene and isoniazid resistance of *Mycobacterium tuberculosis*, *Nature* 358, 591-593.
- (12) Banerjee, A., Dubnau, E., Quemard, A., Balasubramanian, V., Um, K. S., Wilson, T., Collins, D., de Lisle, G., and Jacobs, W. R., Jr. (1994) inhA, a gene encoding a target for isoniazid and ethionamide in *Mycobacterium tuberculosis*, *Science* 263, 227-230.
- (13) WHO. (2015) Global action plan on antimicrobial resistance.
- (14) Zappia, G., Menendez, P., Monache, G. D., Misiti, D., Nevola, L., and Botta, B. (2007) The contribution of oxazolidinone frame to the biological activity of pharmaceutical drugs and natural products, *Mini Rev. Med. Chem.* 7, 389-409.
- (15) Fenton, C., Keating, G. M., and Curran, M. P. (2004) Daptomycin, *Drugs* 64, 445-455.
- (16) Power, E. (2006) Impact of antibiotic restrictions: the pharmaceutical perspective, *Clin. Microbiol. Infect.* 12, 25-34.
- (17) Page, M. G., and Bush, K. (2014) Discovery and development of new antibacterial agents targeting Gram-negative bacteria in the era of pandrug resistance: is the future promising?, *Curr. Opin. Pharmacol.* 18, 91-97.
- (18) Boucher, H. W., Talbot, G. H., Bradley, J. S., Edwards, J. E., Gilbert, D., Rice, L. B., Scheld, M., Spellberg, B., and Bartlett, J. (2009) Bad bugs, no drugs: no ESKAPE! An update from the Infectious Diseases Society of America, *Clin. Infect. Dis.* 48, 1-12.
- (19) Coates, A. R., and Halls, G. (2012) Antibiotics in phase II and III clinical trials, *Handb. Exp. Pharmacol.*, 167-183.
- (20) Gopal, P., and Dick, T. (2015) The new tuberculosis drug Perchlozone® shows cross-resistance with thiacetazone, *Int. J. Antimicrob. Agents* 45, 430-433.
- (21) Nikaido, H. (2009) Multidrug resistance in bacteria, *Annu. Rev. Biochem.* 78, 119-146.

-
- (22) Blair, J. M. A., Webber, M. A., Baylay, A. J., Ogbolu, D. O., and Piddock, L. J. V. (2015) Molecular mechanisms of antibiotic resistance, *Nat. Rev. Micro.* 13, 42-51.
- (23) Lewis, K. (2010) Persister cells, *Annu. Rev. Microbiol.* 64, 357-372.
- (24) Lewis, K. (2005) Persister cells and the riddle of biofilm survival, *Biochem. (Mosc.)* 70, 267-274.
- (25) Levin, B. R., and Rozen, D. E. (2006) Non-inherited antibiotic resistance, *Nat. Rev. Microbiol.* 4, 556-562.
- (26) Mulcahy, L. R., Burns, J. L., Lory, S., and Lewis, K. (2010) Emergence of *Pseudomonas aeruginosa* strains producing high levels of persister cells in patients with cystic fibrosis, *J. Bacteriol.* 192, 6191-6199.
- (27) LaFleur, M. D., Kumamoto, C. A., and Lewis, K. (2006) *Candida albicans* biofilms produce antifungal-tolerant persister cells, *Antimicrob. Agents Chemother.* 50, 3839-3846.
- (28) Keren, I., Shah, D., Spoering, A., Kaldalu, N., and Lewis, K. (2004) Specialized persister cells and the mechanism of multidrug tolerance in *Escherichia coli*, *J. Bacteriol.* 186, 8172-8180.
- (29) Pandey, D. P., and Gerdes, K. (2005) Toxin-antitoxin loci are highly abundant in free-living but lost from host-associated prokaryotes, *Nuc. Acids Res.* 33, 966-976.
- (30) Laxminarayan, R., Duse, A., Wattal, C., Zaidi, A. K. M., Wertheim, H. F. L., Sumpradit, N., Vlieghe, E., Hara, G. L., Gould, I. M., Goossens, H., Greko, C., So, A. D., Bigdeli, M., Tomson, G., Woodhouse, W., Ombaka, E., Peralta, A. Q., Qamar, F. N., Mir, F., Kariuki, S., Bhutta, Z. A., Coates, A., Bergstrom, R., Wright, G. D., Brown, E. D., and Cars, O. (2013) Antibiotic resistance—the need for global solutions, *Lancet Infect. Dis.* 13, 1057-1098.
- (31) Gill, E. E., Franco, O. L., and Hancock, R. E. (2015) Antibiotic adjuvants: diverse strategies for controlling drug-resistant pathogens, *Chem. Biol. Drug Des.* 85, 56-78.
- (32) Chakravorty, D., and Hensel, M. (2003) Inducible nitric oxide synthase and control of intracellular bacterial pathogens, *Microbes. Infect.* 5, 621-627.
- (33) Khan, S. A., Strijbos, P. J., Everest, P., Moss, D., Stratford, R., Mastroeni, P., Allen, J., Servos, S., Charles, I. G., Dougan, G., and Maskell, D. J. (2001) Early

- responses to *Salmonella typhimurium* infection in mice occur at focal lesions in infected organs, *Microb. Pathog.* 30, 29-38.
- (34) Chan, E. D., Chan, J., and Schluger, N. W. (2001) What is the role of nitric oxide in murine and human host defense against tuberculosis? Current knowledge, *Am. J. Respir. Cell Mol. Biol.* 25, 606-612.
- (35) Stenger, S., Donhauser, N., Thüring, H., Röllinghoff, M., and Bogdan, C. (1996) Reactivation of latent leishmaniasis by inhibition of inducible nitric oxide synthase, *J. Exp. Med.* 183, 1501-1514.
- (36) Scharton-Kersten, T. M., Yap, G., Magram, J., and Sher, A. (1997) Inducible nitric oxide is essential for host control of persistent but not acute infection with the intracellular pathogen *Toxoplasma gondii*, *J. Exp. Med.* 185, 1261-1274.
- (37) Barraud, N., Hassett, D. J., Hwang, S. H., Rice, S. A., Kjelleberg, S., and Webb, J. S. (2006) Involvement of nitric oxide in biofilm dispersal of *Pseudomonas aeruginosa*, *J. Bacteriol.* 188, 7344-7353.
- (38) Barraud, N., Kelso, M. J., Rice, S. A., and Kjelleberg, S. (2015) Nitric oxide: a key mediator of biofilm dispersal with applications in infectious diseases, *Curr. Pharm. Des.* 21, 31-42.
- (39) Kuang, Z., Lewis, R. S., Curtis, J. M., Zhan, Y., Saunders, B. M., Babon, J. J., Kolesnik, T. B., Low, A., Masters, S. L., Willson, T. A., Kedzierski, L., Yao, S., Handman, E., Norton, R. S., and Nicholson, S. E. (2010) The SPRY domain-containing SOCS box protein SPSB2 targets iNOS for proteasomal degradation, *J. Cell Biol.* 190, 129-141.
- (40) Pautz, A., Art, J., Hahn, S., Nowag, S., Voss, C., and Kleinert, H. (2010) Regulation of the expression of inducible nitric oxide synthase, *Nitric Oxide* 23, 75-93.
- (41) Kolodziejska, K. E., Burns, A. R., Moore, R. H., Stenoien, D. L., and Eissa, N. T. (2005) Regulation of inducible nitric oxide synthase by aggresome formation, *Proc. Natl. Acad. Sci. U S A* 102, 4854-4859.
- (42) Pandit, L., Kolodziejska, K. E., Zeng, S., and Eissa, N. T. (2009) The physiologic aggresome mediates cellular inactivation of iNOS, *Proc. Natl. Acad. Sci. U S A* 106, 1211-1215.

- (43) Wang, T., and Xia, Y. (2012) Inducible nitric oxide synthase aggresome formation is mediated by nitric oxide, *Biochem. Biophys. Res. Commun.* 426, 386-389.
- (44) Musial, A., and Eissa, N. T. (2001) Inducible nitric-oxide synthase is regulated by the proteasome degradation pathway, *J. Biol. Chem.* 276, 24268-24273.
- (45) Sha, Y., Pandit, L., Zeng, S., and Eissa, N. T. (2009) A critical role for CHIP in the aggresome pathway, *Mol. Cell. Biol.* 29, 116-128.
- (46) Chen, L., Kong, X., Fu, J., Xu, Y., Fang, S., Hua, P., Luo, L., and Yin, Z. (2009) CHIP facilitates ubiquitination of inducible nitric oxide synthase and promotes its proteasomal degradation, *Cell. Immunol.* 258, 38-43.
- (47) Kolodziejcki, P. J., Musial, A., Koo, J. S., and Eissa, N. T. (2002) Ubiquitination of inducible nitric oxide synthase is required for its degradation, *Proc. Natl. Acad. Sci. U S A* 99, 12315-12320.
- (48) Matsumoto, K., Nishiya, T., Maekawa, S., Horinouchi, T., Ogasawara, K., Uehara, T., and Miwa, S. (2011) The ECS(SPSB) E3 ubiquitin ligase is the master regulator of the lifetime of inducible nitric-oxide synthase, *Biochem. Biophys. Res. Commun.* 409, 46-51.
- (49) Kleiber, M. L., and Singh, S. M. (2009) Divergence of the vertebrate sp1A/ryanodine receptor domain and SOCS box-containing (Spsb) gene family and its expression and regulation within the mouse brain, *Genomics* 93, 358-366.
- (50) Wang, D., Li, Z., Messing, E. M., and Wu, G. (2005) The SPRY domain-containing SOCS box protein 1 (SSB-1) interacts with MET and enhances the hepatocyte growth factor-induced Erk-Elk-1-serum response element pathway, *J. Biol. Chem.* 280, 16393-16401.
- (51) Masters, S. L., Yao, S., Willson, T. A., Zhang, J. G., Palmer, K. R., Smith, B. J., Babon, J. J., Nicola, N. A., Norton, R. S., and Nicholson, S. E. (2006) The SPRY domain of SSB-2 adopts a novel fold that presents conserved Par-4-binding residues, *Nat. Struct. Mol. Biol.* 13, 77-84.
- (52) Styhler, S., Nakamura, A., and Lasko, P. (2002) VASA localization requires the SPRY-domain and SOCS-box containing protein, GUSTAVUS, *Dev. Cell* 3, 865-876.
- (53) Woo, J. S., Suh, H. Y., Park, S. Y., and Oh, B. H. (2006) Structural basis for protein recognition by B30.2/SPRY domains, *Mol. Cell* 24, 967-976.

-
- (54) de Castro, E., Sigrist, C. J., Gattiker, A., Bulliard, V., Langendijk-Genevaux, P. S., Gasteiger, E., Bairoch, A., and Hulo, N. (2006) ScanProsite: detection of PROSITE signature matches and ProRule-associated functional and structural residues in proteins, *Nucleic Acids Res.* *34*, W362-365.
- (55) Filippakopoulos, P., Low, A., Sharpe, T. D., Uppenberg, J., Yao, S., Kuang, Z., Savitsky, P., Lewis, R. S., Nicholson, S. E., Norton, R. S., and Bullock, A. N. (2010) Structural basis for Par-4 recognition by the SPRY domain- and SOCS box-containing proteins SPSB1, SPSB2, and SPSB4, *J. Mol. Biol.* *401*, 389-402.
- (56) Lewis, R. S., Kolesnik, T. B., Kuang, Z., D'Cruz, A. A., Blewitt, M. E., Masters, S. L., Low, A., Willson, T., Norton, R. S., and Nicholson, S. E. (2011) TLR regulation of SPSB1 controls inducible nitric oxide synthase induction, *J. Immunol.* *187*, 3798-3805.
- (57) Nishiya, T., Matsumoto, K., Maekawa, S., Kajita, E., Horinouchi, T., Fujimuro, M., Ogasawara, K., Uehara, T., and Miwa, S. (2011) Regulation of inducible nitric-oxide synthase by the SPRY domain- and SOCS box-containing proteins, *J. Biol. Chem.* *286*, 9009-9019.
- (58) Foster, M. W., Thompson, J. W., Forrester, M. T., Sha, Y., McMahon, T. J., Bowles, D. E., Moseley, M. A., and Marshall, H. E. (2013) Proteomic analysis of the NOS2 interactome in human airway epithelial cells, *Nitric Oxide* *34*, 37-46.
- (59) Kugler, J. M., Woo, J. S., Oh, B. H., and Lasko, P. (2010) Regulation of *Drosophila vasa in vivo* through paralogous cullin-RING E3 ligase specificity receptors, *Mol. Cell. Biol.* *30*, 1769-1782.
- (60) Kuang, Z., Yao, S., Xu, Y., Lewis, R. S., Low, A., Masters, S. L., Willson, T. A., Kolesnik, T. B., Nicholson, S. E., Garrett, T. J. P., and Norton, R. S. (2009) SPRY domain-containing SOCS box protein 2: crystal structure and residues critical for protein binding, *J. Mol. Biol.* *386*, 662-674.
- (61) Sells, S. F., Wood, D. P., Jr., Joshi-Barve, S. S., Muthukumar, S., Jacob, R. J., Crist, S. A., Humphreys, S., and Rangnekar, V. M. (1994) Commonality of the gene programs induced by effectors of apoptosis in androgen-dependent and -independent prostate cells, *Cell Growth Differ.* *5*, 457-466.
- (62) Peng, H. M., Morishima, Y., Jenkins, G. J., Dunbar, A. Y., Lau, M., Patterson, C., Pratt, W. B., and Osawa, Y. (2004) Ubiquitylation of neuronal nitric-oxide

- synthase by CHIP, a chaperone-dependent E3 ligase, *J. Biol. Chem.* 279, 52970-52977.
- (63) Jiang, J., Cyr, D., Babbitt, R. W., Sessa, W. C., and Patterson, C. (2003) Chaperone-dependent regulation of endothelial nitric-oxide synthase intracellular trafficking by the co-chaperone/ubiquitin ligase CHIP, *J. Biol. Chem.* 278, 49332-49341.
- (64) Arkin, M. R., Tang, Y., and Wells, J. A. (2014) Small-molecule inhibitors of protein-protein interactions: progressing toward the reality, *Chem. Biol.* 21, 1102-1114.
- (65) Wójcik, P., and Berlicki, L. (2015) Peptide-based inhibitors of protein-protein interactions, *Bioorg. Med. Chem. Lett.*
- (66) Visintin, M., Melchionna, T., Cannistraci, I., and Cattaneo, A. (2008) *In vivo* selection of intrabodies specifically targeting protein-protein interactions: a general platform for an "undruggable" class of disease targets, *J. Biotechnol.* 135, 1-15.
- (67) Murray, J. K., and Gellman, S. H. (2007) Targeting protein-protein interactions: lessons from p53/MDM2, *Biopolymers* 88, 657-686.
- (68) Mignani, S., El Kazzouli, S., Bousmina, M. M., and Majoral, J. P. (2014) Dendrimer space exploration: an assessment of dendrimers/dendritic scaffolding as inhibitors of protein-protein interactions, a potential new area of pharmaceutical development, *Chem. Rev.* 114, 1327-1342.
- (69) Bayraktar, H., Ghosh, P. S., Rotello, V. M., and Knapp, M. J. (2006) Disruption of protein-protein interactions using nanoparticles: inhibition of cytochrome c peroxidase, *Chem. Commun.*, 1390-1392.
- (70) Kritzer, J. A., Zutshi, R., Cheah, M., Ran, F. A., Webman, R., Wongjirad, T. M., and Schepartz, A. (2006) Miniature protein inhibitors of the p53-hDM2 interaction, *ChemBioChem* 7, 29-31.
- (71) Laraia, L., McKenzie, G., Spring, D. R., Venkitaraman, A. R., and Huggins, D. J. (2015) Overcoming chemical, biological, and computational challenges in the development of inhibitors targeting protein-protein interactions, *Chem. Biol.* 22, 689-703.
- (72) Zinzalla, G., and Thurston, D. E. (2009) Targeting protein-protein interactions for therapeutic intervention: a challenge for the future, *Future Med. Chem.* 1, 65-93.

- (73) Vassilev, L. T., Vu, B. T., Graves, B., Carvajal, D., Podlaski, F., Filipovic, Z., Kong, N., Kammlott, U., Lukacs, C., Klein, C., Fotouhi, N., and Liu, E. A. (2004) *In vivo* activation of the p53 pathway by small-molecule antagonists of MDM2, *Science* 303, 844-848.
- (74) Clark, R. C., Lee, S. Y., Searcey, M., and Boger, D. L. (2009) The isolation, total synthesis and structure elucidation of chlorofusin, a natural product inhibitor of the p53-mDM2 protein-protein interaction, *Nat. Prod. Rep.* 26, 465-477.
- (75) Izumikawa, M., Hashimoto, J., Hirokawa, T., Sugimoto, S., Kato, T., Takagi, M., and Shin-Ya, K. (2010) JBIR-22, an inhibitor for protein-protein interaction of the homodimer of proteasome assembly factor 3, *J. Nat. Prod.* 73, 628-631.
- (76) Sperl, B., Seifert, M. H., and Berg, T. (2009) Natural product inhibitors of protein-protein interactions mediated by Src-family SH2 domains, *Bioorg. Med. Chem. Lett.* 19, 3305-3309.
- (77) Winter, A., Higuieruelo, A. P., Marsh, M., Sigurdardottir, A., Pitt, W. R., and Blundell, T. L. (2012) Biophysical and computational fragment-based approaches to targeting protein-protein interactions: applications in structure-guided drug discovery, *Q. Rev. Biophys.* 45, 383-426.
- (78) Karatas, H., Townsend, E. C., Cao, F., Chen, Y., Bernard, D., Liu, L., Lei, M., Dou, Y., and Wang, S. (2013) High-affinity, small-molecule peptidomimetic inhibitors of MLL1/WDR5 protein-protein interaction, *J. Am. Chem. Soc.* 135, 669-682.
- (79) Azzarito, V., Long, K., Murphy, N. S., and Wilson, A. J. (2013) Inhibition of α -helix-mediated protein-protein interactions using designed molecules, *Nat. Chem.* 5, 161-173.
- (80) Lao, B. B., Drew, K., Guarracino, D. A., Brewer, T. F., Heindel, D. W., Bonneau, R., and Arora, P. S. (2014) Rational design of topographical helix mimics as potent inhibitors of protein-protein interactions, *J. Am. Chem. Soc.* 136, 7877-7888.
- (81) Moon, H., and Lim, H. S. (2015) Synthesis and screening of small-molecule α -helix mimetic libraries targeting protein-protein interactions, *Curr. Opin. Chem. Biol.* 24, 38-47.
- (82) Whitby, L. R., and Boger, D. L. (2012) Comprehensive peptidomimetic libraries targeting protein-protein interactions, *Acc. Chem. Res.* 45, 1698-1709.

- (83) Barnard, A., Long, K., Martin, H. L., Miles, J. A., Edwards, T. A., Tomlinson, D. C., Macdonald, A., and Wilson, A. J. (2015) Selective and potent proteomimetic inhibitors of intracellular protein-protein interactions, *Angew. Chem. Int. Ed.* *54*, 2960-2965.
- (84) Kritzer, J. A., Stephens, O. M., Guarracino, D. A., Reznik, S. K., and Schepartz, A. (2005) β -Peptides as inhibitors of protein-protein interactions, *Bioorg. Med. Chem.* *13*, 11-16.
- (85) Checco, J. W., Lee, E. F., Evangelista, M., Sleebs, N. J., Rogers, K., Pettikiriarachchi, A., Kershaw, N. J., Eddinger, G. A., Belair, D. G., Wilson, J. L., Eller, C. H., Raines, R. T., Murphy, W. L., Smith, B. J., Gellman, S. H., and Fairlie, W. D. (2015) α/β -peptide foldamers targeting intracellular protein-protein interactions with activity in living cells, *J. Am. Chem. Soc.* *137*, 11365-11375.
- (86) Sadowsky, J. D., Fairlie, W. D., Hadley, E. B., Lee, H. S., Umezawa, N., Nikolovska-Coleska, Z., Wang, S., Huang, D. C., Tomita, Y., and Gellman, S. H. (2007) ($\alpha/\beta+\alpha$)-peptide antagonists of BH3 domain/Bcl-x(L) recognition: toward general strategies for foldamer-based inhibition of protein-protein interactions, *J. Am. Chem. Soc.* *129*, 139-154.
- (87) Lim, H. S., Archer, C. T., and Kodadek, T. (2007) Identification of a peptoid inhibitor of the proteasome 19S regulatory particle, *J. Am. Chem. Soc.* *129*, 7750-7751.
- (88) Lee, S. G., and Chmielewski, J. (2010) Cross-linked peptoid-based dimerization inhibitors of HIV-1 protease, *ChemBioChem* *11*, 1513-1516.
- (89) Milech, N., and Watt, P. (2012) The construction of "phylomer" peptide libraries as a rich source of potent inhibitors of protein/protein interactions, *Methods Mol. Biol.* *899*, 43-60.
- (90) Cromm, P. M., Spiegel, J., and Grossmann, T. N. (2015) Hydrocarbon stapled peptides as modulators of biological function, *ACS Chem. Biol.* *10*, 1362-1375.
- (91) Zhang, Z., Lin, Z., Zhou, Z., Shen, H. C., Yan, S. F., Mayweg, A. V., Xu, Z., Qin, N., Wong, J. C., Zhang, Z., Rong, Y., Fry, D. C., and Hu, T. (2014) Structure-based design and synthesis of potent cyclic peptides inhibiting the YAP-TEAD protein-protein interaction, *ACS Med. Chem. Lett.* *5*, 993-998.

- (92) Lian, W., Upadhyaya, P., Rhodes, C. A., Liu, Y., and Pei, D. (2013) Screening bicyclic peptide libraries for protein-protein interaction inhibitors: discovery of a tumor necrosis factor- α antagonist, *J. Am. Chem. Soc.* *135*, 11990-11995.
- (93) Robinson, J. A. (2009) Design of protein-protein interaction inhibitors based on protein epitope mimetics, *ChemBioChem* *10*, 971-973.
- (94) Fasan, R., Dias, R. L., Moehle, K., Zerbe, O., Obrecht, D., Mittl, P. R., Grutter, M. G., and Robinson, J. A. (2006) Structure-activity studies in a family of β -hairpin protein epitope mimetic inhibitors of the p53-HDM2 protein-protein interaction, *ChemBioChem* *7*, 515-526.
- (95) Jubb, H., Blundell, T. L., and Ascher, D. B. (2015) Flexibility and small pockets at protein-protein interfaces: New insights into druggability, *Prog. Biophys. Mol. Biol.* *119*, 2-9.
- (96) Cherry, M., and Mitchell, T. (2008) Introduction to fragment-based drug discovery, In *Fragment-based drug discovery*, pp 1-13, John Wiley & Sons, Ltd.
- (97) Fink, T., Bruggesser, H., and Reymond, J. L. (2005) Virtual exploration of the small-molecule chemical universe below 160 Daltons, *Angew. Chem. Int. Ed.* *44*, 1504-1508.
- (98) Fink, T., and Reymond, J. L. (2007) Virtual exploration of the chemical universe up to 11 atoms of C, N, O, F: assembly of 26.4 million structures (110.9 million stereoisomers) and analysis for new ring systems, stereochemistry, physicochemical properties, compound classes, and drug discovery, *J. Chem. Inf. Model.* *47*, 342-353.
- (99) Hann, M. M., Leach, A. R., and Harper, G. (2001) Molecular complexity and its impact on the probability of finding leads for drug discovery, *J. Chem. Inf. Comput. Sci.* *41*, 856-864.
- (100) Wyss, D. F., Wang, Y. S., Eaton, H. L., Strickland, C., Voigt, J. H., Zhu, Z., and Stamford, A. W. (2012) Combining NMR and X-ray crystallography in fragment-based drug discovery: discovery of highly potent and selective BACE-1 inhibitors, *Top. Curr. Chem.* *317*, 83-114.
- (101) Murray, C. W., Verdonk, M. L., and Rees, D. C. (2012) Experiences in fragment-based drug discovery, *Trends Pharmacol. Sci.* *33*, 224-232.
- (102) Erlanson, D. A. (2012) Introduction to fragment-based drug discovery, *Top. Curr. Chem.* *317*, 1-32.

- (103) Congreve, M., Carr, R., Murray, C., and Jhoti, H. (2003) A 'rule of three' for fragment-based lead discovery?, *Drug Discov. Today* 8, 876-877.
- (104) Farmer, B. T., and Reitz, A. B. (2008) Fragment-based drug discovery, In *The practice of medicinal chemistry* (Camille-Georges, Ed.) 3rd ed., pp 228-243, Academic Press, New York.
- (105) Murray, C. W., and Rees, D. C. (2009) The rise of fragment-based drug discovery, *Nat. Chem.* 1, 187-192.
- (106) Jerabek-Willemsen, M., André, T., Wanner, R., Roth, H. M., Duhr, S., Baaske, P., and Breitsprecher, D. (2014) MicroScale Thermophoresis: Interaction analysis and beyond, *J. Mol. Struct.* 1077, 101-113.
- (107) Zartler, E. R., and Shapiro, M. J. (2008) Designing a fragment process to fit your needs, In *Fragment-based drug discovery*, pp 15-37, John Wiley & Sons, Ltd.
- (108) Mayer, M., and Meyer, B. (2001) Group epitope mapping by saturation transfer difference NMR to identify segments of a ligand in direct contact with a protein receptor, *J. Am. Chem. Soc.* 123, 6108-6117.
- (109) Mayer, M., and Meyer, B. (1999) Characterization of ligand binding by saturation transfer difference NMR spectroscopy, *Angew. Chem. Int. Ed.* 38, 1784-1788.
- (110) Carr, H. Y., and Purcell, E. M. (1954) Effects of diffusion on free precession in nuclear magnetic resonance experiments, *Phys. Rev.* 94, 630-638.
- (111) Meiboom, S., and Gill, D. (1958) Modified spin-echo method for measuring nuclear relaxation times, *Rev. Sci. Instrum.* 29, 688-691.
- (112) Hajduk, P. J., Olejniczak, E. T., and Fesik, S. W. (1997) One-dimensional relaxation- and diffusion-edited NMR methods for screening compounds that bind to macromolecules, *J. Am. Chem. Soc.* 119, 12257-12261.
- (113) Dalvit, C., Fogliatto, G., Stewart, A., Veronesi, M., and Stockman, B. (2001) WaterLOGSY as a method for primary NMR screening: practical aspects and range of applicability, *J. Biomol. NMR* 21, 349-359.
- (114) Dalvit, C., Pevarello, P., Tato, M., Veronesi, M., Vulpetti, A., and Sundstrom, M. (2000) Identification of compounds with binding affinity to proteins *via* magnetization transfer from bulk water, *J. Biomol. NMR* 18, 65-68.
- (115) Yao, S., Masters, S. L., Zhang, J. G., Palmer, K. R., Babon, J. J., Nicola, N. A., Nicholson, S. E., and Norton, R. S. (2005) Backbone ^1H , ^{13}C and ^{15}N assignments

- of the 25 kDa SPRY domain-containing SOCS box protein 2 (SSB-2), *J. Biomol. NMR* 31, 69-70.
- (116) Leung, E. W., Yagi, H., Harjani, J. R., Mulcair, M. D., Scanlon, M. J., Baell, J. B., and Norton, R. S. (2014) ^{19}F NMR as a probe of ligand interactions with the iNOS binding site of SPRY domain-containing SOCS box protein 2, *Chem. Biol. Drug Des.* 84, 616-625.
- (117) Dalvit, C. (2009) NMR methods in fragment screening: theory and a comparison with other biophysical techniques, *Drug Discov. Today* 14, 1051-1057.
- (118) Hennig, M., Ruf, A., and Huber, W. (2012) Combining biophysical screening and X-ray crystallography for fragment-based drug discovery, *Top. Curr. Chem.* 317, 115-143.
- (119) Gozalbes, R., Carbajo, R. J., and Pineda-Lucena, A. (2010) Contributions of computational chemistry and biophysical techniques to fragment-based drug discovery, *Curr. Med. Chem.* 17, 1769-1794.
- (120) Chen, Y., and Pohlhaus, D. T. (2010) *In silico* docking and scoring of fragments, *Drug Discov. Today Technol.* 7, e149-e156.
- (121) Villar, H. O., and Hansen, M. R. (2007) Computational techniques in fragment based drug discovery, *Curr. Top. Med. Chem.* 7, 1509-1513.
- (122) Desjarlais, R. L. (2011) Using computational techniques in fragment-based drug discovery, *Methods Enzymol.* 493, 137-155.
- (123) Sandor, M., Kiss, R., and Keseru, G. M. (2010) Virtual fragment docking by Glide: a validation study on 190 protein-fragment complexes, *J. Chem. Inf. Model.* 50, 1165-1172.
- (124) Friesner, R. A., Banks, J. L., Murphy, R. B., Halgren, T. A., Klicic, J. J., Mainz, D. T., Repasky, M. P., Knoll, E. H., Shelley, M., Perry, J. K., Shaw, D. E., Francis, P., and Shenkin, P. S. (2004) Glide: a new approach for rapid, accurate docking and scoring. 1. Method and assessment of docking accuracy, *J. Med. Chem.* 47, 1739-1749.
- (125) Halgren, T. A., Murphy, R. B., Friesner, R. A., Beard, H. S., Frye, L. L., Pollard, W. T., and Banks, J. L. (2004) Glide: a new approach for rapid, accurate docking and scoring. 2. Enrichment factors in database screening, *J. Med. Chem.* 47, 1750-1759.

- (126) Loving, K., Salam, N. K., and Sherman, W. (2009) Energetic analysis of fragment docking and application to structure-based pharmacophore hypothesis generation, *J. Comput. Aided Mol. Des.* 23, 541-554.
- (127) Fukunishi, Y. (2010) Post processing of protein-compound docking for fragment-based drug discovery (FBDD): *in-silico* structure-based drug screening and ligand-binding pose prediction, *Curr. Top. Med. Chem.* 10, 680-694.
- (128) Madhavi Sastry, G., Adzhigirey, M., Day, T., Annabhimoju, R., and Sherman, W. (2013) Protein and ligand preparation: parameters, protocols, and influence on virtual screening enrichments, *J. Comput. Aided Mol. Des.* 27, 221-234.
- (129) Kawatkar, S., Wang, H., Czerminski, R., and Joseph-McCarthy, D. (2009) Virtual fragment screening: an exploration of various docking and scoring protocols for fragments using Glide, *J. Comput. Aided Mol. Des.* 23, 527-539.
- (130) Tyndall, J. D., Nall, T., and Fairlie, D. P. (2005) Proteases universally recognize β strands in their active sites, *Chem. Rev.* 105, 973-999.
- (131) Craik, D. J. (2006) Seamless proteins tie up their loose ends, *Science* 311, 1563-1564.
- (132) Fletcher, J. M., and Hughes, R. A. (2009) Modified low molecular weight cyclic peptides as mimetics of BDNF with improved potency, proteolytic stability and transmembrane passage *in vitro*, *Bioorg. Med. Chem.* 17, 2695-2702.
- (133) Hess, S., Linde, Y., Ovadia, O., Safrai, E., Shalev, D. E., Swed, A., Halbfinger, E., Lapidot, T., Winkler, I., Gabinet, Y., Faier, A., Yarden, D., Xiang, Z., Portillo, F. P., Haskell-Luevano, C., Gilon, C., and Hoffman, A. (2008) Backbone cyclic peptidomimetic melanocortin-4 receptor agonist as a novel orally administrated drug lead for treating obesity, *J. Med. Chem.* 51, 1026-1034.
- (134) Byk, G., Halle, D., Zeltser, I., Bitan, G., Selinger, Z., and Gilon, C. (1996) Synthesis and biological activity of NK-1 selective, *N*-backbone cyclic analogs of the *C*-terminal hexapeptide of substance P, *J. Med. Chem.* 39, 3174-3178.
- (135) Hayouka, Z., Hurevich, M., Levin, A., Benyamini, H., Iosub, A., Maes, M., Shalev, D. E., Loyter, A., Gilon, C., and Friedler, A. (2010) Cyclic peptide inhibitors of HIV-1 integrase derived from the LEDGF/p75 protein, *Bioorg. Med. Chem.* 18, 8388-8395.
- (136) Piserchio, A., Salinas, G. D., Li, T., Marshall, J., Spaller, M. R., and Mierke, D. F. (2004) Targeting specific PDZ domains of PSD-95: structural basis for

- enhanced affinity and enzymatic stability of a cyclic peptide, *Chem. Biol.* *11*, 469-473.
- (137) Kwon, Y.-U., and Kodadek, T. (2007) Quantitative comparison of the relative cell permeability of cyclic and linear peptides, *Chem. Biol.* *14*, 671-677.
- (138) Clark, R. J., Jensen, J., Nevin, S. T., Callaghan, B. P., Adams, D. J., and Craik, D. J. (2010) The engineering of an orally active conotoxin for the treatment of neuropathic pain, *Angew. Chem. Int. Ed.* *49*, 6545-6548.
- (139) White, C. J., and Yudin, A. K. (2011) Contemporary strategies for peptide macrocyclization, *Nat. Chem.* *3*, 509-524.
- (140) Gilon, C., Halle, D., Chorev, M., Selinger, Z., and Byk, G. (1991) Backbone cyclization: A new method for conferring conformational constraint on peptides, *Biopolymers* *31*, 745-750.
- (141) Hayouka, Z., Levin, A., Hurevich, M., Shalev, D. E., Loyter, A., Gilon, C., and Friedler, A. (2012) A comparative study of backbone versus side chain peptide cyclization: Application for HIV-1 integrase inhibitors, *Bioorg. Med. Chem.* *20*, 3317-3322.
- (142) Malesevic, M., Strijowski, U., Bachle, D., and Sewald, N. (2004) An improved method for the solution cyclization of peptides under pseudo-high dilution conditions, *J. Biotechnol.* *112*, 73-77.
- (143) Fujita, Y., Fujita, S., Okada, Y., and Chiba, K. (2013) Soluble tag-assisted peptide head-to-tail cyclization: total synthesis of mahafacyclin B, *Org. Lett.* *15*, 1155-1157.
- (144) Stanger, K., Maurer, T., Kaluarachchi, H., Coons, M., Franke, Y., and Hannoush, R. N. (2014) Backbone cyclization of a recombinant cystine-knot peptide by engineered Sortase A, *FEBS Lett.* *588*, 4487-4496.
- (145) Jia, X., Kwon, S., Wang, C. I., Huang, Y. H., Chan, L. Y., Tan, C. C., Rosengren, K. J., Mulvenna, J. P., Schroeder, C. I., and Craik, D. J. (2014) Semienzymatic cyclization of disulfide-rich peptides using Sortase A, *J. Biol. Chem.* *289*, 6627-6638.
- (146) Conlan, B. F., and Anderson, M. A. (2011) Circular micro-proteins and mechanisms of cyclization, *Curr. Pharm. Des.* *17*, 4318-4328.
- (147) Baeza, J. L., de la Torre, B. G., Santiveri, C. M., Almeida, R. D., García-López, M. T., Gerona-Navarro, G., Jaffrey, S. R., Jiménez, M. A., Andreu, D., González-

- Muñiz, R., and Martín-Martínez, M. (2012) Cyclic amino acid linkers stabilizing key loops of brain derived neurotrophic factor, *Bioorg. Med. Chem. Lett.* 22, 444-448.
- (148) Wang, B., Nimkar, K., Wang, W., Zhang, H., Shan, D., Gudmundsson, O., Gangwar, S., Siahaan, T., and Borchardt, R. T. (1999) Synthesis and evaluation of the physicochemical properties of esterase-sensitive cyclic prodrugs of opioid peptides using coumarinic acid and phenylpropionic acid linkers, *J. Pept. Res.* 53, 370-382.
- (149) Bak, A., Siahaan, T. J., Gudmundsson, O. S., Gangwar, S., Friis, G. J., and Borchardt, R. T. (1999) Synthesis and evaluation of the physicochemical properties of esterase-sensitive cyclic prodrugs of opioid peptides using an (acyloxy)alkoxy linker, *J. Pept. Res.* 53, 393-402.
- (150) Rosengren, K. J., Goransson, U., Otvos, L., Jr., and Craik, D. J. (2004) Cyclization of pyrrhocoricin retains structural elements crucial for the antimicrobial activity of the native peptide, *Biopolymers* 76, 446-458.
- (151) Halai, R., Callaghan, B., Daly, N. L., Clark, R. J., Adams, D. J., and Craik, D. J. (2011) Effects of cyclization on stability, structure, and activity of α -conotoxin RgIA at the $\alpha 9\alpha 10$ nicotinic acetylcholine receptor and GABA_B receptor, *J. Med. Chem.* 54, 6984-6992.
- (152) Clark, R. J., Fischer, H., Dempster, L., Daly, N. L., Rosengren, K. J., Nevin, S. T., Meunier, F. A., Adams, D. J., and Craik, D. J. (2005) Engineering stable peptide toxins by means of backbone cyclization: stabilization of the α -conotoxin MII, *Proc. Natl. Acad. Sci. U S A* 102, 13767-13772.
- (153) Taylor, P. W., and Howes, C. (1991) Rationale for targeted drug delivery, *Biotherapy* 3, 1-8.
- (154) Ye, X., and Yang, D. (2009) Recent advances in biological strategies for targeted drug delivery, *Cardiovasc. Hematol. Disord. Drug Targets* 9, 206-221.
- (155) Jain, N. K., Mishra, V., and Mehra, N. K. (2013) Targeted drug delivery to macrophages, *Expert Opin. Drug Deliv.* 10, 353-367.
- (156) Costa, A., Sarmiento, B., and Seabra, V. (2015) Targeted drug delivery systems for lung macrophages, *Curr. Drug Targets* 16, 1565-1581.

- (157) Takahashi, K., Donovan, M. J., Rogers, R. A., and Ezekowitz, R. A. (1998) Distribution of murine mannose receptor expression from early embryogenesis through to adulthood, *Cell Tissue Res.* 292, 311-323.
- (158) Gazi, U., and Martinez-Pomares, L. (2009) Influence of the mannose receptor in host immune responses, *Immunobiology* 214, 554-561.
- (159) Azad, A. K., Rajaram, M. V., and Schlesinger, L. S. (2014) Exploitation of the macrophage mannose receptor (CD206) in infectious disease diagnostics and therapeutics, *J. Cytol. Mol. Biol.* 1.
- (160) van Vliet, S. J., van Liempt, E., Saeland, E., Aarnoudse, C. A., Appelmelk, B., Irimura, T., Geijtenbeek, T. B., Blixt, O., Alvarez, R., van Die, I., and van Kooyk, Y. (2005) Carbohydrate profiling reveals a distinctive role for the C-type lectin MGL in the recognition of helminth parasites and tumor antigens by dendritic cells, *Int. Immunol.* 17, 661-669.
- (161) Higashi, N., Fujioka, K., Denda-Nagai, K., Hashimoto, S., Nagai, S., Sato, T., Fujita, Y., Morikawa, A., Tsuiji, M., Miyata-Takeuchi, M., Sano, Y., Suzuki, N., Yamamoto, K., Matsushima, K., and Irimura, T. (2002) The macrophage C-type lectin specific for galactose/N-acetylgalactosamine is an endocytic receptor expressed on monocyte-derived immature dendritic cells, *J. Biol. Chem.* 277, 20686-20693.
- (162) Higashi, N., Morikawa, A., Fujioka, K., Fujita, Y., Sano, Y., Miyata-Takeuchi, M., Suzuki, N., and Irimura, T. (2002) Human macrophage lectin specific for galactose/N-acetylgalactosamine is a marker for cells at an intermediate stage in their differentiation from monocytes into macrophages, *Int. Immunol.* 14, 545-554.
- (163) van Vliet, S. J., Saeland, E., and van Kooyk, Y. (2008) Sweet preferences of MGL: carbohydrate specificity and function, *Trends Immunol.* 29, 83-90.
- (164) Schweizer, A., Stahl, P. D., and Rohrer, J. (2000) A di-aromatic motif in the cytosolic tail of the mannose receptor mediates endosomal sorting, *J. Biol. Chem.* 275, 29694-29700.
- (165) van Vliet, S. J., Aarnoudse, C. A., Broks-van den Berg, V. C., Boks, M., Geijtenbeek, T. B., and van Kooyk, Y. (2007) MGL-mediated internalization and antigen presentation by dendritic cells: a role for tyrosine-5, *Eur. J. Immunol.* 37, 2075-2081.

- (166) Varkouhi, A. K., Scholte, M., Storm, G., and Haisma, H. J. (2011) Endosomal escape pathways for delivery of biologicals, *J. Control. Release* 151, 220-228.
- (167) Shete, H. K., Prabhu, R. H., and Patravale, V. B. (2014) Endosomal escape: a bottleneck in intracellular delivery, *J. Nanosci. Nanotechnol.* 14, 460-474.
- (168) Nishimura, Y., Takeda, K., Ezawa, R., Ishii, J., Ogino, C., and Kondo, A. (2014) A display of pH-sensitive fusogenic GALA peptide facilitates endosomal escape from a Bio-nanocapsule *via* an endocytic uptake pathway, *J. Nanobiotechnology* 12, 11.
- (169) Niikura, K., Horisawa, K., and Doi, N. (2015) A fusogenic peptide from a sea urchin fertilization protein promotes intracellular delivery of biomacromolecules by facilitating endosomal escape, *J. Control. Release* 212, 85-93.
- (170) Jayakumar, M. K., Bansal, A., Huang, K., Yao, R., Li, B. N., and Zhang, Y. (2014) Near-infrared-light-based nano-platform boosts endosomal escape and controls gene knockdown *in vivo*, *ACS nano* 8, 4848-4858.
- (171) Richard, J. P., Melikov, K., Vives, E., Ramos, C., Verbeure, B., Gait, M. J., Chernomordik, L. V., and Lebleu, B. (2003) Cell-penetrating peptides. A reevaluation of the mechanism of cellular uptake, *J. Biol. Chem.* 278, 585-590.
- (172) Erazo-Oliveras, A., Muthukrishnan, N., Baker, R., Wang, T. Y., and Pellois, J. P. (2012) Improving the endosomal escape of cell-penetrating peptides and their cargos: strategies and challenges, *Pharmaceuticals (Basel)* 5, 1177-1209.
- (173) Feng, J., and Tang, L. (2015) The cell-type specificity and endosomal escape of cell-penetrating peptides, *Curr. Pharm. Des.* 21, 1351-1356.
- (174) Salomone, F., Cardarelli, F., Di Luca, M., Boccardi, C., Nifosi, R., Bardi, G., Di Bari, L., Serresi, M., and Beltram, F. (2012) A novel chimeric cell-penetrating peptide with membrane-disruptive properties for efficient endosomal escape, *J. Control. Release* 163, 293-303.
- (175) Raagel, H., Hein, M., Kriiska, A., Saalik, P., Floren, A., Langel, U., and Pooga, M. (2013) Cell-penetrating peptide secures an efficient endosomal escape of an intact cargo upon a brief photo-induction, *Cell. Mol. Life Sci.* 70, 4825-4839.
- (176) Mellert, K., Lamla, M., Scheffzek, K., Wittig, R., and Kaufmann, D. (2012) Enhancing endosomal escape of transduced proteins by photochemical internalisation, *PloS one* 7, e52473.

- (177) Qian, Z., LaRochelle, J. R., Jiang, B., Lian, W., Hard, R. L., Selner, N. G., Luechapanichkul, R., Barrios, A. M., and Pei, D. (2014) Early endosomal escape of a cyclic cell-penetrating peptide allows effective cytosolic cargo delivery, *Biochemistry* 53, 4034-4046.
- (178) Li, M., Tao, Y., Shu, Y., LaRochelle, J. R., Steinauer, A., Thompson, D., Schepartz, A., Chen, Z. Y., and Liu, D. R. (2015) Discovery and characterization of a peptide that enhances endosomal escape of delivered proteins *in vitro* and *in vivo*, *J. Am. Chem. Soc.* 137, 14084-14093.
- (179) Ma, D. (2014) Enhancing endosomal escape for nanoparticle mediated siRNA delivery, *Nanoscale* 6, 6415-6425.
- (180) Wang, M., Li, X., Ma, Y., and Gu, H. (2013) Endosomal escape kinetics of mesoporous silica-based system for efficient siRNA delivery, *Int. J. Pharm.* 448, 51-57.
- (181) Narayanan, K., Yen, S. K., Dou, Q., Padmanabhan, P., Sudhakaran, T., Ahmed, S., Ying, J. Y., and Selvan, S. T. (2013) Mimicking cellular transport mechanism in stem cells through endosomal escape of new peptide-coated quantum dots, *Sci. Rep.* 3, 2184.
- (182) Shahbazi, M. A., Almeida, P. V., Makila, E. M., Kaasalainen, M. H., Salonen, J. J., Hirvonen, J. T., and Santos, H. A. (2014) Augmented cellular trafficking and endosomal escape of porous silicon nanoparticles *via* zwitterionic bilayer polymer surface engineering, *Biomaterials* 35, 7488-7500.
- (183) Gujrati, M., Malamas, A., Shin, T., Jin, E., Sun, Y., and Lu, Z. R. (2014) Multifunctional cationic lipid-based nanoparticles facilitate endosomal escape and reduction-triggered cytosolic siRNA release, *Mol. Pharm.* 11, 2734-2744.
- (184) Chu, Z., Miu, K., Lung, P., Zhang, S., Zhao, S., Chang, H. C., Lin, G., and Li, Q. (2015) Rapid endosomal escape of prickly nanodiamonds: implications for gene delivery, *Sci. Rep.* 5, 11661.
- (185) Muro, S. (2014) A DNA-device that mediates selective endosomal escape and intracellular delivery of drugs and biologicals, *Adv. Funct. Mater.* 24, 2899-2906.
- (186) Lukianova-Hleb, E. Y., Belyanin, A., Kashinath, S., Wu, X., and Lapotko, D. O. (2012) Plasmonic nanobubble-enhanced endosomal escape processes for selective and guided intracellular delivery of chemotherapy to drug-resistant cancer cells, *Biomaterials* 33, 1821-1826.

- (187) El-Sayed, A., Masuda, T., Akita, H., and Harashima, H. (2012) Stearylated INF7 peptide enhances endosomal escape and gene expression of PEGylated nanoparticles both *in vitro* and *in vivo*, *J. Pharm. Sci.* *101*, 879-882.
- (188) Chen, J., Luo, J., Zhao, Y., Pu, L., Lu, X., Gao, R., Wang, G., and Gu, Z. (2015) Increase in transgene expression by pluronic L64-mediated endosomal/lysosomal escape through its membrane-disturbing action, *ACS Appl. Mater. Interfaces* *7*, 7282-7293.
- (189) Wen, Y., Guo, Z., Du, Z., Fang, R., Wu, H., Zeng, X., Wang, C., Feng, M., and Pan, S. (2012) Serum tolerance and endosomal escape capacity of histidine-modified pDNA-loaded complexes based on polyamidoamine dendrimer derivatives, *Biomaterials* *33*, 8111-8121.
- (190) Gu, J., Wang, X., Jiang, X., Chen, Y., Chen, L., Fang, X., and Sha, X. (2012) Self-assembled carboxymethyl poly (*L*-histidine) coated poly (β -amino ester)/DNA complexes for gene transfection, *Biomaterials* *33*, 644-658.
- (191) Lachelt, U., Kos, P., Mickler, F. M., Herrmann, A., Salcher, E. E., Rodl, W., Badgajar, N., Brauchle, C., and Wagner, E. (2014) Fine-tuning of proton sponges by precise diaminoethanes and histidines in pDNA polyplexes, *Nanomed. Nanotechnol. Biol. Med.* *10*, 35-44.
- (192) Liu, H. Y., and Gao, X. (2013) A universal protein tag for delivery of siRNA-aptamer chimeras, *Sci. Rep.* *3*, 3129.
- (193) Lo, S. L., and Wang, S. (2008) An endosomolytic Tat peptide produced by incorporation of histidine and cysteine residues as a nonviral vector for DNA transfection, *Biomaterials* *29*, 2408-2414.
- (194) Chu, D., Xu, W., Pan, R., Ding, Y., Sui, W., and Chen, P. (2015) Rational modification of oligoarginine for highly efficient siRNA delivery: structure-activity relationship and mechanism of intracellular trafficking of siRNA, *Nanomed. Nanotechnol. Biol. Med.* *11*, 435-446.
- (195) Johnson, R. P., Jeong, Y. I., John, J. V., Chung, C. W., Choi, S. H., Song, S. Y., Kang, D. H., Suh, H., and Kim, I. (2014) Lipo-poly(*L*-histidine) hybrid materials with pH-sensitivity, intracellular delivery efficiency, and intrinsic targetability to cancer cells, *Macromol. Rapid Commun.* *35*, 888-894.
- (196) Hwang, H. S., Hu, J., Na, K., and Bae, Y. H. (2014) Role of polymeric endosomolytic agents in gene transfection: a comparative study of poly(*L*-lysine)

- grafted with monomeric *L*-histidine analogue and poly(*L*-histidine), *Biomacromolecules* 15, 3577-3586.
- (197) Ramachandran, G. N., Ramakrishnan, C., and Sasisekharan, V. (1963) Stereochemistry of polypeptide chain configurations, *J. Mol. Biol.* 7, 95-99.
- (198) Friesner, R. A., Murphy, R. B., Repasky, M. P., Frye, L. L., Greenwood, J. R., Halgren, T. A., Sanschagrin, P. C., and Mainz, D. T. (2006) Extra precision glide: docking and scoring incorporating a model of hydrophobic enclosure for protein-ligand complexes, *J. Med. Chem.* 49, 6177-6196.
- (199) Tubert-Brohman, I., Sherman, W., Repasky, M., and Beuming, T. (2013) Improved docking of polypeptides with Glide, *J. Chem. Inf. Model.* 53, 1689-1699.
- (200) Rehm, T., Huber, R., and Holak, T. A. (2002) Application of NMR in structural proteomics: screening for proteins amenable to structural analysis, *Structure* 10, 1613-1618.
- (201) Atherton, E., Logan, C. J., and Sheppard, R. C. (1981) Peptide synthesis. Part 2. Procedures for solid-phase synthesis using *N*^α-fluorenylmethoxycarbonylamino-acids on polyamide supports. Synthesis of substance P and of acyl carrier protein 65-74 decapeptide, *J. Chem. Soc., Perkin. Trans. 1*, 538-546.
- (202) Cooper, M. A. (2002) Optical biosensors in drug discovery, *Nat. Rev. Drug Discov.* 1, 515-528.
- (203) Hwang, T. L., and Shaka, A. J. (1995) Water suppression that works. Excitation sculpting using arbitrary wave-forms and pulsed-field gradients, *J. Magn. Reson. A* 112, 275-279.
- (204) Piotto, M., Saudek, V., and Sklenar, V. (1992) Gradient-tailored excitation for single-quantum NMR spectroscopy of aqueous solutions, *J. Biomol. NMR* 2, 661-665.
- (205) Sklenar, V., Piotto, M., Leppik, R., and Saudek, V. (1993) Gradient-tailored water suppression for ¹H-¹⁵N HSQC experiments optimized to retain full sensitivity, *J. Magn. Reson., Series A* 102, 241-245.
- (206) Shaka, A. J., Lee, C. J., and Pines, A. (1988) Iterative schemes for bilinear operators; application to spin decoupling, *J. Magn. Reson. (1969)* 77, 274-293.
- (207) Bax, A., and Davis, D. G. (1985) Practical aspects of two-dimensional transverse NOE spectroscopy, *J. Magn. Reson. (1969)* 63, 207-213.

- (208) Hwang, T. L., and Shaka, A. J. (1992) Cross relaxation without TOCSY: transverse rotating-frame Overhauser effect spectroscopy, *J. Am. Chem. Soc.* *114*, 3157-3159.
- (209) Derome, A. E., and Williamson, M. P. (1990) Rapid-pulsing artifacts in double-quantum-filtered COSY, *J. Magn. Reson. (1969)* *88*, 177-185.
- (210) Schanda, P., Kupče, E., and Brutscher, B. (2005) SOFAST-HMQC experiments for recording two-dimensional heteronuclear correlation spectra of proteins within a few seconds, *J. Biomol. NMR* *33*, 199-211.
- (211) Wishart, D. S., Bigam, C. G., Yao, J., Abildgaard, F., Dyson, H. J., Oldfield, E., Markley, J. L., and Sykes, B. D. (1995) ^1H , ^{13}C and ^{15}N chemical shift referencing in biomolecular NMR, *J. Biomol. NMR* *6*, 135-140.
- (212) Wormald, S., Zhang, J. G., Krebs, D. L., Mielke, L. A., Silver, J., Alexander, W. S., Speed, T. P., Nicola, N. A., and Hilton, D. J. (2006) The comparative roles of suppressor of cytokine signaling-1 and -3 in the inhibition and desensitization of cytokine signaling, *J. Biol. Chem.* *281*, 11135-11143.
- (213) Nicholson, S. E., Novak, U., Ziegler, S. F., and Layton, J. E. (1995) Distinct regions of the granulocyte colony-stimulating factor receptor are required for tyrosine phosphorylation of the signaling molecules JAK2, Stat3, and p42, p44MAPK, *Blood* *86*, 3698-3704.
- (214) Greenwood, J. R., Calkins, D., Sullivan, A. P., and Shelley, J. C. (2010) Towards the comprehensive, rapid, and accurate prediction of the favorable tautomeric states of drug-like molecules in aqueous solution, *J. Comput. Aided Mol. Des.* *24*, 591-604.
- (215) Shelley, J. C., Cholleti, A., Frye, L. L., Greenwood, J. R., Timlin, M. R., and Uchimaya, M. (2007) Epik: a software program for pK_a prediction and protonation state generation for drug-like molecules, *J. Comput. Aided Mol. Des.* *21*, 681-691.
- (216) Lipinski, C. A., Lombardo, F., Dominy, B. W., and Feeney, P. J. (2001) Experimental and computational approaches to estimate solubility and permeability in drug discovery and development settings, *Adv. Drug Deliv. Rev.* *46*, 3-26.
- (217) Köster, H., Craan, T., Brass, S., Herhaus, C., Zentgraf, M., Neumann, L., Heine, A., and Klebe, G. (2011) A small nonrule of 3 compatible fragment library

- provides high hit rate of endothiapepsin crystal structures with various fragment chemotypes, *J. Med. Chem.* *54*, 7784-7796.
- (218) Bloembergen, N., Purcell, E. M., and Pound, R. V. (1948) Relaxation effects in nuclear magnetic resonance absorption, *Phys. Rev.* *73*, 679-712.
- (219) Halgren, T. (2007) New method for fast and accurate binding-site identification and analysis, *Chem. Biol. Drug Des.* *69*, 146-148.
- (220) Kozakov, D., Grove, L. E., Hall, D. R., Bohnuud, T., Mottarella, S. E., Luo, L., Xia, B., Beglov, D., and Vajda, S. (2015) The FTMap family of web servers for determining and characterizing ligand-binding hot spots of proteins, *Nat. Protoc.* *10*, 733-755.
- (221) Halgren, T. A. (2009) Identifying and characterizing binding sites and assessing druggability, *J. Chem. Inf. Model.* *49*, 377-389.
- (222) Kozakov, D., Hall, D. R., Chuang, G. Y., Cencic, R., Brenke, R., Grove, L. E., Beglov, D., Pelletier, J., Whitty, A., and Vajda, S. (2011) Structural conservation of druggable hot spots in protein-protein interfaces, *Proc. Natl. Acad. Sci. U S A* *108*, 13528-13533.
- (223) Collins, J., Tanaka, J., Wilson, P., Kempe, K., Davis, T. P., McIntosh, M. P., Whittaker, M. R., and Haddleton, D. M. (2015) In situ conjugation of dithiophenol maleimide polymers and oxytocin for stable and reversible polymer-peptide conjugates, *Bioconjug. Chem.* *26*, 633-638.
- (224) Jones, M. W., Strickland, R. A., Schumacher, F. F., Caddick, S., Baker, J. R., Gibson, M. I., and Haddleton, D. M. (2012) Highly efficient disulfide bridging polymers for bioconjugates from radical-compatible dithiophenol maleimides, *Chem. Commun.* *48*, 4064-4066.
- (225) Rostovtsev, V. V., Green, L. G., Fokin, V. V., and Sharpless, K. B. (2002) A stepwise Huisgen cycloaddition process: copper(I)-catalyzed regioselective "ligation" of azides and terminal alkynes, *Angew. Chem. Int. Ed.* *41*, 2596-2599.
- (226) Zhang, Q., Wilson, P., Li, Z., McHale, R., Godfrey, J., Anastasaki, A., Waldron, C., and Haddleton, D. M. (2013) Aqueous copper-mediated living polymerization: exploiting rapid disproportionation of CuBr with Me₆TREN, *J. Am. Chem. Soc.* *135*, 7355-7363.
- (227) Schindelin, J., Arganda-Carreras, I., Frise, E., Kaynig, V., Longair, M., Pietzsch, T., Preibisch, S., Rueden, C., Saalfeld, S., Schmid, B., Tinevez, J. Y., White, D.

- J., Hartenstein, V., Eliceiri, K., Tomancak, P., and Cardona, A. (2012) Fiji: an open-source platform for biological-image analysis, *Nat. Methods* 9, 676-682.
- (228) Yap, B. K., Leung, E. W., Yagi, H., Galea, C. A., Chhabra, S., Chalmers, D. K., Nicholson, S. E., Thompson, P. E., and Norton, R. S. (2014) A potent cyclic peptide targeting SPSB2 protein as a potential anti-infective agent, *J. Med. Chem.* 57, 7006-7015.
- (229) Borel, J. F., Feurer, C., Gubler, H. U., and Stahelin, H. (1976) Biological effects of cyclosporin A: a new antilymphocytic agent, *Agents Actions* 6, 468-475.
- (230) Augustijns, P. F., Bradshaw, T. P., Gan, L. S., Hendren, R. W., and Thakker, D. R. (1993) Evidence for a polarized efflux system in CACO-2 cells capable of modulating cyclosporin A transport, *Biochem. Biophys. Res. Commun.* 197, 360-365.
- (231) Makino, K., Yamamoto, N., Higuchi, K., Harada, N., Ohshima, H., and Terada, H. (2003) Phagocytic uptake of polystyrene microspheres by alveolar macrophages: effects of the size and surface properties of the microspheres, *Colloids Surf. B Biointerfaces* 27, 33-39.
- (232) Fernandez, N., Alonso, S., Valera, I., Vigo, A. G., Renedo, M., Barbolla, L., and Crespo, M. S. (2005) Mannose-containing molecular patterns are strong inducers of cyclooxygenase-2 expression and prostaglandin E2 production in human macrophages, *J. Immunol.* 174, 8154-8162.
- (233) Potocky, T. B., Menon, A. K., and Gellman, S. H. (2003) Cytoplasmic and nuclear delivery of a TAT-derived peptide and a β -peptide after endocytic uptake into HeLa cells, *J. Biol. Chem.* 278, 50188-50194.
- (234) Pack, D. W., Putnam, D., and Langer, R. (2000) Design of imidazole-containing endosomolytic biopolymers for gene delivery, *Biotechnol. Bioeng.* 67, 217-223.
- (235) Elmore, S. (2007) Apoptosis: a review of programmed cell death, *Toxicol. Pathol.* 35, 495-516.
- (236) Gottlieb, R. A., Nordberg, J., Skowronski, E., and Babior, B. M. (1996) Apoptosis induced in Jurkat cells by several agents is preceded by intracellular acidification, *Proc. Natl. Acad. Sci. U S A* 93, 654-658.
- (237) Nguyen, D. G., and Hildreth, J. E. K. (2003) Involvement of macrophage mannose receptor in the binding and transmission of HIV by macrophages, *Eur. J. Immunol.* 33, 483-493.

- (238) Upham, J. P., Pickett, D., Irimura, T., Anders, E. M., and Reading, P. C. (2010) Macrophage receptors for influenza A virus: role of the macrophage galactose-type lectin and mannose receptor in viral entry, *J. Virol.* *84*, 3730-3737.
- (239) Wahrenbrock, M. G., and Varki, A. (2006) Multiple hepatic receptors cooperate to eliminate secretory mucins aberrantly entering the bloodstream: are circulating cancer mucins the “tip of the iceberg”?, *Cancer Res.* *66*, 2433-2441.
- (240) Magae, J., Nagi, T., Takaku, K., Kataoka, T., Koshino, H., Uramoto, M., and Nagai, K. (1994) Screening for specific inhibitors of phagocytosis of thioglycollate-elicited macrophages, *Biosci. Biotechnol. Biochem.* *58*, 104-107.
- (241) Choi, K. Y., Swierczewska, M., Lee, S., and Chen, X. (2012) Protease-activated drug development, *Theranostics* *2*, 156-178.
- (242) Takemoto, H., Miyata, K., Hattori, S., Ishii, T., Suma, T., Uchida, S., Nishiyama, N., and Kataoka, K. (2013) Acidic pH-responsive siRNA conjugate for reversible carrier stability and accelerated endosomal escape with reduced IFN α -associated immune response, *Angew. Chem. Int. Ed.* *52*, 6218-6221.
- (243) Mosmann, T. (1983) Rapid colorimetric assay for cellular growth and survival: application to proliferation and cytotoxicity assays, *J. Immunol. Methods* *65*, 55-63.
- (244) Weaver, J. C., and Chizmadzhev, Y. A. (1996) Theory of electroporation: A review, *Bioelectrochem. Bioenerget.* *41*, 135-160.
- (245) Wiese, M., Castiglione, K., Hensel, M., Schleicher, U., Bogdan, C., and Jantsch, J. (2010) Small interfering RNA (siRNA) delivery into murine bone marrow-derived macrophages by electroporation, *J. Immunol. Methods* *353*, 102-110.
- (246) Ma, S., Schroeder, B., Sun, C., Loufakis, D. N., Cao, Z., Sriranganathan, N., and Lu, C. (2014) Electroporation-based delivery of cell-penetrating peptide conjugates of peptide nucleic acids for antisense inhibition of intracellular bacteria, *Integr. Biol.* *6*, 973-978.

APPENDIX I

Other cyclic peptide and peptidomimetic analogues targeting SPSB2

AI Introduction

A brief summary of other cyclic peptide and cyclic peptidomimetic analogues generated in this study but not included in the main chapters are further outlined in this appendix. These analogues are not part of the main chapters as the current data for the analogues are still in preliminary stages and thus insufficient for either a chapter or a publication. Some of these analogues were generated as part of proof-of-principle studies to investigate the plausibility of some substitutions to explore the structure-activity relationship of the analogues. These include the substitution with an *N*-methylated amino acid residue or a fluorophore dye such as fluorescein isothiocyanate (FITC) or acridone (Acd) at specific positions to explore the effect of the substitution on the overall binding of the analogues on the SPSB2 protein. In general, the cyclic peptide or cyclic peptidomimetics analogues were classified and named according to their parent compound. To illustrate, an analogue of the disulphide-bridged cyclic peptide, **CP0** was named as **CP0-x**, in which **x** is an integer. Similarly, the first analogue of mimetic **M1** was named as **M1-1** (**Table AI.1**). Briefly, each of this cyclic peptide or peptidomimetic was synthesised and purified according to the protocol described for its parent compound. The identity and purity of the analogues, as well as their binding profile on SPSB2 protein, were characterised by LC-MS and SPR assays, respectively (**Figure AI.1-AI.7**), again according to the protocol described for their parent compound.

Table AI.1. A brief summary of other cyclic peptide and peptidomimetic analogues generated in this study.

Parent	Analogues	
	Name	Peptide sequence
Ac-c[CVDINNNC]-NH ₂ (CP0)	CP0-1	Ac-c[CKDINNNC]-NH ₂
	CP0-2	Ac-c[CVDINHNC]-NH ₂
	CP0-3	NH ₂ -c[C(<i>N</i> ^α -Methyl-V)DINNNC]-NH ₂
	CP0-4	FITC- βA-c[CVDINNNC]-NH ₂
c[WDINNNβA] (CP2)	CP2-1	c[5hwDINNNβA]
	CP2-2	c[AcdDINNNβA]
c[BzDINNN] (M1)	M1-1	c[BzDAcdNNN]

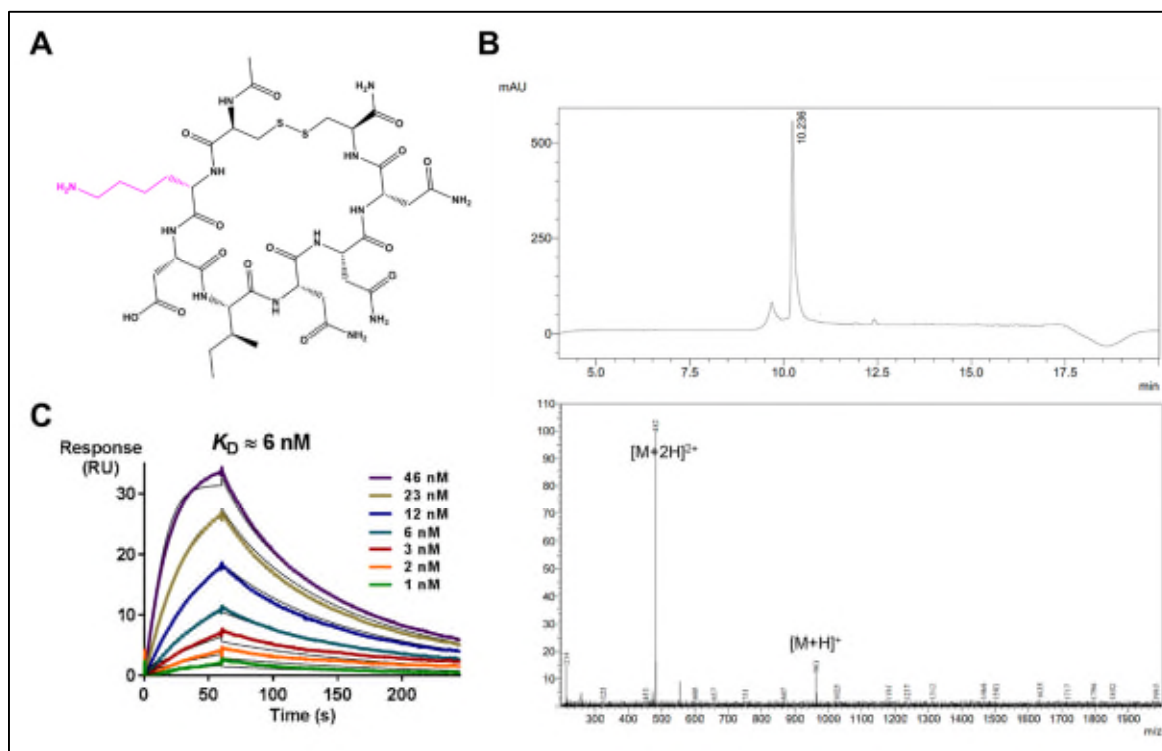
CP0-1Category: Disulphide-bridged cyclic peptide; analogue of Ac-c[CV_DIN_NNC]-NH₂Peptide sequence: Ac-c[CK_DIN_NNC]-NH₂

Figure AI.1. (A) Chemical structure of **CP0-1** with substituted side chain highlighted in magenta. (B) Liquid chromatography (upper panel) and mass spectroscopy (bottom panel) of purified **CP0-1** with the deconvoluted mass (by ESIprot) = 962.09 (theoretical mass = 962.06). (C) Representative SPR sensorgrams of immobilised SPSB2 exposed to increasing concentrations of **CP0-1** in 10 mM HEPES, 150 mM NaCl, 3 mM EDTA and 0.05% Tween 20, pH 7.4 at 25 °C. The data were fitted using a single-site binding model. Binding constant, K_D was determined from double-referenced subtracted SPR sensorgrams fitted to a steady-state 1:1 interaction model.

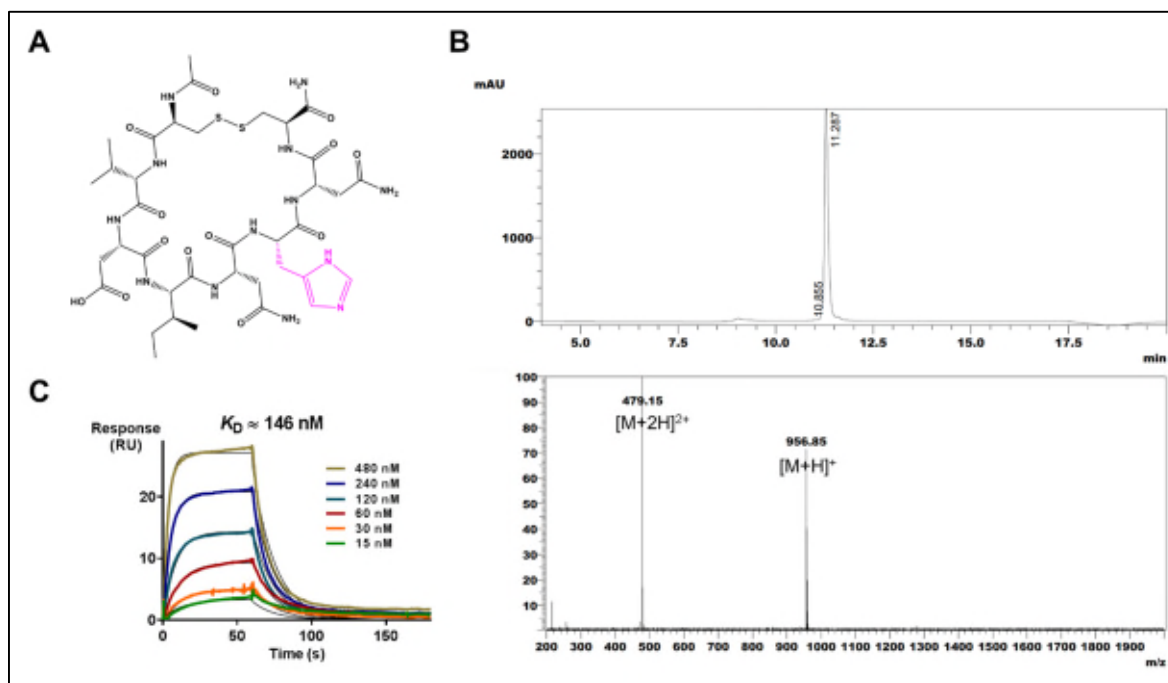
CP0-2Category: Disulphide-bridged cyclic peptide; analogue of Ac-c[CV_DIN_NNC]-NH₂Peptide sequence: Ac-c[CV_DINH_NC]-NH₂

Figure AI.2. (A) Chemical structure of **CP0-2** with substituted side chain highlighted in magenta. (B) Liquid chromatography (upper panel) and mass spectrometry (bottom panel) of purified **CP0-2** with the deconvoluted mass (by ESIprot) = 956.06 (theoretical mass = 956.06). (C) Representative SPR sensorgrams of immobilised SPSB2 exposed to increasing concentrations of **CP0-2** in 10 mM HEPES, 150 mM NaCl, 3 mM EDTA and 0.05% Tween 20, pH 7.4, at 25 °C. The data were fitted using a single-site binding model. Binding constant, K_D was determined from double-referenced subtracted SPR sensorgrams fitted to a steady-state 1:1 interaction model.

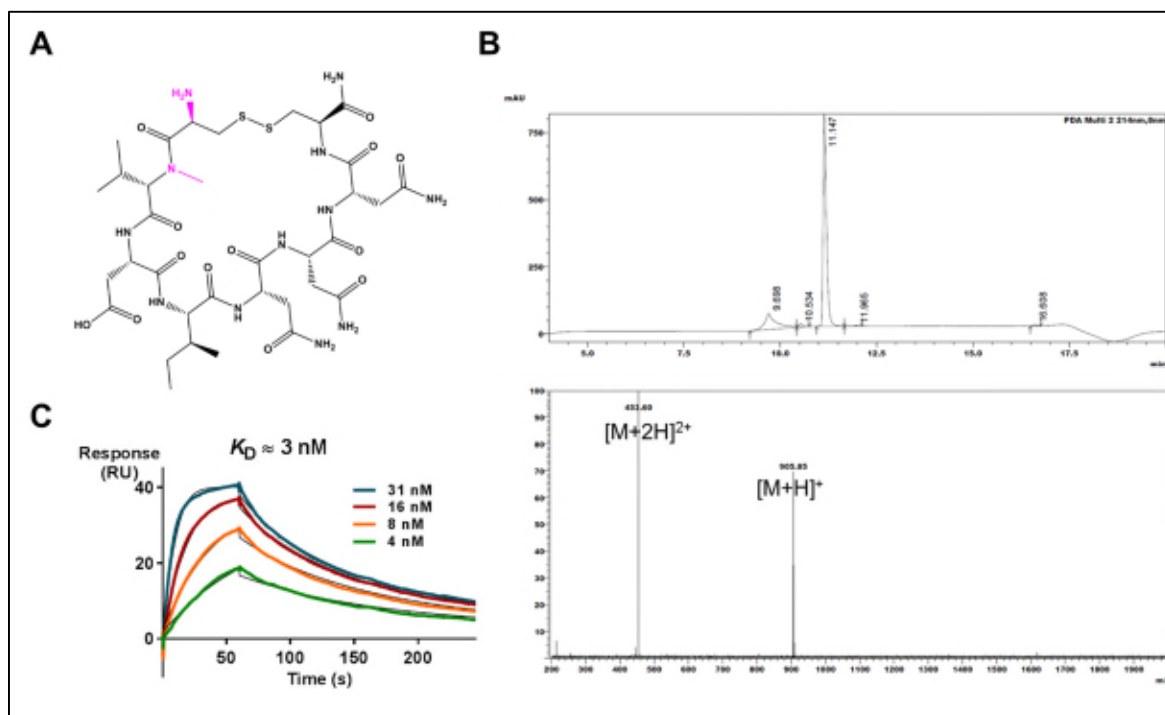
CP0-3Category: Disulphide-bridged cyclic peptide; analogue of Ac-c[CV_DINNNC]-NH₂Peptide sequence: NH₂-c[C(N^α-Methyl-V)DINNNC]-NH₂

Figure AI.3. (A) Chemical structure of **CP0-3** with substituted side chain highlighted in magenta. (B) Liquid chromatography (upper panel) and mass spectrometry (bottom panel) of purified **CP0-3** with the deconvoluted mass (by ESIprot) = 905.01 (theoretical mass = 905.01). (C) Representative SPR sensorgrams of immobilised SPSB2 exposed to increasing concentrations of **CP0-3** in 10 mM HEPES, 150 mM NaCl, 3 mM EDTA and 0.05% Tween 20, pH 7.4, at 25 °C. The data were fitted using a single-site binding model. Binding constant, K_D was determined from double-referenced subtracted SPR sensorgrams fitted to a steady-state 1:1 interaction model.

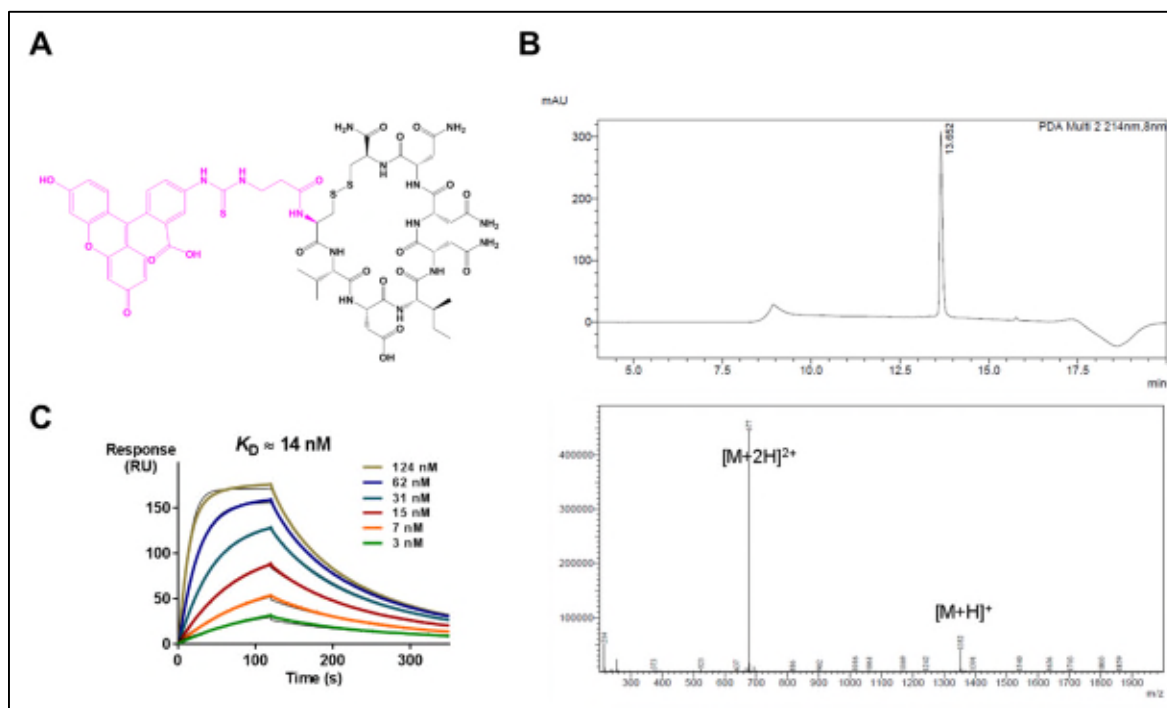
CP0-4Category: Disulphide-bridged cyclic peptide; analogue of Ac-c[CV_DIN_NNC]-NH₂Peptide sequence: FITC-βA-c[CV_DIN_NNC]-NH₂

Figure AI.4. (A) Chemical structure of **CP0-4** with substituted side chain highlighted in magenta. (B) Liquid chromatography (upper panel) and mass spectrometry (bottom panel) of purified **CP0-4** with the deconvoluted mass (by ESIprot) = 1351.59 (theoretical mass = 1351.45). (C) Representative SPR sensorgrams of immobilised SPSB2 exposed to increasing concentrations of **CP0-4** in 10 mM HEPES, 150 mM NaCl, 3 mM EDTA and 0.05% Tween 20, pH 7.4, at 25 °C. The data were fitted using a single-site binding model. Binding constant, K_D was determined from double-referenced subtracted SPR sensorgrams fitted to a steady-state 1:1 interaction model.

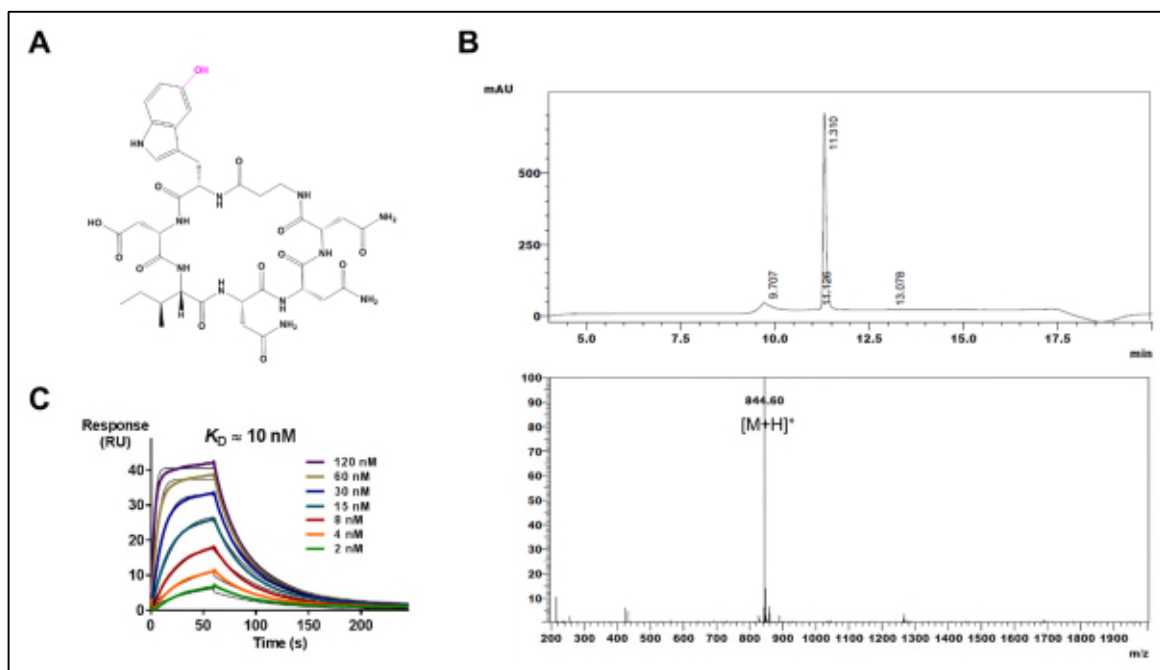
CP2-1Category: Lactam-bridged cyclic peptide; analogue of c[WDINNN β A]Peptide sequence: c[5hwDINNN β A]

Figure AI.5. (A) Chemical structure of **CP2-1** with substituted side chain highlighted in magenta. (B) Liquid chromatography (upper panel) and mass spectroscopy (bottom panel) of purified **CP2-1** with the deconvoluted mass (by ESIprot) = 843.79 (theoretical mass = 843.85). (C) Representative SPR sensorgrams of immobilised SPSB2 exposed to increasing concentrations of **CP2-1** in 10 mM HEPES, 150 mM NaCl, 3 mM EDTA and 0.05% Tween 20, pH 7.4, at 25 °C. The data were fitted using a single-site binding model. Binding constant, K_D was determined from double-referenced subtracted SPR sensorgrams fitted to a steady-state 1:1 interaction model.

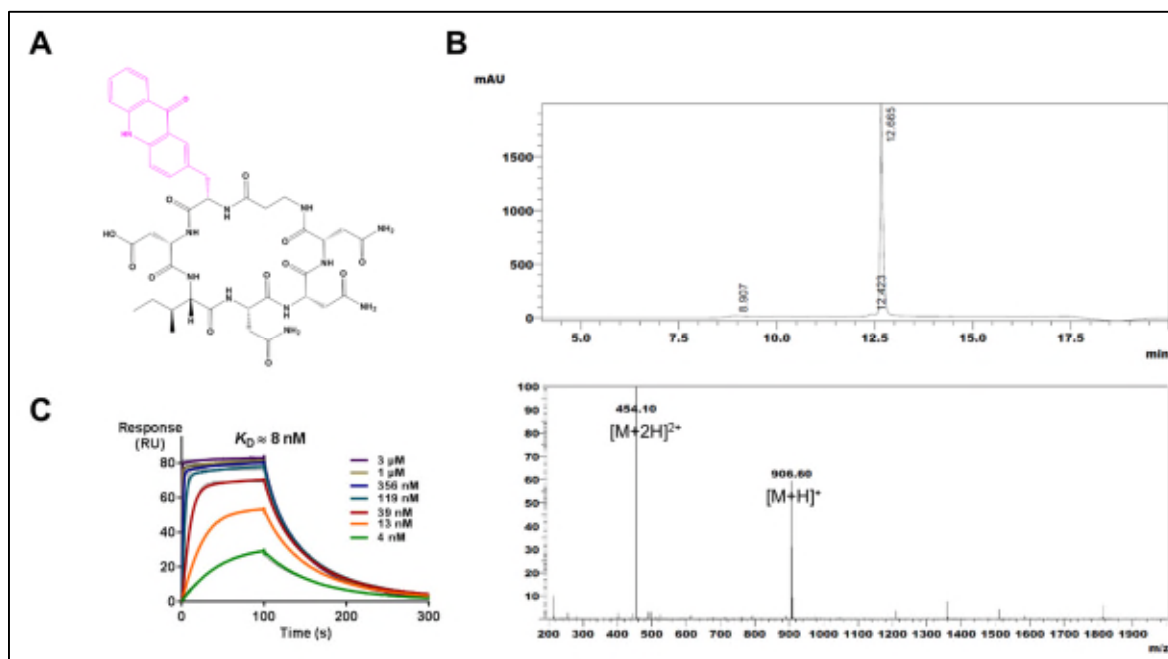
CP2-2Category: Lactam-bridged cyclic peptide; analogue of c[WDINNN β A]Peptide sequence: c[AcDINNN β A]

Figure AI.6. (A) Chemical structure of **CP2-2** with substituted side chain highlighted in magenta. (B) Liquid chromatography (upper panel) and mass spectrometry (bottom panel) of purified **CP2-2** with the deconvoluted mass (by ESIprot) = 905.89 (theoretical mass = 905.92). (C) Representative SPR sensorgrams of immobilised SPSB2 exposed to increasing concentrations of **CP2-2** in 10 mM HEPES, 150 mM NaCl, 3 mM EDTA and 0.05% Tween 20, pH 7.4, at 25 °C. The data were fitted using a single-site binding model. Binding constant, K_D was determined from double-referenced subtracted SPR sensorgrams fitted to a steady-state 1:1 interaction model.

Mimetic M1-1

Category: Benzyl-linked cyclic peptidomimetic; analogue of c[BzDINNN]

Peptide sequence: c[BzDAcDNNN]

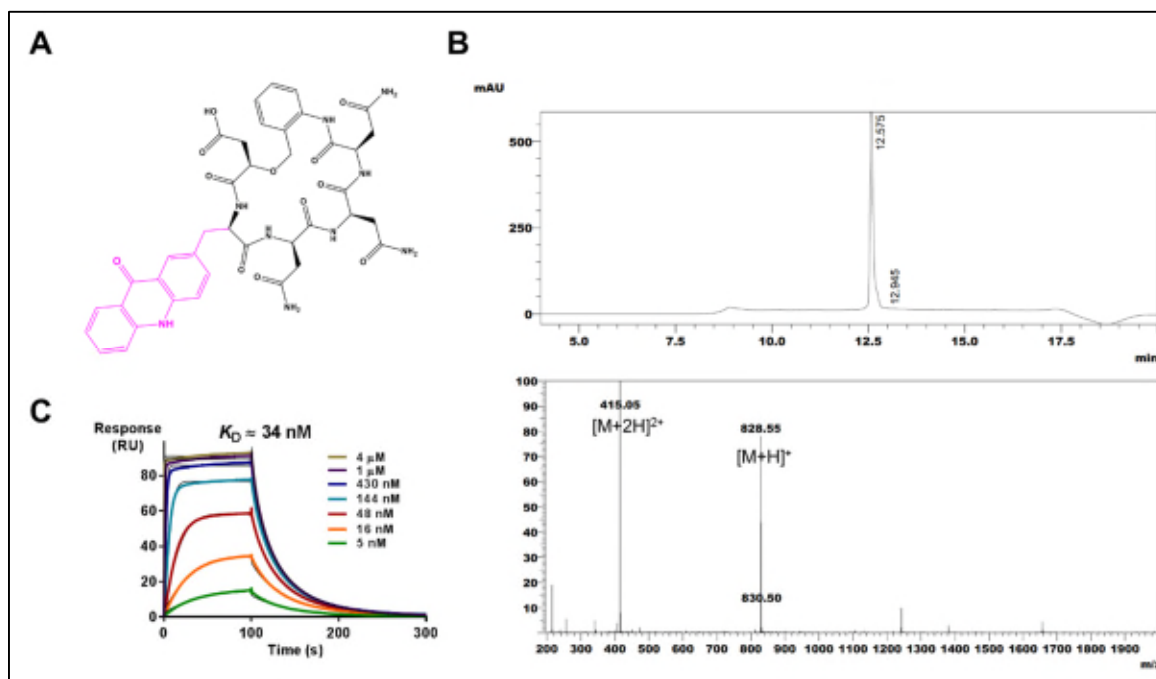


Figure AI.7. (A) Chemical structure of mimetic **M1-1** with substituted side chain highlighted in magenta. (B) Liquid chromatography (upper panel) and mass spectroscopy (bottom panel) of purified mimetic **M1-1** with the deconvoluted mass (by ESIprot) = 827.81 (theoretical mass = 827.81). (C) Representative SPR sensorgrams of immobilised SPSB2 exposed to increasing concentrations of mimetic **M1-1** in 10 mM HEPES, 150 mM NaCl, 3 mM EDTA and 0.05% Tween 20, pH 7.4, at 25 °C. The data were fitted using a single-site binding model. Binding constant, K_D was determined from double-referenced subtracted SPR sensorgrams fitted to a steady-state 1:1 interaction model.

APPENDIX II
Other co-authored publication



An alternative approach to the synthesis of peptides containing a cystathionine bridge



Jitendra R. Harjani, Beow Keat Yap, Raymond S. Norton, Jonathan B. Baell*

Medicinal Chemistry, Monash Institute of Pharmaceutical Sciences, Parkville, VIC 3052, Australia

ARTICLE INFO

Article history:

Received 5 February 2016

Received in revised form 31 March 2016

Accepted 20 April 2016

Available online 22 April 2016

Keywords:

Cystathionine

Cyclopeptides

SPSB2-iNOS

ABSTRACT

A new method for the synthesis of cystathionine containing cyclic peptides has been developed. Conventionally such systems are typically made with relatively late-stage on-resin cyclisation involving reaction between a chlorohomoalanine and cysteine residue. We offer a different approach involving early incorporation of a cystathionine residue through on-resin reaction between a cysteine residue and an *N*-Alloc iodohomoalanine cumyl ester. Subsequent cyclisation then involves amide bond formation. The success of this method was demonstrated by applying it to the synthesis of a cystathionine analogue of the disulfide bridge cyclic peptide, *N*-acetylated cyclic peptide c[CVDINNNC]-NH₂, a biologically active iNOS binding epitope mimetic that binds tightly to the protein, SPSB2. Our method expands the repertoire of synthetic options towards the construction of cystathionine containing cyclic peptides.

© 2016 Elsevier Ltd. All rights reserved.

1. Introduction

Peptides, as drugs offer potential advantages such as greater specificity, high potency and low toxicity.¹ As drug candidates, however they suffer from disadvantages such as low oral bio-availability, short circulation half-life and poor proteolytic stability.² Overcoming these disadvantages is critical for drug development. Disulfide bonds play key roles in the structural stability and biological activity of a number of bioactive molecules.^{3–6} The structural constraints conferred by disulfide bonds are associated with desirable properties such as enhanced proteolytic stability and higher binding affinities for biological targets.⁷ Nonetheless, disulfide bonds are known to be vulnerable towards intra- and extra-cellular reducing agents,⁸ as well as scrambling with the –SH containing molecules such as glutathione or serum albumin.⁹ Although a number of replacements of the disulfide bridge are known in literature, replacement of the –S–S– linkage with the –CH₂–S– (cystathionine, Cth, bridge) offers the advantage that it involves modification at just one atom, resulting in minimal structural perturbation and overcoming the reductive susceptibility of the peptide.¹⁰ Several studies have described the results of replacing the –S–S– linkage with a Cth bridge in oxytocin,¹¹ vasopressin,¹² anti-cardiolipin antibody binders,¹³ VCAM/VLA-4 antagonists¹⁴ and analogues of compstatin.¹⁵

Our group has been involved in the development of cyclic peptides as inhibitors of SPSB2 at the SPSB2-iNOS binding site.¹⁶ Our initial studies indicated that the *N*-acetylated, cyclic peptide c [CVDINNNC]-NH₂, which contains a linkage disulfide bridge, exhibited a *K_D* of about 4 nM for SPSB2, which represents a nearly 70-fold improvement in the affinity when compared with its linear counterpart.¹⁶ The disulfide-bridged cyclic peptide was preferred because of its synthetic ease, and proved to be an important first step in demonstrating that reduced entropy (caused by cyclisation) has a favourable impact on the binding properties of the peptide. However, to be effective in inhibiting the interaction between SPSB2 and iNOS in cytoplasm, an analogue of *N*-acetylated c [CVDINNNC]-NH₂ that would be resistant to reduction was desirable. We have therefore investigated the incorporation of a Cth bridge into this peptide in place of the disulfide.

Incorporation of the Cth bridge in cyclic peptides has been carried out by two distinct approaches. The first exploits the reactivity of the –SH group as a nucleophile that is known to add to alkenes or substitute good leaving groups, creating the cyclic thioether system.^{11,14,17} The other approach uses the integration of an appropriately protected bis α,α' -amino acid, cystathionine.^{10,13,15} Irrespective of which method is preferred, the selection of orthogonal protecting groups becomes crucial as the –NH₂ and –COOH groups on at least one amino acid functional group are required to be resilient towards certain chemistries that are commonly used for peptide synthesis and cleavage under conditions that do not affect the other protecting groups commonly employed during peptide synthesis. Given the popularity and use of

* Corresponding author

cystathionine analogues of disulfide-containing therapeutic peptides, we have explored an alternative approach to known methods of their synthesis. We describe a new method for synthesis of the Cth bridge-containing cyclic peptide that depends on building its architecture via *S*-alkylation, creating orthogonally protected amino acid groups at the terminal position that allow for on-resin cyclisation and functional group interconversion.

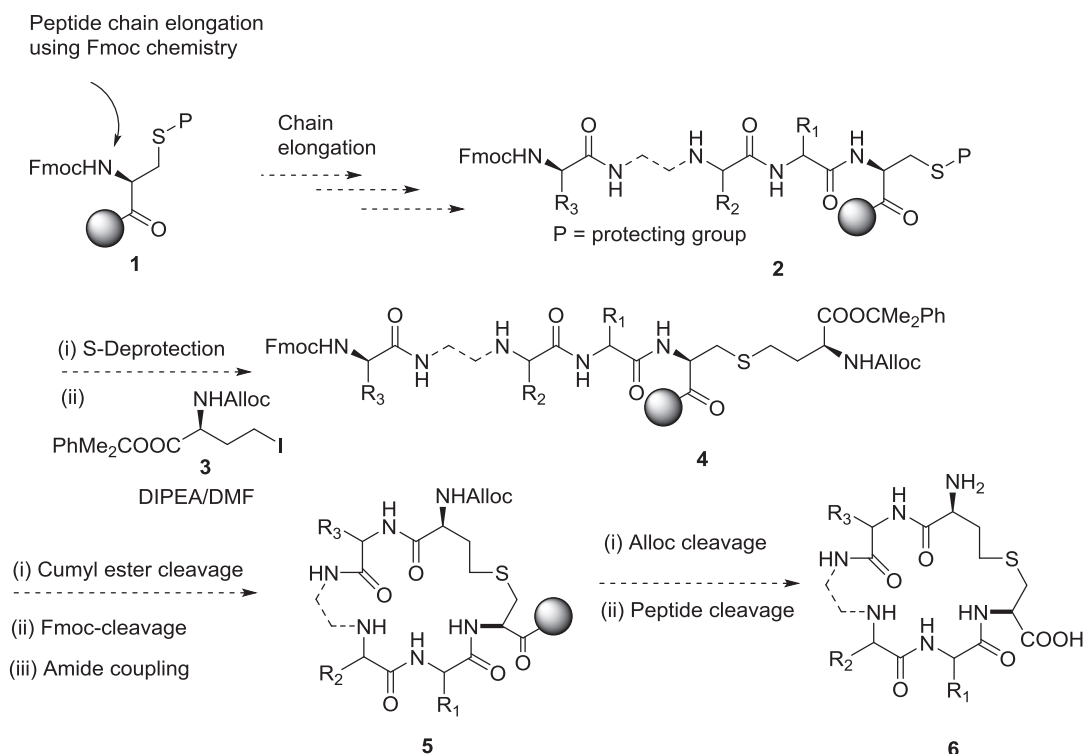
2. Results and discussion

We envisioned that a compound such as **3** would offer an opportunity to incorporate the cystathionine moiety in cyclic peptides. If we start with the Fmoc-protected, C-terminus resin-bound cysteine that has a protected $-SH$ group as in **1**, we might be able to use the N-terminus to elongate the chain as required, using standard Fmoc peptide chemistry as in **2** (Scheme 1). Release of the $-SH$ group should provide an opportunity to *S*-alkylate, establishing the cystathionine core in the peptide as in **4**. Once the desired sequence of amino acids is linked, the cumyl ester may be selectively cleaved to release the corresponding $-COOH$, while not affecting other Fmoc compatible acid-sensitive groups such as trityl and *tert*-Bu that protect the amide and acid groups on the amino acids in the peptide chain. The Fmoc protection on the terminal amino acid can be removed, releasing the $-NH_2$ group. While still resin-bound, the free $-COOH$ and $-NH_2$ groups at the opposite end of the chain could be coupled to cyclise the peptide chain as in **5**. This is likely to result in the formation of cyclic peptide on resin. Similar on-resin cyclisation leading to the generation of cyclic structures has been reported to work well in the past.¹⁸ Removal of protecting groups followed by cleavage of the peptide from the resin should afford the cyclic peptide with the cystathionine moiety **6**.

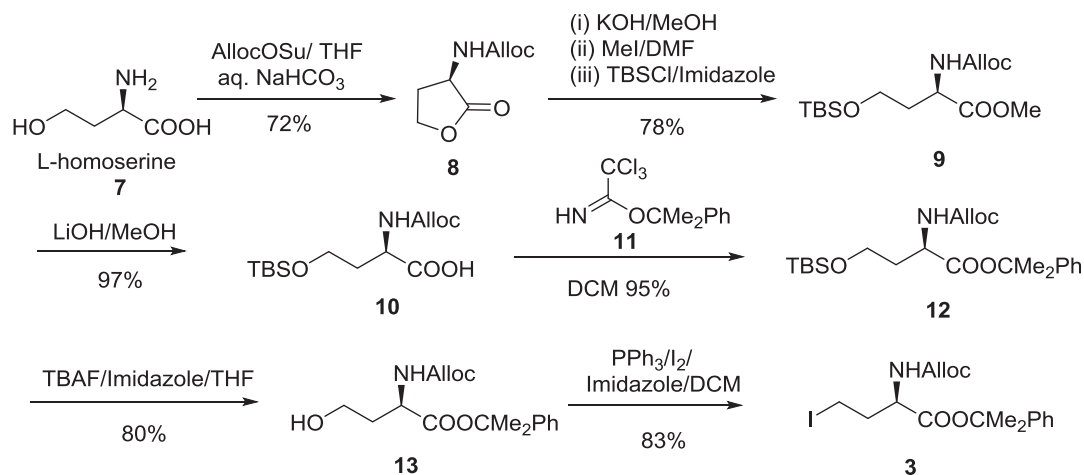
L-Homoserine was *N*-Alloc protected using AllocOSu and $NaHCO_3$ in aq THF. Not surprisingly, the *N*-Alloc protection also resulted in closure of the five-membered lactone ring as in **8** (Scheme 2). This propensity to lactonise offered challenges in the

synthetic manipulation of *L*-homoserine. We found that the most convenient way to functionalise *L*-homoserine with the desired orthogonal protecting groups was to protect all the remaining functional groups ($-OH$ and $-COOH$) with protecting groups. The terminally protected functional groups were deprotected one group at a time and the required functional group interconversion/transprotection was achieved.

The lactone **8** was subjected to the OH^- ion mediated ring opening reaction that presumably leads to the formation of α,ω -hydroxy carboxylate (Scheme 2). The carboxylate was subjected to methylation using iodomethane followed by silylation of the terminal $-OH$ group with TBSCl to form the methyl carboxylate with the terminal $-OTBS$ group as in **9**. The carboxylate group in **9** was transprotected by first using LiOH mediated deprotection of the $-COOMe$ group to yield the carboxylic acid **10**, followed by subsequent esterification of the $-COOH$ group in **10** using the imidate reagent **11**, to yield the corresponding cumyl ester **12**. The next step was deprotection of the $-OTBS$ group in **12** followed by conversion of the alcoholic hydroxyl group to the iodo group as in **3** (Scheme 2). Substantial by-product formation, was apparent when the fluoride mediated cleavage of $-OTBS$ was conducted. The deprotection of the $-OTBS$ group in **12** was achieved with TBAF in the presence of a two-fold excess of imidazole to yield appropriately functionalised *L*-homoserine with the $-NHAlloc$ and $-COOCMe_2Ph$ groups. Even in the presence of a two-fold excess of imidazole, the best outcome from the reaction was accomplished by monitoring it regularly with TLC to assure that the product was separated before any noticeable quantity of by-product began to appear on the TLC. The role of imidazole in this reaction appears to be to reduce the rate of the reaction that leads to the formation of the by-product that we were not able to characterise. Iodination of the alcoholic $-OH$ group in **13** was achieved using iodine as an iodinating agent in the presence of triphenyl phosphine and imidazole, to yield the *L*-homoserine derivative with $-NHAlloc$ and $-COOCMe_2Ph$ groups and a terminal iodo group as in **3**.



Scheme 1. Proposed plan for synthesis of cystathionine-bridge containing cyclic peptide **6**.



Scheme 2. Synthesis of 2-phenylpropan-2-yl (R)-2-((allyloxy)carbonyl)amino-4-iodobutanoate **3**.

To demonstrate the utility of the iodo homologue of L-homoserine **3** in the synthesis of Cth-bridge containing peptides we utilised it to synthesise a known peptide that contained a disulfide bridge.¹⁶ Rink amide AM resin was identified to be compatible with the proposed synthetic plan and was known to offer a clear advantage of stability under basic conditions required during amide coupling procedures, stability under mild acidic conditions required for the cumyl ester group removal and its ability to cleave the peptide protecting groups and peptide from the resin in the final step of the proposed synthesis. The peptide chain CNNNIDV was built on resin using standard Fmoc chemistry (Scheme 3). HCTU was used as a coupling agent. The $-S^t$ Bu protecting group was removed using DTT as a reducing agent followed by S-alkylation of the free cysteine $-SH$ with **3**. This was followed by deprotection of the cumyl ester group under mildly acidic conditions to release the $-COOH$ group at one end of the peptide chain. Scavengers such as triisopropylsilane (TIPS) and ethanedithiol (EDT) are added to the reagents during deprotection of the cumyl ester group as they are known to maintain a reductive environment that prevents oxidation of the divalent sulfur of the thioether bridge (Scheme 3). They also prevent the reaction of released 2-phenylisopropyl cation and its by-products with the thioether group, a process that is known to result in the formation of L-homoserine lactone via a thermodynamically favourable cyclisation step.¹⁹ The $-NH$ Fmoc deprotection at the other end of the peptide chain was performed to release the free $-NH_2$ group. An HCTU mediated amide coupling procedure commonly used in the peptide synthesis was employed to connect the aforementioned $-COOH$ and $-NH_2$ groups and enable the lactam-bridge cyclisation. This was followed by functional group interconversion that involved homogenous catalytic reductive cleavage of the $-NH$ Alloc group to release the free $-NH_2$ group, followed by the acetylation of the free $-NH_2$ group. In the final synthetic manipulation, a one-step deprotection of all acid-sensitive amino and carboxylic acid protecting groups and cleavage of the peptide from resin was achieved at the same time. The crude product was then subjected to purification by RP-HPLC. To establish the identity and purity of **20** (Scheme 3), the purified peptide was analysed by 1H NMR and LC-MS. A single peak was observed in the UV trace in the LCMS spectra, with a deconvoluted mass of 914.60, which matched the theoretical mass m/z of $915.60 (M+H)^+$, $458.55 (M+2H)^{2+}$, indicating the desired cyclic peptide. The chemical shifts and integration of protons in the aliphatic versus amide protons in the 1H NMR spectra confirm the purity of **20**. These observations attest to the success of the use of **3** in the proposed method as a feasible alternative to

generating cyclic peptides that contain the cystathionine group. Although halo homoserine analogues have been used in the synthesis of Cth bridge containing analogues, we present an orthogonal amino group protecting strategy allowing for selective functionalisation of the peptide, prior to global deprotection.^{11,20}

3. Conclusions

Our new method uses the assembly of the thioether-bridge at the end of the peptide synthesis sequence after most of the peptide chain has been assembled. It depends on the use of either mildly acidic or catalytic reductive conditions required for selective deprotection of the $-COOH$ and $-NH_2$ groups, while not affecting the other acid or base sensitive groups on the peptide sequence that are compatible with the Fmoc chemistry. The orthogonality of the protecting groups used in this approach allows for better control of selectively cleaving one protecting group at a time and exploiting its reactivity.

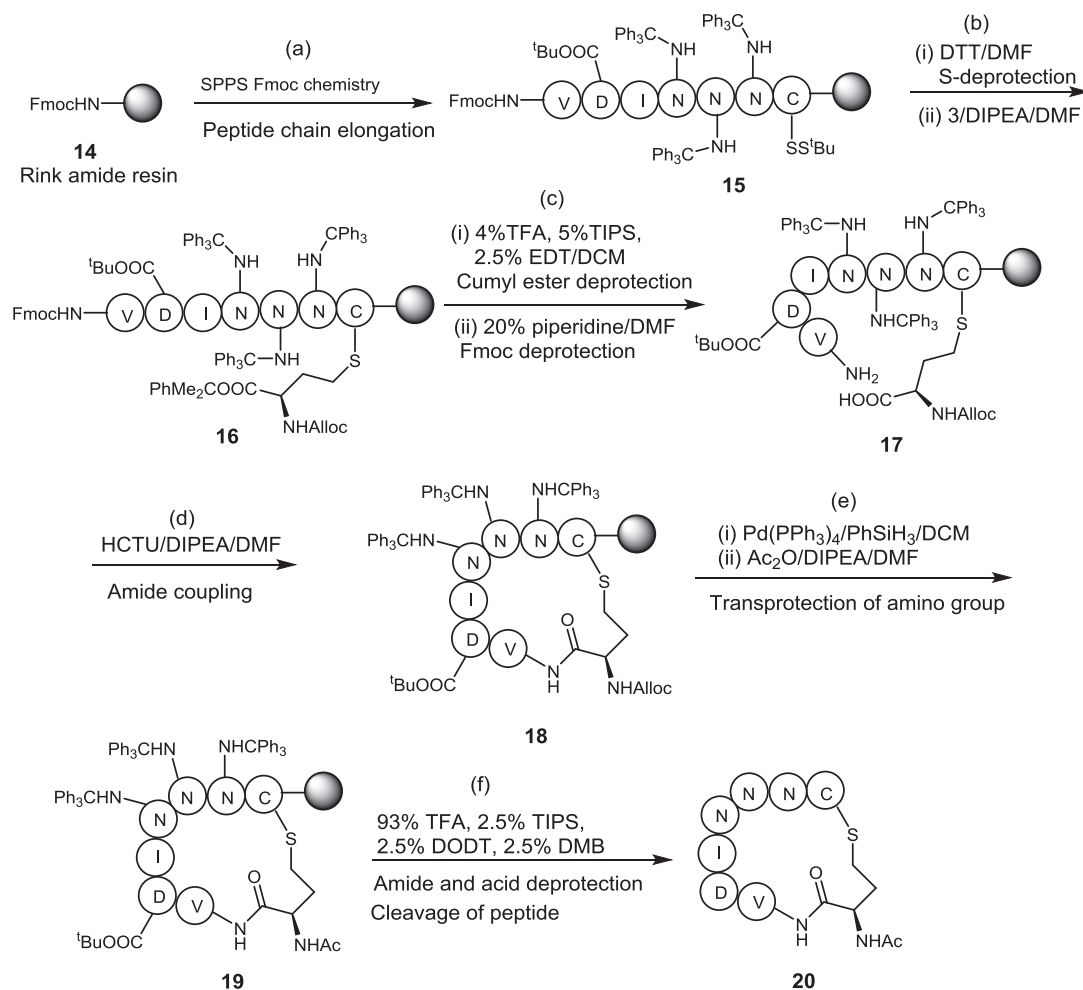
We have deliberately targeted the cystathionine analogue of *N*-acetylated cyclic peptide c[CVDINNNC]- NH_2 because we have recently determined that the Cth bridge-based cyclic peptide is a redox-stable ligand that binds tightly to SPSB2 and is of interest as a potential anti-infective.²¹

We believe that this method represents a valuable alternative that might complement the known methods used for the synthesis of the Cth bridge containing cyclic peptides.

4. Experimental

4.1. General

Commercially available reagents were used without further purification. Column chromatography was performed using silica gel 60 (40–60 μ m). The solvents for chromatography were used without purification. The reactions were monitored by TLC on Silica Gel 60F-254 plates with detection by $KMnO_4$ stain (1.50 g of $KMnO_4$, 10.0 g K_2CO_3 , and 1.25 mL 10% NaOH in 200 mL water). Melting points were determined using Mettler Toledo MP50 melting point system. The optical rotations were measured using a Jasco P-2000 polarimeter at room temperature in a 10 cm, 1 mL cell. The Attenuated Total Reflection-Fourier Transform Infrared Spectroscopy (ATR-FTIR) measurements were performed using a Shimadzu IRTracer-100 Fourier transform spectrometer by averaging 128 scans with a resolution of 4 cm^{-1} . For the small molecules, 1H and ^{13}C NMR spectra were recorded at 400.13 and



Scheme 3. Reagents and conditions: (a) SPPS; (b) (i) DTT (3000 mol %), DIPEA (2.5%, v/v), DMF, 16 h; (ii) **3** (150 mol %), DIPEA (300 mol %), DMF, dark, 16 h; (c) (i) TFA (4%, v/v), TIPS (5%, v/v), EDT (2.5%, v/v), DCM, 15 min \times 3 times; (ii) piperidine (20%, v/v), DMF, 30 min; (d) HCTU (300 mol %), DIPEA (600 mol %), DMF, 16 h; (e) (i) Pd(PPh₃)₄ (200 mol %), PhSiH₃ (2000 mol %), dry DCM, dark, 2 h; (ii) Acetic anhydride (1000 mol %), DIPEA (1500 mol %), DMF, 3 h; (f) TFA (92.5%, v/v), TIPS (2.5%, v/v), DODT (2.5%, v/v), DMB (2.5%, v/v), 2 h.

100.62 MHz, respectively, on a Bruker Avance III Nanobay spectrometer with a BACS 60 sample changer. Proton resonances are annotated as: chemical shift (δ), multiplicity (s, singlet; d, doublet; m, multiplet), coupling constant (J , Hz), and the number of protons. For peptide analysis, the ¹H NMR spectrum was recorded at 600 MHz on a Bruker Avance spectrometer equipped with a 5 mm TCI cryoprobe. High resolution MS was performed with an Agilent 6224 TOF LCMS coupled to an Agilent 1290 Infinity LC. The peptide LCMS was performed with a Shimadzu LCMS2020. The peptide purification was performed using Phenomenex[®] Luna C8 column (100 Å, 3 μ m, 100 \times 2 mm), 30 °C; sample was eluted using a binary gradient (solvent A: 0.05% aq TFA; solvent B: 0.05% TFA in CH₃CN; 0–60% B [10 min], 0.2 mL min⁻¹).

4.2. Synthesis

4.2.1. Allyl (*R*)-(2-oxotetrahydrofuran-3-yl)carbamate (8**).** Water (200 mL) was added to mixture of L-homoserine **7** (9.00 g, 75.63 mmol) and NaHCO₃ (9.58 g, 114 mmol). The reaction mixture was stirred for 10 min until the initial gas evolution subsided. A solution of AllocOSu (15.05 g, 75.6 mmol) in THF (150 mL) was added dropwise over a 1 h duration to the solution of L-homoserine, while being stirred. The reaction mixture was stirred at room temperature for 16 h, after which it was evaporated to almost complete dryness. A citric acid (150 mL of aq 10%) solution was added to the residual mass and the acidic pH of the aq layer was

verified. Sodium chloride was added in small portions, while the reaction mixture was stirred until no more sodium chloride appeared to dissolve in the solution. EtOAc (2 \times 100 mL) was used for the extraction of the product. The organic layers were combined, dried over anhydrous MgSO₄, and evaporated under reduced pressure to yield the crude product. Analytically pure **8** was separated from the crude product using column chromatography (50% EtOAc in hexanes) as a white solid (10.07 g, 72%). R_f (50% EtOAc in hexanes) 0.41; mp 69–71 °C (crystallised from methanol); [α]_D²⁵ –26.14 ($c=1$, THF); IR (neat) 802, 922, 1003, 1161, 1258, 1285, 1362, 1385, 1420, 1451, 1535, 1651, 1694, 1694, 1775, 2338, 2361, 2882, 2943, 3329 cm⁻¹; ¹H NMR (400 MHz, DMSO-*d*₆): δ =7.75 (d, $J=8.4$ Hz, 1H), 5.91 (ddd, $J=17.2$, 10.6, 5.4 Hz, 1H), 5.29 (ddd, $J=17.2$, 3.3, 1.6 Hz, 1H), 5.20 (dd, $J=10.5$, 1.4 Hz, 1H), 4.50 (d, $J=5.4$ Hz, 2H), 4.42 (dt, $J=11.2$, 8.8 Hz, 1H), 4.32 (td, $J=8.7$, 1.1 Hz, 1H), 4.19 (ddd, $J=10.8$, 8.7, 6.3 Hz, 1H), 2.40 (m, 1H), 2.17 (m, 1H); ¹³C NMR (101 MHz, DMSO-*d*₆): δ =175.4, 155.6, 133.4, 117.3, 65.1, 64.7, 49.5, 28.1; HRMS (EI) calcd for C₈H₁₂NO₄ [M+H]⁺: m/z 186.0761; found: m/z 186.0749.

4.2.2. Methyl *N*-((allyloxy)carbonyl)-*O*-(*tert*-butyldimethylsilyl)-*D*-homoserinate (9**).** KOH (2.270 g, 40.54 mmol) was dissolved in MeOH (100 mL) by stirring at room temperature for 20 min. Lactone **8** (7.507 g, 40.54 mmol) was added in small portions, to the alkaline methanolic solution over a 20 min period, while it was being stirred at room temperature. The reaction mixture was

stirred at room temperature for 1 h after which the methanolic solution was evaporated under reduced pressure to get rid of most of the methanol. DMF (100 mL) was added to the residual mass to obtain a clear solution. MeI (6.910 g, 48.65 mmol) was added dropwise to this DMF solution. The reaction mixture was stirred at room temperature for 16 h, after which imidazole (3.40 g, 50 mmol) and TBSCl (7.536 g, 50 mmol) were added. The reaction mixture was stirred at room temperature for 3 h. The DMF was evaporated under reduced pressure and the resulting viscous liquid was treated with water (100 mL). The crude product was extracted from the resultant using DCM (2×100 mL). The DCM extracts were combined, dried over anhydrous MgSO₄ and evaporated under reduced pressure to yield the crude product. Pure **9** was separated from the crude product using column chromatography (20% EtOAc in hexanes) as a colourless viscous liquid (10.46 g, 78%). *R_f* (20% EtOAc in hexanes) 0.62; $[\alpha]_D^{21}$ –1.87 (*c*=1, THF); IR (neat) 833, 934, 995, 1096, 1165, 1211, 1250, 1339, 1389, 1435, 1470, 1508, 1724, 2361, 2855, 2928, 2951 cm⁻¹; ¹H NMR (400 MHz, CDCl₃): δ=5.90 (m, 2H), 5.30 (dd, *J*=17.2, 1.3 Hz, 1H), 5.19 (ddd, *J*=10.5, 2.8, 1.4 Hz, 1H), 4.56 (d, *J*=5.4 Hz, 2H), 4.45 (dd, *J*=12.1, 6.6 Hz, 1H), 3.71 (m, 5H), 2.02 (m, 2H), 0.89 (s, 9H), 0.05 (m, 6H); ¹³C NMR (101 MHz, CDCl₃): δ=172.9, 156.0, 132.9, 117.5, 65.7, 60.1, 52.7, 52.4, 33.9, 26.0, 18.3, –5.5, –5.5; HRMS (EI) calcd for C₁₅H₃₀NO₅Si [M+H]⁺: *m/z* 332.1888; found: *m/z* 332.1891.

4.2.3. N-((Allyloxy)carbonyl)-O-(tert-butyl dimethylsilyl)-D-homoserine (10). A solution of LiOH (0.648 g, 27 mmol) in MeOH (10 mL) was added dropwise to the solution of **9** (4.47 g, 13.5 mmol) in MeOH (100 mL) at room temperature. The reaction mixture was stirred at room temperature for 16 h after which the methanol was evaporated under reduced pressure to obtain a viscous material to which water (50 mL) was added to obtain a clear solution. This was followed by the addition of the aqueous citric acid (30 mL of 10%) solution. After an acidic pH of the solution was verified, the crude product was extracted with DCM (3×50 mL). The organic extracts are combined, dried over anhydrous MgSO₄ and evaporated under reduced pressure to yield the crude product as a colourless viscous liquid that appears to be practically pure by analytical methods (4.15 g, 97%). *R_f* (40% EtOAc, 1% AcOH in hexanes) 0.53; $[\alpha]_D^{21}$ –0.62 (*c*=1, THF); IR (neat) 806, 833, 930, 995, 1015, 1065, 1169, 1211, 1246, 1277, 1339, 1404, 1431, 1458, 1508, 1659, 1701, 2855, 2886, 2928, 3094, 3113, 3240 cm⁻¹; ¹H NMR (400 MHz, CDCl₃): δ=6.01 (d, *J*=7.0 Hz, 1H), 5.90 (ddt, *J*=17.1, 10.8, 5.5 Hz, 1H), 5.30 (dd, 17.2, 1.5 Hz, 1H), 5.20 (ddd, *J*=10.5, 2.7, 1.3 Hz, 1H), 4.57 (d, *J*=5.4 Hz, 2H), 4.44 (dd, *J*=12.4, 5.5 Hz, 1H), 3.80 (t, *J*=5.4 Hz, 2H), 2.08 (m, 2H), 0.89 (s, 9H), 0.07 (s, 6H); ¹³C NMR (101 MHz, CDCl₃): δ=176.3, 156.3, 132.7, 117.7, 65.9, 60.7, 52.9, 33.6, 25.9, 18.3, –5.5; HRMS (EI) calcd for C₁₄H₂₈NO₅Si [M+H]⁺: *m/z* 318.1731; found: *m/z* 318.1732.

4.2.4. 2-Phenylpropan-2-yl N-((allyloxy)carbonyl)-O-(tert-butyl dimethylsilyl)-D-homoserinate (12). The trichloroacetimidate reagent **11** (4.02 g, 14.4 mmol) was added to a solution of the carboxylic acid **10** (3.500 g, 11.04 mmol) in DCM (50 mL). The reaction mixture was stirred at room temperature for 16 h, during which time a crystalline precipitate separated from the reaction mixture. The reaction mixture was concentrated and dry loaded on silica gel. Pure **12** was separated using silica gel column chromatography (10% EtOAc in hexanes) as a colourless viscous liquid (4.56 g, 95%). *R_f* (10% EtOAc in hexanes) 0.56; $[\alpha]_D^{21}$ –8.45 (*c*=1, THF); IR (neat) 833, 934, 1030, 1096, 1138, 1196, 1215, 1254, 1339, 1366, 1447, 1470, 1497, 1724, 2855, 2882, 2951 cm⁻¹; ¹H NMR (400 MHz, CDCl₃): δ=7.45 (m, 1H), 7.30 (m, 4H), 7.20 (m, 1H), 5.83 (m, 1H), 5.24 (dd, *J*=17.2, 1.4 Hz, 1H), 5.13 (d, *J*=10.4 Hz, 1H), 4.51 (d, *J*=5.2 Hz, 2H), 4.38 (td, *J*=7.4, 4.5 Hz, 1H), 3.67 (m, 2H), 2.05 (m, 1H), 1.90 (m, 1H), 1.75 (m, 6H), 0.85 (s, 9H), 0.00 (s, 6H); ¹³C NMR (101 MHz, CDCl₃): δ=170.9, 156.0, 145.4, 132.9, 128.4, 127.3, 124.4, 117.3, 83.0, 65.6, 60.3, 53.2, 34.1, 31.9, 28.6,

28.4, 26.0, 18.3, –5.5; HRMS (EI) calcd for C₂₃H₃₈NO₅Si [M+H]⁺: *m/z* 436.2514; found: *m/z* 436.2486.

4.2.5. 2-Phenylpropan-2-yl((allyloxy)carbonyl)-D-homoserinate (13). Imidazole (0.506 g, 7.45 mmol) was added in small portions to a solution of **12** (1.625 g, 3.73 mmol) in THF (30 mL), while being stirred. A solution of TBAF (1.0 M solution in THF, 3.73 mL, 3.73 mmol) was added dropwise to the mixture of **12** and imidazole in THF. The reaction mixture was monitored every 15 min by TLC (30% EtOAc in hexanes, alkaline KMnO₄ as TLC stain) to ensure that the product was isolated before noticeable quantities of by-product formation became apparent by TLC (2 h in this case). The reaction mixture was loaded on silica gel, evaporated under reduced pressure and eluted with 30% EtOAc in hexanes to obtain **13** as a colourless viscous liquid (0.958 g, 80%). *R_f* (30% EtOAc in hexanes) 0.49; $[\alpha]_D^{21}$ –10.66 (*c*=1, THF); IR (neat) 837, 930, 991, 1049, 1099, 1138, 1215, 1269, 1366, 1447, 1512, 1701, 2886, 2936, 2978, 3333 cm⁻¹; ¹H NMR (400 MHz, CDCl₃): δ=7.27 (m, 4H), 7.18 (m, 1H), 5.82 (m, 1H), 5.51 (d, *J*=7.6 Hz, 1H), 5.22 (dd, *J*=17.2, 1.4 Hz, 1H), 5.14 (dd, *J*=10.4, 1.3 Hz, 1H), 4.45 (m, 3H), 3.61 (m, 2H), 2.17 (m, 1H), 1.72 (m, 6H), 1.59 (m, 1H); ¹³C NMR (101 MHz, CDCl₃): δ=171.1, 157.0, 144.9, 132.5, 128.4, 127.4, 124.3, 118.0, 83.6, 66.1, 58.3, 51.5, 36.0, 28.7, 28.3; HRMS (EI) calcd for C₁₇H₂₃NO₅Na [M+Na]⁺: *m/z* 344.1468; found: *m/z* 344.1467.

4.2.6. 2-Phenylpropan-2-yl (R)-2-(((allyloxy)carbonyl)amino)-4-iodobutanoate (3). A mixture of imidazole (0.230 g, 3.45 mmol) and triphenyl phosphine (0.904 g, 3.45 mmol) in DCM (20 mL) was cooled to –40 °C. Iodine (0.876 g, 3.45 mmol) was added in small portions to this cold solution, while the solution was being stirred at –40 °C. The stirring was continued at –40 °C for 30 min. A solution of **13** (0.742 g, 2.31 mmol) in DCM (10 mL) was added dropwise into the above reagent mixture in DCM, while still continuing to maintain the reaction temperature at –40 °C. The reaction mixture was slowly allowed to warm up to room temperature and then maintained at the room temperature for 3 h, while continuously stirring during the process. The reaction mixture was concentrated and dry loaded on silica gel. Pure **3** was separated as a white solid using silica gel column chromatography and 20% EtOAc in hexanes as an eluent (0.826 g, 83%). *R_f* (20% EtOAc in hexanes) 0.69; mp 50–52 °C (crystallised from methanol); $[\alpha]_D^{21}$ –2.80 (*c*=1, THF); IR (neat) 841, 910, 926, 988, 1038, 1076, 1130, 1165, 1207, 1246, 1277, 1366, 1431, 1447, 1497, 1543, 1686, 1732, 2940, 2978, 3059, 3283 cm⁻¹; ¹H NMR (400 MHz, DMSO-*d*₆): δ=7.68 (d, *J*=8.1 Hz, 1H), 7.35 (m, 5H), 5.91 (ddd, *J*=17.2, 10.5, 5.3 Hz, 1H), 5.30 (dd, *J*=17.2, 1.6 Hz, 1H), 5.18 (ddd, *J*=10.5, 2.8, 1.3 Hz, 1H), 4.50 (m, 2H), 4.11 (td, *J*=9.8, 4.4 Hz, 1H), 3.26 (m, 2H), 2.24 (m, 1H), 2.10 (m, 1H), 1.70 (m, 6H); ¹³C NMR (101 MHz, CDCl₃): δ=169.8, 155.9, 144.8, 132.6, 128.6, 127.6, 124.4, 118.1, 83.9, 66.1, 55.3, 37.4, 31.9, 28.8, 28.2; HRMS (EI) calcd for C₁₇H₂₂INO₄Na [M+Na]⁺: *m/z* 454.0486; found: *m/z* 454.0488.

4.2.7. Peptide 20. All reactions were carried out at room temperature. Rink amide AM resin (179 mg, 0.1 mmol, 0.56 mmol g⁻¹) was swelled in DMF (5 mL) for 30 min. The peptide side-chain with protected –NHfmoc was assembled on resin using an automated Peptide Synthesizer 3 (PS3™), employing Fmoc chemistry using 50 min for each coupling cycle. Fmoc amino acid (0.3 mmol, 300 mol%), HCTU (0.3 mmol, 300 mol%) and DIPEA (7%, v/v) in DMF (5 mL) were used for each coupling procedure (Scheme 3). Double coupling was used to couple the second Asn to the first Asn as well as the third Asn to the second Asn, as this double coupling protocol was found to be superior in our earlier studies. After each coupling step, Fmoc deprotection was achieved with piperidine in DMF (5 mL, 20%, v/v, 2×5 min treatments). After the complete assembly of the linear protected peptide chain with the Fmoc-N-

terminus, the *tert*-butylthiol ($-S-tBu$) protecting group of the Cys residue at the C-terminus was removed with DTT (10%, w/v) and DIPEA (2.5%, v/v) in DMF (5 mL) for 16 h. The resin was washed with DMF (6×5 mL) to remove any residual DTT prior to 16 h coupling with **3** (150 mol%) and DIPEA (300 mol%) in DMF (5 mL). The coupling was carried out in the dark as most iodo compounds such as **3** are likely to be light sensitive. After washing the resin with DMF (3×5 mL) and DCM (3×5 mL), the cumyl ester protecting group was removed using a cocktail mixture containing TFA (4%, v/v), TIPS (5%, v/v) and EDT (2.5%, v/v) in DCM (3×5 mL, 15 min wait each time). The resin was washed with DCM (3×5 mL) followed by DMF (3×5 mL) before it was treated with piperidine (20%, v/v) in DMF (5 mL) for 30 min to remove the Fmoc protecting group at the N-terminus of the linear peptide. After washing the excess reagent from the resin using DMF (3×5 mL), the lactam bridge cyclisation between the free amino and carboxyl groups was achieved with HCTU (300 mol%) and DIPEA (600 mol%) in DMF (5 mL) for 12 h. To remove the Alloc protecting group, the resin was first washed with DMF (3×5 mL), followed by dry DCM (3×5 mL). Nitrogen was bubbled through the suspension of resin in DCM prior to the addition of Pd(PPh₃)₄ (200 mol%, solution in dry DCM, 5 mL) and PhSiH₃ (2000 mol%). The Alloc deprotection was carried out for 2 h in the dark. To remove the excess palladium catalyst, the resin was washed with DIPEA (0.5%, v/v, in DMF, 2×5 mL), followed by sodium diethyldithiocarbamate (0.2 M in DMF, 3×5 mL) and DMF:DCM (1:1, 5×5 mL). This was followed by N-acetylation with Ac₂O (1000 mol%) and DIPEA (1500 mol%) in DMF (5 mL) for 3 h. The crude peptide was cleaved from the resin with a 5 mL solution containing TFA (92.5%, v/v), TIPS (2.5%, v/v), dimethoxybenzene (2.5%, v/v) and 3,6-dioxo-1,8-octanedithiol (DODT, 2.5%, v/v) for 2 h. After cleavage, the peptide was precipitated using cold diethyl ether (2×30 mL), dissolved in a 1:1, H₂O:MeCN (10 mL) mixture and lyophilised. The crude peptide was purified by RP-HPLC on a Phenomenex[®] Luna C18 (2) column (100 Å, 5 µm, 100×10 mm) using a gradient of 20–50% B (A: 99.9% H₂O, 0.1% TFA; B: 80% MeCN, 19.9% H₂O, 0.1% TFA) over 30–60 min. The purity and molecular mass of the purified peptide **20** were confirmed with LC-MS on a Shimadzu LCMS2020 instrument, incorporating a Phenomenex[®] Luna C8 column (100 Å, 3 µm, 100×2 mm) and using a linear gradient of 100% H₂O (0.05% TFA) for 4 min, followed by 0–60% MeCN (0.05% TFA) in water over 10 min at a flow rate of 0.2 mL min⁻¹. ¹H NMR (600 MHz, 10% ²H₂O): δ=8.61 (d, *J*=9.5 Hz, 1H), 8.49 (d, *J*=9.5 Hz, 1H), 8.43 (m, 3H), 8.38 (br s, 1H), 8.17 (d, *J*=7.6 Hz, 1H), 8.10 (d, *J*=9.5 Hz, 1H), 7.86 (br s, 1H), 7.81 (br s, 1H), 7.77 (br s, 1H), 7.68 (br s, 1H), 7.28 (br s, 1H), 7.00 (br s, 1H), 6.95 (br s, 2H), 4.47 (m, 1H), 4.42 (m, 1H), 4.13 (br s, 1H), 4.07 (m, 1H), 2.80 (m, 12H), 2.02 (m, 6H), 1.42 (m, 1H), 1.24 (m, 1H), 0.92 (m, 12H).

Acknowledgements

BKY acknowledges fellowship support received from Academic Staff Training Scheme Fellowship of Universiti Sains Malaysia. RSN

and JBB acknowledge fellowship support from the National Health and Medical Research Council of Australia. This study was supported by the Australian National Health Medical Research Council (NHMRC) Grants 1022693 and 487922, as well as an NHMRC IRIISS grant 361646 and a Victorian State Government Operational Infrastructure Scheme grant.

Supplementary data

Supplementary data associated with this article can be found in the online version, at <http://dx.doi.org/10.1016/j.tet.2016.04.051>.

References and notes

- (a) Fosgerau, K.; Hoffmann, T. *Drug Discov. Today* **2015**, *20*, 122–128; (b) Uhlig, T.; Kyprianou, T.; Martinelli, F. G.; Oppici, C. A.; Heiligers, D.; Hills, D.; Calvo, X. R.; Verhaert, P. *EuPA Open Proteomics* **2014**, *4*, 58–69; (c) Kaspar, A. A.; Reichert, J. M. *Drug Discov. Today* **2013**, *18*, 807–817; (d) Sato, A. K.; Viswanathan, M.; Kent, R. B.; Wood, C. R. *Curr. Opin. Biotechnol.* **2006**, *17*, 638–642.
- (a) Kumar, T. R. S.; Soppimath, K.; Nachaegari, S. K. *Curr. Pharm. Biotechnol.* **2006**, *7*, 261–276; (b) Hamman, J. H.; Enslin, G. M.; Kotze, A. F. *BioDrugs* **2005**, *19*, 165–177.
- Woycechowsky, K. J.; Raines, R. T. *Curr. Opin. Chem. Biol.* **2000**, *4*, 533–539.
- In defensins: Ganz, T. *Nat. Rev. Immunol.* **2003**, *3*, 710–720.
- In conotoxins: Terlau, H.; Olivera, B. M. *Physiol. Rev.* **2004**, *84*, 41–68.
- In SHK¹ toxin: Pennington, M. W.; Lanigan, M. D.; Kalman, K.; Mahnir, V. M.; Rauer, H.; McVaugh, C. T.; Behm, D.; Donaldson, D.; Chandy, K. G.; Kem, W. R.; Norton, R. S. *Biochemistry* **1999**, *38*, 14549–14558.
- (a) Katsara, M.; Tselios, T.; Deraos, S.; Deraos, G.; Matsoukas, M. T.; Lazoura, E.; Matsoukas, J.; Apostolopoulos, V. *Curr. Med. Chem.* **2006**, *13*, 2221–2232; (b) Craik, D. J.; Cemazar, M.; Daly, N. L. *Curr. Opin. Drug Discov. Devel.* **2006**, *9*, 251–260.
- (a) Gehrmann, J.; Alewood, P. F.; Craik, D. J. *J. Mol. Biol.* **1998**, *278*, 401–415; (b) Rabenstein, D. L.; Weaver, K. H. *J. Org. Chem.* **1996**, *61*, 7391–7397; (c) Laboisiere, M. C.; Sturley, S. L.; Raines, R. T. *J. Biol. Chem.* **1995**, *270*, 28006–28009.
- (a) Gilbert, H. F. *Meth. Enzymol.* **1995**, *251*, 8–28; (b) Holmgren, A.; Bjornstedt, M. *Meth. Enzymol.* **1995**, *252*, 199–208.
- Muttenthaler, M.; Andersson, A.; de Araujo, A. D.; Dekan, Z.; Lewis, R. J.; Alewood, P. F. *J. Med. Chem.* **2010**, *53*, 8585–8596.
- Mayer, J. P.; Heil, J. R.; Zhang, J.; Munson, M. C. *Tetrahedron Lett.* **1995**, *36*, 7387–7390.
- Jost, K.; Prochazka, Z.; Cort, J. H.; Barth, T.; Skopkova, J.; Prusik, Z.; Sorm, F. *Collect. Czech. Chem. Commun.* **1974**, *39*, 2835–2856.
- Jones, D. S.; Gamino, C. A.; Randow, M. E.; Victoria, E. J.; Yu, L.; Coutts, S. M. *Tetrahedron Lett.* **1998**, *39*, 6107–6110.
- Fotouhi, N.; Joshi, P.; Tilley, J. W.; Rowan, K.; Schwinge, V.; Wolitzky, B. *Bioorg. Med. Chem. Lett.* **2000**, *10*, 1167–1169.
- Knerr, P. J.; Tzekou, A.; Ricklin, D.; Qu, H.; Chen, H.; van der Donk, W. A.; Lambiris, J. D. *ACS Chem. Biol.* **2011**, *6*, 753–760.
- Yap, B. K.; Leung, E. W.; Yagi, H.; Galea, C. A.; Chhabra, S.; Chalmers, D. K.; Nicholson, S. E.; Thompson, P. E.; Norton, R. S. *J. Med. Chem.* **2014**, *57*, 7006–7015.
- Paul, M.; van der Donk, W. A. *Mini Rev. Org. Chem.* **2005**, *2*, 23–37.
- Dekan, Z.; Vetter, I.; Daly, N. L.; Craik, D. J.; Lewis, R. J.; Alewood, P. F. *J. Am. Chem. Soc.* **2011**, *133*, 15866–15869.
- (a) Gairí, M.; Lloyd-Williams, P.; Albericio, F.; Giral, E. *Tetrahedron Lett.* **1994**, *35*, 175–178; (b) Isidro-Llobet, A.; Álvarez, M.; Albericio, F. *Chem. Rev.* **2009**, *109*, 2455–2504.
- Campiglia, P.; Gomez-Monterrey, O.; Longobardo, L.; Lama, T.; Novellino, E.; Grieco, P. *Tetrahedron Lett.* **2004**, *45*, 1453–1456.
- Yap, B. K.; Harjani, J. R.; Leung, E. W. W.; Nicholson, S. E.; Scanlon, M. J.; Chalmers, D. K.; Thompson, P. E.; Baell, J. B.; Norton, R. S. *FEBS Lett.* **2016**, *590*, 696–704.

Supporting Information

An alternative approach to the synthesis of a cystathionine bridge containing cyclic peptide

Jitendra R. Harjani, Beow Keat Yap, Raymond S. Norton and Jonathan B. Baell *

Medicinal Chemistry, Monash Institute of Pharmaceutical Sciences, Monash University, Parkville VIC 3052, Australia.

Synthetic procedures and copies of ^1H NMR, ^{13}C NMR and HRMS spectra.

*Corresponding author. Tel: +61 3 9903 9044, fax: +61 3 9903 9143, e-mail: Jonathan.Baell@monash.edu

Page number	Contents
4	Materials and methods
7	¹ H NMR of Allyl (<i>R</i>)-(2-oxotetrahydrofuran-3-yl)carbamate 8
8	¹³ C NMR of Allyl (<i>R</i>)-(2-oxotetrahydrofuran-3-yl)carbamate 8
9	HRMS of Allyl (<i>R</i>)-(2-oxotetrahydrofuran-3-yl)carbamate 8
10	¹ H NMR of Methyl <i>N</i> -((allyloxy)carbonyl)- <i>O</i> -(<i>tert</i> -butyldimethylsilyl)- <i>D</i> -homoserinate 9
11	¹³ C NMR of Methyl <i>N</i> -((allyloxy)carbonyl)- <i>O</i> -(<i>tert</i> -butyldimethylsilyl)- <i>D</i> -homoserinate 9
12	HRMS of Methyl <i>N</i> -((allyloxy)carbonyl)- <i>O</i> -(<i>tert</i> -butyldimethylsilyl)- <i>D</i> -homoserinate 9
13	¹ H NMR of <i>N</i> -((allyloxy)carbonyl)- <i>O</i> -(<i>tert</i> -butyldimethylsilyl)- <i>D</i> -homoserine 10
14	¹³ C NMR of <i>N</i> -((allyloxy)carbonyl)- <i>O</i> -(<i>tert</i> -butyldimethylsilyl)- <i>D</i> -homoserine 10
15	HRMS of <i>N</i> -((allyloxy)carbonyl)- <i>O</i> -(<i>tert</i> -butyldimethylsilyl)- <i>D</i> -homoserine 10
16	¹ H NMR of 2-phenylpropan-2-yl <i>N</i> -((allyloxy)carbonyl)- <i>O</i> -(<i>tert</i> -butyldimethylsilyl)- <i>D</i> -homoserinate 12
17	¹³ C NMR of 2-phenylpropan-2-yl <i>N</i> -((allyloxy)carbonyl)- <i>O</i> -(<i>tert</i> -butyldimethylsilyl)- <i>D</i> -homoserinate 12
18	HRMS of 2-phenylpropan-2-yl <i>N</i> -((allyloxy)carbonyl)- <i>O</i> -(<i>tert</i> -butyldimethylsilyl)- <i>D</i> -homoserinate 12
19	¹ H NMR of 2-phenylpropan-2-yl ((allyloxy)carbonyl)- <i>D</i> -homoserinate 13

20	¹³ C NMR of 2-phenylpropan-2-yl ((allyloxy)carbonyl)-D-homoserinate 13
21	HRMS of NMR of 2-phenylpropan-2-yl ((allyloxy)carbonyl)-D-homoserinate 13
22	¹ H NMR of 2-phenylpropan-2-yl (<i>R</i>)-2-(((allyloxy)carbonyl)amino)-4-iodobutanoate 3
23	¹³ C NMR of 2-phenylpropan-2-yl (<i>R</i>)-2-(((allyloxy)carbonyl)amino)-4-iodobutanoate 3
24	HRMS of 2-phenylpropan-2-yl (<i>R</i>)-2-(((allyloxy)carbonyl)amino)-4-iodobutanoate 3
25	LCMS of crude 18
26	LCMS of purified 20
27	1D ¹ H NMR spectrum of purified 20
28	Notes and References

Experimental

Materials and methods

For synthesis of **3**, a number of chemicals were procured from commercial suppliers: *N*-(allyloxycarbonyloxy)succinimide (AllocOSu, Chem Impex, 98%), sodium hydrogen carbonate (NaHCO₃, Merck Millipore, ACS reagent grade), anhydrous magnesium sulfate (MgSO₄, Merck Millipore, ACS reagent grade), L-homoserine (Chem Impex, 98%), potassium hydroxide (KOH, EMSURE®, Merck Millipore), Iodo methane (MeI, Sigma Aldrich, reagent grade, > 99%), *tert*-butyldimethylchlorosilane (TBSCl, Alfa Aesar, 97%), imidazole (Sigma Aldrich, LR, > 99%), lithium hydroxide (Sigma Aldrich, reagent grade, 98%), α,α -dimethylbenzyl alcohol (Sigma Aldrich, 97%), trichloroacetonitrile (Sigma Aldrich, reagent grade, 98%), *tetra-n*-butylammonium fluoride (1 M solution in THF, Alfa Aesar), sodium hydride (60 w% dispersion in mineral oil, Sigma Aldrich), iodine (Alfa Aesar, 99%), triphenyl phosphine (Chem Impex, >99%), anhydrous citric acid (Merck Millipore, EMPROVE®), sodium chloride (Merck Millipore, EMPROVE®). 2-Phenylpropan-2-yl 2,2,2-trichloroacetimidate **11** was prepared using method reported elsewhere.¹

Analytical grade solvents dichloromethane (DCM), Chloroform (CHCl₃), diethyl ether (Et₂O), methanol (MeOH), ethyl acetate (EtOAc), ethanol (EtOH), tetrahydrofuran (THF), dimethyl formamide (DMF) and hexanes, supplied by Merck were used during synthetic manipulations, workups and separations.

Analytical TLC was performed on silica gel 60/F254 pre-coated aluminium sheets (0.25 mm, Merck). Celite® S (Sigma Aldrich) was used as a filter aid. Flash chromatography was carried out with the SiliaFlash® P 60 (SiliCycle, 40–64 μ m, 230–400 mesh).

Rink Amide AM Resin (Chem-Impex, 0.56 mEq/g, 1% DVB, 100- 200 mesh), piperidine (Sigma-Aldrich, reagent plus, 99%), dithiothreitol (DTT, Astral Scientific), trifluoroacetic acid (TFA, Auspep, peptide synthesis grade), ethanedithiol (EDT, Sigma-Aldrich, purum, \geq 98%), tetrakis(triphenylphosphine)palladium(0) (Pd(PPh₃)₄, Sigma-Aldrich, 99%), phenylsilane (PhSiH₃, Sigma-Aldrich, 97%), sodium diethyldithiocarbamate (Sigma-Aldrich, \geq 98%), acetic anhydride (Ac₂O, Sigma-Aldrich, ACS reagent), triisopropylsilane (TIPS, Sigma-Aldrich, 99%), dimethoxy benzene (Sigma-Aldrich, \geq 98%), 2,2'-(ethylenedioxy)diethanethiol (DODT, Sigma-Aldrich, 95%), Fmoc-L-Asn(Trt)-OH (Mimotopes, 99.05%), Fmoc-L-Val-OH (Chem-Impex, 100%), Fmoc-L-Cys(S-S-^tBu)-OH (Chem-Impex, \geq 98%), Fmoc-L-Asp(O-^tBu)-OH (Mimotopes, 100%), Fmoc-L-Ile-OH (Chem-Impex, 99%). Dimethyl formamide (DMF, Merck Millipore, Emsure, ACS reagent grade), Dichloromethane (DCM, Merck Millipore, Emsure, ACS reagent grade), Diethyl ether (Et₂O, Merck Millipore, Emsure, ACS reagent grade), Methanol (MeOH, Merck Millipore, Emsure, ACS reagent grade) and Acetonitrile (ACN, Merck Millipore, Lichlorosolv

Isocratic Grade for Liquid Chromatography) were used for peptide synthesis and purification.

NMR

For the small molecules, ^1H and ^{13}C NMR spectra were recorded at 400.13 and 100.62 MHz respectively, on a Bruker Avance III Nanobay spectrometer with a BACS 60 sample changer. The NMR solvents were purchased from Cambridge Isotope Laboratories. Chemical shifts (δ , ppm) are reported relative to the solvent peak (CDCl_3): 7.26 [^1H] or 77.16 [^{13}C]; $\text{DMSO } d_6$: 2.50 [^1H] or 39.52 [^{13}C]). Proton resonances are annotated as: chemical shift (δ), multiplicity (s, singlet; d, doublet; m, multiplet), coupling constant (J , Hz), and the number of protons.

For peptide analysis, the ^1H NMR spectra was recorded at 600 MHz on a Bruker Avance spectrometer equipped with a 5 mm TCI cryoprobe. The NMR solvent deuterium oxide was purchased from Sigma Aldrich. The ^1H chemical shifts (δ , ppm) are referenced to 3-trimethylsilyl-1-propanesulfonic acid sodium sulfate (DSS) purchased from Sigma Aldrich.

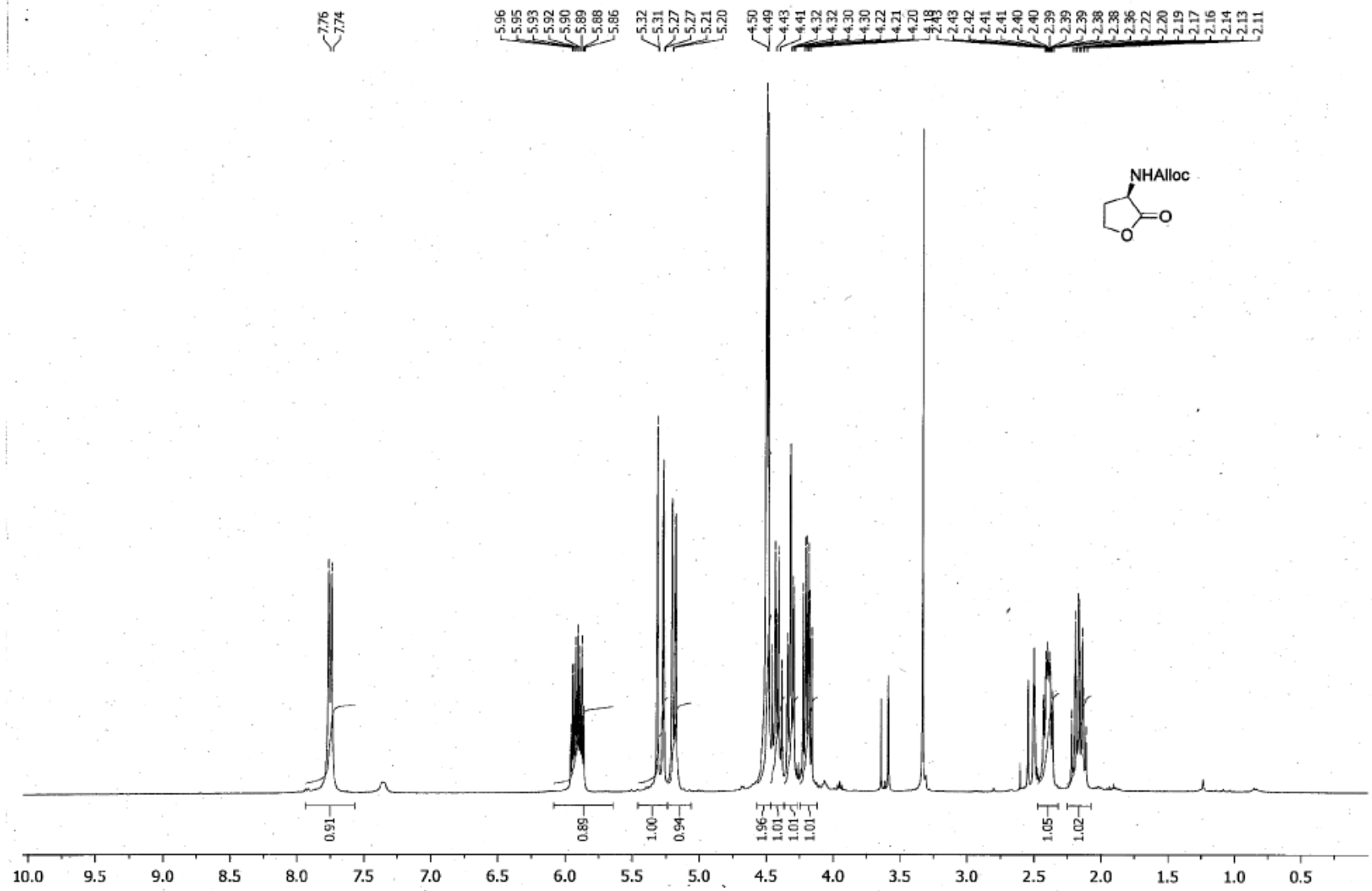
HRMS

High resolution MS was performed with an Agilent 6224 TOF LC/MS coupled to an Agilent 1290 Infinity LC. All data were acquired and reference mass corrected via a dual-spray electrospray ionisation (ESI) source. Each scan or data point on the total ion chromatogram (TIC) is an average of 13,700 transients, producing a spectrum every second. Mass spectra were created by averaging the scans across each peak and subtracting the background from the first 10 s of the TIC. Acquisition was performed using the Agilent Mass Hunter Data Acquisition software ver. B.05.00 Build 5.0.5042.2 and analysis was performed using Mass Hunter Qualitative Analysis ver. B.05.00 Build 5.0.519.13. Acquisition parameters: mode, ESI; drying gas flow, 11 L/min; nebuliser pressure, 45 psi; drying gas temperature, 325 °C; voltages: capillary, 4000 V; fragmentor, 160 V; skimmer, 65 V; octapole RF, 750 V; scan range, 100–1500 m/z; positive ion mode internal reference ions, m/z 121.050873 and 922.009798. LC conditions: Agilent Zorbax SB-C18 Rapid Resolution HT (2.1 × 50 mm, 1.8 mm column), 30 °C; sample (5 μL) was eluted using a binary gradient (solvent A: 0.1% aq. HCO_2H ; solvent B: 0.1% HCO_2H in CH_3CN ; 5–100% B [3.5 min], 0.5 mL/min).

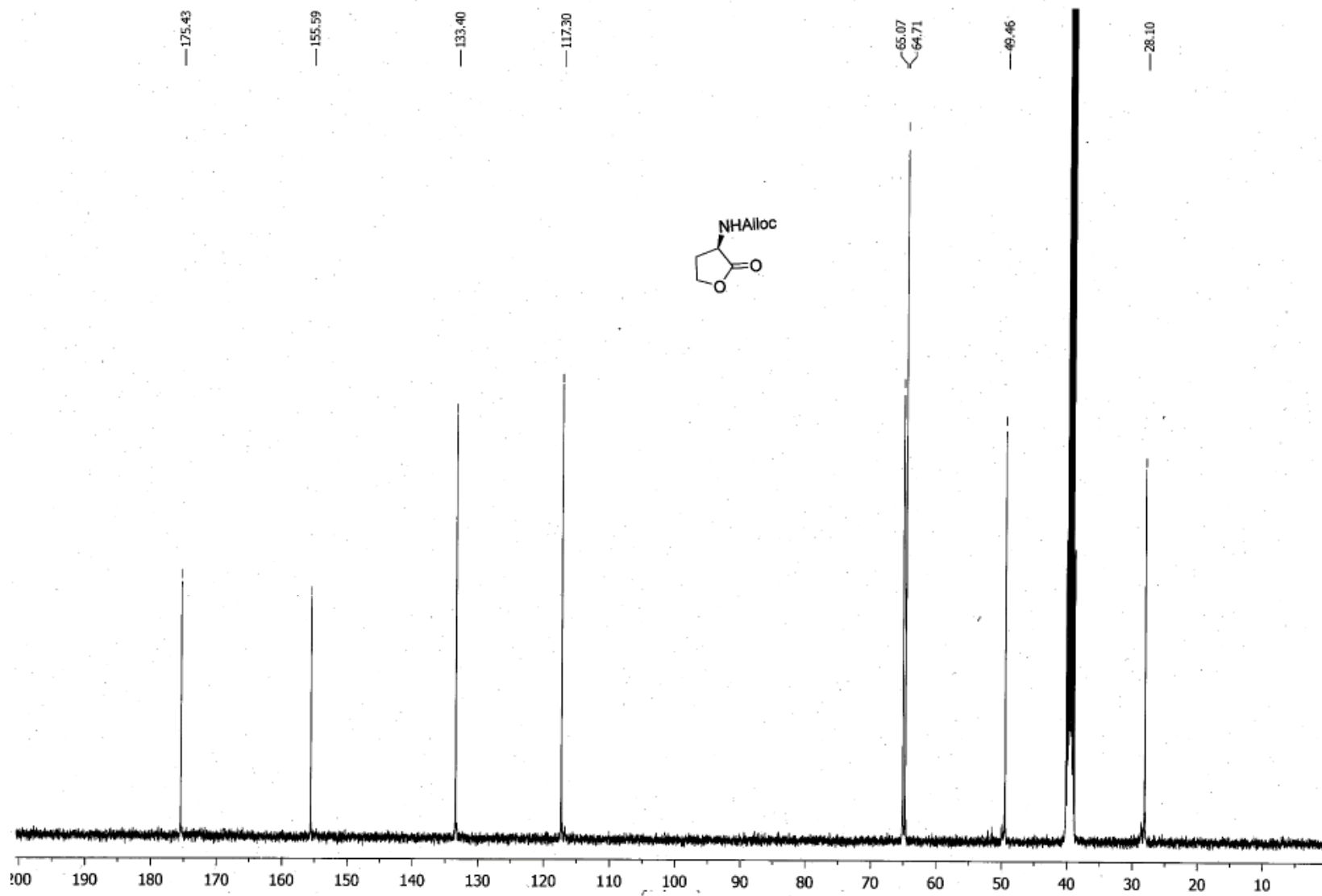
LCMS

The peptide LCMS was performed with a Shimadzu LCMS2020 instrument. All data were acquired and reference mass corrected via an electrospray ionisation (ESI) source. Acquisition and analysis were performed using the LabSolutions software ver. 5.53 SP3. Acquisition parameters: mode, ESI; drying gas flow, 10 L/min; nebulizing gas flow, 1.5 L/min; interface temperature, 350 °C; DL temperature, 250 °C; Heat block, 200 °C; voltages: interface, 4500 V; DL, 0 V; Qarray DC, 0 V; Qarray RF, 60 V; detector, -50 V; scan range, 200–2000 m/z; scan speed,

1875 μ /s; positive ion mode. LC conditions: Phenomenex® Luna C8 column (100 Å, 3 μ m, 100 x 2 mm), 30 °C; sample was eluted using a binary gradient (solvent A: 0.05% aq. TFA; solvent B: 0.05% TFA in CH₃CN; 0–60% B [10 min], 0.2 mL/min).



¹H NMR of Allyl (*R*)-(2-oxotetrahydrofuran-3-yl)carbamate **8**



^{13}C NMR of Allyl (*R*)-(2-oxotetrahydrofuran-3-yl)carbamate **8**

Qualitative Compound Report

Data File	JRH-361-032-01.d	Sample Name	JRH-361-032-01
Sample Type	Sample	Position	P1-B3
Instrument Name	Instrument 1	User Name	Dr Jason Dang
Acq Method	Monash_Direct.m	Acquired Time	11-Aug-15 5:17:20 PM
IRM Calibration Status		DA Method	Monash_Accuracy.m
Comment			

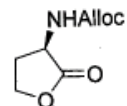
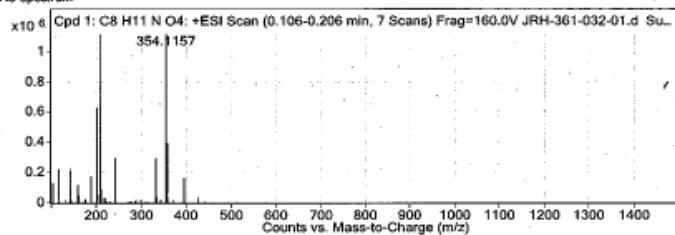
Sample Group	C8H11NO4	Info.	
Formula		Acquisition SW	6200 series TOF/6500 series
		Version	Q-TOF B.05.01 (B5125.1)

Compound Table

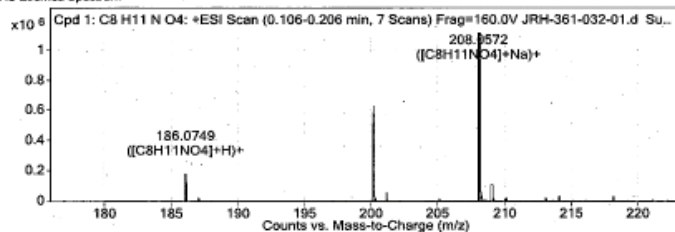
Compound Label	RT	Mass	Abund	Formula	Tgt Mass	Diff (ppm)	MFG Formula	DB Formula
Cpd 1: C8 H11 N O4	0.122	185.068	1117079	C8 H11 N O4	185.0688	-4.32	C8 H11 N O4	C8 H11 N O4

Compound Label	m/z	RT	Algorithm	Mass
Cpd 1: C8 H11 N O4	208.0572	0.122	Find By Formula	185.068

MS Spectrum



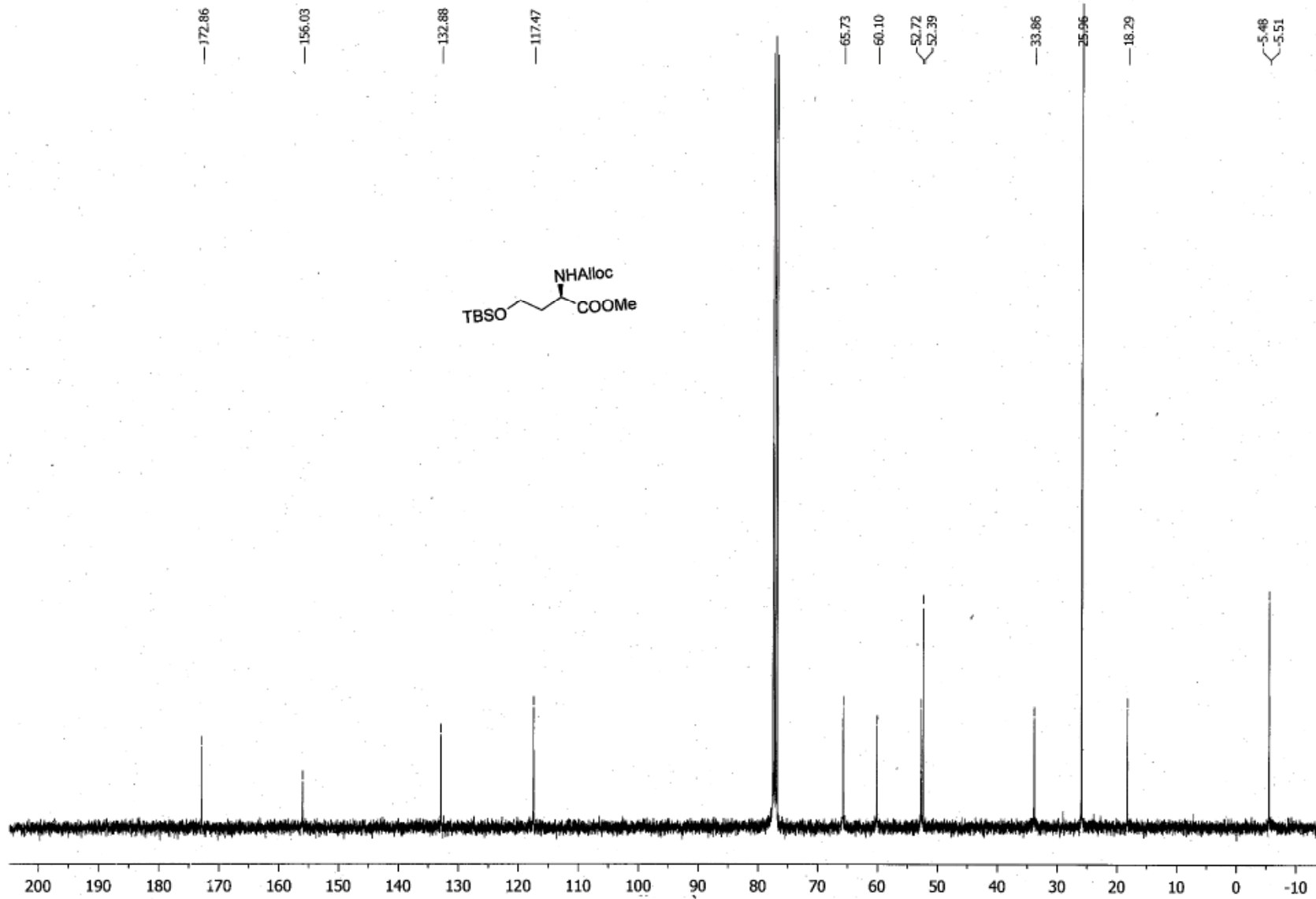
MS Zoomed Spectrum



MS Spectrum Peak List

m/z	Calc m/z	Diff (ppm)	z	Abund	Formula	Tot
186.0749	186.0761	6.22	1	179890.96	C8H11NO4	(M+H)+
208.0572	208.058	4	1	1117079.37	C8H11NO4	(M+Na)+
354.1157				2437344.82		

HRMS of Allyl (*R*)-(2-oxotetrahydrofuran-3-yl)carbamate **8**



¹³C NMR of Methyl *N*-((allyloxy)carbonyl)-*O*-(*tert*-butyl dimethylsilyl)-*D*-homoserinate **9**

Qualitative Compound Report

Data File	JRH-361-060-01.d	Sample Name	JRH-361-060-01
Sample Type	Sample	Position	P1-84
Instrument Name	Instrument 1	User Name	Dr Jason Dang
Acq Method	Monash_Direct.m	Acquired Time	11-Aug-15 5:20:37 PM
IRM Calibration Status		DA Method	Monash_Accuracy.m
Comment			

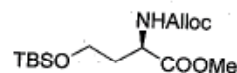
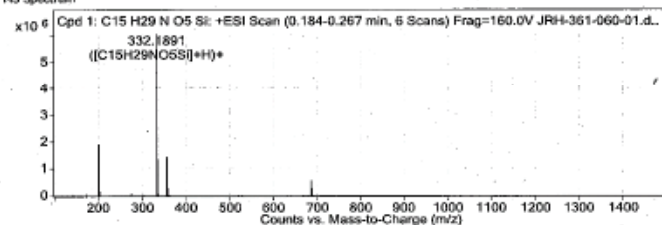
Sample Group		Info.	
Formula	C15H29NO5Si	Acquisition SW	6200 series TOF/6500 series
		Version	Q-TOF 8.05.01 (B5125.1)

Compound Table

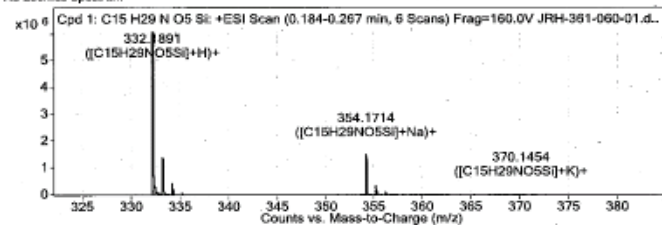
Compound Label	RT	Mass	Abund	Formula	Tgt Mass	Diff (ppm)	MFG Formula	DB Formula
Cpd 1: C15 H29 N O5 Si	0.117	331.182	6107804	C15 H29 N O5 Si	331.1815	1.45	C15 H29 N O5 Si	C15 H29 N O5 Si

Compound Label	m/z	RT	Algorithm	Mass
Cpd 1: C15 H29 N O5 Si	332.1891	0.117	Find By Formula	331.182

MS Spectrum



MS Zoomed Spectrum

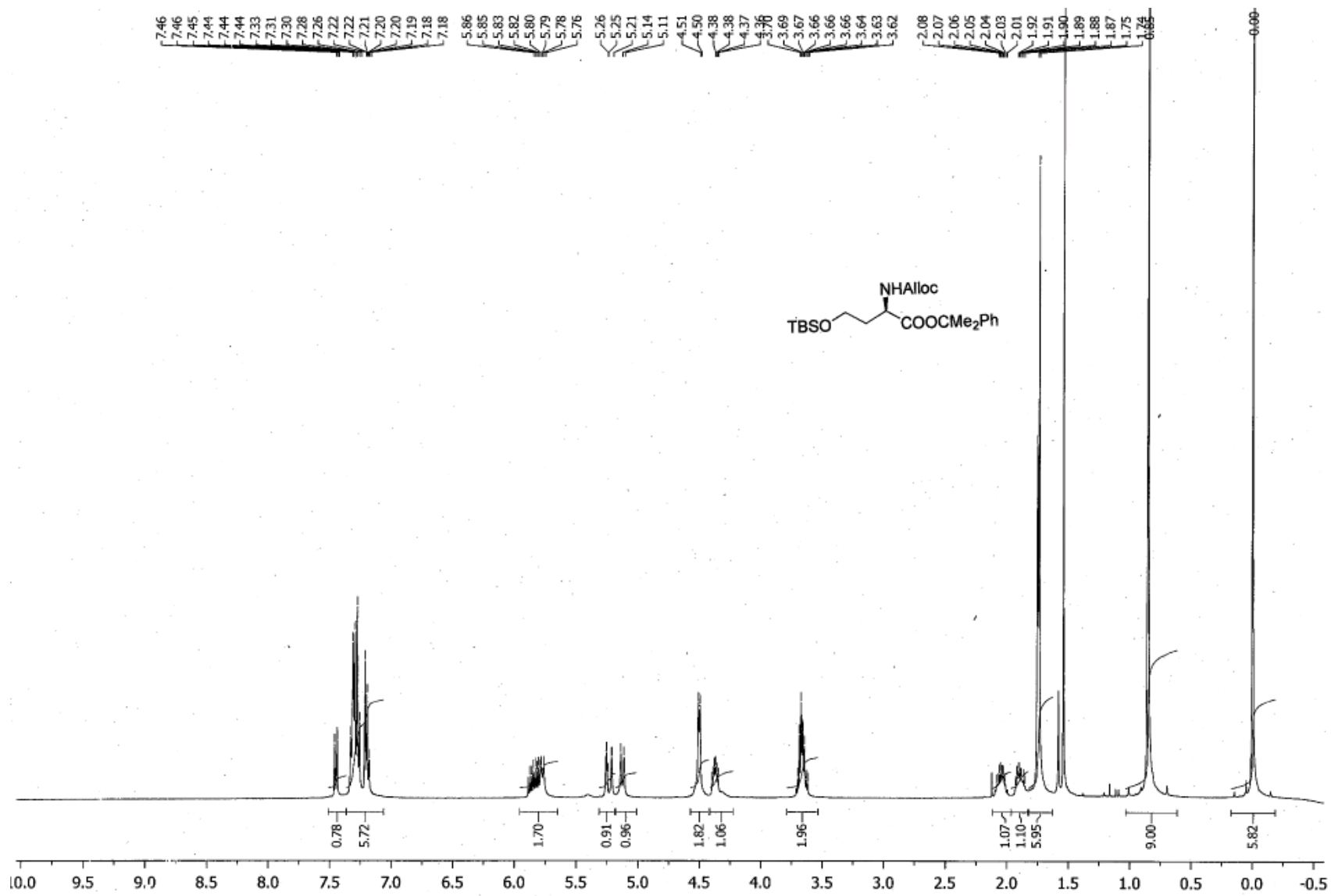


MS Spectrum Peak List

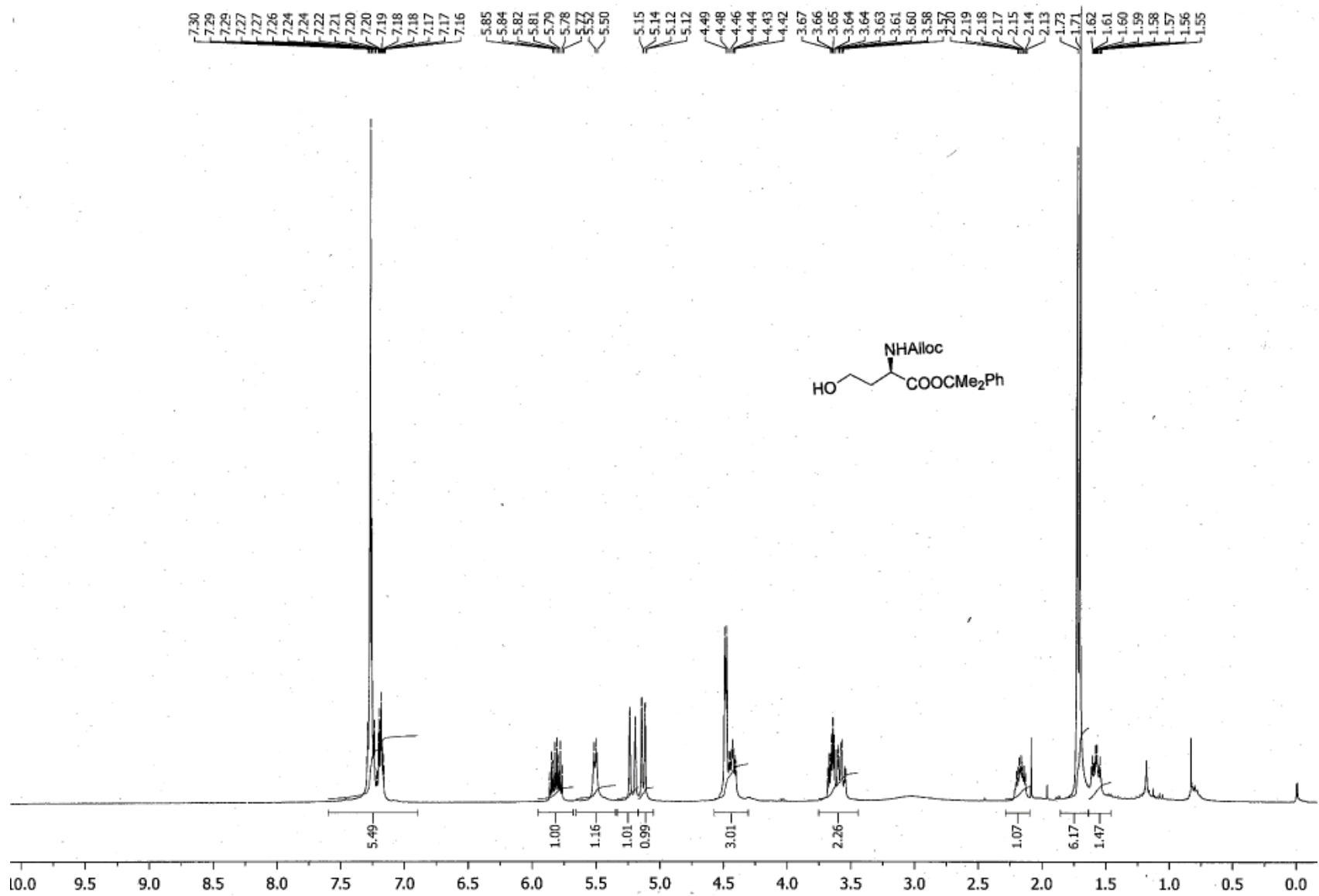
m/z	Calc m/z	Diff(ppm)	z	Abund	Formula	Ion
332.1891	332.1888	-1.04	1	6107804.46	C15H29NO5Si	(M+H)+
354.1714	354.1707	-1.85	1	1479865.97	C15H29NO5Si	(M+Na)+
370.1454	370.1447	-2.08	1	12138.59	C15H29NO5Si	(M+K)+

--- End Of Report ---

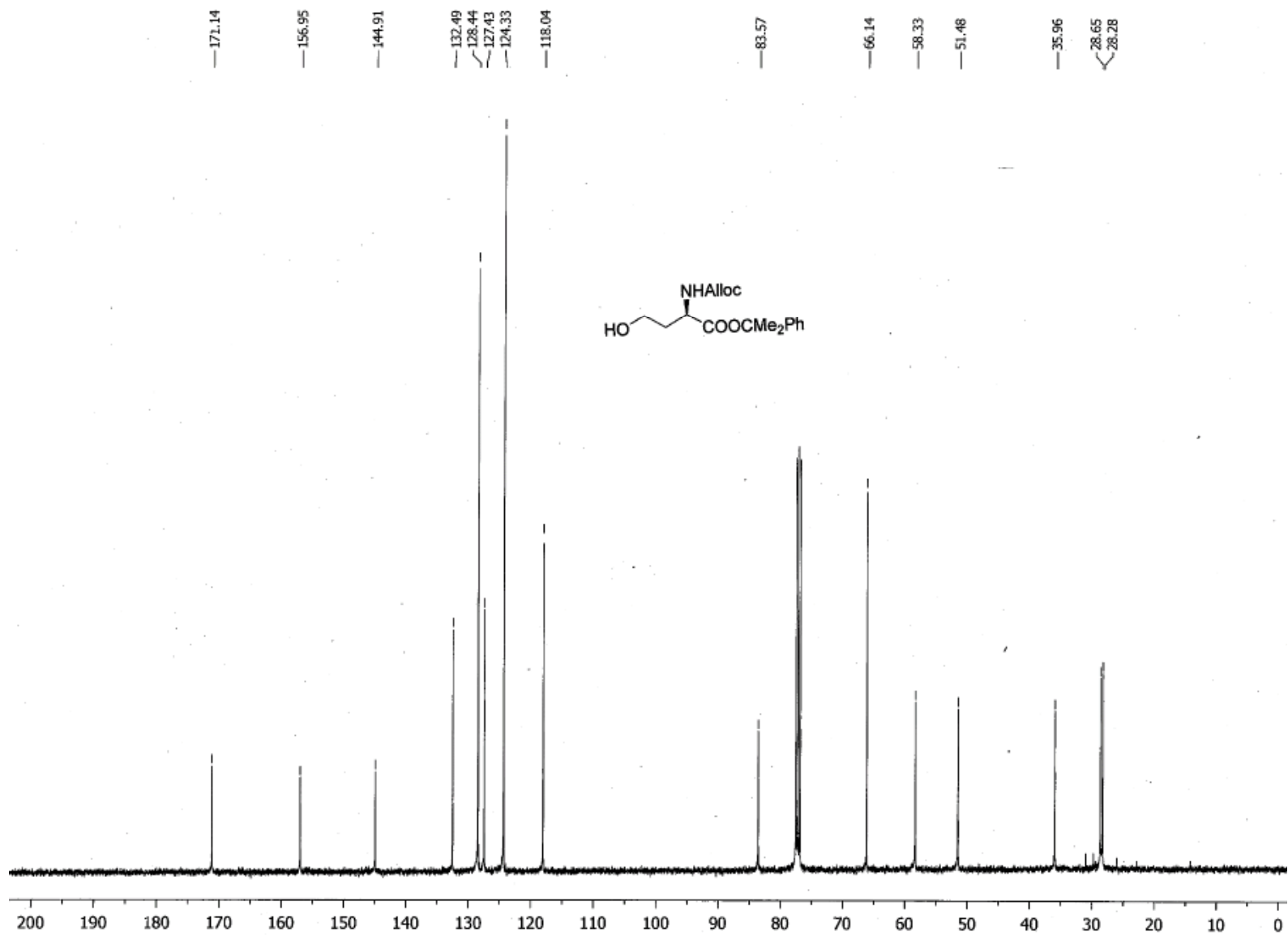
HRMS of Methyl *N*-((allyloxy)carbonyl)-*O*-(*tert*-butyldimethylsilyl)-*D*-homoserinate **9**



¹H NMR of 2-phenylpropan-2-yl N-((allyloxy)carbonyl)-O-(tert-butyl dimethylsilyl)-D-homoserinate 12



¹H NMR of 2-phenylpropan-2-yl ((allyloxy)carbonyl)-D-homoserinate **13**



¹³C NMR of 2-phenylpropan-2-yl ((allyloxy)carbonyl)-D-homoserinate **13**

Qualitative Compound Report

Data File	JRH-361-072-01.d	Sample Name	JRH-361-072-01
Sample Type	Sample	Position	P1-B7
Instrument Name	Instrument 1	User Name	Dr Jason Dang
Acq Method	Monash_Direct.m	Acquired Time	11-Aug-15 5:30:24 PM
IRM Calibration Status	██████████	DA Method	Monash_Accuracy.m
Comment			

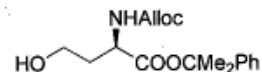
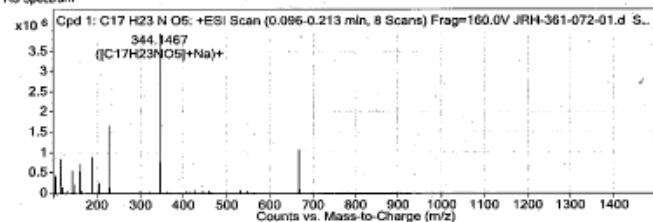
Sample Group		Info.	
Formula	C17H23NO5	Acquisition SW	6200 series TOF/6500 series
		Version	Q-TOF 8.05.01 (85125.1)

Compound Table

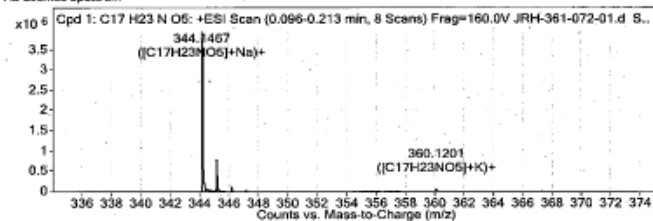
Compound Label	RT	Mass	Abund	Formula	Tgt Mass	Diff (ppm)	MFG Formula	DB Formula
Cpd 1: C17 H23 N O5	0.113	321.1576	3953544	C17 H23 N O5	321.1576	-0.21	C17 H23 N O5	C17 H23 N O5

Compound Label	m/z	RT	Algorithm	Mass
Cpd 1: C17 H23 N O5	344.1467	0.113	Find By Formula	321.1576

MS Spectrum



MS Zoomed Spectrum

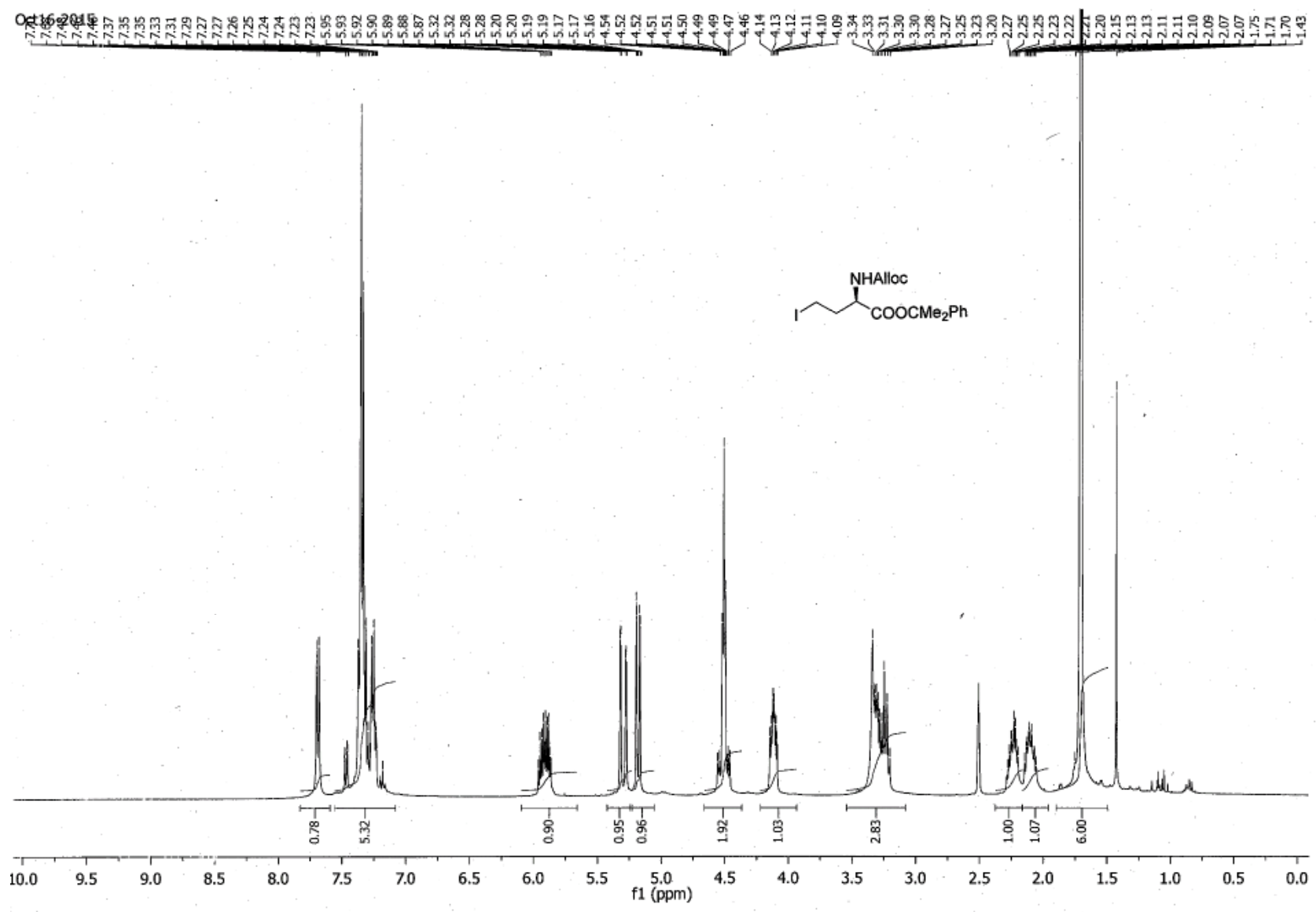


MS Spectrum Peak List

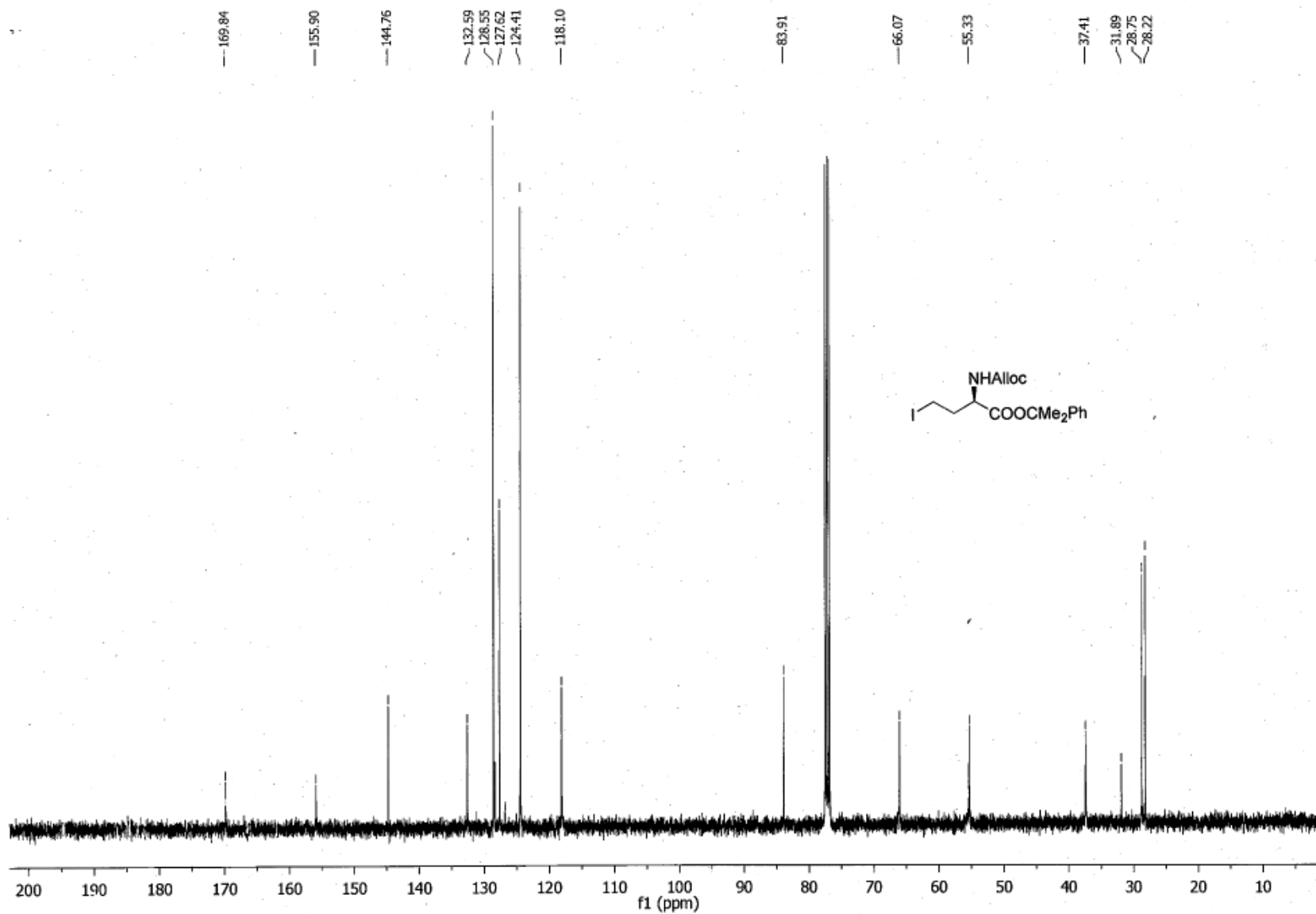
m/z	Calc m/z	Diff(ppm)	z	Abund	Formula	Ion
344.1467	344.1468	0.3	1	3953544.11	C17H23NO5	(M+Na)+
345.1503	345.1501	-0.47	1	779157.12	C17H23NO5	(M+Na)+
360.1201	360.1208	1.85	1	32780.29	C17H23NO5	(M+K)+

--- End Of Report ---

HRMS of 2-phenylpropan-2-yl ((allyloxy)carbonyl)-D-homoserinate **13**



¹H NMR of 2-phenylpropan-2-yl (R)-2-(((allyloxy)carbonyl)amino)-4-iodobutanoate **3**



^{13}C NMR of 2-phenylpropan-2-yl (*R*)-2-(((allyloxy)carbonyl)amino)-4-iodobutanoate **3**

Qualitative Compound Report

Data File	JRH-361-076-01.d	Sample Name	JRH-361-076-01
Sample Type	Sample	Position	P1-B8
Instrument Name	Instrument 1	User Name	Dr Jason Dang
Acq Method	Monash_DirectLim	Acquired Time	11-Aug-15 5:33:41 PM
IRM Calibration Status		DA Method	Monash_Accuracy.m
Comment			

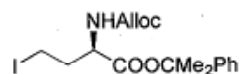
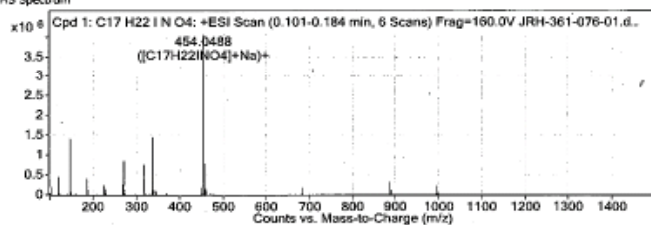
Sample Group		Info.	
Formula	C17H22INO4	Acquisition SW	6200 series TOF/6500 series
		Version	Q-TOF B.05.01 (B5125.1)

Compound Table

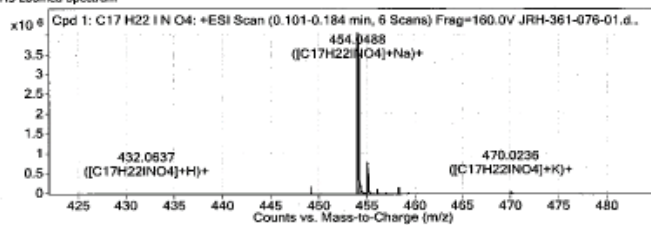
Compound Label	RT	Mass	Abund	Formula	Tgt Mass	Diff (ppm)	MFG Formula	DB Formula
Cpd 1: C17 H22 I N O4	0.118	431.0597	4059136	C17 H22 I N O4	431.0594	0.76	C17 H22 I N O4	C17 H22 I N O4

Compound Label	m/z	RT	Algorithm	Mass
Cpd 1: C17 H22 I N O4	454.0488	0.118	Find By Formula	431.0597

MS Spectrum



MS Zoomed Spectrum

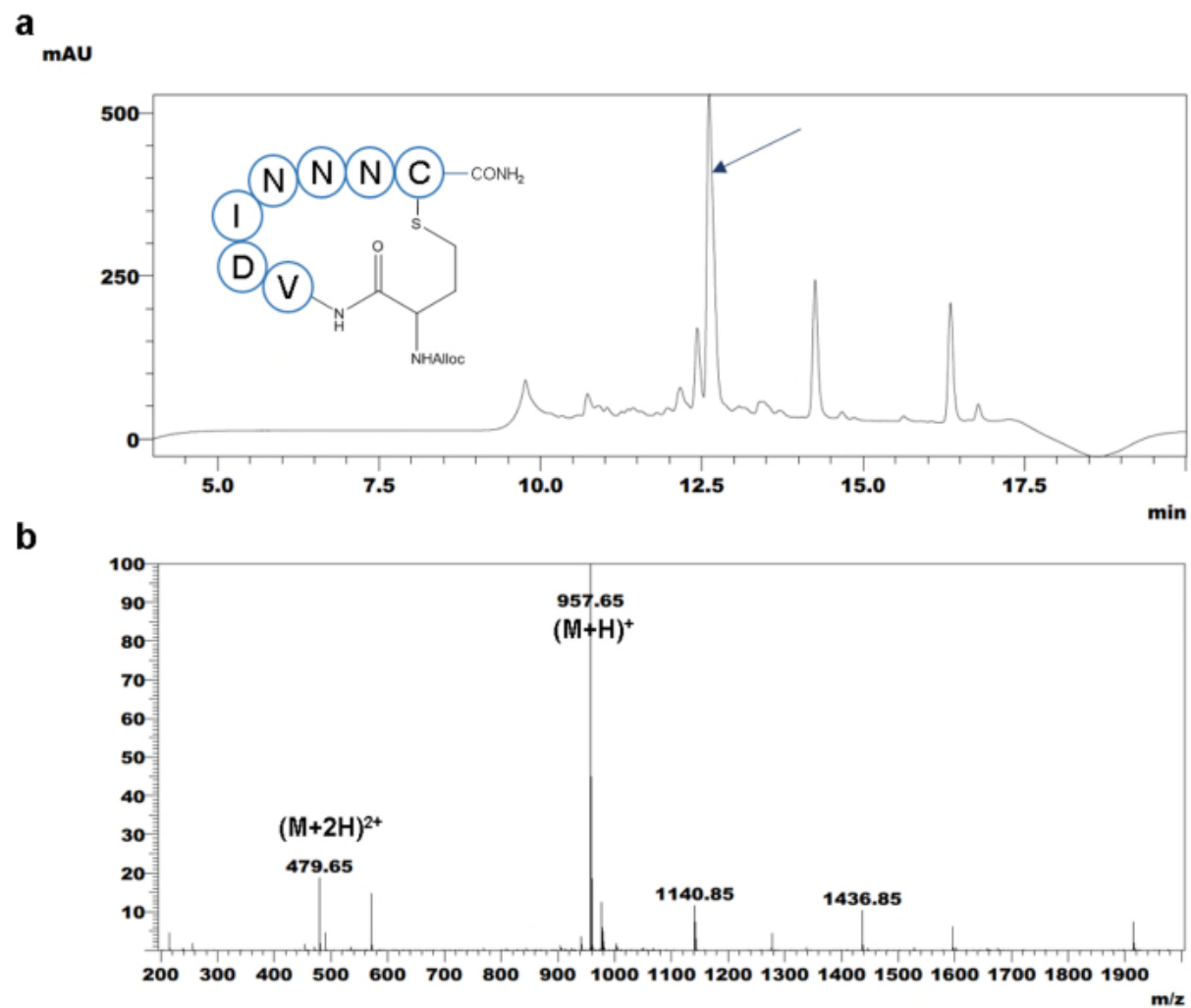


MS Spectrum Peak List

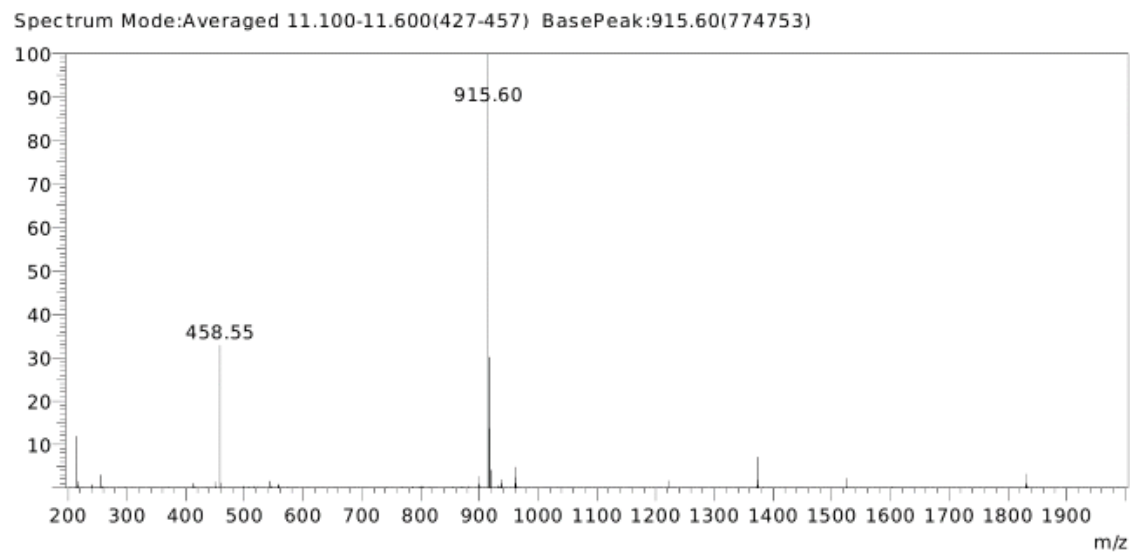
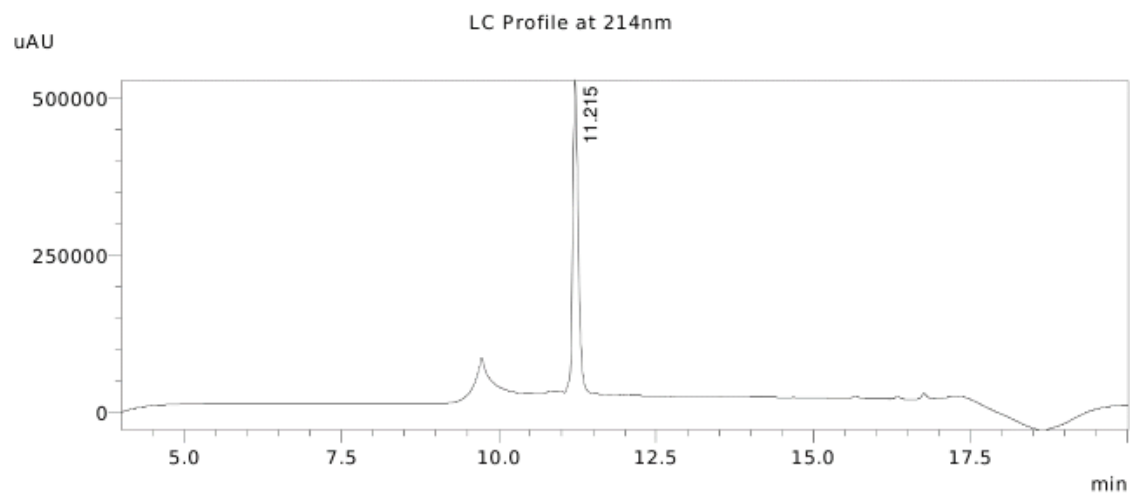
m/z	Calc m/z	Diff(ppm)	z	Abund	Formula	Ion
432.0637	432.0666	6.89	1	361.95	C17H22INO4	(M+H)+
454.0488	454.0486	-0.57	1	4059135.67	C17H22INO4	(M+Na)+
470.0236	470.0225	-2.34	1	43416.63	C17H22INO4	(M+K)+

--- End Of Report ---

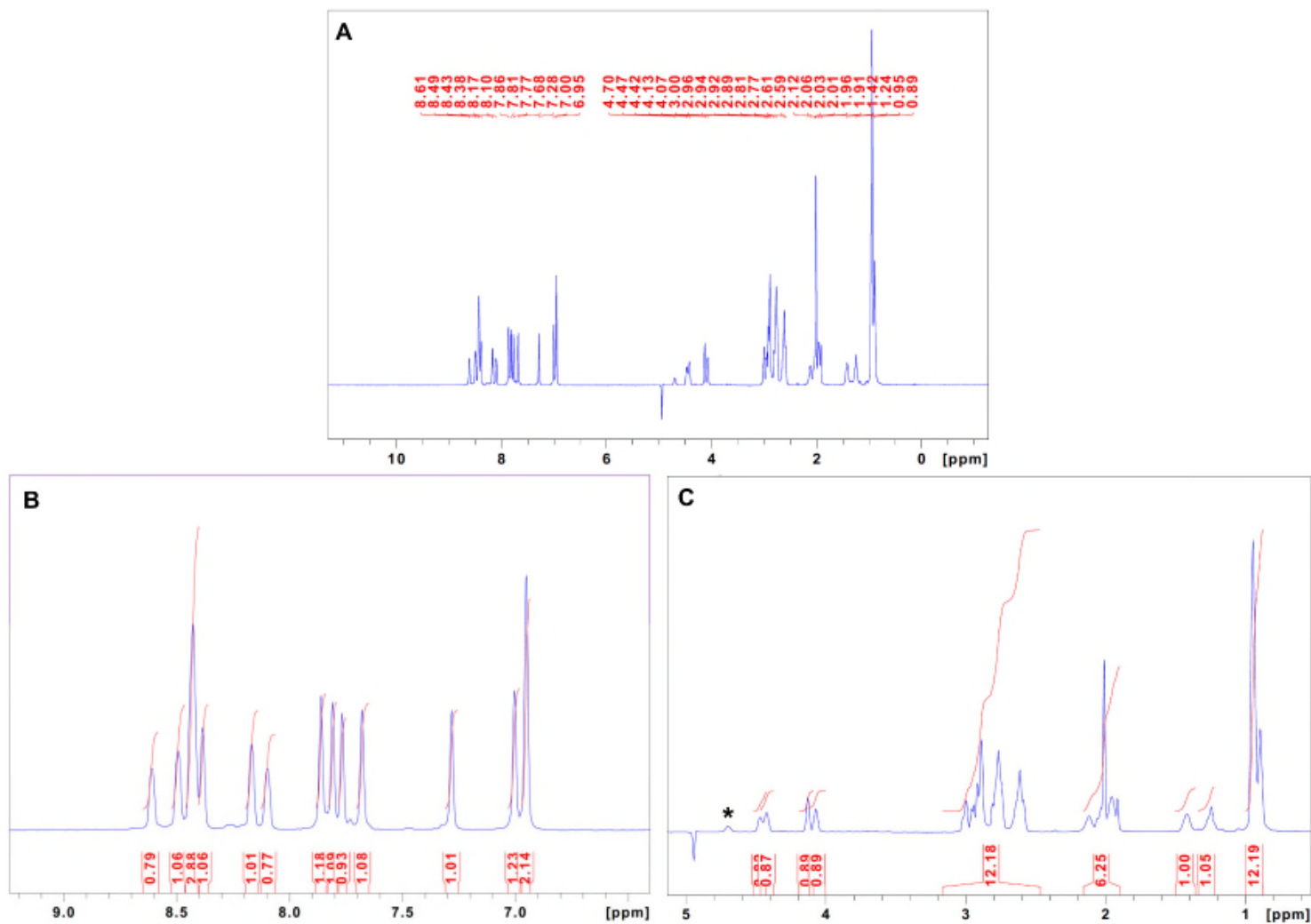
HRMS of 2-phenylpropan-2-yl (*R*)-2-(((allyloxy)carbonyl)amino)-4-iodobutanoate **3**



UV trace in the LC and MS profiles of the crude sample from test cleavage of cyclized Alloc-protected cystathionine analogue in 92.5% (v/v) TFA, 2.5% (v/v) TIPS, 2.5% (v/v) DODT and 2.5% (v/v) DMB. The deconvoluted mass i.e. 947.65 of the major peak (blue arrow) matches the theoretical mass, suggesting that proposed synthesis steps **a-f** were successful



UV trace in LC and MS profiles of the purified **20**. Purity is ~95%, based on the peak area in the chromatogram



1D ^1H NMR spectrum of purified **20** in water, pH 4.8, with 10% $^2\text{H}_2\text{O}$, acquired at 10 °C on a 600 MHz spectrometer. (A) Chemical shifts of each proton resonance are labeled, with integration of peaks in both (B) amide and (C) aliphatic regions shown. Peak in aliphatic region that are close to the suppressed water peak at 4.94 ppm (labeled as asterick), however, was not integrated.

Notes and References:

1. T. Respondek, E. Cueny, J. J. Kodanko, *Org. Lett.*, 2012, **14**, 150.